Doctoral Dissertation
Doctoral Program in Bioengineering and Medical-Surgical sciences (31st Cycle)

Development of 3D skin model and 3D skin infection model, as advanced testing tools for the bio-evaluation of antimicrobial biomaterials for wound healing

Ayesha Idrees
* * * * * *

Supervisors
Prof. Valeria Chiono, Supervisor
Dr. Jochen Salber, Co-Supervisor

Politecnico di Torino
April 28, 2019

I hereby declare that, the contents and organization of this dissertation constitute my own original work and does not compromise in any way the rights of third parties, including those relating to the security of personal data.

Ayesha Idrees.

.....

Ayesha Idrees
Turin, April 28, 2019

Summary

Infected wounds still represent a great challenge in public health. With an increasing need for novel strategies to combat wounds colonized with resistant microbes, more reliable preclinical data are needed to bioanalyze antimicrobial polymeric biomaterials (AMPBs). A 3D human skin equivalent (HSE) and wound infection model (c-HSE) are highly demanded to serve as biomimetic system for the testing of AMPBs.

Initially, murine *in vitro* dermal construct and human *in vitro* dermal construct (HDC) were generated, leading to evaluation of different viability assays to optimize the best suited assay to the respective cell type and 3D system (Chapter 02). Then, in-house reconstructed human epidermis (RHE) and reconstructed murine epidermis (RME) were developed with the aim to use them as test systems for biological evaluation (to understand the relevance of outcomes obtained from human- and animal-based systems) and as basis to develop more complex 3D skin models (Chapter 03).

The dermal and epidermal-based full-thickness human skin equivalent (HSE) was developed by optimizing three-dimensional cell culture conditions (3D-CCs) to obtain the epidermal differentiation mimicking as closely as possible native human skin (NHS). The HSE was fully characterised for its morphology, proteins' tissue distribution (Ki-67, K10, K14, Laminin 5, filaggrin and loricin), ultrastructure tissue architecture, and barrier function properties. The dermis showed uniformly distributed fibroblasts all along the dermal length. The epidermis showed characteristic multi-layered well-differentiated epidermis, right level of expression of epidermal differentiation markers at correct anatomical locations, basement membrane features with lamina lucida (LL), lamina densa (LD), interwoven ECM network, and contact angle of 82.5° ± 8.9°, closely imitating the properties of NHS (Chapter 04). The *in vitro S. aureus* colonized HSE model was coded as c-HSE. Bacterial aggregations and early biofilm formation were observed at wound site on c-HSE. Moreover, fibroblasts/keratinocytes cell lysis, *S. aureus* induced ECM degradation, and bacterial internalization by keratinocytes were also observed (Chapter 05). To validate the 3D systems, Ag^{+} as an antibacterial agent and commercially available Ag containing antimicrobial wound dressings (Ag-dressings) were tested for cytocompatibility and antimicrobial properties using HSE and c-HSE. On the other hand, murine fibroblast & epidermal cell lines and human primary fibroblasts & keratinocytes were used as 2D cytocompatibility evaluation systems. Ag^{+} and Ag-dressings were evaluated for their antibacterial activities (e.g. MIC, MBC, CFU percentage reduction) against clinically relevant pathogens under different growth media. 3D tissue culture models indicated an 'environmental effect' on Ag^{+} induced cytotoxicity, with decreased sensitivity for cells in 3D with respect

to cells in 2D cultures. The considerable variation in antibacterial outcomes obtained using different growth media indicated that antibacterial ability of Ag^+ was highly dependent on wound extracellular micro-environment, affecting Ag^+ availability. This variation also reflects that various media may support bacterial growth differently. The bio-evaluation results of tested Ag-dressings demonstrated that as the cell viability decreased, the antibacterial effect increased. Among the tested Ag-dressings, Biatain® Ag was able to significantly reduce bacteria in c-HSE without significantly compromising cell viability of HSE in our advanced experimental set-ups. Also, it is worth noticing that the bio-evaluation outcomes were different in 2D monolayer vs. 3D cell culture systems and conventionally used microbial methods vs. advanced c-HSE system. With an increasing need for reliable *in vitro* testing systems, we were successfully able to verify our advanced 3D models, to serve as a risk assessment platform for cytocompatibility and antibacterial properties (Chapter 06).

Additional efforts were addressed to the evaluation of the antibacterial properties and cytotoxicity of novel drug-free antibacterial biomaterials (developed by project collaborators ESR01 and ESR07, https://hymedpoly.eu/project-and-researchers/) intended for infected wound healing applications:

(1) Chitosan/Ag-doped mesoporous bioactive glass composite films (CS/ Ag-MBG) (either using ordered or non-ordered MBGs). Owing to observed antibacterial and cytocompatibility properties, Ag-doped composites especially with ordered MBG might have a potential for wound application (Chapter 07).

(2) H_2O_2 releasing hydrogels HB-PEGDA (hyperbranched polyethylene glycol with numerous acrylate groups)/HA-SH (thiolated hyaluronic acid) and PLGA (poly L-lactide-co-glycolide)-PEG (poly ethylene glycol)-PLGA copolymer hydrogels, both containing glucose and various concentrations of glucose oxidase (G/GO). The suitability of a certain hydrogel matrix for G/GO encapsulation and GO distribution within the hydrogel need to be carefully studied.

As a conclusion, H_2O_2 as an antibacterial agent should be used carefully for wound cleaning to kill pathogens, as at high concentrations it might damage newly proliferating cells surrounding the wound area (Chapter 08, Chapter 09, Chapter 09-Appendix D).

Acknowledgment

I would like to thank both of my supervisors Prof. Valeria Chiono and Dr. Jochen Salber for their continued support and valuable guidance from day one throughout my PhD.

My supervisors Prof. Valeria Chiono from Department of Mechanical and Aerospace Engineering (DIMEAS), Politecnico di Torino, Turin, Italy; and Dr. Jochen Salber (Senior Physician Surgery, HOD – Experimental Surgery) from Clinic of Surgery, UMC Knappschaftskrankenhaus Bochum, Hospital of the RUHR University Bochum and Centre for Clinical Research, RUHR University Bochum, Germany, have provided great encouragement in my PhD journey.

I would like to thank Prof. Gianluca Ciardelli (Group Leader - Materials in Bio-nanotechnology and Biomedical Lab) and PhD coordinator, DIMEAS, Politecnico di Torino, Turin, Italy for his valuable support throughout and advices time to time.

I would like to thank Dr. Sandra Pacharra, my former colleague at Centre for Clinical Research, RUHR University Bochum, Germany for being there as a friend and as a senior.

I would like to thank Ms. Susanna Sartori from DIMEAS, Politecnico di Torino, Turin, Italy for being supportive in administrative responsibilities.

I would like to thank Dr. Inge Schmitz, Ms. Mahnaz Ferrera & Ms. Anja Koch (both as technical staff persons), and Prof. Andrea Tannapfel (HOD) from Institute of Pathology, RUHR University Bochum, Germany for a great support in electron microscopy.

I would like to thank Dr. Lennart Marlinghaus and Prof. Sören G. Gatermann (HOD) from Department of Medical Microbiology, Institute for Hygiene and Microbiology, RUHR University Bochum, Germany for providing us the microbiology facility and technical support.

I would like to thank Ms. Wenfa Yu (PhD student) and Prof. Axel Rosenhahn (Group Leader - analytical chemistry-biointerfaces) from Faculty of Chemistry and Biochemistry, RUHR University Bochum, Germany for providing us contact angle measurement facility.

I would like to thank Mr. Björn Thielker, workshop manager, Workshop of Medical Institution, RUHR University Bochum, Germany for being helpful in designing our in-house built spacers for 3D cell culture system.

Our collaboration partners for providing us biomaterials (Chitosan/Ag-doped mesoporous bioactive glass based composite films) Ms. Seray Schmitz (PhD student), Prof. Aldo R. Boccaccini (her supervisor) from Institute of Biomaterials, Friedrich Alexander University (FAU) Erlangen-Nuremberg, Germany, and Dr. Mark Cresswell (her external supervisor) from Lucideon Ltd., Stoke-on-Trent, UK.

Our collaboration partners for providing us biomaterials (glucose and glucose oxidase encapsulated hydrogels) Ms. Jeddah Marie Vasquez (PhD student), Prof. Valeria Chiono (our supervisor) from Department of Mechanical and Aerospace Engineering, Politecnico di Torino, Turin, Italy, Dr. Udo Greiser and Prof. Wenxin Wang (both as her external advisors) from Vornia Ltd., Dublin, Ireland.

The work was supported by European Union's Horizon 2020 research and innovation programme under the Marie Skłodowska-Curie grant agreement No 643050 (HyMedPoly Project). I highly acknowledge our funding source as well as whole HyMedPoly consortium team, Prof. Xiang Zhang (Project Coordinator) from Lucideon Ltd., and Prof. Ipsita Roy (Scientific Coordinator) from Department of Life Science, University of Westminster, London, UK.

Last but not the least I would like to thank my beloved husband Nabeel Ahmed Ansari and my parents (Mr. Mirza Idrees Baig and Mrs. Shafqat Idrees) for their unconditional love and support to keep me going through this bumpy path.

I would also like to thank my family and friends.

I would like to dedicate this thesis to my loving husband and parents

"The dissertation is dedicated to my loving husband ***Nabeel Ahmed Ansari*** *and my parents Mrs. Shafqat Idrees and Mr. Mirza Idrees Baig, who instilled in me the virtues of perseverance and commitment and relentlessly encouraged me to strive for excellence. I proudly dedicate my work to their unconditional love and support.*

Table of chapters

Chapter 01: A Review on Three-dimensional (3D) *In vitro* Human Skin Models – *In vitro* and *In vivo* Applications and Concepts: State-of-the-art and Future Trends

Table of contents

List of figures

List of tables

Abbreviations

2D: Two-dimensional
3D: Three-dimensional
Autologous: Patient's own cells
Allogeneic: Genetically different source (i.e. another individual of same species with human leukocyte antigens or HLA matches)
A. baumannii: Acinetobacter baumannii
A. junii: Acinetobacter junii
AFM: Atomic force microscopy
ALI: air-liquid interface
ASTM: American society for testing and materials
ATCC: American Type Culture Collection
BRAF: v-Rafmurine sarcoma viral oncogene homolog B1
C. albicans: Candida albicans
CAM: Cell adhesion molecules
CDFF: Constant depth film fermenter
c-KIT: v-Kit Hardy-Zuckerman 4 feline sarcoma viral oncogene homolog
CYPs: Cytochrome Proteins
DARPA: Defense Advanced Research Project Agency
DCs: Dendritic cells
ECM: Extracellular matrix
ECs: Endothelial cells
ECVAM: European Centre for the Validation of Alternative Methods
EDNRB: Endothelin receptor type b
EGFR: Epidermal growth factor receptor
EGFR: Epidermal growth factor receptor
ERK1/2: Extracellular signal-regulated kinases
FLIM: Fluorescence lifetime imaging microscopy
FT: Full-thickness
GI: Gastrointestinal
GM-CSF: Granulocyte macrophage-colony stimulating factor
GM-CSF: Granulocyte-monocyte colony-stimulating factor
H & E: Haematoxylin and eosin
HSV: Herpes simplex virus
IGFR: Insulin-like growth factor receptor
IHC: Immunohistochemistry
IL-1 α: Inteleukin1 α
INK4a: Cyclin-dependent kinase inhibitor 2a
iPS: Induced pluripotent stem cells
JIS Z-2801: Japanese industrial standards Z-2801
K: Keratins
KGF: Keratinocyte growth factor
LCs: Langerhans cells

MAPKs: Mitogen-activated protein kinases
Mel-CA: Melanoma Cell Adhesion molecule
MITF: Microphthalmia-associated transcription factor
MMPs: Matrix metalloproteinases
MOC: Multi-organ-chip
MSL: Melanoma cell line
mTOR: Mechanistic target of rapamycin
MTT: 5-dimethylthiazol-2-yl-2,5-diphenyltetrazolium bromide
NIH: National Institutes of Health
NKs: Natural killer cells
NMF: Natural moisturizing factors
P. aeruginosa: Pseudomonas aeruginosa
PCL: Polycaprolactone
PDGF: Platelet derived growth factor
PLGA: Polylactic-co-glycolic acid
PTM: Post-translational modification
REACH: European regulatory program for Registration, Evaluation, Authorization and Restriction of Chemicals
RHE: Reconstituted human epithelia (SkinEthic Laboratories, Nice, France)
RNA FISH: Fluorescence RNA *In Situ* hybridization
ROS: Reactive oxygen species
S. aureus: Staphylococcus aureus
SB: Stratum basale (stratum germinativum).
SC: Stratum corneum
SC-A: Cyclosporine-A
SEM: Scanning electron microscopy
SG: Stratum granulosum
SHG: Second harmonic generation microscopy
SL: Stratum lucidum
SLUG: Snail homolog 2
SS: Stratum spinosum
TBSA: Total body surface area
TEM: Transmission electron microscopy
TER: Transcutaneous electrical resistances
TG: Test guidelines
TGF: Transforming growth factor
TGF-β: Platelets release tumour growth factor-β
THG: Third harmonic generation microscopy
TNF-α: Tumour necrosis factor-α
VBNC: Viable but not culturable bacteria
VEGF: Vascular endothelial growth factor
VZV: Varicella zoster virus
WHO: World Health Organization

α-MSH: α-melanocyte stimulating hormone
Xenogeneic: Genetically and immunologically different source (i.e. from another species)

Chapter 01: Review on Three-dimensional (3D) *In vitro* Human Skin Models – *In vitro* and *In vivo* Applications and Concepts: State-of-the-art and Future Trends

Abstract

Significant progress has been made over >40 years in the development of three-dimensional (3D) *in vitro* human skin models to mimic the native human skin. Skin is the protective layer of the body that functions in insulation, body temperature regulation, and sensation, etc.; and impairment in any of the skin functions results in a pathological alteration. Therefore, the development of well-characterized skin models has significant implications. The motivation to achieve organotypic structures was first driven by the clinics to enable transplantation of *in vitro* grown skin grafts. World Health Organization (WHO) estimates that 180,000 people die worldwide from burns per year (excluding the number of non-fatal burns that are a leading cause of morbidity) [1]. The economic burden measured in 2000 in US, revealed a direct cost of more than 211 million US$ for care of burnt children [1]. The availability and efficacy of skin grafts remain limited for severely burnt patients. Alternative grafting techniques are effective in short-term treatment only, besides are susceptible to immune rejection and disease transmission. Therefore, autologous Full-Thickness (FT) skin constructs offer a permanent graft solution.

Cells within an organized three-dimensional (3D) matrix as compared to standard monolayer (2D) cell cultures, recapitulate the physiological architecture and function of the skin. Several companies (e.g. L'Oreal, Henkel, and Mattek Corporation) have been investing to develop 3D human skin models to meet the European restrictions on the animal experimentation (Decree 76/768 / EEC, and then EU Cosmetic Regulation 1223/2009) [2]. Thus, the inspiration to develop skin constructs was further led by cosmetic industry as an alternative test system of animal trials. In this context, besides the development of closely mimicking human skin model, other issues are not less important: standardized procedures of skin model production, process automation, establishment of reliable & significant analytical methods, and data correlation.

This review summarizes the organotypic skin models in different applications. We further highlight the ongoing efforts in developing the complex skin models with more cell types as well as diseased skin models for studies of skin pathology, drug & biomaterials development, and screening.

Keywords: Skin grafts in clinics, EU regulations, three-dimensional (3D) *in vitro* human skin models, an alternative test system of animal trials, drug development, biomaterials testing, drug-free alternatives

1.1 General architecture of skin

The skin is the largest and a complex organ of the body that works as a protective interface between the surrounding environment and underlying organs. The skin comprises of three layers: epidermis, dermis, and hypodermis (also known as subcutaneous) (Figure 1.1).

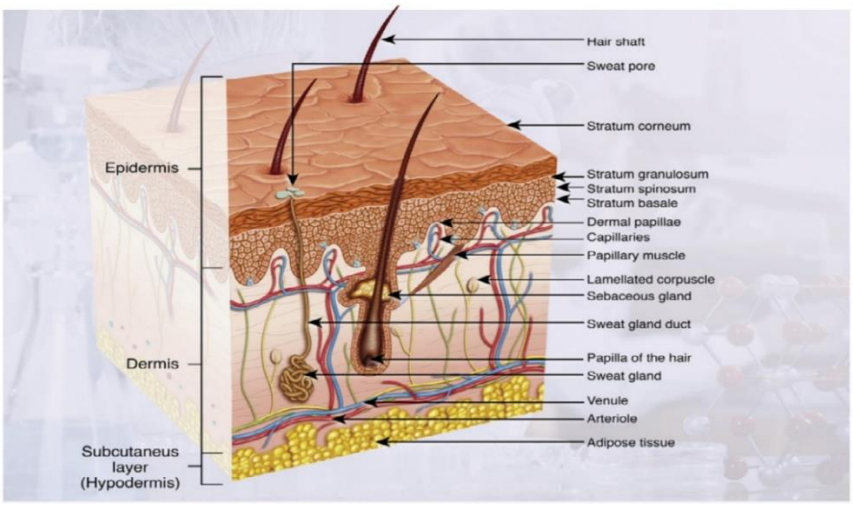

Figure 1.1 Schematic overview of human skin consists of three compartments including epidermis, dermis, and hypodermis; along with skin appendages. The image was used with copyright permission [3].

The epidermis is a stratified squamous epithelium consisting of 95% of keratinocytes as a major cell type [4]. The epidermis is further divided into layers (strata) namely stratum corneum (SC), stratum lucidum (SL) (only in palms and soles), stratum granulosum (SG), stratum spinosum (SS), and stratum basale (SB) (stratum germinativum). These layers result from a balanced differentiation process with each particular layer presenting a specific set of molecular markers (Figure 1.2). The process initiates as a result of cell division (mitosis) by the progenitor cells in the basal layer, pushing the newly formed keratinocytes apically, while moving up, the cells undergo differentiation process changing their shape and composition until they reach the top most anucleated layer of cells in SC. The barrier properties of the skin are due to SC comprising corneocytes (protein rich dead cells) embedded in the lipid matrix, that eventually shed OFF from the surface (desquamation). Other cell types include melanocytes (melanin producing cells in SB), Langerhans cells (dendritic cells, as antigen presenting cells, present in all layers of epidermis while more prominent in stratum spinosum and in papillary dermis particularly close to vessels), Merkels cells (tactile-epithelial cells found in SB working as mechanoreceptor for touch and light sensation).

The epidermis is connected to the dermis through a thin sheet called basement membrane which controls the trafficking between dermis and epidermis [5].

Basement membrane consists of laminins, type IV collagen, nidogen, and the proteoglycan perlecan.

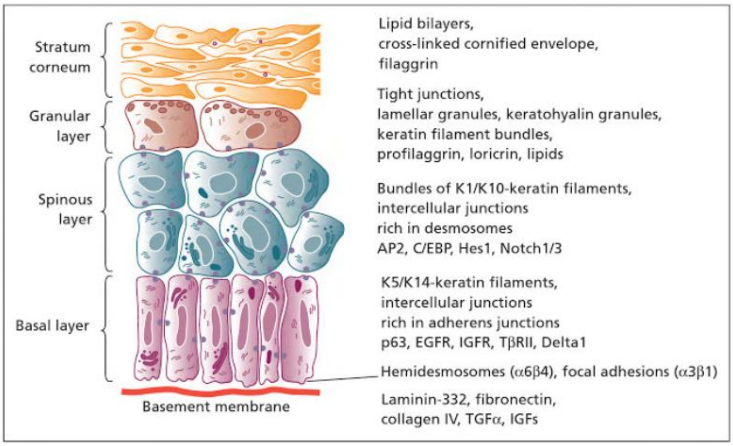

Figure 1.2 Epidermal differentiation and associated molecular expression in different keratinocytes layers. EGFR: Epidermal growth factor receptor, IGFR: Insulin-Like Growth Factor Receptor, TGF: Transforming Growth Factor. The image was used with copyright permission [4].

Beneath the epidermis, dermis is the connective tissue composed of extracellular matrix (ECM) produced by fibroblasts. The dermis is divided into two layers: upper papillary layer (papillae projections extending towards epidermis) consisting of loosely arranged collagen fibres; and a deeper and thicker reticular layer consisting of dense collagen fibres. The elastic properties of skin come from the presence of elastin in the dermis. Unlike epidermis being avascular, the dermis layer is full of blood & lymph vessels, nerves, sweat & sebaceous glands, and hair follicles. The third layer of skin is known as hypodermis that work as shock absorber and body's heat insulator. The prominent cell types in this compartment include fibroblasts and adipocytes.

1.2 *In vivo* applications - Autologous, allogeneic, and tissue-engineered skin substitutes

Skin substitutes are divided into the ones used for transplantation in clinic (*in vivo* applications) and the ones for testing/investigating the drugs or skin products (*in vitro* application). The questions and problems related to these two types of applications differ considerably.

1.2.1 Autologous and allogeneic skin substitutes

Thermal trauma is a major and the most common type of skin injury. Patients with 50-98% lost or burnt total body surface area (TBSA) have a significantly higher survival rate due to the use of skin grafts compared to the ones only treated with antimicrobials [6]. However, the wound healing process can be negatively affected because of the temporarily induced-suppression of immunity resulting in slowing down the healing process and leading to chronic wound conditions. The best skin graft is the one that is readily available, does not trigger an immune response, protects

wound bed safely, reduces the pain, and increases the wound healing process with almost no scar formation. Based on the depth of wound, skin injuries are divided into four degrees namely epidermal (I), superficial partial-thickness (II), deep partial-thickness (III), and full-thickness (IV) [7]. Full-thickness (FT) skin wounds have completely lost epithelial regeneration and the best way to treat them is transplantation of autologous skin grafts (clinical gold standard method) along with the techniques of early excision, and infection control. This increase the survival rate (by 50%) of patients with as high as 98% lost TBSA [8]. In case of more extensive injury, the harvesting of enough autologous skin is extremely limited. Then, use of allogeneic skin grafts (cadaveric skin) from European skin banks is another option as a temporary treatment. However, despite the ethical and safety issues regarding viral disease transmission (HBV, HCV, or HIV), there is not enough tissue available. The major disadvantages include the resulting wound complications and eventual immune rejections later on [9].

Epidermal skin substitutes

Epidermal substitutes are either based on cultured autologous or allogeneic keratinocytes. Autologous keratinocytes are taken from patient's own biopsy and after careful isolation of single cells, keratinocytes are propagated in the lab, possibly in a xenogeneic-free cell expansion media. However, the process is slow and time consuming. On the other hand, allogeneic products [10-14], (as mentioned above) offer an advantage of reduced cost but retain the risk of safety [15]. Examples of both types of commercially available epidermal substitutes used in the clinics are summarized in Table 1.1. Nevertheless, main challenge associated with epidermal substitutes either autologous or allogeneic, is the difficulty in attachment with the wounded skin resulting in blister formation [16].

Table 1.1 Commercially available epidermal constructs for clinical use.

Brand name/manufacturer	Incorporated human cells and cell source	Scaffold material and scaffold source	Duration of cover
Epicel® GENZYME BIOSURGERY, CAMBRIDGE, MA, USA	Cultured keratinocytes. Autologous. Confluent cell sheet.	-----	Permanent
EpiDex® MODEX THERAPEUTIQUES, LAUSANNE, SWITZERLAND	Cultured keratinocytes. Autologous from outer root sheath (ORS) of scalp hair follicles. Confluent cell sheet.	-----	Permanent
Epibase® LABORATOIRES GENEVRIER, SOPHIA-ANTIPOLIS, NICE, FRANCE	Cultured keratinocytes. Autologous. Confluent cell sheet.	-----	Permanent
MySkin® CELLTRAN LTD, SHEFFIELD, UK	Cultured keratinocytes. Autologous. Sub-confluent cell sheet.	Specific surface-coated silicon support layer.	Permanent
Laser Skin or Vivoderm FIDIA ADVANCED BIOPOLYMERS, PADUA, ITALY	Cultured keratinocytes. Autologous.	Microperforated hyaluronic acid	Permanent

	Confluent cell sheet.	membrane (HAM). Recombinant.	
BioSeed®-S BIOTISSUE TECHNOLOGIES GMBH, FREIBURG, GERMANY	Cultured keratinocytes. Autologous. Sub-confluent cell suspension.	Fibrin sealant.	Permanent
CellSpray CLINICAL CELL CULTURE (C3), PERTH, AUSTRALIA	Cultured/non-cultured keratinocytes. Autologous. Sub-confluent cell suspension.	-----	Permanent

Dermal skin substitutes

In full-thickness burns both epidermal and dermal parts of the skin need to be substituted and treatment with cultured epidermal sheets alone would result in poor outcomes. This is because dermal constructs greatly help in maintaining the mechanical stability and prevent wound contraction. Dermal constructs allow dermal vascularization before the application of an epidermal sheet [6]. Available dermal constructs are either based on natural or biodegradable synthetic materials and may be loaded with fibroblasts. The presence of fibroblasts [17] helps in the formation of new ECM and the secretion of growth factors in the wounds until cells undergo natural cell death. On the other hand, the complete absence of cells in the product help preventing the immune rejection [18]. The commercially available dermal substitutes used in the clinics are summarized in Table 1.2.

Table 1.2 Commercially available dermal constructs for clinical use.

Brand name/manufacturer	Incorporated human cells and cell source	Scaffold material and scaffold source	Duration of cover
AlloDerm LIFECELL CORPORATION, BRANCHBURG, NJ, USA	----	Human acellular lyophilized dermis. Allogeneic.	Permanent
Karoderm KAROCELL TISSUE ENGINEERING AB, KAROLINSKA UNIVERSITY HOSPITAL, STOCKHOLM, SWEDEN	-----	Human acellular dermis. Allogeneic.	Permanent
SureDerm HANS BIOMED CORPORATION, SEOUL, KOREA	-----	Human acellular lyophilized dermis. Allogeneic.	Permanent
Graftjacket WRIGHT MEDICAL TECHNOLOGY, INC., ARLINGTON, TN, USA	-----	Human acellular pre-meshed dermis. Allogeneic.	Permanent
Matriderm DR SUWELACK SKIN AND HEALTHCARE AG, BILLERBECK, GERMANY	-----	α-elastin hydrolysate coated bovine non-cross-linked lyophilized dermis. Xenogeneic.	Permanent
Permacol Surgical Implant TISSUE SCIENCE LABORATORIES PLC, ALDERSHOT, UK	-----	Porcine acellular diisocyanite cross-linked dermis. Xenogeneic.	Permanent

OASIS Wound Matrix COOK BIOTECH INC, WEST LAFAYETTE, IN, USA	-----	Porcine acellular lyophilized small intestine submucosa. Xenogeneic.	Permanent
Ez Derm BRENNEN MEDICAL, INC., MN, USA	-----	Porcine aldehyde cross-linked reconstituted dermal collagen. Xenogeneic.	Temporary
Integra Dermal Regeneration Template INTEGRA NEUROSCIENCES, PLAINSBORO, NJ, USA	-----	Bovine cross-linked tendon collagen, Glycosaminoglycan (GAG), polysiloxane. Xenogeneic and synthetic.	Semi-Permanent
Terudermis OLYMPUS TERUMO BIOMATERIAL CORP., TOKYO, JAPAN	-----	Bovine lyophilized cross-linked collagen sponge composed of heat-denatured collagen, silicone. Xenogeneic and synthetic.	Semi-Permanent
Pelnac Standard/Pelnac Fortified GUNZE LTD, MEDICAL MATERIALS CENTER, KYOTO, JAPAN	-----	Atelocollagen derived from pig tendon, silicone/silicone fortified with silicone gauze TREX. Xenogeneic and synthetic.	Semi-Permanent
Biobrane/Biobrane-l UDL LABORATORIES, INC., ROCKFORD, IL, USA	-----	Porcine collagen, silicon film, nylon fabric. Xenogeneic and synthetic.	Temporary
Hyalomatrix PA FIDIA ADVANCED BIOPOLYMERS, ABANO TERME, ITALY	-----	HYAFF (a derivative of hyaluronan) layered on silicone membrane. Allogeneic and synthetic.	Semi-Permanent
TransCyte (DermagraftTC) ADVANCED BIOHEALING, INC., NEW YORK, NY AND LA JOLLA, CA, USA	Cultured neonatal fibroblasts. Allogeneic.	Porcine dermal collagen, silicon film, nylon mesh. Xenogeneic and synthetic.	Temporary
Dermagraft ADVANCED BIOHEALING, INC., NEW YORK, NY AND LA JOLLA, CA, USA	Cultured neonatal fibroblasts. Allogeneic.	Polyglycolic acid (PGA) / polylactic acid (PLA), extracellular matrix (ECM) derived from fibroblasts. Allogeneic and synthetic.	Temporary
Hyalograft 3D FIDIA ADVANCED BIOPOLYMERS, ABANO TERME, ITALY	Cultured fibroblasts. Autologous.	Microperforated hyaluronic acid membrane (HAM). Allogeneic.	Permanent

Dermal-epidermal skin substitutes

The skin substitutes comprising both dermal and epidermal layers are either composed of autologous or allogeneic cells [19], mimic skin architecture and serve as the most sophisticated option in the clinics. However, they should still be considered as temporary wound dressings [20] releasing growth factors, secreting ECM proteins, and promoting wound healing. The main disadvantages include high manufacturing cost as well as failure of wound closure due to tissue rejection. Long term use of allogeneic fibroblasts and immunogenic tolerance is a controversial topic with some reports supporting [21-27] and others not supporting [17] cell use. However, grafting allogeneic keratinocytes have been found to be rejected by the host [21, 28], suggesting the use of autologous keratinocytes as the most adequate solution e.g. TissueTech Autograft System [22-25] is the only available option right

now allowing the complete wound closure. PermaDerm™, another substitute under investigation provides permanent wound closure. Despite all ongoing research, a full-thickness substitute is still not available as an off-the-shelf solution.

Another challenge encountered is poor vascularization of transplanted skin. Addition of growth factors like vascular endothelial growth factor (VEGF) [26] and endothelial cells [29] might help in improving the angiogenesis. However, having a very short lifespan [27, 30], VEGF incorporation was not successful. Genetically modified cells [31] can be used for a controlled release of growth factors. Uniform pigmentation [32] and UV protection in the grafted skin, have been addressed by incorporating melanocytes. Skin function involving wound healing is highly affected by skin appendages (hair follicles, seat/sebaceous glands). Hair follicles [33-36] and sweat glands [37] have been included in skin substitutes in some works. Use of Porcine Embryonic Skin Precursors (PESP) provided hopeful outcomes, resulting in the generation of epidermis, dermis, rete ridges, hair follicles, sweat/sebaceous glands [37] without any observable teratoma signs. This gives a strong hope of using autologous derived stem or progenitor cells [38-40] to serve as a promising approach for the reconstruction of extensive burns. The commercially available dermal-epidermal substitutes used in the clinics are summarized in Table 1.3.

Table 1.3 Commercially available dermal-epidermal constructs for clinical use.

Brand name/manufacturer	Incorporated human cells and cell source	Scaffold material and scaffold source	Duration of cover
Apligraf ORGANOGENESIS INC., CANTON, MASSACHUSETTS, CA, USA	Cultured keratinocytes and fibroblasts. Allogeneic.	Bovine collagen. Xenogeneic.	Temporary
OrCel INTERNATIONAL, INC., NEW YORK, NY, USA	Cultured keratinocytes and fibroblasts. Allogeneic.	Bovine collagen sponge. Xenogeneic.	Temporary
PolyActive HC IMPLANTS BV, LEIDEN, THE NETHERLANDS	Cultured keratinocytes and fibroblasts. Autologous.	Polyethylene oxide terephthalate (PEO) / Polybutylene terephthalate (PBT). Synthetic.	Temporary
TissueTech Autograft System (Laserskin and Hyalograft 3D) FIDIA ADVANCED BIOPOLYMERS, ABANO TERME, ITALY	Cultured keratinocytes and fibroblasts. Autologous.	Microperforated Hyaluronic Acid Membrane (HAM). Recombinant.	Permanent

1.2.2 Tissue-engineered skin substitutes

Tissue-engineered grafts, either cell-free or allogeneic cell-containing, offer possibility of delivering cytokines, growth factors and ECM components at wound site to promote wound healing. However, biomaterial-based skin substitutes can also be used with autologous grafts [41, 42], to help engraftment at the sites with high mechanical stress e.g. joints [43]. As described above, in comparison with autologous-based, tissue-engineered allogeneic-based skin grafts have the risk of disease transmission, however, they have a reduced cost. The commercially available

skin grafts used in the clinics include dermal, epidermal and dermal-epidermal constructs [19, 44].

Bell et al. first described the generation of *in vitro* skin models containing dermal and epidermal compartments [45, 46]. To date, different techniques have been done to improve the generation of skin grafts. Use of natural matrix as dermis e.g. gels based on collagen [47] and fibrin [48], scaffolds of collagen/chitosan/chondroitin-4-6 sulfate [49], and Small Intestine Submucosa (SIS) [50] have been described. Other approach involves the build-up of fibroblasts' own matrix (self-assembly method) without the use of cross-species matrix material [2, 51]. Besides, synthetic polymers including polylactic-co-glycolic acid (PLGA) [52], polycaprolactone (PCL) [53], or a mixture of PLGA/PCL [53], or PLGA/PCL with natural collagen [54, 55] have also been used to generate dermal layer. This helps in providing great mechanical stability as well as prevents pathogen transmission. However, addition of adhesion and signaling molecules is necessary to promote their bioactivity.

1.3 *In vitro* skin models - Tools for the assessment of toxicity in drug development and biomaterials safety

Besides their use in the clinics for *in vivo* applications, skin substitutes have emerged as advanced tools for preclinical assessments of cytotoxicity [56] of topically applied chemicals and in drug development, replacing the need for animal experiments. Based on different types of chemicals, skin might get exposed to a reversible damage (irritancy) [57] or an irreversible skin damage [58]. On the other hand, the safety assessment performed on human cells based monolayer cultures (two-dimensional or 2D trials) has low relevance [59]. Three-Dimensional (3D) systems provide a complex 3D physiological environment: they exhibit cell to cell & cell to ECM interactions and close relevance to *in vivo* situation; thus they respond differently than monolayer systems [59, 60]. For these reasons, skin substitutes would serve as a reliable model system in pharmacological and basic research. In drug development, skin models are being used to evaluate the irritancy, corrosivity, and toxicity of chemical agents [61]. The commercially available models are described in Table 1.4. Other under development systems to be used as skin models include epiCS & EPI-MODEL 24 [3].

Table 1.4 Commercially available in vitro epidermal and full-thickness skin substitutes for in vitro testing.

Brand name/manufacturer	Human skin cells	Scaffold material	Test method
Episkin™ L'OREAL NICE, FRANCE	Keratinocytes (mammary/abdominal samples during plastic surgery).	Collagen.	Skin irritation Skin corrosion*
Skinethic™ RHE L'OREAL, NICE, FRANCE	Keratinocytes (neonatal foreskin or adult breast tissue).	Polycarbonate membrane.	Skin irritation Skin corrosion*

Epiderm™ MATTEK CORPORATION, ASHLAND MA, USA	Keratinocytes (neonatal foreskin or adult breast skin).	Polycarbonate membrane coated with collagen.	Skin irritation Skin corrosion*
EpiDermFT™ MATTEK CORPORATION, ASHLAND MA, USA	Keratinocytes (neonatal foreskin or adult breast skin). Fibroblasts (neonatal foreskin or adult skin).	Collagen. Dermis present.	(To be determined)
EST-1000 CELLSYSTEMS, TROISDORF, GERMANY	Keratinocytes (neonatal foreskin).	Polycarbonate membrane.	Skin corrosion*
AST-2000 CELLSYSTEMS, TROISDORF, GERMANY	Keratinocytes. Fibroblasts.	Collagen Dermis present.	(To be determined)
Phenion® FT Model HENKEL AG&CO.KGAA DUESSELDORF, GERMANY	Primary Keratinocytes (neonatal foreskin). Fibroblasts (neonatal foreskin).	Bovine cross-linked lyophilized collagen. Dermis present.	(To be determined)
StrataTest® STRATATECH CORPORATION MADISON WI, USA	Immortalized keratinocytes (NIKS®). Dermal fibroblasts.	Collagen I Dermis present.	(To be determined)

* indicates TG 431 that is the test No. assigned by OECD test guidelines for testing chemicals. Test methods not marked with *, the OECD test No. has yet to be determined.

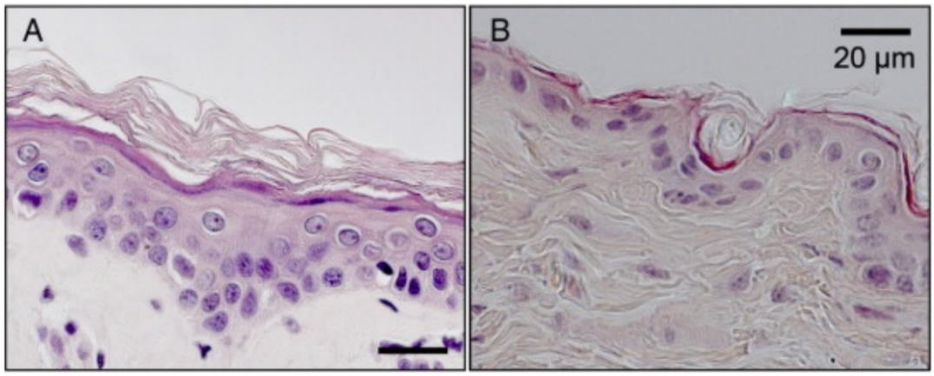

Figure 1.3 Morphological differences between (A) human and (B) mouse skin. Scale bar=20µm. The image was used with copyright permission [44].

Results obtained from animal trials often have limited value because of the differences between animal and human skin in terms of skin anatomical architecture and metabolism (Figure 1.3). As an example, Draize assay is performed by applying the test substance on albino rabbit skin for 4-48 hours to analyze the tissue harm [62]. Apart from being ethically questionable the test has provided incorrect information in the past [51, 63]. Although murine models have been widely used for skin biology experiments and skin cancer study [64-66], however, the dissimilarity between mouse and human skin restricts this approach. Mouse skin being furry is densely packed with hair follicles that are synchronized during the initial months of life. On the contrary, human skin has large interfollicular spaces with scarce hair follicles and the hair cycle is not a synchronized process. Moreover, murine epidermis is quite thin, composed of only three layers with a high turnover rate. On the other hand,

human epidermis is thick composed of 6 to 10 layers (Figure 1.4). Another basic difference is the anatomical location of melanocytes; melanocytes are located in the basal layer of human epidermis and in dermal hair follicles of mice. Another difference lies in the presence of a cutaneous muscle layer (panniculous carnosus) that is present in mice but absent in human skin. These interspecies inconsistences in skin structure exist and lead to variability in results [67].

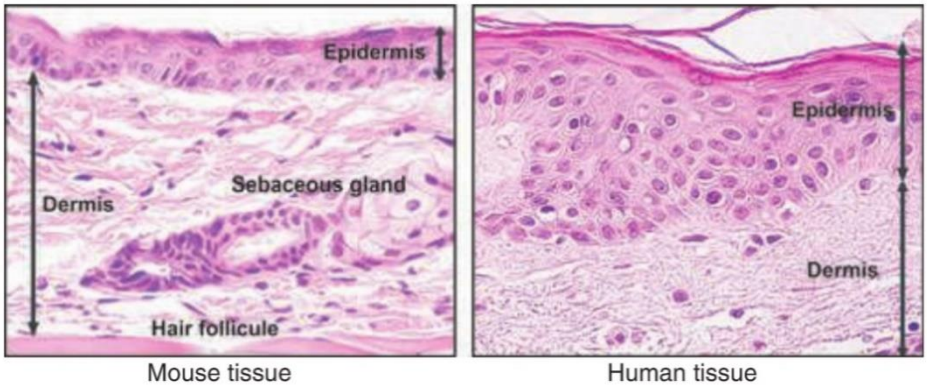

Figure 1.4 Morphological differences between mouse and human (artificial) skin displaying thin dermis and only 3 cell layers of epidermis compared to human skin with thicker dermis and 6-10 layers of epidermis cells. Magnification=60X. The image was used with copyright permission [68].

Amendments in EU regulations and current policies have pushed the development of *in vitro* test systems as an alternative to animal testing. According to the evolving regulations, the European Union (EU) 7th amendment (Dir. 2003/15/EC) of the "Cosmetics Directive" (76/768/EEC) imposed to replace all animal trials on cutaneous resorption with reliable and consistent *in vitro* tests by the year 2009 [2]. This led to the development of the 3Rs principle of "Replacement, Reduction and Refinement" [69]. Additionally, REACH, a European regulatory program for Registration, Evaluation, Authorization and Restriction of Chemicals promotes early characterization of chemicals' properties for hazard assessment [70, 71].

In this regard, skin substitutes have enabled to understand the fundamental processes that are involved in skin homeostasis or in skin pathology. In basic research, skin substitutes have allowed to unveil the basic mechanisms of skin formation in a more controllable and tunable environment for example the formation of the epidermis [72, 73], the molecular interactions between cell types [74, 75], wound healing [76], role of stem cells [74], and skin interaction with pathogens. Researchers have controlled the 3D environment of the skin by tailoring its cell population to specifically answer the biological question under investigation. Different types of *in vitro* skin models have been developed so far [51, 58, 62, 63, 74, 76]. The most relevant types are collected in Table 1.5: some of them are commercially available and used in *in vitro* testing (Table 1.4). These skin substitutes are either consisted of dermal or epidermal or dermal-epidermal both layers and based on various kinds of scaffolds of natural

or synthetic origin. Figure 1.5 shows the morphological similarities between *in vivo* and *in vitro* human skin [68].

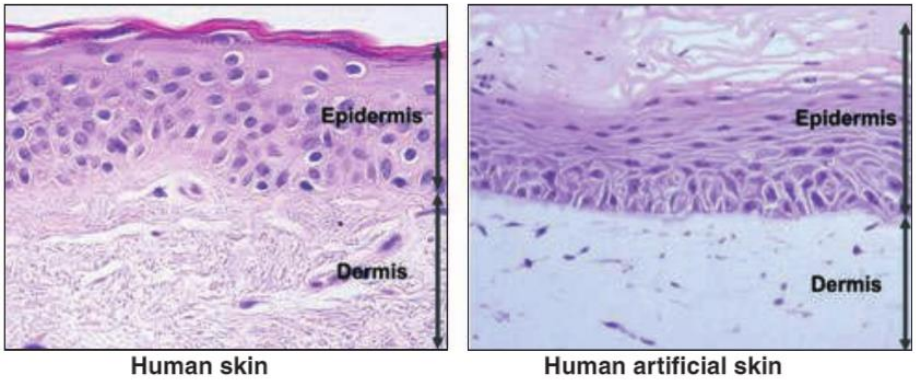

Figure 1.5 Optical micrographs of human facial skin and human artificial skin showing the similar thickness. Human artificial skin demonstrating well differentiated and all layers of epidermis. Maginification=60X. The image was used with copyright permission [68].

Table 1.5 Summary of existing 3D skin models and their applications [3].

Type of human skin model	Application	Advantage	Disadvantage
RHE	Skin irritation [77, 78], skin corrosion [79], phototoxicity [80], epidermal genotoxicity [81], trans-dermal drug delivery [82], skin sensitization [83, 84], and metabolization [85].	Standardized systems with available validated models of EpiDerm™, EpiSkin®, epiCS & EPI-MODEL 24.	Impaired barrier function, less complex, narrow test window of 2-3day after skin model arrives.
RHE plus **Melanocytes**	Skin Lightening [86], and pigmentation.	Standardized system for skin pigmentation.	Less relevant in drug development.
FT	Percutaneous absorption [87, 88], wound healing [89], and bacterial adhesion [89]	Standardized system, and relevant for wound healing process.	Costly, and no possibility of long-term culture.
FT plus **Melanocytes**	Vitiligo pathogenesis [90], and melanogenetic proteins' expression [91-94].	Melanogenesis research, and drug development for vitiligo.	Non-standardized model.
FT plus **Langerhans cells**	Maturation & migration of Langerhans Cells (LCs) [95], evaluation of allergens [96]	Immunocompetent model to evaluate sensitization potential.	Cell line used, and non-standardized model.
FT plus **Endothelial cells & Hypodermis**	angiostatic therapies [97], and adipose metabolism [98].	Drugs' evaluation on adipose tissue & angiogenesis, and Long period cultivation possible.	Technically immature, and non-standardized model.
FT plus **Stem cells**	Epidermal development [99, 100], autologous transplantation [101], wound healing [102, 103], and pigmentation disorders [104, 105].	Progress towards the development of broad spectrum of skin models, and disease models with standardized cell sources.	Low feasibility, and technically difficult.

FT plus **Hair follicles**	Penetration studies [106].	Effect of hair follicles on substance penetration, and absence of artificial matrix.	Other skin appendages are missing, and poor throughput analysis of the method.
Explants	Compound screening [107-111], neuronal interaction [112-114], effect of microbes on skin inflammation [115], stimulation & migration of Antigen Presenting Cells (APCs) [116-118], and epithelial migration [119-121].	Presence of all cell types, and possibility of diseased skin conditions for drug development.	Donor variability, and limited availability of viable tissue.
Explants plus **Hair follicles**	Hair follicle formation at molecular level [122].	Physiologically closely relevant, and thus studying *de novo* development of hair follicle.	Irregularity in stages of hair follicles development, no influence of skin in reorganizing hair follicles, and small sized hair follicles.

RHE=Reconstructed human epidermis, FT=Full-thickness.

1.4 Different approaches towards *in vitro* skin models - Skin models with additional cell types

The existing 3D models have been obtained by a variety of different approaches with different levels of complexity (Table 1.5). However, when the complexity of a system increases, the efficacy of a test system becomes harder to be standardized due to complex construction and readouts. A 3D system for risk assessment application based on one cell type (e.g. a reconstructed epidermis made of keratinocytes) would exhibit high reproducibility. The full-thickness skin models based on dermal and epidermal compartments exhibit a cross-talk between fibroblasts and keratinocytes. Incorporation of other cell types e.g. melanocytes, and Langerhans cells etc. further increases the complexity of the model but appears necessary to answer the question under investigation or to prove the efficacy of drugs in drug development. Table 1.5 collects the different types of *in vitro* 3D skin models with an overview of their advantages and disadvantages.

1.4.1 In vitro skin models - Role of fibroblasts and keratinocytes

Although most of the skin models used in pharmaceutical research are epidermal skin models, addition of fibroblast-containing dermal layer would greatly increase the value to skin models. It is known that the skin fibroblasts are not homogeneous and changes in the populations of fibroblasts is one of reasons behind chronicity of wounds [123]. Fibroblasts secrete growth factors to directly influence the growth [124] and differentiation of keratinocytes [74, 75]. Additionally, the interaction between these two cell types is highly important in the formation of dermal-epidermal junction (basement membrane) [125, 126] On the other hand, keratinocytes also directly influence the proliferation of fibroblasts [74]. Thus, this

interaction is named as double-paracrine mechanism [127, 128]. Based on that, keratinocytes secrete IL-1, that stimulates fibroblasts to secret keratinocyte growth factor (KGF) and granulocyte-monocyte colony-stimulating factor (GM-CSF) that in turn influence keratinocytes proliferation. Besides, fibroblasts have an important role in enhancing the keratinocytes resistances towards toxic compounds [60]. This suggests that epidermal model alone is not enough to predict *in vitro* toxicological studies.

1.4.2 In vitro skin wound models - Role of fibroblasts and keratinocytes

Fibroblasts have an important role in skin remodelling, wound healing [129] and acute wound contraction [45, 130]. Wound repair mechanism sequentially involves homeostasis, inflammation, granulation tissue formation and scar formation. After an injury, platelets aggregate and make a plug to prevent blood loss; additionally, platelets release transforming growth factor-β (TGF-β), and platelet derived growth factor (PDGF) that activates the surrounding cells. As inflammation starts, neutrophils arrive at the site of the injury and release antimicrobial substances like cationic peptides, & reactive oxygen species (ROS) and thus help in wound cleaning as well as protection from microbial attack [131]. If there are more free radicals, as happens in chronic wounds, ROS cause harm to healthy cells as well [132]. Two days later, macrophages appear releasing more cytokines and start digesting matrix elements and cellular debris [133]. Besides this, macrophages have shown to promote angiogenesis [134][a]. Other cells including mast cells (derived from basophils) and leukocytes also appear as they are attracted by specific chemotactic stimuli for which they express the corresponding receptors and release more cytokines supporting tissue repair [134][b]. Apart from inflammatory cells, endothelial cells also enter the site of injury. During granulation phase, keratinocytes and fibroblasts come into action by re-epithelializing and synthesizing new ECM (glycosaminoglycans, proteoglycans, collagen III, fibronectin, vitronectin etc.) respectively. This promotes angiogenesis that causes fibroblasts to convert into myofibroblasts bringing the wound edges closer (wound closure). Finally, as the inflammation reduces, the granulation tissue transforms into scar tissue. Myofibroblasts go through apoptosis and temporary matrix is replaced by new collagenous matrix [132, 135, 136]. This cascade of events is named as normal wound healing process and finally ends with scar tissue remodelling. However, pathological conditions can lead to fibrosis (that is an extra matrix deposition and thus loss in function) [137] or chronicity of wounds. Wound chronicity is related with phenotypic differences of fibroblasts present at the wound site having an affected proliferation rate, flattened morphology and excessive matrix production, that causes a non-healing condition [123]. To understand the underlying processes and for testing treatment options, synthesis of *in vitro* wound models is highly needed and challenging.

1.4.3 In vitro Immunocompetent skin models - Role of Langerhans cells

Besides fibroblasts and keratinocytes, which are fundamental cells of full-thickness skin model, incorporation of Langerhans cells (LCs) may help these models to serve as tools for immunological reactions. LCs are special dendritic cells (DCs) that reside as immature cells in epidermal niches, and upon exposure to antigen, they migrate to dermal lymph nodes. During migration, LCs change into mature DCs that present the antigens to T-cells in lymph nodes [138]. Many attempts reported to integrate LCs remained an important challenge. In an effort, skin models were seeded with CD34+ hematopoietic progenitors, and their differentiation was allowed using granulocyte macrophage-colony stimulating factor (GM-CSF) and tumour necrosis factor-α (TNF-α) that resulted in supra-basally situated cells displaying LCs typical markers [139]. These results also demonstrated the involvement of keratinocytes in LCs differentiation [139]. In another study, an epidermal biopsy was deposited over an *in vitro* dermal model that resulted in the formation of functional epidermis containing phenotypically immature LCs. To test the response against allergens, this model was stimulated with GM-CSF and immunosuppressed using cyclosporine-A (SC-A). GM-CSF showed an increase in LCs migration with no effect on LCs density, while SC-A neither affected the LCs migration nor density [140].

1.4.4 In vitro vascularized skin models - Role of endothelial cells

An important issue related with the grafting of full-thickness skin substitutes is "necrosis" due to the absence or failure of new vessels formation [141]. *In vivo*, a capillary network is supplied to skin through the dermis. In wounds, this network is destroyed, and new capillaries are formed via sprouting out of endothelial cells (ECs), the process is called angiogenesis [140]. Many efforts have been performed [141-145] to promote neovascularization in skin grafts or in *in vitro* angiogenesis models by studying the effect of pro-angiogenic [141, 142] or anti-angiogenic factors, matrix metalloproteinases (MMPs) [143], and cell adhesion molecules (CAM) [144, 145]. The incorporation of ECs in dermal substitutes [146-148] demonstrated the interaction among ECs, ECM, and surrounding cells, resulting in the formation of capillary-like structures but failed to develop mature blood vessels. *In vivo*, shear stress (due to blood flow) works as a stimulator for ECs to display a natural phenotype [149], however the physiological shear conditions are currently lacking in *in vitro* models.

1.4.5 In vitro skin phototoxicity models - Role of melanocytes

The natural skin prevents harmful effects of UV radiation (UVA and UVB) by producing melanin that scavenges the free radical oxygen species [150[a,b]]. Melanin pigment is produced in melanocytes and distributed to the surrounding keratinocytes. To successfully recreate the pigmentation process *in vitro* [151, 152] as well as to understand skin response to sunlight [153, 154], the incorporation of melanocytes is highly required. These models can also be used as *in vitro* test systems [155, 156] to

develop photo protective agents. Different phototypes are also possible to be simulated by using cells from donors of high phototype (dark skin) and low phototype (fair or pale skin) [156]. *In vitro* chimeric skin reconstructs were produced by using keratinocytes and melanocytes combinations from Caucasian and Negroid donors, that demonstrated that melanocytes control the pigmentation and have role in sunlight protection.

1.4.6 In vitro melanoma models - Role of melanoma cells

Amongst the pathological alterations of phototoxicities, malignant melanoma is highly aggressive and the most prominent type in humans. Melanocytes are located in the stratum basale and disease develops when they lose their contact from surrounding keratinocytes entering in a radial growth phase followed by a vertical growth phase and thus penetrating through the basement membrane [157]. Metastases formation starts when cells enter in vertical growth phase and leads to severe disease progression. Genes associated with this transformation include v-Rafmurine sarcoma viral oncogene homolog B1 (BRAF), cyclin-dependent Kinase Inhibitor 2A (INK4a), microphthalmia-associated transcription factor (MITF), v-kit Hardy-Zuckerman 4 feline sarcoma viral oncogene homolog (c-KIT), snail homolog 2 (SLUG) and endothelin receptor type B (EDNRB) [158]. The invasive behaviour is also associated with the alteration of homoeostasis between melanocytes and keratinocytes [159]. This involves the changes in the molecular interaction of metastatic cells with surrounding keratinocytes. These melanocytes get higher proliferation potential (even without the presence of keratinocytes) and express melanoma Cell Adhesion molecule (Mel-CAM/MUC18) receptors [160]. The molecular interactions have been investigated in 2D cell culture systems [159], in *in vivo* animal models [161], and recently in 3D culture as an alternative to *in vivo* system [162]. Many efforts have been performed to incorporate melanoma cells in skin substitutes serving as a controlled experimental melanoma model to study growth behaviour of and growth factors produced by melanoma cell lines (MSL). MSL depending on their origin were found to behave differently in disease progression e.g. MSL from radial growth phase couldn't penetrate basement membrane while MSL from vertical growth phase were easily able to cross the basement membrane [163]. Moreover, different MSL due to their different genetic backgrounds responded differently to therapeutics e.g. towards α-melanocyte stimulating hormone (α-MSH) [164]. The cross-talk between MSL and surrounding skin cells contributes to the invasive behaviour of melanoma cells [165]. It was shown the keratinocytes secreted metalloproteinase-9 help MSL to cross the basement membrane [166].

1.4.7 In vitro vascularized melanoma models - Role of melanoma and endothelial cells

These melanoma skin models would make possible the development of new antimelanoma drugs by revealing the new signalling pathways. The combined

administration of drugs sorafenib (zinc fingers & homeoboxes 2 (RAF) inhibitor) and rapamycin (mechanistic target of rapamycin (mTOR) inhibitor), stops melanoma cell line invasion [167]. Angiogenesis is highly associated with tumours *in vivo*; tumour cells attract ECs to make capillaries by secreting growth factors (tumour angiogenesis) [168]. Moreover, melanoma cells spread into the body through penetrating the blood vessels to form secondary tumours (metastasis) [169]. *In vitro* melanoma models lack vascularization: in order to grow *in vitro* tumour models with a size of 2 to 3mm, and to simulate the critical barrier function by ECs, vascularized skin substitutes are under investigation to unveil the new anti-melanoma drug's targets.

1.4.8 In vitro psoriasis models - Role of fibroblasts and immune cells

Psoriasis is a skin inflammatory condition causing red patched scaly skin. Hyper-proliferated keratinocytes and thickened epidermis extending into the dermis are amongst the typical features of psoriasis [170]. Initially, it was believed that this pathological condition was due to an affected proliferation and differentiation of the keratinocytes [171]. New insights arose from attempts to build psoriatic skin models using fibroblasts and keratinocytes from psoriatic patients. This demonstrated that fibroblasts isolated from psoriatic donors stimulated keratinocytes of healthy donors to hyper-proliferate [172], this was found to be associated with fibroblasts induced expression of either interferon-γ receptor on keratinocytes [173] or an induced high IL-8 secretion by keratinocytes [174]. On the other hand, it was found that drugs targeting immune cells reduce the psoriatic symptoms [175], e.g. antibodies against CD3/4 [176] and a fusion protein (IL-2-diphtheria-toxin) targeting T-cells [177] decreased the clinical symptoms, demonstrating an important role of immune cells in psoriasis. Several efforts were made to develop psoriatic skin substitutes by self-assembly method [178], decellularized dermis [179], disease induction by transglutaminase inhibitors [180] or by cytokines (TNF-α, IL-1α, Il-6 and IL-2) [181]. However, the role of the immune system has not been investigated within models yet. In an effort to address this issue, a psoriatic skin model was grafted in immune-deficient mice and dosed with natural killer cells (NKs) to induce the disease phenotype [182].

1.4.9 In vitro skin models - Role of skin appendages

The skin substitutes are being used in drug development and cosmetic industry for the substances applied on the skin e.g. to know the risk/benefit ratio of chemicals like glucocorticoids [183]. Artificial stratum corneum (SC) [184], epidermal substitutes [185] and dermal-epidermal [186] substitutes are used for penetration studies. However, how much of the substance penetrates through the epidermis [185], and its local & systemic effects (transdermal delivery) [186] are still unclear. The major difference in penetration between *in vitro* and *in vivo* situation is due to the absence of hair follicles and sweat/sebaceous glands [187, 188]. These skin appendages enhance skin permeability. Percutaneous drug absorption either make use of trans-

epidermal diffusion (using inter- or trans-cellular transport through the SC) or trans-appendageal diffusion (transport through hair follicles and their sebaceous glands) [189]. In an effort to incorporate skin appendages to channel the drug transport across SC, thermolysin digested-hairy skin derived pilosebaceous units were obtained in a skin substitute based on fibroblasts and keratinocytes [106]. During penetration study this model demonstrated an increased penetration of hydrocortisone than the control group without hair insertion. However, development of skin model with follicular appendages still represents a challenge.

1.4.10 In vitro skin infection models

Due to the widespread prevalence of skin infections an understanding of how pathogens attach, grow, and breache the stratified layers of the epidermis is highly crucial. 3D skin models would serve as precious tools to investigate pathogenesis of host cells-pathogens molecular interaction to explore new antimicrobial targets. Initial efforts have been made to simulate the skin infection by inoculating different pathogens (including virus, bacteria, and yeast) in 3D skin substitutes. However, there are many shortcomings in the state-of-the-art model of improvement. These models are summarized in Table 1.6.

Table 1.6 3D keratinocytes-based cell culture systems with microbes.

Type of model	Application	Comments
S. aureus (ATCC6538), *P. aeruginosa* (PAO0001) on rat-tail collagen type I matrix (without any eukaryotic cells) with serum mimicking wound bed *[190]*.	*In vitro* development of biofilms attached to solid polymeric surface.	Cell components are missing.
P. aeruginosa MCS5-lite, S. aureus (NTCC 8325) on cellulose matrix (without any eukaryotic cells) in a flat-bed perfusion growth chamber [191, 192].	Evaluation of antimicrobial efficacy of wound dressings.	As above.
-Oral and vaginal candidiasis models on RHE. [193, 194] [195], -Cutaneous candidiasis model on RHE [196, 197], and -Oesophageal candidiasis model on RHE [198, 199].	Development of *in vitro C. albicans* biofilm models [193, 194] to study cellular interactions between *C. albicans* and epithelial tissue; protein & gene expression in a non-complicated environment by non-epithelial factors [200-202]; immunological interactions between C. albicans & keratinocytes [203]; Candidiasis pathology [204], and drugs development [198, 199].	Commensal flora, and humoral &cell-mediated immune responses are missing.
S. aureus (ATCC6538) and *P. aeruginosa* (ATCC 27317) on a 3D human skin model (Graftskin/Apligraf from Organogenesis, MA, USA based on neonatal allogeneic fibroblasts and keratinocytes) [205].	Biofilm formation.	Other cell types are missing. At early stage study, needs more investigation.
A. baumannii (ATCC19606), and *A. junii* (RUH2228) on a 3D human epidermis model (allogeneic	Bacterial adherence, colonization, biofilm formation, and skin's response.	As above and fibroblasts are missing.

keratinocytes from plastic surgery) [206].		
S. aureus (USA 300) on a 3D human skin model (neonatal foreskin fibroblasts and keratinocytes, cadaveric devitalized human dermis as matrix) [207].	Bacterial colonization and infection.	Other cell types are missing. At an early stage study and needs more investigation.
Herpes simplex virus type 1 (HSV-1, type 2 (HSV-2), varicella-zoster virus (VZV) on human skin model (Foreskin and ectocervical keratinocytes on J2 3T3 fibroblasts seeded collagen matrix) [208, 209].	Initial viral infectious process & spread, to evaluate the efficacy of new anti-VZV antivirals (No animal model is yet available for testing anti-VZV antivirals).	Presence of fibroblast cell line.
HSV-1 on human skin model (HaCaT keratinocytes, human fibroblasts seeded collagen matrix) [210, 211].	Establishment of HSV-1 as a function of epithelial maturation, and infection by both latent & lytic HSV.	Presence of keratinocyte cell line.
HSV on "Dual Chamber Neuron-Epidermal Cell System" (human foetal Dorsal Root Ganglia (DRG) in one chamber, autologous skin explants in the other chamber, and chambers are separated by agarose gel) [212][A].	HSV transmission from axon to epidermal cell.	Exact mechanism of HSV emergence from axons is unclear.
MRSA and MDR A. baumannii infected *ex vivo* human skin infection model [212][B].	Development of antimicrobial peptides.	*In vitro* skin models are flexible and tunable. Limited availability of e*x vivo* human skin grafts.

RHE=Reconstituted human epithelia (SkinEthic Laboratories, Nice, France), 3D=Three-dimensional, ATCC=American Type Culture Collection, *S. aureus=Staphylococcus aureus, MRSA=Methicillin-resistant Staphylococcus aureus P. aeruginosa=Pseudomonas aeruginosa, A. junii=Acinetobacter junii, A. baumannii=Acinetobacter baumannii, C. albicans=Candida albicans, HSV=Herpes simplex virus; VZV=Varicella zoster virus, MDR= Multidrug resistant.*

1.5 Analysis of *in vitro* skin models

1.5.1 Molecular analytic methods

In response to external stimuli (e.g. cytotoxicity testing), variations in cellular signalling pathways can be investigated by molecular and biochemical methods (Figure 1.6). Different readouts at various cellular levels allow meaningful way to answer the relevant question. Homogenous cell populations can be extracted from the 3D skin substitute by any purification technique e.g. Fluorescence Activated Cell Sorting (FACS) to conduct spatio-temporal studies. Isolated cells can be characterized for their stem or differentiated nature. On the other hand, different cell

types in 3D skin substitute can be studied in total to investigate a specific information in an interdependence environment of mixed cell types.

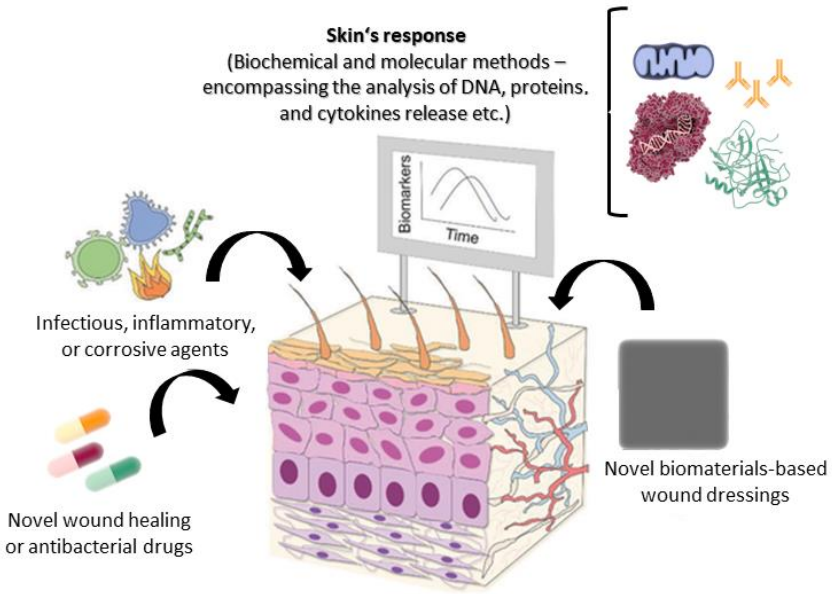

Figure 1.6 The variations in cellular behavior and biomarkers expression can be monitored in organotypic human skin models – advanced in vitro bio-evaluation tools. The image was used and modified with copyright permission [213].

Relative quantitative and qualitative molecular analyses of nucleic acids (RNA, DNA), proteins, lipids, carbohydrates at sub-cellular level is essential to understand functional consequences of these molecules in a skin model. Changes of gene expression can be analysed by measuring relative mRNA levels by qRT-PCR (a low throughput method performed on particular genes) and microarray studies (can be performed on a multitude of genes) [214]. RNA-Seq analyses the transcriptomes with great accuracy [215] measuring mRNA isoforms, mRNA mutations, gene editing and fusions [214, 216-218]. Microarray and RNA-Seq methods require high knowledge for data processing and analysis where minor variations in experimental handling can result in dramatic variations of results. Among *in situ* hybridization techniques, fluorescence RNA *In Situ* hybridization (RNA FISH) on 3D sections offer visualization of RNA expression at spatial level [219]. Keratinocytes proliferation in the basal layer can be detected by using radioactively/fluorescently labelled nucleosides considering signal proportional to the rate of DNA synthesis [220, 221]. Modified nucleosides (which are either radioactively labelled or can be specifically detected via fluorescently labelled antibodies) or click reaction reagents, are added to keratinocytes [220, 221].

Proteins are the direct mRNA translational products, and always function in a dynamic fashion by engaging themselves with other proteins. Changes in protein biology in 3D skin models involve studying protein complex composition, cellular localization, relative abundance, and post-translational modification (PTM). Immunohistochemistry (IHC) analysis is performed to assess these various aspects of proteins by using specific antibodies against antigenic epitopes; e.g. Ki-67 and p63

proteins [222] are associated with cell proliferation, while distinct cytokeratins' expression is associated with epidermal differentiation in different layers of epidermis. Precise recognition of "transient proteins alterations" e.g. the phosphorylation of histone H2AX due to (double-stranded) ds-DNA breaks, can be monitored as well [223].

As compare to IHC that is subjected to score variability due to sample preparation and image analysis, Western blot is more suitable method to analyse extent of PTMs of proteins e.g. due to downregulation of tight junctions using siRNAs in 3D skin models [224, 225], however it is a low throughput method because it needs high cell number. Comparative analysis of normal and diseased skin tissue can be performed by flow cytometry to understand differences in epidermal growth in normal and pathologic conditions [226, 227]. Single-cell mass cytometry measures complex network signalling at single cell level in mixed cellular population investigating the communication among these cell types [228, 229]. This can lead to an approach to assess the effect of therapeutics on patient derived 3D skin substitutes to enable personalized medicinal intervention. However, the preparation of single cell population prior to analysis can introduce cellular alterations due to experimental cell isolation processes. Also, careful sample preparation is important to avoid destruction of weak epitopes e.g. transient phosphorylation episodes. Moreover, antibodies displaying highest affinity towards respective antigens are needed; novel nucleic acid-based agents offer promising replacements of antibodies-based methods [230].

1.5.2 Structural analytic methods

After molecular analysis, structural analysis is another set of informative methods to investigate alterations in skin architecture in terms of skin maturation being directly linked with skin structure. Haematoxylin and eosin (H & E) is the most commonly used staining approach while phalloidin (for staining F-actin) and Hoechst 33342 (for staining DNA) are used see cellular networks inside the matrix [231]. Fluorescence microscopy including epifluorescence and laser scanning generates fluorescent images. The latter category allows good spatial resolution through optical sectioning. However, confocal laser microscopy has limited penetration depth, photobleaching, and phototoxicity effects that prevent its use for visualizing large 3D tissue [232]. Two-photon/multi-photon microscopy has low resolution but provides higher penetration, low photobleaching and phototoxicity allowing long-term fluorescence imaging [233, 234]. To study 3D structures as deep as zebrafish or Drosophila embryos, light sheet fluorescence microscopy is an amazing option having high penetration depth with minimum photobleaching and phototoxicity [232, 235, 236]. Based on basic physical properties, all optical microscopes have their own limitations. Fluorescence lifetime imaging microscopy (FLIM) based on the differences in decay rate of fluorescence (fluorescence lifetime) with respect to its microenvironment (and not from its local intensity), allows high resolution [237]. Different cellular parameters including pH, ion concentration, oxygen concentration,

viscosity and cellular metabolism can be assessed using FLIM [238]. FLIM can be combined with two-photon scanning microscopy to produce highly resolved 3D spatial images e.g. pH gradient in the epidermis of 3D skin was measured [238]. However, FILM limits the study of dynamic events in a living system. Second harmonic generation (SHG) and third harmonic generation microscopy (THG) work like a multiphoton laser scanning microscopy, however, it makes use of label-free imaging by obtaining contrasts from variations in sample's ability to produce second or third harmonic light from incident light and has high penetration to create high resolution 3D reconstruction. This technique was used to analyze the migration of leukocytes in an explanted tissue [239]. SHG is limited to the analysis of structural proteins having crystalline-like lattices e.g. fibrillar collagen, and thus is a less sensitive approach.

Electron microscopy is used to study the 3D structures at a very high resolution down to an ultrastructural level which needs a complicated sample preparation, and this excludes the analysis of living system. Transmission electron microscopy (TEM) can be used to analyze the effect of keratinocytes on skin maturation and elastin presence in dermis [240]. Scanning electron microscopy (SEM) provides the information about topography, composition as well as morphology e.g. interaction of fibroblasts with collagen fibrils [241].

Another structural analysis involves studying mechanical properties of skin (traction, and torsion etc.) by rheological analysis. For example, shear strength of skin adhesives that were applied on skin tissue, was measured by rheometer [242]. The viscosity and elasticity of distinct skin layers can be measured using atomic force microscopy (AFM) [243]. Dermis of an excised mouse skin showed higher mechanical stiffness than stratum corneum and the living epidermis, while living epidermis displayed highest visco-elasticity. This analysis would help in improving micro-devices to work inside the skin. A bio-tribometer was recently used to measure indentation and friction in a human dermal substitute made of a collagen, chitosan matrix, and dermal fibroblasts [244] providing similar Young's modulus and shear modulus values of human skin. This analysis will help determining and comparing the mechanical properties of in vitro skin models to improve the performance of scaffold materials for dermis reconstruction.

1.5.3 In vitro assays

In vitro methods – Bio-evaluation of skin's response

Cultured skin models replicate many aspects of natural skin biology, while diseased skin models imitate the disease state and perturbations demonstrating a specific pathophysiological skin condition. The *in vitro* skin models serve to measure the damaging capacity or the curative potential of applied substances (Figure 1.7). Transcutaneous electrical resistances (TER) method was one of the initially developed *in vitro* test methods to discriminate between corrosive and non-corrosive effect of materials on dermal substitute [245]. The sample is applied to three skin

discs for a duration not exceeding 24 hours. This approach measures the ability of a substance to affect the function of stratum corneum (SC), resulting in the reduction of TER below a threshold level. A combined method "dye-binding step" allows to understand if the increase in ionic permeability was caused by destroying SC. Initially a macromolecular membrane named Corrositex™ served the purpose [246, 247], and later on the assay was developed for *in vitro* skin substitutes [248].

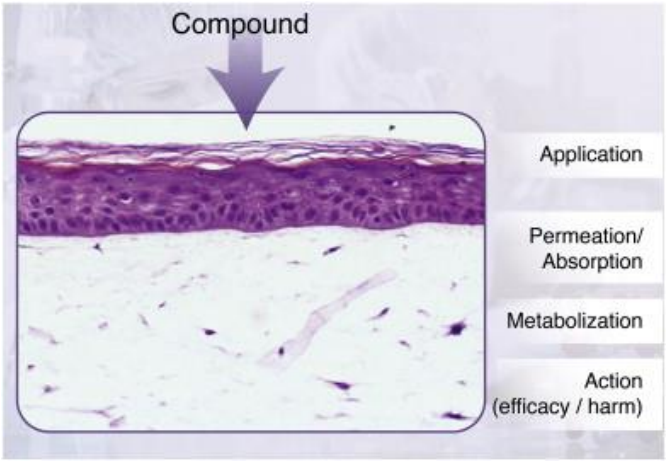

Figure 1.7 Potential actions of tested compound on organotypic human skin models. The image was used with copyright permission [3].

MTT assay (5-dimethylthiazol-2-yl-2,5-diphenyltetrazolium bromide) as well as optical visualization through histological staining (H & E) can serve as effective analysis methods to determine corrosive capacity of a substance. Many efforts have been performed to apply these methods on substituted skin (e.g. Episkin™ and Skin2™) to get standardized assays to finally replace the Draize test for corrosivity measurement. The European Centre for the Validation of Alternative Methods (ECVAM) validates these methods to replace animal experiments [249]. Since then, more efforts have been invested to improve corrosion assays based on skin substitutes (EpiDerm™, SkinEthic™, EST-1000) [250-252]. However, skin irritation test methods are not easily applied as they require not only cytotoxicity measurements but also metabolic reactions [57, 78]. Keratinocytes are very important in immunomodulation and release several cytokines in response to physical or chemical stimuli including (IL-1 α, IL-6, IL-7, IL-8, IL-15, TNF-α) (Figure 1.8). Cell membrane integrity can be measured by the release of cytosolic enzymes e.g. lactate dehydrogenase (LDH) [251, 253, 254]. Many ongoing efforts helped in validation of irritation tests when performed according to ECVAM guidelines (EpiSkin™, Epiderm SIT™ and SkinEthic™ RHE) [255, 256]. This would be of great help in

replacing the animal experiments, however, the systemic response of an applied substance is missing so far.

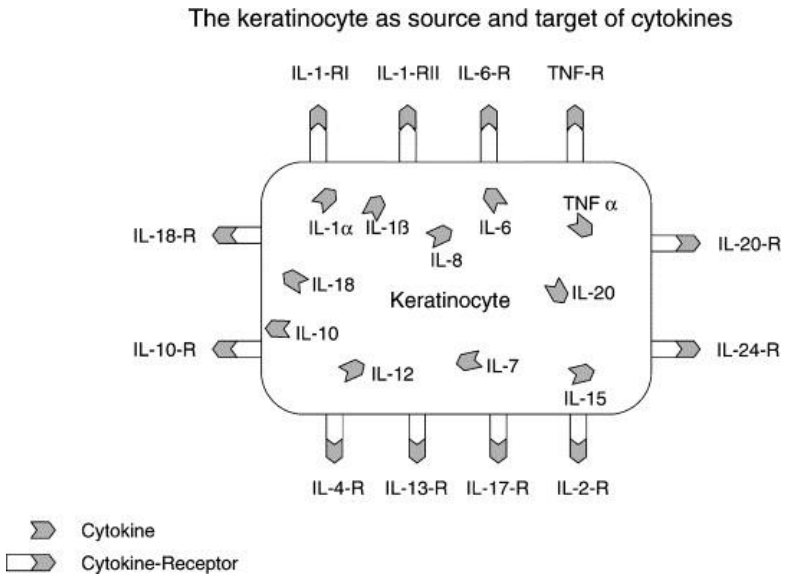

Figure 1.8 Keratinocytes as both source and target of cytokines. The image was used with copyright permission [257].

For percutaneous absorption testing or *in vitro* penetration study, skin substitutes can be suitable to determine the permeability of a substance through the skin. Experimental set-up based on a skin substitute separating a donor from an acceptor compartment was used for this purpose. Alternatively, the use of an epidermal substitute demonstrates a better leak-proof connection than a full-thickness model by sealing the whole surface area and providing the mechanical resilience [186].

Wound healing process is complex involving many cell types and response, there is an ongoing improvement on skin substitutes for studying wound healing. There are several methods to create a wound: scratching, abrading or burning. Different instruments are used to introduce a skin injury, including scalpels, biopsy punches, liquid nitrogen, laser [76] or brass string heated at 150°C for burn models [258]. Laser is the most precise method to achieve a reproducible wound size e.g. Vaughan et al. demonstrated a wound of 6mm length, 1mm width and 400µm depth for studying aging and re-epithelialization *in vitro* [259].

In vitro microbiological methods – Bio-evaluation of antibacterial properties

Commonly used *in vitro* microbiological methods include broth inoculation method [that measures minimum inhibitory concentration (MIC) or minimum bactericidal concentration (MBC) of antimicrobial agents], and Kirby-Bauer disc diffusion method [that measures antibacterial activity as a measure of zone of inhibition (ZOI)]. Microbiological methods that are used to evaluate antimicrobial properties, depend on the "mode of action" of antibacterial agents (Figure 1.9) and how their action is affected after their addition to the polymers (physically incorporation or chemically immobilization). This defines whether bacteria are going to be killed

either from eluting antibacterial agent or by direct contact with the surface of the material (through a biocidal effect or by inhibiting the bacterial adherence).

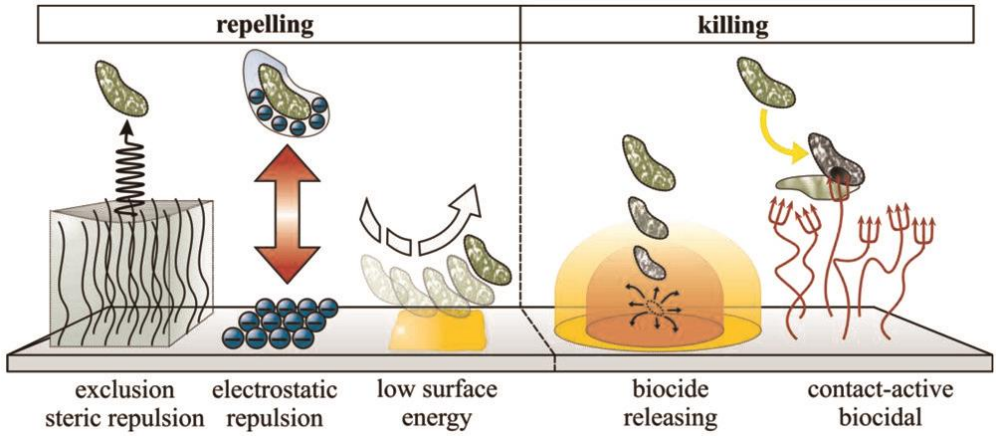

Figure 1.9 Strategies to induce antimicrobial surfaces. The image was used with copyright permission [260].

For example, immersion inoculation method, as described by ASTM (American Society for Testing and Materials), is used for testing of immobilized antimicrobial agents [261]. The direct inoculation method, as described by JIS Z-2801 (Japanese Industrial Standards), is used for the testing of active surface of antimicrobial biomaterials [262]. The methods for analyzing viable but not culturable (VBNC) bacteria include, ATP bioluminescence method, Live/Dead assay, and flow cytometry, etc. [263, 264].

Among *in vivo* biofilm models, murine cutaneous wound systems have been developed to demonstrate delayed re-epithelialization and evaluation of antimicrobial treatments with increased throughput and reproducibility [265, 266]. Recent studies have shown the development of *in vitro* biofilm models, especially chronic wound models for the evaluation of antibacterial properties. Lubbock chronic wound biofilm was the first chronic wound biofilm model used to evaluate the inhibiting efficacy of various biofilm effectors [267, 268]. Other examples of such models based on constant depth film fermenter (CDFF) [269] and colony-drip flow reactor, were used to evaluate the antibacterial effect of wound dressings [270].

Besides the above methods, the development of *in vitro* human based wound infection systems would unravel the poorly understood interactions between pathogenic bacteria and human skin tissue. For example, *in vitro* models of oral & vaginal candidiasis [201, 202, 271, 272], and skin graft-based infections (*S. aureus* and *P. aeruginosa*); studied the biofilm formation [205]. These systems are summarized in Table 1.6.

1.6 Requirements and limitations of 3D *in vitro* skin models

Legal authorities and new EU rules & regulations have pushed the cosmetic industry to develop as well as improve existing epidermal and full-thickness skin models. Model development and characterization are not the only challenges: analytical methods and procedures are also required. As the complexity of an *in vitro* living

system increases, the analytics become complicated. Despite an intensive research in this area, 3D skin models are advanced complex tools that highly need a comprehensive understanding of their development and application in cosmetic or drug development industry. To serve as a successful routinely used tool, skin models need major requirements (as described below) to be defined.

1.6.1 Standardization of production process of 3D in vitro skin models

Concerning the production processes of 3D skin models, a standardized production process is highly needed to better compare the existing and newly developing skin tissue equivalents. Usually in R & D, tissue equivalents are produced manually as traditional way of creating organotypic skin models involving the seeding of human dermal fibroblasts into a matrix material or scaffold (mainly consists of collagen I). After the cells contract the collagen gel, human keratinocytes are seeded on the top to cover the surface and later raised to air-liquid interface (ALI) to start epidermal differentiation process. The collagen contraction is an uncontrollable event that depends on many factors including collagen source, and culture conditions e.g. presence & concentration of serum etc. Many attempts are under investigation to standardize the collagen contraction e.g. rapid expulsion of water from polymerized gels to reconstitute the compressed gels [273]. Additionally, to introduce air-lifted cultures, use of trans-well inserts is cost intensive but necessary, e.g. skin equivalents generated in submerged conditions resulted in less natural moisturizing factors (NMF) and more free water content [274]. Another feature of culture conditions that need to be introduced is dynamic cultivation that applies a pressure and shear force on *in vitro* skin. For performing tests, the time window is 3-4 days because desquamation is missing in *in vitro* skin models [275, 276] resulting in increasing height of stratum corneum (SC) with time. The desquamation process is associated with water level [277] that is usually higher in *in vitro* skin models than *in vivo* skin [278]. Long-term cultures (over 3 months) is another important aspect of epidermal maturation (especially in terms of lipid barrier) resulting in keratin expression pattern and ultrastructure features (presence of lamellar bodies) more similar to *in vivo* skin [48, 74].

Among automated production approaches, ink-jet bioprinting [279] and laser-assisted bioprinting [280] are becoming promising for collagen based dermal compartment, however, the development of stratified epidermis is still in process.

1.6.2 Correlation of in vitro skin models to in vivo models

Several studies have been performed in *in vitro* skin models and data were correlated with the results obtained from human skin biopsies [281]. However, the correlation between data obtained from *in vitro* skin models and *in vivo* models (using animal trials) is still missing. This correlation could be derived by testing compounds in *in vitro* models with a known dose-dependent action in both models. A great amount of investigation is required to fill the gap between preclinical animal trials and *in vitro* skin models and will help to know the relevance of *in vitro* skin models for testing

substance's predictability as well as mode of action. Along with the use of well-known effective drugs, use of false positive and false negative drugs is one possible strategy to compare the results between animal models and 3D *in vitro* skin models as performed with hepatotoxic drugs in toxicological studies [282].

The *in vitro* skin models are used for multiple applications including drug discovery, cosmetic industry, aging, skin immunity, and diseased models such as carcinogenesis [68]. For drug delivery studies of trans-dermal and topical drugs, skin permeation of these models is a very important feature, therefore 3D skin models having poor barrier function are not optimal for penetration studies [283]. To address this issue, investigation is going to improve the barrier function of models similarly to *in vivo* skin.

Validated models for different applications, e.g. corrosion, irritation, and permeation analysis; offer a pre-defined set of standard compounds. Hence, standard compounds and their threshold value should be defined for each type of model e.g. calcipotriol is the standard drug for psoriasis.

As an example, data relevancy about toxicity and metabolism of tested compounds, was assessed by gene expression of enzymes for drug metabolism in *in vitro* skin models (EpiDerm™) showing 87% consistency with human skin [85], suggesting model similarity to *in vivo* skin metabolic pathways and function. However, the basal expression of cytochrome proteins (CYPs) was found low in EpiDerm™, and (specifically CYP1A1/1B1) increased after treatment with 3-methylcholanthrene. Moreover, after stimulation with all-trans retinoic acid [284], strong CYP26AI expression was detected in *in vitro* skin and normal skin that was very weakly detectable in monolayer culture. This expression was even localized the similar way in basal keratinocytes and sweat/sebaceous glands in *in vitro* skin model and normal skin demonstrating the validity of *in vitro* skin models for metabolism and toxicity studies of tested compounds.

1.6.3 Importance of dynamic cultivation

In vivo skin from external surface is subjected to mechanical stimuli, that cause keratinocytes activation (by stimulating mitogen-activated protein kinases or MAPKs) and their increased proliferation [285]. In the body, mechanically stressed areas of skin have thicker epidermis and hyperkeratosis. This response is controlled by calcium influx, phosphorylation of epidermal growth factor receptor (EGFR), and extracellular signal-regulated kinases (ERK1/2). In this respect, mechanical stimulation of *in vivo* skin is a crucial factor. However, little is known about the effect of mechanical stimuli on the skin developmental process. It was recently shown that uniaxial strain applied resulted in enhanced epidermal cell proliferation and differentiation as well as enhanced ECM production [286]. Stretched keratinocytes expressed more cytokeratin 6 and 10 that is a molecular feature of wound edges [287]. Release of proinflammatory cytokines (IL-1α, TNF-α, CXCL8/IL-8 etc.) was already shown when pressure is applied on skin models explaining the situation of

pressure ulcers in skin [288, 289]. Another marker, Tenascin-c, is poorly expressed by keratinocytes in healthy skin, however, inflammation and hyperproliferation increase its expression. Tenascin-c controls proliferation & differentiation and decreases the immune response [290]. It is expressed *in vivo* during wound healing process while in *in vitro* condition it is induced by TNF-α [291]. Fibroblasts are also able to express it in tissue regeneration stimulated by dynamic stimulation [292]. Thus, the incorporation of biomechanical stimulation has significant role to optimize the skin models in the future.

1.6.4 Need of a systemic approach

To investigate the systemic effect of tested compounds on *in vitro* skin models, this system should be connected with other organotypic models. Effect of barrier functions e.g. skin, epithelium of gastrointestinal (GI) tract or lungs, and blood-brain barrier, determine the bioavailability of a drug to the target tissue [293]. A human skin explant was connected with human artificial liver on a chip that was or was not exposed to flow in the system, demonstrated different levels of liver sensitivity towards compound testing [294, 295]. Human skin model was also integrated in a multi-organ-chip (MOC) in dynamic condition, resulting in an improved spatio-temporal cellular microenvironment of dermal matrix [296]. Moreover, the presence of vasculature in MOC better correlated to the *in vivo* situation by contributing to shear stress [295].

The approaches based on multi-human-organs on a chip are of high interest [293, 297-301], and presumably will replace animals and shorten the preclinical trials in future. The National Institutes of Health (NIH) and Defense Advanced Research Project Agency (DARPA) are investing on the development of “organ-on-a-chip” systems to enhance discovery of drugs that are safe and efficient. With special focus to *in vitro* skin models, NIH and DARPA are funding the establishment of skin models from induced pluripotent stem (iPS) cells to produce disease-specific cells for building various skin models. This will lead to a renovation in skin modelling by producing new devices aimed at the study of drugs for pharmacokinetics and pharmacodynamics, as well as mechanical, and biological characterizations.

Conclusion

In conclusion, the 3D skin models offer benefit to the clinics (regenerative medicine following burns/wounds), industry (cosmetics/drugs/therapeutics/biomaterials - development), and basic research (fundamental biology of cell-cell interactions, skin morphogenesis, aging, carcinogenesis/pathologies, etc.). With the advances in stem cell research, it would be possible to generate large number of donor-match backgrounds to ensure autologous skin implants for the severely burnt patients in the coming years.

Moreover, the 3D human skin constructs represent valuable tools, and future efforts for implementation of these models must focus on: 1) Improvement of already existing skin constructs to enhance the reproducibility 2) development of more complex systems to increase the model predictability 3) defining the relevant standards to correlate to *in vivo* results 4) development and improvement of analytical methods to be implemented. These issues offer a challenge to make the routine application of 3D skin models, realistic.

The balance between biological complexity of 3D skin constructs and handling to analyse the 3D system, is a critical point. High complexity is not always important than the flexibility on the ease of use. Therefore, we suggest that the merit of new approaches to incorporate the complexity in the system, has to be taken only case-by-case basis depending on the requirements for application.

References

1. (WHO), W.H.O., *Burns.* 6 March 2018.
2. *Council of the European Union. Seventh Amendment to the EU and Cosmetics Directive 76/768/EEC. Brussels: The European Parliament and the Council of the European Union.* 2003.
3. Mathes, S.H., H. Ruffner, and U. Graf-Hausner, *The use of skin models in drug development.* Advanced drug delivery reviews, 2014. 69: p. 81-102.
4. Griffiths, C., et al., *Rook's textbook of dermatology*. 2016: John Wiley & Sons.
5. Iozzo, R.V., *Basement membrane proteoglycans: from cellar to ceiling.* Nature reviews Molecular cell biology, 2005. 6(8): p. 646.
6. Herndon, D.N., et al., *A comparison of conservative versus early excision. Therapies in severely burned patients.* Annals of surgery, 1989. 209(5): p. 547.
7. Papini, R., *ABC of burns: management of burn injuries of various depths.* BMJ: British Medical Journal, 2004. 329(7458): p. 158.
8. Rose, J. and D. Herndon, *Advances in the treatment of burn patients.* Burns, 1997. 23: p. S19-S26.
9. Eisenburg, D., *Skin substitutes and wound healing: current status and challenges.* Wounds, 2004. 16: p. 1-17.
10. Bolívar-Flores, Y.J. and W. Kuri-Harcuch, *Frozen allogeneic human epidermal cultured sheets for the cure of complicated leg ulcers.* Dermatologic surgery, 1999. 25(8): p. 610-617.
11. Rheinwatd, J.G. and H. Green, *Seria cultivation of strains of human epidemal keratinocytes: the formation keratinizin colonies from single cell is.* Cell, 1975. 6(3): p. 331-343.
12. Bolivar-Flores, J., et al., *Use of cultured human epidermal keratinocytes for allografting burns and conditions for temporary banking of the cultured allografts.* Burns, 1990. 16(1): p. 3-8.
13. Duinslaeger, L., et al., *Cultured allogeneic keratinocyte sheets accelerate healing compared to Op-site treatment of donor sites in burns.* The Journal of burn care & rehabilitation, 1997. 18(6): p. 545-551.
14. Madden, M.R., et al., *Transplantation of cryopreserved cultured epidermal allografts.* Journal of Trauma and Acute Care Surgery, 1996. 40(5): p. 743-750.
15. Khachemoune, A., Y.M. Bello, and T.J. Phillips, *Factors that influence healing in chronic venous ulcers treated with cryopreserved human epidermal cultures.* Dermatologic surgery, 2002. 28(3): p. 274-280.
16. Woodley, D.T., et al., *Burn wounds resurfaced by cultured epidermal autografts show abnormal reconstitution of anchoring fibrils.* Jama, 1988. 259(17): p. 2566-2571.

17. Kolokol'chikova, E., et al., *Morphological changes in burn wounds after transplantation of allogenic fibroblasts.* Bulletin of experimental biology and medicine, 2001. 131(1): p. 89-93.
18. Wainwright, D., *Use of an acellular allograft dermal matrix (AlloDerm) in the management of full-thickness burns.* Burns, 1995. 21(4): p. 243-248.
19. Shevchenko, R.V., S.L. James, and S.E. James, *A review of tissue-engineered skin bioconstructs available for skin reconstruction.* Journal of the Royal Society Interface, 2009: p. rsif20090403.
20. Supp, D.M. and S.T. Boyce, *Engineered skin substitutes: practices and potentials.* Clinics in dermatology, 2005. 23(4): p. 403-412.
21. Clark, R.A., K. Ghosh, and M.G. Tonnesen, *Tissue engineering for cutaneous wounds.* Journal of Investigative Dermatology, 2007. 127(5): p. 1018-1029.
22. Campoccia, D., et al., *Semisynthetic resorbable materials from hyaluronan esterification.* Biomaterials, 1998. 19(23): p. 2101-2127.
23. Caravaggi, C., et al., *HYAFF 11-based autologous dermal and epidermal grafts in the treatment of noninfected diabetic plantar and dorsal foot ulcers: a prospective, multicenter, controlled, randomized clinical trial.* Diabetes care, 2003. 26(10): p. 2853-2859.
24. Uccioli, L., *A clinical investigation on the characteristics and outcomes of treating chronic lower extremity wounds using the tissuetech autograft system.* The international journal of lower extremity wounds, 2003. 2(3): p. 140-151.
25. Myers, S., et al., *A hyaluronic acid membrane delivery system for cultured keratinocytes: clinical "take" rates in the porcine kerato-dermal model.* The Journal of burn care & rehabilitation, 1997. 18(3): p. 214-222.
26. Nomi, M., et al., *Principals of neovascularization for tissue engineering.* Molecular aspects of medicine, 2002. 23(6): p. 463-483.
27. Eppler, S.M., et al., *A target-mediated model to describe the pharmacokinetics and hemodynamic effects of recombinant human vascular endothelial growth factor in humans.* Clinical Pharmacology & Therapeutics, 2002. 72(1): p. 20-32.
28. Strande, L., et al. *In vitro bioartificial skin culture model of tissue rejection and inflammatory/immune mechanisms*. in *Transplantation proceedings*. 1997.
29. Tremblay, P.L., et al., *Inosculation of tissue-engineered capillaries with the host's vasculature in a reconstructed skin transplanted on mice.* American journal of transplantation, 2005. 5(5): p. 1002-1010.
30. George, M.L., et al., *Correlation of plasma and serum vascular endothelial growth factor levels with platelet count in colorectal cancer: clinical evidence of platelet scavenging?* Clinical Cancer Research, 2000. 6(8): p. 3147-3152.
31. Richardson, T.P., et al., *Polymeric system for dual growth factor delivery.* Nature biotechnology, 2001. 19(11): p. 1029.

32. Swope, V.B., et al., *Regulation of pigmentation in cultured skin substitutes by cytometric sorting of melanocytes and keratinocytes.* Journal of investigative dermatology, 1997. 109(3).
33. Huang, S., et al., *In vitro constitution and in vivo implantation of engineered skin constructs with sweat glands.* Biomaterials, 2010. 31(21): p. 5520-5525.
34. Philpott, M.P., M.R. Green, and T. Kealey, *Human hair growth in vitro.* Journal of cell science, 1990. 97(3): p. 463-471.
35. Weinberg, W.C., et al., *Growth factors specifically alter hair follicle cell proliferation and collagenolytic activity alone or in combination.* Differentiation, 1990. 45(3): p. 168-178.
36. Rogers, G., et al., *Cultivation of murine hair follicles as organoids in a collagen matrix.* Journal of investigative dermatology, 1987. 89(4): p. 369-379.
37. Huang, Z., et al., *Embryonic porcine skin precursors can successfully develop into integrated skin without teratoma formation posttransplantation in nude mouse model.* PloS one, 2010. 5(1): p. e8717.
38. Ohyama, M., *Hair follicle bulge: a fascinating reservoir of epithelial stem cells.* Journal of dermatological science, 2007. 46(2): p. 81-89.
39. Taylor, G., et al., *Involvement of follicular stem cells in forming not only the follicle but also the epidermis.* Cell, 2000. 102(4): p. 451-461.
40. Roh, C. and S. Lyle, *Cutaneous stem cells and wound healing.* Pediatric research, 2006. 59(S4): p. 100R.
41. Waymack, P., et al., *The effect of a tissue engineered bilayered living skin analog, over meshed split-thickness autografts on the healing of excised burn wounds.* Burns, 2000. 26(7): p. 609-619.
42. Hansbrough, J.F., et al., *Clinical trials of a biosynthetic temporary skin replacement, Dermagraft-Transitional Covering, compared with cryopreserved human cadaver skin for temporary coverage of excised burn wounds.* The Journal of burn care & rehabilitation, 1997. 18(1): p. 43-51.
43. Pham, C., et al., *Bioengineered skin substitutes for the management of burns: a systematic review.* Burns, 2007. 33(8): p. 946-957.
44. Groeber, F., et al., *Skin tissue engineering—in vivo and in vitro applications.* Advanced drug delivery reviews, 2011. 63(4-5): p. 352-366.
45. Bell, E., et al., *Living tissue formed in vitro and accepted as skin-equivalent tissue of full thickness.* Science, 1981. 211(4486): p. 1052-1054.
46. Bell, E., et al., *The reconstitution of living skin.* Journal of investigative dermatology, 1983. 81(1): p. S2-S10.
47. Parenteau, N.L., et al., *The organotypic culture of human skin keratinocytes and fibroblasts to achieve form and function.* Cytotechnology, 1992. 9(1-3): p. 163-171.
48. Stark, H.-J., et al. *Epidermal homeostasis in long-term scaffold-enforced skin equivalents*. in *Journal of Investigative Dermatology Symposium Proceedings*. 2006. Elsevier.

49. Sahuc, F., et al., *Mesenchymal-epithelial interactions regulate gene expression of type VII collagen and kalinin in keratinocytes and dermal-epidermal junction formation in a skin equivalent model.* Wound repair and Regeneration, 1996. 4(1): p. 93-102.
50. Lindberg, K. and S.F. Badylak, *Porcine small intestinal submucosa (SIS): a bioscaffold supporting in vitro primary human epidermal cell differentiation and synthesis of basement membrane proteins.* Burns, 2001. 27(3): p. 254-266.
51. Phillips II, L., et al., *A comparison of rabbit and human skin response to certain irritants.* Toxicology and Applied Pharmacology, 1972. 21(3): p. 369-382.
52. Ng, K.W. and D.W. Hutmacher, *Reduced contraction of skin equivalent engineered using cell sheets cultured in 3D matrices.* Biomaterials, 2006. 27(26): p. 4591-4598.
53. Bruin, P., et al., *Biodegradable lysine diisocyanate-based poly (glycolide-co-ϵ-caprolactone)-urethane network in artificial skin.* Biomaterials, 1990. 11(4): p. 291-295.
54. Dai, N.-T., et al., *Human single-donor composite skin substitutes based on collagen and polycaprolactone copolymer.* Biochemical and biophysical research communications, 2009. 386(1): p. 21-25.
55. Chen, G., et al., *Culturing of skin fibroblasts in a thin PLGA–collagen hybrid mesh.* Biomaterials, 2005. 26(15): p. 2559-2566.
56. Ponec, M., *Skin constructs for replacement of skin tissues for in vitro testing.* Advanced drug delivery reviews, 2002. 54: p. S19-S30.
57. Welss, T., D.A. Basketter, and K.R. Schröder, *In vitro skin irritation: facts and future. State of the art review of mechanisms and models.* Toxicology in vitro, 2004. 18(3): p. 231-243.
58. Roguet, R., *Use of skin cell cultures for in vitro assessment of corrosion and cutaneous irritancy.* Cell biology and toxicology, 1999. 15(1): p. 63-75.
59. Idrees, A., et al., *Validation of in vitro assays in three-dimensional human dermal constructs.* The International journal of artificial organs, 2018: p. 0391398818775519.
60. Sun, T., et al., *Culture of skin cells in 3D rather than 2D improves their ability to survive exposure to cytotoxic agents.* Journal of biotechnology, 2006. 122(3): p. 372-381.
61. Robinson, M.K., R. Osborne, and M.A. Perkins, *Strategies for the assessment of acute skin irritation potential.* Journal of pharmacological and toxicological methods, 1999. 42(1): p. 1-9.
62. Draize, J.H., G. Woodard, and H.O. Calvery, *Methods for the study of irritation and toxicity of substances applied topically to the skin and mucous membranes.* Journal of pharmacology and Experimental Therapeutics, 1944. 82(3): p. 377-390.

63. Campbell, R.L. and R.D. Bruce, *Comparative dermatotoxicology: I. Direct comparison of rabbit and human primary skin irritation responses to isopropylmyristate.* Toxicology and applied pharmacology, 1981. 59(3): p. 555-563.
64. Youssef, K.K., et al., *Identification of the cell lineage at the origin of basal cell carcinoma.* Nature cell biology, 2010. 12(3): p. 299.
65. Paulitschke, V., et al., *3, 3', 4, 4', 5, 5'-hexahydroxystilbene impairs melanoma progression in a metastatic mouse model.* Journal of Investigative Dermatology, 2010. 130(6): p. 1668-1679.
66. Mancuso, M., et al., *Modulation of basal and squamous cell carcinoma by endogenous estrogen in mouse models of skin cancer.* Carcinogenesis, 2008. 30(2): p. 340-347.
67. Donahue, B.A., et al., *Selective uptake and sustained expression of AAV vectors following subcutaneous delivery.* The journal of gene medicine, 1999. 1(1): p. 31-42.
68. Brohem, C.A., et al., *Artificial skin in perspective: concepts and applications.* Pigment cell & melanoma research, 2011. 24(1): p. 35-50.
69. Becker, R.A., et al., *Report of an ISRTP Workshop: Progress and barriers to incorporating alternative toxicological methods in the US.* Regulatory Toxicology and Pharmacology, 2006. 46(1): p. 18-22.
70. Kuroyanagi, Y., et al., *Establishment of banking system for allogeneic cultured dermal substitute.* Artificial organs, 2004. 28(1): p. 13-21.
71. UNION, P., *Regulation (EC) No 1907/2006 of the european parliament and of the council*. 2006.
72. Asselineau, D., et al., *Human epidermis reconstructed by culture: is it" normal"?* Journal of Investigative Dermatology, 1986. 86(2).
73. Johnson, E.W., et al., *Serial cultivation of normal human keratinocytes: a defined system for studying the regulation of growth and differentiation.* In Vitro Cellular & Developmental Biology-Animal, 1992. 28(6): p. 429-435.
74. Boehnke, K., et al., *Effects of fibroblasts and microenvironment on epidermal regeneration and tissue function in long-term skin equivalents.* European journal of cell biology, 2007. 86(11-12): p. 731-746.
75. El-Ghalbzouri, A., et al., *Effect of fibroblasts on epidermal regeneration.* British Journal of Dermatology, 2002. 147(2): p. 230-243.
76. Xie, Y., et al., *Development of a three-dimensional human skin equivalent wound model for investigating novel wound healing therapies.* Tissue Engineering Part C: Methods, 2010. 16(5): p. 1111-1123.
77. Alépée, N., et al., *A catch-up validation study on reconstructed human epidermis (SkinEthic™ RHE) for full replacement of the Draize skin irritation test.* Toxicology in Vitro, 2010. 24(1): p. 257-266.
78. Kandárová, H., et al., *In vitro skin irritation testing: improving the sensitivity of the EpiDerm skin irritation test protocol.* ATLA-Alternatives to Laboratory Animals, 2009. 37(6): p. 671.

79. Fentem, J.H. and P.A. Botham, *ECVAM's activities in validating alternative tests for skin corrosion and irritation.* ATLA-NOTTINGHAM-, 2002. 30: p. 61-68.
80. Netzlaff, F., et al., *The human epidermis models EpiSkin®, SkinEthic® and EpiDerm®: an evaluation of morphology and their suitability for testing phototoxicity, irritancy, corrosivity, and substance transport.* European Journal of Pharmaceutics and Biopharmaceutics, 2005. 60(2): p. 167-178.
81. Reus, A.A., et al., *Comet assay in reconstructed 3D human epidermal skin models—investigation of intra-and inter-laboratory reproducibility with coded chemicals.* Mutagenesis, 2013. 28(6): p. 709-720.
82. Van Gele, M., et al., *Three-dimensional skin models as tools for transdermal drug delivery: challenges and limitations.* Expert opinion on drug delivery, 2011. 8(6): p. 705-720.
83. McKim Jr, J.M., D.J. Keller III, and J.R. Gorski, *An in vitro method for detecting chemical sensitization using human reconstructed skin models and its applicability to cosmetic, pharmaceutical, and medical device safety testing.* Cutaneous and ocular toxicology, 2012. 31(4): p. 292-305.
84. Gibbs, S., et al., *An epidermal equivalent assay for identification and ranking potency of contact sensitizers.* Toxicology and applied pharmacology, 2013. 272(2): p. 529-541.
85. Hu, T., et al., *Xenobiotic metabolism gene expression in the EpiDerm™ in vitro 3D human epidermis model compared to human skin.* Toxicology in Vitro, 2010. 24(5): p. 1450-1463.
86. Jain, P., et al., *Formulation optimization, skin irritation, and efficacy characterization of a novel skin-lightening agent.* Journal of cosmetic dermatology, 2012. 11(2): p. 101-110.
87. Asbill, C., et al., *Evaluation of a human bio-engineered skin equivalent for drug permeation studies.* Pharmaceutical research, 2000. 17(9): p. 1092-1097.
88. Pappinen, S., et al., *Organotypic cell cultures and two-photon imaging: tools for in vitro and in vivo assessment of percutaneous drug delivery and skin toxicity.* Journal of controlled release, 2012. 161(2): p. 656-667.
89. Heilmann, S., et al., *A thermosensitive morphine-containing hydrogel for the treatment of large-scale skin wounds.* International journal of pharmaceutics, 2013. 444(1-2): p. 96-102.
90. Duval, C., et al., *Human skin model containing melanocytes: essential role of keratinocyte growth factor for constitutive pigmentation—Functional response to α-Melanocyte stimulating hormone and forskolin.* Tissue Engineering Part C: Methods, 2012. 18(12): p. 947-957.
91. Kuphal, S. and A.K. Bosserhoff, *E-cadherin cell–cell communication in melanogenesis and during development of malignant melanoma.* Archives of biochemistry and biophysics, 2012. 524(1): p. 43-47.

92. Haass, N.K., et al., *Adhesion, migration and communication in melanocytes and melanoma.* Pigment cell research, 2005. 18(3): p. 150-159.
93. Duval, C., et al., *Keratinocytes control the pheo/eumelanin ratio in cultured normal human melanocytes.* Pigment cell research, 2002. 15(6): p. 440-446.
94. Kippenberger, S., et al., *Quantification of tyrosinase, TRP-1, and Trp-2 transcripts in human melanocytes by reverse transcriptase-competitive multiplex PCR–regulation by steroid hormones.* Journal of investigative dermatology, 1998. 110(4): p. 364-367.
95. Ouwehand, K., et al., *CCL5 and CCL20 mediate immigration of Langerhans cells into the epidermis of full thickness human skin equivalents.* European journal of cell biology, 2012. 91(10): p. 765-773.
96. Ouwehand, K., et al., *Technical Advance: Langerhans cells derived from a human cell line in a full-thickness skin equivalent undergo allergen-induced maturation and migration.* Journal of leukocyte biology, 2011. 90(5): p. 1027-1033.
97. Tremblay, P.-L., et al., *In vitro evaluation of the angiostatic potential of drugs using an endothelialized tissue-engineered connective tissue.* Journal of Pharmacology and Experimental Therapeutics, 2005. 315(2): p. 510-516.
98. Bellas, E., et al., *In vitro 3D full-thickness skin-equivalent tissue model using silk and collagen biomaterials.* Macromolecular bioscience, 2012. 12(12): p. 1627-1636.
99. Laco, F., et al., *The dose effect of human bone marrow-derived mesenchymal stem cells on epidermal development in organotypic co-culture.* Journal of dermatological science, 2009. 55(3): p. 150-160.
100. van de Kamp, J., et al., *Epithelial morphogenesis of germline-derived pluripotent stem cells on organotypic skin equivalents in vitro.* Differentiation, 2012. 83(3): p. 138-147.
101. Hoeller, D., et al., *An improved and rapid method to construct skin equivalents from human hair follicles and fibroblasts.* Experimental dermatology, 2001. 10(4): p. 264-271.
102. Collawn, S.S., et al., *Adipose-derived stromal cells accelerate wound healing in an organotypic raft culture model.* Annals of plastic surgery, 2012. 68(5): p. 501.
103. Gharzi, A., A. Reynolds, and C. Jahoda, *Plasticity of hair follicle dermal cells in wound healing and induction.* Experimental dermatology, 2003. 12(2): p. 126-136.
104. Li, L., et al., *Human dermal stem cells differentiate into functional epidermal melanocytes.* Journal of Cell Science, 2010: p. jcs. 061598.
105. Nissan, X., et al., *Functional melanocytes derived from human pluripotent stem cells engraft into pluristratified epidermis.* Proceedings of the National Academy of Sciences, 2011: p. 201019070.

106. Michel, M., et al., *Characterization of a new tissue-engineered human skin equivalent with hair.* In Vitro Cellular & Developmental Biology-Animal, 1999. 35(6): p. 318.
107. Forsberg, S. and O. Rollman, *Re-epithelialization from human skin explant cultures is promoted by ligand-activated HER3 receptor.* Journal of dermatological science, 2010. 59(1): p. 7-15.
108. Gandham, V., et al., *Effects of Y27632 on keratinocyte procurement and wound healing.* Clinical and experimental dermatology, 2013. 38(7): p. 782-786.
109. Attia-Vigneau, J., et al., *Regeneration of human dermis by a multi-headed peptide.* Journal of Investigative Dermatology, 2014. 134(1): p. 58-67.
110. Bodó, E., et al., *Dissecting the impact of chemotherapy on the human hair follicle: a pragmatic in vitro assay for studying the pathogenesis and potential management of hair follicle dystrophy.* The American journal of pathology, 2007. 171(4): p. 1153-1167.
111. Peramo, A. and C.L. Marcelo, *Visible effects of rapamycin (sirolimus) on human skin explants in vitro.* Archives of dermatological research, 2013. 305(2): p. 163-171.
112. Lebonvallet, N., et al., *Effects of the re-innervation of organotypic skin explants on the epidermis.* Experimental dermatology, 2012. 21(2): p. 156-158.
113. Lebonvallet, N., et al., *Effect of human skin explants on the neurite growth of the PC 12 cell line.* Experimental dermatology, 2013. 22(3): p. 224-225.
114. Lebonvallet, N., et al., *The evolution and use of skin explants: potential and limitations for dermatological research.* European Journal of Dermatology, 2010. 20(6): p. 671-684.
115. Gueniche, A., et al., *Lactobacillus paracasei CNCM I-2116 (ST11) inhibits substance P-induced skin inflammation and accelerates skin barrier function recovery in vitro.* European journal of dermatology, 2010. 20(6): p. 731-737.
116. Oosterhoff, D., et al., *Intradermal delivery of TLR agonists in a human explant skin model: preferential activation of migratory dendritic cells by polyribosinic-polyribocytidylic acid and peptidoglycans.* The Journal of Immunology, 2013: p. 1200598.
117. Schneider, L.P., et al., *Intradermally administered TLR4 agonist GLA-SE enhances the capacity of human skin DCs to activate T cells and promotes emigration of Langerhans cells.* Vaccine, 2012. 30(28): p. 4216-4224.
118. Flacher, V., et al., *Epidermal Langerhans cells rapidly capture and present antigens from C-type lectin-targeting antibodies deposited in the dermis.* Journal of Investigative Dermatology, 2010. 130(3): p. 755-762.
119. Stenn, K. and I. Dvoretzky, *Human serum and epithelial spread in tissue culture.* Archives of dermatological research, 1979. 264(1): p. 3-15.

120. Stoll, S.W., S. Kansra, and J.T. Elder, *Keratinocyte outgrowth from human skin explant cultures is dependent upon p38 signaling.* Wound Repair and Regeneration, 2003. 11(5): p. 346-353.
121. Lu, H. and O. Rollman, *Fluorescence imaging of reepithelialization from skin explant cultures on acellular dermis.* Wound repair and regeneration, 2004. 12(5): p. 575-586.
122. Krugluger, W., et al., *Reorganization of hair follicles in human skin organ culture induced by cultured human follicle-derived cells.* Experimental dermatology, 2005. 14(8): p. 580-585.
123. Nolte, S.V., et al., *Diversity of fibroblasts–a review on implications for skin tissue engineering.* Cells Tissues Organs, 2008. 187(3): p. 165-176.
124. Freshney, R.I., *Culture of animal cells: a manual of basic technique*. Wiley, New York1994.
125. Andriani, F., et al., *Analysis of microenvironmental factors contributing to basement membrane assembly and normalized epidermal phenotype.* Journal of investigative dermatology, 2003. 120(6): p. 923-931.
126. Lee, D.-Y. and K.-H. Cho, *The effects of epidermal keratinocytes and dermal fibroblasts on the formation of cutaneous basement membrane in three-dimensional culture systems.* Archives of dermatological research, 2005. 296(7): p. 296-302.
127. Maas-Szabowski, N., A. Shimotoyodome, and N.E. Fusenig, *Keratinocyte growth regulation in fibroblast cocultures via a double paracrine mechanism.* Journal of cell science, 1999. 112(12): p. 1843-1853.
128. Maas-Szabowski, N., H.-J. Stark, and N.E. Fusenig, *Keratinocyte growth regulation in defined organotypic cultures through IL-1-induced keratinocyte growth factor expression in resting fibroblasts.* Journal of investigative dermatology, 2000. 114(6): p. 1075-1084.
129. Falanga, V., et al., *Wounding of bioengineered skin: cellular and molecular aspects after injury.* Journal of investigative dermatology, 2002. 119(3): p. 653-660.
130. Coulomb, B., et al., *The collagen lattice: a model for studying the physiology, biosynthetic function and pharmacology of the skin.* British Journal of Dermatology, 1984. 111: p. 83-87.
131. Weiss, S.J., *Tissue destruction by neutrophils.* New England Journal of Medicine, 1989. 320(6): p. 365-376.
132. Martin, P. and S.J. Leibovich, *Inflammatory cells during wound repair: the good, the bad and the ugly.* Trends in cell biology, 2005. 15(11): p. 599-607.
133. Leibovich, S. and R. Ross, *The role of the macrophage in wound repair. A study with hydrocortisone and antimacrophage serum.* The American journal of pathology, 1975. 78(1): p. 71.
134[a]. Polverini, P.J., et al., *Activated macrophages induce vascular proliferation.* Nature, 1977. 269(5631): p. 804.

134[b]. Oliver, R., Does a cognate receptor know its own effector? Trends in plant science, 2010. 15(10).
135. Eming, S.A., et al., *Regulation of angiogenesis: wound healing as a model.* Progress in histochemistry and cytochemistry, 2007. 42(3): p. 115-170.
136. Midwood, K.S., L.V. Williams, and J.E. Schwarzbauer, *Tissue repair and the dynamics of the extracellular matrix.* The international journal of biochemistry & cell biology, 2004. 36(6): p. 1031-1037.
137. Diegelmann, R.F. and M.C. Evans, *Wound healing: an overview of acute, fibrotic and delayed healing.* Front Biosci, 2004. 9(1): p. 283-289.
138. Williams, I.R. and T.S. Kupper, *Immunity at the surface: homeostatic mechanisms of the skin immune system.* Life sciences, 1996. 58(18): p. 1485-1507.
139. Régnier, M., et al., *Integration of Langerhans cells into a pigmented reconstructed human epidermis.* Journal of Investigative Dermatology, 1997. 109(4).
140. Linder, T., *Culture of human epidermal Langerhans cells in a skin equivalent.* British Journal of Dermatology, 1998. 139(4): p. 598-604.
141. Koblizek, T.I., et al., *Angiopoietin-1 induces sprouting angiogenesis in vitro.* Current Biology, 1998. 8(9): p. 529-532.
142. Nör, J.E., et al., *Vascular endothelial growth factor (VEGF)-mediated angiogenesis is associated with enhanced endothelial cell survival and induction of Bcl-2 expression.* The American journal of pathology, 1999. 154(2): p. 375-384.
143. Trochon, V., et al., *Endothelial metalloprotease-disintegrin protein (ADAM) is implicated in angiogenesis in vitro.* Angiogenesis, 1998. 2(3): p. 277-285.
144. Bach, T.L., et al., *Endothelial cell VE-cadherin functions as a receptor for the β15–42 sequence of fibrin.* Journal of Biological Chemistry, 1998. 273(46): p. 30719-30728.
145. Bayless, K.J., R. Salazar, and G.E. Davis, *RGD-dependent vacuolation and lumen formation observed during endothelial cell morphogenesis in three-dimensional fibrin matrices involves the αvβ3 and α5β1 integrins.* The American journal of pathology, 2000. 156(5): p. 1673-1683.
146. Black, A.F., et al., *In vitro reconstruction of a human capillary-like network in a tissue-engineered skin equivalent.* The FASEB Journal, 1998. 12(13): p. 1331-1340.
147. Donovan, D., et al., *Comparison of three in vitro human 'angiogenesis' assays with capillaries formed in vivo.* Angiogenesis, 2001. 4(2): p. 113-121.
148. Ponec, M., et al., *Endothelial network formed with human dermal microvascular endothelial cells in autologous multicellular skin substitutes.* Angiogenesis, 2004. 7(4): p. 295-305.
149. Dewey, C., et al., *The dynamic response of vascular endothelial cells to fluid shear stress.* Journal of biomechanical engineering, 1981. 103(3): p. 177-185.

150[a]. Brenner, M. and V.J. Hearing, *The protective role of melanin against UV damage in human skin.* Photochemistry and photobiology, 2008. 84(3): p. 539-549.
150[b]. Różanowska, M., et al., Free radical scavenging properties of melanin: interaction of eu-and pheo-melanin models with reducing and oxidising radicals. Free Radical Biology and Medicine, 1999. 26(5-6): p. 518-525.
151. Bertaux, B., et al., *Growth of melanocytes in a skin equivalent model in vitro.* British Journal of Dermatology, 1988. 119(4): p. 503-512.
152. Topol, B.M., et al., *Transfer of melanosomes in a skin equivalent model in vitro.* Journal of investigative dermatology, 1986. 87(5).
153. Bernerd, F. and D. Asselineau, *Successive Alteration and Recovery of Epidermal Differentiation and Morphogenesis after Specific UVB-Damages in Skin Reconstructedin Vitro.* Developmental biology, 1997. 183(2): p. 123-138.
154. Garibyan, L. and D.E. Fisher, *How sunlight causes melanoma.* Current oncology reports, 2010. 12(5): p. 319-326.
155. Bernerd, F. and D. Asselineau, *An organotypic model of skin to study photodamage and photoprotection in vitro.* Journal of the American Academy of Dermatology, 2008. 58(5): p. S155-S159.
156. Lelièvre, D., et al., *The EpiSkin phototoxicity assay (EPA): development of an in vitro tiered strategy using 17 reference chemicals to predict phototoxic potency.* Toxicology in vitro, 2007. 21(6): p. 977-995.
157. Bandarchi, B., et al., *From melanocyte to metastatic malignant melanoma.* Dermatology research and practice, 2010. 2010.
158. Uong, A. and L.I. Zon, *Melanocytes in development and cancer.* Journal of cellular physiology, 2010. 222(1): p. 38-41.
159. Hsu, M.Y., F. Meier, and M. Herlyn, *Melanoma development and progression: a conspiracy between tumor and host.* Differentiation: REVIEW, 2002. 70(9-10): p. 522-536.
160. Shih, I., et al., *Regulation of Mel-CAM/MUC18 expression on melanocytes of different stages of tumor progression by normal keratinocytes.* The American journal of pathology, 1994. 145(4): p. 837.
161. Grindon, C., et al., *A review of the status of alternative approaches to animal testing and the development of integrated testing strategies for assessing the toxicity of chemicals under REACH--a summary of a DEFRA-funded project conducted by Liverpool John Moores University and FRAME.* Alternatives to laboratory animals: ATLA, 2006. 34: p. 149-158.
162. Walles, T., et al., *The potential of bioartificial tissues in oncology research and treatment.* Oncology Research and Treatment, 2007. 30(7): p. 388-394.
163. Meier, F., et al., *Human melanoma progression in skin reconstructs: biological significance of bFGF.* The American journal of pathology, 2000. 156(1): p. 193-200.

164. Eves, P., et al., *Anti-inflammatory and anti-invasive effects of α-melanocyte-stimulating hormone in human melanoma cells.* British Journal of Cancer, 2003. 89(10): p. 2004.
165. Eves, P., et al., *Melanoma invasion in reconstructed human skin is influenced by skin cells–investigation of the role of proteolytic enzymes.* Clinical & experimental metastasis, 2003. 20(8): p. 685-700.
166. Van Kilsdonk, J.W., et al., *Keratinocytes drive melanoma invasion in a reconstructed skin model.* Melanoma research, 2010. 20(5): p. 372-380.
167. Meier, F., et al., *Combined targeting of MAPK and AKT signalling pathways is a promising strategy for melanoma treatment.* British Journal of Dermatology, 2007. 156(6): p. 1204-1213.
168. Folkman, J., *What is the evidence that tumors are angiogenesis dependent?* JNCI: Journal of the National Cancer Institute, 1990. 82(1): p. 4-7.
169. Liotta, L.A., J. Kleinerman, and G.M. Saidel, *Quantitative relationships of intravascular tumor cells, tumor vessels, and pulmonary metastases following tumor implantation.* Cancer research, 1974. 34(5): p. 997-1004.
170. Danilenko, D., *Preclinical models of psoriasis.* Veterinary pathology, 2008. 45(4): p. 563-575.
171. Bowcock, A.M. and J.G. Krueger, *Getting under the skin: the immunogenetics of psoriasis.* Nature Reviews Immunology, 2005. 5(9): p. 699.
172. Saiag, P., et al., *Psoriatic fibroblasts induce hyperproliferation of normal keratinocytes in a skin equivalent model in vitro.* Science, 1985. 230(4726): p. 669-672.
173. Fransson, J., et al., *Proliferation and interferon-γ receptor expression in psoriatic and healthy keratinocytes are influenced by interactions between keratinocytes and fibroblasts in a skin equivalent model.* Archives of dermatological research, 1995. 287(6): p. 517-523.
174. Konstantinova, N.V., et al., *Interleukin-8 is induced in skin equivalents and is highest in those derived from psoriatic fibroblasts.* Journal of investigative dermatology, 1996. 107(4).
175. BAKER, B.S., et al., *The effects of cyclosporin A on T lymphocyte and dendritic cell sub-populations in psoriasis.* British Journal of Dermatology, 1987. 116(4): p. 503-510.
176. Prinz, J., et al., *Chimaeric CD4 monoclonal antibody in treatment of generalised pustular psoriasis.* The Lancet, 1991. 338(8762): p. 320-321.
177. Gottlieb, S.L., et al., *Response of psoriasis to a lymphocyte-selective toxin (DAB389IL-2) suggests a primary immune, but not keratinocyte, pathogenic basis.* Nature medicine, 1995. 1(5): p. 442-447.
178. Jean, J., et al., *Development of an in vitro psoriatic skin model by tissue engineering.* Journal of dermatological science, 2009. 53(1): p. 19-25.

179. Barker, C.L., et al., *The development and characterization of an in vitro model of psoriasis.* Journal of investigative dermatology, 2004. 123(5): p. 892-901.
180. Harrison, C., et al., *Transglutaminase inhibitors induce hyperproliferation and parakeratosis in tissue-engineered skin.* British Journal of Dermatology, 2007. 156(2): p. 247-257.
181. Tjabringa, G., et al., *Development and validation of human psoriatic skin equivalents.* The American journal of pathology, 2008. 173(3): p. 815-823.
182. Kalish, R.S., et al., *Skin equivalent and natural killer cells: a new model for psoriasis and GVHD.* The Journal of investigative dermatology, 2009. 129(3): p. 773-776.
183. Gysler, A., et al., *Skin penetration and metabolism of topical glucocorticoids in reconstructed epidermis and in excised human skin.* Pharmaceutical research, 1999. 16(9): p. 1386-1391.
184. de Jager, M., et al., *Preparation and characterization of a stratum corneum substitute for in vitro percutaneous penetration studies.* Biochimica et Biophysica Acta (BBA)-Biomembranes, 2006. 1758(5): p. 636-644.
185. Gabbanini, S., et al., *In vitro evaluation of the permeation through reconstructed human epidermis of essentials oils from cosmetic formulations.* Journal of pharmaceutical and biomedical analysis, 2009. 50(3): p. 370-376.
186. Ackermann, K., et al., *The Phenion® full-thickness skin model for percutaneous absorption testing.* Skin pharmacology and physiology, 2010. 23(2): p. 105-112.
187. Kao, J., J. Hall, and G. Helman, *In vitro percutaneous absorption in mouse skin: influence of skin appendages.* Toxicology and applied pharmacology, 1988. 94(1): p. 93-103.
188. Illel, B., et al., *Follicles play an important role in percutaneous absorption.* Journal of pharmaceutical sciences, 1991. 80(5): p. 424-427.
189. Scheuplein, R.J., *Mechanism of percutaneous absorption: II. Transient diffusion and the relative importance of various routes of skin penetration.* Journal of Investigative Dermatology, 1967. 48(1): p. 79-88.
190. WerthÉn, M., et al., *An in vitro model of bacterial infections in wounds and other soft tissues.* Apmis, 2010. 118(2): p. 156-164.
191. Thorn, R., S. Nelson, and J. Greenman, *Use of a bioluminescent Pseudomonas aeruginosa strain within an in vitro microbiological system, as a model of wound infection, to assess the antimicrobial efficacy of wound dressings by monitoring light production.* Antimicrobial agents and chemotherapy, 2007. 51(9): p. 3217-3224.
192. Thorn, R. and J. Greenman, *A novel in vitro flat-bed perfusion biofilm model for determining the potential antimicrobial efficacy of topical wound treatments.* Journal of applied microbiology, 2009. 107(6): p. 2070-2079.
193. Schaller, M., et al., *Models of oral and vaginal candidiasis based on in vitro reconstituted human epithelia.* Nature protocols, 2006. 1(6): p. 2767.

194. Green, C.B., et al., *RT-PCR detection of Candida albicans ALS gene expression in the reconstituted human epithelium (RHE) model of oral candidiasis and in model biofilms.* Microbiology, 2004. 150(2): p. 267-275.
195. Coenye, T. and H.J. Nelis, *In vitro and in vivo model systems to study microbial biofilm formation.* Journal of microbiological methods, 2010. 83(2): p. 89-105.
196. Schaller, M., et al., *Invasion of Candida albicans correlates with expression of secreted aspartic proteinases during experimental infection of human epidermis.* Journal of investigative dermatology, 2000. 114(4): p. 712-717.
197. Schaller, M., R. Mailhammer, and H.C. Korting, *Cytokine expression induced by Candida albicans in a model of cutaneous candidosis based on reconstituted human epidermis.* Journal of medical microbiology, 2002. 51(8): p. 672-676.
198. Bernhardt, J., et al., *Influence of voriconazole and fluconazole on reconstituted multilayered oesophageal epithelium infected by Candida albicans.* Mycoses, 2004. 47(7): p. 330-337.
199. Bernhardt, J., et al., *Adherence and invasion studies of Candida albicans strains, using in vitro models of esophageal candidiasis.* The Journal of infectious diseases, 2001. 184(9): p. 1170-1175.
200. Jayatilake, J., Y. Samaranayake, and L. Samaranayake, *An ultrastructural and a cytochemical study of candidal invasion of reconstituted human oral epithelium.* Journal of oral pathology & medicine, 2005. 34(4): p. 240-246.
201. Malic, S., et al., *Characterization of Candida albicans infection of an in vitro oral epithelial model using confocal laser scanning microscopy.* Oral microbiology and immunology, 2007. 22(3): p. 188-194.
202. Nailis, H., et al., *Real-time PCR expression profiling of genes encoding potential virulence factors in Candida albicans biofilms: identification of model-dependent and-independent gene expression.* BMC microbiology, 2010. 10(1): p. 114.
203. Schaller, M., et al., *Polymorphonuclear leukocytes (PMNs) induce protective Th1-type cytokine epithelial responses in an in vitro model of oral candidosis.* Microbiology, 2004. 150(9): p. 2807-2813.
204. Zakikhany, K., et al., *In vivo transcript profiling of Candida albicans identifies a gene essential for interepithelial dissemination.* Cellular microbiology, 2007. 9(12): p. 2938-2954.
205. Charles, C.A., et al., *Use of tissue-engineered skin to study in vitro biofilm development.* Dermatologic Surgery, 2009. 35(9): p. 1334-1341.
206. de Breij, A., et al., *A 3D human skin equivalent as a tool to study Acinetobacter baumannii colonization.* Antimicrobial agents and chemotherapy, 2012: p. AAC. 05975-11.
207. Popov, L., et al., *Three-dimensional human skin models to understand Staphylococcus aureus skin colonization and infection.* Frontiers in immunology, 2014. 5: p. 41.

208. Visalli, R.J., R.J. Courtney, and C. Meyers, *Infection and replication of herpes simplex virus type 1 in an organotypic epithelial culture system.* Virology, 1997. 230(2): p. 236-243.
209. Andrei, G., et al., *Organotypic epithelial raft cultures as a model for evaluating compounds against alphaherpesviruses.* Antimicrobial agents and chemotherapy, 2005. 49(11): p. 4671-4680.
210. Syrjänen, S., et al., *In vitro establishment of lytic and nonproductive infection by herpes simplex virus type 1 in three-dimensional keratinocyte culture.* Journal of virology, 1996. 70(9): p. 6524-6528.
211. Hukkanen, V., et al., *Herpes simplex virus type 1 infection has two separate modes of spread in three-dimensional keratinocyte culture.* Journal of general virology, 1999. 80(8): p. 2149-2155.
212[A]. Penfold, M., P. Armati, and A.L. Cunningham, *Axonal transport of herpes simplex virions to epidermal cells: evidence for a specialized mode of virus transport and assembly.* Proceedings of the National Academy of Sciences, 1994. 91(14): p. 6529-6533.
212[B]. de Breij, A., et al., The antimicrobial peptide SAAP-148 combats drug-resistant bacteria and biofilms. Science translational medicine, 2018. 10(423): p. eaan4044.
213. Pupovac, A., et al., *Toward Immunocompetent 3D Skin Models.* Advanced healthcare materials, 2018: p. 1701405.
214. McHale, C.M., et al., *Analysis of the transcriptome in molecular epidemiology studies.* Environmental and molecular mutagenesis, 2013. 54(7): p. 500-517.
215. Wang, Z., M. Gerstein, and M. Snyder, *RNA-Seq: a revolutionary tool for transcriptomics.* Nature reviews genetics, 2009. 10(1): p. 57.
216. Huang, R., et al., *An RNA-Seq strategy to detect the complete coding and non-coding transcriptome including full-length imprinted macro ncRNAs.* PloS one, 2011. 6(11): p. e27288.
217. Joyce, C.E., et al., *Deep sequencing of small RNAs from human skin reveals major alterations in the psoriasis miRNAome.* Human molecular genetics, 2011. 20(20): p. 4025-4040.
218. Eddy, S.R., *Non–coding RNA genes and the modern RNA world.* Nature Reviews Genetics, 2001. 2(12): p. 919.
219. Itzkovitz, S. and A. Van Oudenaarden, *Validating transcripts with probes and imaging technology.* Nature methods, 2011. 8(4s): p. S12.
220. Kalyanaraman, B. and S.T. Boyce, *Wound healing on athymic mice with engineered skin substitutes fabricated with keratinocytes harvested from an automated bioreactor.* Journal of Surgical Research, 2009. 152(2): p. 296-302.
221. Garlick, J.A. and L.B. Taichman, *Fate of human keratinocytes during reepithelialization in an organotypic culture model.* Laboratory

investigation; a journal of technical methods and pathology, 1994. 70(6): p. 916-924.
222. Koster, M.I., et al., *p63 is the molecular switch for initiation of an epithelial stratification program.* Genes & development, 2004. 18(2): p. 126-131.
223. Paull, T.T., et al., *A critical role for histone H2AX in recruitment of repair factors to nuclear foci after DNA damage.* Current Biology, 2000. 10(15): p. 886-895.
224. Mildner, M., et al., *Knockdown of filaggrin impairs diffusion barrier function and increases UV sensitivity in a human skin model.* Journal of Investigative Dermatology, 2010. 130(9): p. 2286-2294.
225. Rachow, S., et al., *Occludin is involved in adhesion, apoptosis, differentiation and Ca2+-homeostasis of human keratinocytes: implications for tumorigenesis.* PLoS One, 2013. 8(2): p. e55116.
226. Scholzen, T. and J. Gerdes, *The Ki-67 protein: from the known and the unknown.* Journal of cellular physiology, 2000. 182(3): p. 311-322.
227. Van Erp, P., et al., *Flow cytometric analysis of epidermal subpopulations from normal and psoriatic skin using monoclonal antibodies against intermediate filaments.* The American journal of pathology, 1989. 135(5): p. 865.
228. Bodenmiller, B., et al., *Multiplexed mass cytometry profiling of cellular states perturbed by small-molecule regulators.* Nature biotechnology, 2012. 30(9): p. 858.
229. Bendall, S.C., et al., *Single-cell mass cytometry of differential immune and drug responses across a human hematopoietic continuum.* Science, 2011. 332(6030): p. 687-696.
230. Brody, E., et al., *Life's simple measures: unlocking the proteome.* Journal of molecular biology, 2012. 422(5): p. 595-606.
231. Braziulis, E., et al., *Modified plastic compression of collagen hydrogels provides an ideal matrix for clinically applicable skin substitutes.* Tissue Engineering Part C: Methods, 2012. 18(6): p. 464-474.
232. Pampaloni, F., E.G. Reynaud, and E.H. Stelzer, *The third dimension bridges the gap between cell culture and live tissue.* Nature reviews Molecular cell biology, 2007. 8(10): p. 839.
233. Squirrell, J.M., et al., *Long-term two-photon fluorescence imaging of mammalian embryos without compromising viability.* Nature biotechnology, 1999. 17(8): p. 763.
234. Diaspro, A., et al., *Multi-photon excitation microscopy.* Biomedical engineering online, 2006. 5(1): p. 36.
235. Santi, P.A., *Light sheet fluorescence microscopy: a review.* Journal of Histochemistry & Cytochemistry, 2011. 59(2): p. 129-138.
236. Keller, P.J., et al., *Digital scanned laser light-sheet fluorescence microscopy (DSLM) of zebrafish and Drosophila embryonic development.* Cold Spring Harbor Protocols, 2011. 2011(10): p. pdb. prot065839.

237. Lakowicz, J.R., et al., *Fluorescence lifetime imaging.* Analytical biochemistry, 1992. 202(2): p. 316-330.
238. Niesner, R., et al., *3D-resolved investigation of the pH gradient in artificial skin constructs by means of fluorescence lifetime imaging.* Pharmaceutical research, 2005. 22(7): p. 1079-1087.
239. Rehberg, M., et al., *Label-free 3D visualization of cellular and tissue structures in intact muscle with second and third harmonic generation microscopy.* PloS one, 2011. 6(11): p. e28237.
240. Duplan-Perrat, F., et al., *Keratinocytes Influence the Maturation and Organization of the Elastin Network in a Skin Equivalent1.* Journal of investigative dermatology, 2000. 114(2): p. 365-370.
241. Jiang, H. and F. Grinnell, *Cell–matrix entanglement and mechanical anchorage of fibroblasts in three-dimensional collagen matrices.* Molecular biology of the cell, 2005. 16(11): p. 5070-5076.
242. Wang, M. and J.A. Kornfield, *Measuring shear strength of soft-tissue adhesives.* Journal of Biomedical Materials Research Part B: Applied Biomaterials, 2012. 100(3): p. 618-623.
243. Crichton, M.L., et al., *The viscoelastic, hyperelastic and scale dependent behaviour of freshly excised individual skin layers.* Biomaterials, 2011. 32(20): p. 4670-4681.
244. Zahouani, H., et al., *Characterization of the mechanical properties of a dermal equivalent compared with human skin in vivo by indentation and static friction tests.* Skin research and technology, 2009. 15(1): p. 68-76.
245. Oliver, G., M. Pemberton, and C. Rhodes, *An in vitro model for identifying skin-corrosive chemicals. I. Initial validation.* Toxicology in vitro, 1988. 2(1): p. 7-17.
246. Scala, R., et al., *Corrositex: An In Vitro Test Method for Assessing Dermal Corrosivity Potential of Chemicals*. 1999.
247. Stobbe, J.L., K.D. Drake, and K.J. Maier, *Comparison of in vivo (Draize method) and in vitro (Corrositex assay) dermal corrosion values for selected industrial chemicals.* International journal of toxicology, 2003. 22(2): p. 99-107.
248. Perkins, M.A., R. Osborne, and G.R. Johnson, *Development of an in vitro method for skin corrosion testing.* Toxicological Sciences, 1996. 31(1): p. 9-18.
249. Fentem, J., et al., *The ECVAM international validation study on in vitro tests for skin corrosivity. 2. Results and evaluation by the Management Team.* Toxicology in vitro, 1998. 12(4): p. 483-524.
250. Kandárová, H., et al., *Assessment of the human epidermis model SkinEthic RHE for in vitro skin corrosion testing of chemicals according to new OECD TG 431.* Toxicology in vitro, 2006. 20(5): p. 547-559.

251. Kidd, D., M. Johnson, and J. Clements, *Development of an in vitro corrosion/irritation prediction assay using the EpiDerm™ skin model.* Toxicology in vitro, 2007. 21(7): p. 1292-1297.
252. Balls, M. and E. Helisten, *Statement on the application of the EpiDerm™ human skin model for skin corrosivity testing.* European Centre for the Validation of Alternative Methods, 2000. 21.
253. Perkins, M.A., et al., *Comparison of in vitro and in vivo human skin responses to consumer products and ingredients with a range of irritancy potential.* Toxicological sciences: an official journal of the Society of Toxicology, 1999. 48(2): p. 218-229.
254. Coquette, A., et al., *Analysis of interleukin-1α (IL-1α) and interleukin-8 (IL-8) expression and release in in vitro reconstructed human epidermis for the prediction of in vivo skin irritation and/or sensitization.* Toxicology in vitro, 2003. 17(3): p. 311-321.
255. Eskes, C., et al., *The ECVAM international validation study on in vitro tests for acute skin irritation: selection of test chemicals.* ATLA-Alternatives to Laboratory Animals, 2007. 35(6): p. 603.
256. Spielmann, H., et al., *The ECVAM international validation study on in vitro tests for acute skin irritation: report on the validity of the EPISKIN and EpiDerm assays and on the Skin Integrity Function Test.* ATLA-Alternatives to Laboratory Animals, 2007. 35(6): p. 559.
257. Gröne, A., *Keratinocytes and cytokines.* Veterinary immunology and immunopathology, 2002. 88(1-2): p. 1-12.
258. Emanuelsson, P. and G. Kratz, *Characterization of a new in vitro burn wound model.* Burns, 1997. 23(1): p. 32-36.
259. Vaughan, M.B., et al., *A reproducible laser-wounded skin equivalent model to study the effects of aging in vitro.* Rejuvenation research, 2004. 7(2): p. 99-110.
260. Siedenbiedel, F. and J.C. Tiller, *Antimicrobial polymers in solution and on surfaces: overview and functional principles.* Polymers, 2012. 4(1): p. 46-71.
261. ASTM, *American Society for Testing & Materials, ASTM E 2149-01, Standard Test Method for Determining the Antimicrobial Activity of Immobilized Antimicrobial Agents Under Dynamic Contact Conditions (American Society for Testing & Materials) West Conshohocken, PA*. 2001.
262. JIS, Z., *2801. Antimicrobial products—test for antimicrobial activity and efficacy. Tokyo, Japan: Japanese Standards Association.* JIS, 2000(2801).
263. Gião, M.S., et al., *Validation of SYTO 9/propidium iodide uptake for rapid detection of viable but noncultivable Legionella pneumophila.* Microbial ecology, 2009. 58(1): p. 56-62.
264. Sachidanandham, R., K. Yew-Hoong Gin, and C. Laa Poh, *Monitoring of active but non-culturable bacterial cells by flow cytometry.* Biotechnology and bioengineering, 2005. 89(1): p. 24-31.

265. Schierle, C.F., et al., *Staphylococcal biofilms impair wound healing by delaying reepithelialization in a murine cutaneous wound model.* Wound Repair and Regeneration, 2009. 17(3): p. 354-359.
266. Kugelberg, E., et al., *Establishment of a superficial skin infection model in mice by using Staphylococcus aureus and Streptococcus pyogenes.* Antimicrobial agents and chemotherapy, 2005. 49(8): p. 3435-3441.
267. Sun, Y., et al., *In vitro multispecies Lubbock chronic wound biofilm model.* Wound repair and regeneration, 2008. 16(6): p. 805-813.
268. Dowd, S., et al., *Effects of biofilm treatments on the multi-species Lubbock chronic wound biofilm model.* Journal of wound care, 2009. 18(12).
269. Hill, K.E., et al., *An in vitro model of chronic wound biofilms to test wound dressings and assess antimicrobial susceptibilities.* Journal of Antimicrobial Chemotherapy, 2010: p. dkq105.
270. Lipp, C., et al., *Testing wound dressings using an in vitro wound model.* Journal of wound care, 2010. 19(6): p. 220.
271. Dongari-Bagtzoglou, A., *Mucosal biofilms: challenges and future directions.* Expert Review of Anti-Infective Therapy, 2008. 6(2): p. 141-144.
272. Schaller, M. and G. Weindl, *Models of oral and vaginal candidiasis based on in vitro reconstituted human epithelia for the study of host-pathogen interactions.* Host-Pathogen Interactions: Methods and Protocols, 2009: p. 327-345.
273. Hu, K., et al., *Compressed collagen gel as the scaffold for skin engineering.* Biomedical microdevices, 2010. 12(4): p. 627-635.
274. Thakoersing, V.S., M. Ponec, and J.A. Bouwstra, *Generation of human skin equivalents under submerged conditions—mimicking the in utero environment.* Tissue Engineering Part A, 2010. 16(4): p. 1433-1441.
275. Ponec, M., et al., *Characterization of reconstructed skin models.* Skin Pharmacology and Physiology, 2002. 15(Suppl. 1): p. 4-17.
276. Ponec, M., J. Kempenaar, and A. Weerheim, *Lack of desquamation–the Achilles heel of the reconstructed epidermis.* International journal of cosmetic science, 2002. 24(5): p. 263-272.
277. Watkinson, A., et al., *Water modulation of stratum corneum chymotryptic enzyme activity and desquamation.* Archives of dermatological research, 2001. 293(9): p. 470-476.
278. Bouwstra, J.A., et al., *Water distribution and natural moisturizer factor content in human skin equivalents are regulated by environmental relative humidity.* Journal of Investigative Dermatology, 2008. 128(2): p. 378-388.
279. Hahn, M.S., et al., *Photolithographic patterning of polyethylene glycol hydrogels.* Biomaterials, 2006. 27(12): p. 2519-2524.
280. Koch, L., et al., *Skin tissue generation by laser cell printing.* Biotechnology and bioengineering, 2012. 109(7): p. 1855-1863.

281. Fernández, Y., et al., *Chemical Blockage of the Proteasome Inhibitory Function of Bortezomib IMPACT ON TUMOR CELL DEATH.* Journal of Biological Chemistry, 2006. 281(2): p. 1107-1118.
282. Kostadinova, R., et al., *A long-term three dimensional liver co-culture system for improved prediction of clinically relevant drug-induced hepatotoxicity.* Toxicology and applied pharmacology, 2013. 268(1): p. 1-16.
283. Godin, B. and E. Touitou, *Transdermal skin delivery: predictions for humans from in vivo, ex vivo and animal models.* Advanced drug delivery reviews, 2007. 59(11): p. 1152-1161.
284. Heise, R., et al., *Skin retinoid concentrations are modulated by CYP26AI expression restricted to basal keratinocytes in normal human skin and differentiated 3D skin models.* Journal of investigative dermatology, 2006. 126(11): p. 2473-2480.
285. Nishimura, K., et al., *The effect of different frequencies of stretch on human dermal keratinocyte proliferation and survival.* Journal of Surgical Research, 2009. 155(1): p. 125-131.
286. Powell, H.M., et al., *Uniaxial strain regulates morphogenesis, gene expression, and tissue strength in engineered skin.* Tissue Engineering Part A, 2009. 16(3): p. 1083-1092.
287. Wong, P. and P.A. Coulombe, *Loss of keratin 6 (K6) proteins reveals a function for intermediate filaments during wound repair.* J Cell Biol, 2003. 163(2): p. 327-337.
288. Bronneberg, D., et al., *An in vitro model system to study the damaging effects of prolonged mechanical loading of the epidermis.* Annals of biomedical engineering, 2006. 34(3): p. 506-514.
289. Bronneberg, D., et al., *Cytokine and chemokine release upon prolonged mechanical loading of the epidermis.* Experimental dermatology, 2007. 16(7): p. 567-573.
290. Lightner, V.A., *Tenascin: does it play a role in epidermal morphogenesis and homeostasis?* Journal of investigative dermatology, 1994. 102(3): p. 273-277.
291. Latijnhouwers, M.A., et al., *Tenascin-C expression in human epidermal keratinocytes is regulated by inflammatory cytokines and a stress response pathway.* Matrix biology, 1998. 17(4): p. 305-316.
292. Mathes, S.H., et al., *A bioreactor test system to mimic the biological and mechanical environment of oral soft tissues and to evaluate substitutes for connective tissue grafts.* Biotechnology and bioengineering, 2010. 107(6): p. 1029-1039.
293. Esch, M., T. King, and M. Shuler, *The role of body-on-a-chip devices in drug and toxicity studies.* Annual review of biomedical engineering, 2011. 13: p. 55-72.
294. Wagner, I., et al., *A dynamic multi-organ-chip for long-term cultivation and substance testing proven by 3D human liver and skin tissue co-culture.* Lab on a Chip, 2013. 13(18): p. 3538-3547.

295. Schimek, K., et al., *Integrating biological vasculature into a multi-organ-chip microsystem.* Lab on a Chip, 2013. 13(18): p. 3588-3598.
296. Ataç, B., et al., *Skin and hair on-a-chip: in vitro skin models versus ex vivo tissue maintenance with dynamic perfusion.* Lab on a chip, 2013. 13(18): p. 3555-3561.
297. Huh, D., G.A. Hamilton, and D.E. Ingber, *From 3D cell culture to organs-on-chips.* Trends in cell biology, 2011. 21(12): p. 745-754.
298. Coleman, R.A., *Human tissue in the evaluation of safety and efficacy of new medicines: a viable alternative to animal models?* ISRN pharmaceutics, 2011. 2011.
299. Ghaemmaghami, A.M., et al., *Biomimetic tissues on a chip for drug discovery.* Drug discovery today, 2012. 17(3-4): p. 173-181.
300. Huh, D., et al., *Microengineered physiological biomimicry: organs-on-chips.* Lab on a Chip, 2012. 12(12): p. 2156-2164.
301. Marx, U., et al., *'Human-on-a-chip'developments: a translational cutting-edge alternative to systemic safety assessment and efficiency evaluation of substances in laboratory animals and man?* Alternatives to Laboratory Animals-ATLA, 2012. 40(5): p. 235.

Chapter 02: Development of Three-dimensional Human Dermal Construct (HDC) and *In vitro* Assays

Table of contents

List of figures

Abbreviations

2D: Two-dimensional
3D: Three-dimensional
ATP: Adenosine triphosphate
Col. I: Collagen type I
CTB: CellTiter-Blue® assay
CTG: CellTiter-Glo® assay
CTO: CytoTox-ONE™ assay
DSMZ: German collection of microorganisms and cell cultures
ECM: Extracellular matrix
EDTA: Ethylenediaminetetraacetic acid
EthD-III: Ethidium homodimer III
FBS: Foetal Bovine Serum
FGM2: Fibroblasts growth media 2
H & E stain: Haematoxylin and eosin stain
HDC: Human *in vitro* dermal construct
HEPES BSS: 4-(2-hydroxyethyl)-1-piperazineethanesulfonic acid buffered saline solution
ISO: international organization for standardization
L929: Mouse fibroblasts cell line
LDH: Lactate dehydrogenase
NADPH: Nicotinamide adenine dinucleotide phosphate
NaHCO3: Sodium bicarbonate
NHDF: Primary normal human dermal fibroblasts
NHEK: Primary normal human epidermal keratinocytes
PE: Polyethylene
RPMI: Roswell park memorial institute medium
RTG MT: RealTime-Glo™ MT assay
TCPS: Tissue culture polystyrene
TNS: Trypsin Neutralizing Solution
ZDEC-PU: Zinc diethyldithiocarbamate containing polyurethane

Chapter 02: Development of Three-dimensional Human Dermal Construct (HDC) and *In vitro* Assays

Abstract

Three-dimensional (3D) cell culture systems are extremely needed for cytocompatibility testing of biomaterials. This work aimed at the development of 3D *in vitro* dermal skin models and their optimization for cytocompatibility evaluation. Initially "murine *in vitro* dermal construct" based on L929 cells was generated, leading to the development of "human *in vitro* dermal construct" consisting of normal human dermal fibroblasts (NHDF) in rat tail tendon collagen type I. To assess the viability of the cells, different assays CellTiter-Blue®, RealTime-Glo™ MT, and CellTiter-Glo® (Promega) were evaluated to optimize the best suited assay to the respective cell type and 3D system. Z-stack imaging (Live/Dead and Phalloidin/DAPI-Promokine) was performed to visualize NHDF inside matrix revealing filopodia like morphology and a uniform distribution of NHDF in matrix. CellTiter-Glo® was found to be the optimal cell viability assay among those analysed. CellTiter-Blue® reagent affected cell morphology of NHDF (unlike L929) suggesting an interference with cell biological activity, resulting in less reliable viability data. On the other hand, RealTime-Glo™ provided a linear signal only with a very low cell density, that made this assay unsuitable for this system. CellTiter-Glo® adapted to 3D dermal construct by optimizing the "shaking time" to enhance the reagent penetration and maximum ATP release indicating 2.4 times higher viability value by shaking for 60 min than for 5 min. Additionally, viability results showed that cells were viable inside the matrix. This model would be further advanced with more layers of skin to make a full thickness model.

Keywords: Three-dimensional (3D) cell culture, Two-dimensional (2D) cell culture, Cytocompatibility evaluation, Human *in vitro* dermal construct, Human dermal fibroblasts.

2.1 Introduction

Before testing new drugs, theranostics or medical devices containing one or more new bioactive biomaterials in "First-in-Man Phase 1 Clinical Trials", highly valid and reliable data is required. Lack of transferability of experimental data of *in vivo* animal trials and their inequivalency to human biology necessitate the use of human cell-derived model systems that can range from single cells via three-dimensional (3D) models to Organs-on-Chips [1-6]. Taking this into consideration, human tissue-related 3D cell cultures have the ability to recapitulate characteristics of tissue physiology and pathophysiology and are emerging as an attractive model system to provide more reliable preclinical outcomes.

Autologous skin or tissue-engineered skin grafts have been used as epidermal/dermal substitutes to treat burns and wounds [7-10]. Commercially available dermal constructs for clinical use include either chemically treated allografts (e.g. AlloDerm®) [11] or *in vitro* cultured human fibroblasts in a matrix (Dermagraft®) [12, 13]. One recent application of grafts is in the field of *in vitro* testing systems [14, 15]. Skin substitutes have been used in pharmacological and basic research either for hazard assessment of chemical compounds (e.g. skin irritation/absorption/corrosion) [14, 16-19] or to understand fundamental processes (e.g. the effect of fibroblasts on microenvironment for epidermal regeneration) [20, 21]. The development of *in vitro* tools for testing has also been stimulated by evolving regulations: the EU 7th amendment of the "Cosmetics Directive" has imposed to replace all animal experiments on cutaneous resorption with reliable *in vitro* tests by the year 2009 [22]. This has led to the development of 3Rs-principle "replacement, reduction and refinement" [23]. In agreement with this principle, cell lines are used to assess general *in vitro* cytotoxicity based on DIN EN ISO 10993-5, while any specific cytotoxicity should be tested using specific primary cells [24]. Additionally, *in vitro* bioevaluation is more accurate using 3D testing systems than 2D cultures [25-27]. Cell-based assays being routinely used for therapeutic screening are the methods based on a specific biomarker for detecting cell viability and cytotoxicity with established 2D cell culture system.There have been precise adaptations of these assays to spheroids-based 3D systems [28-32], however, to evaluate the viability of primary cells-based 3D model, it is crucial to select best suited assay for each cell type in 2D and then in 3D system.

In this work, a human dermal skin model was developed and aimed at the future preclinical testing of new biomaterials for wound healing, reducing the number of needed animal experiments. Human skin is composed of three layers: epidermis, dermis, and the underlying hypodermis, also called subcutaneous connective tissue [33]. A preliminary 3D dermal model using L929 cells (mouse fibroblast cell line) was constructed and named as "murine *in vitro* dermal construct". Knowledge arising from this model allowed the subsequent development of human dermal skin model using primary Normal Human Dermal Fibroblasts (NHDF), named as "human *in vitro* dermal construct". The models were characterised for cell viability and morphology as a function of time. Different viability assays were applied on the models

under different conditions to select the best one as advanced testing system for preclinical evaluation. There is a need for more than one type of test methods to imply in the 3D cell culture system based on different parameters, for example, NADPH enzyme activity, ATP content of cells, and /or DNA content to reveal all the different aspects of non-physiologic or pathophysiologic reactions occurring in this system.

2.2 Materials and Methods

2.2.1 Cell source and materials

L929 cells were obtained from DSMZ (German Collection of Microorganisms and Cell Cultures). Primary cells including normal human dermal fibroblasts (NHDF) and normal human epidermal keratinocytes (NHEK) were obtained from PromoCell. ISO standardized materials i.e. polyethylene (PE) and zinc diethyldithiocarbamate containing polyurethane (ZDEC-PU) were obtained from Goodfellow and Hatano Research Institute respectively used as control materials for cytotoxicity testing. Collagen type I (Col. I) from rat tail tendons was obtained from Ibidi. Lysis Solution of 9% Triton® X-100 in water from Promega was used to create "Lysis control".

2.2.2 Dermal construct fabrication

Gelation of Col. I solution was performed in 10X media (M199-Sigma), in the presence of additives (L-glutamine) and sodium bicarbonate ($NaHCO_3$) resulting a final Col. I concentration of 1.5 mg/mL (containing a final salt concentration of 1X mixture with a pH of 7.2–7.4).

L929 cells maintained in cell culture media RPMI 1640 with stable glutamine (PAN Biotech) containing 10% foetal bovine serum (FBS, PAN Biotech) under physiological culture conditions (37°C, 5% CO_2), and sub-cultured using 0.25% trypsin (Gibco).

NHDF were maintained in fibroblasts growth media 2 (FGM2, Promocell) under the physiological culture conditions (37°C, 5% CO_2), and sub-cultured using DetachKit-Promocell HEPES BSS (2-[4-(2-hydroxyethyl)piperazine-1-yl] ethanesulfonic acid buffered saline solution); 0.04% Trypsin/0.03% EDTA (ethylenediaminetetraacetic acid); and TNS (trypsin neutralizing solution) containing 0.05% trypsin inhibitor from soybean/0.1% bovine serum albumin.

Dermal constructs were prepared by fabricating acellular (200µL) and cellular layers (400µL) of Col. I matrix on polyester membrane of 12 well insert (Corning) constituting a 5mm thick dermal construct.

Cellular layers: Actively dividing mitotic cells (8 x 10^5 L929 cells/mL to obtain the murine *in vitro* dermal construct; 8 x 10^4 NHDF cells/mL to obtain the human *in vitro* dermal construct) were embedded in Col. I solution and poured onto the top of the previously deposited acellular Col. I layer. When the cellularised matrix underwent gelation, the system was fed with fresh cell culture medium. The system was incubated for 5 to 7 days to allow hydrogel remodelling by the embedded cells.

2.2.3 Morphological analysis

Morphological appearance of cells in 2D (cells grown on Tissue Culture Polystyrene or TCPS) and 3D Col. I matrix was assessed using bright field and fluorescent microscopy (Olympus IX51). Fluorescent staining was performed using Live/Dead staining kit-Promokine containing calcein-AM and ethidium homodimer III (EthD-III) to see live and dead cells in 2D and/or 3D matrix. F-actin/nuclei staining was performed using Phalloidin/DAPI stain-Promokine.

2.2.4 Cell viability analysis

To assess the viability of the cells in 2D and 3D system quantitatively, different cell viability and cytotoxicity assays e.g. CellTiter-Blue® (CTB), CytoTox-ONE™ (CTO), RealTime-Glo™ MT (RTG MT), CellTiter-Glo® (CTG)-Promega, were evaluated to monitor cell viability of respective cell types according to standard protocols and for their 3D dermal constructs with modified standard protocols.

The CTG assay was used for matrix-based 3D cultured cells for the first time after optimizing the shaking time using the reagent at the same concentration as described in the standard protocol with monolayer culture. The parallel Z-stack microscopic observation showed, that 60 mins shaking time (10 min for signal stabilization) was enough to lyse cells and release maximum ATP content. The effect on the decay of signal over time was confirmed by recording the luminescence over time.

The CTB assay was used for matrix-based 3D cultured cells for the first time after optimizing the test design using the reagent at the same concentration as described in the standard protocol with monolayer culture. The reagent was added only on the top of the construct, shaken for few minutes and incubated for 2 hours at 37°C. The tiny seeping reagent was transferred every 40 minutes ($T_{40\ min}$, $T_{80\ min}$, $T_{120\ min}$) back to the insert during the incubation period. As compare to higher incubation times, 2 hours were also good enough to reduce blue resazurin to pink resorufin in this 3D system.

2.2.5 Statistical analysis

Experiments were carried out in triplicates (n=3) and results were expressed as mean ± standard deviation. For statistical analysis, GraphPad Prism 5.00.288 (Inc., San Diego, CA, USA) was used to evaluate the significance of the differences in cell viability data. T-test was used when the comparison involved two groups. Significance between groups was considered for $p < 0.05$.

2.3 Results

2.3.1 L929 cells in 2D & 3D models: cytocompatibility evaluation

Morphology of cells changed depending if they had been cultured on 2D flat surface or within a 3D Col. I matrix: a well-connected network of L929 cells was found in 3D matrix (Figure 2.1b) while in 2D cultures cells showed flat morphology (Figure 2.1a).

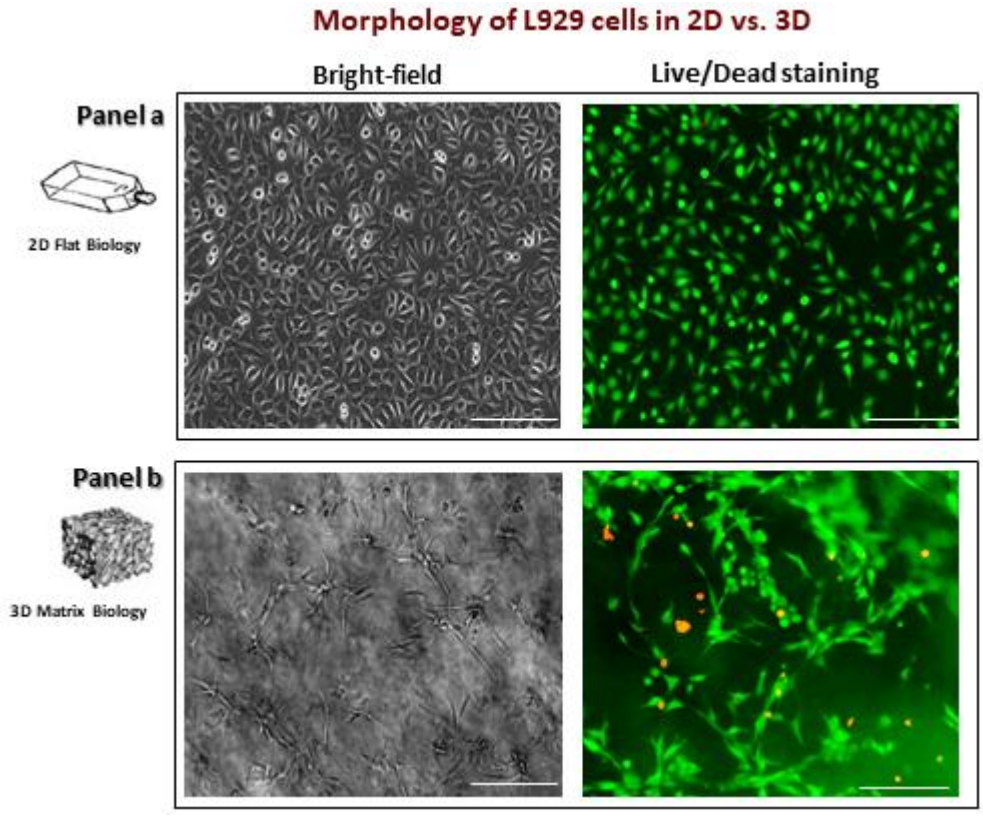

Figure 2.1 Morphology of L929 cells in 2D vs. 3D. Bright field (Left) and fluorescence micrographs (right) of L929 on 2D flat surface (Panel a) and inside 3D Col. I matrix (Panel b). Fluorescent staining was performed using Live/Dead staining kit (calcein-AM and EthD-III). Scale bar=200 µm.

We intended to develop an *in vitro* human dermal skin model for the bio-evaluation of novel drug-free antibacterial hybrid biopolymers for medical applications. Therefore, apart from the company's recommended controls, we used according to the DIN EN ISO 10993-5 standardized positive (PE) and negative control materials (ZDEC-PU), since we intend to analyse the novel biomaterials' interaction with our 3D system.

CTB assay measures cell viability and is based on the ability of living cells to convert a redox dye (resazurin) into a fluorescent end-product (resorufin), while CTO assay evaluates the cytotoxicity by measuring the release of lactate dehydrogenase (LDH) from cells with a damaged membrane. Both assays were performed in multiplexed format to get more information from the same sample. As a proof of concept, the performed

experiment (Figure 2.2 a) showed that CTB assay works well with L929 cells indicating an increasing viability signal with an increase in cell number.

This was also confirmed by monitoring the cytocompatibility of ISO standardized positive (PE) and negative control materials (ZDEC-PU) with L929 cells, indicating cell viability and cytotoxicity signals, respectively (Figure 2.2 b). The fluorescent micrographs using Live/Dead staining of L929 cells (Figure 2.2 c) showed dead cells (red) as a result of exposure with ZDEC-PU and live cells (green) with well-preserved morphology when exposed to PE. This data completely correlated with cytocompatibility data obtained by CTB assay shown in Figure 2.2 b.

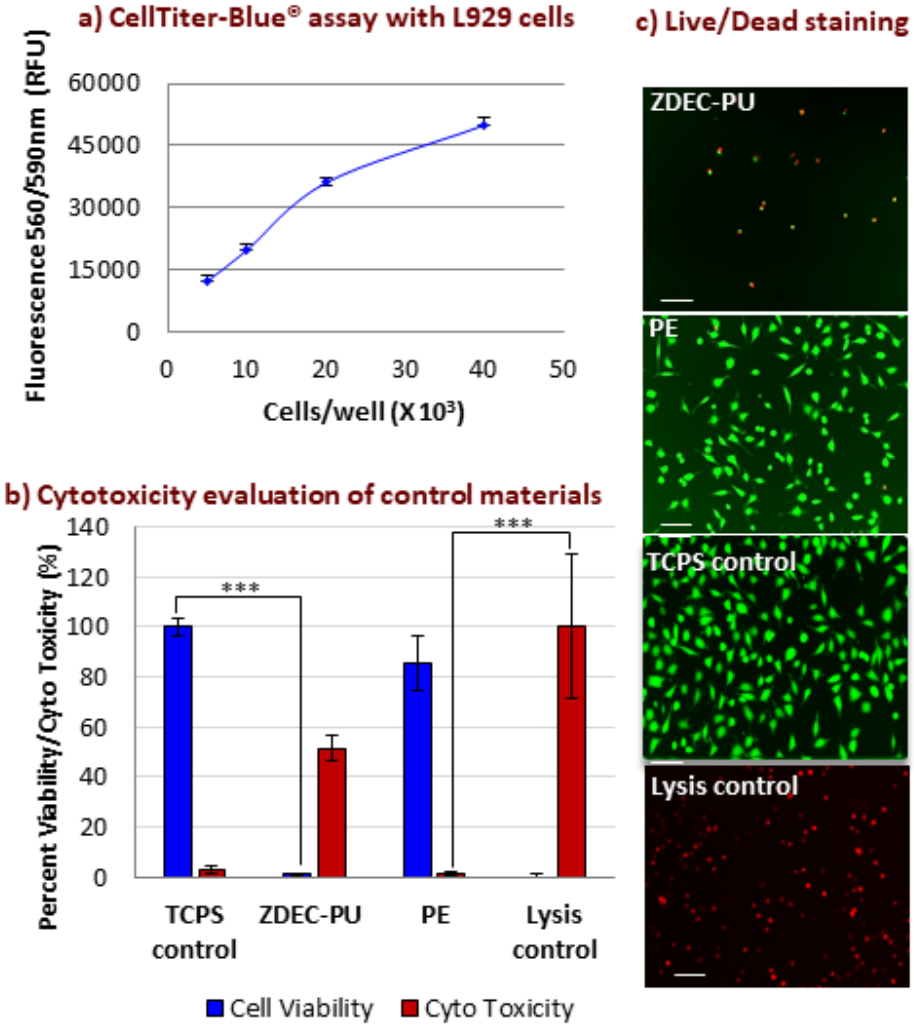

Figure 2.2 a) CellTiter-Blue® assay with L929 cells (in 2D format). The graph shows cell viability data of L929 cells analyzed by using CTB assay. b) Cytotoxicity evaluation of control materials. The cytocompatibility of ISO standardized positive and negative control materials with L929 cells monitored by using CTB and CTO assay. PE indicated polyethylene, ZDEC-PU indicated zinc diethyldithiocarbamate containing polyurethane while TCPS is tissue culture polystyrene. c) Live/Dead staining. The fluorescent micrographs show L929 cells after exposure with the control materials. Staining was performed using Live/Dead staining kit showing dead cells as red and live cells as green. Scale

bar=100 µm. Significant difference between viability values of TCPS control and ZDEC-PU was p=0.0001, and between viability values of Lysis control and PE was p=0.0009.

The assays were optimized in murine *in vitro* dermal construct demonstrating that both assays can be adapted to this 3D system (Figure 2.3 a). This experiment was performed to know if the cell viability can be assessed for the same sample at multiple time points. For this, the reagent exposure time was 2 hours only, at every two days, leading to washing and feeding with fresh media until the following measurement. The results of repeated reagent exposure and as an end point reagent exposure were compared. Cells were viable for at least 20 days in matrix which was a prerequisite for *in vitro* experiments. Furthermore, effect of repeated CTB reagent exposure on viability of L929 cells in 3D matrix demonstrated that this reagent had no toxic effect for at least 18 days exposure (Figure 2.3 b). Therefore, this assay can be used as a method to monitor cytotoxic effect of the same sample in this 3D system over an extended period, at multiple time points.

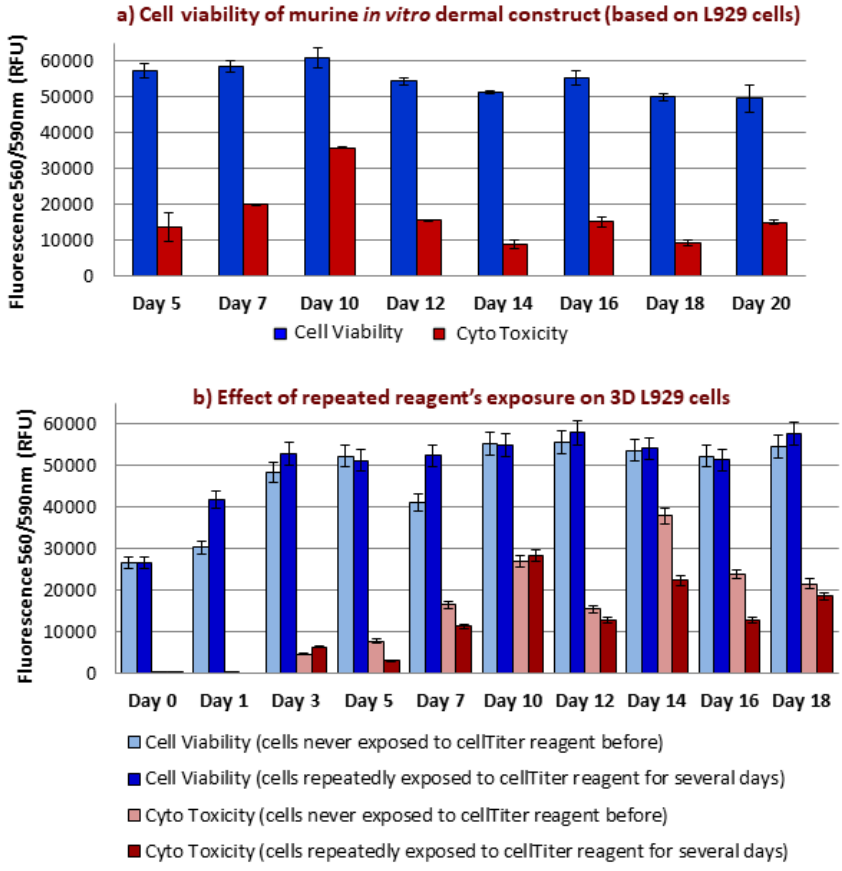

Figure 2.3 a) Cell viability of 3D murine in vitro dermal construct. The graph shows cell viability (blue bars) and cytotoxicity (red bars) assessment of murine 3D dermal construct (based on L929 cells) over time analyzed by CellTiter-Blue® (CTB) and CytoTox-ONE™ (CTO) assays. b) Effect of repeated reagent's exposure on 3D L929 cells. The viability of constructs that were repeatedly exposed to CTB reagent was measured for 18 days.

2.3.2 NHDF cells in 2D & 3D models: cytocompatibility evaluation

CTB assay was performed with primary cells of skin i.e. NHDF and NHEK (Figure 2.4 a). The experiment showed an increasing viability signal with an increase in cell number showing that CTB assay is suitable on these cell types. This concept was further demonstrated by monitoring the cytocompatibility of ISO standardized positive (PE) and negative control materials (ZDEC-PU) with NHDF (Figure 2.4 b). However, microscopic observations (Figure 2.4 c) showed that CTB reagent affected cell morphology (shrunken cells) of NHDF, suggesting reagent interference with cell normal biological activity and possibly resulting less reliable data.

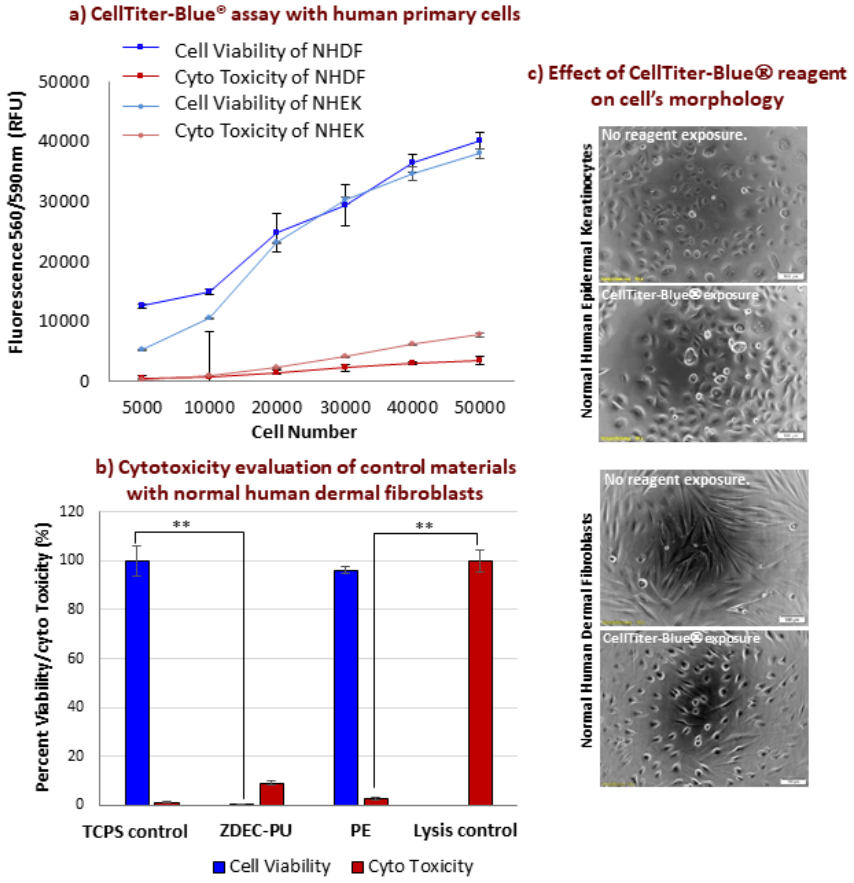

Figure 2.4 a) CellTiter-Blue® assay with human primary cells (in 2D format). The graph shows cell viability data of human skin primary cells i.e. Normal Human Dermal Fibroblasts (NHDF) and Normal Human Epidermal Keratinocytes (NHEK) analyzed by CellTiter-Blue® (CTB) and CytoTox-ONE™ (CTO) assays. b) Cytotoxicity evaluation of control materials with human dermal fibroblasts. The cytocompatibility of ISO standardized positive and negative control materials with NHDF monitored by using CTB and CTO assays. PE indicated polyethylene, ZDEC-PU indicated zinc diethyldithiocarbamate containing polyurethane while TCPS is tissue culture polystyrene. Significant difference between viability values of TCPS control and ZDEC-PU was p=0.0022; and between viability values of Lysis control and PE was p=0.0016. c) Effect of CellTiter-Blue® reagent on cell's morphology. Bright field micrographs show NHEK and NHDF with and without CTB reagent exposure. Scale bar=100 µm.

In an exploration of an appropriate viability assay for NHDF, RTG MT assay was selected because of its continuous-read format to analyse cell viability in real time. The assay is based on the ability of viable cells to reduce a substrate to produce a luminescent signal by NanoLuc® luciferase. This assay did not show linearity of luminescence signal with an increasing time (Figure 2.5). Similar results were obtained with L929 cells (data shown in Appendix A-Figure 2.15), demonstrating that the linearity in the signal was only present when using a lower cell number than 1250, irrespective of cell type. For this reason, this assay was not suitable for 3D systems that involve higher cell number.

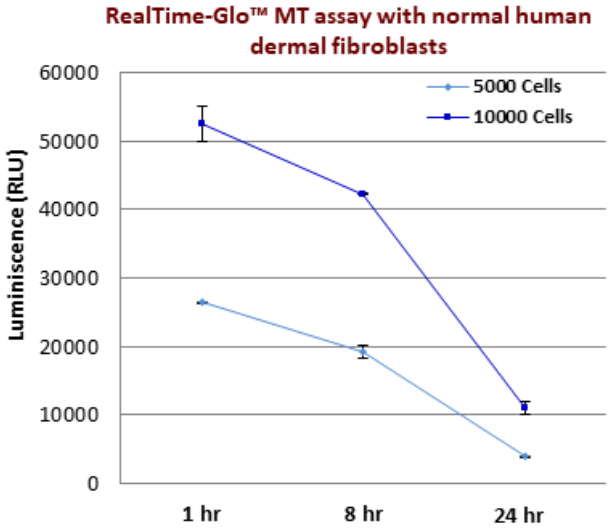

Figure 2.5 RealTime-Glo™ MT assay with human dermal fibroblasts (in 2D format). The graph shows the cell viability data of Normal Human Dermal Fibroblasts (NHDF) analyzed by RealTime-Glo™ MT assay (RTG MT assay) at different time points of 0h, 8h and 24h (T0h T8h T24h).

Finally, CTG assay was performed: it is based on the generation of luminescent signal, proportional to the amount of ATP (Adenosine triphosphate) present in cells. The assay showed an increasing viability signal with an increase in cell number (Figure 2.6 a). Half-life of luminescent signal was assessed as >4h (data shown in Appendix A - Figure 2.14) CTG assay was found to be an optimal cell viability assay among those analysed.

Human *in vitro* dermal construct showed the filopodia-like morphology with dendritic extensions in the matrix and a uniform distribution of NHDF in different planes inside the matrix (Figure 2.6 b).

After selecting CTG assay as an appropriate assay for this cell type, the assay adapted to 3D system by changing the shaking time to optimise the cell lysing ability for ATP release. Increased shaking time resulted in higher cell lytic capacity for maximum ATP release: 60 min shaking time for a cultured dermal construct on Day-7 showed 2.4 times higher luminescent signal for ATP release than shaking for 5 min (Figure 2.6 c). This demonstrated that, NHDF were viable inside the matrix. If an increased ATP content

with time was due to proliferating NHDF inside the matrix needs further exploration using a proliferation assay (Figure 2.6 d).

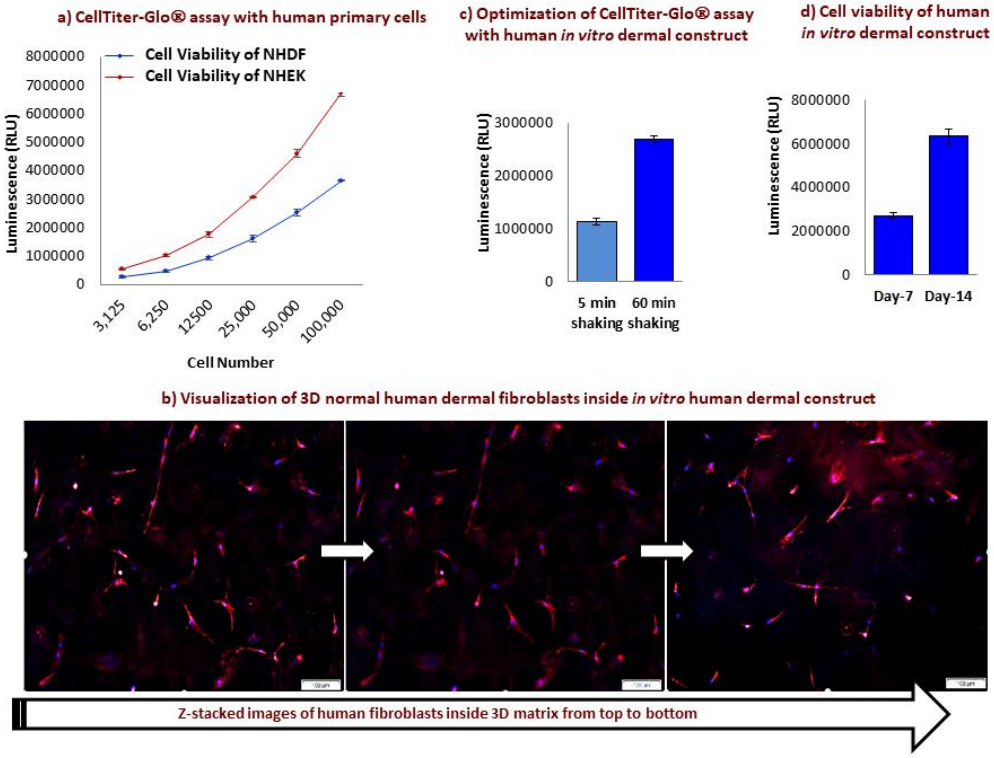

Figure 2.6 a) CellTiter-Glo® assay with human primary cells (in 2D format). The graph shows the cell viability data of human skin primary cells i.e. Normal Human Dermal Fibroblasts (NHDF) and Normal Human Epidermal Keratinocytes (NHEK) analyzed by CellTiter-Glo® (CTG) assay. b) Visualization of 3D normal human dermal fibroblasts inside human in vitro dermal construct. The fluorescent micrographs from top to bottom show the Z-stacked images of in vitro human dermal construct revealing the NHDF inside the matrix. Staining was performed using DAPI and Phalloidin. Scale bar=100 µm. c) Optimization of CellTiter-Glo® assay with 3D human in vitro dermal construct. The graph shows the results of viability of NHDF in 3D matrix of dermal construct demonstrating the optimization of shaking time. d) Cell viability of 3D human in vitro dermal construct. The bar graph shows the cell viability of 3D dermal construct analyzed by optimized CTG assay at different time points of 7 and 14 days of culture.

2.4 Discussion

Type I collagen is a fibrous protein and a major structural component of extracellular matrix (ECM) in skin and thus can simulate the three-dimensional *in vivo* cell environment. Collagen type I from "rat tail tendons" well serves the purpose of ECM because of its irregular fibrils formation that resembles more *in vivo*-like reconstitution. Interactions between fibroblasts and ECM is the core of 3D cell cultures that is different from the focal and fibrillar adhesions on 2D surfaces [34]. Cells in 3D have enhanced cell biological activities and narrowed integrin usage [34] displaying a distinctive morphology (as seen in Figure 2.1 and Figure 2.6 b).

Among the cytocompatibility assays, resazurin-based assay recognized as the alamarBlue® or CellTiter-Blue® is exceedingly used because it is sensitive as well as cost effective [35]. This assay works well with established 2D cell culture system, however to assess the cytotoxic effect of therapeutics in 3D cell culture system, it has to be re-evaluated to get more reliable results. The test has been previously used to screen cytocompatibility of cell spheroids after treatment with an agent, e.g. staurosporine, able to distrup the tight cell junctions for resazurin uptake [36]. In this study, the test was succesfully adapted to matrix-based 3D system of "murine *in vitro* dermal construct" measuring the cell viability at different time intervals (Figure 2.3).

Resazurin is reported nontoxic to cells for short term incubation times but can affect cell survivability for extended exposure times (in terms of days) by interfering the cell's metabolic activity, DNA content and glucose consumption depending on the cell line [37]. Changes in morphology is a cell's stress response to an environmental insult that can result in fragmentation of Golgi complex, swelling of mitochondria, compromised integrity of nucleoli, or alterations in cytoskeleton especially in intermediate filaments [38-40]. In this study, an altered morphology of NHDF that might be resulting from a collapsed cytoskeleton was observed after a short-term exposure ($\leq$1 hour when the reduction of the blue resazurin to pink resorufin has not fully occurred yet) of CTB reagent ((Figure 2.4 c). Therefore, to provide definitive viability data in a clinically relevant 3D model based on human primary cells (that is more sensitive than a model based on cell lines), a panel of cytocompatibility assays were tested for NHDF. In this regard, RTG MT assay lost (Figure 2.5) its linearity at a very low cell seeding density. Here, the substrate concentration can be a limiting factor as well as the cell itself, based on the fact that the number of cells (and the subsequent metabolism) does not change any more. In this case an increase in the substrate concentration would not solve that effect. As per company's recommendation, it was strongly needed to test the best cell number for each respective cell type for RTG MT assay. This non-linearity effect was further tested with L929 cell line. The effect stayed similar (results not shown); and thus, was not suitable to our 3D system.

However, the most advanced and sensitive assay for testing viability of 3D systems has been the CellTiter-Glo® (CTG) assay, based on the quantification of intracellular ATP content [28]. This assay can be employed on 3D spheroids after optimizing the lysis conditions [29-32, 41]. For the "human *in vitro* dermal construct" developed in this work, CTG assay was selected and experimental parameters for reagent penetration were optimised. In 3D systems there is strong cell to cell and cell to matrix interactions resulting in tight junctions that hinder the reagent uptake. In this study, CTG assay was used for "human *in vitro* dermal construct" (matrix-based) for the first time, by optimizing the "shaking time" to enhance reagent penetration for maximum ATP release (Figure 2.6 c) and thus cell viability of NHDF was measured inside the matrix (Figure 2.6 d). However, shaking times varied for the measurement of cell viability of matrix-based 3D system at different time points, indicating the varying matrix-cell interaction with increasing culture time. CTG assay was found to be the optimal cell viability assay for 3D matrix based dermal system among those studied in this work.

The modified protocol for 3D system used a longer shaking time of 60 min in our 3D system to improve reagent penetration in comparison with 5min shaking time (as described by company for monolayer cell culture). Therefore it was important that half-life showed the stability of the signal over time, thus providing the flexibility for measuring time.

The parameters that are important in optimizing an assay in a 3D system include type of cells, number of cells, period of cultivation, frequency of media exchange, culture conditions, type of assay, reagent interaction with cells, assay conditions, detection range of assay, signal half-life etc. Depending on the intrinsic characteristics of 3D system e.g. spheroids are different from cells embedded in a 3D matrix; extrinsic parameters has to be defined differently for each system. For this reason, a portfolio of assays is crucial to be tested for each cell type in 2D and then in 3D system.

Conclusion

Development of human-based three-dimensional *in vitro* systems will serve as an advanced and more complex system in future, to perform more reliable *in vitro* preclinical studies for the bio-evaluation of cytotoxicity of biomedical materials. Although a 3D model based on human primary cells is clinically more relevant, it is also more sensitive. In this study, the differences in morphology were shown when cells were grown on a 2D surface and inside the 3D matrix. Moreover, different cell viability assays were tested to adapt to the matrix-based 3D systems. The CellTiter-Blue® assay was adapted by optimizing the test design to 3D system. It worked well with 3D murine *in vitro* dermal constructs (based on L929 cells) but affected cell morphology of NHDF (unlike L929). In an exploration of the assays tested with NHDF, CellTiter-Glo® was found the most optimal in this study. This assay was adapted to 3D human *in vitro* dermal constructs by optimizing the "shaking time" to enhance the reagent penetration and thus, the maximum ATP release (assisted by parallel Z-stack microscopic observation for confirmation of cell lysis throughout the depth of human *in vitro* dermal construct) indicating 2.4 times higher viability value by shaking it for 60 min as compared to 5 min, a time stated in the standard protocol of the respective assay for monolayer cell cultures. There is a need for more than one type of test methods to reveal all the different aspects of non-physiological or pathophysiological reactions respectively occurring in this system. Measuring more than one parameter would offer more valid data.

On the other hand, we intend to replace the rat tail collagen I used to construct dermal construct with human-based collagen matrix. For this purpose, we have initiated the experiments using transgenic plants derived human collagen from an Israeli company CollPlant Ltd.

Acknowledgments

The work was supported by European Union's Horizon 2020 research and innovation programme under the Marie Sklodowska-Curie grant agreement No 643050 (HyMedPoly Project). The authors declare no conflict of interest.

Published work

The work presented in this chapter, have already been published [42] as an open access article "Validation of *in vitro* assays in three-dimensional human dermal constructs" in "The International Journal of Artificial Organs" (https://doi.org/10.1177/0391398818775519). The content of our published article was used in this chapter as it is. However, the appendix section (Appendix A) of this chapter was added to provide the supplementary information and detailed protocols.

References

1. Campbell, R.L. and R.D. Bruce, *Comparative dermatotoxicology: I. Direct comparison of rabbit and human primary skin irritation responses to isopropylmyristate.* Toxicology and applied pharmacology, 1981. 59(3): p. 555-563.
2. Phillips, L., et al., *A comparison of rabbit and human skin response to certain irritants.* Toxicology and applied pharmacology, 1972. 21(3): p. 369-382.
3. Hartung, T., *Food for thought look back in anger–What clinical studies tell us about preclinical work.* Altex, 2013. 30(3): p. 275.
4. Leist, M. and T. Hartung, *Inflammatory findings on species extrapolations: humans are definitely no 70-kg mice.* Archives of toxicology, 2013. 87(4): p. 563-567.
5. Seok, J., et al., *Genomic responses in mouse models poorly mimic human inflammatory diseases.* Proceedings of the National Academy of Sciences, 2013. 110(9): p. 3507-3512.
6. Hartung, T., *Food for thought… on animal tests.* Altex, 2008. 25(1): p. 3-9.
7. Hansbrough, J.F., et al., *Clinical trials of a biosynthetic temporary skin replacement, Dermagraft-Transitional Covering, compared with cryopreserved human cadaver skin for temporary coverage of excised burn wounds.* Journal of Burn Care & Research, 1997. 18(1): p. 43-51.
8. Hansen, S.L., et al., *Using skin replacement products to treat burns and wounds.* Advances in skin & wound care, 2001. 14(1): p. 37-46.
9. Pham, C., et al., *Bioengineered skin substitutes for the management of burns: a systematic review.* Burns, 2007. 33(8): p. 946-957.
10. OHTANI, T., et al., *Digital gangrene associated with idiopathic hypereosinophilia: treatment with allogeneic cultured dermal substitute (CDS).* European Journal of Dermatology, 2004. 14(3): p. 168-171.
11. Wainwright, D., *Use of an acellular allograft dermal matrix (AlloDerm) in the management of full-thickness burns.* Burns, 1995. 21(4): p. 243-248.
12. Supp, D.M. and S.T. Boyce, *Engineered skin substitutes: practices and potentials.* Clinics in dermatology, 2005. 23(4): p. 403-412.
13. Kolokol'chikova, E., et al., *Morphological changes in burn wounds after transplantation of allogenic fibroblasts.* Bulletin of experimental biology and medicine, 2001. 131(1): p. 89-93.
14. Ponec, M., *Skin constructs for replacement of skin tissues for in vitro testing.* Advanced drug delivery reviews, 2002. 54: p. S19-S30.
15. Hartung, T., *Food for thought… on alternative methods for cosmetics safety testing.* Altex, 2008. 25(3): p. 147-162.

16. Robinson, M.K., R. Osborne, and M.A. Perkins, *Strategies for the assessment of acute skin irritation potential.* Journal of pharmacological and toxicological methods, 1999. 42(1): p. 1-9.
17. Welss, T., D.A. Basketter, and K.R. Schröder, *In vitro skin irritation: facts and future. State of the art review of mechanisms and models.* Toxicology in vitro, 2004. 18(3): p. 231-243.
18. Roguet, R., *Use of skin cell cultures for in vitro assessment of corrosion and cutaneous irritancy.* Cell biology and toxicology, 1999. 15(1): p. 63-75.
19. Tornier, C., M. Rosdy, and H.I. Maibach, *In vitro skin irritation testing on reconstituted human epidermis: reproducibility for 50 chemicals tested with two protocols.* Toxicology in vitro, 2006. 20(4): p. 401-416.
20. Boehnke, K., et al., *Effects of fibroblasts and microenvironment on epidermal regeneration and tissue function in long-term skin equivalents.* European journal of cell biology, 2007. 86(11): p. 731-746.
21. El-Ghalbzouri, A., et al., *Effect of fibroblasts on epidermal regeneration.* British Journal of Dermatology, 2002. 147(2): p. 230-243.
22. *EU, Seventh Amendment to the EU Cosmetics Directive 76/768/EEC, in: The European Parliament and the Council of the European Union (Ed.), Brussels, 2003.*, EU, Editor. 2003. p.
.23. Becker, R.A., et al., *Report of an ISRTP Workshop: Progress and barriers to incorporating alternative toxicological methods in the US.* Regulatory Toxicology and Pharmacology, 2006. 46(1): p. 18-22.
24. Lin, Z. and Y. Will, *Evaluation of drugs with specific organ toxicities in organ-specific cell lines.* Toxicological Sciences, 2011. 126(1): p. 114-127.
25. Astashkina, A., B. Mann, and D.W. Grainger, *A critical evaluation of in vitro cell culture models for high-throughput drug screening and toxicity.* Pharmacology & therapeutics, 2012. 134(1): p. 82-106.
26. Roth, A. and T. Singer, *The application of 3D cell models to support drug safety assessment: opportunities & challenges.* Advanced drug delivery reviews, 2014. 69: p. 179-189.
27. Grainger, D.W., *Cell-based drug testing; this world is not flat.* Advanced drug delivery reviews, 2014. 69: p. vii.
28. Kijanska, M. and J. Kelm, *In vitro 3D spheroids and microtissues: ATP-based cell viability and toxicity assays.* 2016.
29. Rimann, M., et al., *An in vitro osteosarcoma 3D microtissue model for drug development.* Journal of biotechnology, 2014. 189: p. 129-135.
30. Fey, S.J. and K. Wrzesinski, *Determination of drug toxicity using 3D spheroids constructed from an immortal human hepatocyte cell line.* Toxicological Sciences, 2012. 127(2): p. 403-411.

31. Messner, S., et al., *Multi-cell type human liver microtissues for hepatotoxicity testing.* Archives of toxicology, 2013. 87(1): p. 209-213.
32. Riss, T.L., et al., *Validation of in vitro assays to measure cytotoxicity in 3D cell cultures.* Toxicology Letters, 2014. 229: p. S145.
33. Lever, W.F., *Histopathology of the Skin.* Histopathology of the skin., 1949.
34. Cukierman, E., et al., *Taking cell-matrix adhesions to the third dimension.* Science, 2001. 294(5547): p. 1708-1712.
35. O'brien, J., et al., *Investigation of the Alamar Blue (resazurin) fluorescent dye for the assessment of mammalian cell cytotoxicity.* The FEBS Journal, 2000. 267(17): p. 5421-5426.
36. Walzl, A., et al., *The resazurin reduction assay can distinguish cytotoxic from cytostatic compounds in spheroid screening assays.* Journal of biomolecular screening, 2014. 19(7): p. 1047-1059.
37. Pace, R.T. and K.J.L. Burg, *Toxic effects of resazurin on cell cultures.* Cytotechnology, 2015. 67(1): p. 13-17.
38. Lin, J.J.-C. and J.R. Feramisco, *Disruption of the in vivo distribution of the intermediate filaments in fibroblasts through the microinjection of a specific monoclonal antibody.* Cell, 1981. 24(1): p. 185-193.
39. Sanger, J.W., et al., *Reversible translocation of cytoplasmic actin into the nucleus caused by dimethyl sulfoxide.* Proceedings of the National Academy of Sciences, 1980. 77(9): p. 5268-5272.
40. Welch, W.J. and J.P. Suhan, *Morphological study of the mammalian stress response: characterization of changes in cytoplasmic organelles, cytoskeleton, and nucleoli, and appearance of intranuclear actin filaments in rat fibroblasts after heat-shock treatment.* The Journal of cell biology, 1985. 101(4): p. 1198-1211.
41. Rimann, M., et al., *Automation of 3D cell culture using chemically defined hydrogels.* Journal of laboratory automation, 2014. 19(2): p. 191-197.
42. Idrees, A., et al., *Validation of in vitro assays in three-dimensional human dermal constructs.* The International journal of artificial organs, 2018. 41(11): p. 779-788.

2.5 Appendix A

2.5.1 Preliminary experiments for choosing Col. I matrix concentration and cell seeding density to be embedded in dermal constructs

Visualization of 3D L929 (at different cell seeding densities) inside murine dermal constructs (of different concentrations of Col. I matrix)

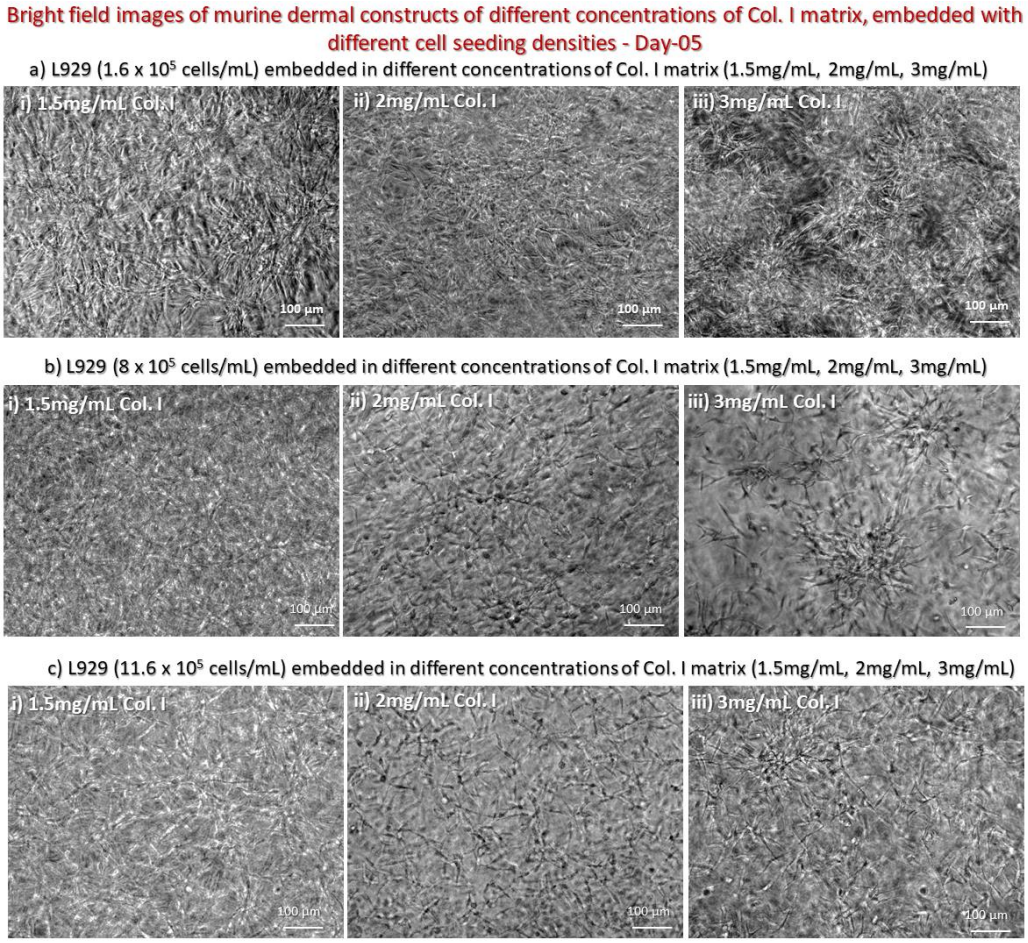

Figure 2.7 Bright field images of 3D murine dermal constructs of different concentrations of Col. I matrix, embedded with different cell seeding densities - Day-05. The images showed L929 at seeding densities of 1.6 x 10^5 cells/mL (sub-images a-i to a-iii), 8 x 10^5 cells/mL (sub-images b-i to b-iii), and 11.6 x 10^5 cells/mL (sub-images c-i to c-iii) were embedded in Col. I matrix of 1.5mg/mL, 2mg/mL, and 3mg/mL.

3D L929 were visualized inside murine dermal constructs to observe the effect of different cell seeding densities and Col. I matrix concentrations. Bright field and F- actin stained images demonstrated the results in Figure 2.7, Figure 2.8, Figure 2.9 on Day-05 and Day-07. Apparently, there were no differences observed in cell morphology and distribution. However, flower like cell clusters appeared for 3mg/mL Col. I at all cell seeding densities on Day-05 (Figure 2.7). The observed effect was independent on

suspending cells in collagen matrix very well during the preparation step. And thus, it might be associated with comparatively slower cell movement during proliferation, in more concentrated gel matrix. While this effect was no more seen with the passage of time, as observed on Day 07 (Figure 2.8), where cells were very well distributed. This effect can be due to cells interaction with matrix, reducing its stiffness to ease cells movement to distribute themselves well inside gel. Though, this was only an assumption and it would need further exploration for better understanding. Thus, the effect on matrix stiffness should be studied in future. The cell density and Col. I concentration chosen for experiments were 8 x 10^5 cells/mL in 1.5mg/mL Col. I matrix.

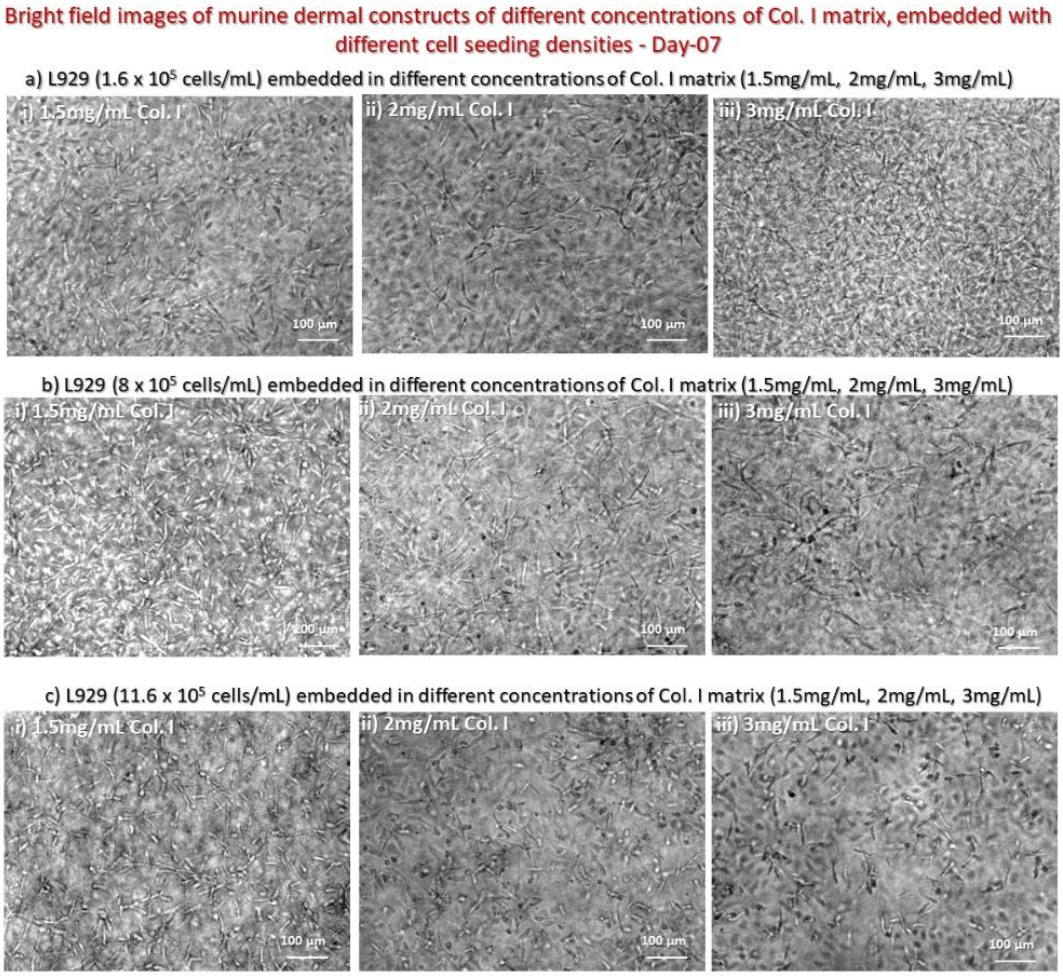

Figure 2.8 Bright field images of 3D murine dermal constructs of different concentrations of Col. I matrix, embedded with different cell seeding densities - Day-07. The images showed L929 at seeding densities of 1.6 x 10^5 cells/mL (sub-images a-i to a-iii), 8 x 10^5 cells/mL (sub-images b-i to b-iii), and 11.6 x 10^5 cells/mL (sub-images c-i to c-iii) were embedded in Col. I matrix of 1.5mg/mL, 2mg/mL, and 3mg/mL.

The dermal construct showed the filopodia-like morphology with dendritic extensions in the matrix and a uniform distribution of cells in different planes inside the matrix (Figure 2.9).

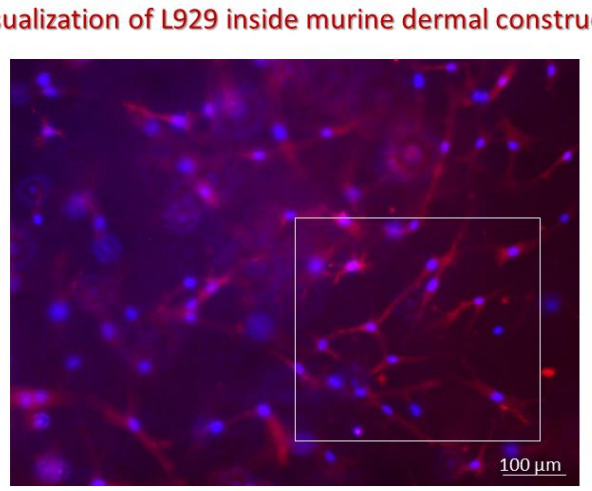

Figure 2.9 Visualization of L929 inside 3D murine dermal construct. F-actin/nuclei staining was performed using Phalloidin/DAPI stain.

Visualization of 3D NHDF (at different cell seeding densities) inside human dermal constructs (of different concentrations of Col. I matrix)

3D NHDF were visualized inside human dermal constructs to observe the effect of different cell seeding densities and Col. I matrix concentrations. Bright field images and Z-stack videos demonstrated the results in Figure 2.10 & Figure 2.11 on Day-05 and Figure 2.12 & Figure 2.13 on Day-07.

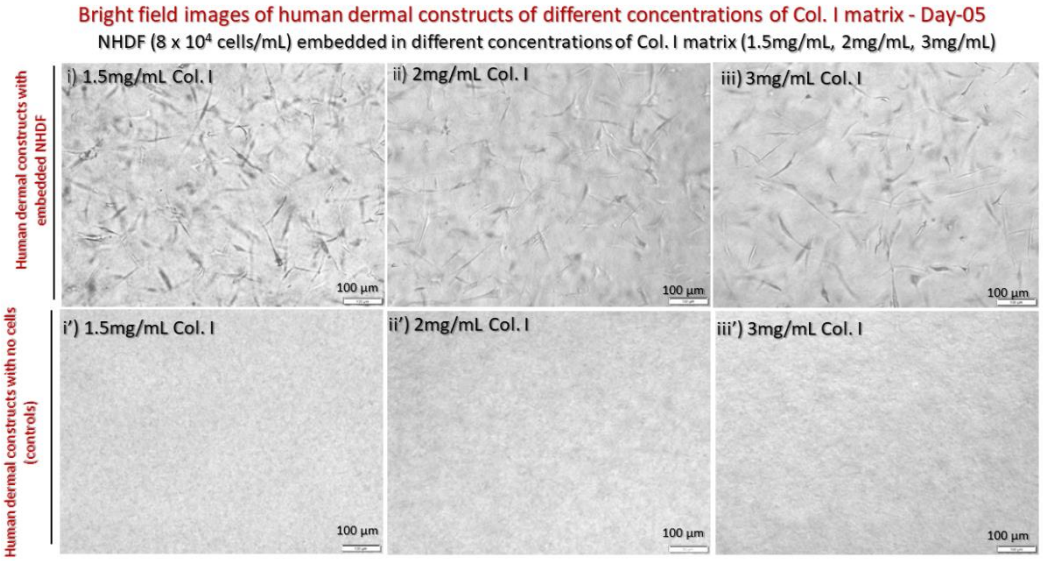

Figure 2.10 Bright field images of 3D human dermal constructs of different concentrations of Col. I matrix - Day-05. The sub-images (i to iii) showed NHDF at seeding density of 8 x 10^4 cells/mL were embedded in Col. I matrix of 1.5mg/mL, 2mg/mL, and 3mg/mL, respectively. The sub-images i' to iii' demonstrated controls without NHDF in Col. I matrix of 1.5mg/mL, 2mg/mL, and 3mg/mL, respectively.

Apparently, there were no differences observed in cell morphology and distribution. However, the effect on matrix stiffness should be investigated in future. The cell density and Col. I concentration chosen for experiments were 8 x 10^4 cells/mL in 1.5mg/mL Col. I matrix.

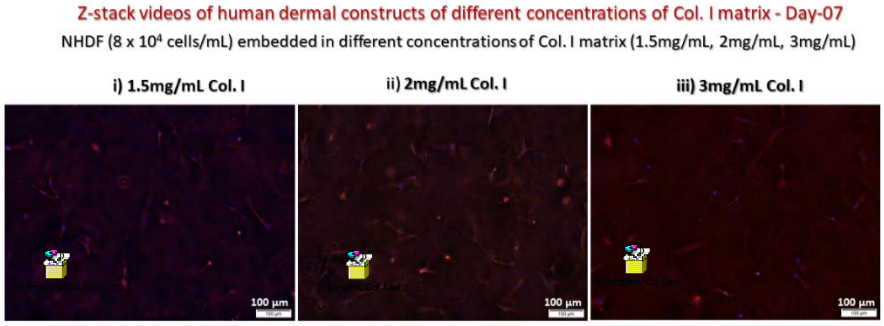

Figure 2.11 Z-stack videos of 3D human dermal constructs of different concentrations of Col. I matrix - Day-07.F-actin/nuclei staining was performed using Phalloidin/DAPI stain. The videos (i to iii) showed NHDF at seeding density of 8 x 10^4 cells/mL were embedded in Col. I matrix of 1.5mg/mL, 2mg/mL, and 3mg/mL, respectively.

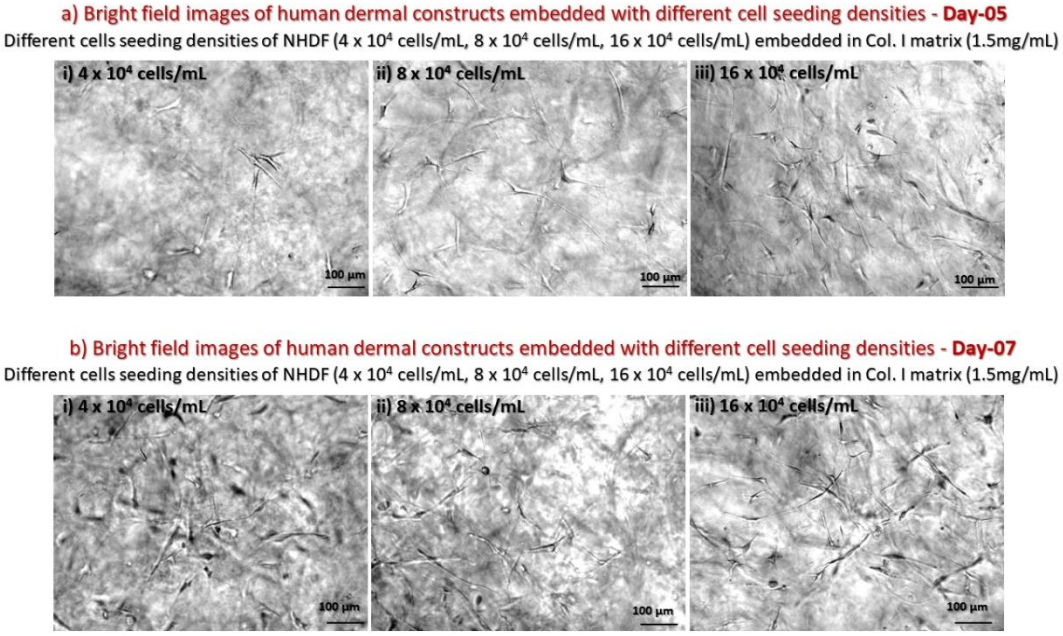

Figure 2.12 Bright field images of 3D human dermal constructs embedded with different cell seeding densities of NHDF on a) Day-05 and b) Day-07. The sub-images (a-i to a-iii and b-i to b-iii)) showed NHDF at seeding densities of 4 x 10^4 cells/mL, 8 x 10^4 cells/mL, 16 x 10^4 cells/mL were embedded in Col. I matrix (1.5mg/mL), respectively.

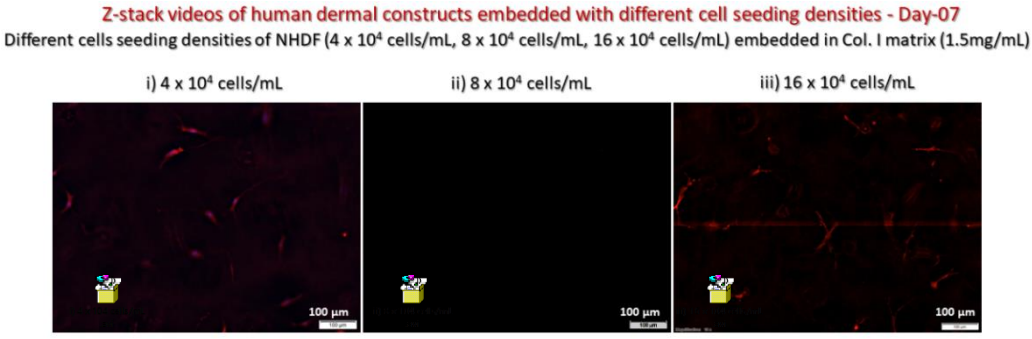

Figure 2.13 Z-stack videos of 3D human dermal constructs embedded with different cell seeding densities of NHDF - Day-07. F-actin/nuclei staining was performed using Phalloidin/DAPI stain. The videos (i to iii) showed NHDF at seeding densities of 4 x 10^4 cells/mL, 8 x 10^4 cells/mL, 16 x 10^4 cells/mL were embedded in Col. I matrix (1.5mg/mL), respectively.

2.5.2 Detailed protocols

Phalloidin staining - protocol for 3D cultured cells in detail

The staining process using Phalloidin and DAPI should be given in more detail.

- Remove cell supernatant.
- Wash constructs twice with 1X Annexin V binding buffer - Promokine (by diluting 5X Binding Buffer 1:5 in distilled water)
- Fix with 4% formaldehyde in 1X Annexin V binding buffer for 30 min at room temperature (RT) in darkness
- Wash with 1X Annexin V binding buffer 1-2 times
- Permeabilize with 0.4% Triton X-100, 10 min at RT in darkness
- Wash with 1X Annexin V binding buffer 1-2 times
- Block with 2% bovine serum albumin (BSA) in PBS for 1 hour at RT in darkness
- Wash with 1X Annexin V binding buffer 1-2 times
- Stain with F-actin stain: Add 5µL Phalloidin per 200µL in 2% BSA (2% BSA gives better results than 1% BSA), 30 min (30 min gives better results than 20 min) at RT in darkness
- Wash with Annexin V binding buffer 1-2 times
- Reconstituted DAPI solution (10mg/mL) is diluted to 1:1000 in PBS and incubated for 10min at RT in darkness
- Wash with 1X Annexin V binding buffer 1-2 times
- Add 1X Annexin V binding buffer for microscopic visualization

Note. (Annexin V binding buffer gives better results in terms of microscopic visualization than PBS).

CellTiter-Glo® assay - standard and modified protocols in detail

The standard protocol CellTiter-Glo ® assay included the following steps:

- Reagent (warmed at room temperature) was mixed with equal volume of media
- Added to cell monolayer culture (also equilibrated at room temperature) in microtiter well plates
- 2 min shaking
- 10 min stabilization time
- Luminescence is read (0.25-1 sec integration time)

This assay for 3D cultured cells was used for the first time. The reagent was used with the same concentration as described in the protocol with monolayer culture, but the shaking time was optimized. This assay was based on measuring total ATP content by lysing the cells. Based on this principle, after exposure with the reagent, morphological changes of cells were observed, from well-spread (in the 3D gel) to rounded form throughout the depth of the gel (Z-stack microscopic observation) with time. For example, for human *in vitro* dermal construct on Day-7, 60 mins shaking (10 min for signal stabilization) was good enough to lyse cells and measure maximum ATP content. And 30 to 45 min shaking was not enough to lyse all cells from the bottom layers of the 3D gel. This also showed the reagents diffusion through the hydrogel, that the reagent was able to penetrate through the hydrogel.

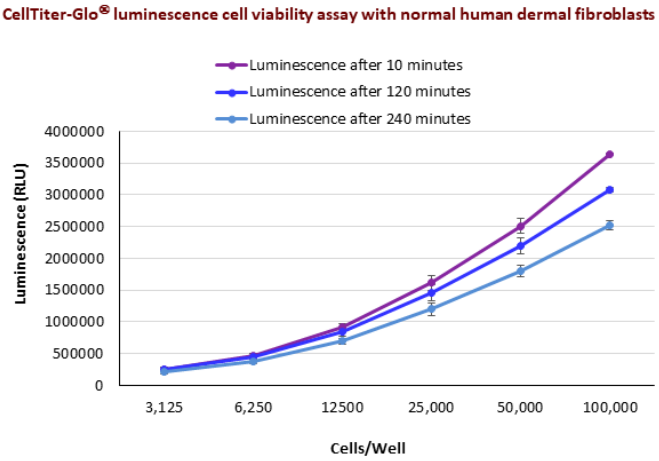

Figure 2.14 CellTiter-Glo ® luminescence cell viability assay with normal human dermal fibroblasts (in 2D format). Decay of signal over time. It is a supplementary figure of Figure 2.6.

Regarding the CTG assay modified for 3D system, the effect on the decay of signal or on signal intensity over time was measured as luminescence over time. There was a linear (directly proportional) relationship between luminescent signal and cell number. The relationship maintained the trend based on the time interval applied to analyse samples (shown in Figure 2.14) providing flexibility for measurement times. Figure 2.14

(a Supplementary image of Figure 2.6) also showed that the half-life of signal is almost more than 4 hours.

CellTiter-Glo ® assay – Determination of half-life of signal

For determination of signal's half-life, the experiment was performed for 2D monolayer cultures as following:

1. Opaque-walled multiwell plates were incubated with cells.
2. Plates were equilibrated at room temperature (RT) for 30 min.
3. CellTiter-Glo® reagent (mainly containing luciferin substrate, luciferase, and lysis buffer) was added to cells (1:1 diluted in cell culture medium)
4. Shaking for 2 minutes to induce cell lysis, and 10 minutes at RT to stabilize signal.
5. The luminescence was recorded after 10, 120, 240 min. (An integration time of 0.25–1 sec)
6. As mentioned before, the results demonstrated that the signal's half-life was >4h and were shown in the Figure 2.14 (a supplementary image of Figure 2.6).

This half-life of the signal showed its stability with time; this was an important investigation as the modified protocol for 3D system used a long shaking time of 60 min. This longer time improved the reagent penetration compared with the 5 min shaking time recommended for the cell culture monolayer.

2.5.3 RealTime-Glo™ MT assay - as a proof of concept

The protocol was performed with cell culture monolayers under the reagent (substrate) concentration recommended by the company. The signal was not linear and also decreasing as a function of time Figure 2.15. The substrate concentration can be a limiting factor as well as the cells themselves, based on the fact that the number of cells (and their subsequent metabolism) does not change any more. In this case an increase in the substrate concentration would not solve the observed effect. To get the clarification regarding this, the company recommended to find the right seeding density for each cell type. Therefore, it was strongly needed to test the best cell number with that assay. As well as to verify this effect, it was important to test this assay with another cell type, e.g. L929 cell line (as a proof of concept). The effect stayed similar as shown in Figure 2.15, a supplementary image of Figure 2.5. Incubation time and cell density affected the assay linearity. Knowing that the assay only worked at very low seeding density, it was decided not to use this assay as it would not be useful for 3D systems.

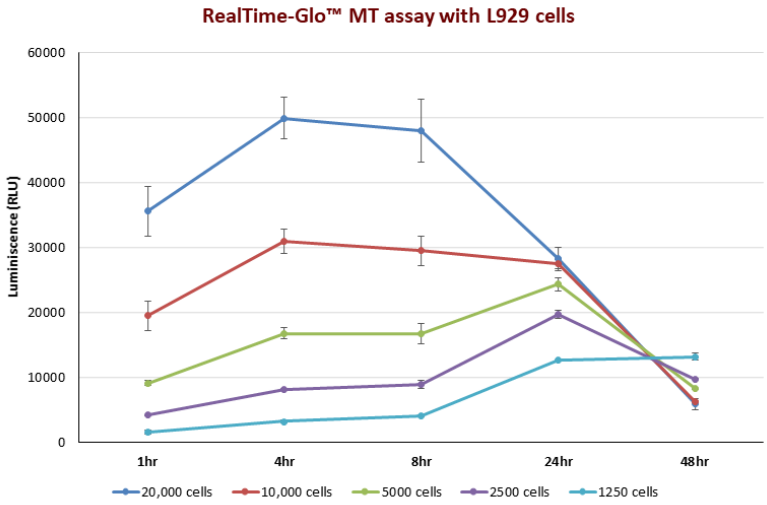

Figure 2.15 RealTime-Glo™ MT assay with L929 cells (in 2D format). It is a supplementary figure of Figure 2.5.

2.5.4 Viability of human and murine dermal constructs

More than one test method would be necessary to reveal all the different aspects of pathophysiological reactions occurring in the cell culture testing system. Measuring more than one parameter, for example, NADPH enzyme activity and ATP content of cells, would offer more valid data. For that reason, we tried to investigate different assays (e.g. based on these two above mentioned parameters) to find the best suitable assay. Assays based on other markers of cell viability (e.g. DNA content by BrdU assay, etc.) should be further explored or developed. The Figure 2.16 demonstrated viability of human and murine dermal construct over a time period of four to eight weeks. Cell viability and cytotoxicity was determined by CellTiter-Blue® and CytoTox-ONE™ assay, respectively.

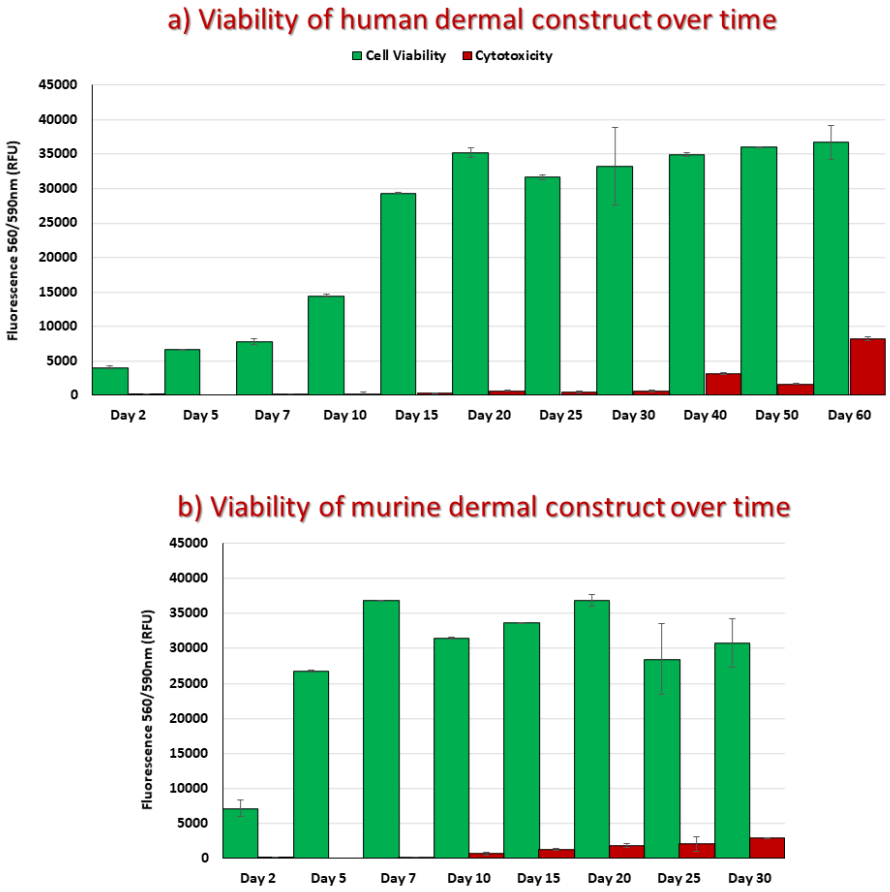

Figure 2.16 Viability of a) 3D human dermal construct and b) 3D murine dermal construct over time. Cell viability and cytotoxicity was determined by CellTiter-Blue® and CytoTox-ONE™ assay respectively.

Chapter 03: Development of Three-dimensional Reconstructed Human Epidermis (RHE)

Table of contents

List of figures

Abbreviations

3D: Three-dimensional
Ab: Antibody
ALI: Air-liquid interface
CnT: CELLnTECH
CnT-PR: CnT-Prime medium
CnT-PR-3D: CnT-Prime 3D barrier culture medium
COCA: Murine epidermal cell line
Col. I: Collagen type I
ECVAM: European centre for the validation of alternative methods
FBS: Foetal bovine serum
Flg: Filaggrin
H & E stain: Haematoxylin and eosin stain
HaCaT: Immortalized human keratinocyte cell line
HSE: Human skin equivalent
IHC: Immunohistochemistry
Inv: Involucrin
K5, 6, 10, 14: Keratin 5, 6, 10, 14
Lor: Loricrin
MTT: 3-(4,5-dimethylthiazol-2-yl)-2,5-diphenyltetrazolium bromide
NHEK: Normal human epidermal keratinocytes
NHS: Native human skin
NMFs: Natural moisturizing factors
NMS: Native mouse skin
OECD: Organisation for economic co-operation and development
PC membrane: Polycarbonate membrane
PCNA: Proliferating cell nuclear antigen
RHE: Reconstructed human epidermis
RME: Reconstructed murine epidermis
SB: Stratum basale
SC: Stratum corneum
SG: Stratum granulosum
SIT: Skin irritation test
SS: Stratum spinosum

Chapter 03: Development of Three-Dimensional Reconstructed Human Epidermis (RHE)

Abstract

Several reconstructed human epidermis (RHE) models have been developed and improved to have better barrier function, morphology, reproducibility, and viability. RHEs have been used as predictive models for skin corrosion, irritancy, and penetration studies. In this work, we developed an in-house RHE model with the aim to use it as a test system for biological evaluation and as a basis to develop more complex 3D skin models.

On the other hand, human pathologies have been successfully modelled in genetically modified mice, however the development of 3D murine skin models have been hindered due to the difficulty in sub-culturing murine epidermal keratinocytes *in vitro*. In this study, in parallel to RHE development, reconstructed murine epidermis (RME) was also developed in accordance with a previously reported study [1]. Developed RHE and RME would serve as key tools to understand the relevance of outcomes obtained from human- and animal-based systems. This would also help to reduce the number of animal trials and the absolute number of sacrificed animals. Moreover, RMEs would also make possible to study the disease pathologies in epidermal models derived from "certain genetically modified murine cell lines".

The RHE was obtained by i-a) seeding 8.3×10^5 NHEKs (normal human epidermal keratinocytes)/mL, while RME was obtained by i-b) seeding 6.6×10^5 COCA cells/mL on polyester membrane. The cells were grown in submerged culture for 3 days to cover the surface and fed with CnT-PR. ii) The culture was then grown in submerged conditions overnight while fed with CnT-PR-3D to allow cells to develop cell-cell adhesion structures before airlift. iii) Finally, the culture was raised to air-liquid interface (ALI) to start tissue differentiation and bottom fed with CnT-PR-3D for 10-20 days. The RHE and RME were characterized by haematoxylin and eosin (H & E) histological staining for morphology analysis, and immunohistochemistry (IHC) for protein tissue distribution analysis. As demonstrated in literature [1], COCA cells retained their capacity to differentiate and stratify in response to increased calcium concentration. Histological results showed the formation of fully organized and well-differentiated RHE and RME epidermal layers of stratum basale (SB), spinosum (SS), granulosum (SG), and corneum (SC). IHC analysis of RHE showed keratin-14 (K14), a marker of early differentiation, as expressed by keratinocytes in SB. Involucrin, a marker of terminal differentiation, was displayed by SC.

RHE can be further advanced to make a more complex skin model. On the other hand, murine epidermal models can be derived from cell lines of genetically modified mice of interest, where RME would serve as a suitable control for studying the biological implications of these alterations.

Keywords: Reconstructed human epidermis (RHE), biological evaluation, Reconstructed murine epidermis (RME), COCA cells, NHEK.

3.1 Introduction

Three-dimensional *in vitro* models serve as great purpose of clinical applications (regenerative medicine), fundamental basic research, and industrial applications for example cytotoxicity analysis, drug targeting studies, testing new therapeutics/treatment approaches. The *in vitro* bio-evaluation is more accurate using 3D testing systems than 2D cell cultures [2-4]. For the past few years, the EU regulations have further emphasized to reduce, refine and replace animal experimentation [5, 6].

3.1.1 *Reconstructed human epidermal (RHE) skin models*

Reconstructed human epidermal sheets have been used as grafts for a number of skin conditions [7-9]. Models of reconstructed human epidermis (RHE) have also been used for *in vitro* bio-evaluation [10]. For example, EpiSkin®, EpiDerm™ and subsequently other models were validated for skin corrosion study by ECVAM (European centre for the validation of alternative methods) [11-13]. Soon after, the models were evaluated for the prediction of skin irritancy test e.g. modified EpiDerm™ SIT and the SkinEthic® RHE were even approved for skin irritancy test [14, 15]. LabCyte EPI-MODEL 24 was also validated for hazard assessment (MTT assay for cell viability and IL-1α release for irritancy determination) [16]. For percutaneous absorption or *in vitro* penetration study, the use of an epidermal substitute demonstrated a better leak-proof connection than a full-thickness model by sealing the whole surface area and providing the mechanical resilience [17].

These RHEs were developed using human keratinocytes (foreskin or mammary skin tissue) under optimal cell culture conditions at the air-liquid interface (ALI) to create a stratified epidermis. Keratinocytes under right cell culture conditions have the tendency to undergo normal differentiation process as happens *in vivo*. In this regard, calcium has a role in inducing the differentiation by supporting the formation of desmosomal contacts [18-20] e.g. it precisely induces type I transglutaminase that is the main enzyme involved in cornified envelope formation [21]. The level of epidermal development is also affected by the physical parameter of ALI resulting in an enhanced tissue organization and differentiation. This is thought to be achieved due to ALI causing chemical gradient formation in epidermal layers [22, 23].

However, to ensure the model reproducibility, the organisation for economic co-operation and development (OECD) has defined the criteria to be satisfied [24]. These include morphology (histological analysis), viability (as untreated or negative control), barrier function (lipid composition), and reproducibility (positive and negative control results) of RHE models. A closer look at the assumed criteria shows that the currently available RHEs do not completely meet the requirements of barrier function. *Van Gele et al.* [25] summarized the total permeation studies performed using different tissue models suggesting the need for improvement in the composition of the lipids in the

stratum corneum. *Schmook et al.* [26] did not support RHE models for penetration analysis. A pre-validation study [27] using EpiDerm™, EpiSkin® and SkinEthic® also showed that the permeation coefficients of these RHEs were different from those of human skin, suggesting the under-developed barrier properties of these models. The permeation of the RHE models exceeded than that of human and pig skins, the SkinEthic® RHE being the most permeable among the ones tested [28]. This was due to the differences in distribution and amount of water, keratins, ceramides and natural moisturizing factors (NMFs).

In this study, we developed an in-house RHE with the aim to use it as a test system for the cytotoxicity evaluation of materials. RHEs are simple models and lack a cross-talk with other cell types. In this PhD work, the developed RHE was further advanced to make more complex skin models.

3.1.2 *3D in vitro murine epidermal skin models*

Over the past years, "genetically modified" mouse models have been developed to study human skin disorders. However, unlike human keratinocytes [29], primary murine keratinocytes are difficult to be cultured *in vitro*, thus reproducible 3D murine epidermal models have not been established up till now. Moreover, efforts to develop fully-defined media have been addressed to improve the culture conditions of primary human epidermal keratinocytes and their 3D models. On the contrary, 3D models using murine keratinocytes are rare and still uses devitalised dermis and complex un-defined cell culture media [30, 31].

Initial efforts were made to encourage a long-term culture of murine keratinocytes using matrix coated dishes, feeder cells, and complex FBS-conditioned media [30, 32, 33]. At high calcium concentration, cells were able to differentiate but at low cell-passages only. *Reichelt & Haase* [34] were successfully able to subculture murine epidermal keratinocytes to higher passages (250 passages), but still needed the feeder cells, collagen-coated dishes, and FBS-conditioned culture media. On the contrary, *Caldelari et al.* [35] were able to subculture cells (50 passages) directly on uncoated dishes and used fully-defined media. When cultures were exposed to high calcium concentration, both approaches [34, 35] showed the differentiation capacity of the applied cell-lines to some extent. *C. Segrelles et al.* [1] established a non-tumorigenic murine keratinocyte cell line, the COCA cells, being able to grow on un-coated dishes and in fully-defined cell culture media, highly retaining the capacity to differentiate (>75 passages) at high calcium concentration. According to their 3D protocols [1], COCA cells had the potential to form epidermis-like structure (also proved *in vivo* when grafted into immunodeficient mice).

Thus, developed epidermal models derived from different genetically modified murine cell lines, would make possible the study of disease pathologies. This would also help to

reduce the number of animal trials and the absolute number of sacrificed animals. In this study, we developed an in-house RME using COCA cells as established by *C. Segrelles et al.* [1], using the same 3D culture conditions that we used to develop our RHE. Developed RHE and RME would serve as great tools to understand the relevance of outcomes obtained from human- and animal-based systems. The obtained data from two epidermal systems would help to understand the relevancy between animal- and human-based systems, as well as would help to fill the unsolved gaps that occur during "data transfer" from animal to human systems.

3.2 Materials and Methods

3.2.1 *Cell source and maintenance*

Primary cells, normal human epidermal keratinocytes (NHEK) were obtained from PromoCell and maintained in CnT-Prime epithelial culture medium (CnT-PR, CELLnTECH) under the physiological culture conditions (37°C, 5% CO_2), subsequently sub-cultured by using DetachKit-Promocell HEPES BSS (2-[4-(2-hydroxyethyl)piperazine-1-yl] ethanesulfonic acid buffered saline solution); 0.04% Trypsin/0.03% EDTA (ethylenediaminetetraacetic acid); and TNS (trypsin neutralizing solution) containing 0.05% trypsin inhibitor from soybean/0.1% bovine serum albumin.

3.2.2 *Fabrication of RHE*

The RHE was obtained by i) seeding 8.3×10^5 cells/mL cell suspension of NHEK (5×10^5 cells per insert) on top of 12-well Transwell inserts (with polyester membrane, pore size 0.4µm, pre-wet in CnT-PR), and grown in submerged culture for 3 days to cover the surface and fed with CnT-PR; ii) the culture was then grown in submerged conditions overnight while now fed with CnT-PR-3D to allow cells to develop cell-cell adhesion structures before airlifted; iii) finally the culture was raised to ALI to start tissue differentiation and bottom fed with CnT-PR-3D for 10 and 20 days, respectively.

3.2.3 *Fabrication of RME*

The RME was obtained by i) seeding 6.6×10^5 cells/mL cell suspension of COCA (4×10^5 cells per insert) on top of 12-well Transwell inserts (with polyester membrane, pore size 0.4µm, pre-wet in CnT-PR), and grown in submerged culture for 3 days to cover the surface and fed with CnT-PR; ii) the culture was then grown in submerged conditions overnight while now fed with CnT-PR-3D to allow cells to develop cell-cell adhesion structures before airlifted; iii) finally the culture was raised to ALI to start tissue differentiation and bottom fed with CnT-PR-3D for 10, 15, and 20 days.

CnT-Prime media are fully-defined and animal component-free media with $CaCl_2$ concentration of 0.07mM along with main growth factors such as EGF, FGF, Insulin, Hydrocortisone, transferrin, T3, and ethanolamine plus 21 different amino acids, 19 minerals and trace elements (including selenium, manganese and zinc), 14 vitamins (including folate, niacinamide and biotin), 10 other ingredients (including glucose, pyruvate, and buffers). They are without cholera toxin, and phenol red. The detailed concentration information for this larger numbers of growth factors is not releasable by the company [36]. CnT-PR-3D contains elevated levels of calcium concentration of 1.2mM and no proliferative factors [36].

3.2.4 *Morphological analysis*

Harvested RHE and RME tissues were fixed in 4% paraformaldehyde (10% formalin) for ≥4h, dehydrated through graded ethanol solutions, cleared in xylol (twice), and infiltrated & embedded in paraffin. ~5µm sections were cut on a microtome, attached to glass slides, dried, deparaffinized and hydrated. For morphological analysis sections were stained with haematoxylin & eosin (H & E) and examined under Olympus BX51 light microscope. The detailed description of tissue processing and staining protocols was described in Chapter 04.

3.2.5 *Immunohistochemical (IHC) analysis*

RHE samples were rinsed in PBS, treated with 2M sucrose solution (Fisher Chemical), and embedded in OCT embedding medium (VWR) by freezing in liquid nitrogen vapor. The samples were cryo-sectioned (~10µm) using Microm HM 550 Cryostat. Primary antibodies included keratin 14 (K14, mouse monoclonal antibodies, Abcam), and involucrin (Inv, mouse monoclonal antibodies, Abcam). Secondary antibodies included Alexa Fluor 594 Donkey anti-Mouse IgG (H+L) (Abcam). Negative controls were performed using secondary antibodies only. Cell nuclei were detected by DAPI staining (1.5µg/mL, VECTASHIELD, Vector labs). Immunohistochemical (IHC) analysis was performed in accordance with the standard protocol from Abcam and the concentrations optimized for primary antibodies were 1:100 for both K14 and Inv. The details of reagents preparation used in IHC staining and the protocol followed was detailed in Chapter 04. The immunostained slides were examined under fluorescent microscope (Olympus XM10 with Alexa 488, 555, 568, & DAPI filters; and Cell Sense Standard software).

3.3 Results & Discussion

3.3.1 *Epidermal differentiation*

Role of calcium in epidermal differentiation

Calcium has been known to have a very significant role in epidermal differentiation. Thus, the commercially available media for 3D culture at air-lift phase are generally supplemented with high calcium concentration of 1.2mM. The calcium receptor (CaR) has a vital role by originating the intracellular signalling events that initiate the differentiation in response to extracellular calcium. The transient increase in intracellular calcium (Cai) is not sufficient and a sustained rise in Cai is mandatory for differentiation, that is made possible by activating PLC-γ1 (Phospholipase C γ1) [37].

Role of ALI in epidermal differentiation

It was evidenced *in vivo* that the calcium gradient formation (due to water loss in the more top layers) is achieved due to air-lift [38]. The ALI also helps in achieving the proper lipid profile (acylglucosylceramides and acylceramides) of stratum corneum (SC) [39]. In this context, the rate of trans-epidermal water loss is related with lipid biosynthesis [40]. Moreover, ALI raised cultures are not in direct contact with cell culture medium components (e.g. retinoids that strongly inhibit epidermal differentiation) and thus are promoted for tissue differentiation [22]. In this study, the epidermal cultures were histologically examined at different time points of ALI culture (i.e. 10-20 days).

Role of growth factors in epidermal differentiation

The traditional culture media used to expand biopsies from human amniotic membrane (HAM) included hydrocortisone, triiodothyronine (T3), adenine and cholera toxin [41-44]. Hydrocortisone has significant role for maintaining epithelial colonies and keratinocyte proliferation [29]. Triiodothyronine has been shown to play a beneficial role in keratinocytes cultivation under minimal levels of foetal calf serum [45]. Cholera toxin (CTX), a protein secreted by *Vibrio cholerae* that causes cholera infection (watery diarrhoea) has been shown to highly stimulate colony growth of cultured human epidermal keratinocytes through increased levels of intracellular cyclic AMP [46]. Adenine also has an effect on epithelial cells by improving their colony forming ability [47-49]. Among several stimuli that cause epidermal keratinocytes differentiation, ascorbic acid (vitamin C) has also been reported to induce epidermal differentiation increasing gene expression for cornified envelop proteins. The pro-differentiating effects of ascorbic acid appear to follow a signaling pathway similar to that mediated by calcium, although, unlike calcium, ascorbic acid-driven differentiation causes an

enhanced ascorbate transport and a prevention of hydrophilic antioxidant depletion [50, 51].

In this study, the knowledge and experience derived from the optimized culture conditions for the development of full-thickness human skin equivalent (HSE) were used to develop RHE and RME. RHE and RME development used the same fully-defined cell culture media as the ones used to optimize the morphogenesis of full-thickness HSE, i.e. CnT-PR for submerged and CnT-PR-3D for airlifted cultures.

3.3.2 *Reconstructed human epidermis (RHE)*

Tissue morphogenesis of RHE

NHEK were able to undergo epithelial differentiation forming an organised epidermis-like structure (Figure 3.1), closely mimicking epithelial differentiation as found in healthy native human skin (NHS) (Figure 3.2). Hence, the construct was termed as reconstructed human epidermis (RHE). Upon a trigger of high calcium concentration in air-lifted phase, the proliferating NHEKs in stratum basale (SB) differentiated forming the different layers of keratinocytes namely stratum spinosum (SS), granulosum (SG), and corneum (SC) (Figure 3.1).

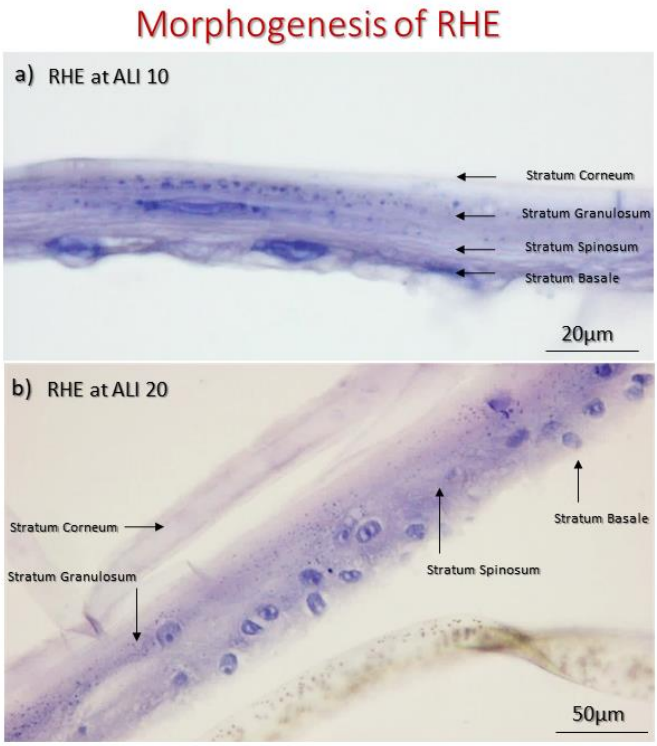

Figure 3.1 Morphogenesis of RHE for a) 10 days and b) 20 days at ALI.

The histological cross-sections at different time points (10 to 20 days) in ALI culture showed increased thickness of upper epidermal layers as a function of time (Figure 3.1).

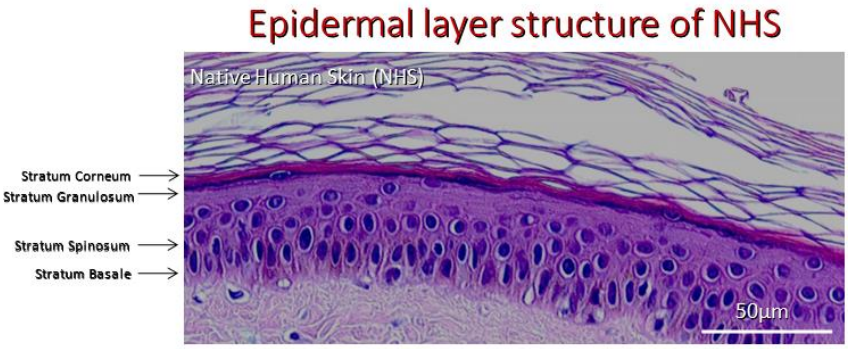

Figure 3.2 Epidermal layer structure of NHS.

IHC of RHE

IHC characterisation of RHE showed that keratin-14 (K14), a marker of early differentiation, was expressed by keratinocytes in basal layer (Figure 3.3 a). Involucrin, a marker of terminal differentiation was present in the stratum corneum (Figure 3.3 b). Cells in stratum spinosum are also known to produce "involucrin" (cornified envelope component) and transglutaminase-K, an enzyme responsible for crosslinking of involucrin in SC [52, 53].

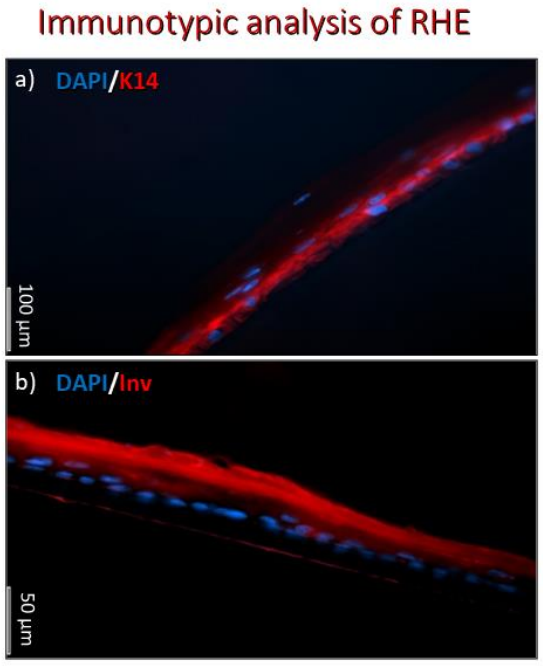

Figure 3.3 Immunotypic analysis of RHE a) K14 as red in basal layer b) Inv as red in stratum corneum.

3.3.3 *Reconstructed murine epidermis (RME)*

Tissue morphogenesis of RME

Human based 3D models allow accurate modelling of skin complex biology *in vitro. Moreover, as advanced biological evaluation tool, they are more predictive in providing reliable outcomes*. However, genetically modified mouse models also have a lot to offer in the area of skin disease study. However, the experimental difficulties to establish long-term murine epidermal cultures have hindered the development of 3D murine skin cultures.

Generally, cell lines (e.g. HaCaT) tend to be highly proliferative, deficient in the intrinsic genetic variability of primary cells and most of them only differentiate poorly, or partially [54-56]. Epidermal tissue formation by HaCaT cells is shown in Figure 3.4 [56] demonstrating delayed differentiation even after 3 weeks. This deficiency was partly compensated by supplementing postmitotic fibroblasts in Col. I (collagen type I) matrix, but the epidermis formation was still incomplete [56]. In 3D culture, cell lines are highly proliferative, resulting in a thick model, with only a thin and partially differentiated cornified top layer. The behavior of cell lines in 3D cultures can be analyzed by histology at different time points, to study how the structure is developing.

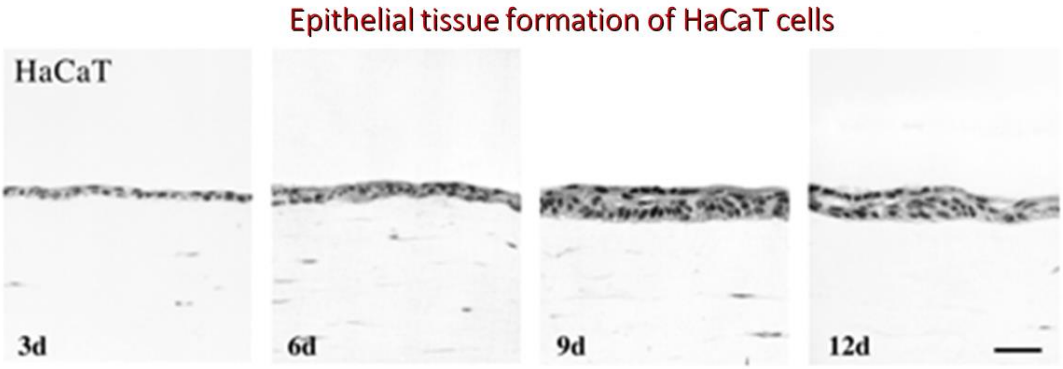

Figure 3.4 Epithelial tissue formation of HaCaT cells. H & E stained histological cross-sections of HaCaT cells organotypic cultures grown on 2×10^5/mL postmitotic fibroblasts containing Col. I gel over a 12-day period. Scale bar measured 100μm. The image was used with copyright permission [56].

C. Segrelles et al. [1] developed COCA cells and showed the non-tumorigenic behaviour of this cell line, by grafting them into immunodeficient mice that showed no signs of tumoral alterations. Moreover, earlier studies [31, 33] showed the tetraploid tendency of COCA cells when sub-cultured. However, COCA cells appeared more stable than earlier reported cells that might be partially due to better and evolving cell culture conditions or to the fact that COCA cells were developed from adult mice instead of new born pups [1]. Nevertheless, these alterations were not appeared to be linked with their differentiation potential at even as late as >75 passages [1]. COCA cells have been reported to arrest their proliferation when exposed to high calcium medium to induce

cell differentiation. Additionally, they barely re-enter cell cycle when re-exposed with low calcium growth medium [57], demonstrating a postmitotic terminally differentiation as it happens *in vivo*. As reported in literature [1], our study also demonstrated that COCA cells, a non-transformed murine keratinocyte cell line showed the capacity to grow in 3D epidermis without the need of feeder cells or coating matrix, under easy-to-use commercially available defined cell culture media. The construct was termed as reconstructed murine epidermis (RME) and the Figure 3.5 demonstrated well differentiated and organised layers of keratinocytes namely SB, SS, SG, SC.

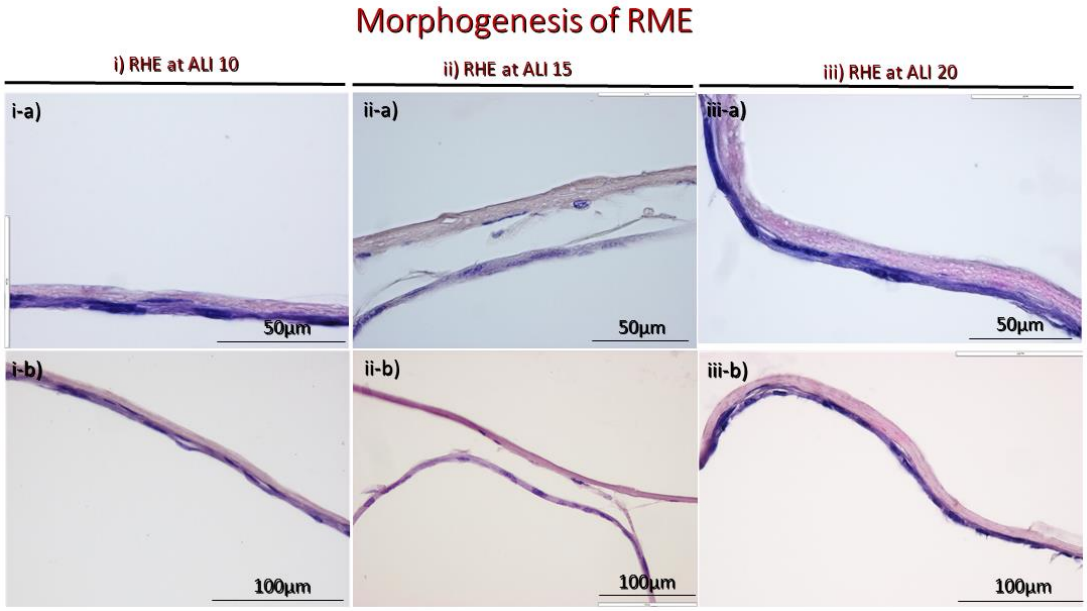

Figure 3.5 Morphogenesis of RME for (sub-images i-a & i-b) 10 days, (sub-images ii-a & ii-b) 15 days, and (sub-images iii-a & iii-b) 20 days at ALI.

The histological cross-sections at different time points (10, 15, and 20 days) in ALI culture, showed increased thickness of upper epidermal layers as a function of time (Figure 3.5).

The obtained morphology of RME was highly comparable with the one reported by *C. Segrelles et al.* [1] (Figure 3.6) that demonstrated the differentiation capacity of COCA cells to develop 3D *in vitro* epidermal model.

Figure 3.6 Morphogenesis of 3D in vitro epidermal model [1] by H & E stained histological cross-sections of 1-3-week 3D cultures (images a, b, c) using passage 76 COCA keratinocytes on polycarbonate membrane. Scale bars measured 100µm. The image was available as public copyright license and was used under Creative Commons License Deed (CC BY 2.00) [1].

The developed morphology of RME can also be compared with the epidermal layers structure of Native Murine Skin (NMS) as shown in Figure 3.7. Murine epidermis is usually quite thin and composed of only three layers with a high turnover rate. On the other hand, human epidermis is thick composed of six to ten layers [58]. This difference can be observed between two images of NHS (Figure 3.2) and NMS (Figure 3.7).

Figure 3.7 Epidermal layer structure of NMS. The image [59] has been used with copyright permission.

We showed the tissue morphogenesis of RME, while the IHC analysis of 3D *in vitro* murine epidermis (also generated by COCA cells) [1] was shown in Figure 3.8.

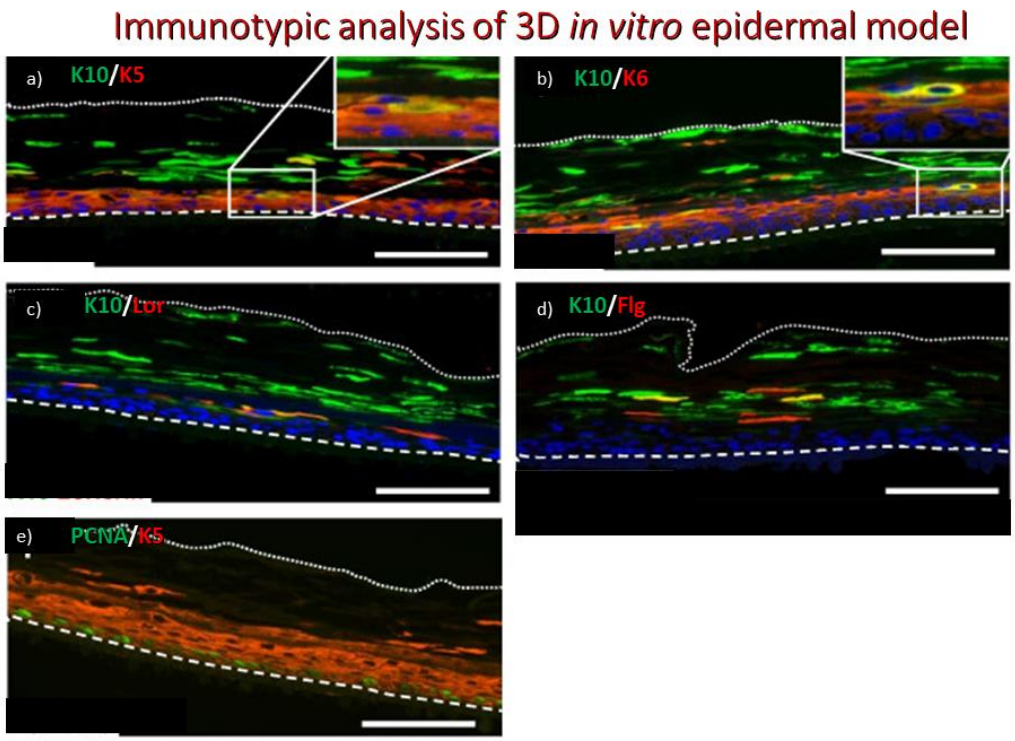

Figure 3.8 Immunotypic analysis of 3D in vitro epidermal model of 3-week 3D cultures using passage 76 COCA keratinocytes. The sub-images (a & b) K5 and K6 expression was expanded to suprabasal layers showing the hyperproliferative nature of the model. a-d) K10 was expressed in suprabasal layers and stratum corneum. The sub-images (c & d) lor and flg were also expressed in suprabasal layers. The sub-image (e) PCNA was mostly restricted to the basal layer demonstrating the proliferation. Dashed lines indicate the contact of basal layer with the polycarbonate membrane. Dotted lines indicate the end of the stratum corneum. Scale bars measured 100µm. The image was available as public copyright license and was used under Creative Commons License Deed (CC BY 2.00) [1].

The Figure 3.8 demonstrated the expression of differentiation markers of K10, loricrin and filaggrin at suprabasal layers. While the expansion in the expression K5 and K6 from basal to suprabasal layers indicated a state of increased proliferation. However, the PCNA staining showed that proliferation was mostly limited to the cells in basal layer. The observed alterations in the normal sequence of differentiation markers might be an experimental limitation of this *in vitro* model, however, these changes were not observed under *in vivo* experiments [1].

Conclusion

In-house RHE was successfully developed from NHEKs under easy-to-use commercially available cell culture media. The epidermal tissue showed well-organised and well-differentiated epidermal layers of keratinocytes. IHC analysis demonstrated K14 expression in basal layer and involucrin expression in corneal/sub-corneal layers as markers of early and terminal differentiation, respectively. The developed RHE might serve as a model to understand epidermal differentiation, *in vitro* cytotoxicity/irritancy testing, as epidermal sheets in regenerative medicine, and as basis to develop more complex skin models.

Human based 3D systems are highly important and predictive, on the other hand, 3D murine epidermal models offer good experimental set-ups to study disease pathologies and treatments, e.g. by growing the tissue from genetically modified mice of interest. In-house RME using COCA cells (murine cell line) were successfully developed in this work, and already reported in the previous literature [1]. COCA cells showed a remarkable capacity to differentiate and construct 3D epidermal tissue. The comparative study between the results obtained from RHE and RME might serve as a link to understand the relevancy of outcomes obtained from animal- and human-based test systems.

References

1. Segrelles, C., et al., *Establishment of a murine epidermal cell line suitable for in vitro and in vivo skin modelling.* BMC dermatology, 2011. 11(1): p. 9.
2. Astashkina, A., B. Mann, and D.W. Grainger, *A critical evaluation of in vitro cell culture models for high-throughput drug screening and toxicity.* Pharmacology & therapeutics, 2012. 134(1): p. 82-106.
3. Roth, A. and T. Singer, *The application of 3D cell models to support drug safety assessment: opportunities & challenges.* Advanced drug delivery reviews, 2014. 69: p. 179-189.
4. Grainger, D.W., *Cell-based drug testing; this world is not flat.* Advanced drug delivery reviews, 2014. 69: p. vii.
5. *Council of the European Union. Seventh Amendment to the EU and Cosmetics Directive 76/768/EEC. Brussels: The European Parliament and the Council of the European Union.* 2003.
6. Becker, R.A., et al., *Report of an ISRTP Workshop: Progress and barriers to incorporating alternative toxicological methods in the US.* Regulatory Toxicology and Pharmacology, 2006. 46(1): p. 18-22.
7. Cooper, M.L., et al., *Direct comparison of a cultured composite skin substitute containing human keratinocytes and fibroblasts to an epidermal sheet graft containing human keratinocytes on athymic mice.* Journal of investigative dermatology, 1993. 101(6): p. 811-819.
8. Olsson, M. and L. Juhlin, *Epidermal sheet grafts for repigmentation of vitiligo and piebaldism, with a review of surgical techniques.* Acta dermato-venereologica, 1997. 77(6): p. 463-466.
9. Yamaguchi, Y., et al., *Epithelial-mesenchymal interactions in wounds: treatment of palmoplantar wounds by nonpalmoplantar pure epidermal sheet grafts.* Archives of dermatology, 2001. 137(5): p. 621-628.
10. El Ghalbzouri, A., et al., *Leiden reconstructed human epidermal model as a tool for the evaluation of the skin corrosion and irritation potential according to the ECVAM guidelines.* Toxicology in Vitro, 2008. 22(5): p. 1311-1320.
11. Fentem, J.H. and P.A. Botham, *ECVAM's activities in validating alternative tests for skin corrosion and irritation.* ATLA-NOTTINGHAM-, 2002. 30: p. 61-68.
12. Hoffmann, J., et al., *Epidermal-skin-test 1000 (EST-1000)—A new reconstructed epidermis for in vitro skin corrosivity testing.* Toxicology in Vitro, 2005. 19(7): p. 925-929.
13. Kidd, D., M. Johnson, and J. Clements, *Development of an in vitro corrosion/irritation prediction assay using the EpiDerm™ skin model.* Toxicology in vitro, 2007. 21(7): p. 1292-1297.

14. Alépée, N., et al., *A catch-up validation study on reconstructed human epidermis (SkinEthic™ RHE) for full replacement of the Draize skin irritation test.* Toxicology in Vitro, 2010. 24(1): p. 257-266.
15. Kandárová, H., et al., *In vitro skin irritation testing: improving the sensitivity of the EpiDerm skin irritation test protocol.* ATLA-Alternatives to Laboratory Animals, 2009. 37(6): p. 671.
16. Kojima, H., et al., *A catch-up validation study of an in vitro skin irritation test method using reconstructed human epidermis LabCyte EPI-MODEL24.* Journal of Applied Toxicology, 2014. 34(7): p. 766-774.
17. Ackermann, K., et al., *The Phenion® full-thickness skin model for percutaneous absorption testing.* Skin pharmacology and physiology, 2010. 23(2): p. 105-112.
18. Mattey, D. and D. Garrod, *Calcium-induced desmosome formation in cultured kidney epithelial cells.* Journal of Cell Science, 1986. 85(1): p. 95-111.
19. Mattey, D. and D. Garrod, *Splitting and internalization of the desmosomes of cultured kidney epithelial cells by reduction in calcium concentration.* Journal of cell science, 1986. 85(1): p. 113-124.
20. Boyce, S.T. and R.G. Ham, *Calcium-regulated differentiation of normal human epidermal keratinocytes in chemically defined clonal culture and serum-free serial culture.* Journal of Investigative Dermatology, 1983. 81(s 1): p. 33-40.
21. Rubin, A.L. and R.H. Rice, *Differential regulation by retinoic acid and calcium of transglutaminases in cultured neoplastic and normal human keratinocytes.* Cancer research, 1986. 46(5): p. 2356-2361.
22. Kopan, R., G. Traska, and E. Fuchs, *Retinoids as important regulators of terminal differentiation: examining keratin expression in individual epidermal cells at various stages of keratinization.* The Journal of cell biology, 1987. 105(1): p. 427-440.
23. Yuspa, S.H., et al., *Expression of murine epidermal differentiation markers is tightly regulated by restricted extracellular calcium concentrations in vitro.* The Journal of cell biology, 1989. 109(3): p. 1207-1217.
24. *GUIDANCE DOCUMENT ON AN INTEGRATED APPROACH ON TESTING AND ASSESSMENT (IATA) FOR SKIN CORROSION AND IRRITATION*, in *OECD TG 439*, O.f.E.C.-o.a. Development, Editor. 2010.
25. Van Gele, M., et al., *Three-dimensional skin models as tools for transdermal drug delivery: challenges and limitations.* Expert opinion on drug delivery, 2011. 8(6): p. 705-720.
26. Schmook, F.P., J.G. Meingassner, and A. Billich, *Comparison of human skin or epidermis models with human and animal skin in in-vitro percutaneous absorption.* International journal of pharmaceutics, 2001. 215(1-2): p. 51-56.

27. Schafer-Korting, M., et al., *Reconstructed human epidermis for skin absorption testing: results of the German prevalidation study.* ATLA-NOTTINGHAM-, 2006. 34(3): p. 283.
28. Schäfer-Korting, M., et al., *The use of reconstructed human epidermis for skin absorption testing: Results of the validation study.* Alternatives to laboratory animals: ATLA, 2008. 36(2): p. 161-187.
29. Rheinwatd, J.G. and H. Green, *Seria cultivation of strains of human epidemal keratinocytes: the formation keratinizin colonies from single cell is.* Cell, 1975. 6(3): p. 331-343.
30. Häkkinen, L., L. Koivisto, and H. Larjava, *An improved method for culture of epidermal keratinocytes from newborn mouse skin.* Methods in cell science, 2001. 23(4): p. 189-196.
31. Bruegel, V.S., et al., *Long-term murine keratinocyte cultures become tetraploid, yet maintain the ability to stratify.* The Journal of investigative dermatology, 2004. 123(2): p. 403-404.
32. Hager, B., P. Fleckman, and J.R. Bickenbach, *Long-term culture of murine epidermal keratinocytes.* Journal of Investigative dermatology, 1999. 112(6): p. 971-976.
33. Yano, S. and H. Okochi, *Long-term culture of adult murine epidermal keratinocytes.* British Journal of Dermatology, 2005. 153(6): p. 1101-1104.
34. Reichelt, J. and I. Haase, *Establishment of spontaneously immortalized keratinocyte lines from wild-type and mutant mice*, in *Epidermal Cells*. 2010, Springer. p. 59-69.
35. Caldelari, R., et al., *Long-term culture of murine epidermal keratinocytes.* The Journal of investigative dermatology, 2000. 114(5): p. 1064.
36. CellnTech, *Medium formulation.*
37. Bikle, D.D., Z. Xie, and C.-L. Tu, *Calcium regulation of keratinocyte differentiation.* Expert review of endocrinology & metabolism, 2012. 7(4): p. 461-472.
38. Menon, G.K., S. Grayson, and P.M. Elias, *Ionic calcium reservoirs in mammalian epidermis: ultrastructural localization by ion-capture cytochemistry.* Journal of Investigative Dermatology, 1985. 84(6): p. 508-512.
39. Ponec, M., et al., *Lipid composition of cultured human keratinocytes in relation to their differentiation.* Journal of lipid research, 1988. 29(7): p. 949-961.
40. Grubauer, G., P.M. Elias, and K.R. Feingold, *Transepidermal water loss: the signal for recovery of barrier structure and function.* Journal of Lipid Research, 1989. 30(3): p. 323-333.
41. Kolli, S., et al., *Loss of corneal epithelial stem cell properties in outgrowths from human limbal explants cultured on intact amniotic membrane.* 2008.

42. Meller, D., R. Pires, and S. Tseng, *Ex vivo preservation and expansion of human limbal epithelial stem cells on amniotic membrane cultures.* British Journal of Ophthalmology, 2002. 86(4): p. 463-471.
43. Pellegrini, G., et al., *Long-term restoration of damaged corneal surfaces with autologous cultivated corneal epithelium.* The Lancet, 1997. 349(9057): p. 990-993.
44. Tsai, R.J.-F., L.-M. Li, and J.-K. Chen, *Reconstruction of damaged corneas by transplantation of autologous limbal epithelial cells.* New England Journal of Medicine, 2000. 343(2): p. 86-93.
45. Hayashi, I., J. Larner, and G. Sato, *Hormonal growth control of cells in culture.* In vitro, 1978. 14(1): p. 23-30.
46. Okada, N., Y. Kitano, and K. Ichihara, *Effects of cholera toxin on proliferation of cultured human keratinocytes in relation to intracellular cyclic AMP levels.* Journal of Investigative Dermatology, 1982. 79(1).
47. Allen-Hoffmann, B.L. and J.G. Rheinwald, *Polycyclic aromatic hydrocarbon mutagenesis of human epidermal keratinocytes in culture.* Proceedings of the National Academy of Sciences, 1984. 81(24): p. 7802-7806.
48. Flaxman, B.A. and R.A. Harper, *In vitro analysis of the control of keratinocyte proliferation in human epidermis by physiologic and pharmacologic agents.* Journal of Investigative Dermatology, 1975. 65(1): p. 52-59.
49. Yu, M., et al., *An important role for adenine, cholera toxin, hydrocortisone and triiodothyronine in the proliferation, self-renewal and differentiation of limbal stem cells in vitro.* Experimental eye research, 2016. 152: p. 113-122.
50. Savini, I., et al., *Characterization of Keratinocyte Differentiation Induced by Ascorbic Acid: Protein Kinase C Involvement and Vitamin C Homeostasis1*. Journal of investigative dermatology, 2002. 118(2): p. 372-379.
51. Pullar, J., A. Carr, and M. Vissers, *The roles of vitamin C in skin health.* Nutrients, 2017. 9(8): p. 866.
52. Thacher, S.M. and R.H. Rice, *Keratinocyte-specific transglutaminase of cultured human epidermal cells: relation to cross-linked envelope formation and terminal differentiation.* Cell, 1985. 40(3): p. 685-695.
53. Warhol, M., et al., *Immuno-ultrastructural localization of involucrin in squamous epithelium and cultured keratinocytes.* Journal of Histochemistry & Cytochemistry, 1985. 33(2): p. 141-149.
54. Lebonvallet, N., et al., *The evolution and use of skin explants: potential and limitations for dermatological research.* European Journal of Dermatology, 2010. 20(6): p. 671-684.
55. Boelsma, E., M.C. Verhoeven, and M. Ponec, *Reconstruction of a human skin equivalent using a spontaneously transformed keratinocyte cell line (HaCaT).* Journal of investigative dermatology, 1999. 112(4): p. 489-498.

56. Maas-Szabowski, N., A. Stärker, and N.E. Fusenig, *Epidermal tissue regeneration and stromal interaction in HaCaT cells is initiated by TGF-α.* Journal of cell science, 2003. 116(14): p. 2937-2948.
57. Ruiz, S., et al., *Unique and overlapping functions of pRb and p107 in the control of proliferation and differentiation in epidermis.* Development, 2004. 131(11): p. 2737-2748.
58. Brohem, C.A., et al., *Artificial skin in perspective: concepts and applications.* Pigment cell & melanoma research, 2011. 24(1): p. 35-50.
59. Groeber, F., et al., *Skin tissue engineering—in vivo and in vitro applications.* Advanced drug delivery reviews, 2011. 63(4-5): p. 352-366.

Chapter 04: Development of Three-Dimensional Dermal-Epidermal based Full-Thickness Human Skin Equivalent (HSE) - Optimization and Characterisation

Table of contents

List of figures

List of tables

Abbreviations

$(Ca^{2+})_i$: Intracellular Ca^{2+}
3D-CCs: Three-dimensional culture conditions
Ab: Antibody
ALI: Air-liquid interface
AREBS: Autosomal recessive EBS
BCIE: Bullous congenital ichthyosiform erythroderma
CaR: Calcium receptor
CnT: CELLnTECH
CnT-PR: CnT-Prime medium
CnT-PR-3D: CnT-Prime 3D barrier culture medium
CnT-PR-F: CnT-Prime fibroblast medium
CnT-PR-FTAL: CnT-Prime full-thickness air-lift medium
Col. I: Collagen I
COTS: Commercial off-the-shelf
CXT: Cholera toxin
DAG: Diacylglycerol
DEJ: Dermal-epidermal junction
Des: Desmosomes
DM-EBS: Dowling-Meara Type EBS
DPR: Dermatopathia pigmentosa reticularis
EBS: Epidermolysis bullosa simplex
ECM: Extracellular matrix
EHK: Epidermolytic hyperkeratosis
FCS & FBS: Foetal calf serum and foetal bovine serum
FGM2: Fibroblast growth media 2
Flg: Filaggrin
Gαq: G protein
H & E stain: Haematoxylin and eosin stain
HDC: Human dermal construct
HSCs: Human skin constructs
HSE: Human skin equivalent
IHC: Immunohistochemistry
IP3: Inositol trisphosphate
IP3: Inositol trisphosphate
IP3R: Inositol trisphosphate receptor
K10: Keratin 10
K14: Keratin 14
K-EBS: Koebner Type EBS

KGM2: Keratinocyte growth media 2
Lam 5: Laminin 5
LD: Lamina densa
LL: Lamina lucida
Lor: Loricrin
NFJS: Naegeli-Franceschetti-Jadassohn Syndrome
NHDF: Normal human dermal fibroblasts
NHEK: Normal human epidermal keratinocytes
NHS: Native human skin
O1O Medium [1]: [43 g DME (dry malt extract powder) containing no glucose and $CaCl_2$ + 0.5 g $MgSO_4$ + 18.5 g $NaHCO_3$ in 5L H_2O]
PBS: Phosphate-buffered saline
PCT: Progenitor cell treated
PES: O-phosphorylethanolamine + ethanolamine + selenium
PKC: Phosphokinase C
PLC: Phospholipase C
PSEK: Progressive symmetric erythrokeratodermia
Rho: Small signalling G proteins
SB: Stratum basale
SC: Stratum corneum
SEM: Scanning electron microscopy
SG: Stratum granulosum
SOC: Store-operated channel
SPCA1: Secretory pathway calcium ATPase 1
Src and Fyn: Families of kinases
SS: Stratum spinosum
T3: Triiodothyronine
TEM: Transmission electron microscopy
TF: Tonofibrils
TJ: Tight junctions
TRI: Masson's trichrome staining
VSI: Vohwinkel syndrome with ichthyosis
WC-EBS: Weber-Cockayne Type EBS

Chapter 04: Development of Three-Dimensional Dermal-Epidermal based Full-Thickness Human Skin Equivalent (HSE) - Optimization and Characterisation

Abstract

Human skin constructs (HSCs) have been intended to meet the needs of clinical applications, fundamental, and applied research. The successful application of HSC requires that the engineered tissue recapitulates the same organization and function of its *in vivo* counterpart. HSC was obtained having both dermal and epidermal compartments by embedding normal human dermal fibroblasts (NHDF) in rat tail tendon collagen type I (Col. I) hydrogel mimicking the dermal extracellular matrix (ECM) to be remodelled by NHDF, and then seeding normal human epidermal keratinocytes (NHEK) on the top to generate the epidermis. Different three-dimensional cell culture conditions (named as 3D-CC-I, II, III, IV) were applied to optimize the epidermal differentiation mimicking as closely as possible native human skin (NHS). The applied 3D-CCs were based on commercially available serum/animal component-free and/or fully-defined media to optimize the development of HSC. Media used were: For NHEK CnT-PR (CELLnTECH), CnT-PR-3D (CELLnTECH), CnT-PR-FTAL (CELLnTECH), KGM2 (PromoCell), High $CaCl_2$ containing KGM2 (PromoCell); and for NHDF CnT-PR-F (CELLnTECH), FGM2 (PromoCell). Each 3D-CC was further carried out with the optimization of a physical parameter, i.e. air-liquid interface (ALI) (10, 15, and 20 days). Tissue morphogenesis of HSCs obtained from four different culture conditions was compared by comparing H & E stained histological sections, selecting "3D-CC-III" as the optimal condition to generate full-thickness *in vitro* skin (that was now named as Human Skin Equivalent or HSE). On the other hand, HSCs obtained from other 3D-CCs (-I, -II, -IV) demonstrated comparatively less organized epidermis with interlayer gaps. The optimized protocol of 3D-CC-III was as following: i) NHDF (~8×10^4 cells/mL) were embedded in Col. I based dermal construct to remodel the ECM for 5-7 days using CnT-PR-F medium; ii) NHEK (8×10^6 cells/mL) were plated and grown in submerged culture for 3 days to cover the dermal substrate using CnT-PR medium; iii) the culture was then continued in submerged conditions overnight using CnT-PR-3D medium to allow cells to develop cell-cell adhesion structures before ALI culture; iv) Finally the culture at ALI was performed for 15-20 days while bottom fed using CnT-PR-3D medium. The HSE was fully characterised by haematoxylin and eosin (H & E) and Masson's trichrome (TRI) histological staining for morphology analysis, immunohistochemistry (IHC) for proteins' tissue distribution analysis, transmission electron microscopy (TEM) for ultrastructure analysis, scanning electron microscopy (SEM) for tissue architecture analysis, and wettability measurement for barrier function

analysis. Histological results showed the formation of a dermal layer demonstrating NHDF with typical elongated filopodia-like morphology, uniformly distributed cells all along the dermal length with the optimal cell density as found in NHS. Histological results for epidermis showed characteristic multi-layered epidermis with well-differentiated layers of stratum basale, spinosum, granulosum, and corneum. IHC results showed that keratinocytes in basal layer were positive for Ki-67 demonstrating their active state of proliferation. Similarly, dermal layer indicated the Ki-67 positive dermal fibroblasts demonstrating proliferative potential of NHDF in dermis. Immunoreactivity for keratins (K) indicated K14 expression was displayed by keratinocytes in the basal layer while K10 (marker of early differentiation) was restricted to the supra-basal layers. Terminal differentiation was demonstrated as spotted expression of filaggrin (Flg) and loricin (Lor) in the sub-corneal and corneal layers of the epidermis. The basement membrane protein Laminin 5 (Lam 5) was displayed as a continuous line at dermal-epidermal junction (DEJ). Likewise, Laminin (Lam) as one of the dermal ECM proteins was actively produced and expressed by human dermal fibroblasts as fainted spots around the cells in dermis. TEM revealed basement membrane with lamina lucida (LL), lamina densa (LD), regular hemidesmosomes and anchoring fibres. The epidermal layers showed abundant intracellular keratin filaments, desmosomes, and tight junction (TJ) between keratinocytes. SEM revealed the interwoven network and architecture of ECM with embedded dermal fibroblasts lying along collagen fibres; while epidermal layers appeared becoming increasingly flattened as they moved to the surface. The contact angle of 82.5±8.9° demonstrated the barrier function of HSE. In this study, we successfully created an *in vitro* three-dimensional dermal-epidermal based interfollicular full-thickness human skin construct recapitulating the skin morphogenesis, epidermal differentiation, ultra-structure features, tissue architecture, and barrier function properties, closely imitating the properties of NHS and thus named as human skin equivalent (HSE). The developed HSE may serve as a strong candidate in the fields of regenerative medicine; a fundamental tool to assess biocompatibility of biomaterials, pharmacotoxicity, safety & effectiveness of cosmetics; to investigate skin biology, skin disease pathogenesis, wound healing, and skin infection.

Keywords: Human skin equivalent (HSE), three-dimensional culture conditions (3D-CCs), normal human dermal fibroblasts (NHDF), normal human epidermal keratinocytes (NHEK), CELLnTECH (CnT).

4.1 Introduction

Human skin constructs (HSCs) are three-dimensional (3D) human based *in vitro* models whom applications range from regenerative medicine to fundamental basic research and industrial uses, for example for cytotoxicity analysis, drug targeting studies and testing new therapeutics / treatment approaches.

4.1.1 In vivo applications

The *in vitro* generation of skin was first reported by pioneering work from Green et al., [2] *Bell et al.,* [3] *Hefton et al.*, [4] for transplantation purposes. Since then the development of a permanent, readily available, and immunologically compatible skin replacement for the treatment of extensive burns represents a challenge. Full-thickness skin wounds can be treated through transplantation of autologous skin grafts (clinical gold standard method) [5]. Due to the extremely limited availability of harvested autologous skin, the use of allogenic skin grafts (cadaveric skin) is the alternative temporary treatment option. However, it has ethical & safety issues regarding viral disease transmission (HBV, HCV, or HIV), it may cause wound complications and possible immune rejection [6]. In this regard, considering that allogenic keratinocytes provoke strong immune rejection but allogenic fibroblasts are well tolerated by the host, commercially available dermal substitutes (either cell-free or allogeneic cell-containing; and either treated or non-treated human or animal dermis e.g. Alloderm® or Matriderm®, respectively) offer possible commercial off-the-shelf (COTS) solutions [7]. Dermal substitutes are important also because treatment with autografts or transplanted keratinocytes alone provides poor stability, excessive wound contracture and scarring. However, use of autologous cells in these substitutes is preferable for better functional and aesthetic outcomes [8]. With progressing research on tissue engineering, cell transplantation, and gene therapy, it is now becoming possible to obtain pure human cell cultures of good amount and best quality. However, the standardization of the procedures especially for proliferative keratinocytes preparation as well as for their maintenance is a major obstacle. On the other hand, the use of serum and the reagents provided by companies offer safety issues, especially in clinical applications. Additionally, the production of animal-free cell therapeutics is greatly on its way, offering recombinant growth factors e.g. trypsin-like dislodging enzyme named TrypLE (Gibco, Invitrogen) etc. [9].

4.1.2 In vitro and industrial applications

Need of a Three-Dimensional (3D) testing system

For industrial applications, *in vitro* bio-evaluation is more accurate using 3D testing systems than 2D cell cultures [10-12]. Extracellular matrix (ECM) is the mechanical

support and main component of 3D tissue microenvironment. It binds to the diffusible molecules, including crucial growth factors, and regulate the intracellular communication via signalling pathways, thus it has a key role in normal tissue homeostasis, growth and differentiation. Furthermore, the interactions between ECM and cells, results in specific cell surface receptor expression (e.g. focal and fibrillar adhesions) [13], metabolic functions, cell proliferative potential, ECM production, release of key regulators, relevant cell density and tissue phenotype [14-21]. 2D cell cultures fail to reproduce these features and result in non-predictive findings [21] mainly due to forcing cells to adapt to an artificial flat 2D surface. Cells grown in 3D environment mimic the relevant complexity and dynamic situation of the *in vivo* microenvironment [21] and cell-cell & cell-ECM interactions define tissue's behaviour towards an external stimulus [14-20]. Thus, the biological response of skin against a toxic agent derives its ability to react as a whole, that is mediated by a cross-talk among multiple cell types and surrounding ECM [6].

Need of an alternative of animal testing

As HSCs are physiologically similar to native human skin (NHS), they offer an advanced 3D testing system as an alternative to animal testing [22] for drugs & cosmetics testing, irritancy & toxicity testing, wound healing studies, cancer research, skin infection biology, mode of action of other skin diseases [23, 24]. The Draize assay is performed on albino rabbit skin for 4-48 hours by applying the test substance to investigate the tissue harm [25]. Despite being ethically questionable (animals suffering pain), the test has provided incorrect information in the past [26, 27]. On the other hand, murine models have also been extensively used for skin biology experiments, wound healing and skin cancer studies [28-30]. However, some basic dissimilarities exist between mouse and human skin architecture [31]. Furry mouse skin is rich of hair follicles and their cycle is synchronized during the initial months of mouse life. On the other hand, human skin has large interfollicular spaces, with scarce hair follicles and hair cycle is not a synchronized process. Moreover, murine epidermis is quite thin composed of only three layers with a high turnover rate. On the other hand, human epidermis is thick, composed of six to ten layers. Another basic difference is the anatomical location of melanocytes as they are located in basal layer of human epidermis, while in dermal hair follicles of murine skin. Another difference lies in the presence of a cutaneous muscle layer (panniculous carnosus) that is present in mice but absent in human skin. These interspecies inconsistences in skin structure exist and lead to different testing outcomes [32]. Moreover, skin functionality and responsiveness are also different in mouse and humans, e.g. mouse skin is effectively able to regenerate after wounding, while human skin damage may lead to hypertrophic scar (keloids) formation, that is completely absent in mouse skin [33]. Also, mouse skin provides more percutaneous absorption because of

lesser water barrier properties of epidermis than human skin and thus is not a valid model for studies involving topical drug-delivery [34].

EU regulations

Amendments in EU regulations and current policies have further pushed the development of *in vitro* testing systems as alternative to animal testing. According to the growing regulations: European union (EU) 7th amendment (Dir. 2003/15/EC) of the "Cosmetics Directive" (76/768/EEC) made it obligatory to replace animal trials for cutaneous resorption with reliable *in vitro* tests by the year 2009 [35]. This ran the development of the 3Rs principle "replacement, reduction and refinement" [36]. Moreover, REACH a European regulatory program for registration, evaluation, authorization and restriction of chemicals emphasizes on human health and environment by early characterisation of chemicals' properties for risk assessment [37, 38]. In this work, a 3D skin model was developed and aimed at the future preclinical testing of new biomaterials for wound healing, reducing the number of needed animal experiments.

4.1.3 Role of culture conditions on keratinocytes' behaviour

Keratinocytes under right cell culture conditions have the tendency to undergo normal differentiation process as it happens *in vivo*. In this regard, calcium has a role in inducing the differentiation by supporting the formation of desmosomal contacts [39-41], e.g. it precisely induces production of type I transglutaminase, the main enzyme involved in cornified envelope formation [42]. The level of epidermal development is also affected by a physical parameter of air-liquid interface (ALI) that cause chemical gradient formation in epidermal layers [43, 44] and thus results in an enhanced tissue organization and differentiation. The goal of this study was to develop *in vitro* dermal-epidermal based full-thickness human interfollicular skin. To this purpose, different 3D cell culture conditions (3D-CCs) were tested to obtain the most physiologically relevant HSC that can sustain the physiological function for more extended time periods and can be used for studying skin development, skin disease pathogenesis, toxicity & efficiency of wound devices, cosmetics, and drugs (short- or long-term studies), or as a skin substitute for transplantation to burnt patients.

4.1.4 Importance of Dermal-Epidermal skin models

Multiple approaches can be employed to develop HSCs e.g. containing dermal, epidermal or both layers as full-thickness skin; either composed of autologous or allogeneic cells; either based on natural or biodegradable synthetic polymers; either fibroblasts loaded or not loaded dermal layer. In this study, we optimized 3D cell culture conditions (3D-CCs) to develop full-thickness human skin equivalent (HSE) using human primary cells. Our HSE was based on fibroblasts-embedded collagen I dermal compartment and a multi-layered well-differentiated epidermal compartment.

Unlike epidermal or dermal skin models, full-thickness skin models comprising both dermal and epidermal compartments have an added value. Fibroblasts secrete growth factors to directly influence the growth [45] and differentiation of keratinocytes [46, 47]. The interaction between these two cell types is also highly important in the formation of the basement membrane as a part of dermal-epidermal junction (DEJ) [48, 49]. Soluble factors secreted by dermal fibroblasts are diffused to the overlying epidermis, influencing the keratinocytes to induce the basement membrane proteins synthesis [47, 50-53]. On the other hand, keratinocytes also directly influence the proliferation of fibroblasts [46]. Thus, this reciprocal interaction works as a double-paracrine mechanism regulating each cell type [54, 55]. According to this, keratinocytes secrete IL-1, stimulating fibroblasts to secret keratinocyte growth factor (KGF) and granulocyte-monocyte colony-stimulating factor (GM-CSF), that in turn influence keratinocytes proliferation. Thus, only in advanced 3D *in vitro* systems, keratinocytes are able to develop well-ordered epidermis and basement membrane features [47, 53, 56], to closely recapitulate the characteristics of native human skin. Besides, fibroblasts have an important role in enhancing the keratinocytes resistance towards toxic compounds [57] This suggests that epidermal model alone is not enough for predictive *in vitro* toxicological studies.

4.1.5 Challenges to meet

In existing 3D skin models, the lack of additional skin cellular components is one of the major limitations. Incorporation of other cell types, such as melanocytes, myofibroblasts, endothelial cells, inflammatory immune cells (Langerhans cells or LC), histiocyte (tissue macrophage or a dendritic cell), and adipocytes is possible depending on the specific application. For instance, the use of mesenchymal stem cells (MSCs) together with dermal fibroblasts in reconstructed skin model has improved wound healing [58]. Incorporation of immune cells would help in understanding the skin immune response, though it has remained a big challenge because of the extreme difficulty in expanding this cell type *in vitro* [59, 60]. Moreover, replacing the dermal part of HSCs with human fibroblasts-derived matrix could help in replicating the features of cutaneous appendages (including hair follicles), that also represents a great challenge, and is one of our future goals to meet.

4.2 Materials and Methods

4.2.1 Cell source and maintenance

Primary cells including normal human dermal fibroblasts (NHDF) and normal human epidermal keratinocytes (NHEK) were obtained from PromoCell.

NHDF and NHEK were maintained in CnT-Prime fibroblast medium (CnT-PR-F, CELLnTECH) and CnT-Prime epithelial culture medium (CnT-PR, CELLnTECH) respectively under the physiological culture conditions (37°C, 5% CO_2), and sub-cultured using DetachKit-Promocell HEPES BSS (2-[4-(2-hydroxyethyl)piperazine-1-yl] ethanesulfonic acid buffered saline solution); 0.04% Trypsin/0.03% EDTA (ethylenediaminetetraacetic acid); and TNS (trypsin neutralizing solution) containing 0.05% trypsin inhibitor from soybean/0.1% bovine serum albumin. Collagen type I (Col. I) from rat tail tendons was obtained from Ibidi at 5mg/mL stock concentration.

Different media used to optimize the development of HSE are: CnT-PR-F (a CnT-Prime fibroblast medium, CELLnTECH) named as Medium A; CnT-PR (a CnT-Prime epithelial culture medium, CELLnTECH) named as Medium B; CnT-PR-3D (a CnT-Prime 3D barrier medium, CELLnTECH) named as Medium C; CnT-PR-FTAL (a CnT-Prime full thickness airlift medium, CELLnTECH); KGM2 (a keratinocyte growth medium 2, Promocell); High calcium containing KGM2 (a keratinocyte growth medium 2, Promocell + 1.2mM $CaCl_2$, Sigma).

Note: The composition of KGM2 is as follows: bovine pituitary extract (0.004 mL/mL), epidermal growth factor (recombinant human) (0.125ng/mL), insulin (recombinant human) (5µg/ml), hydrocortisone (0.33µg/mL), epinephrine (0.39µg/mL), transferrin, holo (human) (10µg/mL), $CaCl_2$ (0.06mM).

The FGM2 is a low serum media (2%v/v) that contains: 0.02mL/mL foetal calf serum, 1ng/mL basic fibroblasts growth factor (FGF) (recombinant human), 5µg/mL insulin (recombinant human) [61].

CnT-Prime media are fully-defined and animal component-free media with $CaCl_2$ concentration of 0.07mM along with main growth factors such as epidermal growth factor (EGF), FGF, insulin, hydrocortisone, transferrin, T3, and ethanolamine plus 21 different amino acids, 19 minerals and trace elements (including selenium, manganese and zinc), 14 vitamins (including folate, niacinamide and biotin), 10 other ingredients (including glucose, pyruvate, and buffers). They are without cholera toxin, and phenol red. The detailed concentration information for this larger numbers of growth factors is not releasable by the company [62].

CnT-PR-3D and CnT-FTAL contains elevated levels of calcium concentration of 1.2mM and no proliferative factors [62].

4.2.2 Fabrication of human skin equivalent (HSE)

In this study a three-dimensional (3D) HSE was generated by successively fabricating dermal and epidermal layers as summarized in Figure 4.1 A.

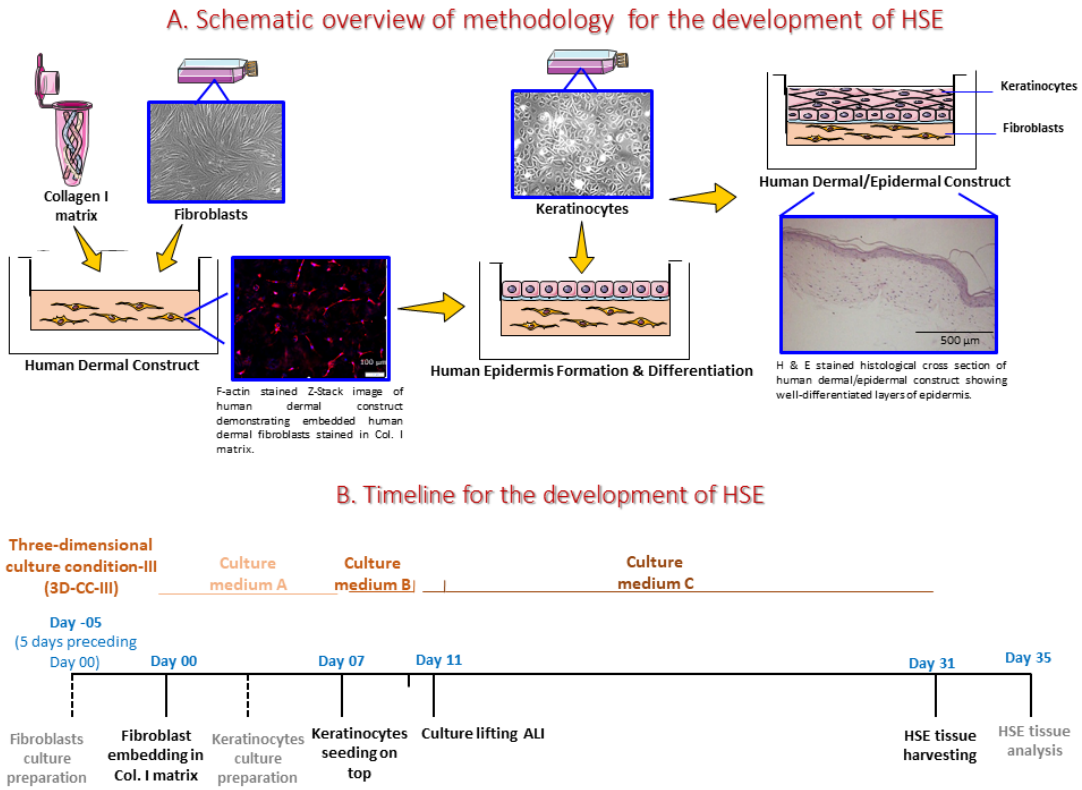

Figure 4.1 A) Schematic overview of methodology for the development of HSE. It starts with the embedding of human dermal fibroblasts in collagen I matrix to contract and remodel the gel to form dermal layer. Then the keratinocytes are seeded on the top to form a monolayer and the culture is raised to ALI under 3D cell culture conditions allowing the keratinocytes to differentiate and form epidermal layers. B) Timeline for the development of HSE.

Fabrication of Human Dermal Construct (HDC)

Gelation of Col. I solution was performed in 10X media (M199, Sigma) in the presence of additives (L-glutamine) and sodium bicarbonate ($NaHCO_3$) resulting in a final Col. I concentration of 1.5mg/mL (containing a salt concentration of 1X in final mixture with pH of 7.2-7.4) (Table 4. 1).

Human Dermal Constructs (HDCs) were prepared by fabricating acellular (200µL) and cellular layers (400µL) of Col. I matrix on polyester membrane of 12 well insert (Corning 3460, with 0.4µm pore size, 12mm diameter, having 1.12cm^2 surface area) to obtain a 5mm thick HDC. A thin layer of acellular collagen served as a substrate for the cellular collagen; and also prevented the cellular collagen from complete contraction from the insert membrane. Actively dividing mitotic cells (5 x 10^4 NHDF cells per 12mm diameter insert to obtain the human *in vitro* dermal construct) were embedded in Col. I

solution and poured onto the top of the previously deposited and gelled acellular Col. I layer (room temperature, 20 min). When the cellularised matrix underwent gelation (37˚C for 30 min), the system was fed with fresh cell culture medium (medium A). The system was incubated for 5-7 days to allow hydrogel remodelling by the embedded cells (Figure 4.2).

Table 4. 1 Guidelines for construction of collagen I (1.5mg/mL) based dermal layer.

Constituents	Calculated vol. of each constituent (µL) Total vol. of **acellular layer** = 200µL per insert	Calculated vol. of each constituent (µL) Total vol. of **cellular layer** = 400µL per insert
10X M199 (Sigma)	20µL (10% of final vol. of 200µL results in 1X M199)	40µL (10% of final vol. of 400µL results in 1X M199)
200mM Glutamine (Biosciences)	0.68µL Formula: M1V1=M2V2 (200mM x V1 = 0.68 x 200µL) (This 0.68µL vol. results in 0.68mM Glutamine in final vol. of 200µL of acellular layer)	1.36µL Formula: M1V1=M2V2 (200mM x V1 = 0.68 x 400µL) (This 1.36µL vol. results in 0.68mM Glutamine in final vol. of 400µL of cellular layer)
ddH_2O	113.32µL (vol. calculated in the end)	176.64µL (vol. calculated in the end)
7.5% of $NaHCO_3$ (Sigma)	6µL (This volume is 10% of the volume of collagen I, that results in a final mixture pH of 7.2–7.4 - optimized)	12µL (This is an optimized volume as 10% of the volume of collagen I, that results in a final mixture pH of 7.2-7.4)
5mg/mL Collagen 1 (Ibidi)	60µL (This volume makes final conc. of 1.5mg/mL in final volume)	120µL (This volume makes final conc. of 1.5mg/mL in final volume)
NHDF (Promocell)	N/A	50µL (This volume should contain 5 x 10^4 NHDF per insert)
Total Vol.	200µL	400µL

Fabrication of the collagen gel needs that all constituents are kept on ice and plastic pipette tips are chilled until the gel mixture is poured onto the insert to prevent the premature gelation of collagen I gel.

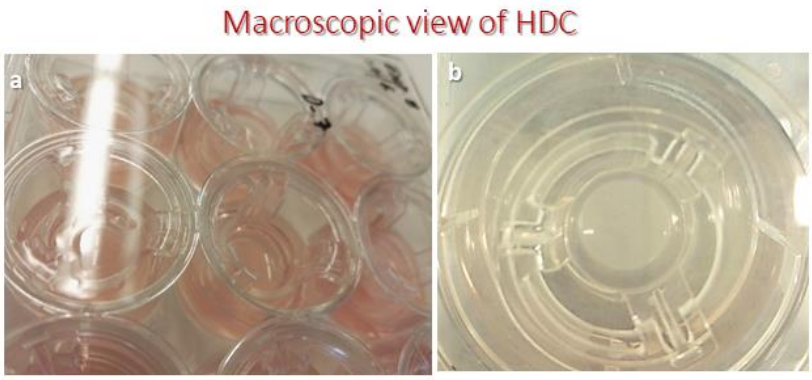

Figure 4.2 Macroscopic view of Human Dermal Construct (HDC). (a) View of experimental set-up of Human Dermal Construct on Day-01 with NHDFs are embedded in collagen I matrix and incubated to allow gel remodeling. (b) Macroscopic top view of contracted collagen on Day-07 retaining its circular shape.

Fabrication of Epidermis onto Human Dermal Construct (HDC)

Media was removed from HDCs 20 minutes before NHEK seeding. NHEK were resuspended (400,000 cells for a surface area of dermal construct of 12mm diameter) in a small volume of 50µL in the centre and plated onto the matrix for epithelialization of cultures. Plates were not moved for 15 min to allow keratinocytes initiate adhesion and then placed at 37°C for 30-60 min without any medium for complete adhesion. Plates were then fed with cell culture medium (medium B). The Transwell inserts were placed in 12 well cell culture plate of special dimensions (Corning 3513), thus providing media volume ~0.3mL media inside + ~1.7mL media outside the insert with equal medium levels inside and outside the insert. Daily media changes were performed by pipetting out media first from outside the insert and then from inside, while feeding fresh media initially inside the insert and then outside. Cultures were maintained in submerged conditions for 3-4 days to allow complete coverage to form a monolayer. Then Medium B was replaced with Medium C and the cultures were kept submerged overnight (15-16 hours) to allow cells to form intercellular adhesion structures. Then the medium was aspirated from inside the insert for ALI culture for 20 days. Medium volume of minimum 1mL and medium change frequency of 3 times per week were used during ALI. For this reason, PMMA (Poly (methyl methacrylate) spacers (2mm thick, custom built for Falcon™ 351146 Polystyrene 6-Well Microplate) were used providing at least 4mL media feeding from bottom with media changes on alternate days. Medium level should be observed carefully as the surface within inserts should remain dry following air-lift for the rest of the cultivation (Figure 4.3).

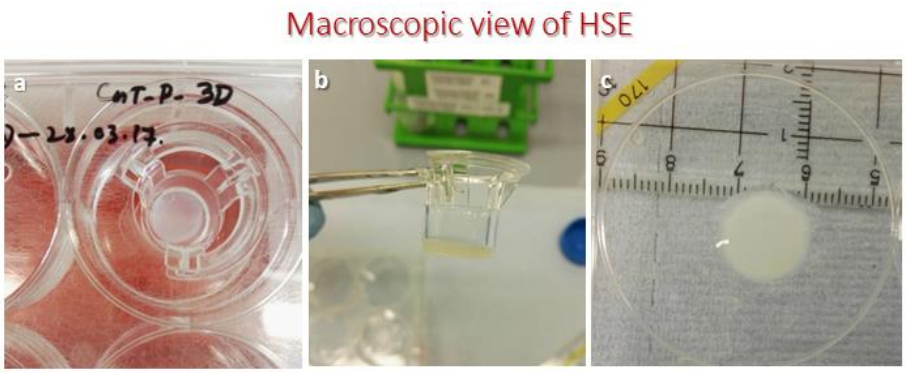

Figure 4.3 Macroscopic view of HSE (a) Top view of experimental set-up of HSE development during incubation at ALI showing the white epidermal layer over the dermal layer. (b) Side view of HSE containing insert at the time of tissue harvesting after 20 days at ALI, showing a thickness of ~2mm. (c) Top view of harvested HSE at the end of ALI period (20 days) retaining the size and diameter of initial mould (12mm in diameter).

Different 3D cell culture conditions (namely 3D-CC-I, -II, -III, -IV) based on different types of commercially available media; were tested to optimize HSE development. The details of the 3D-CC are mentioned in Table 4.2. The test format is described as a timeline in Figure 4.1 B.

Table 4.2 Experimental set-up details of different 3D Culture Conditions (3D-CCs).

Description of 3D culture condition	**3D-CC-I**	**3D-CC-II**	**3D-CC-III**	**3D-CC-IV**
Media used for HDC feeding for 5-7 days	FGM2	FGM2	CnT-PR-F (Medium A)	CnT-PR-F
Media used for epidermal monolayer formation (onto HDC) feeding for 3-4 days	KGM2	KGM2	CnT-PR (Medium B)	CnT-PR-FTAL
Media used for epidermal monolayer formation (onto HDC) feeding for 15-16 hours	----	CnT-PR-3D	CnT-PR-3D	----
Media used for HSC culture at air-lift 10, 15, and/or 20 days	1.2mM $CaCl_2$ containing KGM2	CnT-PR-3D	CnT-PR-3D (Medium C)	CnT-PR-FTAL

CnT-PR-F named as Medium A; CnT-PR named as Medium B; CnT-PR-3D named as Medium C.

Practical considerations regarding "Time" required for fabricating HSE

HSE formation requires ~4 weeks from the time NHDF are embedded in Col. I gel until 3D tissue is fully developed and matured. The preparation involves NHDF seeding in monolayer cultures achieving the confluency two days prior to embedding in collagen gels, and finally passaging at 9:10 ratio to get highly dividing cells for incorporation into collagen gel. The embedded cells take 5-7 days to contract the collagen during which time NHEK monolayers (i.e. 2-3 days before seeding) are cultured and expanded to make them available for seeding on contracted gel. Upon seeding onto HDCs, NHEK are grown under submerged conditions in CnT-PR for 3-4 days; under submerged conditions in CnT-PR-3D media for 15-16 hours (overnight); and then lifted at ALI in CnT-PR-3D media for ~2-3 weeks. The H & E histological analysis takes another 3-4 days including imaging to observe the tissue morphology.

Practical considerations regarding "Strains" of fibroblasts and keratinocytes while fabricating HSE

One critical parameter in the development of HSE include the "strains" of fibroblasts and keratinocytes used to develop HSE. It has been found that fibroblasts support keratinocytes growth and epidermal organization depending upon fibroblasts' ability to "contract" the collagen gel suggesting more the shrinkage of collagen matrix, better would be the keratinocytes' growth. Screening of such fibroblasts strains in prior experiments can help to improve the optimum growth-support. On the other hand, keratinocytes themselves serve as an important parameter to define the tissue architecture of HSE depending on their "proliferative potential". When keratinocytes are seeded onto the dermal construct, most of them adhere to the substrate, however, the ones have already undergone terminal differentiation, would not proliferate anymore. Only the replicating cells would be able to further proliferate and undergo stratification to form HSE. Therefore, the seeded keratinocytes must have an "elevated growth potential", and this can be obtained by growing keratinocytes in small colonies at high density prior to seeding onto dermal construct. Alternatively, passaging the cells in low calcium media also minimizes the terminal differentiation and thus maximize the fraction of replicating cells. The proliferation indices can be directly determined by adding BrdU to the medium. Depending on these parameters when different strains of keratinocyte and fibroblast were incorporated, variations in morphology of HSEs were observed [1, 63].

In this study, we used the same lot of fibroblasts and keratinocytes for optimizing the HSE development under different 3D culture conditions eliminating the variable associated with lot to lot variation.

4.2.3 Morphological analysis

Harvested HSE tissue was rinsed in PBS twice, fixed in 4% paraformaldehyde (10% formalin) for ≥4h, dehydrated through increasing gradient series of ethanol (50%, 70%, 80%, 90%, 95%,100%, 100%, 100%), cleared in xylol (twice), and infiltrated in paraffin using Leica TP1020 Semi-enclosed Benchtop Tissue Processor (over a total period of 12 hours). The processed tissue was paraffin embedded at right orientation using Leica EG1160 Embedding Centre. The sample was thin sliced (~5µm) using Leica RM 2155 microtome leading to sections drying at 37°C overnight to get well adhered and wrinkle-free tissue sections. Morphological analysis was performed on formalin-fixed paraffin-embedded sections through haematoxylin and eosin (H & E) staining. Staining solutions were prepared as: 50% Mayer's haematoxylin (Applicam Panreac) in aqueous water and 0.1% eosin Y solution (Merck) in acetic acid (150µL) containing 70% ethanol. H & E staining involved paraffin dissolution (xylol two times for 10 min each), step-wise rehydration in decreasing gradient series of ethanol (99% for 10 min; and 99%, 90%, 80%, 70%, 50% for 5min each), deionized water for 5 min, haematoxylin staining (for 10 min), bluing & colour differentiation in running water (for 20 min), eosin staining (for 5 min), step-wise dehydration (in increasing gradient series of ethanol), and mounting using Cytoseal (Thermo Fischer). The H & E stained slides were examined under Olympus BX51 light microscope.

The thickness of stratified epidermis and length of DEJ of HSCs was observed qualitatively from H & E stained images and recoded in millimeters (mm). The measurement scale was calibrated using the micron scale of each image.

For Masson's Trichrome (TRI) staining, the staining solutions (Thermo Fischer) include: Goldner's stain I (containing acid fuchsin and xylidine ponceau that stain connective tissue, muscle fibre, & cytoplasm red, and nuclei dark brown respectively); Goldner's stain II (containing Orange G, and phosphotungstic acid that stain erythrocytes orange and decolourises connective tissue respectively); Goldner's stain III (containing Light Green SF yellowish that stains connective tissue green). TRI staining started with dewaxing and rehydration of paraffin sections by dipping in xylol, decreasing gradient series of ethanol (96%, 90%, 80%, 70%), and distilled water for 10 min each. Sections were stained in Weigert iron haematoxylin solution (provided solutions A & B at 1:1 ratio) for 10 min, leading to bluing in running water for 10 min, staining in Goldner's stain I (usually 5-10 min) optimized for 6 min, rinsing in 1% acetic acid solution for 30 sec, staining in Goldner's stain II until connective tissue decolorization (usually 1-30 min with meanwhile microscopic observation) optimized for 2 min, rinsing in 1% acetic acid solution for 30 sec, counterstaining with Goldner's stain III (usually 2-5 min with meanwhile microscopic observation) optimized for 5 min, washing in 1% acetic acid solution (usually 2-5 min) optimized for 30 sec, washing in distilled water to clean acid, dehydration & clearing (for 3-5 min each or only few dips to avoid discoloration of

green stain), mounting, and observing under microscope. As HSE tissue samples are very thin, the staining incubation times were optimized as mentioned above. Moreover, Bouin's solution can be used as a mordant to strengthen the colour reactions.

4.2.4 Immunophenotypic analysis

HSE was rinsed in PBS twice, treated with 2M sucrose solution (Fisher Chemical) at 4°C for at least 1 hour and infiltrated in OCT embedding medium (VWR) for 20-30 min at Room Temperature (RT) leading to embedding in OCT by gradual freezing in liquid nitrogen vapor, leading to storage at -80°C until cryo-sectioned (~10µm) using Microm HM 550 Cryostat. Related to the preservation of tissue architecture during tissue processing, it is important to soak the tissues in sucrose (2M) to replace the water in collagen gels as they are highly hydrated and can result in artefactual damage. Moreover, the HSE tissue is too delicate for snap-freezing, while gradual freezing in liquid nitrogen vapor helps to avoid structural destruction and artefacts.

Immunophenotypic analysis of epidermal markers was performed on cryosections. Specifications on the primary antibodies' concentrations used in this study are listed in Table 4.3. Secondary antibodies included Alexa Fluor 488 Goat anti-Rabbit IgG (H+L) (Abcam), Alexa Fluor 594 Donkey anti-Mouse IgG (H+L) (Abcam), Alexa Fluor 488 Donkey anti-Rabbit IgG (H+L) (Thermo Fischer), Alexa Fluor 568 Goat anti-Mouse IgG (H+L) (Thermo Fischer). Negative controls were performed using secondary antibodies only. Cell nuclei were detected by DAPI staining (1.5µg/mL, VECTASHIELD, Vector labs). Immunohistochemical (IHC) analysis was performed in accordance with the standard protocol from Abcam, with primary antibodies' concentrations optimized for our HSE (as mentioned in Table 4.3). The details of reagents preparation used in IHC staining is detailed in Table 4.4. According to the protocol followed, cryosections were fixed in methanol-free 4% paraformaldehyde (Thermo Scientific) for 10 min leading to rinsing in PBS (2 x 5min). Sections were then permeabilized in 0.2% Triton X-100 for 10 min leading to washing in wash buffer (TBS plus 0.025% Triton X-100) with gentle agitation (2 x 5 min). To avoid secondary antibody cross reaction with tissue's endogenous immunoglobulins, sections were blocked in blocking buffer (10% normal serum from the species in which the secondary antibodies were raised + 1% BSA in TBS) for 2 hours at RT. Slides were drained and applied with primary antibody diluted in antibody diluent buffer (1% BSA in TBS) and incubated in a humidified chamber overnight at 4°C. Fluorophore-conjugated secondary antibody diluted in antibody diluent buffer (1% BSA in TBS) were applied and incubated for 1 hour at RT protected from light to avoid photobleaching. Finally, the sections were rinsed in TBS (3 x 5 min with) and mounted using VECTASHIELD mounting medium. The immuno-stained slides were examined under fluorescent microscope (Olympus XM10 with Alexa 488, 555, 568, & DAPI filters; and Cell Sense Standard software).

The percentage of Ki-67 positive dermal fibroblasts and basal keratinocytes was calculated from IHC images by dividing the Ki-67 positive nuclei (green) by total number of nuclei (blue).

Table 4.3 Primary antibodies used for immunostaining of HSE tissue section.

Primary antibody details and source	Dilution
Ki-67 (Rb, MA) - Cell signal	1:300
Laminin 5 (Rb, PA) - Abcam	1:500
Keratin 14 (Ms, MA) - Abcam	1:100
Keratin 10 (Rb, MA) - Abcam	1:500
Filaggrin (Rb, PA) - Abcam	1:200
β-Tubulin (Ms, MA) - Sigma	1:400
Loricrin (Rb, PA) - Abcam	1:200
Keratin 16 (Rb, PA) - Abcam	1:100 & 2° Ab as 1:200

PA=Polyclonal antibodies; MA=Monoclonal antibodies; Rb=Rabbit; Ms=Mouse; 2° Ab=Secondary antibodies.

Table 4.4 Details of reagents required for Immunostaining.

Reagent Type	Reagent constitution	Reagent Quantity (calculated)
Wash buffer	TBS + 0.025% Triton X-100	250µL (0.25mL) Triton X-100 in 1000mL TBS
Permeabilization reagent	0.2% Triton X-100 in PBS	20µL (0.02mL) Triton X-100 in 10mL TBS
Fixative	4% paraformaldehyde in PBS	10mL of 16% PFA in 30mL PBS
Antibody diluent buffer	TBS + 1% BSA	0.1g BSA in 10mL TBS
Blocking Buffer	10% normal serum + 1% BSA + TBS	1mL normal serum + 0.1g BSA + 9mL TBS
	For double staining:5% normal serum of species in which first secondary antibodies were raised + 5% normal serum of species in which second type of secondary antibodies was raised + 1% BSA + TBS Note: Goat and donkey serum 60mg/mL - Jackson Immuno Research	
Buffers	1X TBS (10X TBS comprised of 500mM tris base + 1.5M NaCl + HCl to set pH to 7.4) 1X PBS	100mL of 10X in 900mL distilled deionized H_2O

BSA is bovine serum albumin, TBS is tris-buffered saline, PBS is phosphate-buffered saline.

4.2.5 Electron microscopy analyses: SEM and TEM

Samples were fixed in 2.5% glutaraldehyde for 1 hour, washed in PBS thrice for 5 min each, and then fixed with 1% osmium tetraoxide for 15 min (Figure 4.4), leading to PBS washing thrice for 5 min each. Then, the samples were dehydrated in an increasing gradient series of ethanol (30% for 5 min, 50% for 5 min, 70% for overnight at 4°C, 96% for 5 min, 96% for 5 min, 96% for 5 min, 100% for 15 min, 100% for 15 min, 100% for 15 min); submerged in polypropylene oxide (PO) for 15 min before submerging in epoxy resin based embedding medium (constituted by combining single components A, B, C, D as per Sigma-Aldrich) with PO (1:1) for 1 hour; and finally embedding in the above mentioned medium in the right orientation (Figure 4.4) leading to heating at 80°C for 8 hours to obtain tissue blocks. These samples were ultrasectioned (~40nm) using Leica Ultracut UCT Ultramicrotome, contrasted with Leica ultrastain 2 (containing 3% lead citrate) & Leica ultrastain (0.5% uranyl acetate), and imaged under JEM-2100 TEM at an accelerating voltage of 200kV.

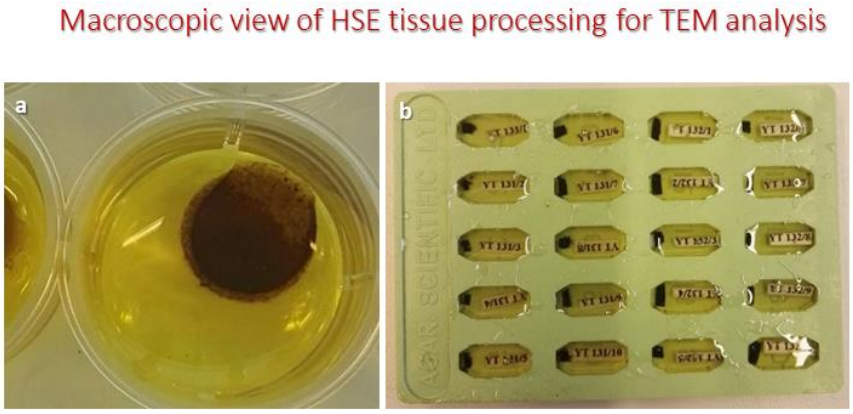

Figure 4.4 Macroscopic view of HSE tissue processing for TEM. (a) Impregnation of osmium tetroxide through human skin equivalent (HSE) turns the samples brown-blackish. Osmium tetroxide works as a strong fixative by acting on proteins and directly stains for lipids. (b) The image shows HSE samples embedded in epoxy resin embedding medium and numbered prior to ultra-sectioning.

For the sample preparation for scanning electron microscopy (SEM), the samples were fixed and dehydrated as described above. Then, the samples were placed in BAL-TEC CPD 030 Critical Point Dryer and dried using CO_2. Cooling CO_2 at 10°C turns gasous CO_2 to liquid CO_2, and heating turns liquid CO_2 into gas, thus removes any left over ethanol. Liquid CO_2 medium was allowed "in and out" 3 times for 10 min. After which, the samples were mounted onto Leit C tabs (electrically conductive, double sided adhesive carbon discs) and gold coated using Edwards S150B Sputter Coater under Argon gas (10^{-1}mbar) at voltage of 15mA for 6 min to create 40nm thick gold (Au) coating. Coated samples were examined under SEM (DSM 982 Gemini, Zeiss). Multiple SEM images were taken at random areas of different samples at 15kV accelerating voltage. The diameter of the collagen fibres was estimated as an average value from multiple TEM images.

4.2.6 Wettability analysis

Static contact angle measurements were performed to investigate wettability of HSE by sessile-drop method using custom-built contact angle goniometer instrument under ambient conditions. An amount of 5µL of MilliQwater was carefully placed on dry samples, multiple images were recorded, and analysed for every drop.

4.2.7 2.7. Statistical analysis

All the experiments were carried out in triplicates (n=3) and results were expressed as mean ± standard deviation. For statistical analysis, GraphPad Prism 5.00.288 (Inc., San Diego, CA, USA) was used to evaluate the significance of the differences in experimental data. T-test was used when the comparison involved two groups. Significance between groups was considered for $p < 0.05$.

4.3 Results & Discussion

4.3.1 Development of dermal layer of HSE

The connective tissue substrate has an important role for the growth of epidermal tissue. Particularly ECM proteins affect skin tissue phenotype [64]. For instance, the use of decellularized dermis e.g. AlloDerm (a commercially available cadaveric dermis for clinical applications); encourages the fast assembly of basement membrane [48]. On the other hand, contracted collagen gels used here might result in a less intact basement membrane, although it greatly supports keratinocyte growth and differentiation. In this study we built a 3D functional HSE by successively fabricating dermal and epidermal layers (Figure 4.1). Fabrication of HDC was discussed in detail in our published article [65] and Chapter 02, demonstrating that Col. I from "rat tail tendons" served the purpose of skin ECM because of its irregular fibrils with *in vivo*-like structure. A thin acellular Col. I layer on well bottom acted as substrate for stable cellularised collagen attachment preventing any possible detachment of contracted cellularised collagen from the insert membrane. Fibroblasts in Col. I gel produced their own ECM proteins (Figure 4.23), remodelled and stabilised the matrix causing gel contraction (Figure 4.2 b).

4.3.2 Optimization of 3D-CCs for the development of HSE

This chapter deals with the development of dermal-epidermal based HSE by optimizing tissue stratification & epithelialization to produce well-differentiated epidermis onto HDC. To this purpose, 3D-CCs based on cell culture media and the physical parameter of ALI (Figure 4.5 and Table 4.2 played an important role on tissue morphogenesis.

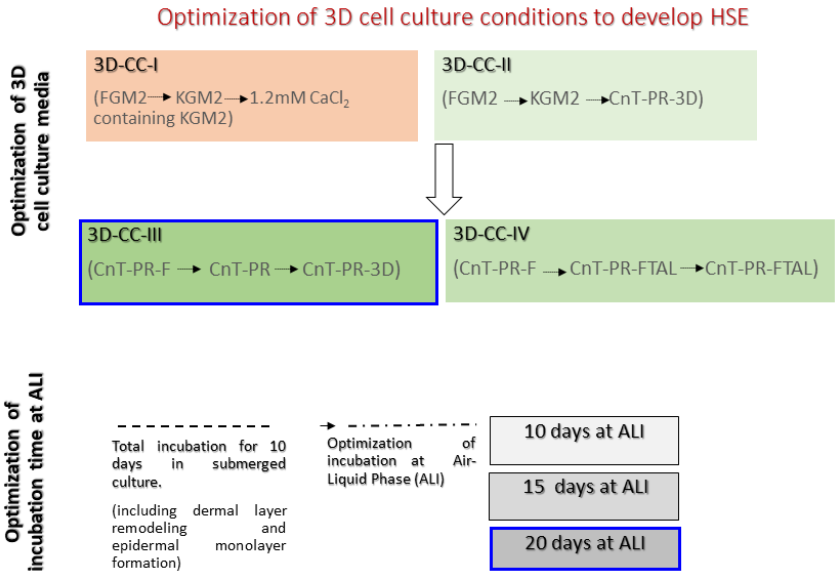

Figure 4.5 Optimization of 3D cell culture conditions to develop HSE. Different 3D cell culture conditions (named as 3D-CC-I, II, III, IV) based on commercially available media were applied to optimize the epidermal differentiation, mimicking as closely as possible NHS. Each 3D-CC was further carried out

with the optimization of ALI, by culturing cells for different time periods of 10, 15, and 20 days at ALI. Blue outlined boxes indicated the optimized and selected culture conditions among the ones tested.

4.3.3 Epidermal differentiation of HSE

Role of calcium in epidermal differentiation

Calcium has been known to have a very significant role in epidermal differentiation. Thus, the media constituted or already available for 3D culture at air-lift phase are generally supplemented with a high calcium concentration of 1.2mM.

In more detail, calcium receptor (CaR) has a key role by starting the intracellular signalling events that initiate differentiation in response to extracellular calcium. Upon activation by calcium, the CaR enhances Cai by stimulating phospholipase C (PLC) activity, leading to phosphatidylinositol-4,5-bisphosphate hydrolysis creating two second messengers: 1) inositol trisphosphate (IP3) and 2) diacylglycerol (DAG), significant for keratinocyte differentiation. IP3 has role in stimulating the release of calcium from intracellular stores, while DAG causes the phosphokinase C (PKC) stimulation. Following this calcium switch, the transient increase in $(Ca^{2+})_i$ is not sufficient and a sustained rise in $(Ca^{2+})_i$ is mandatory for differentiation. PLC-β is mainly responsible for this initial spike in $(Ca^{2+})_i$, while it is PLC-γ1 that sustains the increased $(Ca^{2+})_i$, by raising IP3 levels to release $(Ca^{2+})_i$, and by increasing the influx of calcium via store-operated channels (Figure 4.6) [66].

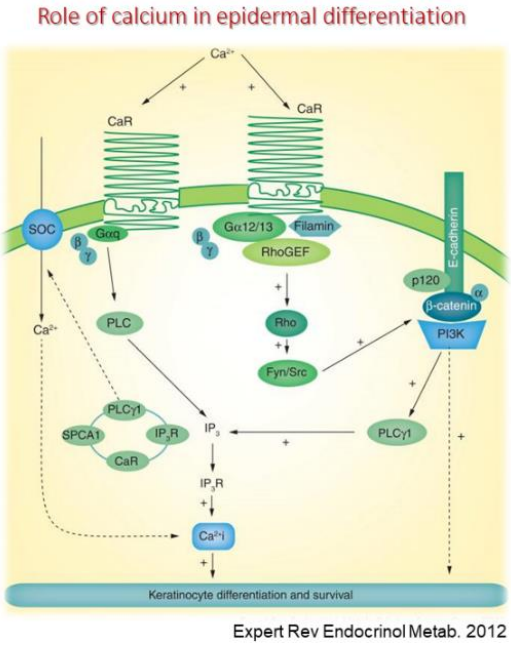

Figure 4.6 Role of calcium in epidermal differentiation. calcium receptor (CaR) after binding with calcium activates its intracellular signaling. According to one pathway; CaR stimulates the G protein (Gαq) causing PLC activation and IP3 generation and thus, releasing calcium from intracellular calcium stores. This pathway results in initial spike of $(Ca^{2+})_i$ (intracellular concentration). Moreover, CaR also triggers Rho that, in turn, stimulates Src and Fyn kinases to phosphorylate the catenins, allowing them to bind and make E-cadherin-catenin complex, that activates PLC-γ1 resulting in a sustained increase in $(Ca^{2+})i$

(along with calcium release from intracellular stores and calcium influx through store-operated channels). Abbreviations: IP3 is inositol trisphosphate, IP3R is inositol trisphosphate receptor, PLC is phospholipase C, SOC is store-operated channel, SPCA1 is secretory pathway Ca^{2+}-ATPase isoform 1 (a Golgi calcium pump). The image from "Expert Rev Endocrinol Metab. 2012" [66] has been used with copyright permission.

Role of ALI in epidermal differentiation

ALI role in epidermal differentiation was evidenced *in vivo* recognizing the calcium gradient formation (due to water loss in the more top layers) is achieved due to air-lift [67]. ALI also helps in achieving the proper lipid profile (acylglucosylceramides and acylceramides) of Stratum Corneum (SC) [68]. In this context, the rate of trans-epidermal water loss is related with lipid biosynthesis [69]. Moreover, ALI raised cultures are not in direct contact with cell culture medium components (e.g. retinoids that strongly inhibit epidermal differentiation) and thus promotes tissue differentiation [43].

Role of growth factors in epidermal differentiation

The traditional culture media used to expand biopsies from human amniotic membrane (HAM) includes hydrocortisone, triiodothyronine (T3), adenine and cholera toxin [70-73]. Hydrocortisone has significant role for maintaining epithelial colonies and keratinocyte proliferation [74].

Another supplement hormone, triiodothyronine has been shown to play a beneficial role in keratinocytes cultivation under minimal levels of foetal calf serum [75].

Cholera toxin (CTX), a protein secreted by *Vibrio cholerae* that causes cholera infection (watery diarrhoea) has been shown to highly stimulate colony growth of cultured human epidermal keratinocytes through increased levels of intracellular cyclic AMP [76].

Adenine also has an effect on epithelial cells by improving their colony forming ability [77-79].

Among several stimuli that cause epidermal keratinocyte differentiation, ascorbic acid (vitamin C) has been reported to induce epidermal differentiation demonstrating an increased gene expression for cornified envelop proteins. The pro-differentiating effects of ascorbic acid appear to follow a similar signaling pathway as the one mediated by calcium, although, unlike calcium, ascorbic acid-associated differentiation is accompanied by an enhanced ascorbate transport and a prevention of hydrophilic antioxidants' depletion [80, 81].

Optimization of 3D-CCs for the development of HSE

Self-constituted cornification media that commonly used for 3D skin culture are still not serum- and animal component-free. They contain bovine calf serum (BCS) or foetal calf serum (FBS) and $CaCl_2$, along with the above mentioned vital growth factors as medium

constituents, namely L-glutamine, adenine, cholera toxin, progesterone, triiodothyronine (T3), PES (O-phosphorylethanolamine + ethanolamine + selenium), transferrin, EGF, hydrocortisone, O1O medium, Ham's F-12 supplements, etc. [1, 63].

Apart from presenting challenging safety issues in clinical applications, the "serum presence at ALI" has reported to impair the terminal differentiation of keratinocyte [82]. In this study, we gradually moved on commercially available media from low-/no-serum to serum-free and animal component-free cell culture media to optimize HSE development. In this work, we studied the differences in tissue morphogenesis when different 3D-CCs based on cell culture media and physical parameter of ALI were applied. Different 3D-CCs namely (-I, -II, -III, -IV) based on commercially available cell culture media are summarized in Table 4.2. ALI was also optimized by comparing the tissue morphogenesis of HSCs obtained from different air-lifts of 10, 15 and 20 days. Figure 4.5 outlines the overview of 3D-CC optimization.

KGM2, a serum-free medium containing 0.06mM $CaCl_2$, was used with keratinocytes at submerged culture conditions (3D-CC-I) and was then supplemented with increased $CaCl_2$ of 1.2mM during air-lift phase [83]. CnT-Prime media are fully-defined and animal component-free media without cholera toxin. The basal CnT medium such as CnT-PR is supplemented with $CaCl_2$ concentration of 0.07mM and a range of progenitor cell treated (PCT) growth factors to extend longevity, and co-factors to improve growth factor binding to membrane-bound receptors. However, the CnT prime media for 3D culture such as CnT-PR-3D and CnT-FTAL contains elevated levels of calcium concentration of 1.2mM. Also, it does not contain PCT growth factors, or other proliferative factors that retard differentiation and thus provides maximal differentiation and increased barrier function [62].

4.3.4 Tissue morphogenesis of HSCs

Tissue morphogenesis in 3D-CC-I and 3D-CC-II

Figure 4.7and Figure 4.8 showed histological images of HSCs obtained using 3D-CC-I and 3D-CC-II. Two structurally distinct compartments epidermis and dermis are present. Epidermis was comparatively better organized in 3D-CC-II than in 3D-CC-I which on the contrary displayed larger gaps between the layers (Figure 4.7). Among some examples of pathological conditions, cells nests formation in dermis depicts malignant behaviour of melanocytes [84], as it happens in early tumour invasion *in vivo* with the melanoma cells getting into dermis through invading the basement membrane [85]. Another example is the formation of thickened scaly skin plaques due to hyperplasia that is an indication of psoriatic skin and is histologically seen as spongiform micropustules and elongated rete ridges [86]. The presence of wide interlayer spaces is one of the abnormal skin appearances and should be avoided to obtain a better morphogenesis with

healthy skin. Furthermore, Figure 4.8 also showed that under 3D-CC-II, the epidermal layers were better organized at air-lift for 15 days than at air-lift for 10 days.

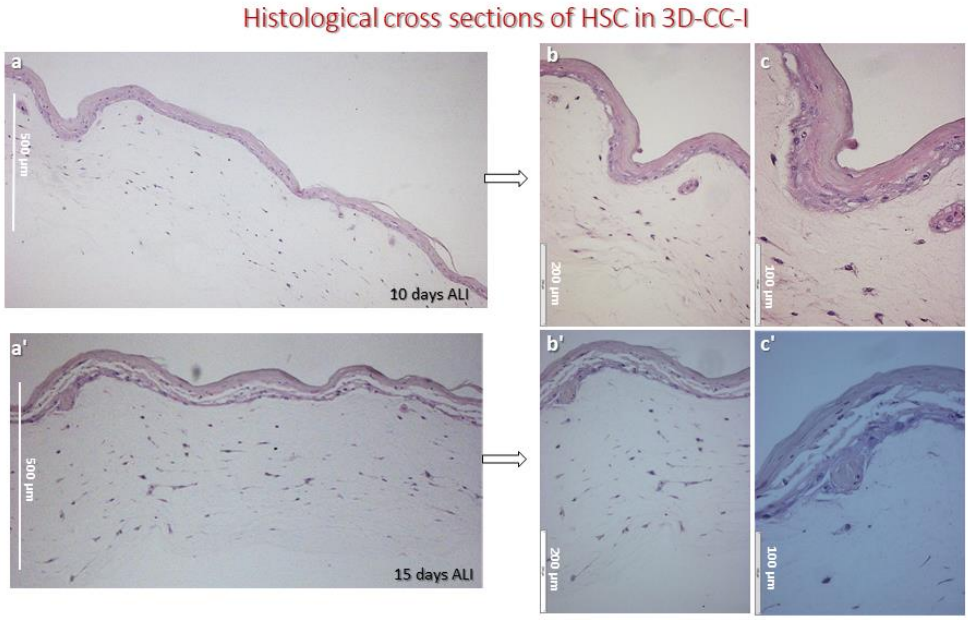

Figure 4.7 Histological cross sections of HSC in 3D-CC-I. Upper panel and lower panel (images at different magnifications) showed H & E stained histological micrographs of HSCs raised for 10 days and 15 days at ALI, respectively.

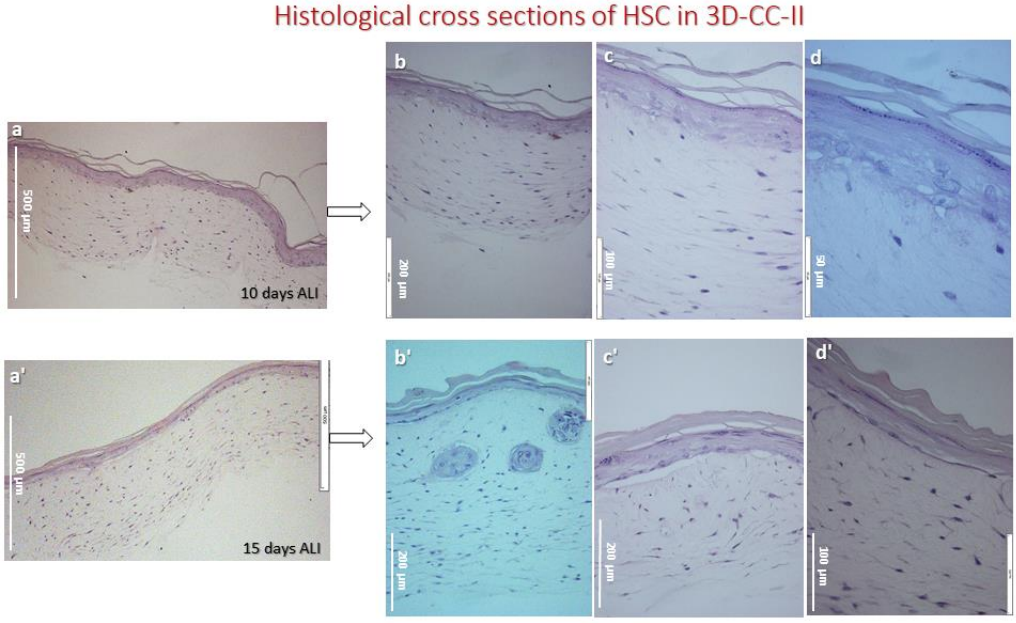

Figure 4.8 Histological cross sections of HSC in 3D-CC-II. Upper panel and lower panel (images at different magnifications) showed H & E stained histological micrographs of HSCs raised for 10 days and 15 days at ALI, respectively.

ALI is a condition exposing the skin cells located at this interface to atmospheric air, that determines spatial organization behaviour and architectural features of HSE as seen *in*

vivo [87, 88]. Exposure to ALI enables keratinocytes to differentiate and recapitulate the morphological as well as biochemical processes of native human epidermis [88]. In this study, we observed that cultures for an extended period at ALI comparatively demonstrated better morphological and biochemical differentiation in terms of tissue differentiation, organization, and stratification.

Tissue morphogenesis in 3D-CC-I and 3D-CC-IV

To optimize the HSE development, among the possible culture conditions, CnT-PR-3D medium is recommended for 3D "epidermal" models at air-lift phase. However, CnT-FTAL is recommended to use during air-lift phase of "Dermal-Epidermal full-thickness skin model" to promote "ECM secretion" by fibroblasts. However, we found comparatively better tissue morphogenesis with "CnT-PR-3D" for developing "full-thickness" skin model than with the company (CELLnTECH) recommended medium for "full-thickness" model named "CnT-FTAL". Figure 4.9 and Figure 4.10 showed the results as histological images of HSCs obtained from 3D-CC-IV and -III respectively. We found well-organized, well-differentiated epidermal formation and best tissue morphogenesis under 3D-CC-III (based on CnT-PR-3D) than under 3D-CC-IV (based on CnT-FTAL).

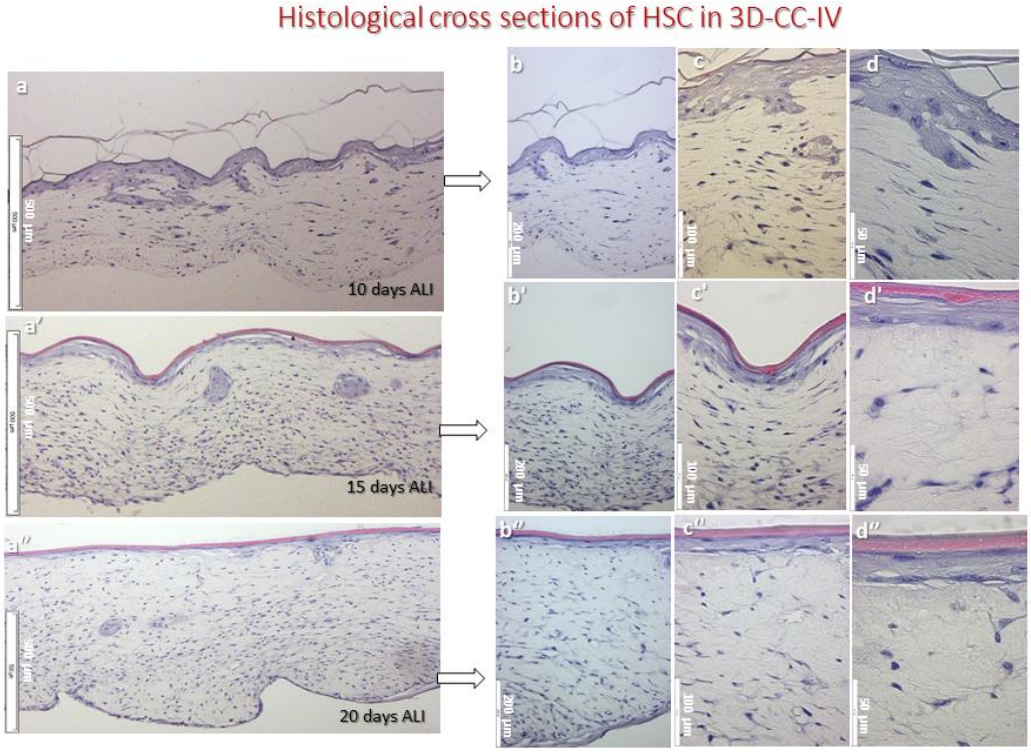

Figure 4.9 Histological cross sections of HSC in 3D-CC-IV. Upper, middle, and lower panels (images at different magnifications) showed H & E stained histological micrographs of HSCs raised for 10 days,15 days, and 20 days at ALI, respectively.

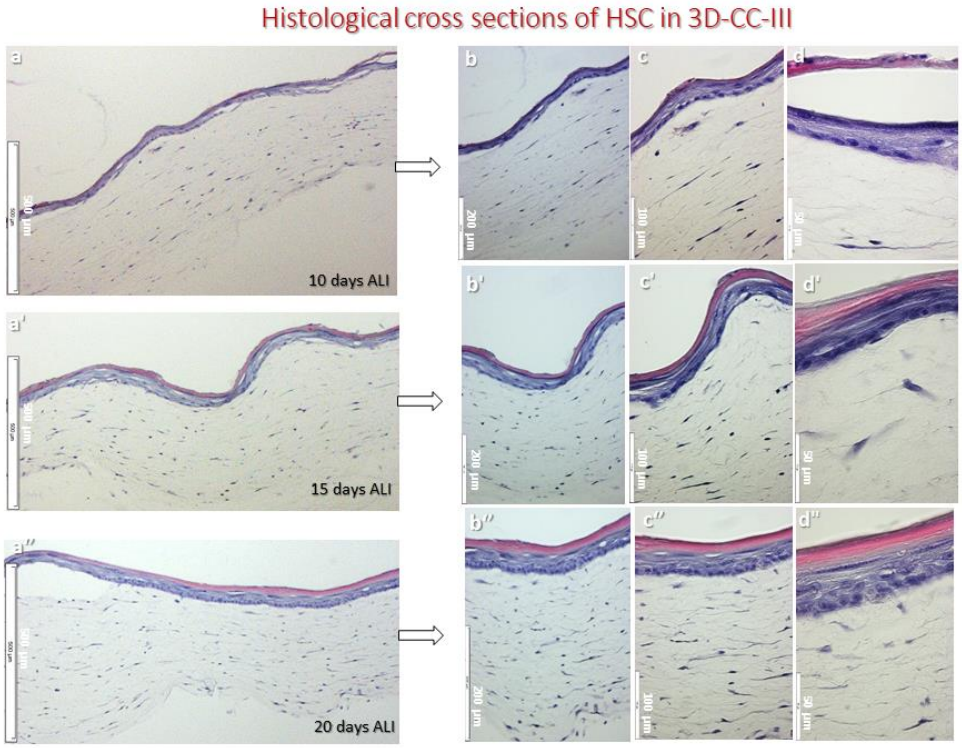

Figure 4.10 Histological cross sections of HSC in 3D-CC-III. Upper, middle, and lower panels (images at different magnifications) showed H & E stained histological micrographs of HSCs raised for 10 days, 15 days and 20 days at ALI, respectively.

Among the tested conditions, best results were obtained under 3D-CC-III and at air-lift for "20 days" with the most closely mimicking epithelial differentiation as found in healthy human skin. Hence this HSC was termed as human skin equivalent (HSE) (Figure 4.11). The innermost cells of the basal layer have the capacity for DNA synthesis and mitosis. Upon a trigger of terminal differentiation, the basal cells begin their journey to the surface, undergoing a series of morphological and biochemical changes associated with the sequential appearance of epidermal layers and subsequent expression of differential markers. The epidermal part showed well differentiated layers of keratinocytes namely stratum basale (SB), spinosum (SS), granulosum (SG), and corneum (SC) (Figure 4.11).

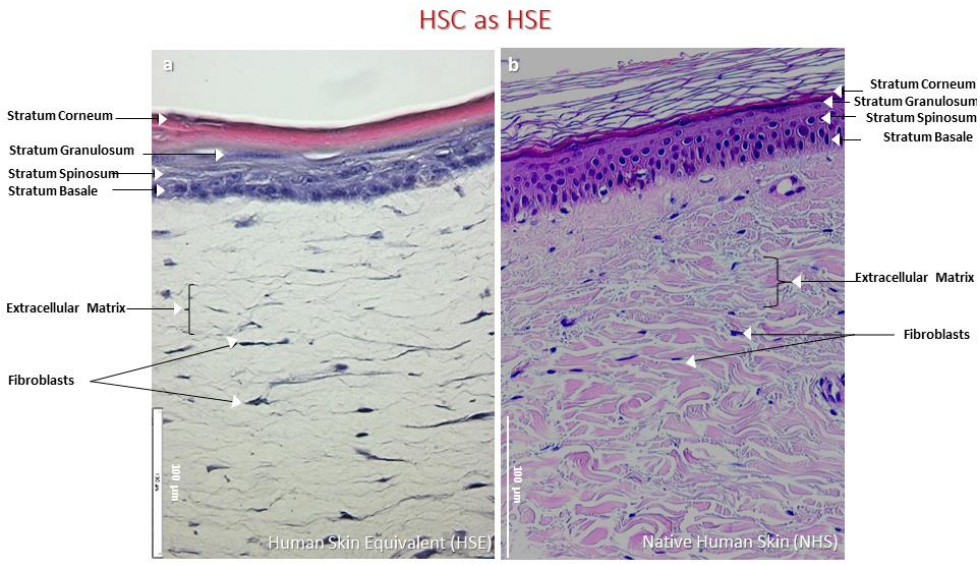

Figure 4.11 HSC as HSE. H & E stained histological image of HSC obtained from (a) 3D-CC-III was able to best recapitulate epidermal differentiation, morphogenesis and organization as found in (b) NHS (origin: human leg) and thus named as HSE. HSE showed two structurally distinct layers of skin the outer epidermal layer, and the underlying thicker dermal layer. The epidermal part showed well differentiated layers of keratinocytes namely stratum basale, spinosum, granulosum, and corneum. The staining differences regarding the visualization of NHS (as compared to HSE) were due to H & E protocol followed to stain NHS in Institute of Pathology, Ruhr University Bochum, Germany, where the NHS tissue was obtained from.

4.3.5 Epidermal thickness and DEJ Length

The thickness of skin varies depending upon its location in the body. The average epidermal thickness is 0.1mm (renewing itself approx. every 28 days); Whereas the average dermal thickness is about 2mm (upper papillary dermis being thinner, and the reticular dermis being thicker) [89]. The total thickness of stratified layers of the epidermis was found statistically different between culture condition III (0.060±0.002mm) and culture condition IV as (0.040±0.003mm) (P=0.022, *) (epidermal thickness indicated as white lines Figure 4.12).

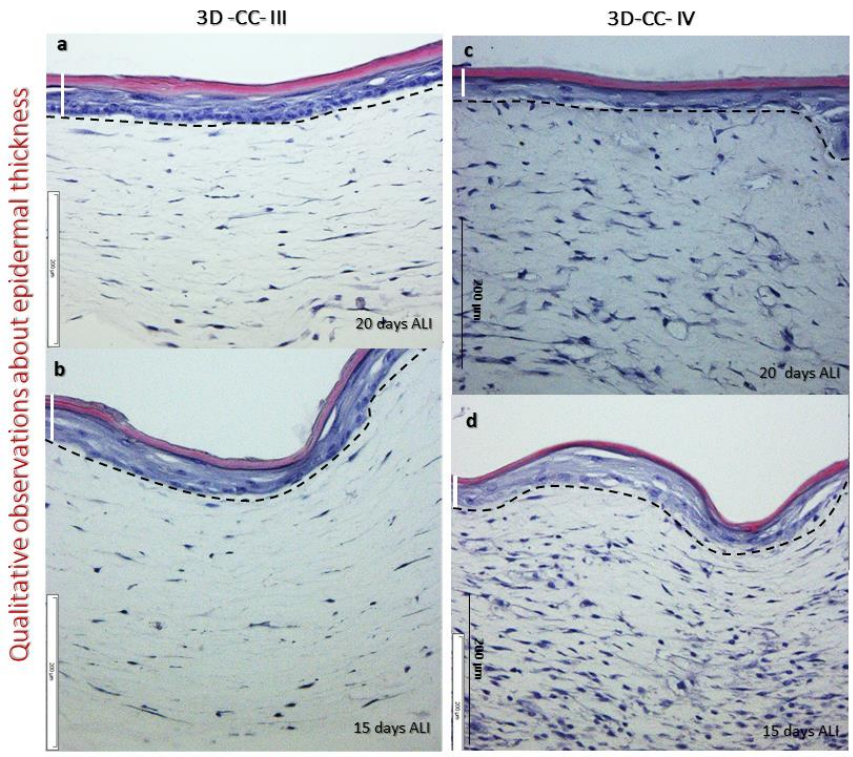

Figure 4.12 Qualitative observations about thickness of stratified epidermis. The values measured for HSE in 3D-CC-III and 3D-CC-IV were 0.060±0.002mm and 0.040±0.003mm with a statistically significant difference of P=0.022 (*) in the epidermal thickness values obtained from these two different culture conditions. But no statistically significant difference was found in epidermal thickness obtained from different incubation periods at ALI. The measurement scale was calibrated using the micron scale of each image.

From a morphological point of view, we observed that contact interface between dermal and epidermal surface was not straight but undulated as in human skin. This dermal epidermal convoluted interface appeared flatter at highest air-lift (i.e. 20 days) than lower air-lift periods. Furthermore, this DEJ interface also appeared comparatively flatter in 3D-CC-IV than in 3D-CC-III. However, there was no statistically significant difference in the calculated length of DEJ either between two culture conditions (1.31±0.001mm in culture condition III and 1.32±0.007mm in culture condition IV); or between two ALI time periods of 15 or 20 days (DEJ length indicated as black dotted lines in Figure 4.13).

Other visible observations include the presence of slight epidermal invaginations-like structures (that under *in vivo* situation is termed as characteristic rete ridge) in case of 3D-CC-IV at air-lift for 20 days (indicated by white arrows in Figure 4.13 d). The rete ridge morphology was observed once in one of the organotypic skin models that was built using acellular dermis (human biopsy) as a supporting connective tissue for epidermis [90].

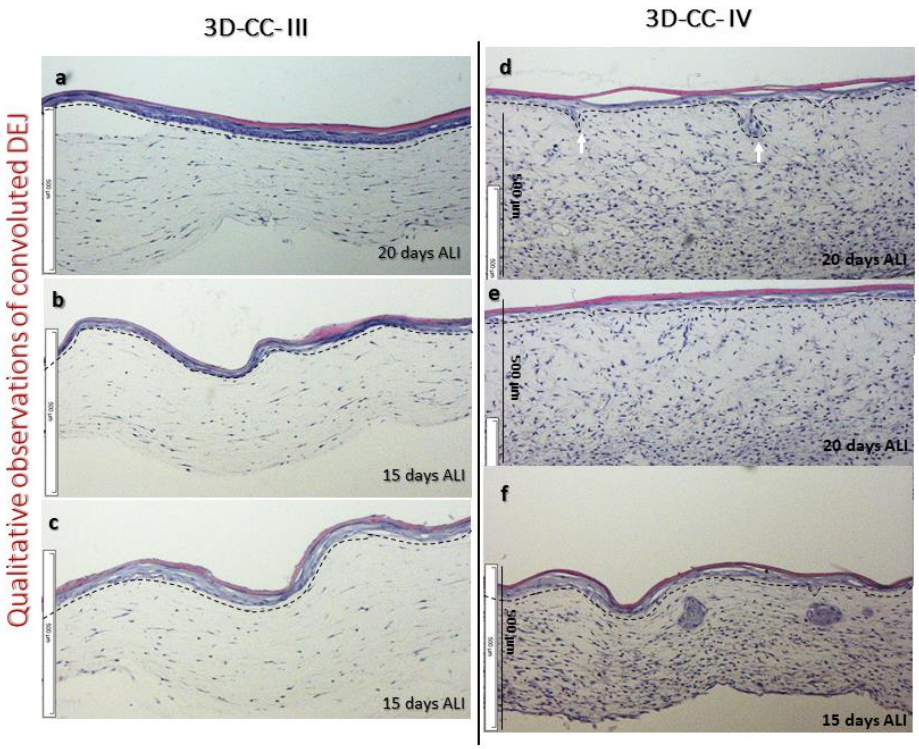

Figure 4.13 Qualitative observations of convoluted DEJ. Length of DEJ measured for HSE in 3D-CC-III is 1.31±0.001mm; and length of DEJ measured for HSC in 3D-CC-IV is 1.32±0.007mm with no statistically significant difference. DEJ values obtained from three different incubation periods at ALI did not change either. The measurement scale was calibrated using the micron scale of each image.

4.3.6 Connective tissue and dermal fibroblasts density in HSE

As supposed, under 3D-CC-IV, the result showed higher number of fibroblasts due to fibroblasts proliferation and thus high levels of ECM secretion by fibroblasts (Figure 4.9). Masson's Trichrome (TRI) staining is used to study histopathological situation in wound healing conditions, to evaluate collagen re-organization and density (together with image analysis and polarized light microscope) [91]. Besides, highlighting collagen formation and amount of collagen deposition, TRI staining is also used to demonstrate fibroblast proliferation and reepithelialisation process in wound healing [91-93]. The TRI stained HSCs histological cross sections confirmed more collagen formation, showing more green stained connective tissue (Figure 4.14 b) in 3D-CC-IV (based on CnT-FTAL) than in 3D-CC-III (based on CnT-PR-3D) (Figure 4.14 a). Moreover, presence of more brown dots in HSC dermis under 3D-CC-IV (Figure 4.14 b), also demonstrated that CnT-FTAL promotes fibroblasts proliferation and thus ECM production. Therefore, the use CnT-FTAL is recommended in HSC development without the need of exogenous collagen matrix. Dermal fibroblasts density in 3D-CC-III (Figure 4.14 a) was comparatively optimal and better comparable to the cell density observed in the dermis of NHS (Figure 4.11 b).

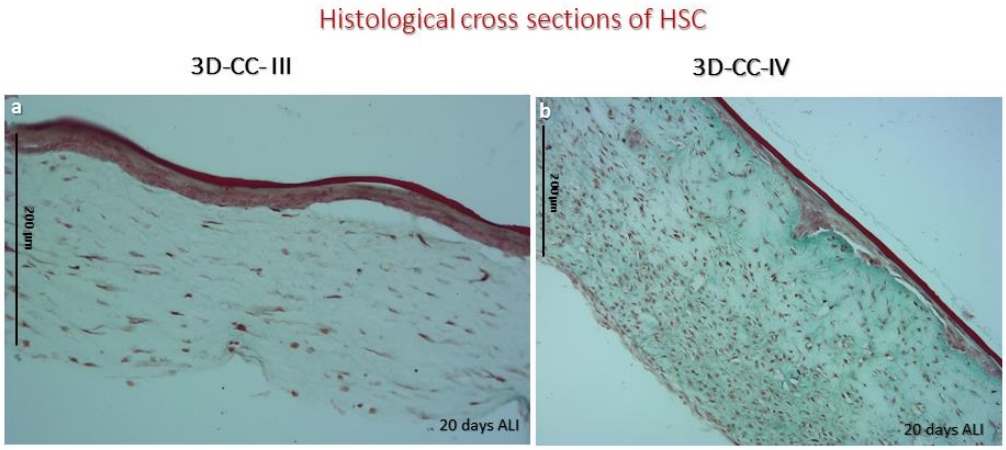

Figure 4.14 TRI stained histological cross sections of HSC. The histological micrographs showed HSE in 3D-CC-III (a) and HSC in 3D-CC-IV (b), both raised for 20 days at ALI. TRI stained connective tissue green, cytoplasm red and nuclei as dark brown.

4.3.7 IHC analysis of HSE

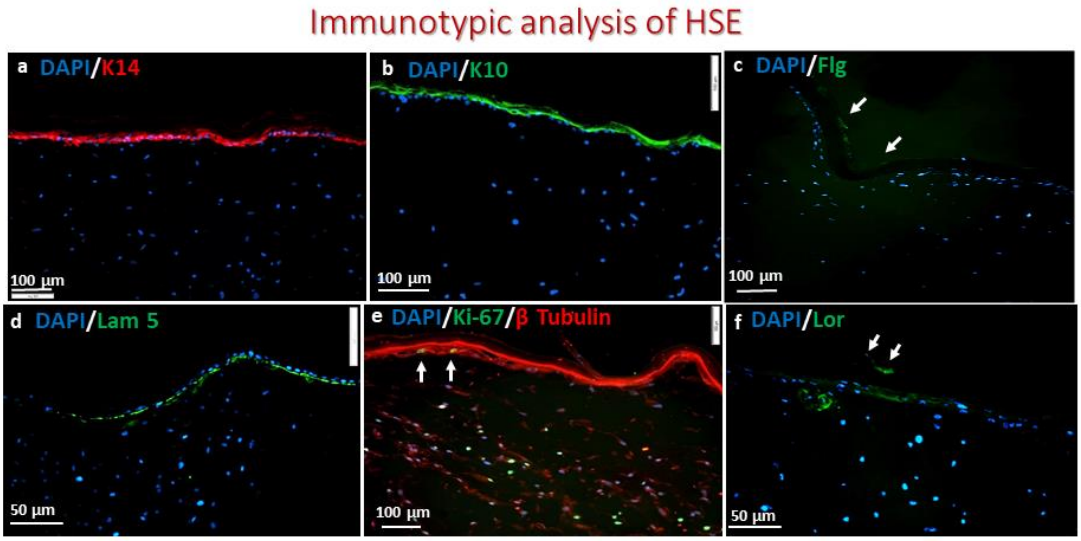

Figure 4.15 Immunotypic analysis of HSE. IHC characterization of HSE showed immunolabelling for specific epidermal differentiation markers namely (a) Keratin 14 (K14) red, (b) Keratin 10 (K10) green, (c) Filaggrin (Flg) green, (d) Laminin 5 (Lam 5) green, (e) Ki-67 green, and (f) Loricrin (Lor) green. Cell nuclei were shown in blue by using DAPI staining and microtubules in cytoplasm were shown in red using β Tubulin staining (e).

Epidermal differentiation in HSE

Describing the sequential expression of differential markers, cytokeratins K5 and K14 are expressed in the mitotically active cells in stratum basale (SB). When these cells leave the SB and enter the differentiation program, they become postmitotic, downregulating K14 mRNAs expression and switching to expression of another set of keratins from K5/K14 to suprabasal keratins K1/K10 in the stratum spinosum (SS). These changes in keratin expression pattern (and keratin pair expression) are particularly

important and provide precise functional requirements to epidermal keratinocytes [94]. Moreover, the expression of differentiation-specific keratins also causes keratin filament network's reorganization resulting in denser bundle formation [95]. In more detail, cells from inner layers of the epidermis have small keratins (46-58K), while the cells from the outer layers also contain large keratins (63-67K) [96]. These changes in keratin composition and synthesis occur during the course of terminal differentiation. Moreover, the keratins for the outermost layer must be synthesized earlier that are then processed post-translationally during the final phases of differentiation, as there is no synthesis happening in stratum corneum (SC) [96].

Immunohistochemistry (IHC) characterisation of HSE (Figure 4.15 a, b) showed results for specific epidermal differentiation markers. Cytokeratin-14 (K14) expressed by epithelial cells (EPCs) in basal layer (Figure 4.15 a) while the suprabasal layers displayed the presence of cytokeratin-10 (K10) (Figure 4.15 b). Both keratins being members of intermediate filaments (IF) superfamily; together with actin microfilaments and microtubules, constitute the cytoskeleton of EPCs.

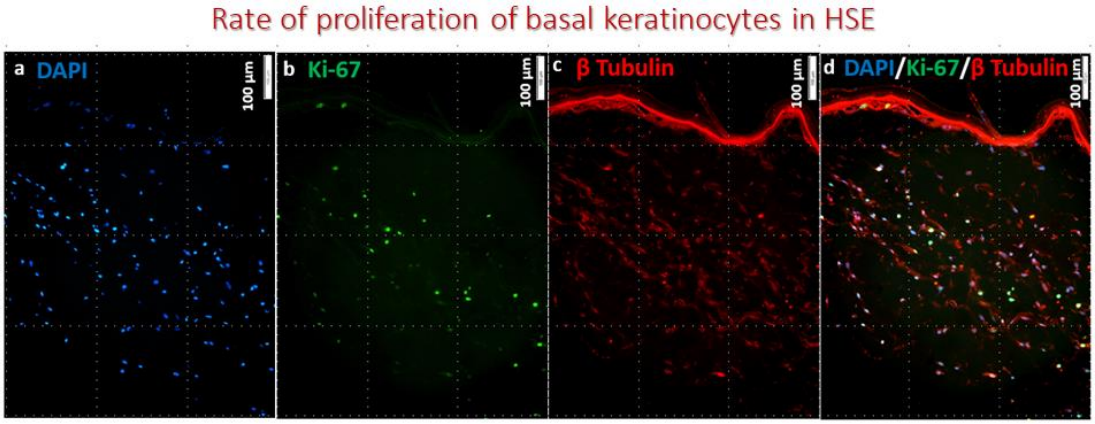

Figure 4.16 Rate of proliferation of basal keratinocytes in HSE. IHC analysis of HSE showed immunolabelling for Ki-67 green. Cell nuclei are shown in blue by using DAPI staining and microtubules in cytoplasm are shown in red using β Tubulin staining. Images (a, b, c) were taken from the same microscopic field. while image (d) represents a merged image of blue, green and red signal. Percent of Ki-67 positive basal keratinocytes were measured as 10.50±0.78%.

Proliferative state of basal keratinocytes in HSE

Ki-67 is a cellular marker for proliferation, is present during all active phases of the cell cycle and is absent in quiescent (G_0) cells. The Ki-67 antigen can be exclusively detected within the cell nucleus (during interphase; relocated on chromosomes during mitosis). Cells in basal layer were found positive for Ki-67 (arrows), demonstrating an active state of proliferation (Figure 4.15 e, Figure 4.16 b). Our HSE displayed 10.5±0.78% of Ki-67 positive basal keratinocytes (Figure 4.16) that is highly comparable to the *in vivo* proliferation rate of 10–12% measured by Ki-67 expression in the stratum basale of NHS [97].

Terminal differentiation in outer layers of HSE

Cells in stratum spinosum (SS) also produce "involucrin" (cornified envelope component) and transglutaminase-K (enzyme responsible for crosslinking of involucrin in stratum corneum (SC) [98, 99]. The stratum granulosum (SG) has electron-dense keratohyalin granules containing profilaggrin (precursor of "filaggrin"), and the smaller granules contain "loricrin" (Lor) that is a major constituent of cornified envelope [100, 101]. During terminal differentiation of EPCs, filaggrin (Flg) is post-translationally produced from a large profilaggrin precursor protein. Flg is a filament-aggregating protein that connects keratin fibres by promoting disulfide-bond formation among the intermediate filaments. The terminal differentiation of epidermis was demonstrated by the spotted expression of Flg (arrows) in the granular layer (SG) (Figure 4.15 c). Lor, a major protein component of cornified envelope, also showed spotted expression (arrows in Figure 4.15 f) in SC and is a marker of terminally differentiated epidermal cells.

Basement membrane in HSE

The stable attachment of the epidermis to the dermis is provided by DEJ suggesting the presence of basement membrane. The epidermal basal cells connect to papillary dermis through anchoring filaments of hemidesmosomes. The proteins within the anchoring complex provide links to both the intracellular cytoskeletal keratins in keratinocytes and connective tissue proteins of the papillary dermis. Laminins, a family of ECM glycoproteins are major non-collagenous components of basement membranes. Laminin 5 (Lam 5) is a key component of this anchoring complex that initiates hemidesmosome formation in the basal lamina (one of the layers of basement membrane), and also has an important role in accelerating the assembly of basement membranes as well as enhancing the recovery of damaged skin [102]. Lam 5 was expressed at DEJ as a thin continuous line (Figure 4.15 d) suggesting stable epidermal-dermal interaction.

Activated state of HSE

HSE displayed a complete morphological differentiation and similar biochemical features respect to *in vivo* skin. However, it showed higher proliferation of keratinocytes with respect to native human skin. When keratinocytes are cultured *in vitro*, they are very responsive to external growth stimuli. Additionally, HSE formation is a de-novo development, with cells undergoing a re-epithelialization process (a process happening upon wounding *in vivo*) [1, 103], causing them to stay in an activated phase. The effect is a hyperproliferative stimuli [104, 105]: where K1/K10 expression is considerably reduced and K6/K16 normally absent in interfollicular epidermis, is induced. The occurrence of this phenomenon is suggested by the expression of K16 in basal layer (Figure 4.17). Another phenotypic difference associated with *in vitro* grown skin is the expression of integrin receptors (α_v integrins) that are not expressed in skin under normal conditions but are constitutively expressed *in vitro* in keratinocytes to form HSEs [1].

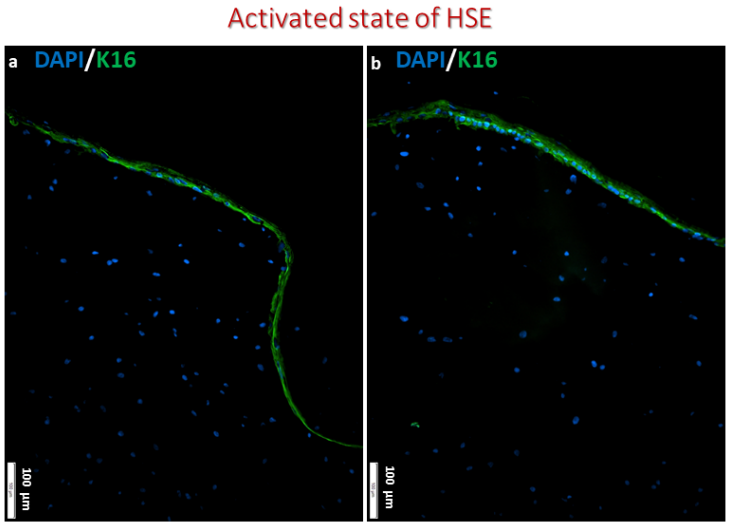

Figure 4.17Activated state of HSE. IHC analysis of HSE showed immunolabelling for epidermal activation marker Keratin 16 (K16) green. Cell nuclei were shown in blue by using DAPI staining.

4.3.8 Comparison of Immunoreactivity among different 3D-CCs

Differences in epidermal differentiation in HSC in 3D-CC-III at air-lift for "15 days" vs. "20 days"

IHC analysis for cytokeratins was performed for HSC at air-lift for "15 days" (obtained from 3D-CC-III), and the results demonstrated that K14 and K10 were expressed by EPCs in basal layer (Figure 4.18 a) and suprabasal layers (Figure 4.18 b) respectively, but in this case, the expression was lower than that of HSE at air-lift for "20 days" (Figure 4.15 a, b). These results are very important in highlighting the role of "longer air-lift phase" on tissue morphogenesis and differentiation.

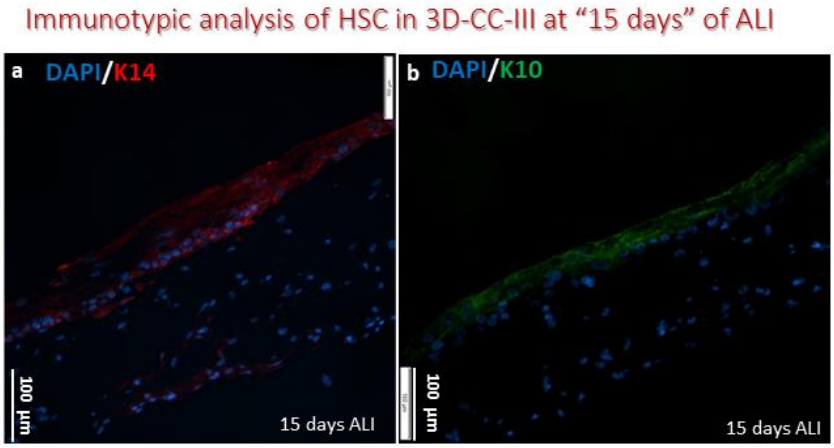

Figure 4.18 Immunotypic analysis of HSC in 3D-CC-III at 15 days of ALI. IHC analysis of HSE showed immunolabelling for specific epidermal differentiation markers, namely (a) Keratin 14 (K14) red, and (b) Keratin 10 (K10) green. Cell nuclei were shown in blue by using DAPI staining.

Differences in epidermal differentiation in HSC in 3D-CC-IV vs. 3D-CC-III

IHC analysis for cytokeratins was also performed for HSC obtained from 3D-CC-IV at ALI for 20 days, and the results demonstrated that K14 and K10 are expressed by EPCs in basal layer (Figure 4.19 a) and suprabasal layers (Figure 4.19 b), respectively. However, K14 and K10 expression was found comparatively lower than in HSE (3D-CC-III, at air-lift for 20 days) (Figure 4.15 a, b), while Ki-67 was found similarly expressed (Figure 4.19 c) as in HSE (Figure 4.15 e).

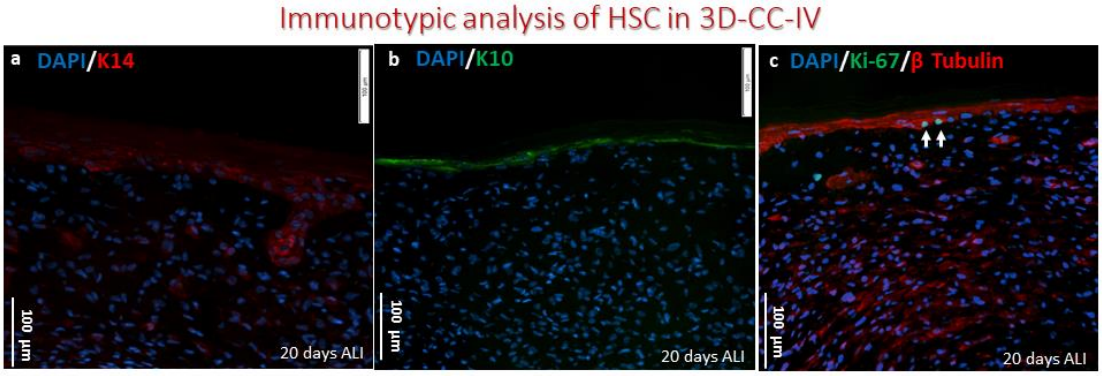

Figure 4.19 Immunotypic analysis of HSC in 3D-CC-IV. IHC analysis of HSE showed immunolabelling for specific epidermal differentiation markers namely (a) Keratin 14 (K14) red, (b) Keratin 10 (K10) green, and (c) Ki-67 green. Cell nuclei are shown in blue by using DAPI staining and microtubule in cytoplasm are shown in red using β Tubulin staining (c).

Normal and abnormal expression of epidermal markers is highly related with the physiological and pathological conditions of skin. For example, a "skin blistering disorder" namely bullous congenital ichthyosiform erythroderma (BCIE) or epidermolytic hyperkeratosis (EHK) is caused by defects in KRT10 gene and histologically seen as diffused epidermolytic degeneration of lower spinous layer in epidermis [106]. Other "skin blistering conditions" involving intraepidermal epidermolysis bullosa named epidermolysis bullosa simplex Dowling-Meara type (DM-EBS), Weber-Cockayne type (WC-EBS), Koebner type (K-EBS), and autosomal recessive (AREBS) are caused by defects in KRT14 [107]. Naegeli-Franceschetti-Jadassohn syndrome (NFJS) and dermatopathia pigmentosa reticularis (DPR) are ectodermal dysplasia conditions, caused by defects in KRT14 [97, 108]. Defects in LOR cause a skin condition with "erythematous plaques" named as progressive symmetric erythrokeratodermia (PSEK) and Vohwinkel syndrome with ichthyosis (VSI) [109]. Therefore, the right level of expression at correct anatomical location is important for defining the morphological and functional characteristics of a tissue. In addition to morphological analysis of histological cross sections (Figure 4.11), IHC results (Figure 4.15) reinforced the choice of HSC obtained from "3D-CC-III" at air-lift for "20days" as "HSE".

4.3.9 Ultrastructure of HSE

TEM was used to investigate the ultrastructure of the HSE. Regarding the dermal compartment, TEM analysis confirm the presence of the embedded fibroblasts in a network of collagen- and immature elastin- based ECM.

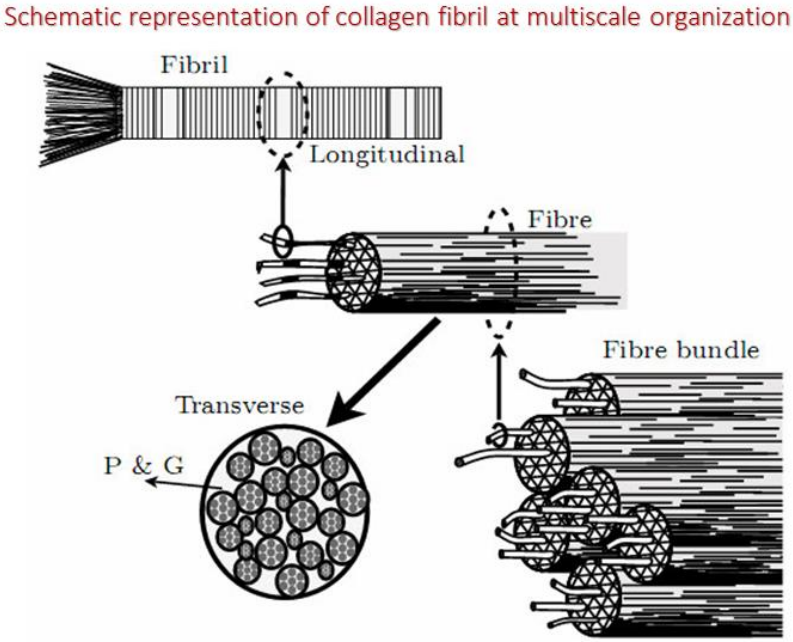

Figure 4.20 Schematic representation of collagen fibril, collagen fibre and fibre bundles in connective tissue. The image [109] has been used with copyright permission.

Collagen fibrils combine each other to form collagen fibres (Figure 4.20). In HSE, collagen formed both fibres and fibrils (Figure 4.21 a, b, c, d) [110] displaying the characteristic banded pattern of with a period of ~65 nm [111]. Elastin was found deposited on collagen fibrils or microfibrils in an amorphous immature form (Figure 4.21 c) [112]. The connection between epidermis and DEJ interface was demonstrated by the presence of hemidesmosomes, connecting basal cells through tonofibrils / keratin filaments and attaching them into dense basal lamina through anchoring filaments (Figure 4.21 a, b). Basal lamina is one of the two layers of basement membrane and is further divided into lamina lucida (LL) and lamina densa (LD) [82]. Regarding the connection of dermis through DEJ, loops of fibrils being perpendicularly arranged to basal lamina, have been reported to anchor into DEJ. They are called oxytalan elastic fibres and their presence suggest a strong cohesion between DEJ and dermal compartment [112].

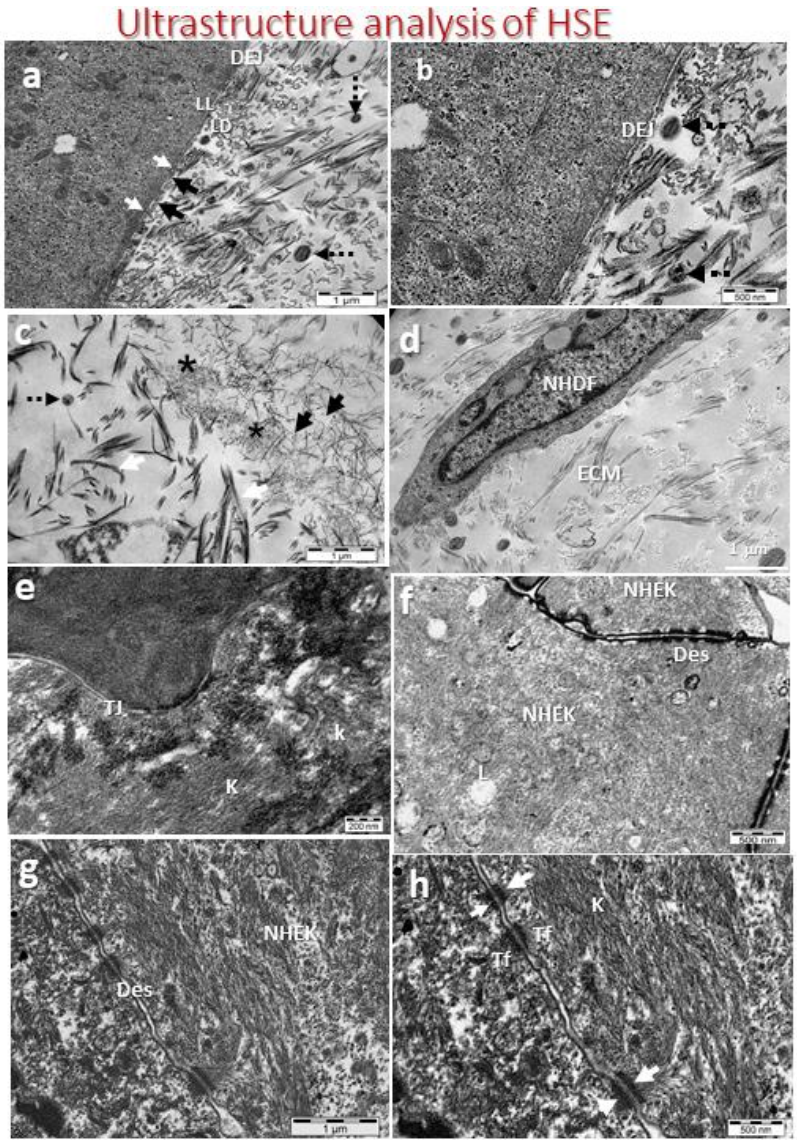

Figure 4.21 Ultrastructure analysis of HSE. TEM images (a, b) revealed DEJ that separates epidermis from the dermis through basement membrane consisting of lamina lucida (LL) and lamina densa (LD). LD was connected with the collagen matrix by loops of anchoring fibrils (black arrows). The hemidesmosomes (white arrows) were connected with tonofibrils (Tf) in keratinocytes. Collagen fibres were shown as black dotted arrows. TEM images (c, d) demonstrated collagen fibrils (Col. I) with their characteristic banded pattern (white arrows). Microfibrils or fibrillins (black arrows) were also secreted by fibroblasts, forming a scaffold that was detected near collagen fibrils. Amorphous or "immature" elastin was secreted and aggregated (asterisks) on microfibrils. Collagen fibres (black dotted arrow) appeared when collagen fibrils combined to form fibres. Normal Human Dermal Fibroblasts (NHDF) were also seen as embedded in ECM. In TEM images (e, f, g, h) epidermis showed TJ between the keratinocytes. Keratinocytes showed abundant intracellular filament of keratins and upper epidermal layers showed lipid droplets (L). Tonofibrils (Tf) in keratinocytes (NHEK) were made of tonofilaments (keratin intermediate filaments), that appear converging to form spot like connections or desmosomes (white arrows).

Regarding the epidermal compartment, we observed abundance of keratins and tonofilaments in keratinocytes, tight junctions (TJ), and lipid (L) droplets in stratum

granulosum (SG) (Figure 4.21 e, f, g, h). *In vivo*, SG contains lamellar bodies and lipid-containing vesicles (as observed in Figure 4.21 f) that secrete lipid content into the connection between SG and SC [113]. The matured outermost layer (SC) is a cornified envelope around bundled keratin filaments which is adherent to the lipid envelope contributed by the SG resulting in an impermeable covering protecting the lower layers [114]. Results also demonstrated the presence of Desmosomes (Des) as spot-like connections for cell-to-cell adhesion of keratinocytes (Figure 4.21 f, g, h). Des enable the skin to bear intense mechanical stresses. Altogether, these findings demonstrated complex ECM network organization (though immature) of HSE dermal compartment, epidermal differentiation, and DEJ maturation (Figure 4.21).

4.3.10 Tissue architecture (SEM) of HSE

Histological analyses highlighted the typical elongated morphology of NHDF (Figure 4.11 a). SEM images confirmed the presence of embedded fibroblasts, with dendritic extensions lying along dense matrix of collagen fibres (Figure 4.22 b). ECM of the dermal compartment of HSE demonstrated the typical interwoven network morphology and architecture (Figure 4.22 a). Indeed, the average diameters of microfibril, collagen fibril, and collagen fibre calculated from multiple TEM images (n=3) were 26±21nm; 65±57nm; and 157±10nm respectively. Fibril-associated molecules on the surface of collagen fibrils play an important role in controlling interactions between the fibrils, and thus the relative frequency of collagen bundles' diameters. ECM showed thinner collagen fibres than mature collagen bundles suggesting an immature state of the dermal compartment [115, 116].

SEM images also showed that epidermal layers become increasingly flattened when approaching SC (Figure 4.22 c, d, e, f). The basal and suprabasal layers of keratinocytes were continuous with less flattened morphology (Figure 4.22 c). When keratinocytes are cultured *in vitro* to develop 3D tissue, one of the main issues is the limited longevity of keratinocytes due to the long culture time at ALI (e.g. two to three weeks). The surface layers of developed epidermis become very thick because of their inability to desquamate causing the compression of the lower layers as observed in SEM results (Figure 4.22 c, d). *In vivo*, the normal desquamation happens unnoticeably: keratinocytes mature moving from SB to SG in 14 days, then they are shed off [117].

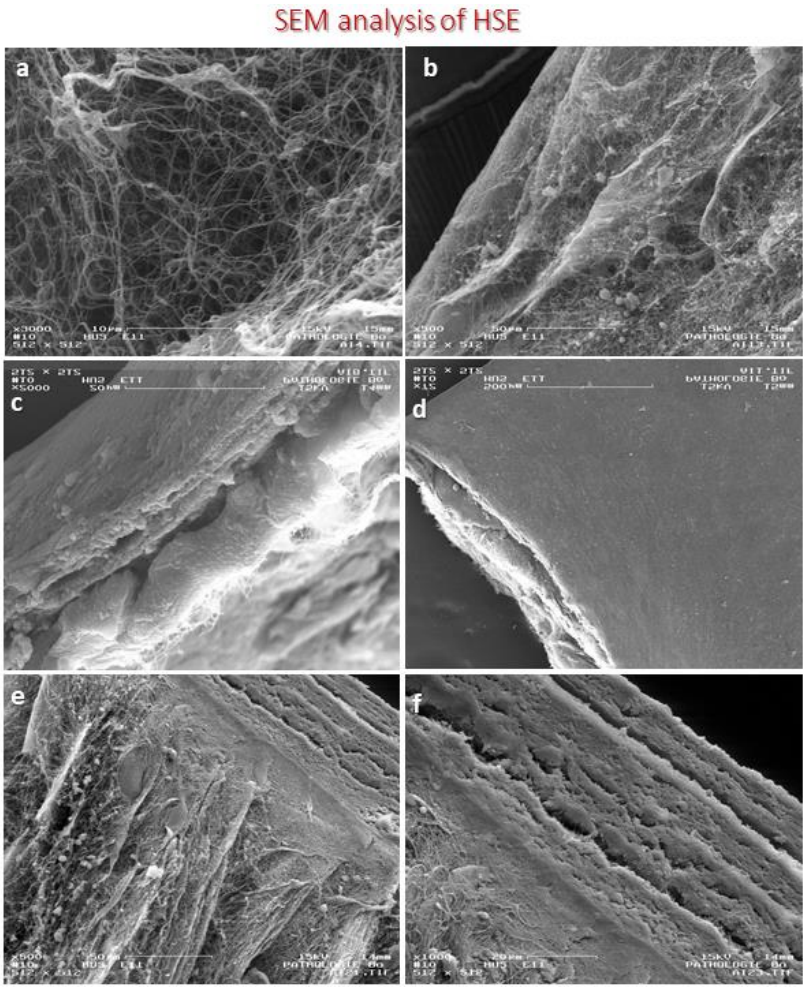

Figure 4.22 SEM analysis of HSE.(a, b) SEM images of dermal compartment of HSE showed ECM with a typical interwoven network morphology and architecture with embedded dermal fibroblasts lying along dense matrix of collagen fibres. (c, d, e, f) Epidermal layers of skin were increasingly flattened as they move to the surface to form SC. The inner layers of keratinocytes were continuous with less flattened morphology.

4.3.11 ECM proteins in dermal compartment of HSE

Dermal ECM contains many components secreted by dermal fibroblasts including collagen, elastin, laminin, fibronectin, and hyaluronic acid. IHC was performed for laminin and results demonstrated that human dermal fibroblasts actively produced laminin, that was detected as fainted spots around the fibroblasts (Figure 4.23). Hence, cells provided a physiological environment by depositing ECM molecules.

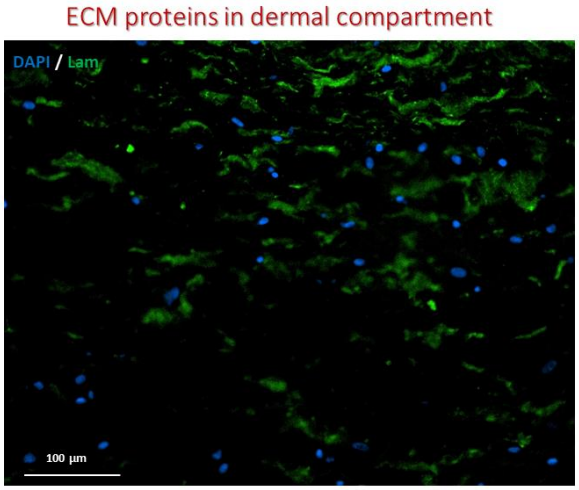

Figure 4.23 ECM proteins in dermal compartment. IHC analysis of HSE showed immunolabelling for one of the ECM proteins laminin in green. Cell nuclei are shown in blue by using DAPI staining.

4.3.12 Proliferative state of dermal fibroblasts and homeostatic equilibrium in dermis of HSE

Another important aspect in 3D cultures is the presence of homeostatic equilibrium that depends on collagen remodelling as well as proportion of proliferative vs. non-proliferative dermal fibroblasts [118, 119]. Collagen remodelling equilibrium can be calculated as degree of collagen assembly indicating the assembled fraction of collagen network. In this study IHC analysis was performed for calculating immunoreactivity of dermal fibroblasts for Ki-67 to demonstrate their active proliferation status. The percentage of Ki-67 positive dermal fibroblasts we calculated was 24.7±7.8%, indicating their proliferative potential (Figure 4.24 & Figure 4.24). This value was not statistically different from the literature value 24.9±6.2% for endogenous human dermal equivalent where dermal fibroblasts secreted their own ECM to constitute dermal microtissues [120].

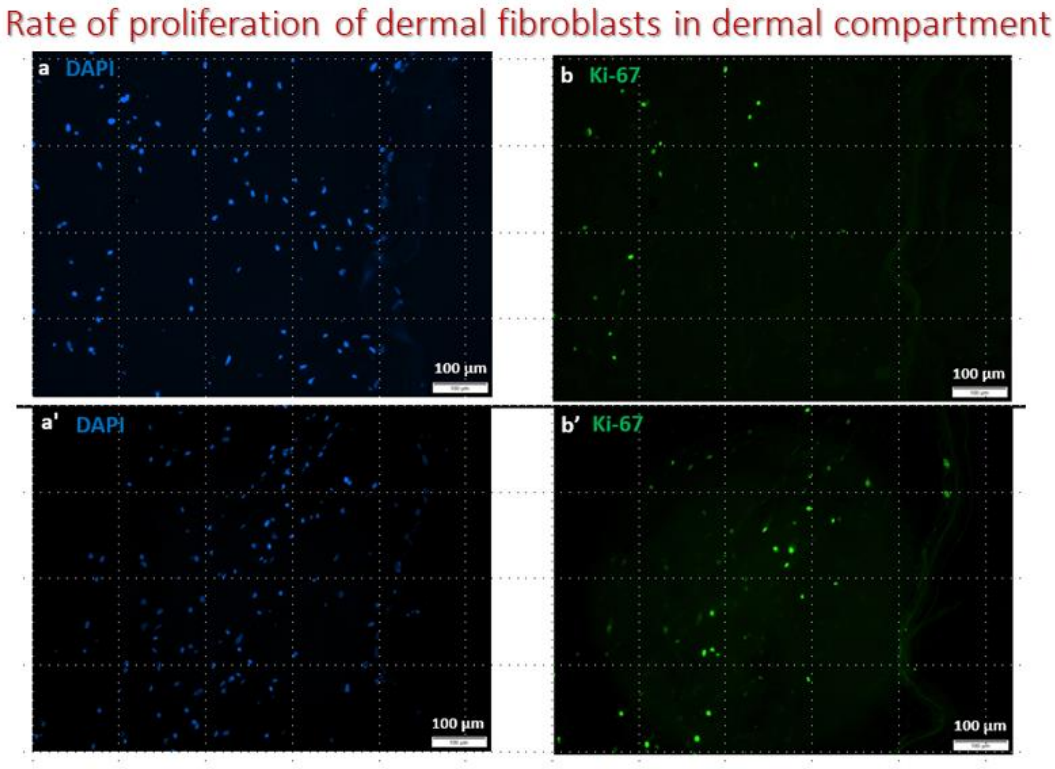

Figure 4.24 Rate of proliferation of dermal fibroblasts in dermal compartment. IHC analysis showed immunolabelling for Ki-67 in green. Cell nuclei are shown in blue by using DAPI staining. Images in (a, b) and (a', b') panels are representing two different microscopic fields. Percentage of Ki-67 positive dermal fibroblasts was 24.7±7.8%.

The proliferative behaviour of fibroblasts explained the non-contraction behaviour of HSE during epidermis formation. It was experimentally observed that HSE retained its size and shape during epidermal development on the top of HDC (Figure 4.2 b & Figure 4.3 c).

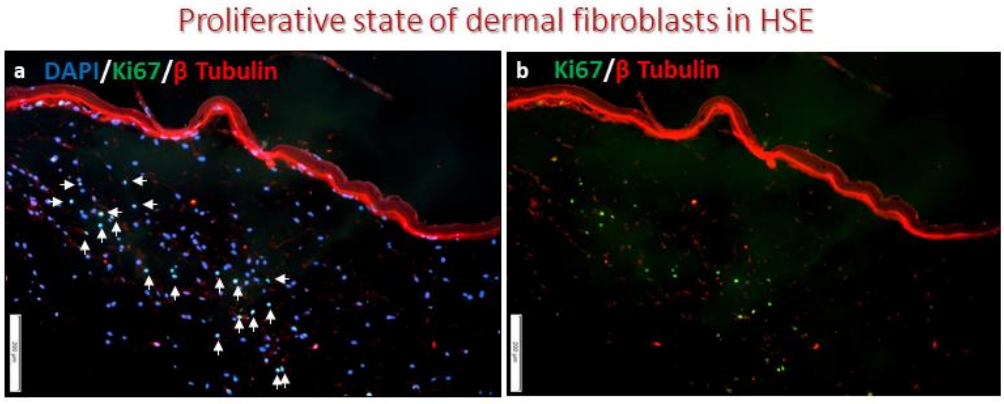

Figure 4.25 Proliferative state of dermal fibroblasts in HSE. IHC analysis showed immunolabelling for Ki-67 green (white arrows). Cell nuclei were shown in blue by using DAPI staining and microtubules in cytoplasm were shown in red using β Tubulin staining. Images (a) and (b) are the same microscopic field.

4.3.13 Barrier function properties of HSE

An important interest associated with well-developed SC is the skin barrier function. This functionality was evaluated by measuring the surface wettability of HSE that is highly related with physiological surface properties of skin. The static contact angle value of HSE was 82.5±8.9° (Table 4.5 and Figure 4.26) that was highly comparable to the value (90.0±5.1°) reported for NHS [120]. This result is in agreement with other results obtained by TEM and SEM analysis demonstrating that SC (Figure 4.22) had formed providing protection because of tight cell junctions (corneo-desmosomes), lipids sealing intercellular spaces, (Figure 4.21) and intracellular keratin filaments (including filaggrin and degradation products) (Figure 4.15 c, f).

Table 4.5 Barrier Properties of HSE. Static contact angle measurements of HSE vs. NHS[117].*

Type	Contact angle (°)
NHS *	90.0±5.1°
HSE	82.5±8.9°

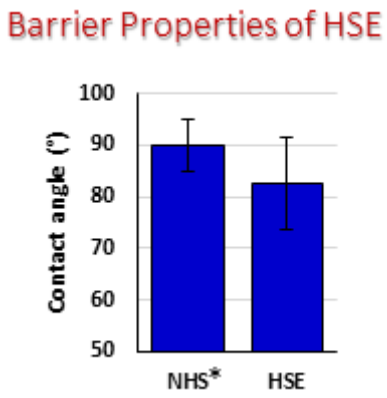

Figure 4.26 Barrier Properties of HSE. Static contact angle measurements of HSE vs. NHS[117].*

Conclusion

In conclusion in this study a dermal-epidermal organotypic model, was tuned by optimizing the 3D cell culture conditions, for presentation of the proper signals to 1) guide cells towards the formation of a well-differentiated and fully-functional epidermal tissue 2) ensure the correct cross-talk signals between dermis and epidermis. Histological results of HSE showed characteristic multi-layered epidermis with well-differentiated layers and immunostaining supported the expression of dermal & epidermal markers at accurate anatomical locations. TEM and SEM revealed ultrastructure features and tissue architecture, respectively. The contact angle demonstrated the barrier function of HSE.

Further experiments on HSE development were recently performed using so-called dermal microtissues as described in Appendix B.

Developed HSE may represent a suitable *in vitro* model for investigations of mechanisms of pathological events, that involve dermis and epidermis interactions. In this regard, our HSE also provides a reliable pre-clinical *in vitro* testing platform for screening novel biomaterials, therapeutics and cosmetics designed to address specific health challenges. It can also be used as allogenic skin graft to fulfil the demand for treating burnt patients or as autologous skin graft by using the patient's own cells.

Moreover, this model represents a fundamental basic construct with the capabilities to add advanced skin features by adding other cell types: e.g. incorporation of Langerhans cells would help this model to serve as a tool for studying skin immunological reactions while the incorporation of skin appendages would help to conduct more reliable drugs/cosmetics penetration studies.

References

1. Carlson, M.W., et al., *Three-dimensional tissue models of normal and diseased skin.* Current protocols in cell biology, 2008. 41(1): p. 19.9. 1-19.9. 17.
2. Green, H., O. Kehinde, and J. Thomas, *Growth of cultured human epidermal cells into multiple epithelia suitable for grafting.* Proceedings of the National Academy of Sciences, 1979. 76(11): p. 5665-5668.
3. Bell, E., et al., *Living tissue formed in vitro and accepted as skin-equivalent tissue of full thickness.* Science, 1981. 211(4486): p. 1052-1054.
4. JM, H., et al., *Grafting of burn patients with allografts of cultured epidermal cells.* Lancet 1983(2): p. 428-430.
5. Rose, J. and D. Herndon, *Advances in the treatment of burn patients.* Burns, 1997. 23: p. S19-S26.
6. Eisenburg, D., *Skin substitutes and wound healing: current status and challenges.* Wounds, 2004. 16: p. 1-17.
7. Coulomb, B., et al., *Advantage of the presence of living dermal fibroblasts within in vitro reconstructed skin for grafting in humans.* Plastic and reconstructive surgery, 1998. 101(7): p. 1891-1903.
8. Atiyeh, B.S. and M. Costagliola, *Cultured epithelial autograft (CEA) in burn treatment: three decades later.* Burns, 2007. 33(4): p. 405-413.
9. De Corte, P., et al., *Feeder layer-and animal product-free culture of neonatal foreskin keratinocytes: improved performance, usability, quality and safety.* Cell and tissue banking, 2012. 13(1): p. 175-189.
10. Astashkina, A., B. Mann, and D.W. Grainger, *A critical evaluation of in vitro cell culture models for high-throughput drug screening and toxicity.* Pharmacology & therapeutics, 2012. 134(1): p. 82-106.
11. Roth, A. and T. Singer, *The application of 3D cell models to support drug safety assessment: opportunities & challenges.* Advanced drug delivery reviews, 2014. 69: p. 179-189.
12. Grainger, D.W., *Cell-based drug testing; this world is not flat.* Advanced drug delivery reviews, 2014. 69: p. vii.
13. Cukierman, E., et al., *Taking cell-matrix adhesions to the third dimension.* Science, 2001. 294(5547): p. 1708-1712.
14. Grinnell, F., *Biochemical analysis of cell adhesion to a substratum and its possible relevance to cell metastasis.* Progress in clinical and biological research, 1976. 9: p. 227-236.
15. Bissell, M.J., H.G. Hall, and G. Parry, *How does the extracellular matrix direct gene expression?* Journal of theoretical biology, 1982. 99(1): p. 31-68.
16. Yang, J., et al., *Different mitogenic and phenotypic responses of human breast epithelial cells grown in two versus three dimensions.* Experimental cell research, 1986. 167(2): p. 563-569.

17. Lin, C.Q. and M.J. Bissell, *Multi-faceted regulation of cell differentiation by extracellular matrix.* The FASEB Journal, 1993. 7(9): p. 737-743.
18. Smalley, K.S., M. Lioni, and M. Herlyn, *Life ins't flat: Taking cancer biology to the next dimension.* In Vitro Cellular & Developmental Biology-Animal, 2006. 42(8-9): p. 242-247.
19. Grinnell, F., *Fibroblast mechanics in three-dimensional collagen matrices.* Journal of bodywork and movement therapies, 2008. 12(3): p. 191-193.
20. Horning, J.L., et al., *3-D tumor model for in vitro evaluation of anticancer drugs.* Molecular pharmaceutics, 2008. 5(5): p. 849-862.
21. Mazzoleni, G., D. Di Lorenzo, and N. Steimberg, *Modelling tissues in 3D: the next future of pharmaco-toxicology and food research?* Genes & nutrition, 2009. 4(1): p. 13.
22. Mertsching, H., et al., *Human skin equivalent as an alternative to animal testing.* GMS Krankenhaushygiene interdisziplinar, 2008. 3(1).
23. Ponec, M., *Skin constructs for replacement of skin tissues for in vitro testing.* Advanced drug delivery reviews, 2002. 54: p. S19-S30.
24. Ponec, M., et al., *Characterization of reconstructed skin models.* Skin Pharmacology and Physiology, 2002. 15(Suppl. 1): p. 4-17.
25. Draize, J.H., G. Woodard, and H.O. Calvery, *Methods for the study of irritation and toxicity of substances applied topically to the skin and mucous membranes.* Journal of pharmacology and Experimental Therapeutics, 1944. 82(3): p. 377-390.
26. Campbell, R.L. and R.D. Bruce, *Comparative dermatotoxicology: I. Direct comparison of rabbit and human primary skin irritation responses to isopropylmyristate.* Toxicology and applied pharmacology, 1981. 59(3): p. 555-563.
27. Phillips II, L., et al., *A comparison of rabbit and human skin response to certain irritants.* Toxicology and Applied Pharmacology, 1972. 21(3): p. 369-382.
28. Youssef, K.K., et al., *Identification of the cell lineage at the origin of basal cell carcinoma.* Nature cell biology, 2010. 12(3): p. 299.
29. Paulitschke, V., et al., *3, 3', 4, 4', 5, 5'-hexahydroxystilbene impairs melanoma progression in a metastatic mouse model.* Journal of Investigative Dermatology, 2010. 130(6): p. 1668-1679.
30. Mancuso, M., et al., *Modulation of basal and squamous cell carcinoma by endogenous estrogen in mouse models of skin cancer.* Carcinogenesis, 2008. 30(2): p. 340-347.
31. Groeber, F., et al., *Skin tissue engineering—in vivo and in vitro applications.* Advanced drug delivery reviews, 2011. 63(4-5): p. 352-366.

32. Donahue, B.A., et al., *Selective uptake and sustained expression of AAV vectors following subcutaneous delivery.* The journal of gene medicine, 1999. 1(1): p. 31-42.
33. Khorshid, F.A., *Comparative study of keloid formation in humans and laboratory animals.* Medical science monitor, 2005. 11(7): p. BR212-BR219.
34. Menon, G.K., *New insights into skin structure: scratching the surface.* Advanced drug delivery reviews, 2002. 54: p. S3-S17.
35. *Council of the European Union. Seventh Amendment to the EU and Cosmetics Directive 76/768/EEC. Brussels: The European Parliament and the Council of the European Union.* 2003.
36. Becker, R.A., et al., *Report of an ISRTP Workshop: Progress and barriers to incorporating alternative toxicological methods in the US.* Regulatory Toxicology and Pharmacology, 2006. 46(1): p. 18-22.
37. Kuroyanagi, Y., et al., *Establishment of banking system for allogeneic cultured dermal substitute.* Artificial organs, 2004. 28(1): p. 13-21.
38. UNION, P., *Regulation (EC) No 1907/2006 of the european parliament and of the council*. 2006.
39. Mattey, D. and D. Garrod, *Calcium-induced desmosome formation in cultured kidney epithelial cells.* Journal of Cell Science, 1986. 85(1): p. 95-111.
40. Mattey, D. and D. Garrod, *Splitting and internalization of the desmosomes of cultured kidney epithelial cells by reduction in calcium concentration.* Journal of cell science, 1986. 85(1): p. 113-124.
41. Boyce, S.T. and R.G. Ham, *Calcium-regulated differentiation of normal human epidermal keratinocytes in chemically defined clonal culture and serum-free serial culture.* Journal of Investigative Dermatology, 1983. 81(s 1): p. 33-40.
42. Rubin, A.L. and R.H. Rice, *Differential regulation by retinoic acid and calcium of transglutaminases in cultured neoplastic and normal human keratinocytes.* Cancer research, 1986. 46(5): p. 2356-2361.
43. Kopan, R., G. Traska, and E. Fuchs, *Retinoids as important regulators of terminal differentiation: examining keratin expression in individual epidermal cells at various stages of keratinization.* The Journal of cell biology, 1987. 105(1): p. 427-440.
44. Yuspa, S.H., et al., *Expression of murine epidermal differentiation markers is tightly regulated by restricted extracellular calcium concentrations in vitro.* The Journal of cell biology, 1989. 109(3): p. 1207-1217.
45. Freshney, R.I., *Culture of animal cells: a manual of basic technique*. Wiley, New York1994.
46. Boehnke, K., et al., *Effects of fibroblasts and microenvironment on epidermal regeneration and tissue function in long-term skin equivalents.* European journal of cell biology, 2007. 86(11-12): p. 731-746.

47. El-Ghalbzouri, A., et al., *Effect of fibroblasts on epidermal regeneration.* British Journal of Dermatology, 2002. 147(2): p. 230-243.
48. Andriani, F., et al., *Analysis of microenvironmental factors contributing to basement membrane assembly and normalized epidermal phenotype.* Journal of investigative dermatology, 2003. 120(6): p. 923-931.
49. Lee, D.-Y. and K.-H. Cho, *The effects of epidermal keratinocytes and dermal fibroblasts on the formation of cutaneous basement membrane in three-dimensional culture systems.* Archives of dermatological research, 2005. 296(7): p. 296-302.
50. Balasubramani, M., T.R. Kumar, and M. Babu, *Skin substitutes: a review.* Burns, 2001. 27(5): p. 534-544.
51. El Ghalbzouri, A., E. Lamme, and M. Ponec, *Crucial role of fibroblasts in regulating epidermal morphogenesis.* Cell and tissue research, 2002. 310(2): p. 189-199.
52. El Ghalbzouri, A., et al., *Basement membrane reconstruction in human skin equivalents is regulated by fibroblasts and/or exogenously activated keratinocytes.* Journal of investigative dermatology, 2005. 124(1): p. 79-86.
53. Wong, T., J. McGrath, and H. Navsaria, *The role of fibroblasts in tissue engineering and regeneration.* British Journal of Dermatology, 2007. 156(6): p. 1149-1155.
54. Maas-Szabowski, N., A. Shimotoyodome, and N.E. Fusenig, *Keratinocyte growth regulation in fibroblast cocultures via a double paracrine mechanism.* Journal of cell science, 1999. 112(12): p. 1843-1853.
55. Maas-Szabowski, N., H.-J. Stark, and N.E. Fusenig, *Keratinocyte growth regulation in defined organotypic cultures through IL-1-induced keratinocyte growth factor expression in resting fibroblasts.* Journal of investigative dermatology, 2000. 114(6): p. 1075-1084.
56. Stark, H.-J., et al., *Organotypic cocultures as skin equivalents: A complex and sophisticated in vitro system.* Biological procedures online, 2004. 6(1): p. 55.
57. Sun, T., et al., *Culture of skin cells in 3D rather than 2D improves their ability to survive exposure to cytotoxic agents.* Journal of biotechnology, 2006. 122(3): p. 372-381.
58. Chioni, A.-M. and R. Grose, *Organotypic modelling as a means of investigating epithelial-stromal interactions during tumourigenesis.* Fibrogenesis & tissue repair, 2008. 1(1): p. 8.
59. Régnier, M., et al., *Integration of Langerhans cells into a pigmented reconstructed human epidermis.* Journal of Investigative Dermatology, 1997. 109(4).

60. Regnier, M., et al., *Reconstructed human epidermis composed of keratinocytes, melanocytes and Langerhans cells.* Medical and Biological Engineering and Computing, 1998. 36(6): p. 821-824.
61. Promocell, *Fibroblast Growth Medium 2.*
62. CellnTech, *Medium formulation.*
63. Egles, C., J.A. Garlick, and Y. Shamis, *Three-dimensional human tissue models of wounded skin*, in *Epidermal Cells*. 2010, Springer. p. 345-359.
64. Segal, N., et al., *The basement membrane microenvironment directs the normalization and survival of bioengineered human skin equivalents.* Matrix Biology, 2008. 27(3): p. 163-170.
65. Idrees, A., et al., *Validation of in vitro assays in three-dimensional human dermal constructs.* The International journal of artificial organs, 2018: p. 0391398818775519.
66. Bikle, D.D., Z. Xie, and C.-L. Tu, *Calcium regulation of keratinocyte differentiation.* Expert review of endocrinology & metabolism, 2012. 7(4): p. 461-472.
67. Menon, G.K., S. Grayson, and P.M. Elias, *Ionic calcium reservoirs in mammalian epidermis: ultrastructural localization by ion-capture cytochemistry.* Journal of Investigative Dermatology, 1985. 84(6): p. 508-512.
68. Ponec, M., et al., *Lipid composition of cultured human keratinocytes in relation to their differentiation.* Journal of lipid research, 1988. 29(7): p. 949-961.
69. Grubauer, G., P.M. Elias, and K.R. Feingold, *Transepidermal water loss: the signal for recovery of barrier structure and function.* Journal of Lipid Research, 1989. 30(3): p. 323-333.
70. Kolli, S., et al., *Loss of corneal epithelial stem cell properties in outgrowths from human limbal explants cultured on intact amniotic membrane.* 2008.
71. Meller, D., R. Pires, and S. Tseng, *Ex vivo preservation and expansion of human limbal epithelial stem cells on amniotic membrane cultures.* British Journal of Ophthalmology, 2002. 86(4): p. 463-471.
72. Pellegrini, G., et al., *Long-term restoration of damaged corneal surfaces with autologous cultivated corneal epithelium.* The Lancet, 1997. 349(9057): p. 990-993.
73. Tsai, R.J.-F., L.-M. Li, and J.-K. Chen, *Reconstruction of damaged corneas by transplantation of autologous limbal epithelial cells.* New England Journal of Medicine, 2000. 343(2): p. 86-93.
74. Rheinwatd, J.G. and H. Green, *Seria cultivation of strains of human epidemal keratinocytes: the formation keratinizin colonies from single cell is.* Cell, 1975. 6(3): p. 331-343.
75. Hayashi, I., J. Larner, and G. Sato, *Hormonal growth control of cells in culture.* In vitro, 1978. 14(1): p. 23-30.

76. Okada, N., Y. Kitano, and K. Ichihara, *Effects of cholera toxin on proliferation of cultured human keratinocytes in relation to intracellular cyclic AMP levels.* Journal of Investigative Dermatology, 1982. 79(1).
77. Allen-Hoffmann, B.L. and J.G. Rheinwald, *Polycyclic aromatic hydrocarbon mutagenesis of human epidermal keratinocytes in culture.* Proceedings of the National Academy of Sciences, 1984. 81(24): p. 7802-7806.
78. Flaxman, B.A. and R.A. Harper, *In vitro analysis of the control of keratinocyte proliferation in human epidermis by physiologic and pharmacologic agents.* Journal of Investigative Dermatology, 1975. 65(1): p. 52-59.
79. Yu, M., et al., *An important role for adenine, cholera toxin, hydrocortisone and triiodothyronine in the proliferation, self-renewal and differentiation of limbal stem cells in vitro.* Experimental eye research, 2016. 152: p. 113-122.
80. Savini, I., et al., *Characterization of Keratinocyte Differentiation Induced by Ascorbic Acid: Protein Kinase C Involvement and Vitamin C Homeostasis1.* Journal of investigative dermatology, 2002. 118(2): p. 372-379.
81. Pullar, J., A. Carr, and M. Vissers, *The roles of vitamin C in skin health.* Nutrients, 2017. 9(8): p. 866.
82. Black, A.F., et al., *Optimization and characterization of an engineered human skin equivalent.* Tissue engineering, 2005. 11(5-6): p. 723-733.
83. Promocell, *Keratinocyte Growth Medium 2.*
84. Della, *HistoQuarterly: SUPERFICIAL SPREADING MALIGNANT MELANOMA* Histology Blog., January 23, 2014
85. Hill, D.S., et al., *A novel fully-humanised 3D skin equivalent to model early melanoma invasion.* Molecular cancer therapeutics, 2015: p. molcanther. 0394.2015.
86. Park, J.-H., et al., *Histopathological differential diagnosis of psoriasis and seborrheic dermatitis of the scalp.* Annals of dermatology, 2016. 28(4): p. 427-432.
87. DiMarco, R.L., et al., *Engineering of three-dimensional microenvironments to promote contractile behavior in primary intestinal organoids.* Integrative Biology, 2014. 6(2): p. 127-142.
88. Sugihara, H., et al., *Reconstruction of the skin in three-dimensional collagen gel matrix culture.* In Vitro Cellular & Developmental Biology-Animal, 1991. 27(2): p. 142-146.
89. Farris, P.K., *Skin anatomy and physiology.* Nu Skin.
90. MacNeil, S., *Progress and opportunities for tissue-engineered skin.* Nature, 2007. 445(7130): p. 874.
91. Suvik, A. and A. Effendy, *The use of modified Masson's trichrome staining in collagen evaluation in wound healing study.* Mal J Vet Res, 2012. 3: p. 39-47.

92. Reddy, B.S., et al., *Evaluation of antimicrobial, antioxidant and wound-healing potentials of Holoptelea integrifolia.* Journal of Ethnopharmacology, 2008. 115(2): p. 249-256.
93. O'connor, W.N. and S. Valle, *A combination Verhoeffs elastic and Masson's trichrome stain for routine histology.* Stain technology, 1982. 57(4): p. 207-210.
94. Santos, M., et al., *The expression of keratin k10 in the basal layer of the epidermis inhibits cell proliferation and prevents skin tumorigenesis.* Journal of Biological Chemistry, 2002. 277(21): p. 19122-19130.
95. Coulombe, P.A., R. Kopan, and E. Fuchs, *Expression of keratin K14 in the epidermis and hair follicle: insights into complex programs of differentiation.* The Journal of cell biology, 1989. 109(5): p. 2295-2312.
96. Fuchs, E. and H. Green, *Changes in keratin gene expression during terminal differentiation of the keratinocyte.* Cell, 1980. 19(4): p. 1033-1042.
97. Al Saif, F., *Dermatopathia pigmentosa reticularis: report of a new cases and literature review.* Indian journal of dermatology, 2016. 61(4): p. 468.
98. Thacher, S.M. and R.H. Rice, *Keratinocyte-specific transglutaminase of cultured human epidermal cells: relation to cross-linked envelope formation and terminal differentiation.* Cell, 1985. 40(3): p. 685-695.
99. Warhol, M., et al., *Immuno-ultrastructural localization of involucrin in squamous epithelium and cultured keratinocytes.* Journal of Histochemistry & Cytochemistry, 1985. 33(2): p. 141-149.
100. Mehrel, T., et al., *Identification of a major keratinocyte cell envelope protein, loricrin.* 1990. 61(6): p. 1103-1112.
101. Steven, A., et al., *Biosynthetic pathways of filaggrin and loricrin—two major proteins expressed by terminally differentiated epidermal keratinocytes.* Journal of structural biology, 1990. 104(1-3): p. 150-162.
102. Nishiyama, T., et al., *The importance of laminin 5 in the dermal–epidermal basement membrane.* Journal of dermatological science, 2000. 24: p. S51-S59.
103. Garlick, J.A. and L.B. Taichman, *Fate of human keratinocytes during reepithelialization in an organotypic culture model.* Laboratory investigation; a journal of technical methods and pathology, 1994. 70(6): p. 916-924.
104. Weiss, R.A., R. Eichner, and T.T. Sun, *Monoclonal antibody analysis of keratin expression in epidermal diseases: a 48- and 56-kdalton keratin as molecular markers for hyperproliferative keratinocytes.* The Journal of Cell Biology, 1984. 98(4): p. 1397-1406.
105. Paladini, R.D. and P.A. Coulombe, *The Functional Diversity of Epidermal Keratins Revealed by the Partial Rescue of the Keratin 14 Null Phenotype by Keratin 16.* The Journal of Cell Biology, 1999. 146(5): p. 1185-1201.

106. Pegu, S., et al., *A novel keratin 10 gene mutation causing epidermolytic hyperkeratosis (bullous congenital ichthyosiform erythroderma) in a term neonate.* Case Reports in Perinatal Medicine, 2017. 6(1).
107. Khani, P., et al., *Keratins and epidermolysis bullosa simplex.* Journal of cellular physiology, 2018.
108. Vats, G., et al., *Dermatopathia pigmentosa reticularis.* Indian Journal of Paediatric Dermatology, 2018. 19(1): p. 77.
109. Maestrini, E., et al., *A molecular defect in loricrin, the major component of the cornified cell envelope, underlies Vohwinkel's syndrome.* Nature genetics, 1996. 13(1): p. 70.
110. Sharma, S., et al., *Effect of vitamin C on collagen biosynthesis and degree of birefringence in polarization sensitive optical coherence tomography (PS-OCT).* African Journal of Biotechnology, 2008. 7(12).
111. Chapman, J.A., *The banding pattern of collagen*, in *Biology of Invertebrate and Lower Vertebrate Collagens*. 1985, Springer. p. 515-537.
112. Duplan-Perrat, F., et al., *Keratinocytes Influence the Maturation and Organization of the Elastin Network in a Skin Equivalent1.* Journal of investigative dermatology, 2000. 114(2): p. 365-370.
113. Elias, P.M., et al., *Membrane structural alterations in murine stratum corneum: relationship to the localization of polar lipids and phospholipases.* 1988. 91(1).
114. Hohl, D.J.D., *Cornified cell envelope.* 1990. 180(4): p. 201-211.
115. Ehrlich, H.P. and T.M. Krummel, *Regulation of wound healing from a connective tissue perspective.* Wound repair and regeneration, 1996. 4(2): p. 203-210.
116. Hur, G.-Y., D.-K. Seo, and J.-W. Lee, *Contracture of skin graft in human burns: effect of artificial dermis.* Burns, 2014. 40(8): p. 1497-1503.
117. Jackson, S.M., et al., *Pathobiology of the stratum corneum.* Western journal of medicine, 1993. 158(3): p. 279.
118. Harrison, C.A., et al., *Use of an in vitro model of tissue-engineered skin to investigate the mechanism of skin graft contraction.* Tissue engineering, 2006. 12(11): p. 3119-3133.
119. Michel, M., et al., *Characterization of a new tissue-engineered human skin equivalent with hair.* In Vitro Cellular & Developmental Biology-Animal, 1999. 35(6): p. 318.
120. Casale, C., et al., *Endogenous human skin equivalent promotes in vitro morphogenesis of follicle-like structures.* Biomaterials, 2016. 101: p. 86-95.

4.4 Appendix B

4.4.1 Tissue morphogenesis of HSE using so-called dermal microtissues

Our results indicate that dermal fibroblasts are able to remodel ECM and to synthesize their own ECM. However, the 3D dermis could also be fabricated by embedding cells in collagen matrix of human origin or allowing cells to completely synthesis their ECM to obtain reconstituted humanized HSE. To evaluate the effect of such dermal layer on HSC tissue morphogenesis, some preliminary experiments were performed for the development of HSC using so-called dermal microtissues with fibroblasts embedded into HDC for 4 weeks instead of 1 week (keeping all other cell culture conditions unchanged as 3D-CC-III). The H & E stained histological cross sections of resulting HSC were shown in Figure 4.27 (at different magnifications). The HSC tissue showed well-differentiated epidermal tissue with similar structure compared to the one of optimized HSE. In the future it will be further characterised by IHC analysis to evaluate matrix proteins in dermal compartment, and protein expression in epidermal compartment.

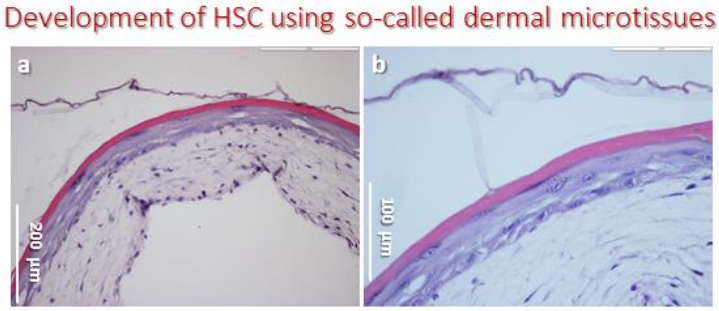

Figure 4.27 Development of HSC using so-called dermal microtissues (remodeled for 4 weeks). H & E stained histological cross sections indicate micrographs of HSCs (at different magnifications) raised for 20 days at ALI.

Chapter 05: Development of *S. aureus* colonized Human Skin Equivalent (c-HSE)

Table of contents

List of figures

Abbreviations

2D and 3D: Two-dimensional and three-dimensional
ALI: Air-liquid interface
AMPBs: Antimicrobial polymeric biomaterials
ATCC: American type culture collection
CDFF: Constant depth film fermenter
CELLnTECH: CnT
CFU: Colony forming unit
c-HDC: Bacterial colonized human dermal construct
c-HSE: *S. aureus* colonized human skin equivalent
CnT-PR: CnT-Prime epithelial culture medium
CnT-PR-3D: CnT-Prime 3D barrier culture medium
CnT-PR-F: CnT-Prime fibroblast medium
Col. I: Rat tail tendon collagen type I
CTB assay: CellTiter-Blue® cell viability assay
CTO: CytoTox-ONE™ assay
CXCR-1: Chemokine receptor for interleukin-8
Dsg: Desmoglein
ECM: Extracellular matrix
EPS: Extracellular polymeric substance
Gram +ve and Gram -ve: Gram positive and Gram negative
H & E stain: Haematoxylin and eosin stain
HDC: Human dermal construct
HSC: Human skin construct
HSE: Human skin equivalent
HSV and VZV: Herpes simplex virus and varicella zoster virus
IL-1, 6, 8: Interleukin-1, 6, and 8
LB: Luria-Bertani broth
LDH: Lactate dehydrogenase
MIC: Minimum inhibitory concentration
MMPs: Matrix metalloproteinases
NF-kB: Nuclear factor kappa-light-chain-enhancer of activated B cells
NHDF: Normal human dermal fibroblasts
NHEK: Normal human epidermal keratinocytes
PAMPs: Pathogen-associated molecular patterns
PPO: Polypropylene oxide
RHE: Reconstructed human epithelia (SkinEthic Laboratories, Nice, France)
S. aureus: Staphylococcus aureus
SC: Stratum corneum
SEM: Scanning electron microscopy

SSSS: Staphylococcal scalded skin syndrome
$T_{0h,}$ T_{1h} and T_{24h}: Time point 0 hour, 1 hour, and 24 hours
TEM: Transmission electron microscopy
TLR2 & 4: Toll-like receptor 2 and 4
TNF-α: Tumour necrosis factor alpha
αifn: Alpha interferon

Chapter 05: Development of *S. aureus* colonized Human Skin Equivalent (c-HSE)

Abstract

Due to widespread prevalence as an asymptomatic skin colonizer, *Staphylococcus aureus* is a major bacterial pathogen in skin and soft tissue infections. In this context, biofilms have been identified to have a potential impact in the chronicity of nonhealing wounds and antibiotic resistance. A better understanding of how *S. aureus* interacts with wounded skin and how it attaches to/grows on /breaches the multi-faceted skin tissue, is of critical importance. Moreover, with an increasing need for novel strategies to combat wounds colonized with resistant microbes, more reliable preclinical data is needed to bioanalyze antimicrobial polymeric biomaterials (AMPBs). In this study, a preliminary dermal infection system (c-HDC) was created by inoculating 1 x 10^5 CFU of *S. aureus*, *P. aeruginosa, or S. aureus* + *P. aeruginosa* onto 12mm diameter human dermal construct (HDC) and incubating it for 24 hours. Moving to an advanced system, a three-dimensional (3D), human dermal/epidermal skin equivalent (HSE) was exploited to study *S. aureus* skin colonization generating an *in vitro S. aureus* colonized HSE model (c-HSE). HSEs were incised to create 2-3mm full-thickness wounds, that were then inoculated with 5 x 10^3 CFU *S. aureus* at wound site; tissues were incubated at various time points and harvested to be visualized under light (hematoxylin & eosin) and electron microscopy.

Bacterial aggregations and early biofilm formation were observed at wound site on c-HSE. Additionally, the results showed that *S. aureus* growth was quite higher on HSE based biotic surface than as a free-floating planktonic form in liquid media conditions. Histological results demonstrated that bacterial colonization hindered the re-epithelialization process, when c-HSE was compared with uninfected wound control. TEM results revealed fibroblasts/keratinocytes cell lysis, *S. aureus* induced ECM degradation, and bacterial internalization by keratinocytes. SEM revealed grape-like bacterial clusters covered within extracellular polymeric substance at wound site in dermis and epidermis.

The c-HDC results suggested that co-existence of *S. aureus* and *P. aeruginosa* may be significant for both bacterial colonization and pathogenicity in wounds. Histology revealed biofilm formation in all c-HDC groups, although demonstrated denser colonized biofilm regions in c-HDC inoculated with *S. aureus* as compared to the c-HDC inoculated with *P. aeruginosa.*

c-HSE and c-HDC cultures would be useful for providing insights about interactions between bacteria and human skin tissue. These models may provide a basis for future studies to unveil therapeutic strategies to prevent biofilm formation. The c-HSE would

also serve as a promising tool to evaluate the antimicrobial and wound healing properties of AMPs and novel therapeutics under an advanced infected wound *in vivo*-like condition.

Keywords: *S. aureus* colonized human skin equivalent (c-HSE), bacterial colonized human dermal construct (c-HDC), biofilm formation, infected wounds.

5.1 Introduction

5.1.1 Need of an *in vitro skin infection system*

Wound management still represents a significant problem. Due to the widespread prevalence of skin infections, an understanding of how pathogens attach and colonize the stratified epidermis, is highly crucial. Furthermore, emerging antibiotic resistance leads to non-healing wound conditions. With an increasing need of novel strategies for treating infected wounds, there is an extreme urgency to develop reliable *in vitro* tools for biological evaluation of novel antimicrobial polymeric biomaterials (AMPBs). Traditional microbiological research has approached bacterial susceptibility considering that bacterial cell exists in a liquid, free-floating medium. However, bacteria have great potential to adhere, colonize, and grow especially in communities enclosed in self-produced polymeric matrix forming biofilms. This is medically important as bacterial colonization and biofilm formation shield bacteria from antimicrobial therapies and thus has a role in resistant microbial infections and chronicity of non-healing wounds. [1]. Traditionally employed method to measure the Minimum Inhibitory Concentration (MIC) uses free-floating bacteria, where number of organisms used is too low with no sufficient organic matter in medium.

Among *in vitro* models of chronic wounds, constant depth film fermenter (CDFF) was used to grow wound biofilms [2]. *Staphylococcus aureus* is a major human bacterial pathogen [3], causing a wide range of skin and soft tissue infections [4, 5]. In the past, *S. aureus* skin interactions have been investigated by inoculating 2D keratinocytes monolayer cultures with bacteria to understand bacterial attachment and keratinocytes' response [6, 7]. Adherence to plastic and adherence to human cells are two distinct events, involving bacterial interactions with abiotic and biotic surfaces. However, these two testing systems may not correctly predict the interaction of bacteria with human skin. This is mainly because bacteria adhere on skin under comparatively dry conditions [8] as compared to the conditions simulated *in vitro*. Moreover, bacterial adherence and subsequent replication are strongly dependent on environmental conditions [9] of skin barrier properties, nutrient availability at skin surface, and triggered & innate inflammatory response of skin.

Considering the 7th amendment [Dir. 2003/15/EC] in the European Cosmetic Directive (76/768/EEC) [10, 11], 3Rs strategy (that aimed at refining, reducing and replacing animal trials) [12, 13], as well as the basic dissimilarities existing between animal and human skins [14-16], *in vitro* human based 3D skin cultures that mimic the complexity and dynamic behavior of the *in vivo* microenvironment [17-24] would represent the basic systems to generate wound infection models.

Ex vivo human skin implants can serve as established models, but they have limited option for experimental manipulations (of host genetics) and have restricted availability.

Tissue engineered and air-exposed 3D human skin constructs (HSCs) closely mimic the native human skin (NHS) [25-27]. Unlike explants, HSCs can be tailored controlling both the cell compartments and infecting pathogens [28-30]. In these models, innate immune response of keratinocytes can be studied by knocking down a gene of interest [31, 32] and by examining how tissues deficient in a particular immune product may alter the *S. aureus* niche. For example, filaggrin contributes to atopic dermatitis that enhances *S. aureus* colonization in patients [33-36] and the knock down approach can help to understand *S. aureus* interaction with filaggrin depleted skin [37].

Efforts were made to simulate skin infection by inoculating different pathogens (including virus, bacteria, and yeast) on the 3D skin substitute. *S. aureus* and *P. aeruginosa* were inoculated on rat-tail collagen type I matrix (without any eukaryotic cells) with serum mimicking wound bed [38], with the aim to investigate *in vitro* development of biofilms. *P. aeruginosa* and *S. aureus* on cellulose matrix (without any eukaryotic cells) in a flat-bed perfusion growth chamber [39, 40] was used to study antimicrobial efficacy of wound dressings. Moreover, RHE (Reconstructed Human Epithelia, SkinEthic™) was used to construct oral, vaginal [41, 42] [43], cutaneous [44, 45], and oesophageal candidiasis [44, 45], to study cellular and immunological interactions between *Candida albicans* (yeast) and epithelial tissue [46]. Some human skin models were used to study viral (*HSV-1/2, and VZV)* infectious process, spread, and efficacy of new anti-VZV antivirals [47-50]. A 3D human epidermal model was applied to study *A. baumannii* and *A. junii* (RUH2228) [51] adherence and colonization. Very recently, *S. aureus* (USA 300) was used on a 3D human dermal-epidermal skin model (using devitalized human dermal tissue) to understand skin colonization and infection [52]. In another work, *S. aureus* and *P. aeruginosa* were inoculated on a commercially available 3D human skin model (Graftskin®/Apligraf®) to study biofilm formation [1].

In this Ph.D. thesis, a full-thickness Human Skin Equivalent (HSE) model (described in more detail in Chapter 04, having dermal and well-differentiated epidermal layers) was applied as an interesting model for studying pathogen-skin interactions. To this aim, *S. aureus* colonized Human Skin Equivalent (c-HSE) was developed using our in-house HSE. The c-HSE may serve as an advanced tool to investigate pathogenesis (host-pathogen molecular interactions) to explore new antimicrobial targets. On the other hand, c-HSE may also serve as a complex *in vitro* tool for antimicrobial evaluation of AMPs against adhered and colonized bacteria on HSE.

5.1.2 Bacterial-keratinocyte interaction

To better understand staphylococcal colonization and the transition to an invasive infection, *S. aureus* should be studied in its natural habitat i.e. 3D human skin culture representing an interface between tissue barrier and *S. aureus.* Bacterial virulence factors have a great effect in promoting bacterial growth and invasion processes. Staphylococcal

virulence factors have well known targets within the human skin, for instance, exfoliative toxins can cleave epidermal desmogleins, as happens in staphylococcal scalded skin syndrome [53, 54]. *S. aureus* virulence factors have a role in asymptomatic colonization as well as in establishing the colonization state. For instance, clumping factor B, a *S. aureus* virulence factor can cause systemic infection and colonization. In bloodstream infections, clumping factor B binds to the α-chain of fibrinogen protein, causing platelet aggregation, and thus staphylococcal attachment to damaged tissue in endocarditis [55, 56]. Nevertheless, it causes nasal colonization by enabling adhesion to the keratinized epithelium by interacting with cytokeratin 10 (K10) that is expressed on squamous cells [7, 57]. Similarly, the secreted toxin α-hemolysin has been shown to promote the cleavage of E-cadherin in lung and skin epithelia of disease models [58]. The *S. aureus* has the ability to modify the biology of host adherens junctions and thus, may contribute to its ability to persist in the skin in a disease-free state.

To examine the role of virulence factors in *S. aureus* colonization, competition experiments can be performed in c-HSE where the same c-HSE tissue is co-infected with wild type and mutant *S. aureus* strains (labelled with fluorophores), observing the fate of wild type and mutant populations within the same stratified human tissue over time.

5.1.3 Keratinocytes and innate immune response

One potential application of c-HSE is represented by the study of the immune response to *S. aureus* cutaneous colonization/infections. The *in vitro* direct interactions between the bacteria and immune cells do not correctly represent a physiologically relevant interaction between immune cells and *S. aureus*. The incorporation of immune cell types (e.g. Langerhans cells or neutrophils) into the 3D skin culture can help to examine how *S. aureus* and immune cells would interact with one another in stratified human skin tissue. However, keratinocytes themselves have an important role in innate immunity [59] and can produce proinflammatory cytokines e.g. TNF-α, IL-1α, IL-1β, IL-6, and IL-8 and anti-inflammatory cytokines e.g. IL-10 in response to bacteria. Moreover, skin equivalents can be examined for antimicrobial peptides production i.e. human beta-defensins [60, 61] that are constitutively expressed in skin, and bacterial strains can induce an enhanced expression of these peptides.

Stratum corneum (SC) is a protective barrier against bacteria and infections. *Duckney et al.* demonstrated that *Staphylococcus epidermidis* and *Propionibacterium acnes* induced an inflammatory response in a reconstructed human epidermal tissue only when applied subcutaneously and not when applied topically [62]. These studies suggested the importance of SC in the evaluation of host-pathogen interactions: simple keratinocyte monolayers (lacking SC) would not truly predict the *in vivo* situation.

Additionally, c-HSE model may also serve as a valuable tool in assessing how immunization against *S. aureus* might alter bacterial colonization behavior on the

epidermis or prevent invasive epidermal infections. Treatment with antibodies directed against *S. aureus* by adding them in the basolateral media of the c-HSE could allow examining the effect of immune response against *S. aureus.*

5.1.4 Biofilms, inflammation, and non-healing chronic wounds

The first and main step of biofilm formation is bacterial attachment. Bacteria can attach to certain molecular patterns of host system called epitopes. For example, bacteria can use their cell wall-anchored adhesins that can bind to epitopes in ECM collagen and fibronectin etc. Or other bacteria can bind to cells by injecting effector proteins into the cells, that result in actin filaments polymerization turning these cells as a support to which bacteria can attach and multiply [63]. During attachment, bacteria must avoid macrophages and neutrophils mediated phagocytosis, as these specialized immune cells can detect pathogen-associated molecular patterns (PAMPs). If bacteria evade this first immune response for a short time, and immune system do not response quickly and firmly at this right moment, biofilm formation would follow. And once established, biofilm is unable to be overcome by host immune system alone without external intervention [63].

Biofilm are bacterial communities that work on the principles of quorum sensing (pheromone approach) by assigning its genotypically/phenotypically-diverse components into specific tasks. This benefits the community by enhancing their nutrient-gathering capacity (minimal survival ability), defense mechanism, and reproduction [64, 65]. Biofilm is composed of bacteria's own produced matrix, called extracellular polymeric substances (EPS) containing self-secreted polysaccharides, proteins, DNA, and host components. This acts as a barrier towards immune cells, antibodies and other antimicrobial strategies. One of the most important features of a biofilm is its "constant flux state", according to which a certain population with planktonic phenotype would slough off to colonize the uncolonized surfaces [66, 67].

Human's adaptive immune system can generate endless number of random sequences against any existing antigen. However, biofilms prevent this immune response by stopping the penetration of immune cells and antibodies [68-70], making the "universality" of host immune system completely irrelevant of biofilm eradication. Immune system develops in such a way that it doesn't respond to self-antigens as well as to mutualistic bacteria. This characteristic is called tolerance, and biofilms maintenance is not based on this feature of tolerance either. Instead, biofilms do not like downregulation of immune system and prevent immune system to develop any kind of tolerance against biofilms. A perpetual inflammatory condition (or lack of appropriateness of immune system) is what sets biofilms to stay and persists with a non-healing condition. This is what makes chronic infections different from acute infection, where rapidly growing bacteria and their produced bacterial virulence factors damage

the host tissue. While in chronic infections, biofilms destroy host tissue using host-originated factors such as by regulating host proteases production (matrix metalloprotease and elastase), raising the pro-inflammatory cytokines to destructive levels, and making the excessive infiltration of neutrophils at wound site, thus balancing the host tissue destruction with host healing [63]. Figure 5.1 represented the biofilm maintenance and associated chronicity of wounds.

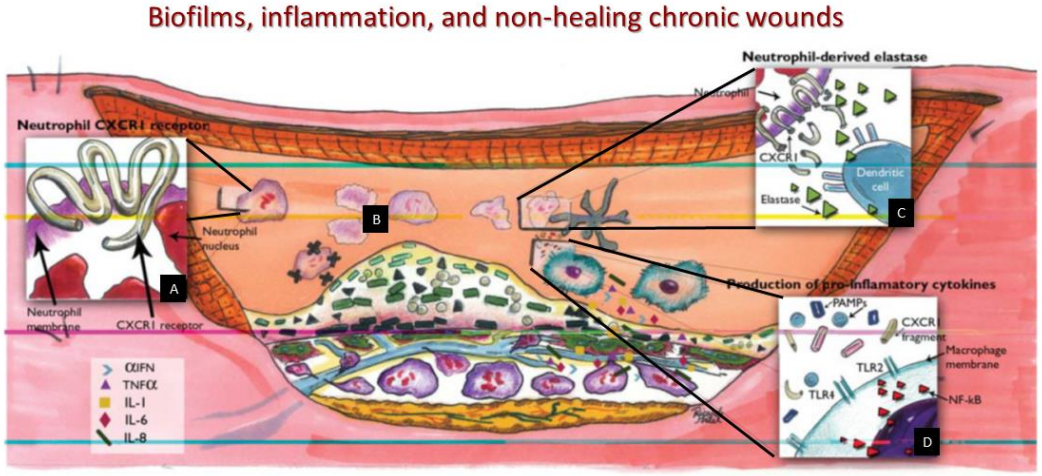

Figure 5.1 Biofilms, inflammation, and non-healing chronic wounds. After bacteria have attached, micro-colonized, and established in a biofilm community within the host tissue, they maintain an inflammatory niche by directing the host immune response. The neutrophils present at wound site contain interleukin-8 receptor (CXCR-1) within their cell membranes that is responsible for neutrophil's activation and migration to wound site (A). Many bacteria can kill neutrophils using their virulence factors (B). If neutrophils are not cleared by macrophages, the dying neutrophils can release elastase into the wound environment, that degrades its own CXCR-1 receptor. This makes neutrophils' phagocytosis by macrophages even more difficult. The fragmented CXCR-1 stimulate Toll-like receptor-2 (TLR2) present on dendritic cells and macrophages. This leads to a burst release of pro-inflammatory cytokines from these cells via a nuclear factor Kappa B pathway (NF-kB) (C & D). Wound-bed cells-produced tissue inhibitors of matrix metalloproteases (or TIMPs) become deficient and thus downregulation of pro-inflammatory cytokines is prevented. The pro-inflammatory cytokines attract excessive neutrophils (diapedesis). This leads to a sustainable cycle where bacteria induce massive neutrophil migration and thus an inflammatory non-healing wound condition persists. The image was used with copyright permission [63].

5.2 Materials and methods

5.2.1 Fabrication of HSE

5.2.1.1 Cells and cell culture maintenance

Primary cells including normal human dermal fibroblasts (NHDF) and normal human epidermal keratinocytes (NHEK) were obtained from PromoCell. NHDF were maintained in CnT-Prime fibroblast medium (CnT-PR-F, CELLnTECH) while NHEK were maintained in CnT-Prime epithelial culture medium (CnT-PR, CELLnTECH) under the physiological culture conditions (37°C, 5% CO_2). The cells were sub-cultured subsequently sub-cultured by using DetachKit-Promocell HEPES BSS (2-[4-(2-hydroxyethyl)piperazine-1-yl] ethanesulfonic acid buffered saline solution); 0.04% Trypsin/0.03% EDTA (ethylenediaminetetraacetic acid); and TNS (trypsin neutralizing solution) containing 0.05% trypsin inhibitor from soybean/0.1% bovine serum albumin.

5.2.1.2 Construction of HSE

HSE was obtained having both dermal and epidermal compartments, by first embedding NHDF in rat tail tendon collagen type I (Col. I) hydrogel from Ibidi (mimicking dermal extracellular matrix or ECM) to generate human dermal construct (HDC) and then later seeding NHEK on it to generate the epidermis. The cell culture conditions were optimized to obtain a closely *in vivo* tissue mimicking HSE. The optimized protocol of 3D cell culture conditions (i.e. 3D-CC-III) was as following: i) NHDF (~8×10^4 cells/mL) were embedded in Col. I (1.5mg/mL) based dermal construct to remodel the ECM for 5-7 days using CnT-PR-F medium; ii) NHEK (8×10^6 cells/mL) were plated and grown in submerged culture for 3 days to cover the dermal substrate using CnT-PR medium; iii) the culture was then continued in submerged conditions overnight using CnT-PR-3D medium to allow cells to develop cell-cell adhesion structures before ALI culture; iv) Finally the culture at ALI was performed for 15-20 days while bottom fed using CnT-PR-3D medium. HDCs development and characterization are described in more detail in Chapter 02. While the HSE development and full characterization are described in more detail in Chapter 04.

5.2.2 Fabrication of c-HSE

5.2.2.1 Preparation of bacterial inoculum

S. aureus (ATCC 29213, wound source) was revived and cultured on fresh blood agar one day before use. The well-isolated colonies were suspended in 0.9% normal saline by direct colony suspension method and adjusted to McFarland 0.5. This suspension was diluted in PBS (pH 7.4) by 1:200 ratio to obtain an inoculum with a concentration of 1

x 10^6 CFU/mL that represented ~1 x 10^3 CFU per µL, as verified afterwards by standard viable counts.

5.2.2.2Bacterial colonization of HDC to construct c-HDC (preliminary experiments)

In an effort to create c-HSE, preliminary experiments were performed using in-house HDCs where *S. aureus* (ATCC 21819) and *Pseudomonas aeruginosa* (ATCC 27853) (alone and together as co-infection) were topically inoculated onto surface of dermal construct with ~70µL bacterial inoculum containing ~10^5 CFU and incubated at 37°C, 5% CO_2 for 24 hours to allow bacteria to adhere to HDC, that now was named as c-HDC.

5.2.2.3S. aureus colonization of HSE to construct c-HSE

Airlifted HSEs were used to create an incisional wound by making a full-thickness incision of 2-3mm (in length) using a scalpel N°10 without damaging the Transwell insert membrane. Skin equivalents were inoculated with 5µL (~5 x 10^3 CFU) bacterial inoculum at incision site and incubated at 37°C, 5% CO_2 for 1 hour and 24 hours to allow bacteria to adhere to HSE, forming c-HSE.

Additionally, some control experiments were also done to examine the bacterial interactions with intact HSE (without any incisional wounds). For this, unwounded skin equivalents were individually inoculated with 5µL (~5 x 10^3 CFU) and 10µL (~2 x 10^4 CFU) of *S. aureus* bacterial inoculum and incubated at 37°C, 5% CO_2 for 1 and 24 hours to investigate how *S. aureus* adheres, colonizes and breaches the stratified human skin tissue. These experiments would also help to understand the effect of increased bacterial burden on HSE.

5.2.3 Cell viability analysis

CytoTox-ONE™ (CTO) assay, a fluorometric method was used to measure cytotoxicity of NHDF in c-HDC. The method evaluated the cytotoxicity by measuring the release of lactate dehydrogenase (LDH) from cells with a damaged membrane. The assay was performed according modified standard protocols [71, 72] for 3D HDCs. The method is based on the conversion of a redox dye (resazurin) into a fluorescent end-product (resorufin) that fluoresces at Ex/Em 560/590.

Lysis solution of 9% Triton® X-100 in water from Promega was used to create "Lysis control". HDC without any bacterial inoculation served as negative control, while HDC treated with lysis solution served as positive control.

The cell viability of HSE was measured by CellTiter-Blue® (CTB) assay, also based on the redox conversion of resazurin into resorufin. After the incubation, the HSEs were transferred to 24 well plate by cutting the Transwell membrane. 400µL CTB reagent

(this vol. is enough to completely dip the HSEs) was pipetted per well and incubated for 3h at 37°C and 5% CO_2 [71, 72]. The cell supernatant was transferred to black microtiter 96-well plates. The fluorescence was measured at Ex/Em 560/590 nm.

5.2.4 Bacterial replication on c-HSE – CFU count

The numbers of bacteria (CFU) per c-HSE were assessed microbiologically. For this, c-HSEs along with the supernatant were collected and homogenized using a manual glass tissue homogenizer. The homogenates were subsequently serially diluted and plated (100µL) onto blood agar plates to determine the reduction in CFU number.

5.2.5 Microscopic analysis of bacterial colonization on c-HSE

Harvested c-HSE tissue were fixed in 4% paraformaldehyde (10% formalin) for ≥4h, dehydrated through graded ethanol solutions, cleared in Xylol (twice), and infiltrated & embedded in paraffin. Sections of ~5µm thickness were cut by a microtome, then attached to glass slides, dried, and then deparaffinized and hydrated. For morphological analysis sections were stained with haematoxylin & eosin (H & E) and examined under Olympus BX51 light microscope. The particulars of tissue processing and staining are described in more detail in Chapter 04.

In an effort to best visualize the bacterial colonization and biofilm formation on the preliminary model, c-HDCs were stained with H&E, Gram, and Alcian blue-PAS staining methods. Alcian blue-PAS staining kit from NovaUltra was used to demonstrate the full features of tissue proteoglycans. It was used to stain biofilm matrix (blue). Generally, it stains acid mucins and nuclei as blue, while neutral mucins, glycogen, and glycoproteins as magenta. The kit comprised: 1) 1% Alcian blue in 3% aq. acetic acid, 2) 0.5% aq. periodic acid, and 3) Schiff's reagent.

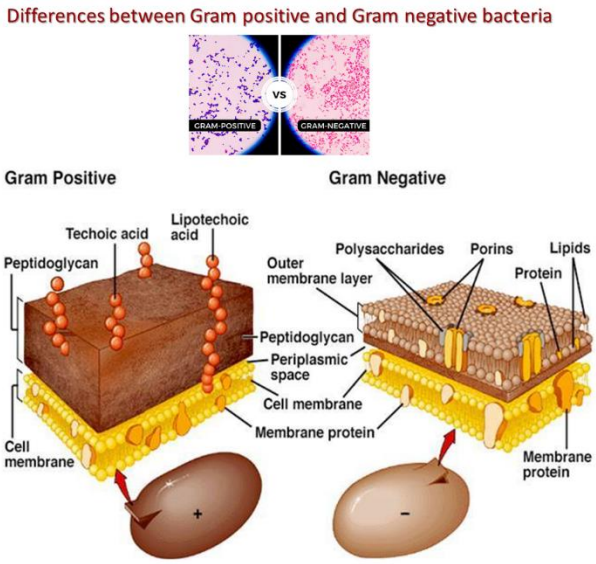

Figure 5.2 Differences between Gram +ve and Gram -ve bacteria. The images have been used with copyright permissions from author and publisher (McGraw-Hill), respectively [73, 74].

Gram staining is a common technique used to distinguish two large groups of bacteria Gram +ve and Gram -ve based on their differences in cell wall constituents (Figure 5.2) by colouring these cells red and violet respectively. Gram staining kit (Sigma-Aldrich) containing crystal violet, iodine, and safranin solutions was used.

5.2.6 Electron microscopy analyses of c-HSE: SEM and TEM

The c-HSE samples were fixed in 2.5% glutaraldehyde, washed in PBS, and then fixed with 1% osmium tetraoxide. Then, the samples were dehydrated in graded ethanols, submerged in polypropylene oxide (PPO), and embedded in epoxy resin (Sigma-Aldrich) leading to heating at 80°C for 8 hours to obtain tissue blocks. These samples were ultrasectioned (~40nm) using Leica Ultracut UCT Ultramicrotome, contrasted with Leica ultrastain II (containing 3% lead citrate) & Leica ultrastain I (0.5% uranyl acetate), and imaged under JEM-2100 TEM at an accelerating voltage of 200kV.

For the sample preparation for scanning electron microscopy (SEM), the c-HSE samples (at T_{1h} and T_{24h} incubation with *S. aureus*) were fixed and dehydrated as described above. Then, the samples were placed in BAL-TEC CPD 030 Critical Point Dryer and dried using CO_2. Liquid CO_2 medium was allowed "in and out" 3 times for 10 min. After which, the samples were mounted onto Leit-C tabs (electrically conductive, double sided adhesive carbon discs) and gold coated using Edwards S150B Sputter Coater under Argon gas (10^{-1}mbar) at voltage of 15mA for 6 min to create a 40nm thick gold (Au) coating. Coated samples were examined under SEM (DSM 982 Gemini, Zeiss) at 15kV accelerating voltage. The particulars of sample preparation for TEM and SEM were described in more detail in Chapter 04.

5.2.7 Statistical analysis

Experiments were carried out in triplicates (n=3) and results were expressed as mean ± standard deviation. For statistical analysis, GraphPad Prism 5.00.288 (Inc., San Diego, CA, USA) was used to evaluate the significance of the differences in cytotoxicity and cell viability data. T-test was used when the comparison involved two groups. Significance between groups was considered for $p < 0.05$.

5.3 Results and discussion

5.3.1 c-HDC

5.3.1.1Microscopic analysis of bacterial colonization - c-HDC

S. aureus and *P. aeruginosa* are two bacteria that are commonly associated with infected wounds [75, 76]. Results for c-HDC inoculated either with *S. aureus* alone, *P. aeruginosa* alone, or co-inoculated with *S. aureus* and *P. aeruginosa*, demonstrated that in all groups, bacteria were able to attach, colonize and initiate biofilm formation on dermal surface as well as to invade deeper areas inside the dermis (Figure 5.3, Figure 5.4, Figure 5.5). *S. aureus* c-HDC group (Figure 5.3) as compared to *P. aeruginosa* one (Figure 5.4) showed heavy biofilm formation with densely stained regions of bacterial clusters (microcolonies). *S. aureus* is one of the well-known and most common pathogens in soft tissue infections that has an inherent ability to form biofilms on biotic and abiotic surfaces [77]. Moreover, *S. aureus* colonized c-HDC showed a smaller number of NHDFs as compared to the other c-HDC groups indicating that cells died by the heavy bacterial colonization and dead cells had been moved or cleared out of dermis (Figure 5.3). On the other hand, the histological sections of c-HDCs on which *S. aureus* and *P. aeruginosa* were co-colonized showed most NHDF with round nuclei, lacking elongated cell morphology (Figure 5.5), suggesting that dead or stressed cells were still in place. The co-existence of multiple strains (Gram +ve and Gram -ve) may be significant for both colonization and pathogenicity in wounds. *Alves PM et al.* reported that these two microorganisms in wounds interact during early co-colonization in a mutual-beneficial manner [78]. *S. aureus* was the one to predominate in biofilm (as also seen in this study) and its aggregates favored *P. aeruginosa* attachment by significantly enhancing adherence to human immortalized keratinocytes cell line (HaCaT); on the other hand, *P. aeruginosa* promoted the invasive phenotype of *S. aureus* [78]. The black arrows indicated bacterial biofilm formation, with the bacterial cocci and rod cells embedded within their own produced extracellular polymeric substance (EPS) (Figure 5.3, Figure 5.4, Figure 5.5).

Histologically, haematoxylin & eosin (H&E) and Gram staining methods were employed to identify the presence of bacteria in infected wounds. Alcian blue-PAS is a special staining method to efficiently analyze biofilm formation. However, in this study no significant difference in microbial visualization was observed among these three staining techniques, suggesting the need for further staining optimization for a delicate tissue like c-HDC. These methods might have a contrasting effect between bacteria and skin tissue visualization, while used for staining full-thickness infected skin wounds. Additionally, modified Gram staining as described by *Sandra Becerra et al*. [79] could also be used to enhance the contrast between bacteria and host tissue for a rapid diagnosis.

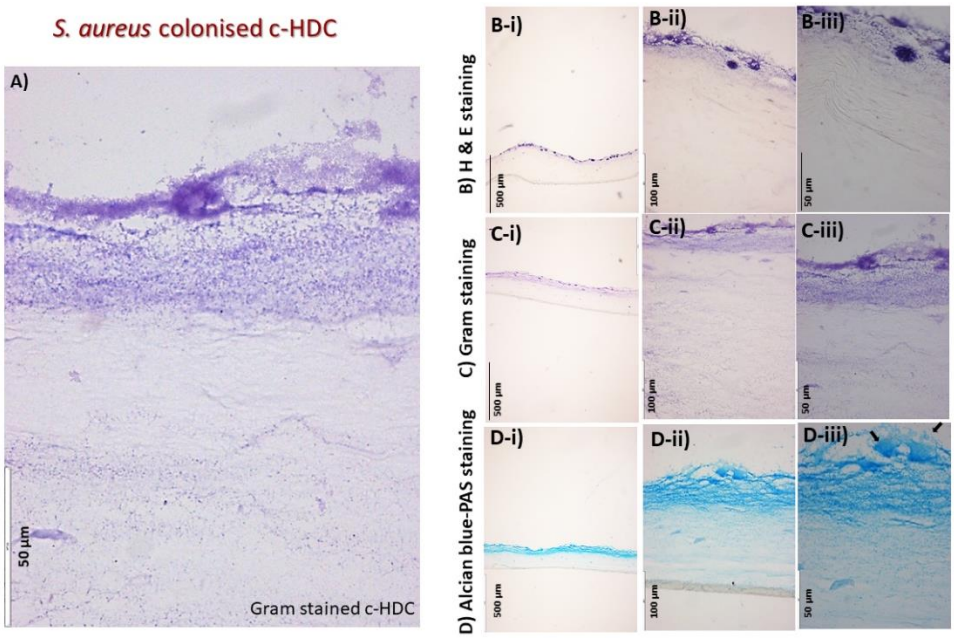

Figure 5.3 A) Histological cross-section of S. aureus colonized c-HDC. The sub-images (B, C, D) displayed S. aureus colonized c-HDC stained by H & E staining (B-i to B-iii), Gram staining (C-i to C-iii), and Alcian blue-PAS staining (D-i to D-iii) shown at different magnifications.

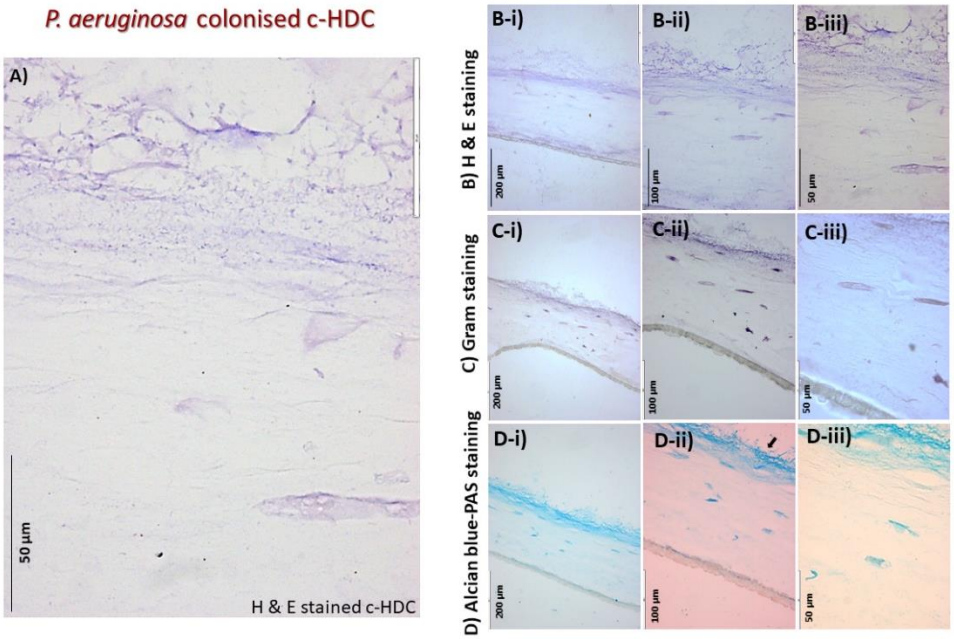

Figure 5.4 A) Histological cross-sections of P. aeruginosa colonized c-HDC. The sub-images (B, C, D) displayed P. aeruginosa colonized c-HDC stained by H & E staining (B-i to B-iii), Gram staining (C-i to C-iii), and Alcian blue-PAS staining (D-i to D-iii) shown at different magnifications.

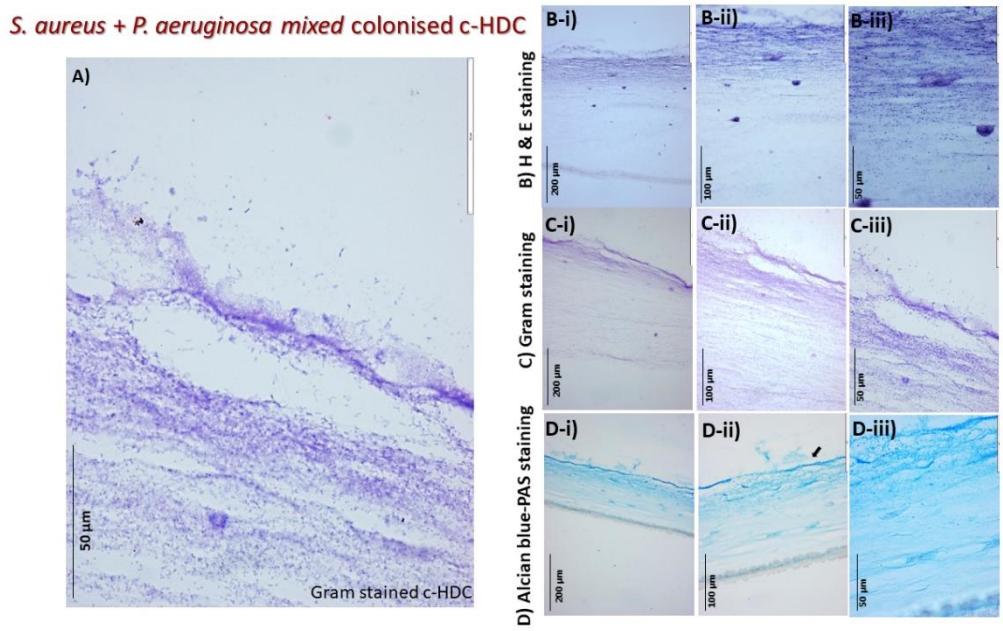

Figure 5.5 A) Histological cross-sections of S. aureus and P. aeruginosa mixed colonized c-HDC. The sub-images (B, C, D) displayed S.aureus and P. aeruginosa mixed colonized c-HDC stained by H & E staining (B-i to B-iii), Gram staining (C-i to C-iii), and Alcian blue-PAS staining (D-i to D-iii) shown at different magnifications.

5.3.1.2Cytotoxicity analysis – c-HDC

A previous study that used an immortalized keratinocyte cell line (HaCaT) to be co-infected with *S. aureus* and *P. aeruginosa* demonstrated an enhanced damage, an impaired wound closure and sustained proinflammatory response allowing persistent microbial colonization [78]. In this study, the cell damage was determined by measuring LDH release using CTO assay. The assay evaluated the cell membrane integrity of NHDF for estimating the number of nonviable cells present in c-HDC. Figure 5.6 showed that the highest cytotoxic effect was observed in c-HDC that was co-colonized with *S. aureus* and *P. aeruginosa* as compared to c-HDC infected either with *S. aureus* or *P. aeruginosa* alone. The statistical analysis showed no significant difference (ns) between cytotoxicity values of "*S. aureus* and *P. aeruginosa* co-colonized c-HDC" and positive control (i.e. lysis control for max. LDH release). However, there were significant difference found between the LDH release values of "*S. aureus* colonized c-HDC" & positive control (P=0.001, **), as well as "*P. aeruginosa* colonized c-HDC" & positive control (P=0.006, **) (Figure 5.6)

As seen in histological cross-sections of *S. aureus* colonized c-HDC group, the presence of a high-density biofilm formation and a very few remaining NHDFs (Figure 5.3) as compared to the other c-HDC groups might indicate NHDF cell damage at an early time point. The half-life of LDH, released from cells into the surrounding medium is almost 9 hours. If the cell damage had occurred at the beginning of an experimental exposure period (i.e. 24 hours), the residual quantity of active LDH in the cell culture medium at

the end of the experiment might underestimate the actual quantity of LDH released and thus the measured (bacterially induced-) cytotoxic effect. This could be one of the explanations while comparing histological results with cytotoxicity data (Figure 5.3 and Figure 5.6)

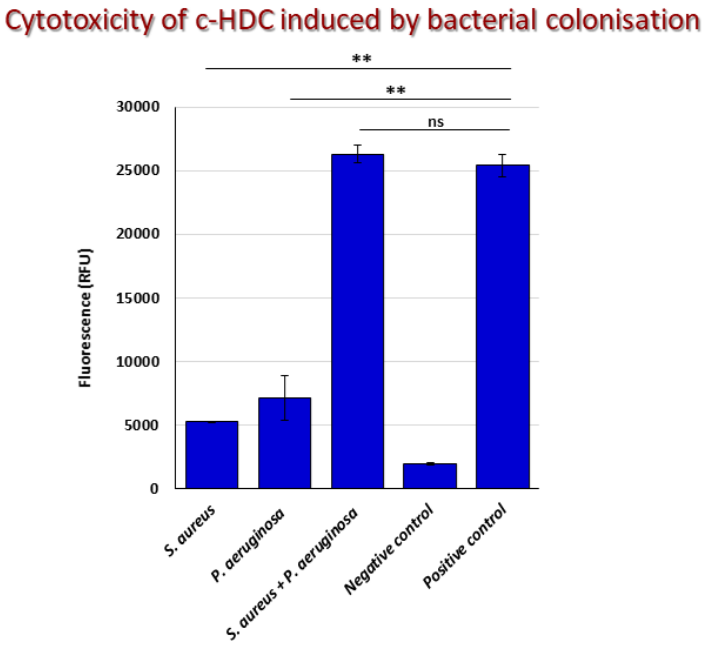

*Figure 5.6 Cytotoxicity of c-HDC induced by bacterial colonization. The cell damage was determined by measuring LDH release using CTO (CytoTox-ONE™ - Promega) assay. Significant difference found between the LDH release values of "S. aureus colonized c-HDC" & positive control (P=0.001, **), as well as* "P. aeruginosa *colonized c-HDC" & positive control (P=0.006, **)*

5.3.2 Wounded HSE

5.3.2.1 Microscopic analysis - wounded HSE

Histological cross-sections of non-inoculated HSE (wounded HSE or wound control) demonstrated the proliferating and migrating basal keratinocytes from the marginal wound edges to cover the wound (Figure 5.7, as indicated by black arrows). This is referred as re-epithelialization that covers the defect and causes wound contraction to reduce the gap volume. Following wounding *in vivo*, during the proliferative phase of damage repair, granulation tissue is formed that is high in fibroblasts number and contains immature ECM with no epidermal surface. Then follows the migration of epidermal cells from surviving epidermis or subepidermal appendages to generate the surface. If the damage is considerable, then cell migration might take significant time retarding the wound closure and enhancing the chances of infection [80-82]. Planktonic or biofilm conditioned media prevented scratch closure by keratinocytes *in vitro,* or wound closure *in vivo* in both murine and rabbit models [83, 84], indicating the negative

effect of microbial wound contamination towards its healing process. *S. aureus* exotoxin, named as ε-cytotoxin, was reported to play an important role in preventing re-epithelialization [85].

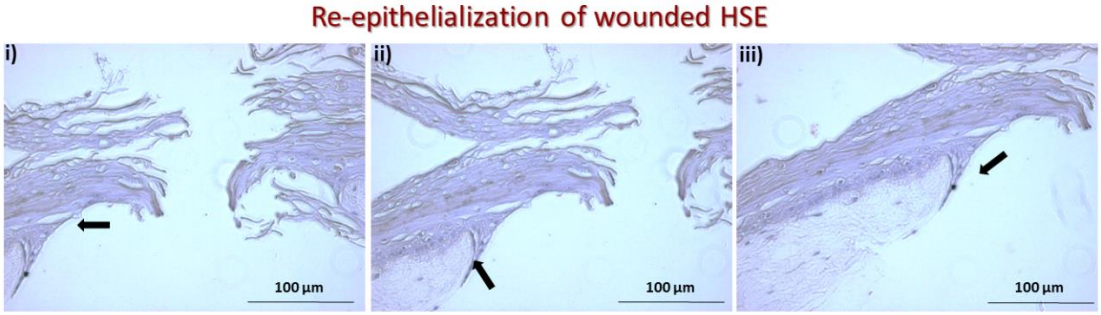

Figure 5.7 Histological cross-sections of re-epithelialization of wounded HSE. The sub-images i, ii, and iii showed different microscopic fields around the wounded HSEs. Black arrows indicated proliferation and migration of basal keratinocytes to cover the wound.

5.3.2.2Cell viability analysis - wounded HSE

Keratinocytes migration plays a central role in wound healing process that starts as early as at 12-24 hours after injury [86] causing cell proliferation until new cell to cell contacts are established. Meanwhile fibroblasts [87] and endothelial cells migration [88, 89], are equally important for granulation tissue formation and angiogenesis respectively. *Eric Teplicki et al.,* reported wound healing properties of therapeutics by measuring the proliferation and migration of fibroblasts and keratinocytes [86]. In this thesis, cell viability was analyzed as a measure of number of living cells in wounded HSE (T_{24h} after wounding) as compared to intact HSE (unwounded) (Figure 5.8). The results demonstrated that the cell viability was lower in wounded HSE as compared to intact HSE (P=0.015, *). This indicated that the loss in viability was due to the damage incurred by full-thickness incision that might need more time to recover. However, histological cross-sections demonstrated that keratinocytes started migrating to cover the gap within 24 hours after incision (Figure 5.7).

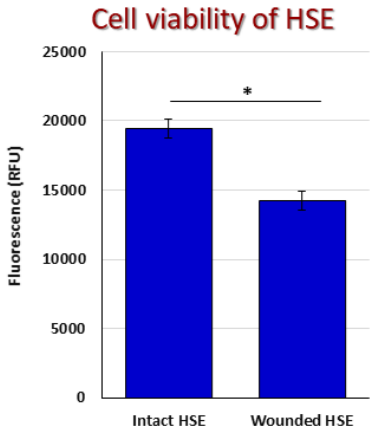

Figure 5.8 Cell viability of intact and wounded HSE. Cell viability was analyzed as a measure of

*number of living cells in wounded HSE (T_{24h} after wounding) as compared to intact HSE (unwounded) by CTB (CellTiter-Blue®) assay. The cell viability was significantly lower in wounded HSE as compared to intact HSE (P=0.015, *).*

5.3.3 c-HSE

5.3.3.1 Microscopic analysis of S. aureus colonization - c-HSE

Histological cross-sections of *S. aureus* colonized c-HSE demonstrated the aggregation of adherent basophilic bacterial cocci along the entire wound edge and the initiation of biofilm formation (Figure 5.9). *S. aureus* surrounded multiple layers of epidermis causing their dissociation and separation (as indicated with *). It also surrounded individual keratinocytes in the basal layer (as indicated with *). *S. aureus* demonstrated big and small colonies formation in dermis near the wound site (as indicated with black arrows) that appeared to invade dermis deeper and sideways dissolving the ECM (as indicated with black dotted arrows). *S. aureus* has been reported to induce the enhanced expression of matrix metalloproteinases (MMPs) of human dermal fibroblasts that take part to degrade their own collagen matrix [90].

Previous *in vivo* studies were performed in animal models of infected skin with multiple aims [91-94]. A study on the effect of methamphetamine in exacerbating susceptibility to *S. aureus* infection used BALB/c mice with full-thickness excisional wounds (5mm in diameter) that were inoculated with 10^7 CFU *S. aureus*. Histological analysis reported the bacterial cluster formation in biofilm-like arrangements *in vivo* [93]. As the rodent skin is not a good representative of wound healing physiology in human skin, other *in vivo* studies made use of infected porcine burns [94, 95]. Partial-thickness burns ($7cm^2$) were inoculated with 1 x 10^6 CFU of either *P. aeruginosa* or *S. aureus* and treated or not treated with antimicrobials. The study reported that the wound debridement was not effective in preventing bacterial colonization, and bacteria were still detected in untreated wounds (debrided but not treated with antibiotic) even after the removal of most of the eschar [94]. An *in vitro* 3D human epidermal model was infected with *A. baumannii* [51] demonstrating that the bacteria were able to colonize and form large biofilms on stratum corneum but did not invade epidermis. Bacterial colonization did not alter keratinocyte proliferation or differentiation [51]. On the contrary, in this Ph.D. thesis, c-HSE cross-sections demonstrated informative visualization of *S. aureus* interaction with epidermal layers and dermal compartment (Figure 5.9). Histological cross-sections of c-HSE (Figure 5.9), compared to wound control (without any *S. aureus*) (Figure 5.7), demonstrated an affected wound closure with no keratinocyte migration suggesting that the presence of bacteria interfered with the normal wound healing process. *Merriman, J.A., et al.,* reported that *S. aureus* exotoxin, named ε-cytotoxin, play an important role in preventing re-epithelialization [85].

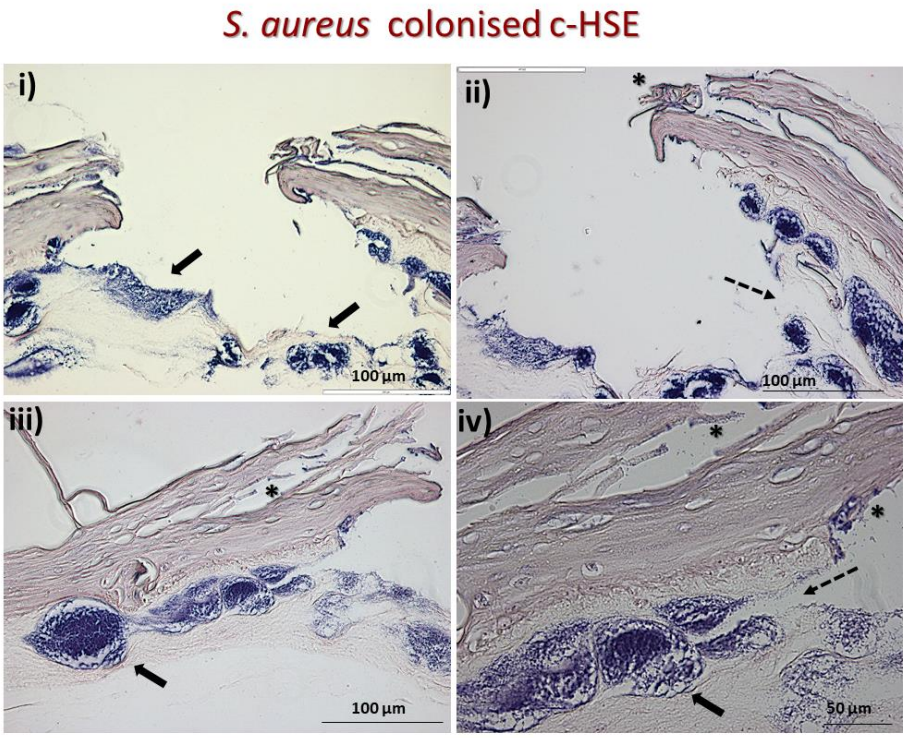

*Figure 5.9 Histological cross-sections of S. aureus colonized c-HSE. The sub-images i, ii, iii, and iv showed different microscopic fields around the S. aureus colonized c-HSE. Big and small colonies formation in dermis near the wound site were indicated with black arrows. S. aureus induced-degradation of ECM was indicated with black dotted arrows). S. aureus surrounding keratinocytes of epidermal layers was indicated with *. "Intact & non-colonized HSE" and "wounded and non-colonized HSE" controls were run, sectioned and compared with c-HSE.*

5.3.3.2S. aureus replication on c-HSE

S. aureus growth rate on c-HSE was measured at T_{0h} (at the time of *S. aureus* inoculation) and T_{24h} (**Error! Reference source not found.** A). Additionally, the differences in *S. aureus* growth under different culture conditions was also recorded (**Error! Reference source not found.** B). The results showed that *S. aureus* growth was much higher on a biotic surface of c-HSE than as a free-floating planktonic form in liquid media conditions of LB broth (a most widely used medium for bacterial growth) and CnT-PR-3D (a media used to bottom feed HSE and c-HSE). The CFU/mL increase in c-HSE was 5.5 x 10^3 times higher as compared to CFU/mL of initial inoculum (**Error! Reference source not found.**). On the other hand, CFU/mL was only 270 and 590 times higher than its initial inoculum, under LB and CnT-PR-3D media, respectively. This result indicated an increased growth rate of *S. aureus* on HSE due to the very well nature-mimicking microenvironment (biotic surface) and thus a more probable cross-communication between bacteria and their hosting HSE-based *in vitro* skin tissue.

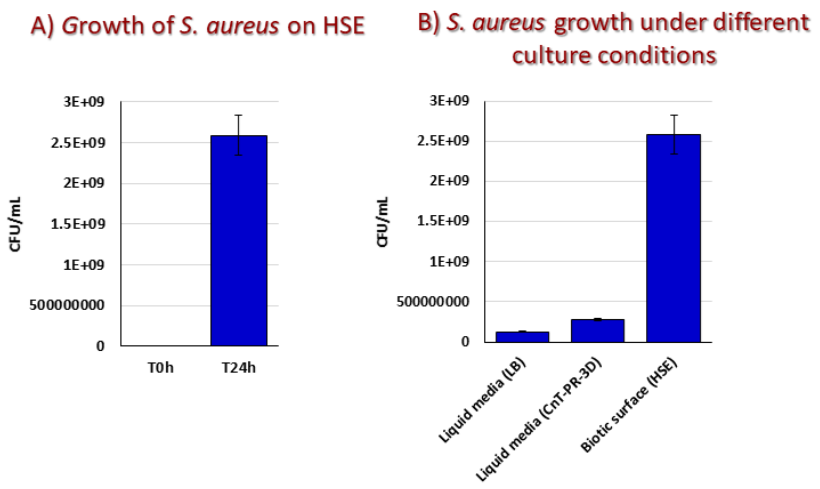

Figure 5. 10 Growth of S. aureus on HSE after 24 hours. The c-HSEs along with the supernatant were collected, homogenized, serially diluted and plated to determine CFU number. The CFU/mL increase in c-HSE was 5.5 x 10^3 times higher as compared to CFU/mL of initial inoculum. While it was 270 and 590 times higher than its initial inoculum, under LB and CnT-PR-3D media, respectively.

5.3.3.3TEM analysis of c-HSE

Transmission electron micrographs revealed ultrastructural interactions of viable *S. aureus* upon contact with keratinocytes and fibroblasts of HSE (**Error! Reference source not found.**). Incomplete cross-walls indicated round and intact dividing cells of *S. aureus* demonstrating their active proliferation and some of the organisms displayed cytoplasm inhomogeneities (with electron light area) in the intracellular DNA region (**Error! Reference source not found.** i, ii, v, & vi).

The dermal compartment of HSE showed a multitude of *S. aureus* bacteria (**Error! Reference source not found.** i & ii), degrading the dermal collagen matrix (**Error! Reference source not found.** i & ii). TEM images also showed bacterial interaction with fibroblasts in dermal layers (**Error! Reference source not found.** iii) and with keratinocytes in epidermal compartments (**Error! Reference source not found.** iv, v, vi, & vii) with the presence of cellular debris and lysed cells around bacteria (**Error! Reference source not found.** iii, iv, & v). The results also demonstrated the separation of epidermal layers, showing the interlayer gaps and filopodia-like extrusions of keratinocyte cell membrane (**Error! Reference source not found.** vi, vii, viii, & ix). Additionally, the internalization of *S. aureus* by keratinocytes was detected (**Error! Reference source not found.** vii). It is known that *S. aureus* has the ability to be internalized by and survive within keratinocytes, contributing to the development of persistent or chronic infections [96].

TEM of c-HSE

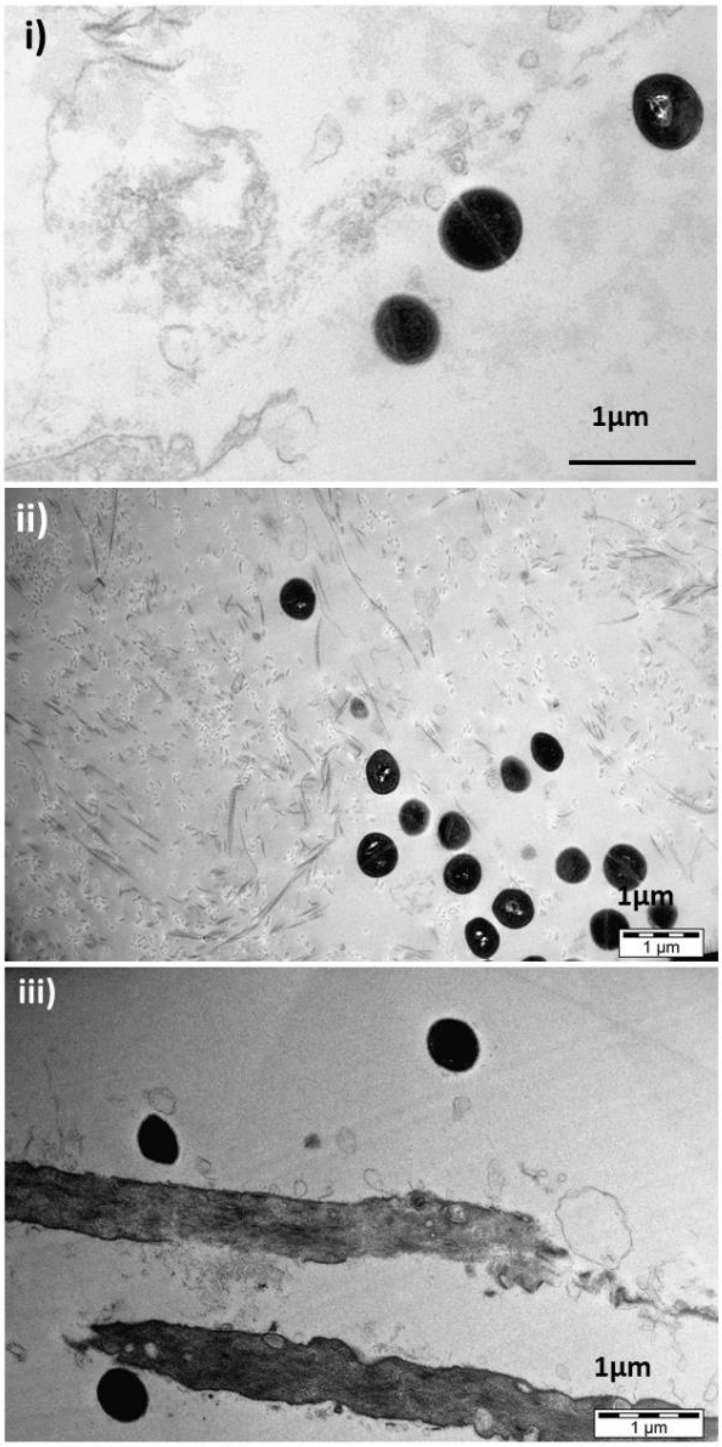

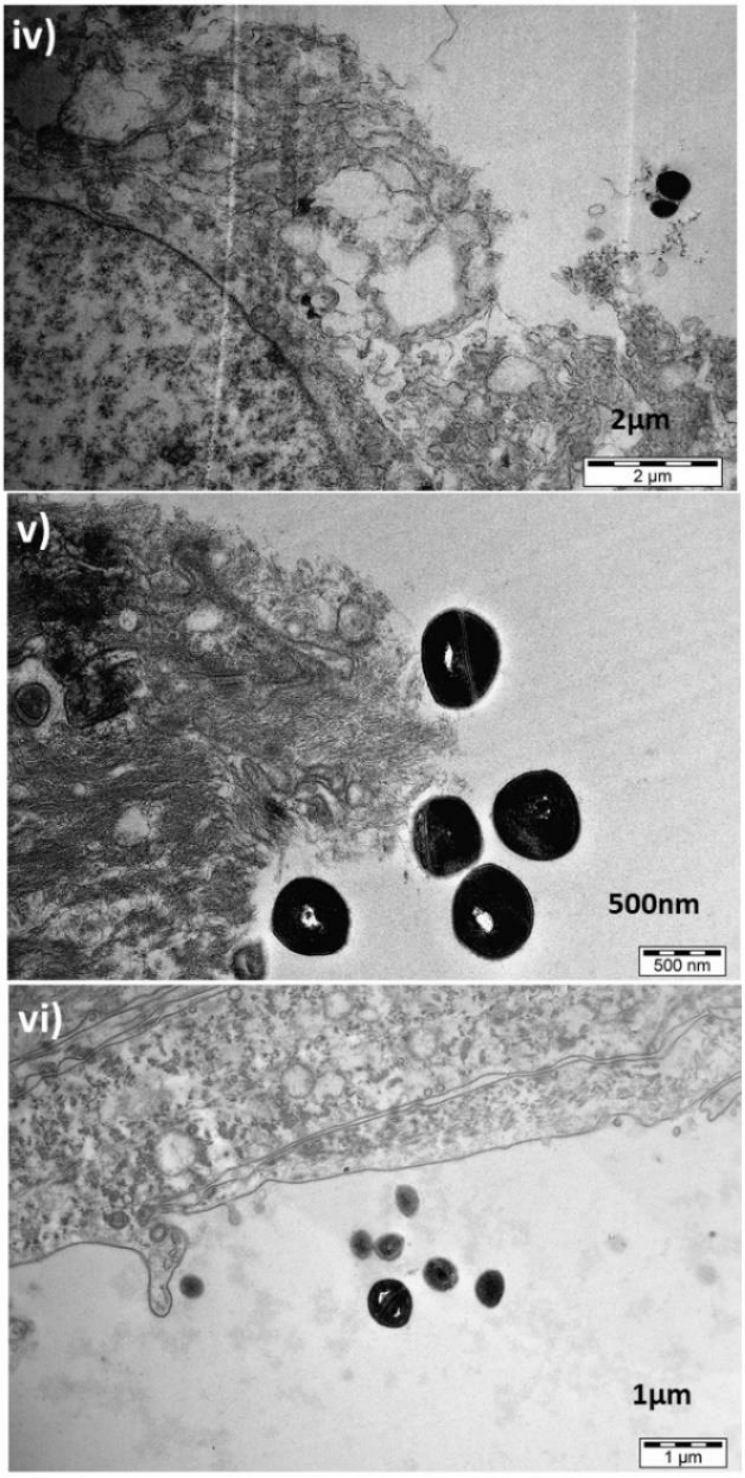
iv)
2µm
2 µm
v)
500nm
500 nm
vi)
1µm
1 µm

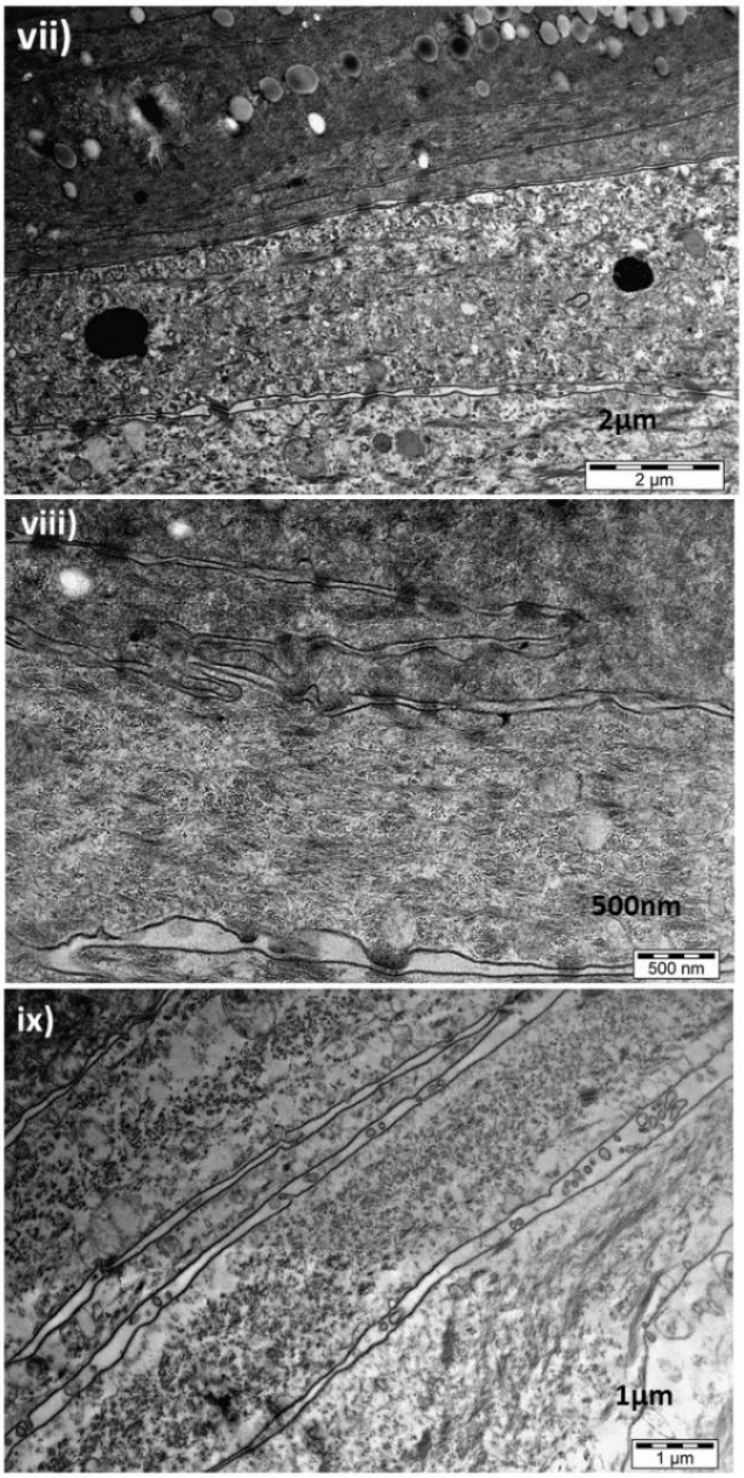

Figure 5. 11 TEM analysis of c-HSE. Images i & ii showed S. aureus (cocci) and their capability to degrade the dermal collagen matrix. The sub-image iii showed bacterial interaction with dermal fibroblasts. The sub-images iv, v, vi, & vii showed bacterial interaction with keratinocytes in epidermal compartments, demonstrating cellular debris/lysed cells around bacteria (sub-images iv & v), bacteria in proximity of keratinocyte (sub-image vi), and internalized bacteria by keratinocytes (sub-image vii). The sub-images viii & ix demonstrated the separation of epidermal layers, showing the interlayer gaps and filopodia-like extrusions of keratinocyte cell membrane.

5.3.3.4 SEM analysis of c-HSE

SEM assessment of c-HSE was shown after 1 hour (T_{1h}) (**Error! Reference source not found.**) and 24 hours (T_{24h}) (**Error! Reference source not found.**) of incubation with *S. aureus*. The results demonstrated *S. aureus* adhesion, proliferation, and biofilm formation at inoculated wound site at indicated times. Grape-like clustering is common to Staphylococcus species as specifically shown in **Error! Reference source not found.** v. **Error! Reference source not found.** i demonstrated bacterial cell clusters, microcolonies, and initiation of relatively immature biofilm formation (as indicated by white arrows) at wound edge. *S. aureus* attached to injured stratum corneum and surrounding the keratinocytes of epidermal layers (causing the layers to dissociate) was shown in **Error! Reference source not found.** ii (as indicated by *). The biofilm formation demonstrated coccoid cells (**Error! Reference source not found.** i, ii, iii, & iv as indicated by white squares) covered and surrounded by EPS (**Error! Reference source not found.** i & ii, as indicated by white arrow heads) at T_{24h}. The NHDF embedded (as indicated by black arrows) in collagen I based ECM (as indicated by white circles) were also seen at the wound site in the dermal compartment, demonstrating their typical elongated morphology (**Error! Reference source not found.**). SEM analysis revealed the *S. aureus* colonization status on HSE in an external appearance perspective.

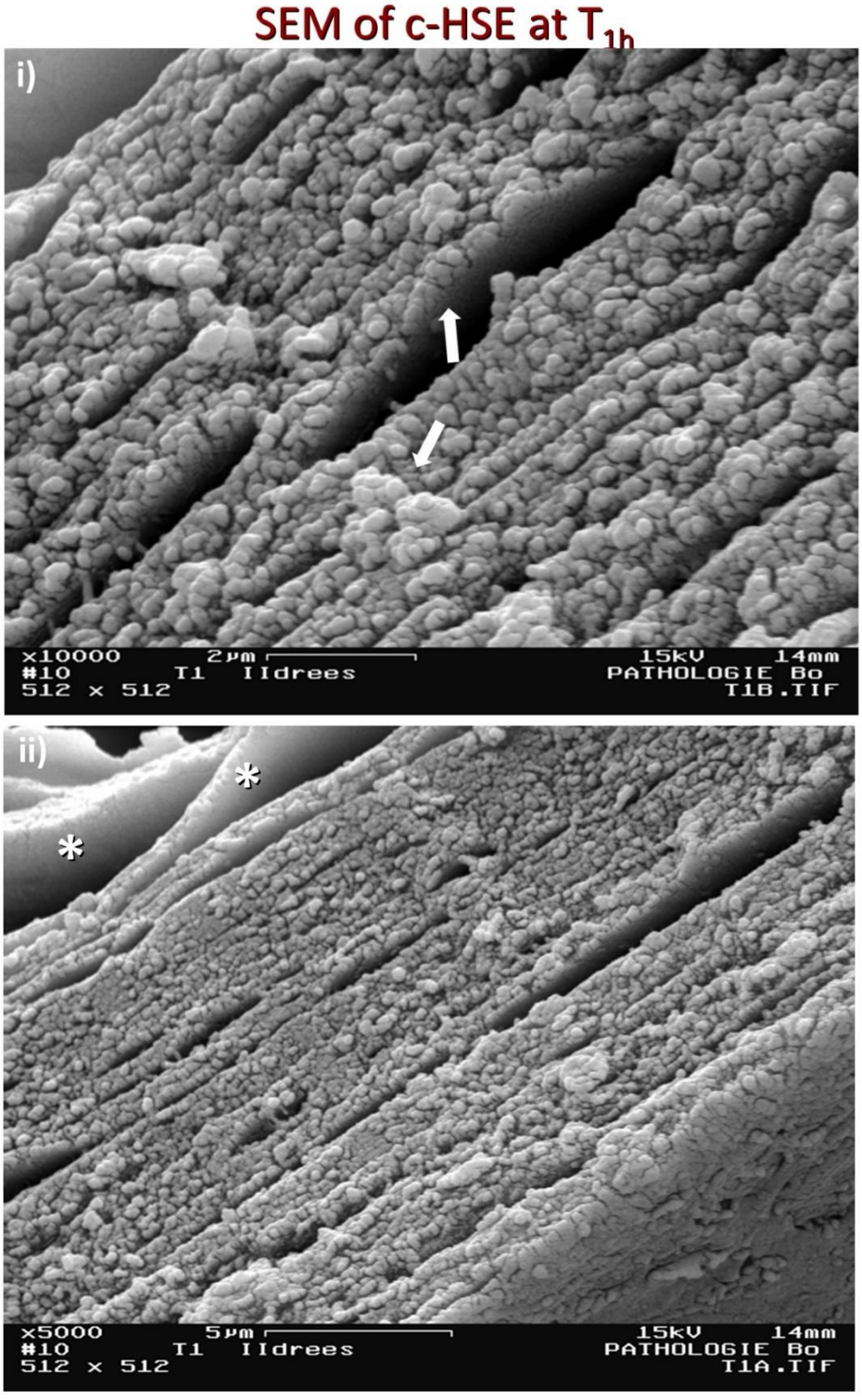

*Figure 5. 12 SEM analysis of c-HSE at T_{1h}. Images i & ii showed different microscopic fields around the S. aureus colonized c-HSE. Bacterial clusters were indicated by white arrows and S. aureus induced epidermal layers dissociation was indicated by *.*

SEM of c-HSE at T_{24h}

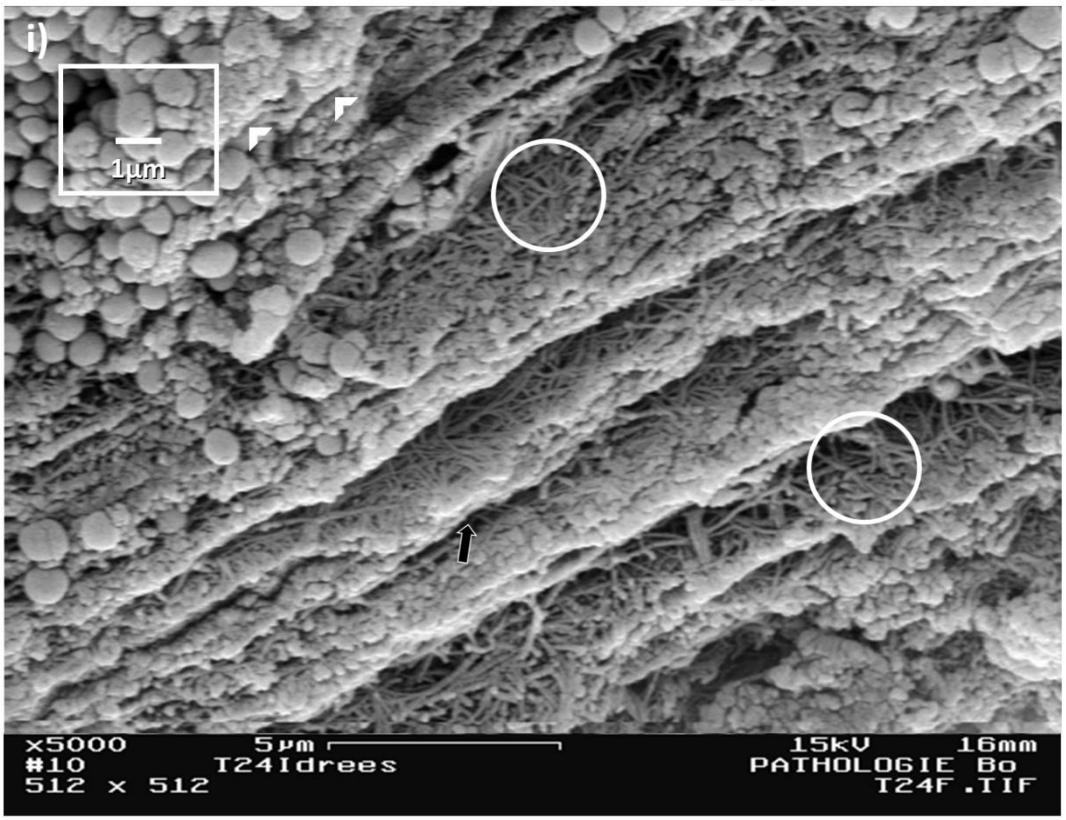

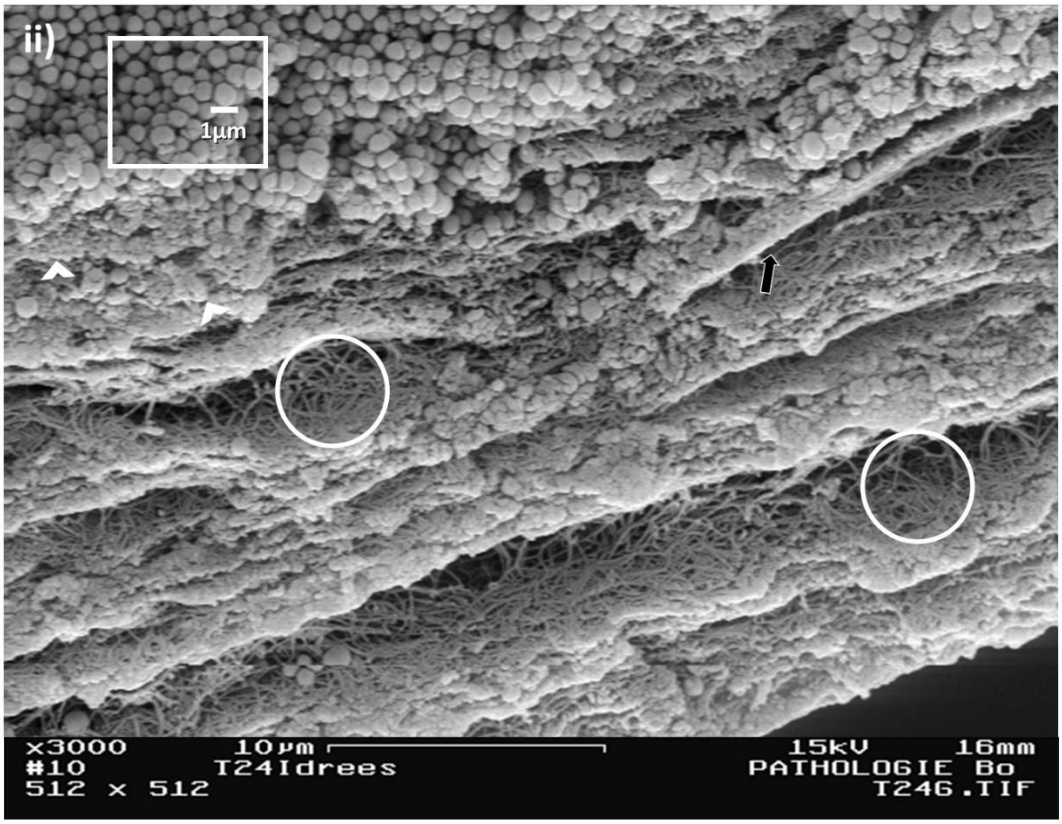

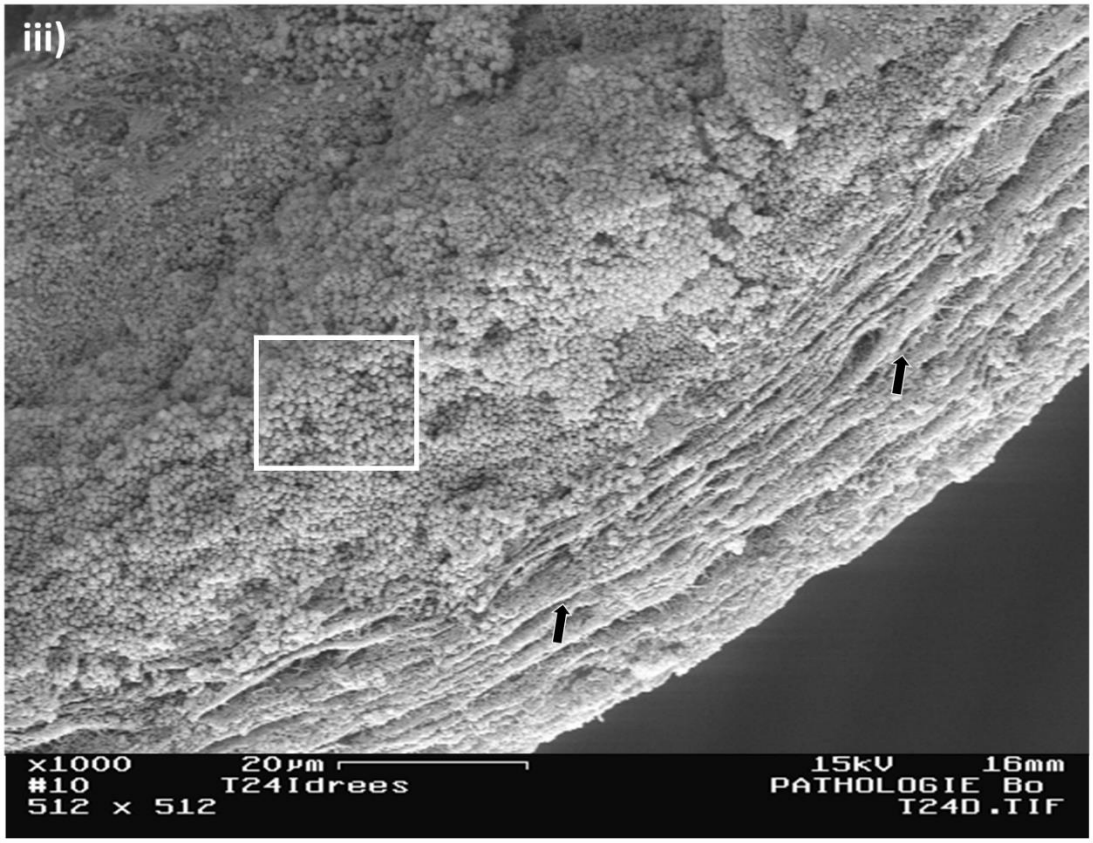
iii)
x1000 20µm 15kV 16mm
#10 T24Idrees PATHOLOGIE Bo
512 x 512 T24D.TIF

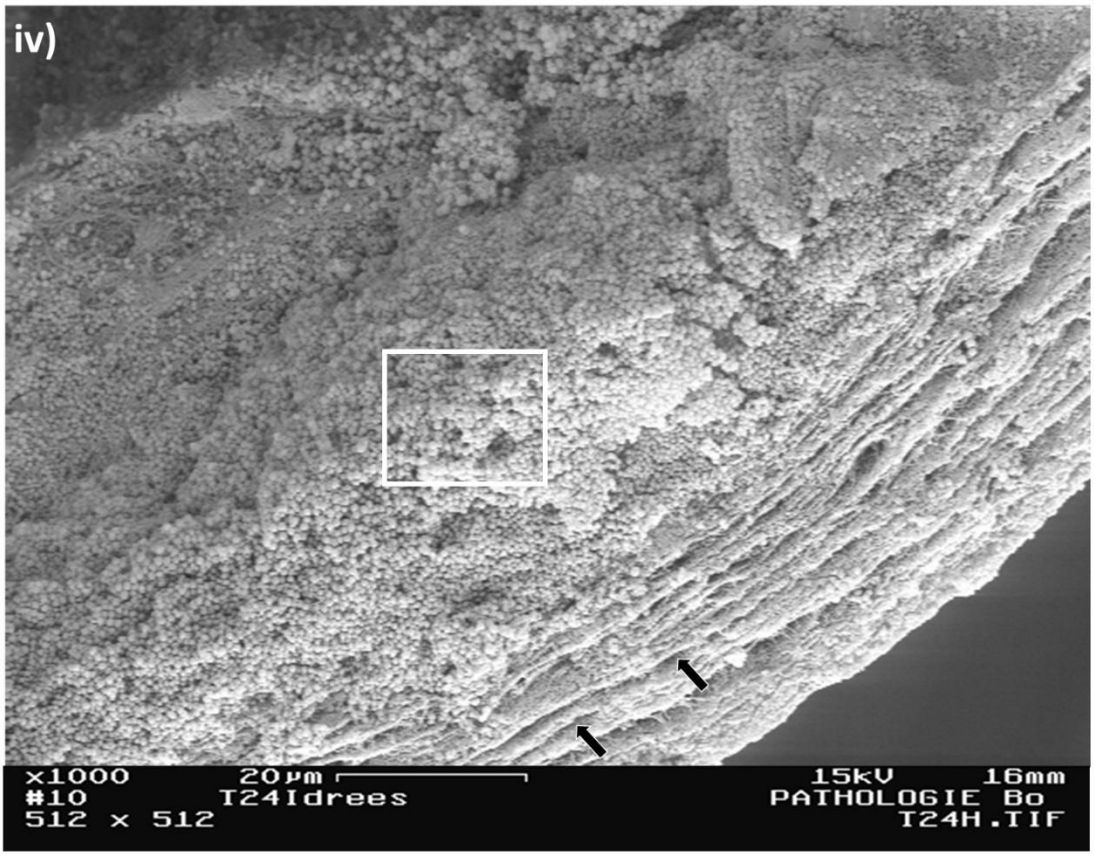
iv)
x1000 20µm 15kV 16mm
#10 T24Idrees PATHOLOGIE Bo
512 x 512 T24H.TIF

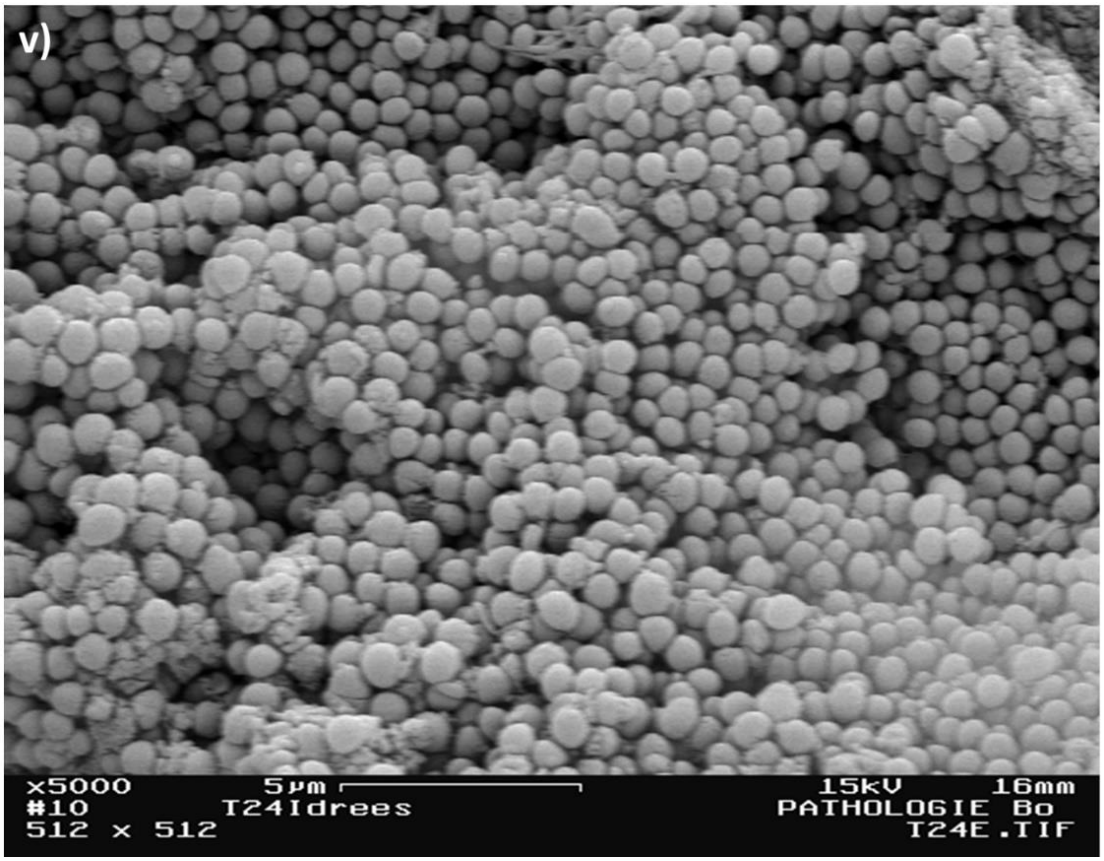

Figure 5. 13 SEM analysis of c-HSE at T_{24h}. The sub-images i, ii, iii, & iv showed different microscopic fields around the S. aureus colonized c-HSE. The biofilm formation and coccoid cells were indicated by white squares that were embedded within EPS (as indicated by white arrow heads). The NHDF (as indicated by black arrows) were embedded within a collagen I based ECM (as indicated by white circles).

5.3.4 S. aureus interaction with intact HSE

Control experiments included the *S. aureus* inoculation on unwounded or intact HSE to examine the interaction between bacteria and HSE at the air-HSE surface interface (**Error! Reference source not found.**). At low bacterial inoculum (i.e. 5000 CFU), bacteria appeared to attach to the top layer (as indicated by black arrows) without invading the deeper layers (**Error! Reference source not found.** A). The results also demonstrated a thickened epidermis (as indicated by black dotted line) (**Error! Reference source not found.** A), that might be due to an induced hyperproliferative state of skin in response to bacteria. Generally, upon barrier disruption, active proliferation state of keratinocytes is important for epidermal reconstruction [97] and, if hindered, it can lead to non-healing wounds [97]. On the other side, *S. aureus* secreted proteins might have a role in altering keratinocyte proliferation [97]. Among the examples of other pathological conditions, thickened scaly skin plaques had been seen in psoriatic skin condition due to hyperplasia [98].

Additionally, the basal cells showed migrating clusters of keratinocytes into the dermis (as indicated by white arrow heads) (**Error! Reference source not found.** A). Among

the examples of other pathological conditions, cells nests formation in dermis depicts malignant behavior of melanocytes [99], through invading the basement membrane *in vivo* [100].

However, despite these observations, bacteria did not invade the epidermis emphasizing the protective barrier function of stratum corneum.

S. aureus colonisation on intact HSE

A) Low inoculum

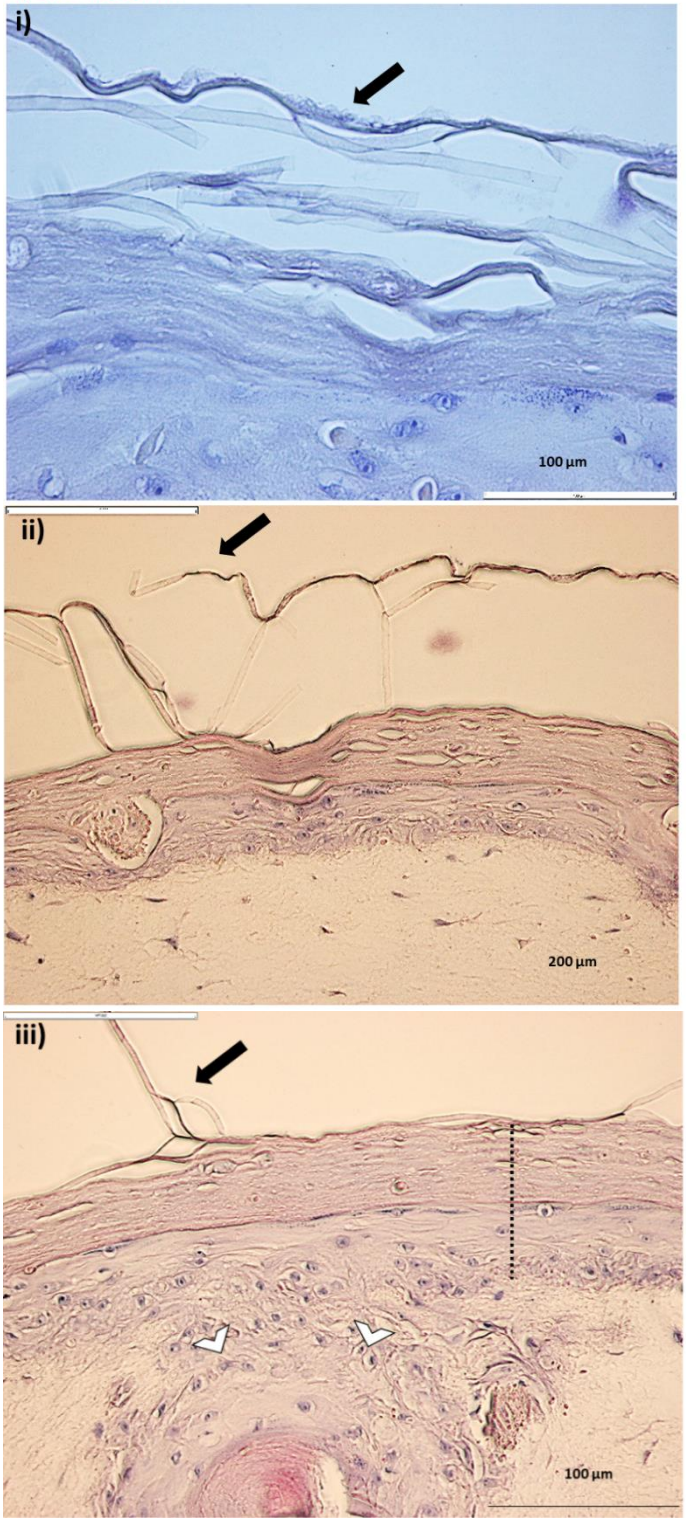

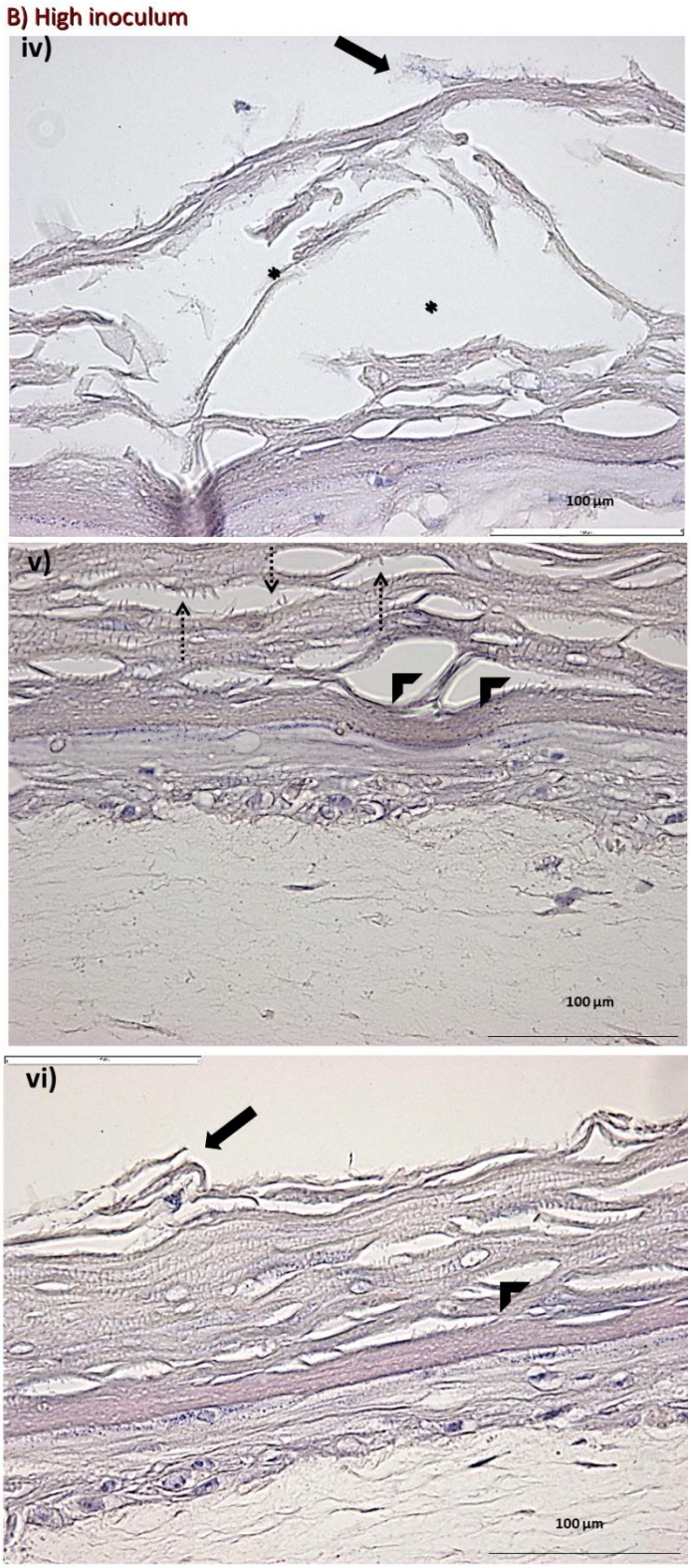

Figure 5. 14 A) Histological cross-sections of S. aureus colonization on intact HSE at low inoculum, demonstrating different aspects of interaction between bacteria and intact HSE, as shown in the sub-images (i, ii, iii). Bacteria attached to the top layer were indicated by black arrows, a thickened epidermis was indicated by black dotted line, and migrating clusters of basal keratinocytes into the dermis were

*indicated by white arrow heads. B) Histological cross-sections of S. aureus colonization on intact HSE at high inoculum, demonstrating different aspects of interaction between bacteria and intact HSE, as shown in the sub-images (iv, v, vi). Bacteria attached to the top epidermal layer were indicated by black arrows, interlayer gaps within epidermal layers were indicated by black arrow heads, epidermal layers dissociation was indicated by *, and serrated demarcations of separating epidermal layers were indicated by black dotted arrows.*

At comparatively higher bacterial inoculum (20,000 CFU), bacteria not only attached to the top epidermal layer (as indicated by black arrows), but they were even able to invade a few epidermal layers (**Error! Reference source not found.** B). Moreover, epidermal layers showed interlayer gaps (as indicated by black arrow heads) as compared to the control without any bacteria. The top epidermal layers clearly appeared to dissociate from each other (as indicated by *) (**Error! Reference source not found.** B). The separating layers showed the serrated demarcations (as indicated by black dotted arrows) suggesting tearing of layers. Skin desquamation can be a type of skin response as its defence mechanism, making it difficult for organisms to establish permanent residence on skin. The *S. aureus* induced epidermal exfoliation observed in **Error! Reference source not found.** B might be due to the exfoliative toxins (ETs) produced by *S. aureus* that can attack the skin defense barrier [101]. ETs are able to digest desmoglein 1 (Dsg1), a keratinocyte cell to cell adhesion molecule [101], resulting in dissociation of keratinocytes in stratum granulosum and spinosum. The loss of adhesive function of Dsg1 cannot be compensated by other Dsgs, as it happens in staphylococcal scalded skin syndrome, cutaneous abscess/furuncles [102] and intraepidermal splitting in impetigo [103]. Thus, changes in the epidermal barrier function can lead to *S. aureus* penetration through epidermis and bacterial entry into the dermis; for example, this happens in atopic dermatitis where filaggrin defects enhance *S. aureus* colonization and dermal dysbiosis results in aggravation of disease condition [104]. Previously, it was observed that bacteria residing on the epidermis may be found within the dermis of healthy human skin [105].

Experiments performed in this Ph.D. thesis demonstrated the barrier function of HSE in preventing the bacterial invasion and showed that the barrier function lost efficiency if the inoculated bacterial number was high enough to damage the stratum corneum. Such experiments helped to understand invasive epidermal infection mechanisms in unwounded skin by *S. aureus*.

Conclusion

An *in vitro* model for *S. aureus* colonization and biofilm formation, using HSE was developed (c-HSE). Preliminary studies were performed on HDC on mixed colonization of *S. aureus* and *P. aeruginosa*. The bacterial co-existence revealed significance for both colonization and pathogenicity in wounds. The biofilm formation demonstrated denser colonized regions in c-HDC inoculated with *S. aureus* as compared to the c-HDC inoculated with *P. aeruginosa.*

The complete c-HSE model identified aspects of bacterial colonization on intact and wounded HSE. The results demonstrated that bacterial colonization on wounded c-HSE hindered the re-epithelialization process by inducing fibroblasts/keratinocytes damage, ECM degradation, and by forming biofilm like structures.

The c-HSE model may be useful in characterizing bacterial growth kinetics and the interaction among different bacterial species on a skin tissue-based biotic surface. Moreover, the c-HSE model might be beneficial for identifying new targets for antimicrobial strategies. Likewise, this model may serve as an advanced tool to evaluate the antimicrobial and wound healing properties of AMPBs and novel therapeutics.

References

1. Charles, C.A., et al., *Use of tissue-engineered skin to study in vitro biofilm development.* Dermatologic Surgery, 2009. 35(9): p. 1334-1341.
2. Hill, K.E., et al., *An in vitro model of chronic wound biofilms to test wound dressings and assess antimicrobial susceptibilities.* Journal of Antimicrobial Chemotherapy, 2010. 65(6): p. 1195-1206.
3. McCaig, L.F., et al., *Staphylococcus aureus–associated skin and soft tissue infections in ambulatory care.* Emerging infectious diseases, 2006. 12(11): p. 1715.
4. Moran, G.J., et al., *Methicillin-resistant Staphylococcus aureus in community-acquired skin infections.* Emerging infectious diseases, 2005. 11(6): p. 928.
5. Eady, E.A. and J.H. Cove, *Staphylococcal resistance revisited: community-acquired methicillin resistant Staphylococcus aureus-an emerging problem for the management of skin and soft tissue infections.* Current opinion in infectious diseases, 2003. 16(2): p. 103-124.
6. Krishna, S. and L.S. Miller, *Host–pathogen interactions between the skin and Staphylococcus aureus.* Current opinion in microbiology, 2012. 15(1): p. 28-35.
7. O'Brien, L.M., et al., *Staphylococcus aureus clumping factor B (ClfB) promotes adherence to human type I cytokeratin 10: implications for nasal colonization.* Cellular microbiology, 2002. 4(11): p. 759-770.
8. Shepherd, J., et al., *Development of three-dimensional tissue-engineered models of bacterial infected human skin wounds.* Tissue Engineering Part C: Methods, 2009. 15(3): p. 475-484.
9. O'Toole, G., H.B. Kaplan, and R. Kolter, *Biofilm formation as microbial development.* Annual Reviews in Microbiology, 2000. 54(1): p. 49-79.
10. Flecknell, P., *Replacement, reduction, refinement.* ALTEX-Alternatives to animal experimentation, 2002. 19(2): p. 73-78.
11. Russell, W.M.S., R.L. Burch, and C.W. Hume, *The principles of humane experimental technique*. Vol. 238. 1959: Methuen London.
12. *Council of the European Union. Seventh Amendment to the EU and Cosmetics Directive 76/768/EEC. Brussels: The European Parliament and the Council of the European Union.* 2003.
13. Commission, E., *THE SCCP'S NOTES OF GUIDANCE FOR THE TESTING OF COSMETIC INGREDIENTS AND THEIR SAFETY EVALUATION (Adopted by the SCCP during the 10th plenary meeting of 19 December 2006)*, E. Commission, Editor. 2006.
14. Campbell, R.L. and R.D. Bruce, *Comparative dermatotoxicology: I. Direct comparison of rabbit and human primary skin irritation responses to*

isopropylmyristate. Toxicology and applied pharmacology, 1981. 59(3): p. 555-563.
15. Phillips II, L., et al., *A comparison of rabbit and human skin response to certain irritants.* Toxicology and Applied Pharmacology, 1972. 21(3): p. 369-382.
16. Groeber, F., et al., *Skin tissue engineering—in vivo and in vitro applications.* Advanced drug delivery reviews, 2011. 63(4-5): p. 352-366.
17. Mazzoleni, G., D. Di Lorenzo, and N. Steimberg, *Modelling tissues in 3D: the next future of pharmaco-toxicology and food research?* Genes & nutrition, 2009. 4(1): p. 13.
18. Cukierman, E., et al., *Taking cell-matrix adhesions to the third dimension.* Science, 2001. 294(5547): p. 1708-1712.
19. Grinnell, F., *Biochemical analysis of cell adhesion to a substratum and its possible relevance to cell metastasis.* Progress in clinical and biological research, 1976. 9: p. 227-236.
20. Yang, J., et al., *Different mitogenic and phenotypic responses of human breast epithelial cells grown in two versus three dimensions.* Experimental cell research, 1986. 167(2): p. 563-569.
21. Lin, C.Q. and M.J. Bissell, *Multi-faceted regulation of cell differentiation by extracellular matrix.* The FASEB Journal, 1993. 7(9): p. 737-743.
22. Smalley, K.S., M. Lioni, and M. Herlyn, *Life ins't flat: Taking cancer biology to the next dimension.* In Vitro Cellular & Developmental Biology-Animal, 2006. 42(8-9): p. 242-247.
23. Grinnell, F., *Fibroblast mechanics in three-dimensional collagen matrices.* Journal of bodywork and movement therapies, 2008. 12(3): p. 191-193.
24. Horning, J.L., et al., *3-D tumor model for in vitro evaluation of anticancer drugs.* Molecular pharmaceutics, 2008. 5(5): p. 849-862.
25. El Ghalbzouri, A., et al., *Replacement of animal-derived collagen matrix by human fibroblast-derived dermal matrix for human skin equivalent products.* Biomaterials, 2009. 30(1): p. 71-78.
26. El Ghalbzouri, A., et al., *Leiden reconstructed human epidermal model as a tool for the evaluation of the skin corrosion and irritation potential according to the ECVAM guidelines.* Toxicology in Vitro, 2008. 22(5): p. 1311-1320.
27. de Breij, A., et al., *Three-dimensional human skin equivalent as a tool to study Acinetobacter baumannii colonization.* Antimicrobial agents and chemotherapy, 2012. 56(5): p. 2459-2464.
28. Holland, D.B., et al., *Differential innate immune responses of a living skin equivalent model colonized by Staphylococcus epidermidis or Staphylococcus aureus.* FEMS microbiology letters, 2009. 290(2): p. 149-155.

29. Corriveau, M.-N., et al., *Detection of Staphylococcus aureus in nasal tissue with peptide nucleic acid–fluorescence in situ hybridization.* American journal of rhinology & allergy, 2009. 23(5): p. 461-465.
30. Ohnemus, U., et al. *Regulation of epidermal Tight Junctions (TJ) during infection with exfoliative-toxin negative staphylococcus strains*. in *JOURNAL OF INVESTIGATIVE DERMATOLOGY*. 2007. NATURE PUBLISHING GROUP 75 VARICK STREET, 9TH FLOOR, NEW YORK, NY 10013-1917 USA.
31. Ridky, T.W., et al., *Invasive three-dimensional organotypic neoplasia from multiple normal human epithelia.* Nature medicine, 2010. 16(12): p. 1450.
32. Kretz, M., et al., *Control of somatic tissue differentiation by the long non-coding RNA TINCR.* Nature, 2013. 493(7431): p. 231.
33. Hauser, C., et al., *Staphylococcus aureus skin colonization in atopic dermatitis patients.* Dermatology, 1985. 170(1): p. 35-39.
34. Leung, D.Y., et al., *New insights into atopic dermatitis.* The Journal of clinical investigation, 2004. 113(5): p. 651-657.
35. LEYDEN, J.J., R.R. MARPLES, and A.M. KLIGMAN, *Staphylococcus aureus in the lesions of atopic dermatitis.* British Journal of Dermatology, 1974. 90(5): p. 525-525.
36. Mildner, M., et al., *Knockdown of filaggrin impairs diffusion barrier function and increases UV sensitivity in a human skin model.* Journal of Investigative Dermatology, 2010. 130(9): p. 2286-2294.
37. McGrath, J.A. and J. Uitto, *The filaggrin story: novel insights into skin-barrier function and disease.* Trends in molecular medicine, 2008. 14(1): p. 20-27.
38. WerthÉn, M., et al., *An in vitro model of bacterial infections in wounds and other soft tissues.* Apmis, 2010. 118(2): p. 156-164.
39. Thorn, R., S. Nelson, and J. Greenman, *Use of a bioluminescent Pseudomonas aeruginosa strain within an in vitro microbiological system, as a model of wound infection, to assess the antimicrobial efficacy of wound dressings by monitoring light production.* Antimicrobial agents and chemotherapy, 2007. 51(9): p. 3217-3224.
40. Thorn, R. and J. Greenman, *A novel in vitro flat-bed perfusion biofilm model for determining the potential antimicrobial efficacy of topical wound treatments.* Journal of applied microbiology, 2009. 107(6): p. 2070-2079.
41. Schaller, M., et al., *Models of oral and vaginal candidiasis based on in vitro reconstituted human epithelia.* Nature protocols, 2006. 1(6): p. 2767.
42. Green, C.B., et al., *RT-PCR detection of Candida albicans ALS gene expression in the reconstituted human epithelium (RHE) model of oral candidiasis and in model biofilms.* Microbiology, 2004. 150(2): p. 267-275.

43. Coenye, T. and H.J. Nelis, *In vitro and in vivo model systems to study microbial biofilm formation.* Journal of microbiological methods, 2010. 83(2): p. 89-105.
44. Schaller, M., et al., *Invasion of Candida albicans correlates with expression of secreted aspartic proteinases during experimental infection of human epidermis.* Journal of investigative dermatology, 2000. 114(4): p. 712-717.
45. Schaller, M., R. Mailhammer, and H.C. Korting, *Cytokine expression induced by Candida albicans in a model of cutaneous candidosis based on reconstituted human epidermis.* Journal of medical microbiology, 2002. 51(8): p. 672-676.
46. Schaller, M., et al., *Polymorphonuclear leukocytes (PMNs) induce protective Th1-type cytokine epithelial responses in an in vitro model of oral candidosis.* Microbiology, 2004. 150(9): p. 2807-2813.
47. Syrjänen, S., et al., *In vitro establishment of lytic and nonproductive infection by herpes simplex virus type 1 in three-dimensional keratinocyte culture.* Journal of virology, 1996. 70(9): p. 6524-6528.
48. Hukkanen, V., et al., *Herpes simplex virus type 1 infection has two separate modes of spread in three-dimensional keratinocyte culture.* Journal of general virology, 1999. 80(8): p. 2149-2155.
49. Visalli, R.J., R.J. Courtney, and C. Meyers, *Infection and replication of herpes simplex virus type 1 in an organotypic epithelial culture system.* Virology, 1997. 230(2): p. 236-243.
50. Andrei, G., et al., *Organotypic epithelial raft cultures as a model for evaluating compounds against alphaherpesviruses.* Antimicrobial agents and chemotherapy, 2005. 49(11): p. 4671-4680.
51. de Breij, A., et al., *A 3D human skin equivalent as a tool to study Acinetobacter baumannii colonization.* Antimicrobial agents and chemotherapy, 2012: p. AAC. 05975-11.
52. Popov, L., et al., *Three-dimensional human skin models to understand Staphylococcus aureus skin colonization and infection.* Frontiers in immunology, 2014. 5: p. 41.
53. Amagai, M. and J.R. Stanley, *Desmoglein as a target in skin disease and beyond.* Journal of Investigative Dermatology, 2012. 132(3): p. 776-784.
54. Bukowski, M., B. Wladyka, and G. Dubin, *Exfoliative toxins of Staphylococcus aureus.* Toxins, 2010. 2(5): p. 1148-1165.
55. Ganesh, V.K., et al., *Structural and biochemical characterization of Staphylococcus aureus clumping factor B/ligand interactions.* Journal of Biological Chemistry, 2011. 286(29): p. 25963-25972.
56. Miajlovic, H., et al., *Both complement-and fibrinogen-dependent mechanisms contribute to platelet aggregation mediated by Staphylococcus aureus clumping factor B.* Infection and immunity, 2007. 75(7): p. 3335-3343.

57. Walsh, E.J., et al., *Clumping factor B, a fibrinogen-binding MSCRAMM (microbial surface components recognizing adhesive matrix molecules) adhesin of Staphylococcus aureus, also binds to the tail region of type I cytokeratin 10.* Journal of Biological Chemistry, 2004. 279(49): p. 50691-50699.
58. Wilke, G.A. and J.B. Wardenburg, *Role of a disintegrin and metalloprotease 10 in Staphylococcus aureus α-hemolysin–mediated cellular injury.* Proceedings of the National Academy of Sciences, 2010. 107(30): p. 13473-13478.
59. Sørensen, O.E., et al., *Differential regulation of β-defensin expression in human skin by microbial stimuli.* The Journal of Immunology, 2005. 174(8): p. 4870-4879.
60. Fulton, C., et al., *Expression of natural peptide antibiotics in human skin.* The Lancet, 1997. 350(9093): p. 1750-1751.
61. Falconer, A., et al., *Expression of the peptide antibiotics human β defensin-1 and human β defensin-2 in normal human skin.* Journal of investigative dermatology, 2001. 117(1): p. 106-111.
62. Duckney, P., et al. *Inflammatory effects of common skin microbial species on cultured keratinocytes*. in *JOURNAL OF INVESTIGATIVE DERMATOLOGY*. 2011. NATURE PUBLISHING GROUP 75 VARICK ST, 9TH FLR, NEW YORK, NY 10013-1917 USA.
63. Wolcott, R.D., D.D. Rhoads, and S.E. Dowd, *Biofilms and chronic wound inflammation.* Journal of wound care, 2008. 17(8): p. 333-341.
64. Williams, P., *Quorum sensing, communication and cross-kingdom signalling in the bacterial world.* Microbiology, 2007. 153(12): p. 3923-3938.
65. Dowd, S.E., et al., *Survey of bacterial diversity in chronic wounds using pyrosequencing, DGGE, and full ribosome shotgun sequencing.* BMC microbiology, 2008. 8(1): p. 43.
66. Stoodley, P., et al., *Growth and detachment of cell clusters from mature mixed-species biofilms.* Appl. Environ. Microbiol., 2001. 67(12): p. 5608-5613.
67. Purevdorj-Gage, B., J.W. Costerton, and P. Stoodley, *Phenotypic differentiation and seeding dispersal in non-mucoid and mucoid Pseudomonas aeruginosa biofilms.* Microbiology, 2005. 151(5): p. 1569-1576.
68. Meluleni, G.J., et al., *Mucoid Pseudomonas aeruginosa growing in a biofilm in vitro are killed by opsonic antibodies to the mucoid exopolysaccharide capsule but not by antibodies produced during chronic lung infection in cystic fibrosis patients.* The Journal of Immunology, 1995. 155(4): p. 2029-2038.
69. Lam, J.S., et al., *Production and characterization of monoclonal antibodies against serotype strains of Pseudomonas aeruginosa.* Infection and Immunity, 1987. 55(5): p. 1051-1057.

70. Lam, J., et al., *Immunogenicity of Pseudomonas aeruginosa outer membrane antigens examined by crossed immunoelectrophoresis.* Infection and immunity, 1983. 42(1): p. 88-98.
71. Idrees, A., et al., *Validation of in vitro assays in three-dimensional human dermal constructs.* The International journal of artificial organs, 2018. 41(11): p. 779-788.
72. Promega, U., *CytoTox-ONE™ Homogeneous Membrane Integrity Assay.*
73. Karki, G., *Difference between Gram positive and Gram negative bacteria*, in *Online Biology Notes*. July 31, 2018.
74. Cowan, M.K., *Microbiology: a systems approach*. 2018: McGraw-Hill.
75. Church, D., et al., *Burn wound infections.* Clinical microbiology reviews, 2006. 19(2): p. 403-434.
76. Laurie, C., et al., *Prevention and management of infections associated with burns in the combat casualty.* Journal of Trauma and Acute Care Surgery, 2008. 64(3): p. S277-S286.
77. Otto, M., *Staphylococcal biofilms*, in *Bacterial biofilms*. 2008, Springer. p. 207-228.
78. Alves, P.M., et al., *Interaction between Staphylococcus aureus and Pseudomonas aeruginosa is beneficial for colonisation and pathogenicity in a mixed biofilm.* Pathogens and disease, 2018. 76(1): p. fty003.
79. Becerra, S.C., et al., *An optimized staining technique for the detection of Gram positive and Gram negative bacteria within tissue.* BMC research notes, 2016. 9(1): p. 216.
80. Ehrlich, H.P. and T.M. Krummel, *Regulation of wound healing from a connective tissue perspective.* Wound repair and regeneration, 1996. 4(2): p. 203-210.
81. Hur, G.-Y., D.-K. Seo, and J.-W. Lee, *Contracture of skin graft in human burns: effect of artificial dermis.* Burns, 2014. 40(8): p. 1497-1503.
82. Pastar, I., et al., *Epithelialization in wound healing: a comprehensive review.* Advances in wound care, 2014. 3(7): p. 445-464.
83. Secor, P.R., et al., *Staphylococcus aureus Biofilm and Planktonic cultures differentially impact gene expression, mapk phosphorylation, and cytokine production in human keratinocytes.* BMC microbiology, 2011. 11(1): p. 143.
84. Gurjala, A.N., et al., *Development of a novel, highly quantitative in vivo model for the study of biofilm-impaired cutaneous wound healing.* Wound repair and regeneration, 2011. 19(3): p. 400-410.
85. Merriman, J.A., et al., *Novel Staphylococcus aureus Secreted Protein Alters Keratinocyte Proliferation and Elicits a Proinflammatory Response In Vitro and In Vivo.* Biochemistry, 2015. 54(31): p. 4855-4862.

86. Teplicki, E., et al., *The Effects of Aloe vera on Wound Healing in Cell Proliferation, Migration, and Viability.* Wounds: a compendium of clinical research and practice, 2018. 30(9): p. 263-268.
87. Werner, S., T. Krieg, and H. Smola, *Keratinocyte–fibroblast interactions in wound healing.* Journal of Investigative Dermatology, 2007. 127(5): p. 998-1008.
88. Freinkel, R.K. and D.T. Woodley, *The biology of the skin*. 2001: CRC Press.
89. Robinson, J.K., et al., *Surgery of the skin: procedural dermatology*. 2014: Elsevier Health Sciences.
90. Kanangat, S., et al., *Induction of multiple matrix metalloproteinases in human dermal and synovial fibroblasts by Staphylococcus aureus: implications in the pathogenesis of septic arthritis and other soft tissue infections.* Arthritis research & therapy, 2006. 8(6): p. R176.
91. Jacobsen, F., et al., *Efficacy of topically delivered moxifloxacin against wound infection by Pseudomonas aeruginosa and methicillin-resistant Staphylococcus aureus.* Antimicrobial agents and chemotherapy, 2011. 55(5): p. 2325-2334.
92. Dai, T., et al., *Animal models of external traumatic wound infections.* Virulence, 2011. 2(4): p. 296-315.
93. Mihu, M.R., et al., *Methamphetamine alters the antimicrobial efficacy of phagocytic cells during methicillin-resistant Staphylococcus aureus skin infection.* MBio, 2015. 6(6): p. e01622-15.
94. Roy, D.C., et al., *Ciprofloxacin-loaded keratin hydrogels reduce infection and support healing in a porcine partial-thickness thermal burn.* Wound Repair and Regeneration, 2016. 24(4): p. 657-668.
95. Wong, V.W., et al., *Surgical approaches to create murine models of human wound healing.* BioMed Research International, 2010. 2011.
96. Kintarak, S., et al., *Internalization of Staphylococcus aureus by human keratinocytes.* Infection and immunity, 2004. 72(10): p. 5668-5675.
97. Bucalo, B., W.H. Eaglstein, and V. Falanga, *Inhibition of cell proliferation by chronic wound fluid.* Wound repair and regeneration, 1993. 1(3): p. 181-186.
98. Park, J.-H., et al., *Histopathological differential diagnosis of psoriasis and seborrheic dermatitis of the scalp.* Annals of dermatology, 2016. 28(4): p. 427-432.
99. Della, *HistoQuarterly: SUPERFICIAL SPREADING MALIGNANT MELANOMA* Histology Blog., January 23, 2014
100. Hill, D.S., et al., *A novel fully-humanised 3D skin equivalent to model early melanoma invasion.* Molecular cancer therapeutics, 2015: p. molcanther. 0394.2015.

101. Nishifuji, K., M. Sugai, and M. Amagai, *Staphylococcal exfoliative toxins:"molecular scissors" of bacteria that attack the cutaneous defense barrier in mammals.* Journal of dermatological science, 2008. 49(1): p. 21-31.
102. Yamasaki, O., et al., *Distribution of the exfoliative toxin D gene in clinical Staphylococcus aureus isolates in France.* Clinical microbiology and infection, 2006. 12(6): p. 585-588.
103. Imanishi, I., et al., *Staphylococcus aureus penetrate the interkeratinocyte spaces created by skin-infiltrating neutrophils in a mouse model of impetigo.* Veterinary dermatology, 2017. 28(1): p. 126-e27.
104. Nakatsuji, T., et al., *Staphylococcus aureus exploits epidermal barrier defects in atopic dermatitis to trigger cytokine expression.* Journal of Investigative Dermatology, 2016. 136(11): p. 2192-2200.
105. Nakatsuji, T., et al., *The microbiome extends to subepidermal compartments of normal skin.* Nature communications, 2013. 4: p. 1431.

Chapter 06: Comparative 2D vs. 3D bio-evaluation Tools: Human Skin Equivalent (HSE) and *S. aureus* colonized HSE (c-HSE) as Advanced Preclinical *In vitro* Risk and Antibacterial Properties' Assessment Platforms

Table of contents

List of figures

List of tables

Abbreviations

2D and 3D: Two-dimensional and three-dimensional
Ag^{+}: Silver ion
Ag-dressings: Antibacterial silver containing wound dressings
$AgNO_3$: Silver nitrate
ALI: Air-liquid interface
AMPB: Antimicrobial polymeric biomaterials
ATCC: American Type Culture Collection
BF: Bright field
CFU: Colony forming unit
c-HSE: Colonized human skin equivalent
CLSI: Clinical & Laboratory Standards Institute
CnT: CELLnTECH
CnT-PR: CnT-Prime medium
CnT-PR-3D: CnT-Prime 3D barrier culture medium
CnT-PR-F: CnT-Prime fibroblast medium
COCA: Mouse epidermal cchapell line
CTB: CellTiter-Blue® cell viability assay
DSMZ: German Collection of Microorganisms and Cell Cultures
ECACC: European Collection of Authenticated Cell Cultures
ECM: Extracellular matrix
E. coli: Escherichia coli
FCS & FBS: Foetal calf serum and foetal bovine serum
GC and SC: Growth control and sterility control
Gram +ve and Gram -ve: Gram positive and negative bacteria
H & E stain: Haematoxylin and eosin stain
HSE: Human skin equivalent
IC50: Half maximal inhibitory concentration (While assaying cytotoxicity, IC50 is the concentration of cytotoxic compound that gives 50% viability)
L929: Mouse fibroblast cell line
MBC: Minimum bactericidal concentration
MHB: Mueller-Hinton broth
MIC: Minimum inhibitory concentration
MODS: Multiple organ dysfunction syndrome
MRD: Maximum recovery diluent
MRSA: Methicillin-resistant Staphylococcus aureus
MRSE: Methicillin-resistant Staphylococcus epidermidis
NHDF: Normal human dermal fibroblasts
NHEK: Normal human epidermal keratinocytes
Ns: Non-significant

PBS: Phosphate-buffered saline
PE: Polyethylene
P. aeruginosa: Pseudomonas aeruginosa
RPMI1640: Roswell Park memorial institute cell culture medium
ROS: Reactive oxygen species
SDS: Sodium dodecyl sulphate
SI: Selectivity index
SIRS: Systemic inflammatory response syndrome
SWF: Simulated wound fluid
S. aureus: Staphylococcus aureus
S. epidermidis: Staphylococcus epidermidis
$T_{4h,\ 24h,\ 48h}$: Time point 4 hours, 24 hours, 48 hours
TCPS: Tissue culture polystyrene
TCPS: Tissue culture polystyrene
TEM: Transmission electron microscopy
TNS: Trypsin neutralizing solution
TSB: Tryptic soy broth
ZDEC-PU: Zinc diethyldithiocarbamate containing polyurethane

Chapter 06: Comparative 2D vs. 3D bio-evaluation tools: Human Skin Equivalent (HSE) and *S. aureus* colonized HSE (c-HSE) as advanced preclinical *in vitro* risk and antibacterial properties' assessment platforms

Abstract

Infected wounds still represent a great challenge in public health. With an increasing need for novel strategies to combat wounds colonized with resistant microbes, more reliable preclinical data are needed to bioanalyze antimicrobial polymeric biomaterials (AMPBs). A 3D human skin equivalent (HSE) and wound infection model (c-HSE) are highly demanded to serve as biomimetic system for the testing of AMPBs.

The HSE was obtained having both a dermal and an epidermal compartment, by embedding normal human dermal fibroblasts (NHDF) in rat tail tendon collagen type I hydrogel (mimicking dermal extracellular matrix) and then seeding normal human epidermal keratinocytes (NHEK) on it to generate the epidermis. The culture conditions were optimized to obtain well-differentiated tissue, closely mimicking *in vivo* skin. Skin infection model was created by full-thickness incision and colonization with relevant skin infectious bacteria (*S. aureus*) at wound site. The *in vitro S. aureus* colonized HSE model was coded as c-HSE. The models were fully characterized by histology staining, immunohistochemistry, confocal microscopy and TEM analysis. To validate the 3D systems, Ag^{+} as an antibacterial agent and commercially available Ag containing antimicrobial wound dressings (Ag-dressings) [namely PolyMem® Ag (Ferris), Biatain® Alginate Ag (Coloplast), Biatain® Ag (Coloplast), Atrauman® Ag (Hartmann)] along with their controls without silver, were tested. The silver sources in wound dressings were either nanocrystalline silver, metallic silver, or Ag containing inorganic salt embedded in a polymer (polyurethane=PU)/ biopolymer (alginate) matrix, releasing Ag^{+}; that were tested for cytocompatibility and antimicrobial properties. Murine fibroblast cell line (L929), murine epidermal cell line COCA, NHDF, and NHEK monolayer cell cultures were used as 2D cytocompatibility evaluation systems. Further *in vitro* experiments were performed using HSE, where tissue culture model allowed cellular behavior evaluation in three-dimensional pattern, which more closely simulates *in vivo* behavior. CellTiter-Blue® (CTB) assay and/or Live/Dead imaging were used to measure cell viability of monolayer and 3D cell cultures after 24 exposure of test material via direct contact method. Bright field microscopy further supplemented cytotoxicity analysis by indicating the changes in cell morphology, if any.

The microdilution method was used to determine MIC and MBC of Ag^{+} against clinically relevant pathogens namely *Staphylococcus aureus* (ATCC 29213), *Staphylococcus epidermidis* (ATCC 12228), *Escherichia coli* (ATCC 25922),

Pseudomonas aeruginosa (ATCC 27853), *Methicillin-resistant Staphylococcus aureus (MRSA)*, and *Methicillin-resistant Staphylococcus epidermidis (MRSE).* Different culture media and testing methods were also evaluated to assess the effects of culture 'environment' on bacterial susceptibility to the toxic action of silver. For this purpose, Ag-dressings were evaluated for their antibacterial activity against *Staphylococcus aureus* (ATCC 29213), *Escherichia coli* (ATCC 25922), and *Pseudomonas aeruginosa* (ATCC 27853) by broth inoculation method in tryptic soy broth (TSB) and simulated wound fluid (SWF) over a time period of 48 hours (T_{4h}, T_{24h}, T_{48h}), to determine bacterial reduction and CFU number of surviving bacteria. Then, we used the c-HSE to test the antibacterial effects of tested materials on *S. aureus* colonized HSE. The materials were microbiologically tested in the infected skin model (c-HSE) and the results allowed calculation of CFU per c-HSE.

Ag^+ showed an IC50 (half maximal inhibitory concentration - while assaying cytotoxicity, IC50 is the concentration of cytotoxic compound that gives 50% viability) of 2.3µg/mL, 10.8µg/mL, 10.3µg/mL and 11.8µg/mL in 2D monolayer cultures of L929, COCA, NHDF and NHEK, respectively, while IC50 was three times higher (34.2µg/mL) when using HSE. Tissue culture models indicated an 'environmental effect' on cytotoxicity, with decreased sensitivity to Ag^+ cytotoxicity for cells in 3D with respect to cells in 2D cultures. Ag^+ showed MIC in a range of 4.2-8.4µg/mL and MBC in a range of 4.2-33µg/mL against mentioned Gram +ve and Gram -ve bacteria. The antibacterial activity of Ag^+ against *S. aureus* in TSB showed 99.99% reduction at T_{24h}, while it was not efficient when tested in SWF. This considerable variation indicated that antibacterial ability of Ag^+ was highly dependent on wound extracellular micro-environment, that could affect Ag^+ availability.

Among tested Ag-dressings, the cytotoxicity tests using NHDF and NHEK indicated that silver released from Biatain® Ag (1% cell viability) and Biatain® Alginate Ag (53% cell viability) was lethal for both fibroblasts and keratinocytes. On the other hand, Biatain® Ag and Biatain® Alginate Ag demonstrated 77±21.8% and 92.5±10.6% cell viability with HSE, that was not significantly different than negative control. Biatain® Ag demonstrated 99.99% bacterial reduction against *S. aureus*, and Gram -ve (e.g. *P. aeruginosa*, and/or *E. coli*) in both TSB and SWF testing environments at all time points. On the contrary, Biatain® Alginate Ag showed 99% bacterial reduction against *S. aureus* and Gram -ve (e.g. *P. aeruginosa*) only in TSB but not in SWF environment at T_{24h}. When tested in a more complex *S. aureus* colonized HSE model (c-HSE), Biatain® Ag was still able to reduce bacterial burden and demonstrated significantly less (P=0.0085, **) Log CFU in Biatain® Ag treated c-HSE, while Biatain® Alginate Ag showed no significant reduction. These results demonstrated that as the cell viability decreased, the antibacterial effect increased. Among the tested Ag-dressings, Biatain® Ag was able to significantly reduce bacteria in c-HSE without significantly compromising cell viability of HSE in our advanced experimental set-ups. Other Ag-products were highly

compatible with cells but were not significantly lethal to bacteria. Also, it is worth noticing that the bio-evaluation outcomes were different in 2D monolayer vs. 3D cell culture systems. Additionally, results obtained from conventionally used microbial methods were different compared to those deriving from advanced c-HSE system. With an increasing need for reliable *in vitro* test systems, we were successfully able to verify our advanced 3D models, to serve as a risk assessment platform for cytocompatibility and antibacterial properties. Moreover, these results also suggested the critical considerations to be taken into account while deciding the use of Ag and Ag-dressings for wound care strategies.

HSE and c-HSE have great potential to develop even more complex skin models for testing skin treatment strategies, as these models allow the study of skin-pathogen interactions, and of novel targets for designing new antibacterial agents.

Keywords: AMPBs, HSE, c-HSE, *S. aureus*, bio-evaluation tools, cytocompatibility, antibacterial activity, Ag-dressings, Ag^{+}, 2D vs. 3D

6.1 Introduction

6.1.1 HSE as an in vitro tool of bio-evaluation and safety assessment

Need of a 3D testing system

In vitro bio-evaluation is more accurate using three-dimensional (3D) testing systems than two-dimensional (2D) cell cultures [1-3]. Extracellular matrix (ECM) is the main component of 3D microenvironment and regulates the intercellular & intracellular communication via distinct signaling pathways. The interactions between ECM and cells in 3D vs 2D cell culture systems result in differences of cell surface receptor expression (e.g. focal and fibrillar adhesions) [4], metabolic functions, proliferative potential, ECM production, release of key regulators, relevant cell density and tissue phenotype [5-11]. 2D cell cultures do not reproduce the natural ECM microenvironment and tissue structure, as they force cells to adhere to flat substrates, resulting in poor model predictivity [11]. The cells grown in 3D environment mimic the complexity and dynamicity of the *in vivo* microenvironment [11]. Thus, the cells-ECM combined interactions (Figure 6.1) define tissue's response to an external stimulus [5-10, 12]. Consequently, the biological response of a 3D skin against a toxic agent, and its ability to react as a whole, are mediated by a cross-talk among multiple cell types and surrounding ECM [13].

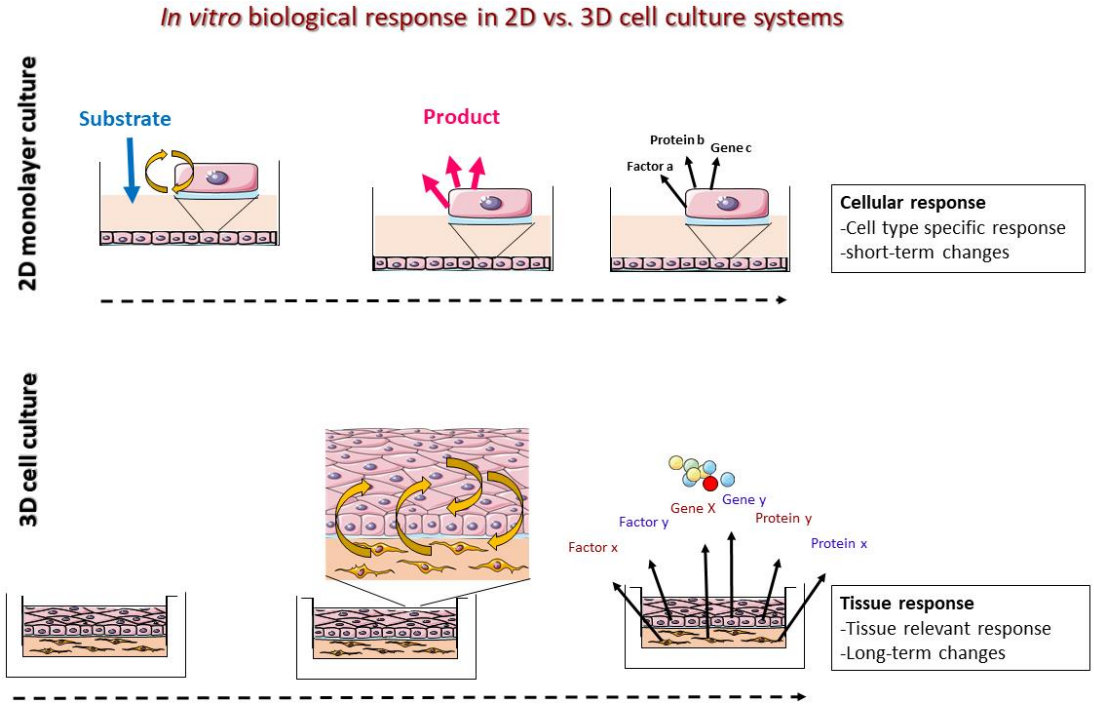

Figure 6.1 In vitro biological response in 2D vs. 3D cell culture systems. Unlike 2D cell culture, the in vitro bio-evaluation in a 3D testing system is a result of a combined interactions of a tissue to better define the cell's behavior towards an external stimulus.

In vitro skin models and diseased skin models imitate the physiological and pathological state respectively and can serve to measure the damaging capacity or the curative potential of applied substances. In this context, organotypic (i.e. tissue) skin cultures consisting of cell lines (e.g. HaCat) do not only lack the skin differentiation capacity but are also deficient in the intrinsic genetic variability of primary keratinocytes [14-16]. Establishing more close, complex, and systemic 3D approaches enhance the predictability of *in vivo* outcomes (Figure 6.2).

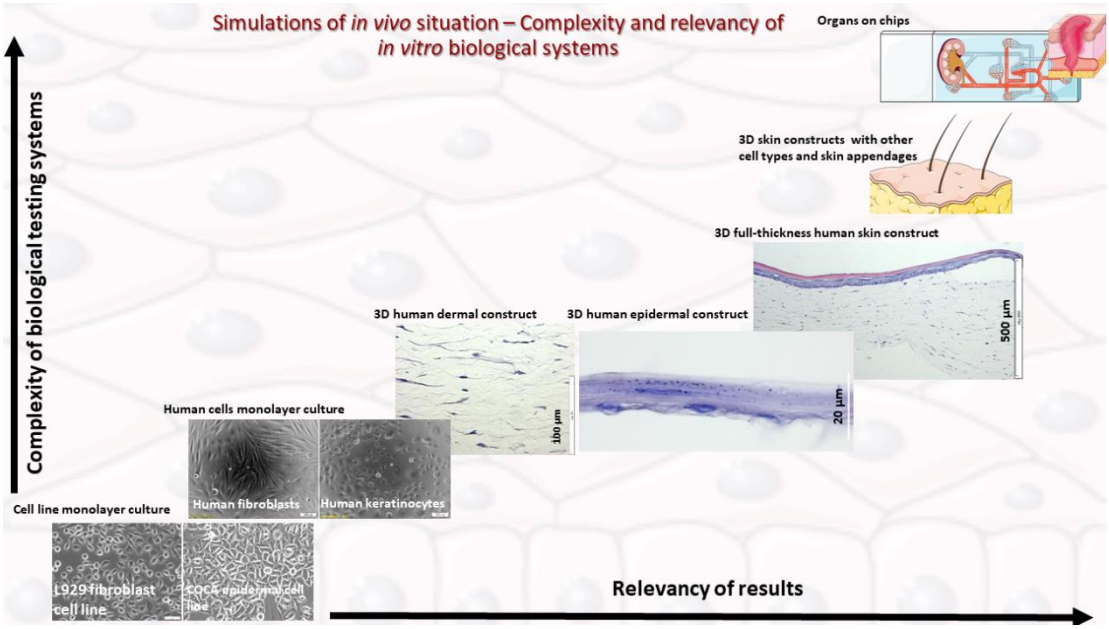

Figure 6.2 Simulations of in vivo situation – Complexity and relevancy of in vitro biological systems. The image showed the general correlation of in vitro testing system's complexity and its relevancy to in vivo outcomes. As the complexity of biological system increases, the challenges associated with its reproducibility, analysis/readout methods, and system validation increase as well.

Need of an alternative of animal testing

The understanding of outcomes occurring during pre-clinical phase (Figure 6.3) often requires a significant amount of exploratory research. For example, in rodents, histopathological assessment may be indicator of potential treatment-related changes, but, in many cases, their exact mechanisms and clinical relevance of the observed effects remain unknown.

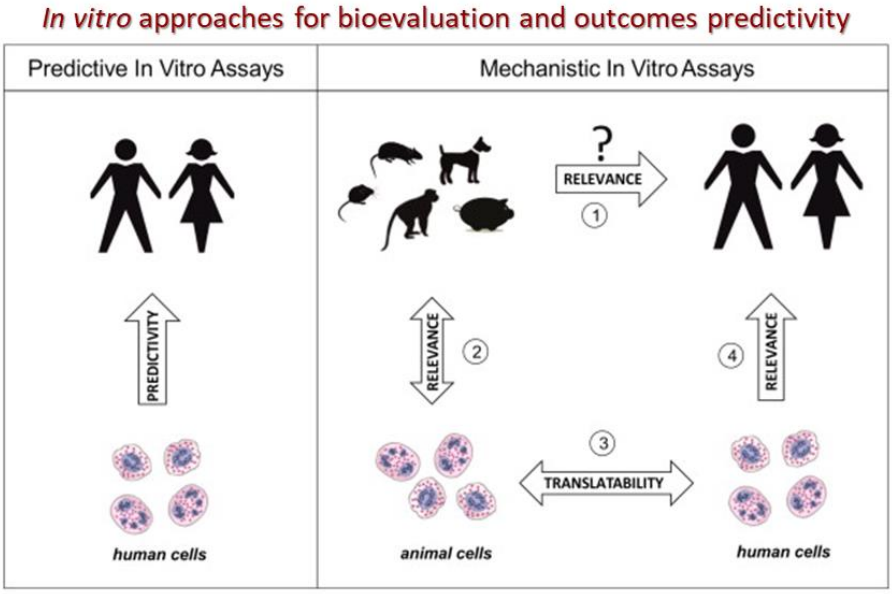

Figure 6.3 In vitro approaches for bio-evaluation and outcomes predictivity. Left side showed the in vitro cellular assays can be directly predictive of the human situation. Right side demonstrated the possible relevance (1) of animal outcomes to humans should be first evaluated (2) in an in vitro assay system, then the observed effects should be transferred (3) to a human cell based in vitro system, and finally the outcomes for human risk assessment should be derived (4). The image was used with copyright permission [17].

HSE being physiologically similar to Native Human Skin (NHS) can not only offer an advanced 3D *in vitro* testing system but can also serve as an alternative to animal experiments [18] for drugs & cosmetics testing, irritancy & toxicity evaluation, wound healing studies, cancer research, skin infection biology, and mode of action of skin diseases [19, 20]. Related to the irritancy evaluation, Draize assay is performed on albino rabbit skin for 4-48 hours by applying the test substance to investigate the tissue harm [21]. Despite being ethically questionable (animals suffering pain), the test has provided incorrect information in the past [22, 23]. On the other hand, murine models have also been extensively used for skin biology experiments, wound healing and skin cancer studies [24-26]. However, there are some basic dissimilarities between mouse and human skin architecture [27]. Mouse skin being furry is densely packed with hair follicles that are synchronized during the initial months of its life, as compared to human skin that has large interfollicular spaces with scarce hair follicles and their hair cycle is not a synchronized process. Moreover, murine epidermis is quite thin composed of only three layers with a high turnover rate. On the other hand, human epidermis is thick composed of six to ten layers. Another basic difference is the anatomical location of melanocytes: they are in the basal layer of human epidermis, and in the dermal hair follicles of mouse skin. Another difference lies in the presence of a cutaneous muscle layer (panniculous carnosus) that is present in mouse skin but absent in human skin. These interspecies inconsistences in skin structure exist and lead to the variations in outcomes [28]. Moreover, skin functionality and responsiveness are also different in

mouse and humans, e.g. mouse skin is effectively able to regenerate after wounding, while human skin damage leads to hypertrophic scar (keloids) formation that is completely absent in mouse skin [29]. Also, mouse skin provides more percutaneous absorption because of lesser water barrier properties of epidermis than human skin and thus is not a true model for the studies on topical drug-delivery [30].

EU regulations

Additionally, amendments in EU regulations and current policies have further pushed the development of *in vitro* testing systems as alternatives to animal testing. The regulations "European Union (EU) 7th amendment (Dir. 2003/15/EC) of the "Cosmetics Directive" (76/768/EEC) made it obligatory to replace animal trials for cutaneous resorption with reliable *in vitro* tests by the year 2009 [31]. This gave rise to the development of the 3Rs principle "replacement, reduction and refinement" [32]. Moreover, REACH, a European regulatory program for "registration, evaluation, authorization and restriction of chemicals" highlights human health and environment by emphasizing early characterization of chemicals' properties for risk assessment [33, 34].

Biological study and analytics using skin equivalents

Skin equivalents have been developed and continuously improved for performing several analyses and to answer specific questions under investigation. For example, Transcutaneous Electrical Resistance (TER) method has served to discriminate between corrosive and non-corrosive effect of materials [35] by measuring the effect on function of stratum corneum, and thus reduction of TER [36, 37]. Moreover, short term contact (e.g. 15 min) of corrosive substances on substituted skin (e.g. Episkin™ and Skin2™) followed by recovery (e.g. for 48 hours) has been used to replace the Draize test. Regarding corrosion test, many efforts have been performed to improve and validate these assays on skin substitutes so far (EpiDerm™, SkinEthic™, EST-1000) [38-43].

The effect of topically applied substances (e.g. cosmetic products) has been evaluated for their penetration into the skin [44]. For this purpose, a model mimicking the lipid organization in stratum corneum has been investigated [45]. Despite the differences observed in the exact composition of the fatty acids and ceramides, the models were used to perform permeation and percutaneous absorption studies [46]. Skin models can also serve to evaluate the skin irritation and toxicity of applied substances. Since long time, skin models have been investigated [47] and improvements have been made for cytotoxicity and inflammation studies e.g. Skin2 and Testskin. Additionally, efforts have been made to investigate phototoxic and photoprotection effects of test substances as well. Ozone or ultraviolet (UV) irradiation produced Reactive Oxygen Species (ROS) in skin and antioxidant effect of sunscreens was tested with StrataTest® [48]. With increasing exposure of nanoparticles to humans, recently, nanoparticle penetration test

has also been investigated at different skin depths and locations [49] to study cytotoxicity and immune responses.

In the context of cell-material interaction studies and *in vitro* analytical methods, the response of a 3D tissue can be evaluated by MTT assay (3-[(4,5-dimethylthiazol-2-yl)-2,5-diphenyltetrazolium bromide]), or luciferin-luciferase ADP/ATP assay to measure the cellular metabolic activity. The changes in integrin expression can be investigated by flow cytometry. H & E histological staining can serve to determine the visual tissue damaging capacity of a substance. Immunohistochemical (IHC) analysis can help determining the effect of a substance on epidermal differentiation. On compounds interaction, the invaded epidermis might trigger an inflammatory response by releasing cytokines and chemokines that can be measured by enzyme-linked immunosorbent assay (ELISA). The relevant changes in gene expression can also be determined by total RNA extraction and quantitative PCR.

In the present study, our fully characterized HSE was used as an advanced 3D model to evaluate the cytotoxic effects of commercially available silver containing antimicrobial wound dressings (Ag-dressings). The toxic effects on constructs were evaluated by CellTiter-Blue® (CTB) assay.

Bacterial study using skin equivalents

Among different strains *Staphylococcus aureus* is a major human bacterial pathogen, *causing* tens of thousands of deaths and millions of emergency room visits per year in the US alone [50]. Among a wide range of *S. aureus* clinical presentations, the vast majority is represented by skin and soft tissue infections [51, 52].

Traditional microbiological research has approached bacterial susceptibility considering that bacterial cell exists in a liquid, free-floating medium. However, bacteria have a great potential to adhere, colonize, and grow in communities enclosed in self-produced polymeric matrix (biofilms). This is medically important biofilm shields bacteria from antimicrobial therapies and thus has a role in resistant microbial infections and chronicity of non-healing wounds. [53]. Traditionally employed methods to measure the Minimum Inhibitory Concentration (MIC) make use of free-floating bacteria, where the number of organisms used is too low and without sufficient organic matter in medium. Among *in vitro* models of chronic wounds, constant depth film fermenter (CDFF) was used to grow wound biofilms [54]. In the past, *S. aureus* skin interactions have been investigated by inoculating 2D keratinocytes monolayer cultures with bacteria to understand bacterial attachment and keratinocyte response [55, 56].

Bacterial adherence and biofilm formation on plastic and human cells are two distinct systems presenting bacterial interactions with abiotic and biotic surfaces. However, these systems do not adequately imitate bacterial interaction with the human skin: the process occurs under relatively dry conditions [57], depends on physicochemical barrier

properties of the skin and is strongly influenced by environmental conditions [58]. Also, the 2D nature of cell monolayers interaction with bacteria do not replicate bacterial effect on 3D epidermal differentiation.

In the present study, *S aureus* colonized human skin equivalent (c-HSE) was used as an advanced model to investigate antibacterial effects of Ag-dressing on HSE adhered and colonized bacteria.

6.1.2 Ag-dressings

Ag-dressings are widely used in wound management of infected wounds as well as those at risk of infection. However, the clinical response varies due to the differences of silver content, silver release, dressings' properties themselves, wound type and condition. Therefore, dressing choice has the main role for successful wound management.

Understanding silver in Ag-dressings

Silver can be found in wound dressings in several forms e.g. as elemental silver (silver metal, nanocrystalline silver), as an inorganic compound (silver oxide, silver phosphate, silver chloride, silver sulphate, silver-calcium-sodium phosphate, silver zirconium compound, etc.), or as an organic complex (silver-zinc-allantoinate, silver alginate, silver carboxymethylcellulose) [59-61].

The silver in wound dressings may be: 1) a coating on the surface (elemental silver); 2) present within the structure of the dressing (elemental silver), inside the pores of the dressing (elemental silver), or in the form of a compound being part of the dressing structure (e.g. silver alginate); and 3) as a combination of above strategies.

Silver on the surface of the dressing exerts its antimicrobial action when it comes in contact with the wound. Silver within the dressing structure exerts its effect on bacteria absorbed into the dressing but can also diffuse around to some extent [62]. The amount of silver delivered to a wound does not really correlate with the amount of silver contained within the dressing [59] as the silver bioavailability depends on the wound environment and its interaction with wound components [62].

Mode of action of silver

Metallic form of silver is unreactive and can become bactericidal only after losing an electron (more readily in an aqueous environment) and converting into positively charged silver ions (Ag^{+}) that can bind to negatively charged molecules. Ag^{+} are highly reactive affecting multiple sites in bacterial cells (Figure 6.4) e.g. binding to cell membranes can result in cell leakage. When transported inside cells, Ag^{+} can bind to proteins disturbing cell energy production, enzymatic function as well as cell replication [63, 64]. Ag^{+} has been found active against a wide range of bacteria [65-70] including antibiotic-resistant strains of *methicillin resistant Staphylococcus aureus* (*MRSA*) and

vancomycin resistant Enterococci (*VRE*) [71]. Some studies have shown that silver might even reduce bacterial adhesion and disrupt the biofilm matrix [72]. Moreover, silver might kill the bacteria within the matrix. to make them susceptible to antibiotics [73-75].

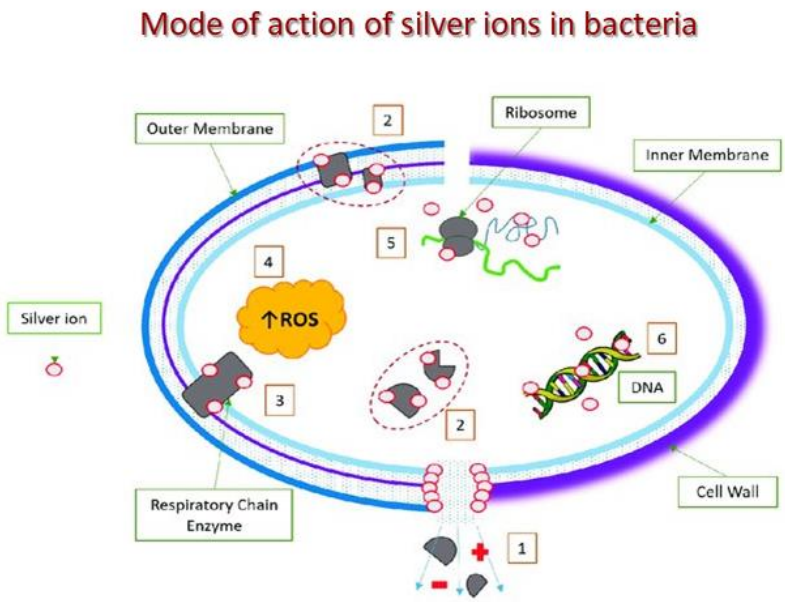

Figure 6.4 Mode of action of silver ions in bacteria. This included pore formation (1), cells metabolites/ions leakage (2), Cytoplasmic & structural protein denaturation (3), raising of intracellular reactive oxygen species (ROS) (4), interaction with ribosome machinery (5), interaction with nucleic acids (6). The image was used with copyright permission [76].

Besides controlling the bioburden, some laboratory work has suggested the beneficial role of silver in wound healing when applied on closed surgical wounds [77]. Moreover, silver nitrate, nanocrystalline silver, and some silver-containing wound dressings have been shown to have anti-inflammatory and neovascularisation effects [61, 78-80]. Interestingly, Ag^{+} at different concentrations might show a duality in function. For example, Ag^{+} ions at low concentration may convert to silver nanoparticle (respiratory nitrate reductase may be involved in nanoparticles production) while at higher concentration silver may induce cell apoptosis due to its direct inhibitory action towards proteins by interacting with their thiol groups (Figure 6.5) [81].

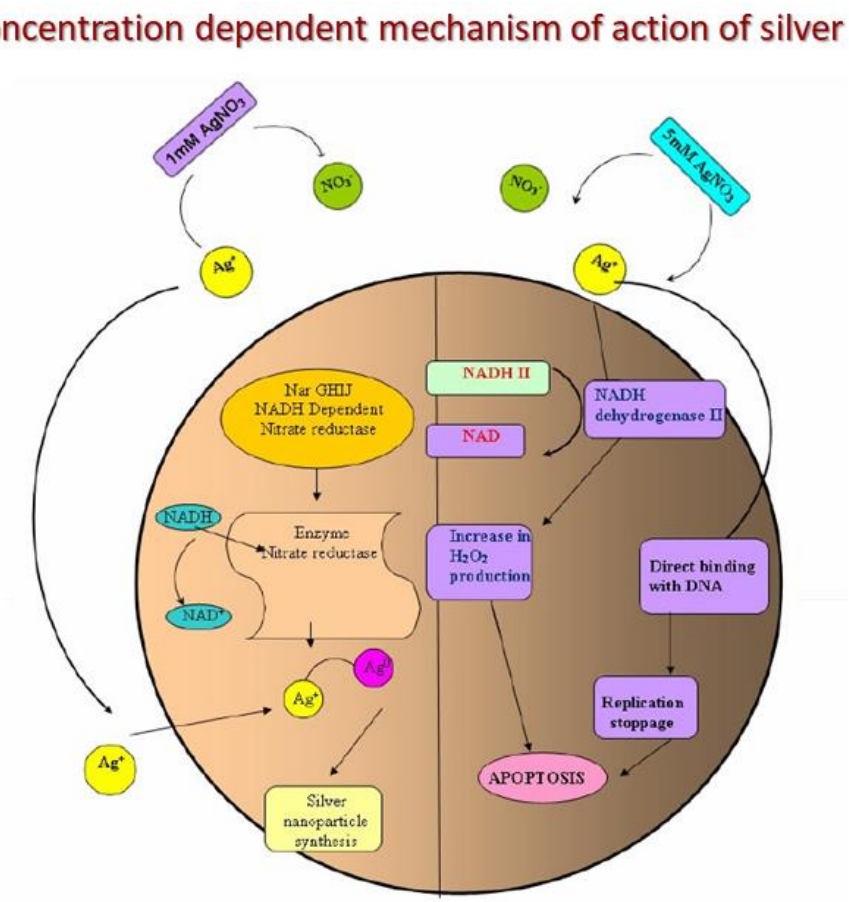

Figure 6.5 Concentration dependent mechanism of action of silver. Left side shows silver nanoparticle synthesis at lower Ag^+ concentration that might involve nitrate reductase enzyme. Right side shows induction of apoptosis by Ag^+ that might involve inactivation of thiol group containing proteins (e. g. NADH dehydrogenase II) and/or direct binding of Ag^+ to DNA. The image was licensed under a Creative Commons License [81].

Recommended use of Ag-dressings

The bacterial infection starts with wound contamination, colonization, and infection [82] that can be localized to the wound or spread to nearby tissues causing a systemic inflammatory response syndrome (SIRS) or multiple organ dysfunction syndrome (MODS). The purpose of silver dressings in wound management is to: 1) decrease the bioburden in acute or chronic wounds or 2) act as an antimicrobial barrier for wounds at high risk of infection or re-infection [82].

Selection of an appropriate dressing depends on the wound condition. For example, high absorbency is a requirement for wounds with high exudate production; low adherence would be preferable for highly painful wounds at dressing change; an enhanced dressing conformability would be needed for an irregular wound bed to prevent exudate pools formation and underneath bacterial growth, etc. Depending on the wound condition, dressing changes are planned (e.g. once weekly). In this regard duration of silver

availability has a significant role and should provide sustained silver delivery over days in this case.

Antimicrobial efficacy of Ag-dressings

In vitro evidence

Silver has been shown antimicrobial activity against a wide range of bacteria *in vitro*. However, the techniques (as summarized in Table 6.1) often used to assess antimicrobial efficacy are not standardised [83]. Therefore, the comparisons among different studies may lead to incorrect conclusions. Moreover, comparisons among different dressings have shown differences in silver content, silver availability at wound, and degree of antibacterial efficacy [62, 69, 71, 84]. In this context, one of the literature studies found no association between silver content, silver release and antimicrobial activity in an *in vitro* assay, demonstrating that silver dissolution from a wound dressing does not predict its antimicrobial activity [71]. On the other hand, other studies have shown the importance of silver content as well as numerous other factors, such as silver distribution within the dressing, silver availability from the dressing, dressing's contact ability with wound surface (i.e. dressing conformability), dressing's absorbency, the dressing structure, and its chemical/physical properties [62, 85, 86]. Keeping this into consideration and understanding the complexity of the wound environment, current *in vitro* tests to measure antimicrobial efficacy of Ag-dressings are not likely to be a true representative of their performance in a wound because of the complexity of the wound environment.

Table 6.1 In vitro tests of the antimicrobial efficacy of dressings. (adapted from [68, 87]).

***In vitro* antimicrobial test**	**Outline of method**	**Advantages**	**Disadvantages**
Zone of inhibition assay (Disc diffusion assay)	A piece of test dressing is placed on the surface of agar medium inoculated with bacteria and incubated for ~24 hours. The result is recorded as a clear zone around the dressing (zone of inhibition).	Simple and widely available.	The test does not differentiate between bacteriostatic and bactericidal activity. Wide variations in the method makes comparisons among different studies difficult.
Minimum inhibitory concentration (MIC) & Minimum bactericidal	A series of concentrations of an antimicrobial agent is tested in the presence of the bacteria and incubated for ~24 hours. The result is examined for the lowest concentrations with no signs of growth (MIC).	Determines the levels of antimicrobial agents for clinical use. MBC does not provide information on rate of killing bacteria.	MIC and MBC values are highly dependent on the type of growth medium (i.e. presence of organic

concentration (MBC)	The concentrations with no growth are plated and incubated for 24 hours. The result is examined for lowest concentration showing complete bacterial growth prevention (MBC).		matter and chloride in media).
Bacterial reduction (or Log reduction) through broth inoculation method	The antimicrobial agent is incubated with bacteria of a known density for different time points e.g. 0.5–24 hours. At various intervals, bacteria are recovered, and viable cell number is counted and expressed as reduction or log reduction by measuring the difference in logs before and after exposure to the test agent. Log reduction of >3 (i.e. >99.9% of bacteria are killed) tells the agent is bactericidal. Log reductions of >1 and <3 tells some of the bacteria have been killed.	The most appropriate *in vitro* test for wound dressing assessment. Can also provide information on rate of killing. Can be comparatively predictive of clinical outcomes.	Though Log reductions are hard to be compared because of different incubation times and media used.
Direct counts	This method uses a microscope to count bacteria following exposure to tested agents for certain times.	Useful in assessing growth inhibition.	The test does not differentiate between bacteriostatic and bactericidal activity due to detection limit of ≤2 log reduction.

Clinical evidence

Silver wound dressings have been evaluated in several different types of studies. These studies involved partial thickness burns, donor site wounds, as well chronic wounds from: pressure ulcers (grades III & IV), venous leg ulcers (at risk of infection, colonised, critically colonised, critically colonised with delayed healing, infected, or infected with critical inflammation), and diabetic foot ulcer. A meta-analysis study combines the results from multiple studies in order to understand the efficacy of silver wound dressings [87]. Some studies have found Ag-dressings to have a positive impact on overall wound healing [88-99], while others have found no significant differences than controls [100, 101]. The difficulties in interpretation and comparisons mainly arise from the small number of patients (problems with randomisation), a wide range of different criteria, study protocols and study endpoints used. Many of the studies have used an endpoint associated with healing. However, more appropriate endpoint should relate to measurement of microbial burden and assessment of clinical indicators of infection [102]. A study that examined pre-specified indicators of infection, observed significant

differences in Ag-dressings treated group showing no signs of heavy bacterial colonisation after 4-8 weeks of treatment [91]. However, another smaller study that used clinical infection scores, observed no significant difference between silver dressing treated and control groups after 2 weeks of treatment [103].

A particularly controversial study called VULCAN study [101, 104] used randomised patients (n=213) of venous leg ulcers receiving Ag- dressings. The main outcome considered was rate of complete wound healing after 12 weeks. The study concluded no significant difference between Ag-dressings treated and the control group, though cost analysis showed a higher cost associated with Ag-dressings. Despite the care involved in the study design, many reported their concerns that the outcomes were potentially misleading [105-107]. The major concern was that the study did not use Ag-dressings in line with existing recommendations, for example, the study did not report the risk of infection, and did not evaluate the wounds for presence of infection. Furthermore, silver dressings are not supposed to be used for extended periods, whereas in the study the dressings were applied for 12 weeks. More importantly, the endpoint or the goal of the care using Ag-dressings should not be wound healing (thus an inappropriate measure of efficacy in the study), rather it should be the reduction in wound bioburden. Some studies generalised the findings suggesting the invalid use of Ag-dressings in clinics. However, the study designs and clinical outcomes must be carefully concluded.

To validate our in-house developed HSE and c-HSE based 3D systems, clinically used Ag-dressings along with their controls without silver, and Ag^+ (as an antibacterial agent) were tested for cytocompatibility and antimicrobial properties. On the other hand, cell monolayer cultures based on L929 cells, COCA cells, NHDF, and NHEK were used as 2D cytocompatibility evaluation systems. Ag^+ and Ag-dressings were also evaluated for their antibacterial activities using most commonly used antibacterial methods (e.g. MIC, MBC, CFU percentage reduction) against clinically relevant pathogens (*Staphylococcus aureus, Pseudomonas aeruginosa* etc.). The antibacterial activity was tested under different growth media conditions such as tryptic soy broth (TSB) and simulated wound fluid (SWF) over time. This helped to assess the effects of culture 'environment' on bacterial susceptibility to the toxic action of silver. In future, we intend to perform the toxicity and antibacterial evaluations of novel and successfully produced antimicrobial polymeric materials in HyMedPoly project using our advanced HSE and c-HSE based 3D systems.

6.2 Materials and Methods

6.2.1 Materials

ISO standardized materials, that is, Polyethylene (PE) and Zinc Diethyldithiocarbamate containing Polyurethane (ZDEC-PU) were obtained from Goodfellow and Hatano Research Institute, respectively, and used as control materials for cytotoxicity testing with cell monolayer cultures. lysis solution of 9% Triton® X-100 in water from Promega was used to create "lysis control". "TCPS control" was cell monolayer attached on Tissue Culture Polystyrene (TCPS) surface. 5 % SDS (Sodium dodecyl sulfate, w/v) solution was prepared in distilled water and allowed 15 min contact time with HSE to obtain positive control for cytotoxicity evaluation in 3D cell culture system. PBS was used to obtain HSE negative control (or untreated control).

Ag^+ was tested as silver nitrate solution ($AgNO_3$) that was obtained from Carl Roth (0.1 mol/L). The Ag-dressings used in this study were PolyMem® Ag (Ferris), Biatain® Alginate Ag (Coloplast), Biatain® Ag (Coloplast), Atrauman® Ag (Hartmann) along with their controls without silver. Ag-dressings' product type, their silver formulation, and recommended uses are detailed in Table 6.2. The product images are shown in Figure 6.6.

Table 6.2 Antibacterial wound dressings used in this study and their properties.

Product Name and Manufacturer	Details of product type	Silver formulation	Recommendation for wound type	Antimicrobial effect
PolyMem® Ag (Ferris) (1788 WIC® and 5733 WIC®)	Hydrophilic polyurethane foam	Nanocrystalline silver	For cavity wounds, and works as wound filler that conforms to the wound cavity. Serves as combined primary and secondary dressing or as a secondary dressing.	Protects the wound from microbes.
Biatain® Alginate Ag (Coloplast)	Alginate (biodegradable) fibrous dressing	Silver complex $AgNaZr[HPO_4]_3$	For open wounds and wound cavities. Works as absorption substrate for medium strong to heavily exuding wounds.	For infected wounds.
Biatain® Ag (Coloplast)	Polyurethane foam	Inorganic silver complex $AgNaZr[HPO_4]_3$ (according to the company's patent no. EP 1 654 013 B1)	Superior absorption for moderate to highly exuding wounds of very fragile skin, for long wear time up to 7 days.	For infected wounds as, continuous antimicrobial effect during entire wear time.

Atrauman® Ag (Hartmann) (499 571 and 499 550)	Polyamide tulle (hydrophobic polyester fibres with 1mm pore size)	Metallic silver	For deep wounds. Prevents granulation tissue from penetrating the dressing. Serves as a primary dressing and used in combination with a secondary dressing.	For treatment of critically colonised or infected wounds. Silver ions on its surface, thus kill bacteria on contact.

Figure 6.6 Antibacterial Ag- dressings along with their controls.

6.2.2 In vitro cytotoxicity testing - 2D cell monolayer culture

Cells and cell culture maintenance

Primary cells including normal human dermal fibroblasts (NHDF) and normal human epidermal keratinocytes (NHEK) were obtained from PromoCell. Cell lines including L929 (mouse fibroblast cell line) and COCA (mouse epidermal cell line) were obtained from DSMZ (German Collection of Microorganisms and Cell Cultures) and ECACC (European Collection of Authenticated Cell Cultures), respectively.

NHDF were maintained in CnT-Prime fibroblast medium (CnT-PR-F, CELLnTECH) while NHEK and COCA were maintained in CnT-Prime epithelial culture medium (CnT-PR, CELLnTECH) under the physiological culture conditions (37°C, 5% CO_2), and sub-cultured using DetachKit-Promocell HEPES BSS (2-[4-(2-hydroxyethyl)piperazine-1-yl] ethanesulfonic acid buffered saline solution); 0.04% Trypsin/0.03% EDTA (ethylenediaminetetraacetic acid); and TNS (trypsin neutralizing solution) containing 0.05% trypsin inhibitor from soybean/0.1% bovine serum albumin. L929 cells were maintained in cell culture media RPMI 1640 with stable glutamine (PAN Biotech, P04-18500), containing 10% foetal bovine serum (FBS; PAN Biotech) under physiological culture conditions (37°C, 5% CO_2), and sub-cultured using 0.25% trypsin (Gibco).

2D cell monolayer culture preparation

Defined aliquots of cell suspensions at early passage numbers (P4 to P6) were pipetted in 24 well plates for cytotoxicity evaluation of Ag-dressings and in 96 well plates for cytotoxicity evaluation of Ag^+. Cell seeding densities to obtain sub-confluent monolayer cultures in 24 hours were pre-determined for each individual cell type and are detailed in Table 6.3. The plates were incubated at 37°C, 5% CO_2 for 24 hours. The cell sub-confluency and morphology were verified before exposing the cells to test samples. Culture medium was removed and replaced with fresh medium before starting the test.

Table 6.3 Cell seeding densities.

Cell type	Cells per well in TC 24 multi-dish (1.8cm² culture area)	Cells per well in TC 96 multi-dish (0.3cm² culture area)
L929	7×10^4	1×10^4
COCA	7×10^4	2×10^4
NHEK	1.5×10^5	3×10^4
NHDF	3×10^4	0.75×10^4

TC=Treated for cell culture.

Test protocols for cytotoxicity evaluation onto 2D cell monolayer culture

$AgNO_3$ solutions (100µL per well) were prepared as two-folds dilutions in respective cell culture media at concentrations of 33µg/mL, 16µg/mL, 8.4µg/mL, 4.2µg/mL, 2.1µg/mL, 1.2µg/mL, 0.56µg/mL, 0.26µg/mL, 0.13µg/mL, 0.06µg/mL and were tested with above mentioned cell types, as monolayer culture, in TC 96 multi-dish.

Ag-dressing samples were freshly punched in a size of 5mm diameter, UV sterilized (at 254 nm UV lamp, and min. 30 minutes each side) and exposed to the above mentioned cell monolayer culture through direct contact method, by placing the samples in the centre of the well of TC 24 multi-dish (1mL media per well) without making unnecessary movements of specimens (Figure 6.7). The wells without any sample exposure served as TCPS control (tissue culture treated polystyrene), while the wells treated with lysis solution (9% Triton® X-100) served as Lysis control. Cells treated with PU-ZDEC and PE films served as positive and negative controls of cytotoxicity analysis, respectively. The well plate was then incubated at 37°C, 5% CO_2 for 24 hours. The next day, supernatant culture medium and specimens were carefully removed, and CellTiter-Blue® (CTB) assay (Promega) was performed for measuring the cell viability according to Promega standard protocol [108]. To this aim, for this 400µL CTB reagent (this vol. is enough to cover the surface of TC 24 well) was pipetted per well for 2h at 37°C and 5% CO_2. The cell supernatant was transferred to black microtiter 96-well plates. The fluorescence was measured at excitation (Ex) of 560 nm and emission (Em) of 590 nm.

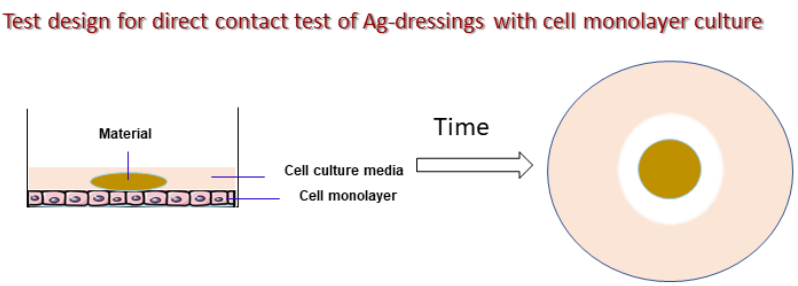

Figure 6.7 Test design for direct contact test of Ag-dressings with cell monolayer culture. Microscopic fields that were right under (U), around/near (N), and far from (F) the exposed specimen would indicate the reactivity grades of cytotoxic effect of materials.

Morphological analysis

Changes in morphological appearance of cells were evaluated using bright field and fluorescent microscopy (Olympus IX51). Fluorescent staining was performed using Live/Dead imaging (Promokine) using calcein-AM and ethidium homodimer III (EthD-III) to see live (green-fluorescence for live cells by enzymatic conversion of non-fluorescent substrate, Ex/Em ~495nm/~515nm) and dead (red-fluorescence for dead cells upon binding to nucleic acid, Ex/Em ~530nm/~635nm) cells.

6.2.3 In vitro cytotoxicity testing - 3D cell culture system

Fabrication of HSE

The human skin equivalent (HSE) was obtained having both a dermal and an epidermal compartment, by first embedding NHDF in rat tail tendon collagen type I (Col. I) hydrogel from Ibidi (mimicking dermal Extracellular Matrix or ECM) to establish dermal construct and then later seeding NHEK on it to generate the epidermis. The cell culture conditions were optimized to obtain a closely *in vivo* tissue mimicking HSE. The optimized protocol followed the procedure as: i) NHDF (~8 × 10^4 cells/mL) were embedded in 1.5mg/mL Col. I based dermal construct to remodel the ECM for 5-7 days using 12-well Transwell inserts (with polyester membrane, pore size 0.4 µm), and were fed with CnT-PR-F; ii) NHEK (8 × 10^6 cells/mL) were seeded on top and grown in submerged culture for 3 days to cover the dermal substrate and fed with CnT-PR; iii) the culture was then grown in submerged conditions overnight while now fed with CnT-PR-3D to allow cells to develop cell-cell adhesion structures before airlifted; iv) finally the culture was raised to air liquid interface (ALI) to start tissue differentiation and bottom fed with CnT-PR-3D for 15-20 days. Human dermal construct development and characterization are described in more detail in Chapter 02. While the HSE development and full characterization are described in more detail in Chapter 04.

Test protocols for cytotoxicity evaluation onto HSE

The cytotoxicity was represented as IC50 (Half maximal inhibitory concentration) which is the concentration of the tested compound that gives 50% viability.

HSEs were used to create full-thickness wound incision of 2-3mm using scalpel N°10 and used to evaluate the cytotoxicity of different silver-containing wound dressings as well as Ag^+ as following:

Depending on the determined IC50 of Ag^+ in 2D cell culture, HSEs were exposed to Ag^+ at concentrations of 66µg/mL, 33µg/mL, 16µg/mL, and 8.4µg/mL (prepared in CnT-PR-3D). For this purpose, HSEs were exposed with tested liquid samples of $AgNO_3$ at apical (200µL) and basal sides (800µL), maintaining the same level outside and inside the Transwell inserts.

Ag-dressings (5mm in diameter) were placed on the top of HSE carefully (as shown in Figure 6.8) using sterile forceps and 500µL CnT-PR-3D medium was pipetted to wet the material. The level of the medium was kept similar outside and inside the HSE containing Transwell inserts.

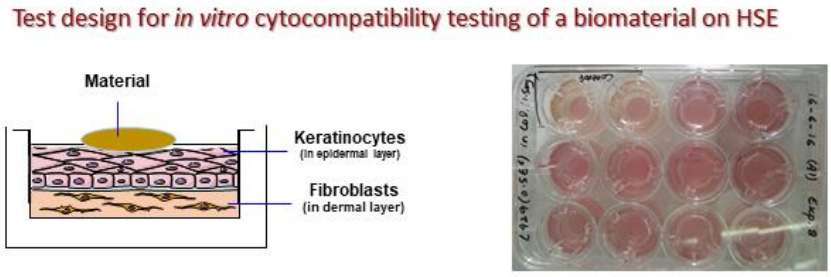

Figure 6.8 Test design for in vitro cytocompatibility testing of a biomaterial on HSE.

The treated HSEs were placed at 37° C and 5% CO_2 for 24 hours. After the incubation, the tested samples were removed using forceps or tested liquid samples were pipetted out. HSEs were rinsed thoroughly with sterile PBS 3 times to remove all the residual material. The remaining PBS was gently removed and HSE were transferred to 24 well plate by cutting the Transwell membrane. The cell viability was measured by CTB assay (Figure 6.9). For this 400µL CTB reagent per well (this vol. is enough to completely dip the HSEs) was pipetted and incubated for 3 h at 37°C and 5% CO_2. The cell supernatant was transferred to black microtiter 96-well plates. The fluorescence was measured at Ex/Em 560/590 nm. PBS treated HSE served as negative control and 5%SDS treated HSE served as positive controls for cytotoxicity evaluation of samples. The relative tissue viability of each tissue was calculated as a percentage of the viability of the mean of the negative controls. The interference (if any) of test samples with the CTB reagent can be checked by applying test chemical onto non-viable (freeze-killed) HSE control tissues. Thus, the binding of the compound to the HSE tissue can be assessed, and also the amount of CTB reagent converted.

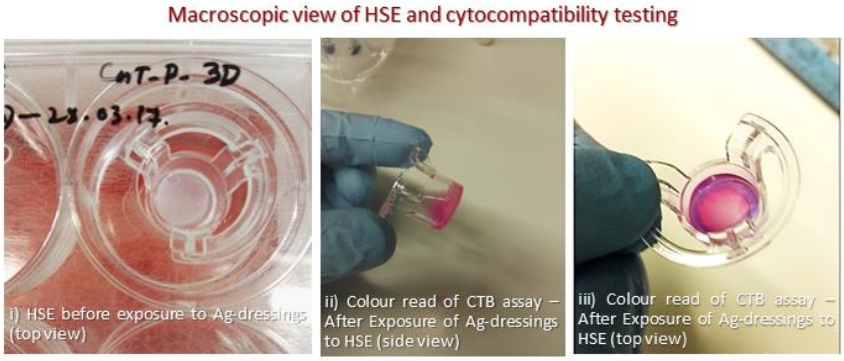

Figure 6.9 Macroscopic view of HSE and cytocompatibility testing. i) HSE before exposure to Ag-dressings (top view). ii) Color read of CTB assay – After Exposure of Ag-dressings to HSE (side view). iii) Color read of CTB assay – After Exposure of Ag-dressings to HSE (top view).

6.2.4 *In vitro antibacterial testing*

Antibacterial activity of Ag^+ - MIC and MBC determination

Staphylococcus aureus (ATCC 29213 of wound source), *Staphylococcus epidermidis* (ATCC 12228), *Escherichia coli* (ATCC 25922), *Pseudomonas aeruginosa* (ATCC 27853), being most relevant in infected wounds, were used to evaluate antibacterial activity of Ag^+. Additionally, resistant strains with most commonly found resistance-phenotypes including *Methicillin-resistant Staphylococcus aureus (MRSA)*, and *Methicillin-resistant Staphylococcus epidermidis (MRSE),* were also tested.

The MIC and MBC determination of Ag^+ was performed by microdilution method (Figure 6.10) according to CLSI (Clinical & Laboratory Standards Institute) guidelines [109]. The detailed protocol is described as following:

1. Bacterial strains were revived by culturing on fresh blood agar one day before testing.

2. The tested antibacterial agent solution of Ag^+ was prepared (fully dissolved) as two times (2X) concentrated of required concentration in MHB (Mueller-Hinton broth from Becton Dickinson, BD 212322) aseptically from stock solution of $AgNO_3$ (Table 6.4).

Table 6.4 Concentration calculation and preparation of Ag^+ from silver nitrate solution ($AgNO_3$) for MIC and MBC determination experiment.

Concentration	Conc. of stock solution	Conc. required for the first dilution	Prepared as: 2X of the concentration required
Molarity (M)	0.1M	800µL=0.0008M	1600µL=0.0016M Calculation: $C_1V_1=C_2V_2$ →(0.1M x V_1=0.0016M x 1mL) → 16µL from stock into in 984µL solvent to obtain 1600µM

Mass concentration (µg/mL)	169.88g/mol ∴ Calculation: 16.98g/0.1mol or 16.98g/100mL or 169.88mg/mL	135.9µg/mL Calculation: (169.88mg/mL x 0.0008M=0.0339mg/mL=33.9µg/mL)	271µg/mL Calculation: (169.88mg/mL x 0.0016M=0.1359mg/mL=135.9µg/mL)

Calculated mass concentrations from molar concentrations: 400µM=~66µg/mL (67.95µg/mL), 200µM=~33µg/mL (33.97µg/mL), 100µM=~16µg/mL (16.98µg/mL), 50µM=8.49µg/ml, 25µM=4.2µg/mL.

3. 50µL MHB was pipetted in all wells.

Note: 50µL MHB was pipetted in the growth control (GC) well and 100µL in the sterility control (SC) well.

4. 50µL of tested compound was pipetted in first well and two-fold dilutions were prepared by pipetting 50µL of each dilution in next respective wells, and 50µL was discarded from the last dilution.

5. The well-isolated colonies were suspended in 0.9% normal saline by direct colony suspension method and adjusted to McFarland 0.5 [110111].

6. Each well containing 50µL of tested compounds dilutions as well as the GC were inoculated with 50µL of the bacterial suspension (using automatic dispensing pipette for accuracy). This resulted in the final desired inoculum of 3.75 X 10^5 CFU ml^{-1} (Table 6.5).

Table 6.5 Calculation for bacterial seeding density according to CLSI standards.

Turbidity		Calculation (according to CLSI standards final bacterial concentration in each well should be between 2 - 8 x 10^5 CFU/mL)	
0.5 McFarland in 0.9% saline 1 - 2 x 10^8 CFU/mL	1 x 10^8 CFU/mL	1:100 → 1 x 10^6 CFU/mL	1:200 → 0.5 x 10^6 CFU/mL
		(50µL inoculum + 50µL compound) 5 x 10^5 CFU/mL or 5 x 10^4 CFU/well	(50µL inoculum + 50µL compound) 2.5 x 10^5 CFU/mL or 2.5 x 10^4 CFU/well
	1.5 x 10^8 CFU/mL	1:100 → 1.5 x 10^6 CFU/mL	1:200 → 0.75 x 10^6 CFU/mL
		(50µL inoculum + 50µL compound) 7.5 x 10^5 CFU/mL or 7.5 x 10^4 CFU/well	(50µL inoculum + 50µL compound) **3.75 x 10^5 CFU/mL or 3.75 x 10^4 CFU/well**
	2 x 10^8 CFU/mL	1:100 → 2 x 10^6 CFU/mL	1:200 → 1 x 10^6 CFU/mL
		(50µL inoculum + 50µL compound) 1 x 10^5 CFU/mL or 1 x 10^4 CFU/well	(50µL inoculum + 50µL compound) 5 x 10^5 CFU/mL or 5 x 10^4 CFU/well

The most likely value for CFU/mL at 0.5 McFarland was bolded.

7. Colony counts of inoculum suspensions: aliquot from the GC immediately after inoculation was diluted as 1:100 and 1:1000 by transferring 10µL aliquot in 990µL and 10µL aliquot in 1990µL of saline. These dilutions were plated by pipetting 100 µL aliquots on blood agar plates in duplicates. After incubation, the presence of approximately 50 colonies indicated an inoculum density of 5×10^5 CFU ml^{-1}.

8. The inoculated microdilution trays were placed at 35±2°C for 16-20 hours in an ambient air incubator. If necessary, each tray can be sealed with plastic tape and placed in a plastic bag to prevent drying.

9. The results can be read next day after wiping off the bottom of the microtiter plate. SC should be clear. The MIC is defined as the lowest concentration of the antimicrobial agent that inhibits visible growth of the tested isolate as observed with the unaided eye. To determine the MBC, the dilution representing the MIC and at least two of the more concentrated dilutions were plated and enumerated next day to determine viable CFU/ml.

Ag^+ at its MIC and MBC was also tested to evaluate the percent reduction in CFU count in this microdilution experimental set-up.

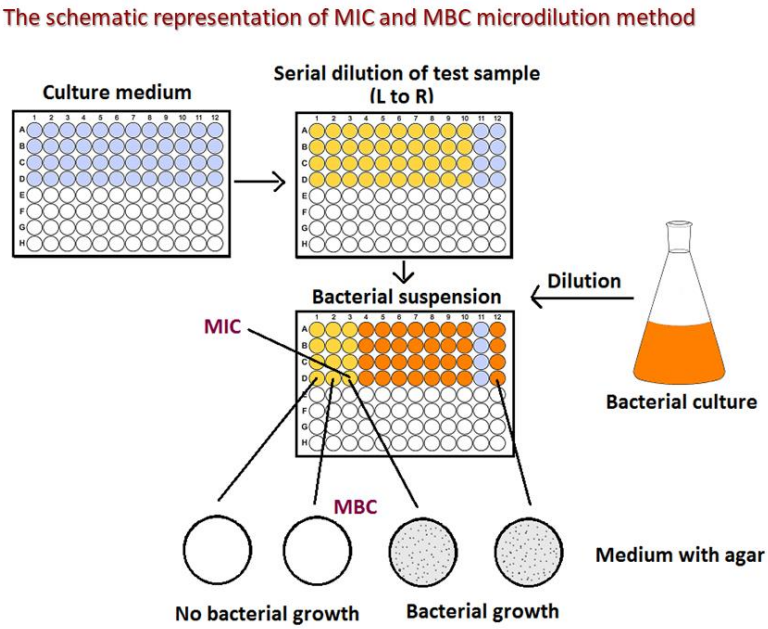

Figure 6.10 The schematic representation of MIC and MBC microdilution assays.

Antibacterial activity of Ag-dressings – Broth inoculation method to determine bacterial reduction

The Ag-dressings were tested against most commonly found wound pathogens namely *S. aureus* (ATCC 29213), *E. coli* (ATCC 25922), and *P. aeruginosa* (ATCC 27853). The revived bacterial cultures were suspended in 0.9% normal saline by direct colony suspension method and adjusted to McFarland 0.5. This suspension was diluted by 1:200

ratio to obtain an inoculum with a concentration of 0.75 x 10^6 CFU/mL. Antibacterial activity of four types Ag-dressings (5mm diameter samples, UV sterilized) was assessed over a period of 4 hours, 24 hours, and/or 48 hours (T_{4h}, T_{24h}, T_{48h}). For this, the samples were transferred to the 1mL inoculum in tryptic soy broth (TSB), and tubes were incubated at 37˚C at the rotation of 90 revolutions/min. To best reproduce the clinical conditions in which these dressings are used, a simulated wound fluid (SWF) was prepared consisting of 50% foetal calf serum (FCS, PAN Biotech, Germany) and 50% maximum recovery diluent (MRD prepared as: 0.1% w/v peptone from beef protein extract and 0.9% w/v sodium chloride). Bacterial inoculum (0.75 x 10^6 CFU/mL) was prepared in SWF and Ag-dressings were incubated the same way as in TSB. 100µl rigorously pipetted aliquots and their diluted solutions were plated for total viable counts at intervals of T_{4h}, T_{24h}, and T_{48h}. Sample replicates were individually incubated for each time interval. The results were calculated as percent reduction in CFU count by comparing the CFU of GC at each time point.

6.2.5 In vitro antibacterial testing - 3D cell culture system

Fabrication of c-HSE

Preparation of bacterial inoculum

S. aureus (ATCC 29213, wound source), was revived and cultured on fresh blood agar one day before use. The well-isolated colonies were suspended in 0.9% normal saline by direct colony suspension method and adjusted to McFarland 0.5. This suspension was diluted in PBS (pH 7.4) by 1:200 ratio to obtain an inoculum with a concentration of 1 x 10^6 CFU/mL that represented ~5 x 10^3 CFU per 5µL, as verified afterwards by standard viable counts.

S. aureus colonization of HSE to construct c-HSE

Airlifted HSEs were used to create an incisional wound by making a full-thickness incision of 2-3mm using scalpel N°10 without damaging the Transwell insert membrane. Skin equivalents were inoculated with 5µL bacterial inoculum at incision site and incubated at 37°C, 5% CO_2 for 1 hour to allow bacteria to adhere to HSE, now named c-HSE. The c-HSE development and characterization is described in more detail in Chapter 05.

Protocol for testing antibacterial activity onto c-HSE

One hour after bacterial inoculation, antibacterial compounds including Ag^+ as well as Ag-dressings were applied along with their controls in separate experiments (Figure 6.11).

Ag^+ solutions were prepared in CnT-PR-3D at the concentrations of 33µg/mL, 16.5µg/mL, and 8.25µg/mL from $AgNO_3$ stock solution; and 1000µL of each concentration was applied by pipetting 200µL on the top and 800µL in the bottom of c-HSE keeping the solution at the same level outside and inside the Transwell insert. 24 hours after the application of the Ag^+ solution, the numbers of bacteria (CFU) per c-HSE were assessed microbiologically. For this, c-HSEs along with the supernatant were collected and homogenized using a manual glass tissue homogenizer. The homogenates were subsequently serially diluted and plated (100µL) onto blood agar plates to determine the reduction in CFU number.

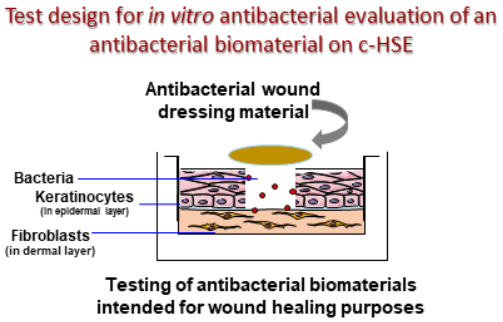

Figure 6.11 Test design for in vitro antibacterial evaluation of an antibacterial biomaterial on c-HSE.

The Ag-dressings (5mm diameter, and UV sterilized), were applied onto c-HSE using sterile forceps. 600µL of CnT-PR-3D was applied onto the material to make it wet, and the bottom CnT-PR-3D media level was kept at the same level (counts a bottom vol. of 1.7mL). The numbers of bacteria were assessed microbiologically, 24 hours after the application of the materials. Briefly, Ag-dressings were removed and handled to extract any attached bacteria by vertexing, and sonication (10-15 min with intervals) in 500µL PBS. These extracts were serially diluted and plated on blood agar plates. The undiluted extracts were also plated. The c-HSEs along with the supernatant were collected and homogenized using a manual glass tissue homogenizer. The homogenates were subsequently serially diluted and plated (100µL) onto blood agar plates to determine the reduction in CFU number. The number of bacteria were recorded as CFU per skin equivalent. The controls included c-HSE applied with PBS and c-HSE applied with oxacillin disc (1µg disc from Oxoid™) using sterile forceps.

6.2.6 Statistical analysis

Independent experiments for cytocompatibility and antibacterial analysis were carried out in triplicates (n=3) and results were expressed as mean ± standard deviation. For statistical analysis, GraphPad Prism 5.00.288 (Inc., San Diego, CA, USA) was used to evaluate the significance of the differences in cell viability and antibacterial data. T-test was used when the comparison involved two groups. Significance between groups was considered for $p < 0.05$.

6.3 Results and discussion

Ag^+ being the active antibacterial agent in Ag-dressings, was first evaluated for its cytocompatibility and antibacterial properties in this study. This was followed by the bioevaluation of Ag-dressings.

6.3.1 Bio-evaluation of Ag^+

Cytocompatibility (Cytotoxicity) evaluation of Ag^+

Cell lines (L929 & COCA) (Figure 6.12) were used to assess general *in vitro* cytotoxicity based on DIN EN ISO 10993-5, while specific cytotoxicity was tested using specific primary cells (NHDF & NHEK) (Figure 6.13). CTB assay was used to measure the metabolic potential as a specific biomarker for detecting cell viability and cytotoxicity of cell culture system after 24 hours exposure with Ag^+ at different concentrations (Figure 6.12 C).

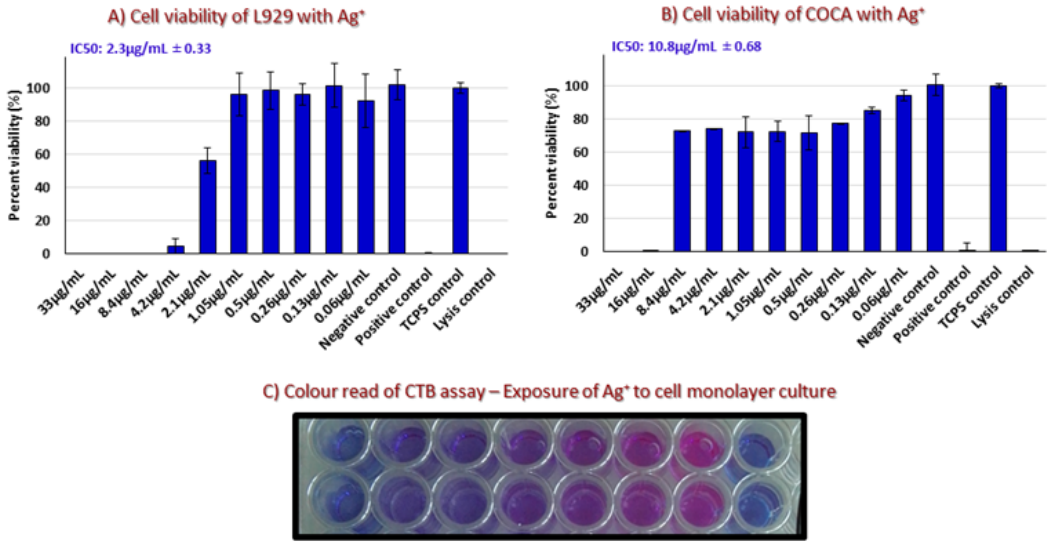

Figure 6.12 (A) Cell viability of L929 and (B) of COCA cell lines with Ag^+. C) Color read of CTB assay – Exposure of Ag^+ to monolayer cell culture in 96 well plate.

Ag^+ showed IC50 of 2.3±0.33µg/mL and 10.8±0.68µg/mL with L929 and COCA cell lines, respectively (Figure 6.12). IC50 was 10.3±0.21µg/mL and 11.8±0.56µg/mL for NHDF and NHEK human primary skin cells, respectively (Figure 6.13). The value was similar for the two primary cell types. The overall data on IC50 values are collected in Table 6.6.

The IC50 was ~5times inferior for L929 cell line with respect to primary human dermal fibroblasts (NHDF). However, in the case of keratinocytes (unlike HaCaT) [15, 16], COCA cell line behaved much more closely to primary human epidermal keratinocytes (NHEK) and IC50 was not much different between the two cell types.

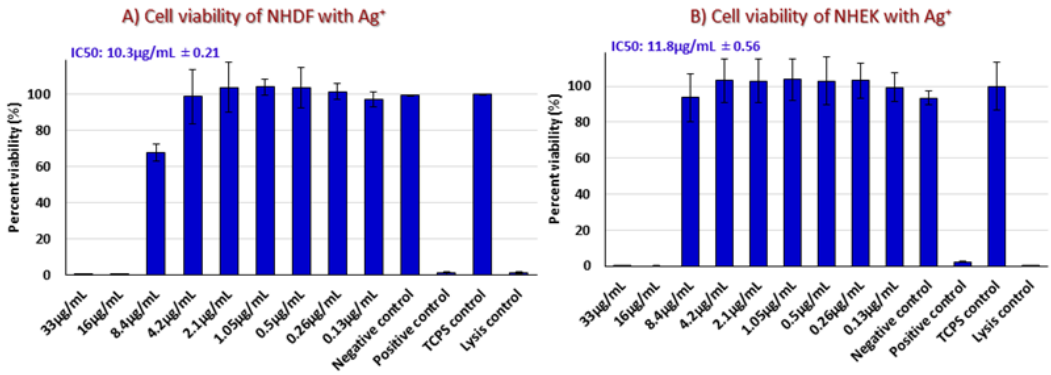

Figure 6.13 A) Cell viability of NHDF and (B) NHEK with Ag^{+}.

Considering *in vitro* bioevaluation being more accurate in 3D testing systems than 2D cell cultures [17, 112, 113], Ag^{+} was also tested at comparatively higher concentrations on HSE based 3D system for 24 hours exposure. The cell viability data showed an IC50 of 34.2±0.56µg/mL on HSE (Figure 6.14). The IC50 values were found significantly different in the two distinct systems, cell monolayer cultures (2D) and HSE (3D), with IC50 value three times higher in HSE system. Cells arranged in a 3D ECM-like system behave similarly to *in vivo* condition [7, 9]. Hence, HSE is an important bio-evaluation tool due to its evident advantages in providing more physiologically relevant information and more predictive data for *in vivo* tests [6, 8, 10, 11, 13].

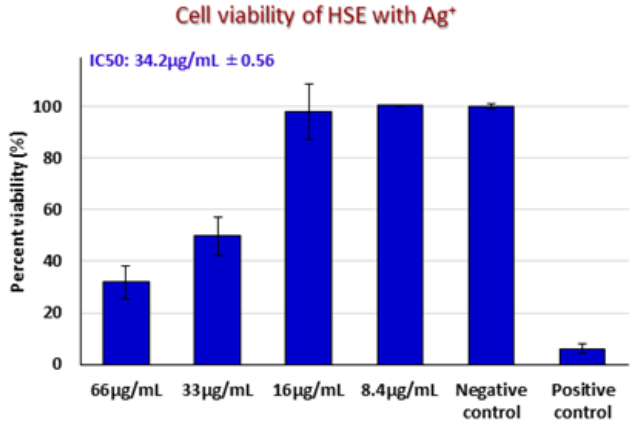

Figure 6.14 Cell viability of Human Skin Equivalent (HSE) with Ag^{+}.

Differences in lethal concentration of Ag^{+} between monolayer culture and 3D culture also indicated that as the complexity of the environment increased, the toxic effect of the Ag^{+} seemed to decrease. This is most probably related to the bioavailability of the Ag^{+}. The presence of high protein content in the culture system can bind Ag^{+} reducing its effective concentration. This can be one of the reasons of reduced susceptibility of HSE, compared to monolayer cultures.

Table 6.6 IC 50 of Ag+ in 2D and 3D cell culture system.

2D and 3D cell culture systems			IC 50 of Ag^+
2D cell culture system	Murine cell lines	L929	2.3µg/mL±0.33
		COCA	10.8µg/mL±0.68
	Human primary skin cells	NHDF	10.3µg/mL±0.21
		NHEK	11.8µg/mL±0.56
3D cell culture system	Human dermal-epidermal skin model	HSE	34.2µg/mL±0.56

IC50: The half maximal inhibitory concentration. For cytotoxicity assay, IC50 is the concentration of tested compound that gives 50% viability.

Antibacterial evaluation of Ag^+

Broth microdilution assay was used as a method to test the susceptibility of bacteria to Ag^+ and the results are reported in Figure 6.15. Ag^+ showed MIC in the range of 4.2-8.4µg/mL and MBC in the range of 4.2-33µg/mL against several Gram +ve and Gram -ve bacteria (

Table 6.7). Additionally, resistant strains with most commonly found resistance-phenotypes (*MRSA* and *MRSE*) were also tested.

Figure 6.15 Experimental results' demonstration - MIC and MBC determination of Ag^+ through microdilution assay.

Table 6.7 MIC and MBC of Ag^+ against wide range of bacteria.

Bacterial Strains	Ag^+	
	MIC (µg/mL)	MBC (µg/mL)
***Staphylococcus aureus* (ATCC 29213)**	**8.4±0.0**	**33±0.0**
MRSA - Methicillin-resistant Staphylococcus aureus	**8.4±0.0**	**30±7.6**
***Staphylococcus epidermidis* (ATCC 12228)**	**3.8±1.1**	**33±0.0**
MRSE - Methicillin-resistant Staphylococcus epidermidis	**3.8±1.1**	**30±7.6**
***Pseudomonas aeruginosa* (ATCC 27853)**	**4.2±0.0**	**4.2±0.0**
***Escherichia coli* (ATCC 25922)**	**4.2±0.0**	**8.4±0.0**

MIC: Minimum inhibitory concentration; MBC: Minimum bactericidal concentration (bacterial reduction of ≥99.9% of initial inoculum).

The antibacterial activity of Ag^+ at its MIC and MBC (against *S. aureus*, *E. coli*, *P. aeruginosa*) was also measured as percent of bacterial reduction and CFU/mL number of surviving bacteria (Figure 6.16). This demonstrated >90% reduction at their MIC and more than >99% reduction at their MBC after 24 hours.

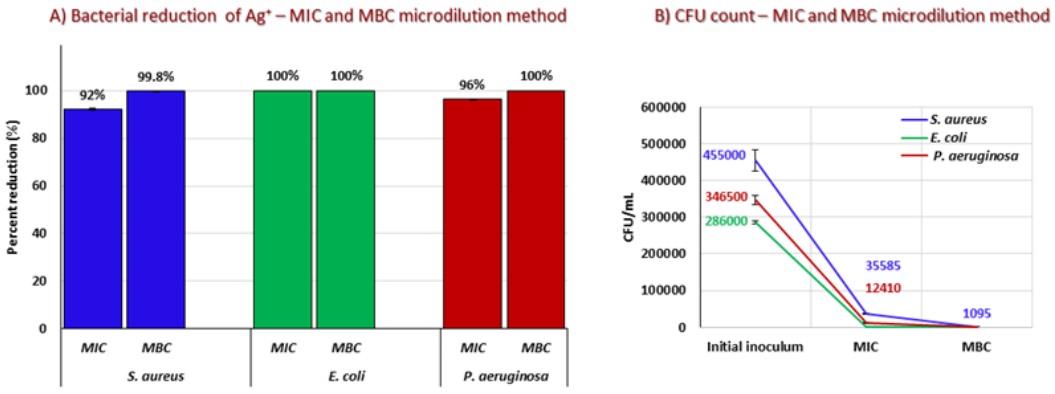

Figure 6.16 Antibacterial activity of Ag^+ as percent reduction (A) and CFU/mL count (B) – MIC and MBC microdilution assay.

S. aureus being one of the most pathogenic bacteria in wounds [114] was further investigated for Ag^+ induced bacterial reduction under different culture media than the one (MHB) used in standard microdilution assay. For this, broth inoculation assay was used to measure percent reduction of *S. aureus* in "TSB" at different time points over a time period of 48 hours (Figure 6.17). These antibacterial results of Ag^+ were also demonstrated as CFU/mL count of surviving *S. aureus*, as well as the growth curve of *S. aureus* in the respective medium of TSB was also shown (Figure 6.17). After 24 hours of exposure Ag^+ in TSB medium, the results demonstrated only 40.4±7.6% *S. aureus* reduction at the pre-determined MIC of Ag^+, while still presented 99.99±0.004% reduction at MBC. This killing effect of Ag^+ at its MBC appeared to decrease to 79±0.3% at T_{48h} demonstrating that a very few surviving bacteria at T_{24h} were still able to grow at T_{48h} as Ag^+ effect decreased with time.

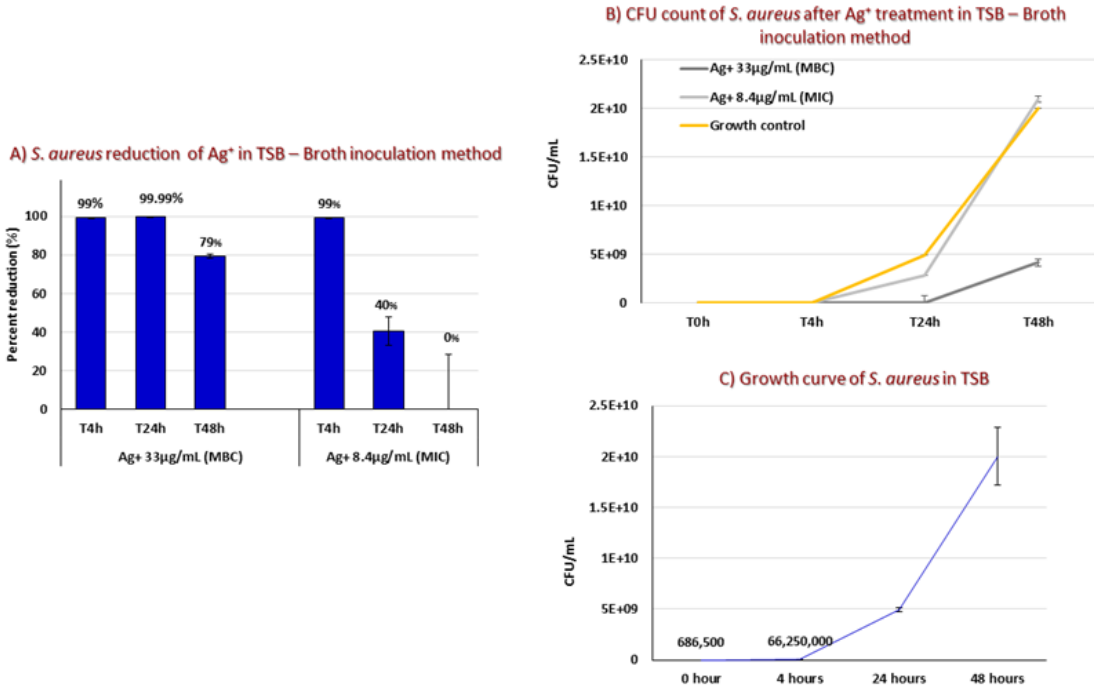

Figure 6.17 Antibacterial activity of Ag^+ against S. aureus in TSB over time as (A) percent reduction and (B) CFU/mL count – Broth inoculation assay. C) Growth curve of S. aureus in TSB.

Though, the antibiotic susceptibility of antibacterial agents has been widely tested in TSB medium by many authors, considering the wound situation, the antibacterial activity of Ag^+ against *S. aureus* was also tested in SWF (Figure 6.18). SWF is higher in protein content and thus is the best representative of wound exudate. Surprisingly, the results demonstrated almost no *S. aureus* reduction in SWF both at Ag^+ MIC and MBC at any time point. This considerable variation in the ability of Ag^+ to interfere with bacterial growth demonstrated the significance of the wound environment. The Ag^+ interaction with serum proteins can be one of the explanations of 0% bacterial reduction in this medium (Figure 6.18).

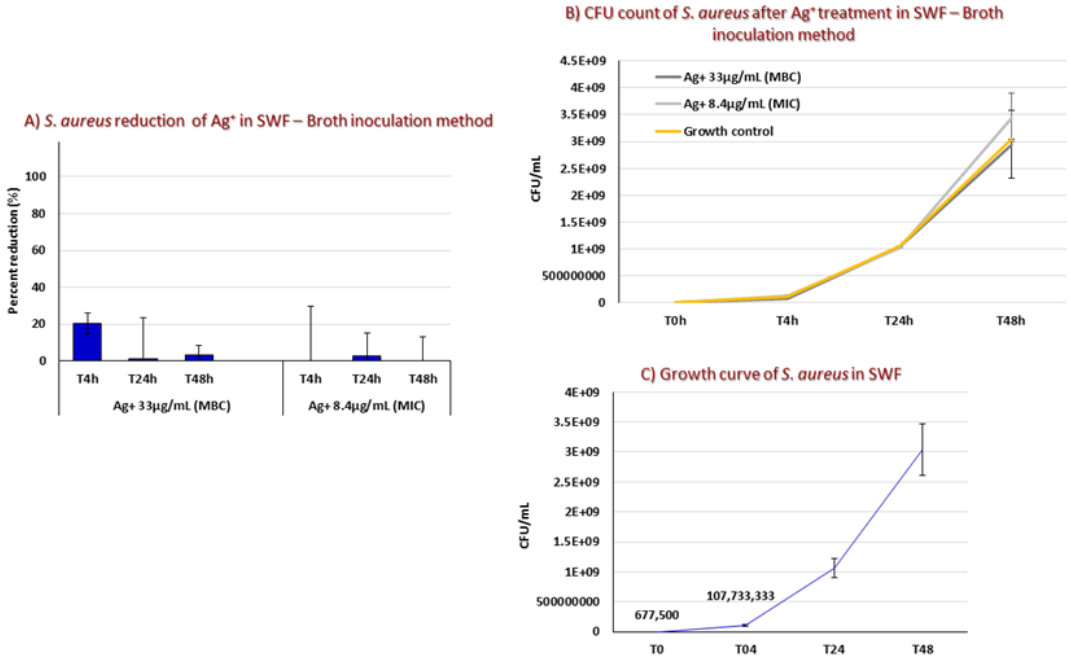

Figure 6.18 Antibacterial activity of Ag^+ against S. aureus in SWF over time as (A) percent reduction and (B) CFU/mL count – Broth inoculation assay. C) Growth curve of S. aureus in SWF.

To understand the complexity of the infected wounds, we used our *S. aureus* colonized HSE model (c-HSE) as a complex 3D system presenting a biotic surface (of *in vitro* skin tissue) with colonized bacteria. To determine any antibacterial effect of Ag^+ on this system, c-HSEs were exposed to higher Ag^+ concentrations than its MIC and MBC. However, the results showed that Ag^+ was no more able to show any bacterial inhibition in c-HSE system at any tested concentration (Figure 6.19). Such results suggested that when bacteria had adhered, colonized and penetrated the deeper layers of skin and/or made biofilm-like structures, they were not inhibited anymore at the doses of antibacterial agent suggested by 2D trials. Results were shown as Log CFU of *S. aureus* per c-HSE and there was no significant difference between the effect of high Ag^+ concentration of 33µg/mL and the negative control (untreated).

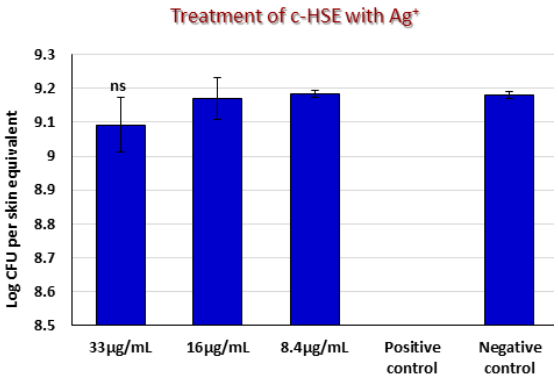

Figure 6.19 Treatment of c-HSE with Ag^+ for 24 hours.

Furthermore, the results showed that bacterial growth was much higher on a biotic surface of c-HSE than in liquid media conditions of MHB (a media used in microdilution assay) and CnT-PR-3D (a media used to bottom feed the HSE) (Figure 6. 20). This showed that the concentration of antibacterial agent required to kill bacteria in c-HSE should be increased and further investigated by using our novel c-HSE mode, as to get more closely *in vivo* values.

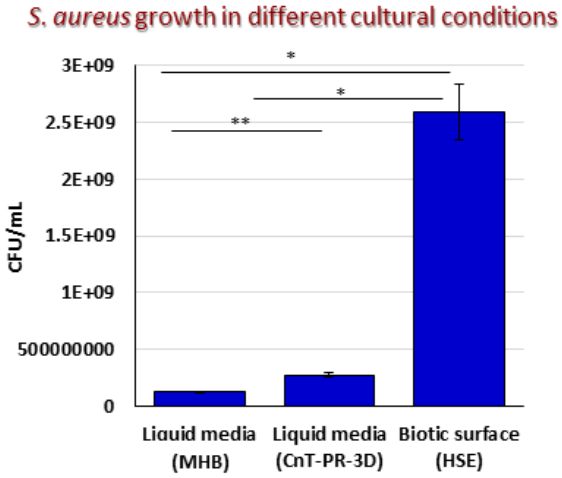

Figure 6. 20 Differences in bacterial growth under different cultural conditions after 24 hours.

The *in vitro* efficacy (the effective concentration window) of a tested sample can be expressed as selectivity index (SI=IC50/MIC50) which is the ratio of 50% cell viability concentration (i.e. IC50, the lowest concentration that shows 50% viable cells) to the 50% antibacterial concentration (i.e. MIC50, which is the lowest concentration to inhibit 50% of bacteria). Ag^{+} showed MIC in a range of 4.2-8.4µg/mL, while IC50 with human primary cells were measured as 10.3-11.8µg/mL (Figure 6.13), that calculated SI of 1.4–2.5.

6.3.2 Bio-evaluation of Ag-dressings

Cytocompatibility (cytotoxicity) evaluation of Ag-dressings

Commercially available Ag-dressings along with their control materials without Ag (the detail of product type and Ag formulation are described in Table 6.2) served the purpose of model materials and were tested in a 2D monolayer cell culture system as well as in our HSE based 3D cell culture system. L929 were used to assess general *in vitro* cytotoxicity (Figure 6.21 A), while NHDF & NHEK were used to test specific cytotoxicity (Figure 6.22) of Ag-dressings via direct contact method. CTB assay and BF microscopy were used to measure the cell viability and morphological changes after 24 hours exposure with Ag-dressings (Figure 6.21 B). The L929 cell viability after application of Biatain® Ag (17.2±0.95%) and Biatain® Alginate Ag (30.9±10.5%) respectively showed a

significant difference of **, P=0.0012 and ***, P=0.0002, compared to the negative control (PE treated, 100±14.5%) (Figure 6.21 A). However, cell viability in the presence of Biatain® and Biatain® Alginate, i.e. dressings without silver (79±19.3% and 76±19.9%, respectively) demonstrated no significant difference, compared to the negative control, indicating that Ag was the responsible agent of reduced cell viability, while the matrix material was cytocompatible in this experimental setting. BF micrographs highly correlate with the cell viability results demonstrating an affected morphology in the wells exposed to Biatain® Ag and Biatain® Alginate Ag (Figure 6.21 B-v & Figure 6.21 B-iii). Change in morphology is a cell stress response to an environmental insult that can result in fragmentation of Golgi complex, swelling of mitochondria, compromised integrity of nucleoli, or alterations in cytoskeleton especially in intermediate filaments [115-117]. L929 cells in wells with positive control (ZDEC-PU treated) and lysis control showed a clear picture of stressed and lysed cells, respectively (Figure 6.21 B-x & Figure 6.21 B-xii).

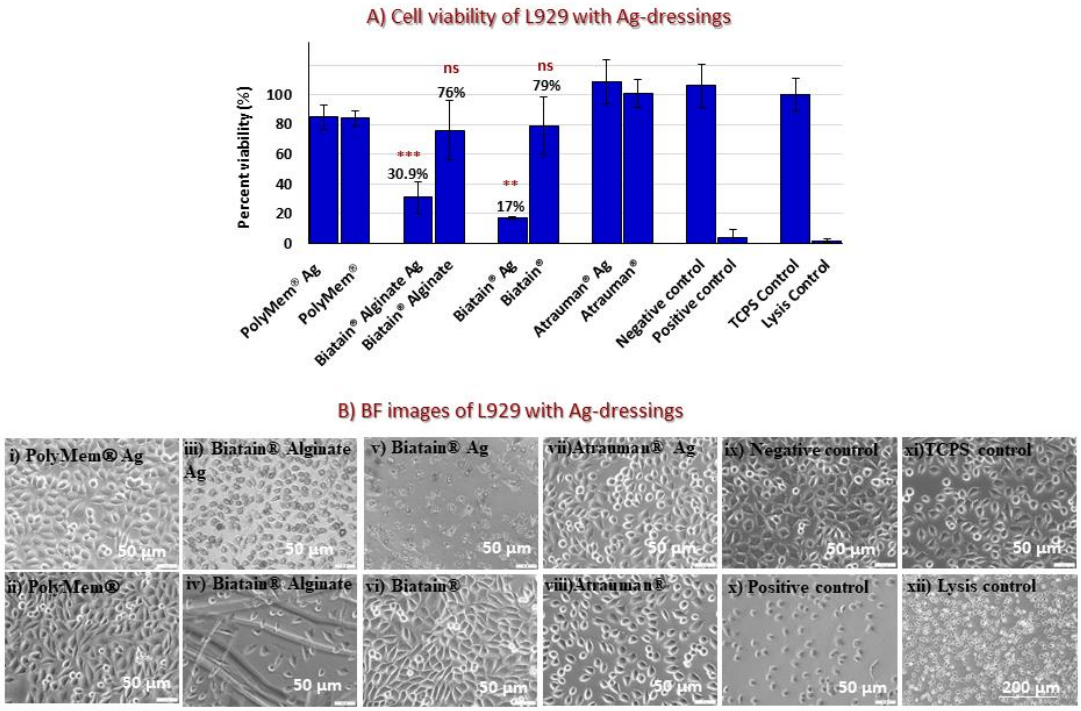

Figure 6.21 A) Cell viability of L929 with Ag-dressings. B) Bright field microscopy of L929 with Ag-dressings

The cytotoxicity of NHDF and NHEK with Ag-dressings indicated that silver released from Biatain® Ag was lethal for both fibroblasts and keratinocytes in our controlled laboratory environment, demonstrating straight 0.7±1.1% and 1.3±1.0% cell viability respectively (Figure 6.22). Biatain® Alginate Ag also demonstrated a considerable decrease of 53.5±1.3% and 52.5±19.8% in cell viability of both NHDF and NHEK, respectively. The similar cytotoxic effect of Biatain® Ag and Biatain® Alginate Ag was also observed in the presence of L929 cells (Figure 6.21). Unlike NHDF, NHEK

appeared to be slightly affected (demonstrated a cell viability of 70.5±14.5%) after exposure with PolyMem® control (without any Ag) which is polyurethane foam-based dressing (Figure 6.22).

The CTB assay colour development gives a quick qualitative readout of cytotoxicity caused by materials exposure to cell monolayer culture as shown in Figure 6.22 C.

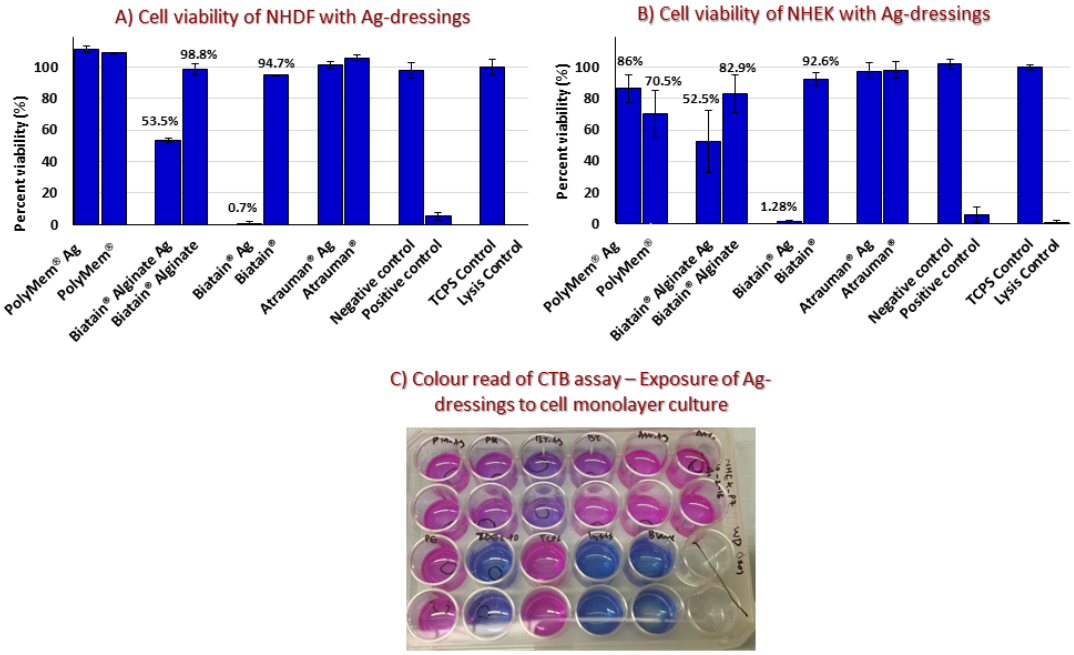

Figure 6.22 Cell viability of (A) NHDF and (B) NHEK with Ag-dressings. C) Color read of CTB assay – Exposure of Ag-dressings to cell monolayer cultures.

After 24 hours exposure with Ag-dressings, fluorescent and BF micrographs of NHEK provided a clear visual evidence about Live/Dead cell signal and cell morphology, respectively (Figure 6.23). These images highly correlated with cell viability data shown in Figure 6.22 B. Though the cells were still attached to the TCPS surface, reduced green signal in the wells exposed to Biatain® Ag (Figure 6.23) was observed as an evidence of the cytotoxic effect of this Ag-dressing. This effect was highly comparable to the images of positive control (ZDEC-PU treated) in Figure 6.23. In case of cells exposed to Biatain® Alginate Ag, a reduced green signal was observed in the test (Figure 6.23). Moreover, Biatain® Alginate (without any Ag) also appeared to have a slightly reduced green signal (Figure 6.23), when compared with negative control (PE treated) and TCPS control. Thus, the Live/Dead images (Figure 6.23) suggested that the resultant cytotoxicity of the material was a combined effect of the matrix material and impregnated antibacterial agent (Ag).

In case of PolyMem® (without any Ag), which caused a reduced cell viability CTB signal of NHEK (Figure 6.22 B), live/dead assay also showed a reduced green signal (Figure 6.23). This decrease was due to a reduced cell density in PolyMem® than

PolyMem® Ag exposed wells. This might be a result due to the detachment of dead cells from the surface after cytotoxic exposure of PolyMem® material to cells.

Furthermore, BF images demonstrated an affected cell morphology of NHEK (shrunken cells) in the wells exposed to Biatain® Ag and Biatain® Alginate Ag (Figure 6.23) and.rounded cells with disintegrated cell boundary were also observed in positive and lysis control.

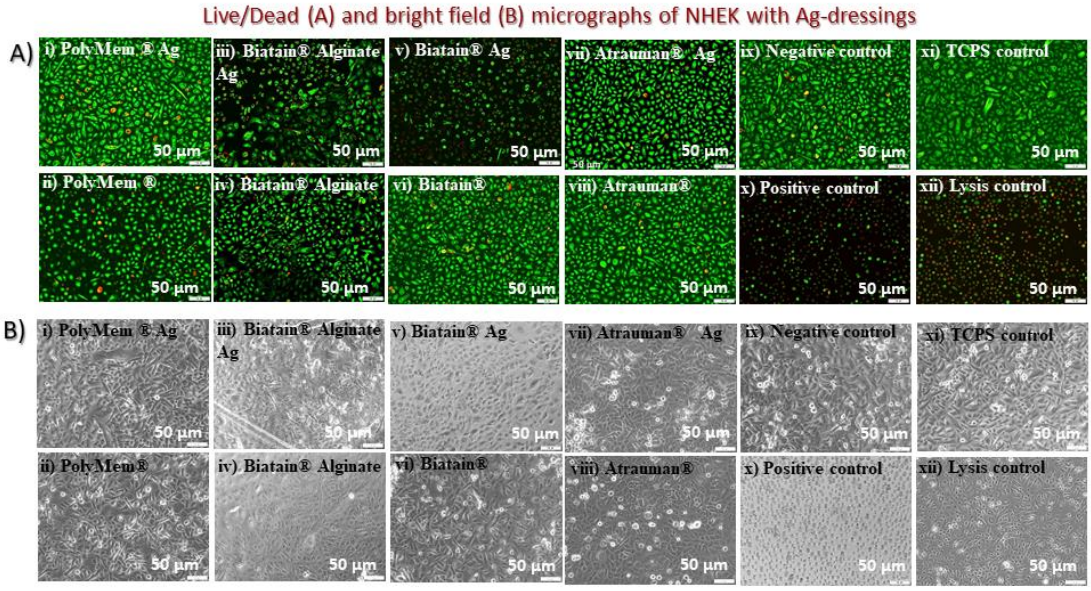

Figure 6.23 Live/Dead (A) imaging and bright field (B) microscopy of NHEK with Ag-dressings.

Taking the cytocompatibility evaluation of Ag-dressings further to an advanced level, Ag-dressings were tested in our HSE based 3D model which full-thickness histological section was shown in Figure 6.24 A. After 24 hours exposure to HSE, the cell viability was measured by CTB assay and the colour read of CTB assay was reported in Figure 6.24 C. Biatain® Ag showed 77±21.8% viability in HSE (Figure 6.24 B) as compared to monolayer cell culture system (NHDF & NHEK) where it was only ~1% (Figure 6.22). However, there was no significant difference found between Biatain® Ag and negative control (Figure 6.24 B). Likewise, Biatain® Alginate Ag demonstrated 92.5±10.6% cell viability in HSE (Figure 6.24 B) as compared to the ~53% cell viability in NHDF & NHEK based monolayer culture (Figure 6.22). Moreover, there was no significant difference found between Biatain® Alginate Ag and the negative control either (Figure 6.24 B).

The literature also supports the role of silver in enhancing the healing when applied on closed surgical wounds [77]. As wound healing can be modulated by many processes, for example, using proliferating keratinocytes [118-121], our concern should be if the silver-based antimicrobial dressings would be suitable for these new strategies in wound management.

Each study has its own test design and experimental set-up, thus results cannot be precisely cross-compared among different testing systems. However, it was evident that silver released from Biatain® Ag was lethal for either fibroblasts or keratinocytes based monolayer systems but was no more cytotoxic when tested in HSE based 3D system, suggesting that as the complexity of the environment increased, the toxic effect of the silver decreased.

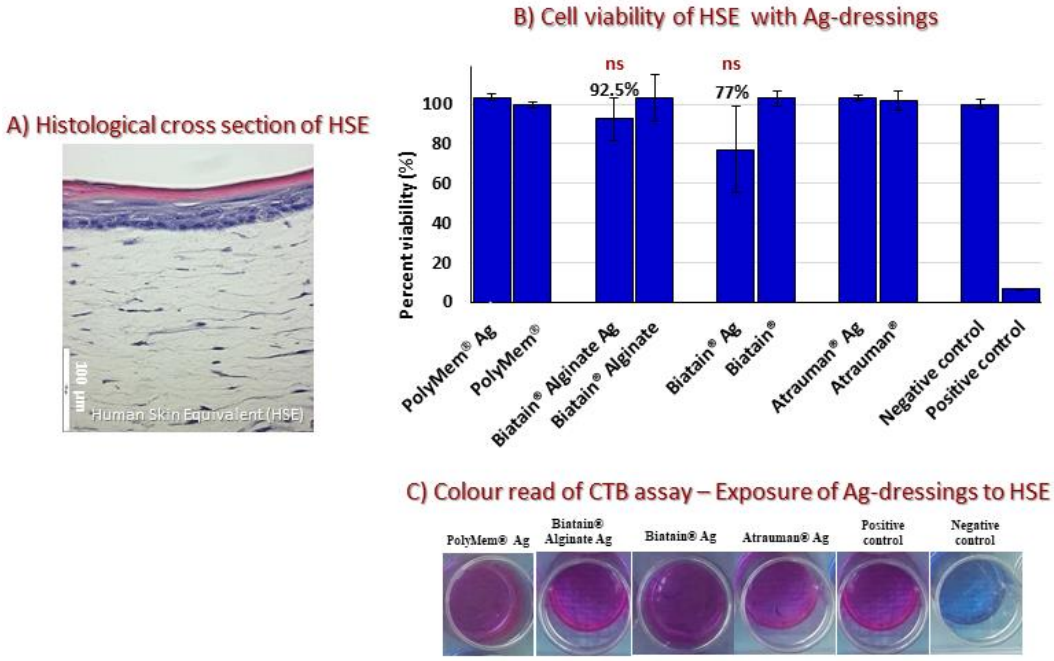

Figure 6.24 A) Histological cross section of HSE. B) Cell viability of HSE with Ag-dressings. C) Color read of CTB assay – Exposure of Ag-dressings to HSE.

Our study also demonstrates that a rapid and too direct extrapolation of results from 2D laboratory experiments to clinical outcomes must be taken with caution. For example, one study [122] evaluated into the toxicity of an antimicrobial called EUSOL (also called Dakin's solution, aq. solution of "sodium hypochlorite" including pH stabilizing agents) on human fibroblasts, despite its widespread use it gained notoriety in the UK. Based on the lab results about devastating effects on cells [123], a number of issues raised on the safety of EUSOL. Following these tests, debates were made about the relevancy of laboratory experiments to clinical experience [124-126], that also highlighted the professional differences between nurses (who pursue evidence-based practice) and doctor (who pursue experience-based practice). This went too far suggesting nurses with a legal right to not follow the EUSOL use even prescribed by a doctor [127]. Result is that EUSOL is no longer used in clinics in UK [128].

In conclusion, Ag^{+} showed three times higher IC50 value using HSE than 2D monolayer based cell culture. Among tested Ag-dressings, the cytotoxicity tests using NHDF and NHEK indicated that silver released from Biatain® Ag (1% cell viability) and Biatain®

Alginate Ag (53% cell viability) was lethal for both fibroblasts and keratinocytes. On the other hand, Biatain® Ag and Biatain® Alginate Ag demonstrated 77±21.8% and 92.5±10.6% cell viability with HSE.

Antibacterial evaluation of Ag-dressings

The challenge is to develop an effective antibacterial product, based on an agent and its delivery system, that is functional for selective killing of bacteria. In the literature, the role of silver *in vivo* had been proven by its contribution for reducing the infection when administered into venous [129, 130] and urethral [131] catheters.

Antibacterial activity of Ag-dressings against *S. aureus* over time was performed by broth inoculation assay in TSB media and the results were measured as percent of bacterial reduction as well as CFU/mL of surviving bacteria (Figure 6.25). The growth curve of *S. aureus* over a time period of 48 hours in TSB was also recorded. Among tested Ag-dressings, Biatain® Ag and Biatain® Alginate Ag were able to show complete bacterial reduction, in which Biatain® Ag showed a continued inhibitory effect even after 48 hours of incubation (Figure 6.25). On the other hand, in the case of PolyMem® Ag and Atrauman® Ag products, the bacterial inhibitory effect appeared to increase with time: it was "22.7±14.9% & 54.5±4.2%" at T_{24h} and "86±1.8% & 92±0.7%" at T_{48h}, respectively (the effect was evidenced with upward arrows in Figure 6.25 A). This effect might be related to the form of silver, silver content, silver release and the dressing matrix material itself of each individual Ag-dressing.

Ag^{+} at its pre-determined MIC and MBC were also tested for *S. aureus* reduction and served as sort of controls in this experimental set-up (Figure 6.25).

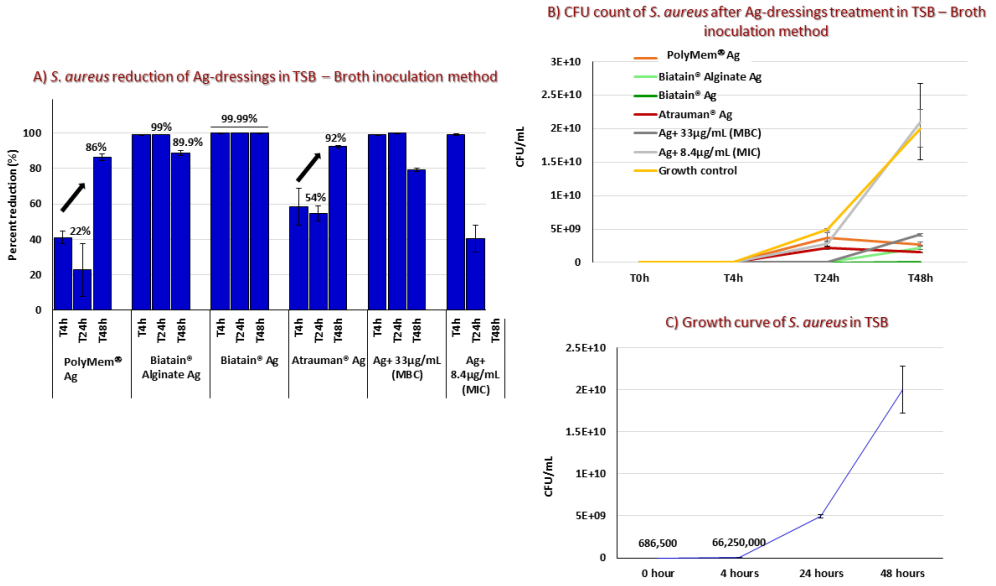

Figure 6.25 Antibacterial activity of Ag-dressings against S. aureus in TSB over time as (A) percent reduction and (B) CFU/mL count – Broth inoculation assay. C) Growth curve of S. aureus in TSB.

Comparing the dressings is logical, provided the question is to test and find the one with highest clinical efficacy. However, whether the silver in different products is efficacious, can indeed not be answered. Though, the comparison among different Ag-dressings is not always appropriate because the total amount of silver in dressings differs considerably [62]. Additionally, the amount of silver delivered to a wound does not really correlate with the amount of silver contained within the dressing [59] because the consumption of silver ions highly depends on wound environment and silver interaction with wound components, e.g. proteins and chloride ions. In this context, laboratory experiments that showed as low concentration as ≤1ppm silver ions [63] to be effective against bacteria, were not really correlated to the clinical performance [74]. Some authors have suggested that the active form of silver released from Ag-dressing is different than the active form of silver released by silver nitrate [132]. Moreover, a study that used PolyMem® Ag along with other Ag-dressings (e.g. AQUACEL® Ag) found no direct correlation between silver content/silver release, and their respective antibacterial activities [71]. However, the studies reported by [64, 133] suggested that higher the silver concentrations in Ag-dressings, higher would be the bactericidal properties. In our study, the correlation between Ag content/release and antibacterial activity can only be investigated by measuring the silver release profile of different Ag-dressings in the respective medium.

The antibacterial effect of Ag-dressings was also tested against Gram -ve bacteria of *P. aeruginosa* in TSB until 24 hours. Biatain® Ag and Biatain® Alginate Ag both demonstrated 99.99±2.1% bacterial reduction against *P. aeruginosa* (Figure 6.26) as they showed against *S. aureus* (Figure 6.25).

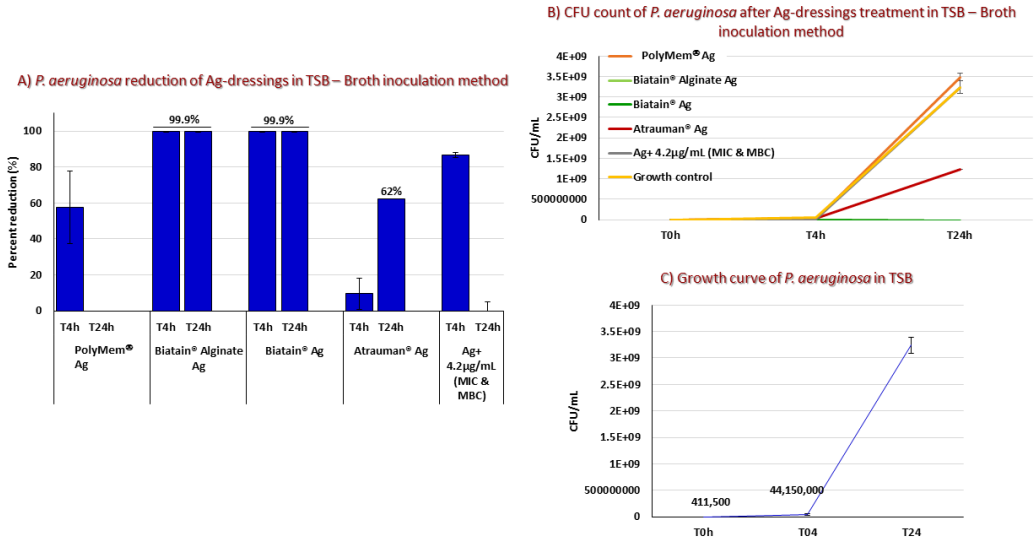

Figure 6.26 Antibacterial activity of Ag-dressings against P. aeruginosa in TSB over time as (A) percent reduction and (B) CFU/mL count – Broth inoculation assay. C) Growth curve of P. aeruginosa in TSB.

The antibacterial activity of Ag-dressings against *S. aureus* was tested the same way as above but this time in a complex high protein medium namely SWF instead of TSB (Figure 6.27). The antibacterial results obtained in SWF medium were compared with the results obtained in TSB medium (Figure 6.25). The considerable variation in the antibacterial ability in each of individual Ag-dressing was observed in SWF environment. For example, Biatain® Alginate Ag showed no bacterial reduction in this medium (Figure 6.27) as compared to 100% bacterial reduction at T_{24h} in TSB (Figure 6.25). The time dependent antibacterial effect of PolyMem® Ag and Atrauman® Ag observed in TSB also did not appear at the similar level in SWF, with PolyMem® Ag demonstrating only 61±1.3% bacterial reduction at T_{24h} that further reduced to 0% at T_{48h} (Figure 6.27).

Most importantly, Biatain® Ag was still able to demonstrate 99.99±0.0% in SWF.

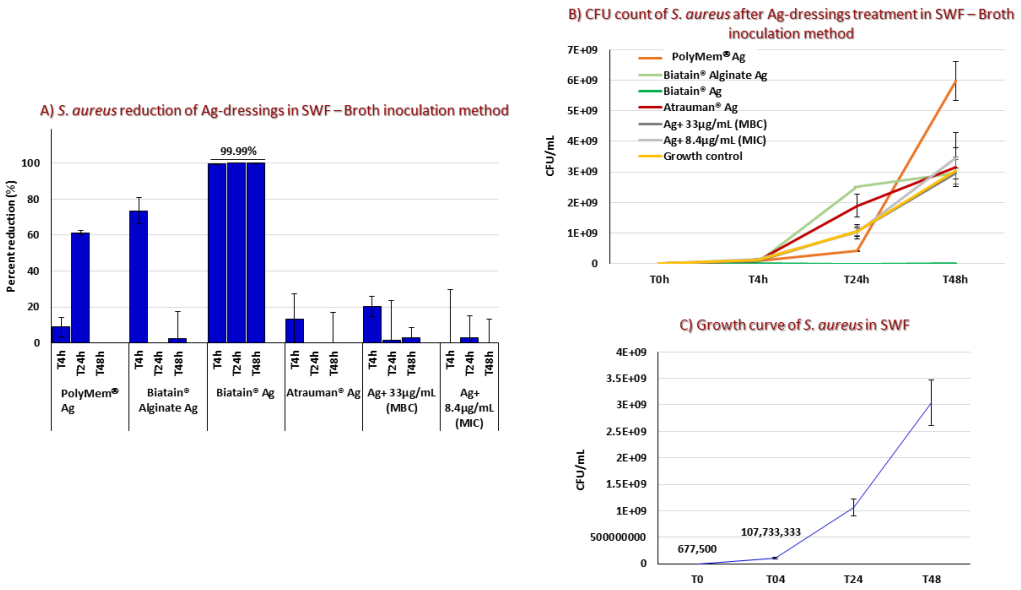

Figure 6.27 Antibacterial activity of Ag-dressings against S. aureus in SWF over time as (A) percent reduction and (B) CFU/mL count – Broth inoculation assay. C) Growth curve of S. aureus in SWF.

The antibacterial effect of Biatain® Ag was also tested against Gram -ve bacteria of *E. coli* until 24 hours that demonstrated 99.99±0.0% bacterial reduction in SWF (Figure 6.28). Biatain® Alginate Ag showed an antibacterial activity of 83±3.4% reduction (Figure 6.28) against *E. coli* compared to 0% reduction against *S. aureus* (Figure 6.27) in SWF at T_{24h}. This suggested that Gram -ve susceptibility is higher with Biatain® Alginate Ag.

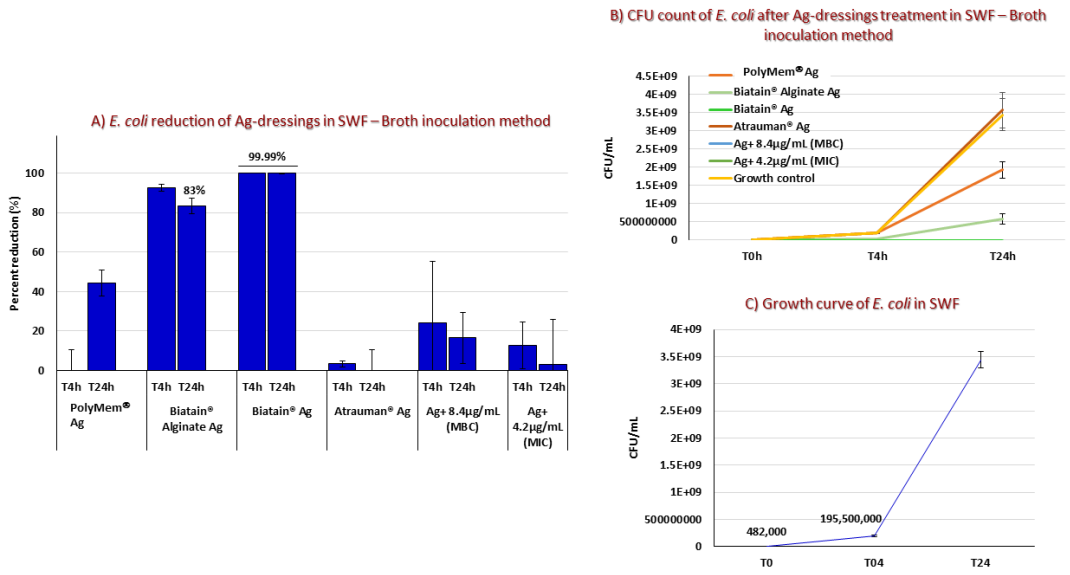

Figure 6.28 Antibacterial activity of Ag-dressings against E. coli in SWF over time as (A) percent reduction and (B) CFU/mL count – Broth inoculation assay. C) Growth curve of E. coli in SWF.

With the aim to understand the complexity of the infected wounds, we then tested commercially available Ag-dressing with our *S. aureus* colonized HSE model (c-HSE) (Figure 6.29 C). Results were shown as Log CFU of *S. aureus* per c-HSE and a significant difference (P=0.0085, **) was found between Biatain® Ag and the negative control (untreated), while no significant difference was found between Biatain® Alginate Ag and the negative control (Figure 6.29 A). Biatain® Ag demonstrated 100% reduction against *S. aureus* in broth inoculation method under both TSB and SWF media (Figure 6.25 and Figure 6.27), however, it showed only 56% reduction (calculated results not shown) in our c-HSE antibacterial-evaluation system. Furthermore, as shown before, the bacterial growth was much higher on a biotic surface of c-HSE than in liquid media conditions of MHB (a medium used in microdilution assay) and CnT-PR-3D (a medium used to bottom feed the HSE) (Figure 6.29 B).

Ag-dressings are widely used to treat the infected wounds. Considering the fact that the clinical intervention strategies have an important role to fight against wound infections, the Ag availability in wounds and the actual role of available Ag against infection is not 100%, thus actual antibacterial efficiency is unclear. For understanding/evaluating antibacterial activities, the developed c-HSE system has great potentiality and would serve as an advanced tool to screen novel antimicrobial biomaterials for infected wound healing.

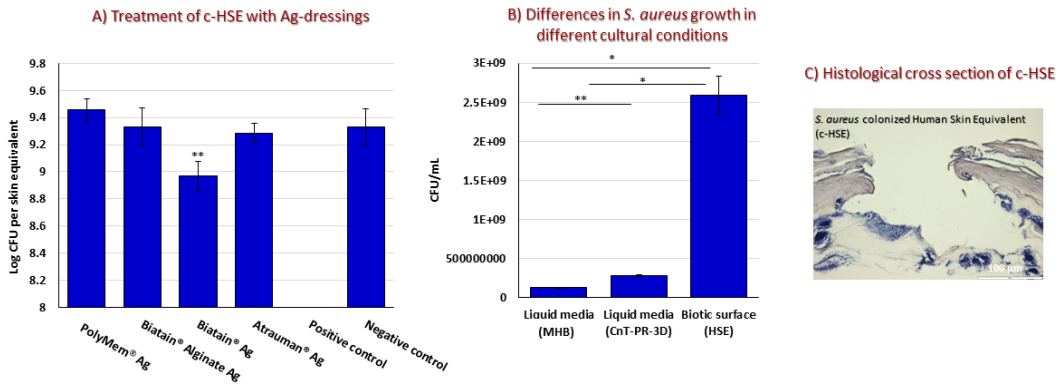

Figure 6.29 A) Treatment of c-HSE with Ag-dressings for 24 hours. B) Differences in S. aureus growth in different cultural conditions. C) Histological cross section of c-HSE.

Antibacterial products cannot exactly distinguish between healthy cells involved in wound healing and pathogenic bacteria involved in wound infection or delayed wound healing. Therefore, the silver-based products should be used with caution in wounds where healing is stimulated by proliferating cells (e.g. in donor sites, or superficial partial thickness wounds or when undifferentiated cultured keratinocyte strategy is applied).

Conclusion

Single-cell assays under submerged culture conditions (cell lines and/or human primary cells), or 3D systems like dermal equivalents, epidermal equivalents, full-thickness skin equivalents and excised skin under ALI culture conditions, serve as different types of model systems with different advantages and disadvantages related to each [134]. Recently in an effort to substitute the animal experiments, several commercially available skin equivalents (e.g. EpiDerm®, Episkin® and SkinEthic®) are going to be used as stand-alone irritancy test replacements of rabbit Draize test [135]. In this regard, our in-house built HSE has shown to have a great potential for the safety assessment of antibacterial biomaterials.

Moreover, antibacterial products may be very effective in a controlled laboratory set-up, but they may not be as effective on patients. The cytotoxicity and antibacterial outcomes of silver vary significantly under different laboratories as well as in clinical situations. The silver sensitivity of the cells and its lethal effect towards bacteria are decreased when the cells and/or bacteria are grown in complex arrangements to simulate the clinical environment. In this study, we investigated the antibacterial agent (Ag^+) and a few antibacterial wound products (Ag-dressings) in our 3D systems (HSE and c-HSE) imitating an *in vivo* like settings. The study verified that our 3D model systems were able to assess the cytotoxicity and antibacterial properties in a more complex environment. Moreover, this study also bio-evaluated the Ag^+ and Ag-products under 2D cell culture and commonly used antibacterial arrangement; the outcomes were compared with the results obtained from advanced 3D testing systems, demonstrating considerable variations among the two set-ups.

IC50 of Ag^+ was three times higher (34.2µg/mL) in HSE cultures than 2D monolayer cultures. The antibacterial activity of Ag^+ showed 99.99% *S. aureus* reduction in TSB, while 0% reduction in SWF indicating the significance of wound extracellular micro-environment. Among tested Ag-dressings, Biatain® Ag indicated 77±21.8% cell viability in HSE as compared to 1% cell viability in 2D monolayer cultures. Biatain® Ag demonstrated 99.99% *S. aureus* reduction in both TSB and SWF testing environments. Biatain® Ag was still able to significantly reduce bacterial burden in c-HSE system as compared to untreated c-HSE control. Among the tested Ag-dressings, Biatain® Ag was able to significantly reduce bacteria in c-HSE without significantly compromising cell viability of HSE in our advanced experimental set-ups. The results suggested the need and importance of advanced *in vitro* bio-evaluation systems to better investigate the biological properties of antibacterial products. In this context, a quick extrapolation of results from laboratory experiments to clinical outcomes must be taken with extreme care. On the other hand, the Ag-products must also be used with high attention depending on the patient and the wound situation.

For the treatment of chronic wounds, the antibacterial products should also be evaluated for anti-inflammatory properties. In this context, Ag^+ and Ag-products have been shown to have anti-inflammatory and neovascularization effects *in vitro* [61, 78-80], though this needs further *in vitro* experimentation to prove clinical relevance. For this purpose, our 3D system can be used as a base to build more complex immunocompetent models.

References

1. Antoni, D., et al., *Three-dimensional cell culture: a breakthrough in vivo.* International journal of molecular sciences, 2015. 16(3): p. 5517-5527.
2. Breslin, S. and L. O'Driscoll, *Three-dimensional cell culture: the missing link in drug discovery.* Drug discovery today, 2013. 18(5-6): p. 240-249.
3. Joseph, J.S., S.T. Malindisa, and M. Ntwasa, *Two-Dimensional (2D) and Three-Dimensional (3D) Cell Culturing in Drug Discovery*, in *Cell Culture*. 2018, IntechOpen.
4. Cukierman, E., et al., *Taking cell-matrix adhesions to the third dimension.* Science, 2001. 294(5547): p. 1708-1712.
5. Grinnell, F., *Biochemical analysis of cell adhesion to a substratum and its possible relevance to cell metastasis.* Progress in clinical and biological research, 1976. 9: p. 227-236.
6. Yang, J., et al., *Different mitogenic and phenotypic responses of human breast epithelial cells grown in two versus three dimensions.* Experimental cell research, 1986. 167(2): p. 563-569.
7. Lin, C.Q. and M.J. Bissell, *Multi-faceted regulation of cell differentiation by extracellular matrix.* The FASEB Journal, 1993. 7(9): p. 737-743.
8. Smalley, K.S., M. Lioni, and M. Herlyn, *Life ins't flat: Taking cancer biology to the next dimension.* In Vitro Cellular & Developmental Biology-Animal, 2006. 42(8-9): p. 242-247.
9. Grinnell, F., *Fibroblast mechanics in three-dimensional collagen matrices.* Journal of bodywork and movement therapies, 2008. 12(3): p. 191-193.
10. Horning, J.L., et al., *3-D tumor model for in vitro evaluation of anticancer drugs.* Molecular pharmaceutics, 2008. 5(5): p. 849-862.
11. Mazzoleni, G., D. Di Lorenzo, and N. Steimberg, *Modelling tissues in 3D: the next future of pharmaco-toxicology and food research?* Genes & nutrition, 2009. 4(1): p. 13.
12. Bissell, M.J., H.G. Hall, and G. Parry, *How does the extracellular matrix direct gene expression?* Journal of theoretical biology, 1982. 99(1): p. 31-68.
13. Coulomb, B., et al., *Advantage of the presence of living dermal fibroblasts within in vitro reconstructed skin for grafting in humans.* Plastic and reconstructive surgery, 1998. 101(7): p. 1891-1903.
14. Lebonvallet, N., et al., *The evolution and use of skin explants: potential and limitations for dermatological research.* European Journal of Dermatology, 2010. 20(6): p. 671-684.
15. Boelsma, E., M.C. Verhoeven, and M. Ponec, *Reconstruction of a human skin equivalent using a spontaneously transformed keratinocyte cell line (HaCaT).* Journal of investigative dermatology, 1999. 112(4): p. 489-498.

16. Maas-Szabowski, N., A. Stärker, and N.E. Fusenig, *Epidermal tissue regeneration and stromal interaction in HaCaT cells is initiated by TGF-α.* Journal of cell science, 2003. 116(14): p. 2937-2948.
17. Roth, A. and T. Singer, *The application of 3D cell models to support drug safety assessment: opportunities & challenges.* Advanced drug delivery reviews, 2014. 69: p. 179-189.
18. Mertsching, H., et al., *Human skin equivalent as an alternative to animal testing.* GMS Krankenhaushygiene interdisziplinar, 2008. 3(1).
19. Ponec, M., *Skin constructs for replacement of skin tissues for in vitro testing.* Advanced drug delivery reviews, 2002. 54: p. S19-S30.
20. Ponec, M., et al., *Characterization of reconstructed skin models.* Skin Pharmacology and Physiology, 2002. 15(Suppl. 1): p. 4-17.
21. Draize, J.H., G. Woodard, and H.O. Calvery, *Methods for the study of irritation and toxicity of substances applied topically to the skin and mucous membranes.* Journal of pharmacology and Experimental Therapeutics, 1944. 82(3): p. 377-390.
22. Campbell, R.L. and R.D. Bruce, *Comparative dermatotoxicology: I. Direct comparison of rabbit and human primary skin irritation responses to isopropylmyristate.* Toxicology and applied pharmacology, 1981. 59(3): p. 555-563.
23. Phillips II, L., et al., *A comparison of rabbit and human skin response to certain irritants.* Toxicology and Applied Pharmacology, 1972. 21(3): p. 369-382.
24. Youssef, K.K., et al., *Identification of the cell lineage at the origin of basal cell carcinoma.* Nature cell biology, 2010. 12(3): p. 299.
25. Paulitschke, V., et al., *3, 3', 4, 4', 5, 5'-hexahydroxystilbene impairs melanoma progression in a metastatic mouse model.* Journal of Investigative Dermatology, 2010. 130(6): p. 1668-1679.
26. Mancuso, M., et al., *Modulation of basal and squamous cell carcinoma by endogenous estrogen in mouse models of skin cancer.* Carcinogenesis, 2008. 30(2): p. 340-347.
27. Groeber, F., et al., *Skin tissue engineering—in vivo and in vitro applications.* Advanced drug delivery reviews, 2011. 63(4-5): p. 352-366.
28. Donahue, B.A., et al., *Selective uptake and sustained expression of AAV vectors following subcutaneous delivery.* The journal of gene medicine, 1999. 1(1): p. 31-42.
29. Khorshid, F.A., *Comparative study of keloid formation in humans and laboratory animals.* Medical science monitor, 2005. 11(7): p. BR212-BR219.
30. Menon, G.K., *New insights into skin structure: scratching the surface.* Advanced drug delivery reviews, 2002. 54: p. S3-S17.

31. *Council of the European Union. Seventh Amendment to the EU and Cosmetics Directive 76/768/EEC. Brussels: The European Parliament and the Council of the European Union.* 2003.
32. Becker, R.A., et al., *Report of an ISRTP Workshop: Progress and barriers to incorporating alternative toxicological methods in the US.* Regulatory Toxicology and Pharmacology, 2006. 46(1): p. 18-22.
33. Kuroyanagi, Y., et al., *Establishment of banking system for allogeneic cultured dermal substitute.* Artificial organs, 2004. 28(1): p. 13-21.
34. UNION, P., *Regulation (EC) No 1907/2006 of the european parliament and of the council*. 2006.
35. Oliver, G., M. Pemberton, and C. Rhodes, *An in vitro model for identifying skin-corrosive chemicals. I. Initial validation.* Toxicology in vitro, 1988. 2(1): p. 7-17.
36. Scala, R., et al., *Corrositex: An In Vitro Test Method for Assessing Dermal Corrosivity Potential of Chemicals*. 1999.
37. Stobbe, J.L., K.D. Drake, and K.J. Maier, *Comparison of in vivo (Draize method) and in vitro (Corrositex assay) dermal corrosion values for selected industrial chemicals.* International journal of toxicology, 2003. 22(2): p. 99-107.
38. Kandárová, H., et al., *Assessment of the human epidermis model SkinEthic RHE for in vitro skin corrosion testing of chemicals according to new OECD TG 431.* Toxicology in vitro, 2006. 20(5): p. 547-559.
39. Kidd, D., M. Johnson, and J. Clements, *Development of an in vitro corrosion/irritation prediction assay using the EpiDerm™ skin model.* Toxicology in vitro, 2007. 21(7): p. 1292-1297.
40. Balls, M. and E. Helisten, *Statement on the application of the EpiDerm™ human skin model for skin corrosivity testing.* European Centre for the Validation of Alternative Methods, 2000. 21.
41. Fentem, J., et al., *A prevalidation study on in vitro tests for acute skin irritation: results and evaluation by the Management Team.* Toxicology in vitro, 2001. 15(1): p. 57-93.
42. Fentem, J., et al., *The ECVAM international validation study on in vitro tests for skin corrosivity. 2. Results and evaluation by the Management Team.* Toxicology in vitro, 1998. 12(4): p. 483-524.
43. Perkins, M.A., R. Osborne, and G.R. Johnson, *Development of an in vitro method for skin corrosion testing.* Toxicological Sciences, 1996. 31(1): p. 9-18.
44. Ponec, M., et al., *Barrier function in reconstructed epidermis and its resemblance to native human skin.* Skin Pharmacology and Physiology, 2001. 14(Suppl. 1): p. 63-71.
45. Bouwstra, J., et al., *New aspects of the skin barrier organization.* Skin Pharmacology and Physiology, 2001. 14(Suppl. 1): p. 52-62.

46. Lotte, C., et al., *Permeation and skin absorption: reproducibility of various industrial reconstructed human skin models.* Skin Pharmacology and Physiology, 2002. 15(Suppl. 1): p. 18-30.
47. Osborne, R. and M. Perkins, *An approach for development of alternative test methods based on mechanisms of skin irritation.* Food and Chemical Toxicology, 1994. 32(2): p. 133-142.
48. Rasmussen, C., et al., *The StrataTest® human skin model, a consistent in vitro alternative for toxicological testing.* Toxicology in vitro, 2010. 24(7): p. 2021-2029.
49. Smijs, T.G. and J.A. Bouwstra, *Focus on skin as a possible port of entry for solid nanoparticles and the toxicological impact.* Journal of biomedical nanotechnology, 2010. 6(5): p. 469-484.
50. McCaig, L.F., et al., *Staphylococcus aureus–associated skin and soft tissue infections in ambulatory care.* Emerging infectious diseases, 2006. 12(11): p. 1715.
51. Moran, G.J., et al., *Methicillin-resistant Staphylococcus aureus in community-acquired skin infections.* Emerging infectious diseases, 2005. 11(6): p. 928.
52. Eady, E.A. and J.H. Cove, *Staphylococcal resistance revisited: community-acquired methicillin resistant Staphylococcus aureus-an emerging problem for the management of skin and soft tissue infections.* Current opinion in infectious diseases, 2003. 16(2): p. 103-124.
53. Charles, C.A., et al., *Use of tissue-engineered skin to study in vitro biofilm development.* Dermatologic Surgery, 2009. 35(9): p. 1334-1341.
54. Hill, K.E., et al., *An in vitro model of chronic wound biofilms to test wound dressings and assess antimicrobial susceptibilities.* Journal of Antimicrobial Chemotherapy, 2010. 65(6): p. 1195-1206.
55. Krishna, S. and L.S. Miller, *Host–pathogen interactions between the skin and Staphylococcus aureus.* Current opinion in microbiology, 2012. 15(1): p. 28-35.
56. O'Brien, L.M., et al., *Staphylococcus aureus clumping factor B (ClfB) promotes adherence to human type I cytokeratin 10: implications for nasal colonization.* Cellular microbiology, 2002. 4(11): p. 759-770.
57. Shepherd, J., et al., *Development of three-dimensional tissue-engineered models of bacterial infected human skin wounds.* Tissue Engineering Part C: Methods, 2009. 15(3): p. 475-484.
58. O'Toole, G., H.B. Kaplan, and R. Kolter, *Biofilm formation as microbial development.* Annual Reviews in Microbiology, 2000. 54(1): p. 49-79.
59. Woo, K., E. Ayello, and R. Sibbald, *SILVER versus other antimicrobial dressings: best practices!* Surgical technology international, 2008. 17: p. 50-71.
60. Leaper, D.J., *Silver dressings: their role in wound management.* International wound journal, 2006. 3(4): p. 282-294.

61. Lansdown, A. and A. Williams, *How safe is silver in wound care?* Journal of wound care, 2004. 13(4): p. 131-136.
62. Thomas, S. and P. McCubbin, *An in vitro analysis of the antimicrobial properties of 10 silver-containing dressings.* Journal of wound care, 2003. 12(8): p. 305-308.
63. Hermans, M.H., *Silver-containing dressings and the need for evidence.* Advances in skin & wound care, 2007. 20(3): p. 166-173.
64. Lansdown, A.B., *Silver I: its antibacterial properties and mechanism of action.* Journal of wound care, 2002. 11(4): p. 125-130.
65. Percival, S.L., P. Bowler, and D. Russell, *Bacterial resistance to silver in wound care.* Journal of hospital infection, 2005. 60(1): p. 1-7.
66. Woodward, M., *Silver dressings in wound healing: what is the evidence?* Primary Intention: The Australian Journal of Wound Management, 2005. 13(4): p. 153.
67. Nadworny, P. and R. Burrell, *A Review of Assessment Techniques for Silver Technology in Wound Care Part 1: In VitroMethods for Assessing Antimicrobial Activity.* Journal of Wound Technology, 2008. 2(I): p. 6-13.
68. Nadworny, P. and R. Burrell, *A Review of Assessment Techniques for Silver Technology in Wound Care Part II.* Journal of Wound Technology, 2008. 2(I): p. 14-22.
69. Ip, M., et al., *Antimicrobial activities of silver dressings: an in vitro comparison.* Journal of medical microbiology, 2006. 55(1): p. 59-63.
70. Bowler, P., et al., *Microbicidal properties of a silver-containing Hydrofiber® dressing against a variety of burn wound pathogens.* Journal of Burn Care & Rehabilitation, 2004. 25(2): p. 192-196.
71. Parsons, D., et al., *Silver antimicrobial dressings in wound management: a comparison of antibacterial, physical, and chemical characteristics.* Wounds-A Compendium of Clinical Research and Practice, 2005. 17(8): p. 222-232.
72. Chaw, K., M. Manimaran, and F.E. Tay, *Role of silver ions in destabilization of intermolecular adhesion forces measured by atomic force microscopy in Staphylococcus epidermidis biofilms.* Antimicrobial agents and chemotherapy, 2005. 49(12): p. 4853-4859.
73. Percival, S.L., P. Bowler, and E.J. Woods, *Assessing the effect of an antimicrobial wound dressing on biofilms.* Wound repair and regeneration, 2008. 16(1): p. 52-57.
74. Thorn, R., et al., *In vitro comparison of antimicrobial activity of iodine and silver dressings against biofilms.* Journal of wound care, 2009. 18(8): p. 343-346.
75. Kostenko, V., et al., *Impact of silver-containing wound dressings on bacterial biofilm viability and susceptibility to antibiotics during prolonged treatment.* Antimicrobial agents and chemotherapy, 2010. 54(12): p. 5120-5131.

76. Kędziora, A., et al., *Similarities and differences between silver ions and silver in nanoforms as antibacterial agents.* International journal of molecular sciences, 2018. 19(2): p. 444.
77. Lansdown, A., et al., *Silver aids healing in the sterile skin wound: experimental studies in the laboratory rat.* British Journal of Dermatology, 1997. 137(5): p. 728-735.
78. Lansdown, A.B., *A pharmacological and toxicological profile of silver as an antimicrobial agent in medical devices.* Advances in pharmacological sciences, 2010. 2010.
79. Wilkinson, L., R. White, and J. Chipman, *Silver and nanoparticles of silver in wound dressings: a review of efficacy and safety.* Journal of wound care, 2011. 20(11): p. 543-549.
80. Walker, M., P.G. Bowler, and C.A. Cochrane, *In vitro studies to show sequestration of matrix metalloproteinases by silver-containing wound care products.* Ostomy Wound Management, 2007. 53(9): p. 18.
81. Pandian, S.R.K., et al., *Mechanism of bactericidal activity of Silver Nitrate-a concentration dependent bi-functional molecule.* Brazilian Journal of Microbiology, 2010. 41(3): p. 805-809.
82. (WUWHS), W.U.o.W.H.S., *Wound infection in clinical practice: a WUWHS international consensus.* 14 October 2009.
83. Siddiqui, A.R. and J.M. Bernstein, *Chronic wound infection: facts and controversies.* Clinics in dermatology, 2010. 28(5): p. 519-526.
84. Thomas, S. and P. McCubbin, *A comparison of the antimicrobial effects of four silver-containing dressings on three organisms.* Journal of wound care, 2003. 12(3): p. 101-107.
85. Walker, M., et al., *Evaluation of low-adherent antimicrobial dressings.* Wounds UK, 2011. 7(2): p. 32-45.
86. Cavanagh, M.H., R.E. Burrell, and P.L. Nadworny, *Evaluating antimicrobial efficacy of new commercially available silver dressings.* International Wound Journal, 2010. 7(5): p. 394-405.
87. Leaper, D., *Appropriate use of silver dressings in wounds: international consensus document.* International wound journal, 2012. 9(5): p. 461-464.
88. Opasanon, S., P. Muangman, and N. Namviriyachote, *Clinical effectiveness of alginate silver dressing in outpatient management of partial-thickness burns.* International wound journal, 2010. 7(6): p. 467-471.
89. Muangman, P., et al., *A prospective, randomized trial of silver containing hydrofiber dressing versus 1% silver sulfadiazine for the treatment of partial thickness burns.* International wound journal, 2010. 7(4): p. 271-276.

90. Dimakakos, E., et al., *Infected Venous Leg Ulcers: Management With Silver-releasing Foam Dressing.* Wounds: a compendium of clinical research and practice, 2009. 21(1): p. 4-8.
91. Lazareth, I., et al., *The Role of a Silver Releasing Lipido-colloid Contact Layer in Venous Leg Ulcers Presenting Inflammatory Signs Suggesting Heavy Bacterial Colonization: Results of a Randomized Controlled Study.* Wounds: a compendium of clinical research and practice, 2008. 20(6): p. 158-166.
92. Munter, K.-C., et al., *Effect of a sustained silver-releasing dressing on ulcers with delayed healing: the CONTOP study.* Journal of wound care, 2006. 15(5): p. 199-206.
93. Jude, E., et al., *Prospective randomized controlled study of Hydrofiber® dressing containing ionic silver or calcium alginate dressings in non-ischaemic diabetic foot ulcers.* Diabetic Medicine, 2007. 24(3): p. 280-288.
94. Jørgensen, B., et al., *The silver-releasing foam dressing, Contreet Foam, promotes faster healing of critically colonised venous leg ulcers: a randomised, controlled trial.* International Wound Journal, 2005. 2(1): p. 64-73.
95. Meaume, S., et al., *Evaluation of a silver-releasing hydroalginate dressing in chronic wounds with signs of local infection.* Journal of wound care, 2005. 14(9): p. 411-419.
96. Romanelli, M. and P. Price, *Health-related quality of life aspects after treatment with a foam dressing and a silver-containing foam dressing in chronic leg ulcers.* Journal of the American Academy of Dermatology, 2005. 52(3): p. P211.
97. Russell, L., *The CONTOP multinational study: preliminary data from the UK arm.* WOUNDS UK, 2005. 1(1): p. 44.
98. Verd Soriano, J., et al., *Effects of an activated charcoal silver dressing on chronic wounds with no clinical signs of infection.* Journal of wound care, 2004. 13(10): p. 419-423.
99. Wunderlich, U. and C. Orfanos, *Treatment of venous ulcera cruris with dry wound dressings. Phase overlapping use of silver impregnated activated charcoal xerodressing.* Der Hautarzt; Zeitschrift fur Dermatologie, Venerologie, und verwandte Gebiete, 1991. 42(7): p. 446-450.
100. Jurczak, F., et al., *Randomised clinical trial of Hydrofiber dressing with silver versus povidone–iodine gauze in the management of open surgical and traumatic wounds.* International wound journal, 2007. 4(1): p. 66-76.
101. Michaels, J., et al., *Randomized controlled trial and cost-effectiveness analysis of silver-donating antimicrobial dressings for venous leg ulcers (VULCAN trial).* British Journal of Surgery: Incorporating European Journal of Surgery and Swiss Surgery, 2009. 96(10): p. 1147-1156.
102. *Best Practice Statement: The use of topical antiseptic/antimicrobial agents in wound management, 2nd edition.* Wounds UK, 2011.

103. Trial, C., et al., *Assessment of the antimicrobial effectiveness of a new silver alginate wound dressing: a RCT.* Journal of Wound Care, 2010. 19(1): p. 20-26.
104. Michaels, J., et al., *A prospective randomised controlled trial and economic modelling of antimicrobial silver dressings versus non-adherent control dressings for venous leg ulcers: the VULCAN trial.* Health Technol Assess, 2009. 13(56): p. 1-114.
105. Leaper, D. and R. Drake, *Should one size fit all? An overview and critique of the VULCAN study on silver dressings.* International wound journal, 2011. 8(1): p. 1-4.
106. Gottrup, F. and J. Apelqvist, *The challenge of using randomized trials in wound healing.* British Journal of Surgery: Incorporating European Journal of Surgery and Swiss Surgery, 2010. 97(3): p. 303-304.
107. White, R., et al., *Randomized controlled trial and cost-effectiveness analysis of silver-donating antimicrobial dressings for venous leg ulcers (VULCAN trial)(Br J Surg 2009; 96: 1147–1156).* British Journal of Surgery: Incorporating European Journal of Surgery and Swiss Surgery, 2010. 97(3): p. 459-460.
108. Doyle, K., J. Miles, and P. Corporation, *Protocols and applications guide*. 1996: Promega Corporation.
109. CLSI, *M26-A: Methods for Determining Bactericidal Activity of Antimicrobial Agnets;Approved Guidline.* (Clinical & Laboratory Standards Institute: CLSI Guidelines), September 1999.
110. Cockerill, F.R., *Performance standards for antimicrobial susceptibility testing: twenty-first informational supplement*. 2011: Clinical and Laboratory Standards Institute (CLSI).
111. Jorgensen, J.H., *Methods for dilution antimicrobial susceptibility tests for bacteria that grow aerobically: approved standard: NCCLS document M7-A3*. 1993: Nccls.
112. Astashkina, A., B. Mann, and D.W. Grainger, *A critical evaluation of in vitro cell culture models for high-throughput drug screening and toxicity.* Pharmacology & therapeutics, 2012. 134(1): p. 82-106.
113. Grainger, D.W., *Cell-based drug testing; this world is not flat.* Advanced drug delivery reviews, 2014. 69: p. vii.
114. Archer, G.L., *Staphylococcus aureus: a well-armed pathogen.* Reviews of Infectious Diseases, 1998. 26(5): p. 1179-1181.
115. Lin, J.J.-C. and J.R. Feramisco, *Disruption of the in vivo distribution of the intermediate filaments in fibroblasts through the microinjection of a specific monoclonal antibody.* Cell, 1981. 24(1): p. 185-193.
116. Sanger, J.W., et al., *Reversible translocation of cytoplasmic actin into the nucleus caused by dimethyl sulfoxide.* Proceedings of the National Academy of Sciences, 1980. 77(9): p. 5268-5272.

117. Welch, W.J. and J.P. Suhan, *Morphological study of the mammalian stress response: characterization of changes in cytoplasmic organelles, cytoskeleton, and nucleoli, and appearance of intranuclear actin filaments in rat fibroblasts after heat-shock treatment.* The Journal of cell biology, 1985. 101(4): p. 1198-1211.
118. Burd, A. and E. Chan, *Keratinocyte-keloid interaction.* Plastic and reconstructive surgery, 2002. 110(1): p. 197-202.
119. Navarro, F., et al., *Sprayed keratinocyte suspensions accelerate epidermal coverage in a porcine microwound model.* The Journal of burn care & rehabilitation, 2000. 21(6): p. 513-518.
120. Wood, F. and M. Stoner, *Implication of basement membrane development on the underlying scar in partial-thickness burn injury.* Burns, 1996. 22(6): p. 459-462.
121. Stoner, M.L. and F.M. Wood, *The treatment of hypopigmented lesions with cultured epithelial autograft.* The Journal of burn care & rehabilitation, 2000. 21(1): p. 50-54.
122. Lineaweaver, W., et al., *Cellular and bacterial toxicities of topical antimicrobials.* Plastic and reconstructive surgery, 1985. 75(3): p. 394-396.
123. Leaper, D.J., *Eusol.* BMJ: British Medical Journal, 1992. 304(6832): p. 930.
124. Patton, M.A., *Eusol: the continuing controversy.* BMJ: British Medical Journal, 1992. 304(6842): p. 1636.
125. Burton, J., *For and against Eusol.* BMJ: British Medical Journal, 1992. 304(6839): p. 1442.
126. Beevers, M., *For and against Eusol.* BMJ: British Medical Journal, 1992. 304(6839): p. 1443.
127. Tingle, J., *Eusol and the law.* Nursing times, 1990. 86(38): p. 70-72.
128. Taks, J., *Eusol management of burns.* Tropical doctor, 2000. 30(1): p. 54-54.
129. Guggenbichler, J.-P., et al., *A new technology of microdispersed silver in polyurethane induces antimicrobial activity in central venous catheters.* Infection, 1999. 27(1): p. S16-S23.
130. Yorganci, K., et al., *Activity of antibacterial impregnated central venous catheters against Klebsiella pneumoniae.* Intensive care medicine, 2002. 28(4): p. 438-442.
131. Newton, T., J.M. Still, and E. Law, *A comparison of the effect of early insertion of standard latex and silver-impregnated latex foley catheters on urinary tract infections in burn patients.* Infection Control & Hospital Epidemiology, 2002. 23(4): p. 217-218.
132. Tredget, E.E., et al., *A matched-pair, randomized study evaluating the efficacy and safety of Acticoat silver-coated dressing for the treatment of burn wounds.* Journal of Burn Care & Rehabilitation, 1998. 19(6): p. 531-537.

133. Castellano, J.J., et al., *Comparative evaluation of silver-containing antimicrobial dressings and drugs.* International wound journal, 2007. 4(2): p. 114-122.
134. Gibbs, S., *In vitro irritation models and immune reactions.* Skin pharmacology and physiology, 2009. 22(2): p. 103-113.
135. McNamee, P., et al., *A tiered approach to the use of alternatives to animal testing for the safety assessment of cosmetics: eye irritation.* Regulatory toxicology and pharmacology, 2009. 54(2): p. 197-209.

Chapter 07: Bio-evaluation of Chitosan/Ag-doped Mesoporous Bioactive Glass Composite Films (CS/ Ag-MBG) for Wound Treatment

Table of contents

List of figures

List of tables

Abbreviations

AFM: Atomic force microscopy
Ag: Silver
Ag-MBG: Ag-doped MBG
$AgNO_3$: Silver nitrate
AgNPs: Silver nanoparticles
ATCC: American Type Culture Collection
bFGF: Basic fibroblast growth factor
BGs: silicate-based bioactive glasses
C_2H_5OH: ethanol
$Ca(NO_3)_2 \cdot 4H_2O$: Calcium nitrate tetrahydrate
CMC: Critical micelle concentration
Col. I: Collagen type I
CS/ non-ord. Ag-MBG composite: CS/non-ordered Ag-doped MBG composite film
CS/ non-ord. und. MBG composite: CS/non-ordered undoped MBG composite film
CS/ ord. Ag-*MBG composite:* CS/ordered Ag-doped MBG composite film
CS/ ord. und. MBG composite: CS/ordered undoped MBG composite film
CS: Chitosan
CTB: CellTiter-Blue® assay
DSMZ: German collection of microorganisms and cell cultures
E. coli: Escherichia coli
ECM: Extracellular matrix
EDS: Energy-dispersive X-ray spectroscopy
EGF: Epidermal growth factor
EISA: Evaporation-induced self-assembly process
EMA: European medicines agency
ESR07: Early Stage Researcher, Seray Schmitz
FBS: Foetal Bovine Serum
HCA: Hydroxy-carbonate apatite
HCL: Hydrochloric acid
HDF: Human Dermal Fibroblasts
HNO_3: Nitric acid
HRTEM: High resolution transmission electron microscopy
ICP-OES: Inductively coupled plasma - Optical emission spectrometry
L929: Murine fibroblast cell line
MBGs: Mesoporous bioactive glasses
MRSA: Methicillin resistant Staphylococcus aureus
NHEK: Normal human epidermal keratinocytes
Non-ord. Ag-MBG: Non-ordered Ag-doped MBG
Non-ord. und. MBG: Non-ordered undoped MBG

Ord. Ag-MBG: Ordered Ag-doped MBG
Ord. und. MBG: Ordered undoped MBG
P. aeruginosa: Pseudomonas aeruginosa
PCL: Polycaprolactone
Ppm: Parts per million (mg/L)
ROS: Reactive oxygen species
S. aureus: Staphylococcus aureus
S. epidermidis: Staphylococcus epidermidis
SBF: Simulated body fluid
SEM: Scanning electron microscopy
StDev: Standard deviation
TEOS: Tetraethyl orthosilicate
TEP: Triethyl phosphate
TGF-β: Transforming growth factor-beta
Tris: Tris(hydroxymethyl)-aminomethane
Und.: Undoped
VCAM: Vascular cell adhesion molecules
VEGF: Vascular endothelial growth factor
VRE: Vancomycin resistant Enterococci
XRD: X-ray diffraction
XRF: X-ray fluorescence
α-SMA: Alpha-smooth muscle actin

Chapter 07: Bio-evaluation of Chitosan/Ag-doped Mesoporous Bioactive Glass Composite Films (CS/ Ag-MBG) for Wound Treatment

Abstract

Bioactive glasses (BGs) have been extensively investigated for mineralized tissue regeneration, however, recently their application in soft tissue repair have demonstrated great potential. Infected wounds represent a great challenge in public health. With an increasing need to develop novel antimicrobial strategies for treating infected wounds, this study aimed at the bio-evaluation of developed chitosan / Ag-doped mesoporous bioactive glass composite films (CS/ Ag-MBG). The cytotoxicity and antibacterial activities of the novel biomaterials are key issues that should be addressed prior to clinical applications. Two types of Ag-doped MBGs (*Ag-MBGs*) were prepared: non-ordered and ordered Ag-MBGs. To achieve an effective antibacterial, drug-free MBG-based biomaterial the surfactant-assisted sol-gel method was applied hypothesizing that this method would provide ordered Ag-MBG particles with a higher surface area, thus a higher bioactivity and suitable Ag-ion release. Results presented were obtained with CS/ Ag-MBG composite films prepared by mixing of 0.3% (w/v) of 5 wt.% Ag-MBG particles with 0.7% (w/v) CS solution. The mixture was vigorously vortexed to achieve an optimal dispersion and was cast into glass petri dishes to form films. The different types of CS/MBG composite films manufactured, were named as "*CS/ non-ord. und. MBG", "CS/ non-ord. Ag-MBG", "CS/ ord. und. MBG"*, and *"CS/ ord. Ag-MBG composites".* These samples were characterized for their surface area & pore size (BET), amorphous nature (XRD), surface topography (SEM), ultra-structure (TEM), surface elemental composition (EDS), particle size distribution (PSD), Ag-incorporation (XRF), Ag-release (ICP-OES), and swelling properties (water uptake). The cytotoxicity analysis was performed by testing extracts of MBGs and CS/MBGs composite films by 1) indirect contact (shaking/ non-shaking conditions), as well as by 2) direct contact with L929 fibroblasts and Normal Human Epidermal Keratinocytes (NHEK). CellTiter-Blue® (CTB) assay and Live/Dead imaging were used to investigate cell viability of cells after 24 hours of direct contact with composites. Bright field microscopy further supplemented cytotoxicity analysis by indicating the changes in cell morphology. The antibacterial activity of composites was determined through disc-diffusion assay by measuring the zone of inhibition (ZOI) against clinically relevant bacteria namely *Staphylococcus aureus* (ATCC 29213), *Staphylococcus epidermidis* (ATCC 12228), *Escherichia coli* (ATCC 25922), and *Pseudomonas aeruginosa* (ATCC 27853).

The *CS/ non-ord. und. MBG composite* demonstrated less regular distributed MBG particles that did not distribute on the film surface uniformly (as indicated by SEM). This

might be due to the big particle size resulting in reduced tendency of MBGs to effectively disperse within the chitosan and distributed on or close to the composite film surface. On the other hand, *CS/ ord. Ag-MBG composite* due to the smaller particle size, resulted in more evenly distributed MBG particles within the chitosan matrix and over the film surface demonstrating a uniformity in films appearance.

Both Ag-doped composites showed a decrease in CTB-derived L929 viability with respect to untreated control (as indicated by direct contact test) of approx. 60% for the *CS/ non-ord. Ag-MBG* and approx. 23% for the *CS/ ord. Ag-MBG composites*. However, in case of NHEK, the cytotoxic effects were reduced to approx. <20% for both Ag-doped composites as compared to their undoped composites counterparts, suggesting that the effect might be related with the Ag release (0.9 ppm from *CS/ ord. Ag-.MBG composite*) affecting the L929 cells more than it did to NHEK. The different cell types are not equally sensitive to Ag^+ toxicity such as IC50 of Ag^+ for NHEK (11.8µg/mL) was approx. 5 times higher than it was for L929 (2.3µg/mL). However, the lowered L929 cell viability by *CS/ non-ord. Ag-MBG composite* could not be explained based on Ag release (0.0ppm) performed in SBF (Simulated body fluid), and there might be other factors associated with L929 cytotoxicity.

The *non-ord. Ag-MBG* was able to incorporate approx. double the amount of Ag (120ppm) with respect to *ord. Ag-MBGs* (66ppm). Both, of these Ag-doped MBGs i.e. non-ordered and ordered ones, exhibited Ag release of 0.38ppm and 0.35ppm, respectively after 24 hours in PBS. However, in case of Ag-doped composite films, the Ag release was evidently reduced in *CS/ non-ord. Ag-MBG composite,* while in case of *CS/ ord. Ag-MBG composite* it was 0.93ppm in SBF after 3 days. This effect might be related with the differences in surface areas of *non-ord. Ag-MBGs* ($307 m^2/g$) and *ord. Ag-MBGs*, ($528 m^2/g$): smaller surface area could lead to a lower ion release. This effect might also be related with the pore size and pore pattern of *ord. Ag-MBGs,* that had comparatively a larger pore size (4.0 to 5.3nm) and higher surface area ($528 m^2/g$), indicating the possibility of an arrangement where all pore sides were exposed. On the other hand, *non-ord. Ag-MBGs* had comparatively a smaller pore size (2.8 to 3.4nm) and lower surface area ($307 m^2/g$), that might be associated with an overlapped and irregular pores structure. Another assumption could be the chemical interaction between Ag^+ ions and components of composite films, subsequently affecting the Ag^+ release from *CS/ non-ord. Ag-MBG composite*. Or most probably, the zero release might be related to SBF interaction: any HA deposition on the surface by SBF immersion might be blocking Ag release.

Both Ag-doped composites demonstrated antibacterial activity against tested bacteria, and ZOI were found similar between *CS/ non-ord. Ag-MBG* and *CS/ ord. Ag-MBG composites.* Thus, due to antibacterial properties, cytocompatibility, and water retaining ability, in general, Ag-doped composites especially *CS/ ord. Ag-MBG composite* might

have a potential for wound healing. However, the materials should be investigated for their hydrophilicity and surface roughness to better understand the mechanism of cytotoxicity and antibacterial activity. Moreover, ion release might depend on the type of dissolution media and thus Ag^{+} release should be investigated in cell culture and microbial growth media, or at least simply in PBS.

Keywords: Mesoporous bioactive glass (MBG), Ag-doping, Chitosan/ mesoporous bioactive glass composites, cytotoxicity, antibacterial activity

7.1 Introduction

7.1.1 Bioglass in wound healing

Since their first development by Dr. Larry Hench in 1969, silicate-based bioactive glasses (BGs) have been considered highly osteo-conductive and -inductive, and thus have been widely studied and used in the repair of mineralized tissues (bones and teeth) [1, 2]. Being a bioactive material [3], BGs have shown to form hydroxy-carbonate apatite (HCA) on the surface in the presence of biological fluid causing their bonding to mineralized tissues [1, 4]. This HCA formation might attribute its interaction with surrounding soft collagenous tissue (reviewed [5]), demonstrating the potential BG applications in wound healing. However, controllably released ions might have an impact in dynamically changing wound environment and thus, mediate cellular functions and soft tissue mechanisms (reviewed [6, 7]). This has led to explore the role of BGs in soft tissue repair and wound healing. Though, little is known about BGs-induced specific mechanisms in complex cascade of wound repair. As a result of glass dissolution in biological fluids, the subsequent ion release might be related with the haemostasis (e.g. Ca^{2+}) [8, 9], antimicrobial effect (e.g. Ag^{+} [10-21]) against *Escherichia coli*, *Staphylococcus aureus* and *Pseudomonas aeruginosa* (that are highly associated with wound infections and biofilm formation [22, 23], anti-inflammatory effect (e.g. Zn^{2+} [23]), and angiogenesis (e.g. B^{3+} [24, 25], Cu^{2+} [26]). BGs have also been reported to induce the expression of certain genes that encode proteins and are involved in tissue healing e.g. vascular endothelial growth factor (VEGF), basic fibroblast growth factor (bFGF), and vascular cell adhesion molecules (VCAM) [6]. The major ionic component released from BGs is Si^{4+}, that has been shown to stimulate collagen production [27] and neovascularization [28-30]. Beside collagen role as an ECM template in bone regeneration, it has a great importance in skin repair and thus its modulation might be important to prevent scar tissue formation (fibrosis) [31]. Moreover, considering the involvement of transforming growth factor-beta (TGF-β) in wound healing (reviewed at [31]), sol-gel derived BG has been reported to down regulate TGF-β signalling and its downstream molecule Smad2 in fibroblasts, suggesting its role in modulating the TGF-β pathway [32] (Figure 7.1). Additionally, the same BGs have shown to regulate the expressions of various collagen types, fibronectin and alpha-smooth muscle actin (α-SMA), hence inhibiting trans-differentiation of fibroblasts to myofibroblast (Figure 7.1). Interestingly, collagen I and α-SMA expressions in fibroblasts were initially up-regulated and then down-regulated suggesting the role of ionically-mediated gene expression in sequential wound healing stages [33]. The HCA deposition on BG has been studied for its role to promote wound healing as well [33-37], however, the direct correlation among HCA deposition, BG degradation and the subsequent rate of wound healing still has to be verified. BG dissolution of its CaO releasing Ca^{2+} might induce blood clot formation, epidermal cell migration, fibroblast proliferation, and collagen

lattice contraction [9, 33, 38]. Calcium and silver-doped mesoporous silica spheres were reported to induce enhanced blood coagulation and antimicrobial activities, respectively [8].

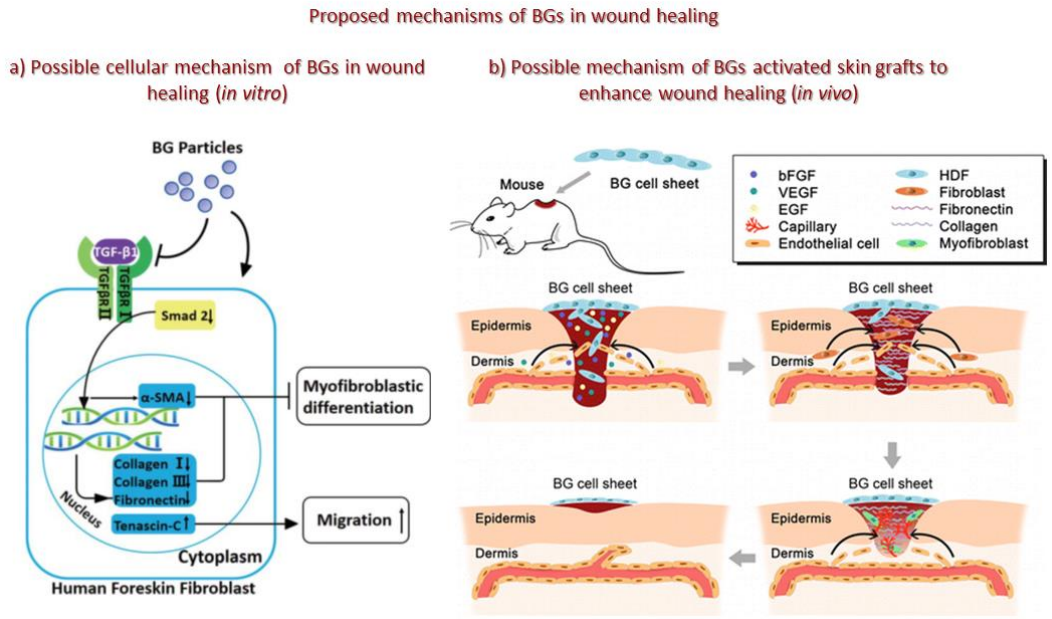

Figure 7.1 Proposed mechanisms of BGs in wound healing. a) Possible cellular mechanism of BGs in wound healing (in vitro). The image has been used with copyright permission [32]. b) Possible mechanism of BGs activated skin grafts to enhance wound healing (in vivo). Reprinted with permission from (Yu H, Peng J, Xu Y, Chang J, Li H. Bioglass activated skin tissue engineering constructs for wound healing. ACS applied materials & interfaces. 2015 Dec 31;8(1):703-15). Copyright (2019) American Chemical Society [33].

Implanted biomaterials might induce an inflammatory response; however a controllable inflammatory response is inevitable and can be accepted [25]. Nevertheless, the biomaterials can be tuned to regulate the inflammation and immune response [39]. Macrophages secrete various chemokines, cytokines, and proteases recruiting endothelial cells, and migrating fibroblasts & keratinocytes to wound site [40, 41] subsequently stimulating angiogenesis, collagen synthesis and wound healing. BG ionic products were reported to activate macrophages towards M2 phenotype stimulating them to express more anti-inflammatory response [42]. BGs were also reported for inducing the secretion of several cytokines by macrophages [43, 44]. Thus, BGs do not only affect the macrophage polarization but are also involved in paracrine action between macrophages and wound repairing cells (e.g. fibroblasts, keratinocytes, and endothelial cells), thus enhancing wound healing.

A major disadvantage of BGs is associated with their high solubility and thus, most of the released ions might be moved away before they can take effect. The surface reactions and, therefore, biodegradation can be obtained by rational design of BG composition tailoring them for specific clinical applications [45].

7.1.2 Chitosan in wound healing

Chitosan (CS), is chemically processed chitin. CS is a linear polycationic polysaccharide consisting of β-(1→4)-linked 2-amino-2-deoxy-d-glucose (D-glucosamine) and 2-acetamido-2-deoxy-d-glucose (N-acetyl-D-glucosamine) units. Due to its adhesive nature, antimicrobial properties, biocompatibility, water absorption, and oxygen permeability, CS is considered a favourable candidate for the treatment of wounds [46]. Chitosan serves as a non-proteinaceous matrix for 3D tissue development providing a histoarchitectural tissue organization. The gradual depolymerization of chitosan at wound site releases N-acetyl-β-D-glucosamine, that can promote fibroblast proliferation, collagen deposition, and natural hyaluronic acid synthesis for faster wound healing preventing scar formation [47]. Chitosan can be easily processed into many forms e.g. hydrogels [48-50], nanofibres [46, 51, 52], nanoparticles [53, 54], and membranes [55-60] etc. Thomas et al. demonstrated great antibacterial activity of developed chitosan/AgNPs films, suggesting a potential application as wound dressings [53, 54]. However, limited information and a few review articles, have reported chitosan and chitosan composite based wound dressings [50, 61-64].

7.1.3 Silver as an antibacterial agent

Ag^+ ions are highly reactive affecting multiple sites in bacterial cells, i.e. binding to cell membranes resulting in cell leakage. When transported inside cells, Ag^+ ions can bind proteins disturbing cell energy production, enzymatic function as well as cell replication [65, 66]. Ag^+ ions have been found active against a wide range of bacteria [67-72] including antibiotic-resistant strains of *methicillin resistant Staphylococcus aureus* (MRSA) and *vancomycin resistant Enterococci* (VRE) [73]. Some studies have shown that Ag^+ ions might even reduce bacterial adhesion, disrupt the biofilm matrix [74], kill the bacteria, and enhance the susceptibility of bacteria against antibiotics as well. [75-77]. Besides controlling the bioburden, some laboratory work has suggested the beneficial role of silver in wound healing when applied on closed surgical wounds [78]. Moreover, some silver-containing wound dressings have also been shown to have anti-inflammatory and neo-vascularization effects [79-82].

7.1.4 Chitosan/bioglass composites

CS/BG composites have been shown to protect against reactive oxygen species (ROS) by enhancing the activity of superoxide dismutase, catalase, and glutathione peroxidase at the graft-implanted site in rats, suggesting the potential of CS/BG composites as anti-oxidant materials for tissue healing [83]. It has also been shown previously that BG addition to CS enhances its protein adsorption for better cell adhesion [84, 85]. Moreover, CS/BG composites were demonstrated to have a higher cell viability as compared to the BG alone due to an accelerated calcium phosphate deposition. CS addition to BG enhances the dissolution rate of glassy network improving the overall

chemical reactivity of CS/BG composite [84-86]. On the other hand, BG decreases the swelling ratio of CS improving its structural stability and thus, the cell migration capabilities [84, 85, 87].

As mentioned, the morphological, chemical, and physical properties of BGs can be tuned by the synthesis parameters. BGs prepared by sol-gel method have higher porosity, better apatite forming ability, and larger surface area in comparison to melt-quenched BG that have an advantage of better mechanical properties [88]. The sol-gel method uses low temperature treatments that results BG with highly-porous structure. To obtain a mesoporous structure (2-50nm), surfactants at its critical micelle concentration (CMC) can play a key role to form micelles as a template for directing pore formation in BG [89, 90]. Thus, a composition of sol-gel-derived and surfactant (P 123)-assisted mesoporous bioactive glasses (MBGs) were synthesized in this study to provide an ordered structure (ord. MBGs) with high surface area and thus, an increased bioactivity and doped-ion releasing. To introduce antibacterial properties, BGs were doped with Ag during sol-gel technique to synthesize Ag-MBGs. Eventually, Ag-MBG were dispersed in chitosan matrix to make composite films as a product for wounds treatment.

7.2 Materials and methods

7.2.1 Materials' synthesis

MBGs preparation

"Ordered" 5wt.% Ag-doped and undoped MBGs (named as: *ord. und. MBG* and *ord. Ag-MBG*), were synthesized by surfactant (Pluronic P 123)-assisted sol-gel method. The "non-ordered" 5wt.% Ag-doped and undoped mesoporous bioactive glasses (named as: *non-ord. und. MBG* and *non-ord. Ag-MBG*), were synthesized by sol-gel method (see the Appendix C for synthesis details).

CS/MBG composite films preparation

0.7% (w/v) chitosan (medium M_w:190,000–310,000Da, 75–85% deacetylated from Sigma-Aldrich) was dissolved in 2 vol.% aq. acetic acid (Sigma-Aldrich) under heating at 50°C overnight. The 0.3% (w/v) MBG was added into the chitosan solution, stirred to disperse MBG, ultra-sonicated, casted to petri dish, and left for drying. The pH measured in SBF was 7.62-7.74. The detailed method to prepare composite films is mentioned below:

CS control film

- 0.3g chitosan was dissolved in 30mL 2 vol% aq. acetic acid at 50ºC and stirred at 250rpm overnight.
- After complete dissolving, solution was poured into glass petri dish.
- Petri dish was left for evaporation under fume hood for ~72 hours.

CS/und. MBG films

- 0.21g chitosan was dissolved in 30mL 2 vol% aq. acetic acid at 50ºC and stirred at 250rpm overnight.
- 0.09g MBGs were added to chitosan solution.
- For und. MBGs an optimum dispersion was achieved at 38ºC and a stirring speed of 480 rpm for 3 hours.
- Ultrasonicated for 2 hours to disperse the MBG particles.
- Right before pouring the CS/MBG suspensions into petri dishes, the mixture was stirred for 5min and poured.
- Left for evaporation for ~72 hours.

CS/Ag-MBG films

- 0.21g chitosan was dissolved in 30mL 2 vol% aq. acetic acid at 50ºC and 250rpm overnight.
- 0.09g Ag-MBGs were added to chitosan solution.
- For Ag-MBGs an optimum dispersion was achieved at RT and a stirring speed of 480rpm for 5 hours.
- Ultrasonicated for 1 hour to disperse the MBG particles.
- Right before pouring the CS/MBG suspensions into petri dishes, the mixture was stirred for 5 min and poured.
- Left for evaporation for ~72 hours.

The detailed synthesis of Ag-MBGs by sol-gel method was described in Appendix C and wt.% of inorganic material in chitosan with respect to the final dry weight of the composite could be find above under the same heading.

7.2.2 Materials' characterization

Ion release analysis

20mg powder samples of *non-ord. Ag-MBG* and *ord. Ag-MBG each*, were immersed in 20mL PBS at 37°C under 100rpm shaking conditions, for 24 and 72 hours (as two sets of independent experiments) and the Ag release was tested as mentioned above.

0.5cm x 0.5cm film of each sample (samples weighed between 11-16mg) was immersed in 25mL SBF at 37°C under 100rpm shaking conditions, for 3 and 7 days (as two sets of independent experiments). Ions released (Si, Ca, P and Ag) in liquid (aliquots of the filtered and un-diluted solutions) were recorded by ICP through taking three measurements per sample. Ca, P and Si analysis were run on the Agilent 5110 ICP-OES machine, while Ag containing samples were tested for Ag release using Varian 720-ES ICP-OES machine.

The obtained values were blank corrected. Table 7.2 showed the values as the average and the standard error of mean (SEM) of three measurements per sample.

SEM/EDS analysis

SEM was performed using JEOL JSM6490-LV SEM (fitted with an Oxford Instruments INCA EDA). It was performed in low vacuum mode without any conductive coating being applied on the films. The working distance and the accelerating voltage for this examination were 10 mm and 20kV, respectively. The film samples were analyzed using Backscattered Electron Imaging, where the brightness of a given feature was proportional to its mean atomic number such that the organic membrane appeared dark

grey and the MBG particles appeared light grey. Microanalysis results were shown as elemental spectra. The obtained spectra from EDS analysis were normalized. This was necessary to compare peak intensities among spectra of different sample surfaces. Furthermore, it was important to compare always peak ratios with each other.

Particle size distributions (PSD) analysis

The particle size distributions of the MBGs were obtained using Malvern Mastersizer 3000 particle size analyzer. PSD results were described as D-values (D10 & D90) that were intercepts for 10% and 90% of the cumulative mass. D10 was the diameter at which 10% of the sample mass included particles with a diameter less than this value. Likewise, D90 was the diameter of the particle at which 90% of the sample mass was smaller than this size value.

7.2.3 Cytotoxicity evaluation

Cell source and maintenance

L929 cells (murine fibroblast cell line) were obtained from DSMZ (German Collection of Microorganisms and Cell Cultures) and maintained in cell culture media RPMI 1640 with stable glutamine (PAN Biotech), containing 10% foetal bovine serum (FBS; PAN Biotech) and 1% Pen/Strep (100U/mL penicillin and 100µg/mL streptomycin) under physiological culture conditions (37°C, 5% CO_2), and sub-cultured using 0.25% trypsin (Gibco).

Primary cells, normal human epidermal keratinocytes (NHEK) were obtained from PromoCell and maintained in keratinocyte growth media 2 (PromoCell) under the physiological culture conditions (37°C, 5% CO_2), and sub-cultured using DetachKit-Promocell HEPES BSS (2-[4-(2-hydroxyethyl)piperazine-1-yl] ethanesulfonic acid buffered saline solution); 0.04% Trypsin/0.03% EDTA (ethylenediaminetetraacetic acid); and TNS (trypsin neutralizing solution) containing 0.05% trypsin inhibitor from soybean/0.1% bovine serum albumin. according to standard subcultivation protocol [91].

Cytotoxicity of materials – Extracts, direct contact, and indirect contact test

A known aliquot of cell suspension (7 X 10^4 cells per well in case of L929 and 1.5 X 10^5 cells per well in case of NHEK) at early passage numbers (P4 to P6) was pipetted in 24 well cell culture plate (1.8cm^2 growth area, 15mm dia.). The plates were incubated at 37°C, 5% CO_2 for 24hours. The cell sub-confluency and morphology were verified before exposing the cells to test samples. Culture medium was removed and replaced with fresh medium before starting the test. The 6mm diameter disks were punched from the composite films and UV-sterilized for 30 min on both sides.

For test on extracts, 5mg powder of *non-ord. Ag-MBG* (Ag-doping concentrations: 1wt.%, 3wt.%, 5wt.%) were weighted and sterilized under UV light for 30 minutes. A volume of 5mL complete RPMI 1640 medium was added to each tube with MBG samples and agitated at 37ºC & 120rpm for 1 day and 3 days. After the incubation, the supernatant (extract) was recovered and tested with L929 in 96 well plate. To this aim, the extracts were added to each well (triplicates), as 3 different setups: direct extract, extract diluted as 1:2 vol.:vol. and extract diluted as 1:4 vol.:vol.

For indirect contact test, the composite film samples were exposed to L929 cells through 24 well Transwell inserts (PET membrane, 1µm pore size, 6.5mm diameter, Sarstedt.), placed into 24 well cell culture plate. This set-up was also run under shaking cell culture conditions to make the uniform distribution of leachables throughout the cell culture media, thus, avoiding its accumulation in the cell culture area right under the insert. The cell culture media volume at apical (250µL) and basal sides (800µL) of inserts was maintained at the same level outside and inside the Transwell inserts.

For direct contact test, the individual composite film samples were placed directly on the cell monolayer (L929 and NHEK) in the center of wells without making unnecessary movements of the specimens. Thus, the films of 6mm diameter covered ~1/3rd area of the well surface of 24-well cell culture plate.

The wells without any sample exposure served as TCPS control (Tissue Culture Treated Polystyrene), while the wells treated with lysis solution (9% Triton® X-100) served as Lysis control. Cells treated with ZDEC-PU and PE films served as positive and negative controls of cytotoxicity analysis, respectively. The well plate was then incubated at 37°C, 5% CO_2 for 24 hours. The next day, supernatant culture medium and specimens were carefully removed, and CellTiter-Blue® (CTB) assay (Promega) was performed for measuring the cell viability according to Promega standard protocol [92]. To this aim, 400µL CTB reagent (this vol. was enough to cover the surface of TC 24 well) was pipetted per well for 2 h at 37°C and 5% CO_2. The cell supernatant was transferred to black microtiter 96-well plates. The fluorescence was measured at excitation (Ex) of 560nm and emission (Em) of 590nm.

Microscopic analysis

Changes in morphological appearance and visualization of live and dead cells, were evaluated using bright field and fluorescent microscopy (Olympus IX51). Fluorescent staining was performed using Live/Dead imaging (Promokine) using calcein-AM and ethidium homodimer III (EthD-III) to see live (green-fluorescence for live cells by enzymatic conversion of non-fluorescent substrate, Ex/Em ~495nm/~515nm) and dead (red-fluorescence for dead cells upon binding to nucleic acid, Ex/Em ~530nm/~635nm) cells.

7.2.4 Antibacterial activity

S. aureus (ATCC 29213), S. epidermidis (ATCC 12228), E. coli (ATCC 25922), and *P. aeruginosa (ATCC 27853),* being most relevant bacteria in infected wounds, were used to evaluate antibacterial activity of composite films. The disc-diffusion method was performed for antimicrobial susceptibility testing according to EUCAST (European Committee on Antimicrobial Susceptibility Testing) guidelines [93]. Bacterial strains were revived and cultured on fresh Mueller-Hinton (MH) agar plate before testing. The well-isolated colonies were picked using sterile loop, suspended in normal saline to an even turbidity and adjusted to McFarland 0.5 [94], [95]. The inoculum was spread evenly over the entire surface of MH agar using a sterile cotton swab. Sterile film samples' discs (6mm) were applied (within 15min of bacterial inoculation). The plates were incubated at 37°C for 16-20hours (within 15min of disk application). The zone of inhibition (mm) was measured using a scale ruler by reading the MH plates from the back against a dark background and zone edges were read at the point of complete inhibition using a scale bar.

7.3 Results & Discussion

The physicochemical characterization of chitosan/Ag-doped mesoporous bioactive glass composite films (CS/ Ag-MBG) have been widely discussed in the PhD thesis by ESR07. The *und. MBGs* (wt.% of $76SiO_2$-$13CaO$-$11P_2O_5$) and *Ag-MBG* (wt.% $71SiO_2$-$13CaO$-$11P_2O_5$-$5Ag_2O$) were amorphous in nature. While *ord. Ag-MBG* also showed metallic Ag phase (as measured by X-ray powder diffraction or XRD) as compared to *non-ord. Ag-MBG*. Ag^+ reduction might be due to ethanol [96] used during surfactant-assisted sol-gel process to synthesize ordered MBGs and was not used in non-ordered MBGs synthesis.

In Chapter 07 CS/MBG composite films (with 6mm diameter, 0.07-0.13mm thickness) were tested for their cytotoxicity and antibacterial properties.

7.3.1 Cytotoxicity of MBGs

Cytotoxicity analysis – Test on MBGs' extracts with L929 fibroblasts

Preliminary antibacterial results (ZOI) showed a higher antibacterial activity for *non-ord. Ag-MBG* than for *ord. Ag-MBGs* (results not shown). For this reason, preliminary cytotoxicity evaluation was performed on *non-ord. Ag-MBG*. To this purpose, L929 fibroblasts were exposed to 1 day and 3 days extracts of *non-ord. Ag-MBG* (1mg/mL), and cell viability was analyzed by CTB assay. The CTB assay assesses the number of viable cells by measuring their ability to reduce resazurin into a highly fluorescent resorufin (cells' metabolic potential). Non-viable cells lose their metabolic ability and cannot reduce the indicator dye. Initially, Ag was incorporated into MBGs at various Ag concentrations of 1, 3, 5wt.%, and all the extracts from these powdered samples were further diluted by 1:2 and 1:4. The samples showed a cell viability between ~70 to 90%, at each Ag-doped concentration and at both 1 day & 3 days extraction time, suggesting that the dissolution products of Ag-MBGs were cytocompatible (Figure 7.2). Considering the high cell viability results even at the highest Ag-dopant concentration of 5wt.% Ag-MBG, the composite films were prepared using only this concentration.

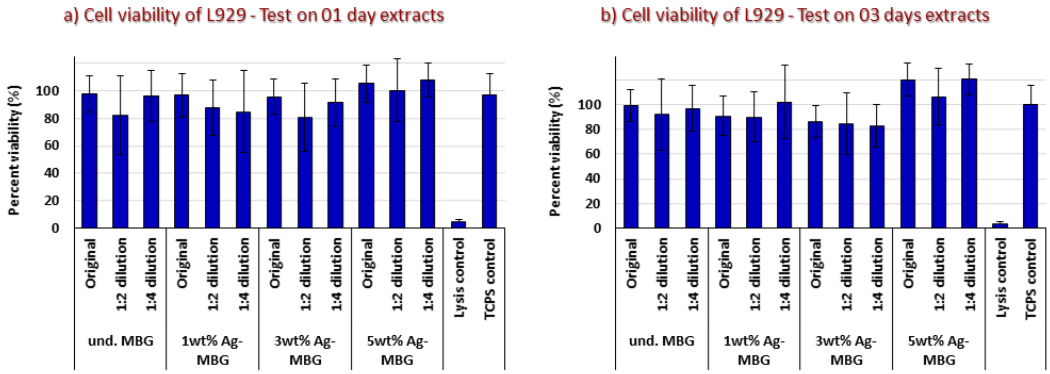

Figure 7.2 L929 cell viability of Ag-doped MBGs: test on extracts after a) 01 day and b) 03 days incubation.

XRF (X-ray fluorescence) results showed that Ag-MBGs prepared with 5 wt.% that were aimed for an ideal 5wt.% (or 150ppm) silver doping, only contained 120ppm (4wt.%) and 66ppm (2.2wt.%) silver in *non-ord.* and *ord. Ag-MBGs*, respectively. Comparatively less dopant incorporation was observed in *ord. Ag-MBG*, where surfactant-assisted sol-gel method was used to provide highly ordered mesoporosity. Probably, some of the Ag-dopants might have interacted with surfactants and have been removed along with surfactant during calcination. Despite the differences in dopant incorporation, the ICP results showed not much differences in Ag release in PBS over the period of 24 h, i.e. 0.38ppm and 0.35ppm from *non-ord.* and *ord. Ag-MBGs*, respectively, (Figure 7.3 and Table 7.1). The release from *non-ord. Ag-MBG* was 0.38ppm over a period of 72 h, while that from *ord. Ag-MBG* increased from 0.35ppm to 0.38ppm in 72 h (Table 7.1 and Figure 7.3).

Table 7.1 ICP analysis for the measurement of ion release by MBG powders (in PBS) using three samples (a, b, c) and their average values at 24 h and 72 h.

Time	**Ag Ion concentration (ppm)**					
	Non-ord. Ag-MBG			*Ord. Ag-MBG*		
	a	b	c	a	b	c
24 h	0.38	0.34	0.41	0.35	0.35	0.35
72 h	0.39	0.38	0.37	0.28	0.56	0.30
24 h Average ± standard error of mean	0.38±0.02			0.35±0.00		
72 h Average ± standard error of mean	0.38±0.01			0.38±0.09		

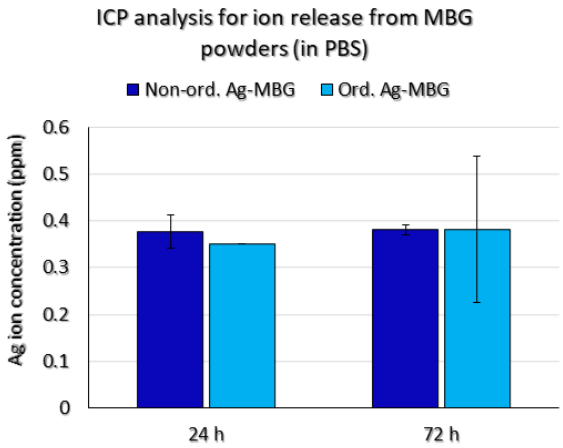

Figure 7.3 ICP analysis for ion release from MBG powders (in PBS) i.e. a) non-ord. Ag-MBG and b) ord. Ag-MBG.

7.3.2 Cytotoxicity of CS/MBG composites

Cytotoxicity analysis – Indirect contact test with L929 fibroblasts

The CS/MBG composite films were initially tested for cytotoxicity through indirect contact tests with L929 fibroblasts (Figure 7.4). L929 fibroblasts showed >80% cell viability in indirect contact with composite films in static conditions (Figure 7.4-a). Similarly, shaking of the culture medium during films' incubation with cells for 24 hours, was performed to enhance the ion dissolution and their distribution in the cell culture media; then cell viability was evaluated (Figure 7.4-b). Cells showed similar cell viability signal as under non-shaking condition, suggesting that released ions and dissolution products (if any) did not induce cytotoxicity.

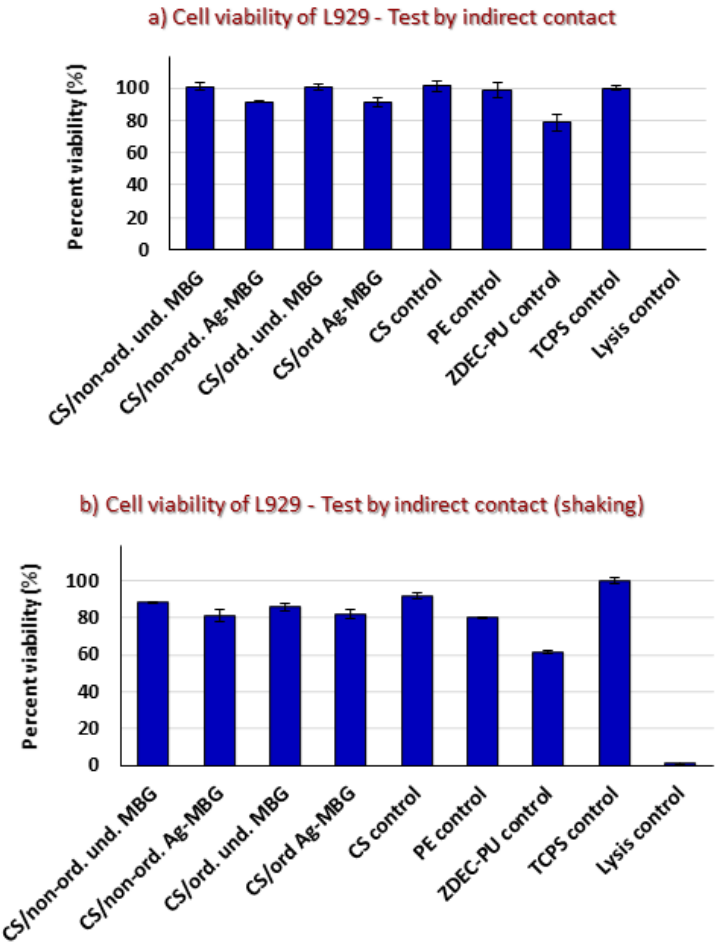

Figure 7.4 Cell viability of CS/MBG composites with L929 - Test by indirect contact under a) normal and b) shaking conditions for 24 hours.

Cytotoxicity analysis – Direct contact test with L929 fibroblasts

The CS/MBG composite films were intended for wound treatment, with material coming in direct contact with cells. Thus, the films were also evaluated by direct contact assays using L929 fibroblasts (Figure 7.5). The viability values were compared with control values and expressed as viability percentage (%). TCPS, being an ideal cell culture surface for adhering cells, and PE, being an "inert" biomaterial, served as negative controls for cytotoxicity evaluation. Respect to both negative controls for L929 viability, pristine chitosan (CS) was identified as highly cytocompatible. Furthermore, cytocompatibility was also observed for the undoped composites i.e. *CS/ non-ord. und. MBG* and *CS/ ord. und. MBG* composites. In contrast both Ag-doped composites showed a decrease in L929 viability of approx. 60% for the *CS/ non-ord. Ag-MBG* and 28% for the *CS/ ord. Ag-MBG composites*. Since showing >70% cell viability, *CS/ ord. Ag-MBG composite* was considered cytocompatible according to recommendations given by DIN EN ISO 10993-5

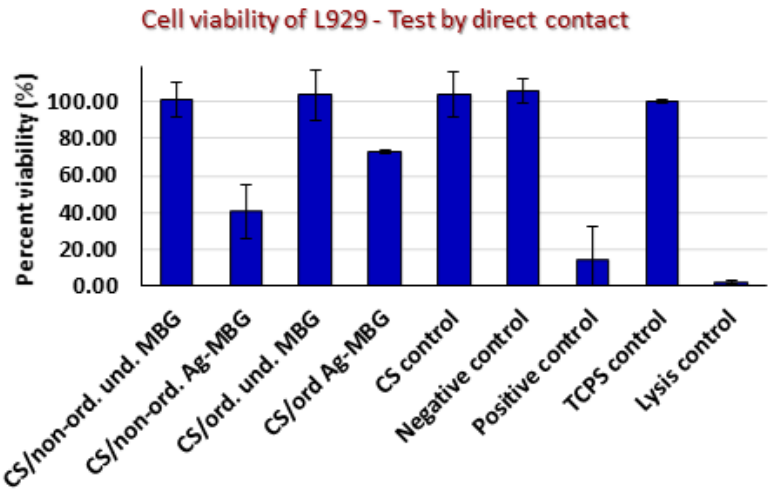

Figure 7.5 Cell viability of CS/MBG composites with L929 - Test by direct contact.

The decreased cell viability of *CS/ ord. Ag-MBG composite* as compared to undoped counterpart i.e. *CS/ ord. und. MBG composite* suggested an effect of its Ag release (0.9ppm Table 7.2) affecting the L929 cells.

It would also be worth noticing that between two Ag-doped composites, *CS/ non-ord. Ag-MBG composite* showed higher StDev in viability data as compared to *ord. Ag-composite*, that might be related with less uniform MBG particle distribution in non-ordered as compared to ordered composites.

Morphological analysis – Direct contact test with L929 fibroblasts

CTB assay measured the cell metabolic potential and thus estimated the number of viable cells. The bright field (BF) images were recorded to visualize the differences in cell morphology of L929 fibroblasts after 24 hours direct interaction with CS/MBG composite films. The L929 cells were imaged in the microscopic fields that were right under (U), around/near (N), and far from (F) the exposed specimen indicating the reactivity grades of cytotoxic effect of materials. Comparing both Ag-doped composites, *CS/ non-ord. Ag-MBG composite* (Figure 7.6 ii-a to -c) showed rounded and shrunken cells in all areas (U-, N-, & F-areas), while in case of *CS/ ord. Ag-MBG composite* (Figure 7.6 iv-a to -c) the effects on morphology were restricted to U- & N-areas. This observation in BF images highly correlated with the cell viability data of two Ag-doped composites (Figure 7.5). In case of undoped composites, the cells appeared to be affected at some extent as well, such as *CS/ non-ord. und. MBG composite* (Figure 7.6 i-a to -c) -exposed wells demonstrated an affected cell morphology in U-area, indicating that the Ag was not the only factor affecting cells but there were also other aspects associated with "non-ordered" composites. For example, coarse morphology, lower surface area, and uneven physicochemical properties associated with non-ordered composites made them comparatively less suitable for cells.

The cytotoxic effect observed with *CS/ non-ord. Ag-MBG composite* could be a combined consequence of Ag and other unknown factors, such as surface roughness, or MBG acting as protein scavenger, that enhanced protein (e.g. growth factors) adsorption, endorsing a nutrition-limiting conditions to cells that were very close to the materials surface. Additionally, the presence of rounded cells was worth noticing in all areas (U-, N-, and F-areas) of wells that were exposed to the cytotoxic material, i.e. ZDEC-PU (positive control) (Figure 7.6 vii-a to -c). The lysed cells were also visible in lysis control (Figure 7.6 xi).

On the other hand, the wells exposed with CS films (CS control) (Figure 7.6 v-a to -c), the cytocompatible material PE (a negative control) (Figure 7.6 vi-a to -c), and untreated (TCPS control) (Figure 7.6 viii) demonstrated well-spread cells with normal morphology.

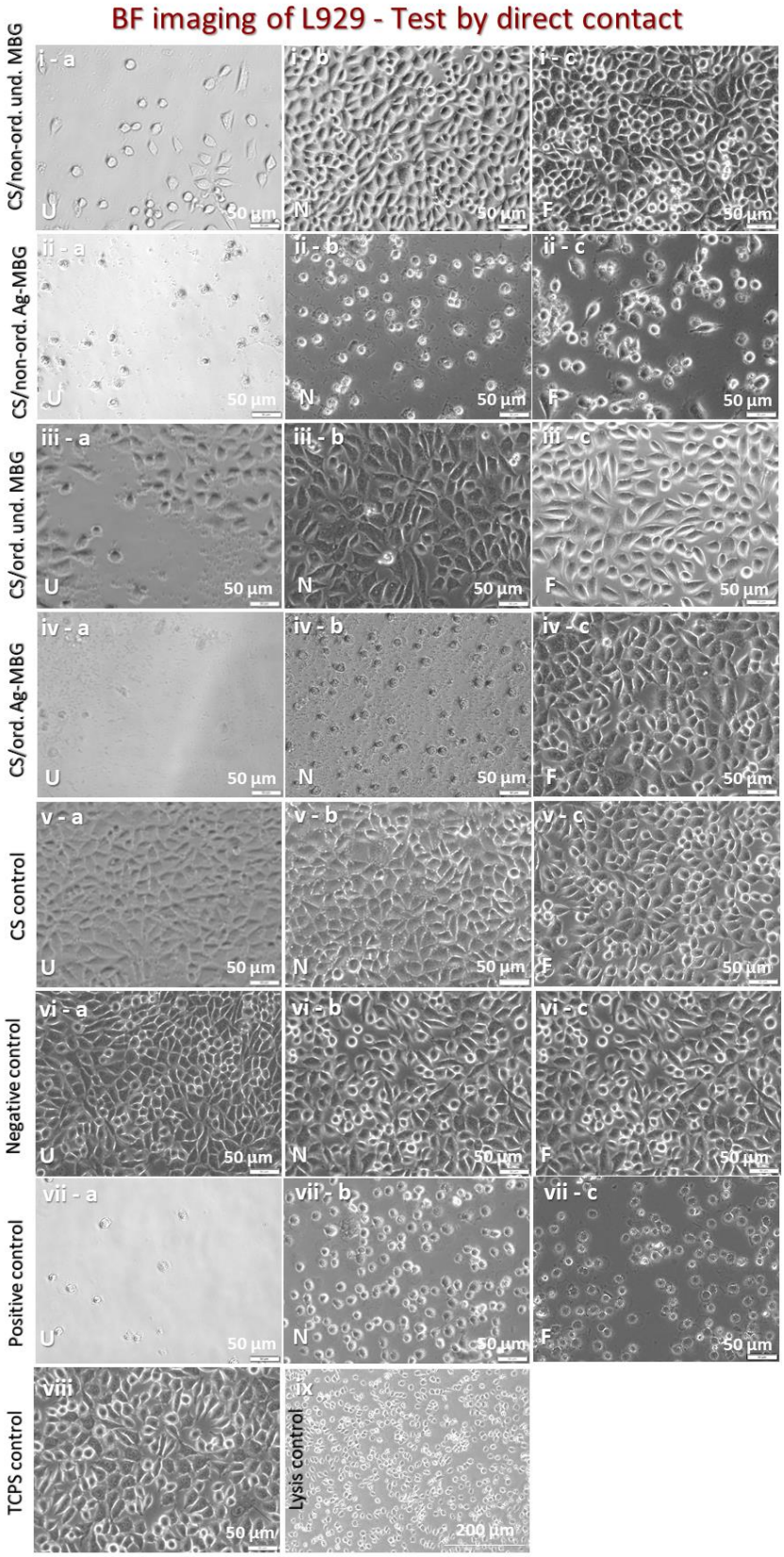

Figure 7.6 BF imaging of L929 after CS/MBG composites exposure - Test by direct contact. Images i-a to i-c displayed the microscopic fields in U-, N-, F-areas exposed by CS/ non-ord. und. MBG; images ii-a to

ii-d displayed the microscopic areas exposed by CS/ non-ord. Ag-MBG; images iii-a to iii-c displayed the microscopic areas exposed by CS/ ord. und. MBG; images iv-a to iv-d displayed the microscopic areas exposed by CS/ ord. Ag-MBG; images v-a to v-c displayed the microscopic areas exposed by CS control; images vi-a to v-c displayed the microscopic areas exposed by negative control, and images vii-a to vii-c displayed the microscopic areas exposed by positive control. Images viii, ix displayed TCPS and lysis controls, respectively.

Between Ag-doped composites, the *CS/ ord. Ag-MBG composites* demonstrated Ag release (0.9ppm in SBF for 3 and 7 days) as compared to its non-ordered counterpart, i.e. *CS/ non-ord. Ag-MBG composite* (Table 7.2) which Ag release was not significant at the analysed time intervals. Between Ag-MBGs, the *ord. Ag-MBG* demonstrated larger surface area of 528m^2/g (pore size of 4.0-5.3nm) (as measured by BET and shown in Table 7.3), than the surface area of 307m^2/g (pore size of 2.8-3.4nm) for *non-ord. Ag-MBG*. The relation between porosity and surface area might be associated with the differences in Ag release between ordered and non-ordered composites. Such as, *ord. Ag-MBGs* might have an ordered pattern of pores (as observed by HRTEM in Figure 7.7) where all pore sides were exposed thus resulting in higher surface area. While *non-ord. Ag-MBGs* might be owing overlapped and irregular structure of pores resulting in comparatively smaller surface area. This suggested that higher silver release by *CS/ ord. Ag-MBG composite* might be associated with its larger surface area due to an ordered porous structure. Besides, a material with larger surface area might have better cytocompatibility, as observed when comparing viability results of *CS/ ord. Ag-MBG composite* (~73%) and *CS/ non-ord. Ag-MBG composite* (~40%) (Figure 7.5). Considering the effect of Ag release on cell viability, *CS/ non-ord. Ag-MBG composite* had no Ag release (Table 7.2) but showed the highest cytotoxic effect (up to ~60%) with L929 (Figure 7.5). This cytotoxic effect cannot be explained in correlation with its Ag release profile (0.0ppm, Table 7.2), suggesting the involvement of other cytotoxic factors. Indeed, BF images (Figure 7.6 i-a) showed that the undoped counterpart of *CS/ non-ord. und. MBG composite* were without any Ag-doping but were still able to affect cells to a certain extent (rounded cells in U area). This effect can be explained by understanding the chemical interaction between Ag^+ ions and chitosan, subsequently affecting the Ag^+ release from *CS/ non-ord. Ag-composite*.

The majority of the Ag^+ ions might had formed chitosan-Ag^+ complexes [97] by interacting with the amino and hydroxyl groups on the chitosan surface, thus restricting Ag^+ mobility. The Ag^+ ions chelation by chitosan amine groups, might be the reason of no Ag^+ release by *CS/ non-ord. Ag-MBG composites*, considering the involvement of additional factors that still enabled these films to possess the antibacterial effect. Moreover, chelation is possible if any negatively charged ion or molecule links with protonated amino groups (positively charged) of chitosan. The assumed chitosan-Ag^+ complexes formation with positively charged Ag ions need further investigation to prove this hypothesis.

Additionally, if this interaction between chitosan-Ag^{+} is assumed true, then it should happen for both Ag-doped composites. Therefore, the inorganic phase structure, rather than its interaction with chitosan, might have more effect on Ag release. Additionally, the distribution Ag-MBGs in the chitosan matrix could be another reason of no release.

Moreover, PBS than SBF could be a better medium to test Ag release for comparison with cell tests, this would be done in future.

Table 7.2 ICP analysis for ion release from CS/MBG composite films (in SBF).

Composites	3 Days Ion concentration (ppm) (Average ± standard error of mean)				7 Days Ion concentration (ppm) (Average ± standard error of mean)			
	Si	Ca	P	Ag	Si	Ca	P	Ag
CS/ non-ord. und. MBG	42.8±0.4	5.8±0.2	2.9±0.1	N/A	29.0±0.4	4.9±0.3	2.3±0.1	N/A
CS/ ord. und. MBG	37.1±0.2	-30.3±0.2	-20.8±0.2	N/A	22.3±0.03	-34.2±0.3	-21.2±0.2	N/A
CS/ non-ord. Ag-MBG	18.9±0.2	4.9±0.2	2.7±0.1	0.0±0.0	24.6±0.2	3.2±0.2	2.2±0.3	0.0±0.0
CS/ ord. Ag-MBG	28.3±0.2	-20.1±0.4	-13.77±0.03	0.932±0.004	41.7±0.5	-30.0±0.2	-19.7±0.2	0.925±0.004

Positive values indicated an increase in ion concentration in SBF, while the negative values referred to a depletion of the ion concentration in the testing solution potentially due to the initiation of CaP phase formation.

Table 7.3 BET surface area and pore size of different MBGs.

MBGs	BET surface area (m^2/g)	Pore size (nm)
non-ord. und. MBG	246.7	2.80
non-ord. Ag-MBG	307.8	3.14
ord. und. MBG	411.9	4.72
ord. Ag-MBG	528.6	5.24

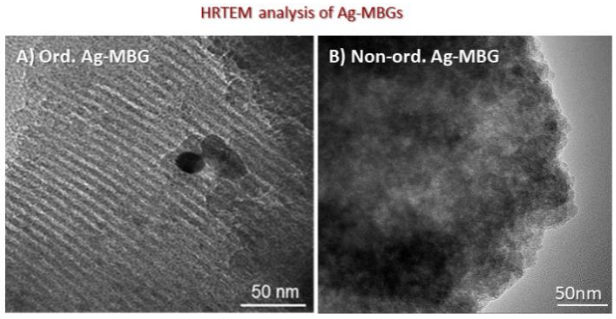

Figure 7.7 HRTEM image of A) ord. Ag-MBG, demonstrating a highly regular channeled structure as compared to B) non-ord. Ag-MBG.

Moreover, the non-uniform distribution of *non-ord. Ag-MBG* particles on chitosan film surfaces might result in variation of local Ag^+ concentration along the thickness of the film and thus might cause the differences in local Ag^+ diffusivity. The CS/MBGs composite films were surface scanned and elemental intensities were detected by EDS (Figure 7.8). CS control films demonstrated typical carbon and oxygen peaks. As compared to other composite films, *CS/ non-ord. und. composites* demonstrated relatively higher carbon content (carbon peaks) coming from the uncovered surface of CS. The *CS/ non-ord. und. MBG composite*s demonstrated agglomerated MBG particles that did not cover the film surface uniformly (as also indicated by SEM in Figure 7.9 i). This might be due to wide particle size distribution (PSD) (Table 7.4) resulting in reduced tendency of MBGs to effectively disperse within the chitosan, and thus, increasing the chances of agglomeration. On the other hand, *CS/ ord. Ag-MBG composite* due to the narrowest PSD (Table 7.4) resulted in evenly distributed MBG particles as a compact film surface (Figure 7.9 iv) demonstrating a uniformity in films appearance (Figure 7.10 iv). These findings were found consistent with EDS of *CS/ ord. Ag-MBG composite* that detected the elements from chitosan e.g. carbon in lower intensity as compared to *CS/ non-ord. und. MBG composite* (Figure 7.8 i & iv). Comparison of peak intensity ratio is a better approach, than intensity of peaks alone.

About both Ag-doped composites, the EDS results did not explain the significant difference between *CS/ non-ord. Ag- MBG* and *CS/ ord. Ag- MBG composites* (similar peaks for both) (Figure 7.8 ii & iv) SEM results indicated that "ordered" composites had more evenly distributed MBG particles with compact homogeneous appearance with respect to the "non-ordered" composites (Figure 7.9 iv); these results were in agreement with PSD data (Table 7.4).

EDS analysis

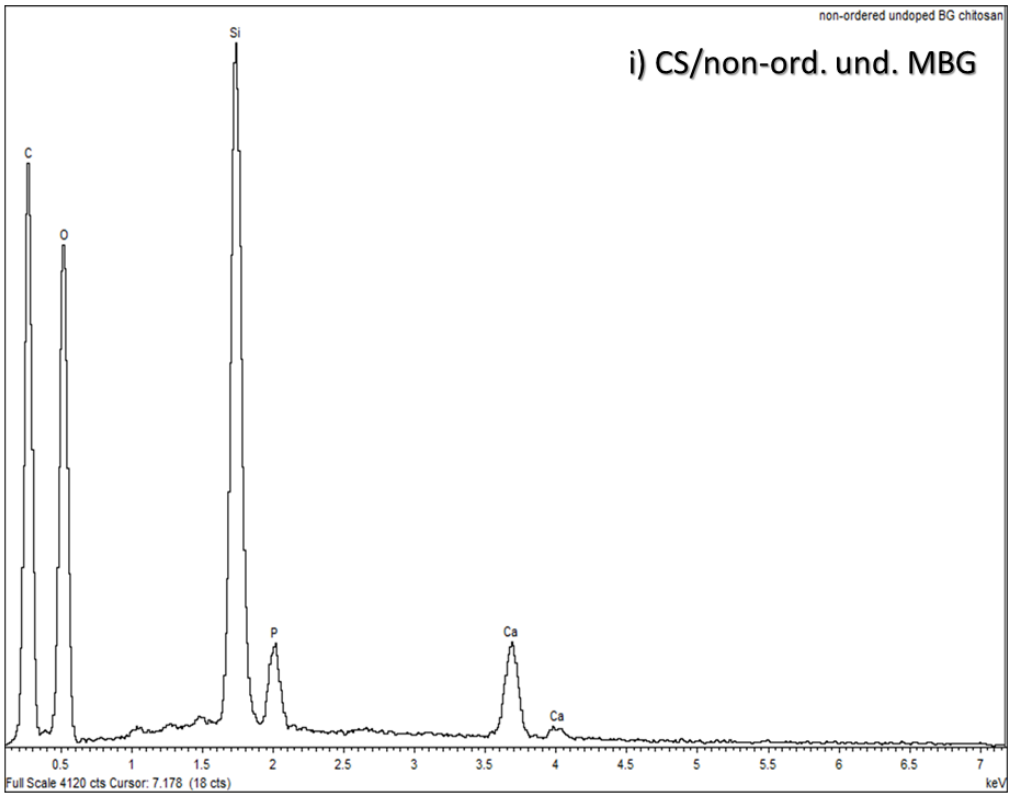

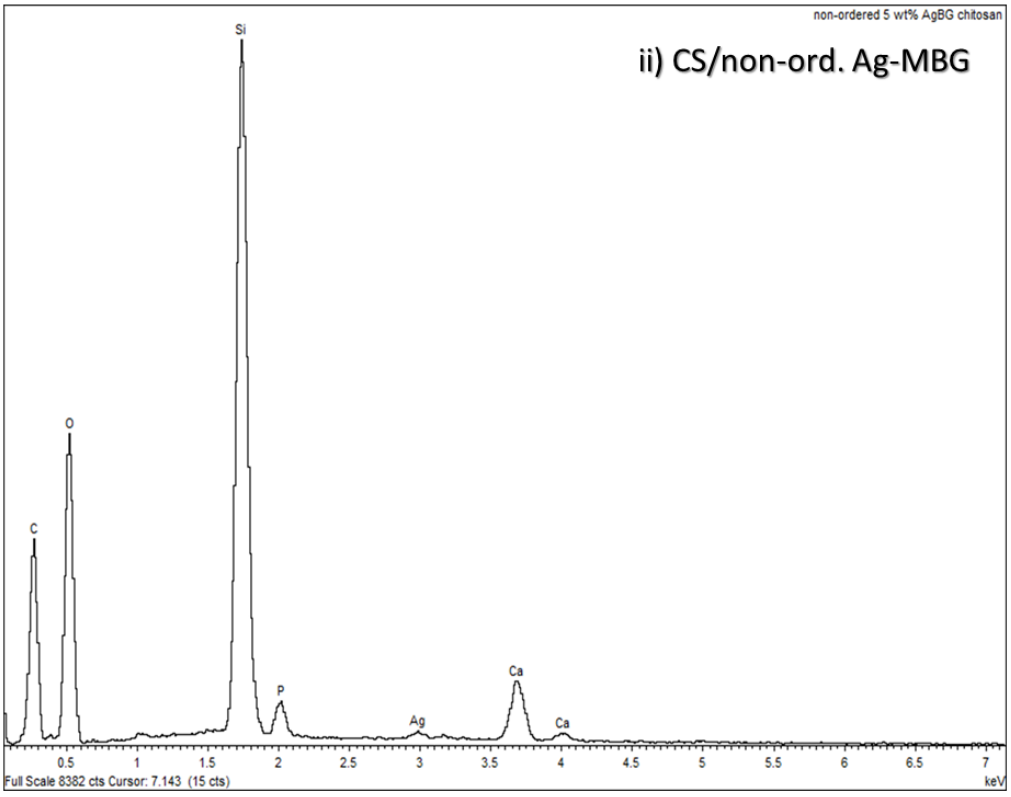

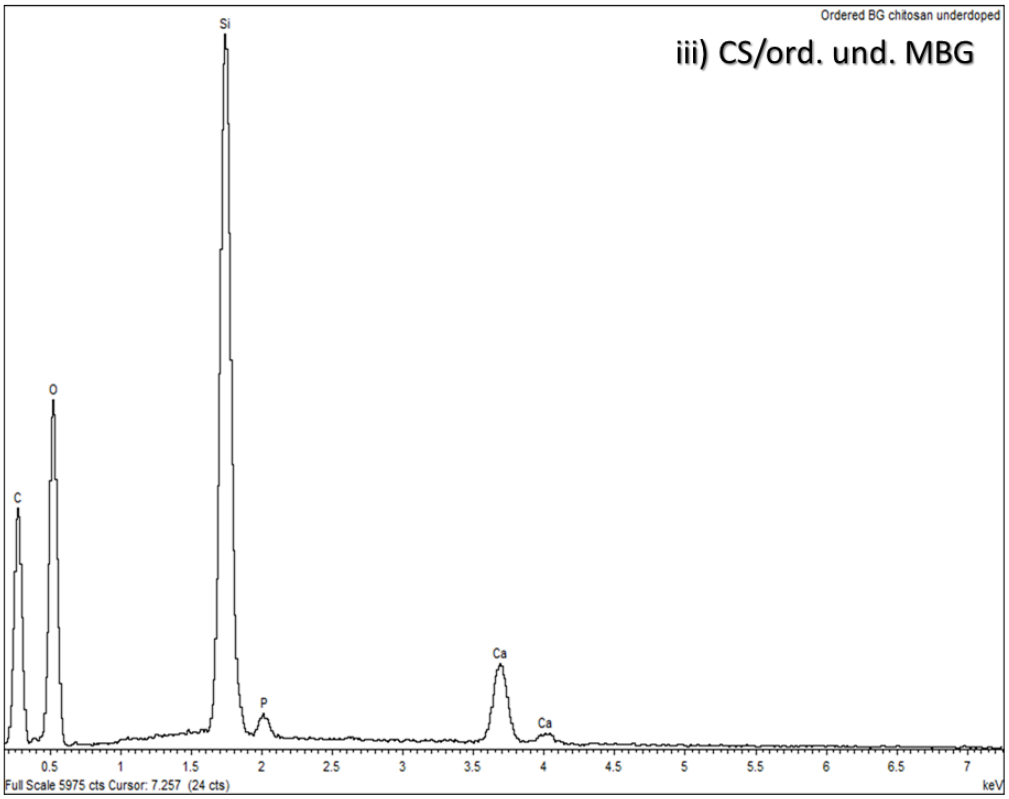
Ordered BG chitosan underdoped
iii) CS/ord. und. MBG
Si
O
C
Ca
P
Ca
0.5 1 1.5 2 2.5 3 3.5 4 4.5 5 5.5 6 6.5 7
Full Scale 5975 cts Cursor: 7.257 (24 cts)
keV

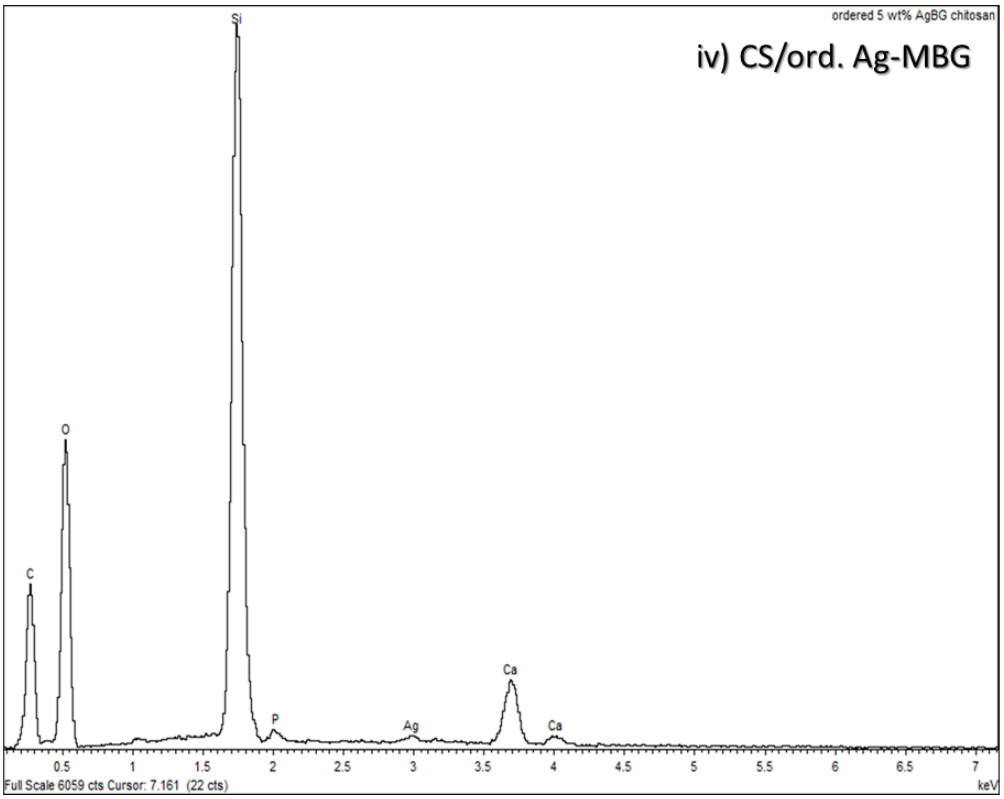
ordered 5 wt% AgBG chitosan
iv) CS/ord. Ag-MBG
Si
O
C
Ca
P
Ag
Ca
0.5 1 1.5 2 2.5 3 3.5 4 4.5 5 5.5 6 6.5 7
Full Scale 6059 cts Cursor: 7.161 (22 cts)
keV

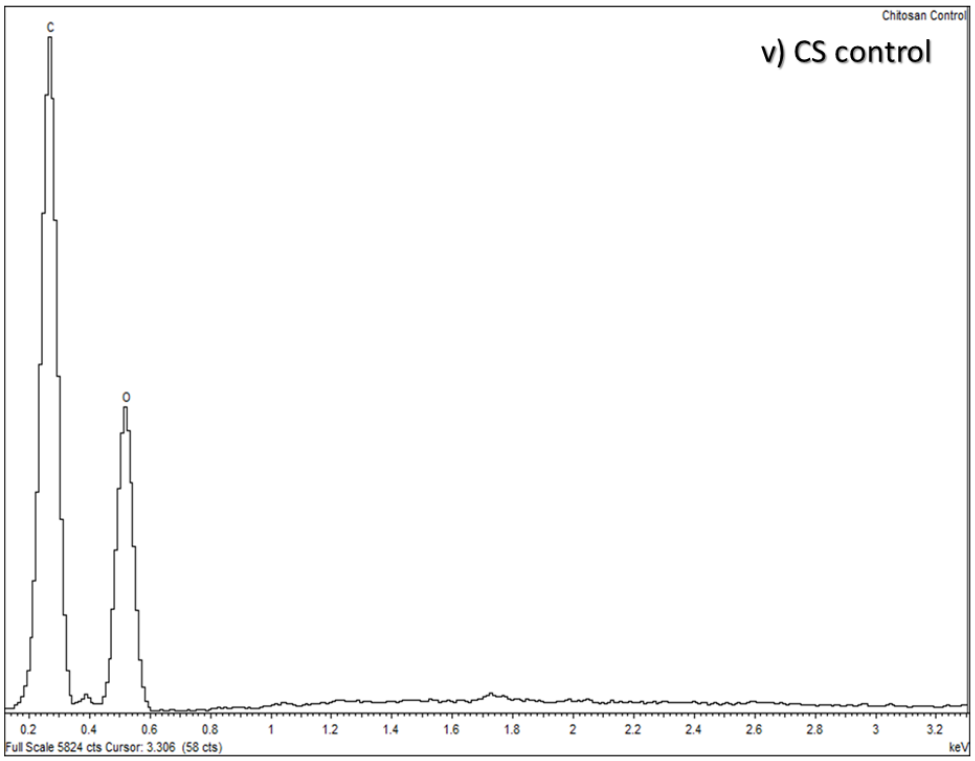

Figure 7.8 EDS analysis of CS/MBG composites: CS/ non-ord. und. MBG (i), CS/ non-ord. Ag-MBG (ii), CS/ ord. und. MBG (iii), CS/ ord. Ag-MBG (iv), and CS control (v). Images were enlarged to make peak attributed values legible.

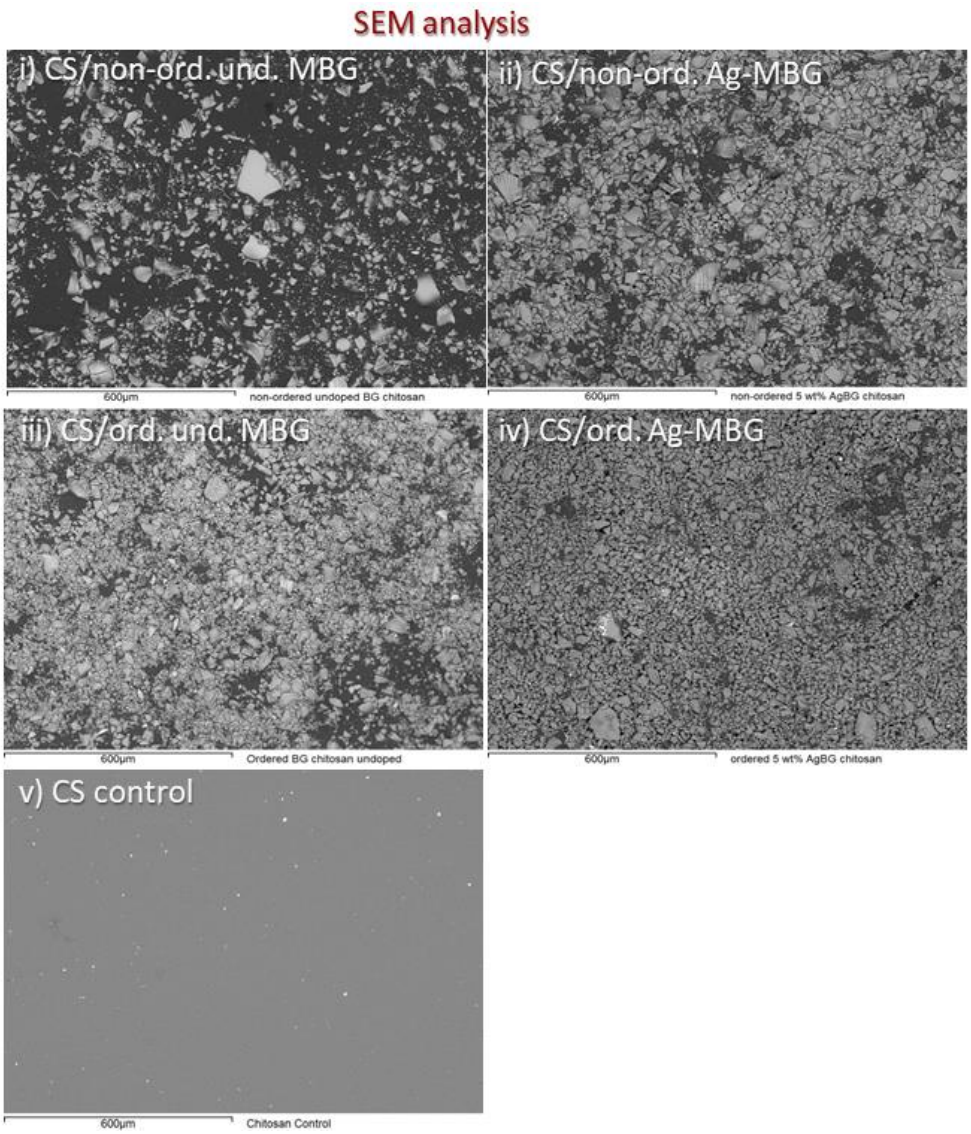

Figure 7.9 SEM images of CS/MBG composites: CS/ non-ord. und. MBG (i), CS/ non-ord. Ag-MBG (ii), CS/ ord. und. MBG (iii), CS/ ord. Ag-MBG (iv), and CS control (v).

Table 7.4 PSD of MBGs used in CS/MBG composite films.

MBGs	Particle size distribution (µm) D10-D90
non-ord. und. MBG	22.9-357
non-ord. Ag-MBG	21.9-308
ord. und. MBG	27.1-352
ord. Ag-MBG	19.7-255

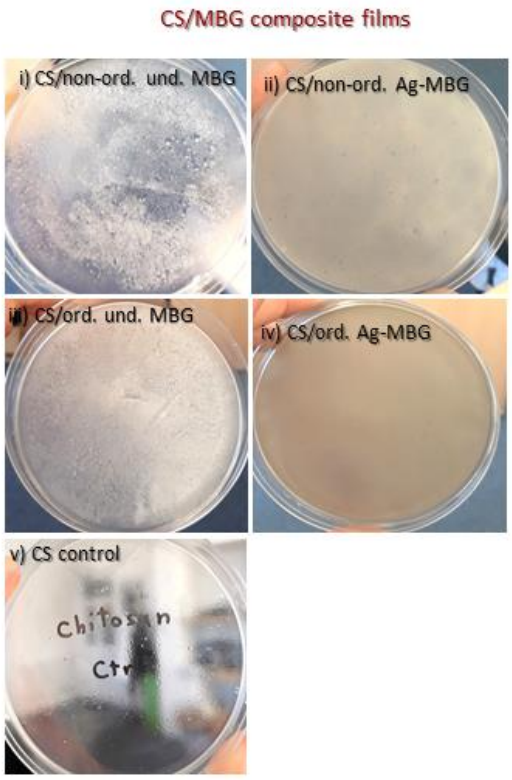

Figure 7.10 Macroscopic appearance of CS/MBG composite films: CS/ non-ord. und. MBG (i), CS/ non-ord. Ag-MBG (ii), CS/ ord. und. MBG (iii), CS/ ord. Ag-MBG (iv), and CS control (v).

Cytotoxicity analysis – Direct contact test with NHEK

The CS/MBGs composite films were also evaluated for their direct interaction with NHEK through direct contact tests (Figure 7.11). Both Ag-doped composites, i.e. *CS/ non-ord. Ag-MBG* and *CS/ ord. Ag-MBG composites* demonstrated high cell viability with NHEK of ~82% and ~87%, respectively. Interestingly, *CS/ non-ord. Ag-MBG composite* that showed only ~40% cell viability with L929 fibroblasts, demonstrated ~82% cell viability with NHEK, suggesting the sensitivity of L929 fibroblasts towards these Ag-doped composites. Different cell types are harmed by Ag^{+} cytotoxic effect to different extents, as was demonstrated in Chapter 06, showing the IC50 of ~2µg/mL (2ppm) and ~12µg/mL (12ppm) when using L929 and NHEK, respectively.

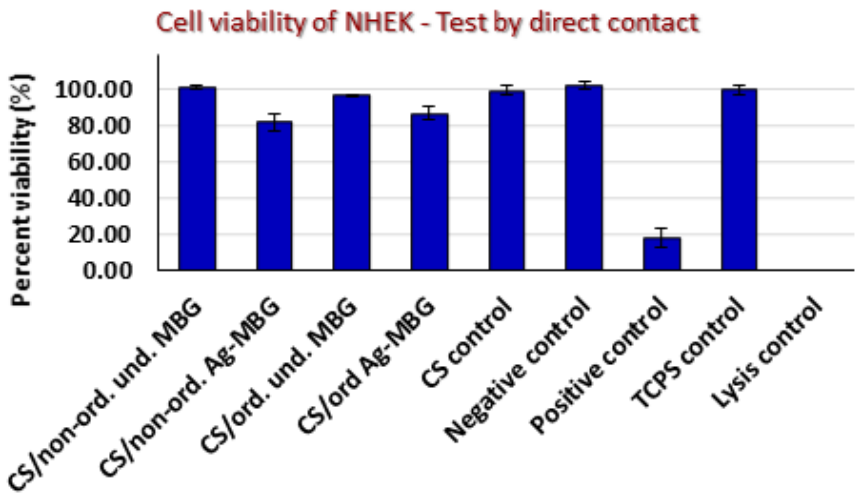

Figure 7.11 Cell viability of CS/MBG composites with NHEK - Test by direct contact.

Live/Dead visualization – Direct contact test with NHEK

The fluorescent micrographs of Live/Dead staining were also recorded to visualize the cytotoxic effects of CS/MBG composites. Both Ag-doped composites, i.e. *CS/ non-ord. Ag-MBG* and *CS/ ord. Ag-MBG composites* affected the cell viability to some extent demonstrating more red fluorescence than green signal right under the specimen (U-area) (Figure 7.12 ii-a, iv-a). However, in case of *CS/ non-ord. Ag-MBG composite*, the cytotoxic signal was not only restricted in U-area but also around the sample in N-area, to some extent (Figure 7.12 ii-b). These fluorescent images highly correlated with cell viability data (Figure 7.11). Both undoped composites i.e. *CS/ non-ord. und. MBG* and *CS/ ord. und. MBG composites* demonstrated green signal of cell viability in all microscopic fields (areas) of the wells (Figure 7.12 i-a to c and iii-a to c). CS control, negative control, and TCPS control demonstrated a uniform green signal as well, while positive control and lysis control showed red signal as an indication of dead cells (Figure 7.12 vii & ix).

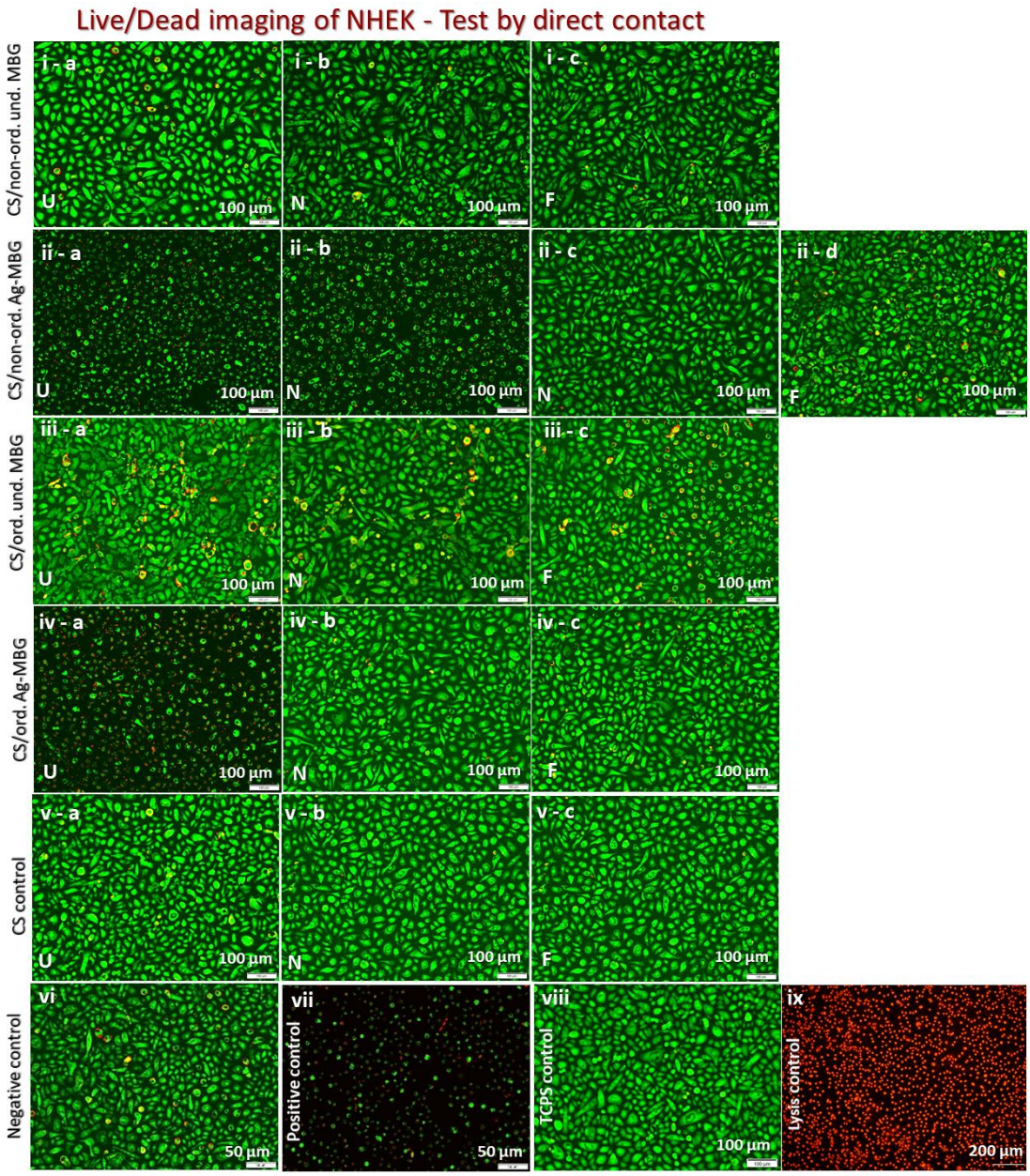

Figure 7.12 Fluorescent micrographs (Live/Dead staining) of NHEK after exposure with CS/MBG composites - Test by direct contact. Images i-a to i-c displayed the microscopic fields in U-, N-, F-areas exposed by CS/ non-ord. und. MBG, images ii-a to ii-d displayed the microscopic areas exposed by CS/ non-ord. Ag-MBG, images iii-a to iii-c displayed the microscopic areas exposed by CS/ ord. und. MBG, images iv-a to iv-d displayed the microscopic areas exposed by CS/ ord. Ag-MBG, and images v-a to v-c displayed the microscopic areas exposed by CS control. Images vi, vii, viii, ix displayed negative, positive, TCPS, and lysis controls, respectively.

7.3.3 Antibacterial activity of CS/MBG composite films

The antibacterial effect of CS/MBGs composite films was evaluated by measuring ZOI through disc-diffusion assay against clinically relevant bacteria involved in wound infections (Figure 7.14). Both Ag-doped composites i.e. *CS/ non-ord. Ag- MBG* and *CS/ ord. Ag- MBG composites* demonstrated antibacterial effect and there were no significant

differences observed in the size of ZOI (Figure 7.13 and Table 7.5). The MIC (minimum inhibitory concentration) of Ag^{+} measured against *S. aureus*, *Methicillin-resistant S. aureus (MRSA), S. epidermidis, Methicillin-resistant S. epidermidis (MRSE), P. aeruginosa, E. coli* (as described in Chapter 06) was in a range of 4.2-8.4µg/mL (4.2ppm-8.4ppm), demonstrating ~90-100% bacterial reduction at their MICs.

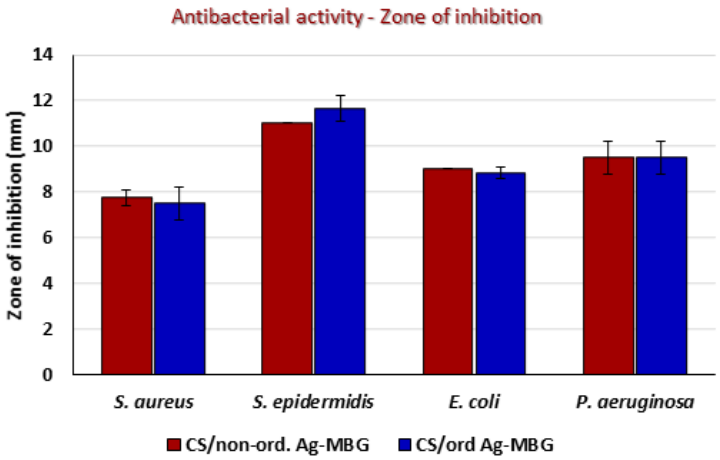

Figure 7.13 Antibacterial activity – ZOI.

Table 7.5 Measurement of ZOI against various bacteria.

Bacterial strains	**CS/non-ord. Ag-MBG** ZOI ± Stdev (mm)	**CS/ord. Ag-MBG** ZOI ± Stdev (mm)
S. aureus	7.75±0.35	7.5±0.7
S. epidermidis	11.0±0	11.6±0.57
E. coli	9.0±0.0	8.83±0.23
P. aeruginosa	9.5±0.7	9.5±0.7

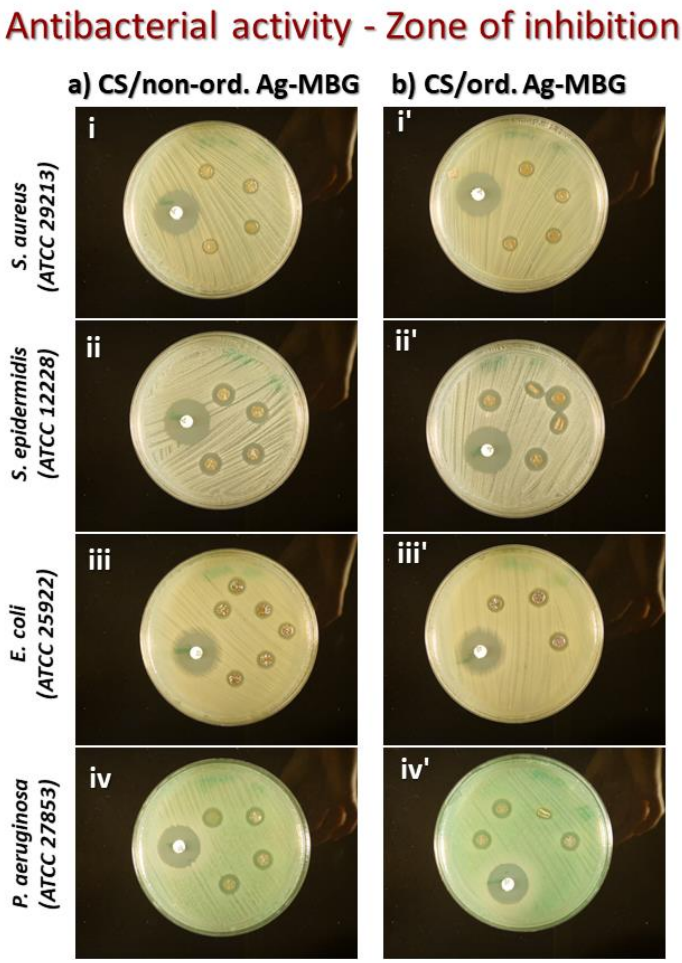

Figure 7.14 Antibacterial activity – ZOI. Images i-iv (in panel a) showed ZOI demonstrated by CS/ ord. Ag-MBG, while images i'-iv' (in panel b) showed ZOI demonstrated by CS/ ord. Ag-MBG against various bacteria. The CS/ ord. Ag-MBG composites had the tendency to fold, while placed on agar surface, thus the test was repeated multiple times to get well spreaded films and thus well-defined round ZOI. The control antibiotic discs are white colored discs: Oxacillin showed 22mm and 23mm against S. aureus and S. epidermidis respectively. While gentamicin showed 20mm and 21mm against E. coli and P. aeruginosa respectively.

Undoped composites did not show any ZOI, neither did chitosan, suggesting Ag being the antibacterial agent. This suggested that Ag was exposed and released by all the Ag-doped composites

Chitosan is generally reported in literature for its antibacterial properties, either by damaging bacterial membrane (the interaction between cationic amine groups of chitosan and anionic groups on bacterial membrane) or by binding with DNA or disabling the enzymes [98]. However, its antibacterial property might depend on multiple factors e.g. on the availability of free protonated amine groups on chitosan, thus, the degree of acetylation and the molecular weight [99^{A}]. Likewise, Ag-doped composites should be investigated for surface roughness, hydrophilicity, Ag release, and

any chemical change on surface that might has happened between material and Ag^+ to better understand the factors behind the respective antibacterial activity.

This effect can be expressed as contact-harming (in case of L929) and contact-killing (in case of susceptible bacteria). Even though no silver release could be observed in experiments for measuring Ag^+ release, it did not mean that there was no Ag^+ on the material surface either, or at the interface of material/medium/cells (L929, bacteria). Therefore, the reason for demonstrated antibacterial was not only related with Ag^+ release, but also with the immediate contact and therefore a very short diffusion distance of Ag^+ ions to the bacteria.

Ion release data in SBF is not predictive due to the interferences with other ions released/exchanged with SBF, and probably hydroxyapatite deposition on the films surface might entrapped Ag avoiding its release. And this was probably more rapid in the case of unordered composites. EDS analysis of SBF incubated samples would be useful to answer this question. Therefore, as previously mentioned that Ag release must be investigated in a medium other than SBF (e.g. PBS or cell culture medium). Ion release in SBF is nor predictive and cannot be directly related with cell and antibacterial tests supposing that SBF medium interfered.

On the basis of bio-evaluation results we concluded that it is not only Ag-release that contributed materials' behaviour towards cells but materials' topography, their ordered/non-ordered structure, and surface area etc. have very important role to play as well. Based on our investigations, we suppose Ag release might present in both Ag-doped composites at first place, as was also suggested in subsequent results on antibacterial tests. Therefore, future investigations have to be made with special concern about Ag ions release in different media.

According to the EUCAST, diameters of ZOI of antibiotics are categorized and interpreted as susceptible, intermediate, or resistant depending on the clinical MIC breakpoints. For most antimicrobials, a good correlation exists between MIC values and ZOI diameters. As a main part of Chapter 06, Ag^+ being an antimicrobial agent of Ag-dressings was evaluated for MIC/MBC determination and percent reduction of bacterial load as a function of time under various type of media. ZOI diameter reported in this chapter though interprets the presence of any sort of antibacterial activity or not. It was not used as absolute measure for the efficacy of the alternative, drug-free antimicrobial. However, establishing MIC breakpoints and ZOI diameters for new antimicrobial agents of systems, the process has to pass a licensing procedure through EMA (European medicines agency) [99^B]. To declare if a novel antimicrobial material is sufficiently antibacterial, depends on the properties of antimicrobial system. For example, antimicrobial agent release from the polymer system, on the type of dissolution media, materials' surface area, porosity, pore size, hydrophilicity, and surface roughness.

7.3.4 Water uptake by CS/MBG composite films

The hydrophilic nature of chitosan made the CS/MBGs films to absorb water up to ~100% of their weight during initial 4 hours, that decreased to an uptake of half of their weight in coming 7 days (Figure 7.15), suggesting the composites as suitable candidates for an optimally moist wound healing environment as well to serve as a candidate for exudating wounds. There was no significant difference in water uptake among different CS/MBG composites.

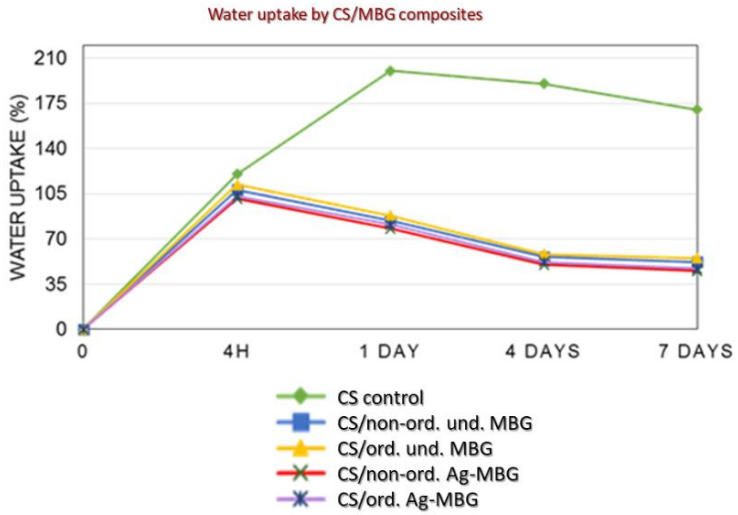

Figure 7.15 Water uptake by CS/MBG composites.

Conclusion

This study aimed the bio-evaluation of CS/Ag-MBG composites for the treatment of infected wounds. In this regard, both Ag-doped composites i.e *CS/ non-ord. Ag-MBG* and *CS/ ord. Ag-MBG composites* demonstrated antibacterial activity against tested bacteria. Cytotoxicity results demonstrated a decrease in L929 fibroblasts viability of approx. 60% for the *CS/ non-ord. Ag-MBG* and approx. 23% for the *CS/ ord. Ag-MBG composites* with respect to untreated control. However, this effect was reduced to only <20% with NHEK for both Ag-doped composites, suggesting higher sensitivity of fibroblasts towards the tested materials as compared to keratinocytes. However, the lowered L929 cell viability by *CS/ non-ord. Ag-MBG composite* could not be explained only on the basis of Ag release profile, suggesting involvement of other factors associated with L929 cytotoxicity. The effect was explained on the basis of surface area, structured porosity (ordered or non-ordered), and particle size distribution of materials. However, the materials should be investigated for their hydrophilicity and surface roughness, and any chemical change on CS/Ag-MBG, to better understand the factors behind the observed antibacterial activity and cytotoxicity. BGs have maximum solubility in plain buffering agent e.g. Tris that does not contain any ions [100]. On the other, SBF (as used in this study for analyzing ion release from composites) has an ion concentration close to human blood plasma and PBS (also used in this study for analyzing ion release from inorganic materials used as fillers in the polymer composites) is more focused on maintaining the pH level (pH 7.4) and isotonic osmolarity. The release behavior of the releasing agent (here: Ag^{+}) depends on the kind of mechanism under investigation. In general, the simpler system would have a better ion release profile but testing the ion release in cell culture and microbial growth media might be helpful in revealing the unanswered questions related to Ag release.

Due to antibacterial properties, cytocompatibility, and water retaining ability, in general, Ag-doped composites especially *CS/ ord. Ag-MBG composite* could be exploited for wound healing application in the future.

HyMedPoly project was a piece of collaborative work. We intend to continue these collaborations to bio-evaluate the successfully produced antimicrobial materials using our advanced 3D based bio-evaluation systems.

Collaboration work

This chapter describes the collaboration work between Ayesha Idrees (ESR14) and Seray Schmitz (ESR07) under HyMedPoly project (Grant agreement No. 643050). The materials synthesis and characterization were performed by Seray Schmitz, a Ph.D. student from Institute of Biomaterials, University of Erlangen-Nuremberg.

Here are the descriptions of ESR07, Seray Schmitz Ph.D. thesis: " Ion doped mesoporous silica-based bioactive glasses for antibiotic-free antibacterial applications " (2019) - Department of Materials Science and Engineering, Institute of Biomaterials, Friedrich-Alexander-University (FAU), Erlangen-Nuremberg, Germany. Supervisor: Prof. Dr. Aldo R. Boccaccini (FAU, Erlangen-Nuremberg, Germany). Co -supervisor: Dr. Mark Cresswell (Lucideon Ltd. Stoke-on-Trent, UK).

.

References

1. Hench, L.L., *Bioceramics: from concept to clinic.* Journal of the american ceramic society, 1991. 74(7): p. 1487-1510.
2. Hench, L.L., *The story of Bioglass®.* Journal of Materials Science: Materials in Medicine, 2006. 17(11): p. 967-978.
3. Williams, D.F.D.F., European Society for Biomaterials, *Definitions in biomaterials : proceedings of a consensus conference of the European Society for Biomaterials, Chester, England, March 3-5, 1986.*
4. Cao, W. and L.L. Hench, *Bioactive materials.* Ceramics international, 1996. 22(6): p. 493-507.
5. Hench, L.L., *The future of bioactive ceramics.* Journal of Materials Science: Materials in Medicine, 2015. 26(2): p. 86.
6. Miguez-Pacheco, V., L.L. Hench, and A.R. Boccaccini, *Bioactive glasses beyond bone and teeth: emerging applications in contact with soft tissues.* Acta biomaterialia, 2015. 13: p. 1-15.
7. Baino, F., et al., *Bioactive glasses: special applications outside the skeletal system.* Journal of Non-Crystalline Solids, 2016. 432: p. 15-30.
8. Dai, C., et al., *Degradable, antibacterial silver exchanged mesoporous silica spheres for hemorrhage control.* Biomaterials, 2009. 30(29): p. 5364-5375.
9. Lansdown, A.B., *Calcium: a potential central regulator in wound healing in the skin.* Wound repair and regeneration, 2002. 10(5): p. 271-285.
10. Hu, G., et al., *Antibacterial hemostatic dressings with nanoporous bioglass containing silver.* International journal of nanomedicine, 2012. 7: p. 2613.
11. Pratten, J., et al., *In vitro attachment of Staphylococcus epidermidis to surgical sutures with and without Ag-containing bioactive glass coating.* Journal of biomaterials applications, 2004. 19(1): p. 47-57.
12. Bellantone, M., H.D. Williams, and L.L. Hench, *Broad-spectrum bactericidal activity of Ag2O-doped bioactive glass.* Antimicrobial agents and chemotherapy, 2002. 46(6): p. 1940-1945.
13. Bellantone, M., N.J. Coleman, and L.L. Hench, *Bacteriostatic action of a novel four-component bioactive glass.* Journal of Biomedical Materials Research: An Official Journal of The Society for Biomaterials, The Japanese Society for Biomaterials, and The Australian Society for Biomaterials and the Korean Society for Biomaterials, 2000. 51(3): p. 484-490.
14. Catauro, M., et al., *Antibacterial and bioactive silver-containing Na 2 O· CaO· 2SiO 2 glass prepared by sol–gel method.* Journal of Materials Science: Materials in Medicine, 2004. 15(7): p. 831-837.

15. Blaker, J., S. Nazhat, and A. Boccaccini, *Development and characterisation of silver-doped bioactive glass-coated sutures for tissue engineering and wound healing applications.* Biomaterials, 2004. 25(7-8): p. 1319-1329.
16. Lohbauer, U., et al. *Antimicrobial treatment of dental osseous defects with silver doped bioglass: osteoblast cell response*. in *Key Engineering Materials*. 2005. Trans Tech Publ.
17. Wren, A., et al., *Silver coated bioactive glass particles for wound healing applications.* Journal of Materials Science: Materials in Medicine, 2012. 23(5): p. 1331-1341.
18. Kawashita, M., et al., *Antibacterial silver-containing silica glass prepared by sol–gel method.* Biomaterials, 2000. 21(4): p. 393-398.
19. Ahmed, I., et al., *Antimicrobial effect of silver-doped phosphate-based glasses.* Journal of Biomedical Materials Research Part A: An Official Journal of The Society for Biomaterials, The Japanese Society for Biomaterials, and The Australian Society for Biomaterials and the Korean Society for Biomaterials, 2006. 79(3): p. 618-626.
20. Mulligan, A., M. Wilson, and J. Knowles, *Effect of increasing silver content in phosphate-based glasses on biofilms of Streptococcus sanguis.* Journal of Biomedical Materials Research Part A: An Official Journal of The Society for Biomaterials, The Japanese Society for Biomaterials, and The Australian Society for Biomaterials and the Korean Society for Biomaterials, 2003. 67(2): p. 401-412.
21. Luo, S.H., et al., *In vitro evaluation of cytotoxicity of silver-containing borate bioactive glass.* Journal of Biomedical Materials Research Part B: Applied Biomaterials, 2010. 95(2): p. 441-448.
22. Valappil, S.P., et al., *Antimicrobial gallium-doped phosphate-based glasses.* Advanced functional materials, 2008. 18(5): p. 732-741.
23. Rai, M., A. Yadav, and A. Gade, *Silver nanoparticles as a new generation of antimicrobials.* Biotechnology advances, 2009. 27(1): p. 76-83.
24. Yao, A., et al., *In vitro bioactive characteristics of borate-based glasses with controllable degradation behavior.* Journal of the American Ceramic Society, 2007. 90(1): p. 303-306.
25. Durand, L.A.H., et al., *In vitro endothelial cell response to ionic dissolution products from boron-doped bioactive glass in the SiO 2–CaO–P 2 O 5–Na 2 O system.* Journal of Materials Chemistry B, 2014. 2(43): p. 7620-7630.
26. Gérard, C., et al., *The stimulation of angiogenesis and collagen deposition by copper.* Biomaterials, 2010. 31(5): p. 824-831.
27. Reffitt, D., et al., *Orthosilicic acid stimulates collagen type 1 synthesis and osteoblastic differentiation in human osteoblast-like cells in vitro.* Bone, 2003. 32(2): p. 127-135.

28. Gerhardt, L.C., et al., *Neocellularization and neovascularization of nanosized bioactive glass-coated decellularized trabecular bone scaffolds.* Journal of Biomedical Materials Research Part A, 2013. 101(3): p. 827-841.
29. Li, J., et al., *A patterned nanocomposite membrane for high-efficiency healing of diabetic wound.* Journal of Materials Chemistry B, 2017. 5(10): p. 1926-1934.
30. Xu, H., et al., *Hierarchically micro-patterned nanofibrous scaffolds with a nanosized bio-glass surface for accelerating wound healing.* Nanoscale, 2015. 7(44): p. 18446-18452.
31. Finnson, K.W., et al., *Dynamics of transforming growth factor beta signaling in wound healing and scarring.* Advances in wound care, 2013. 2(5): p. 195-214.
32. Xie, W., et al., *Regulation of cellular behaviors of fibroblasts related to wound healing by sol–gel derived bioactive glass particles.* Journal of Biomedical Materials Research Part A, 2016. 104(10): p. 2420-2429.
33. Yu, H., et al., *Bioglass activated skin tissue engineering constructs for wound healing.* ACS applied materials & interfaces, 2015. 8(1): p. 703-715.
34. Mao, C., C. Lin, and X. Chen, *Enhanced healing of full-thickness diabetic wounds using bioactive glass and Yunnan baiyao ointments.* Journal of Wuhan University of Technology-Mater. Sci. Ed., 2014. 29(5): p. 1063-1070.
35. Ostomel, T.A., et al., *Spherical bioactive glass with enhanced rates of hydroxyapatite deposition and hemostatic activity.* Small, 2006. 2(11): p. 1261-1265.
36. Yang, Q., et al., *In vitro study of improved wound-healing effect of bioactive borate-based glass nano-/micro-fibers.* Materials Science and Engineering: C, 2015. 55: p. 105-117.
37. Lin, C., et al., *Healing effect of bioactive glass ointment on full-thickness skin wounds.* Biomedical Materials, 2012. 7(4): p. 045017.
38. Kawai, K., et al., *Calcium-based nanoparticles accelerate skin wound healing.* PloS one, 2011. 6(11): p. e27106.
39. Mantovani, A., et al., *Macrophage plasticity and polarization in tissue repair and remodelling.* The Journal of pathology, 2013. 229(2): p. 176-185.
40. Champagne, C., et al., *Macrophage cell lines produce osteoinductive signals that include bone morphogenetic protein-2.* Bone, 2002. 30(1): p. 26-31.
41. Thies, R.S., et al., *Recombinant human bone morphogenetic protein-2 induces osteoblastic differentiation in W-20-17 stromal cells.* Endocrinology, 1992. 130(3): p. 1318-1324.
42. Dong, X., J. Chang, and H. Li, *Bioglass promotes wound healing through modulating the paracrine effects between macrophages and repairing cells.* Journal of Materials Chemistry B, 2017. 5(26): p. 5240-5250.
43. Day, R.M. and A.R. Boccaccini, *Effect of particulate bioactive glasses on human macrophages and monocytes in vitro.* Journal of Biomedical Materials Research

Part A: An Official Journal of The Society for Biomaterials, The Japanese Society for Biomaterials, and The Australian Society for Biomaterials and the Korean Society for Biomaterials, 2005. 73(1): p. 73-79.
44. Bosetti, M., L. Hench, and M. Cannas, *Interaction of bioactive glasses with peritoneal macrophages and monocytes in vitro.* Journal of biomedical materials research, 2002. 60(1): p. 79-85.
45. Anderson, J.M., *Inflammatory response to implants.* ASAIO transactions, 1988. 34(2): p. 101-107.
46. Jayakumar, R., et al., *Biomaterials based on chitin and chitosan in wound dressing applications.* Biotechnology advances, 2011. 29(3): p. 322-337.
47. Paul, W. and C.P. Sharma, *Chitosan and alginate wound dressings: a short review.* Trends Biomater Artif Organs, 2004. 18(1): p. 18-23.
48. Nagahama, H., et al., *Preparation of biodegradable chitin/gelatin membranes with GlcNAc for tissue engineering applications.* Carbohydrate Polymers, 2008. 73(3): p. 456-463.
49. Nagahama, H., et al., *Novel biodegradable chitin membranes for tissue engineering applications.* Carbohydrate Polymers, 2008. 73(2): p. 295-302.
50. Tamura, H., et al., *Biomedical applications of chitin hydrogel membranes and scaffolds.* Carbohydrate Polymers, 2011. 84(2): p. 820-824.
51. Shalumon, K., et al., *Single step electrospinning of chitosan/poly (caprolactone) nanofibers using formic acid/acetone solvent mixture.* Carbohydrate Polymers, 2010. 80(2): p. 413-419.
52. Shalumon, K., et al., *Electrospinning of carboxymethyl chitin/poly (vinyl alcohol) nanofibrous scaffolds for tissue engineering applications.* Carbohydrate Polymers, 2009. 77(4): p. 863-869.
53. Anitha, A., et al., *Development of mucoadhesive thiolated chitosan nanoparticles for biomedical applications.* Carbohydrate Polymers, 2011. 83(1): p. 66-73.
54. Anitha, A., et al., *Synthesis, characterization, cytotoxicity and antibacterial studies of chitosan, O-carboxymethyl and N, O-carboxymethyl chitosan nanoparticles.* Carbohydrate Polymers, 2009. 78(4): p. 672-677.
55. Jayakumar, R., et al. *Synthesis, characterization and biospecific degradation behavior of sulfated chitin*. in *Macromolecular symposia*. 2008. Wiley Online Library.
56. Jayakumar, R., et al., *Sulfated chitin and chitosan as novel biomaterials.* International journal of biological macromolecules, 2007. 40(3): p. 175-181.
57. Jayakumar, R., et al., *Bioactive and osteoblast cell attachment studies of novel α-and β-chitin membranes for tissue-engineering applications.* International journal of biological macromolecules, 2009. 45(3): p. 260-264.

58. Madhumathi, K., et al., *Wet chemical synthesis of chitosan hydrogel–hydroxyapatite composite membranes for tissue engineering applications.* International journal of biological macromolecules, 2009. 45(1): p. 12-15.
59. Marreco, P.R., et al., *Effects of different sterilization methods on the morphology, mechanical properties, and cytotoxicity of chitosan membranes used as wound dressings.* Journal of Biomedical Materials Research Part B: Applied Biomaterials: An Official Journal of The Society for Biomaterials, The Japanese Society for Biomaterials, and The Australian Society for Biomaterials and the Korean Society for Biomaterials, 2004. 71(2): p. 268-277.
60. Yusof, N.L.B.M., et al., *Flexible chitin films as potential wound-dressing materials: Wound model studies.* Journal of Biomedical Materials Research Part A: An Official Journal of The Society for Biomaterials, The Japanese Society for Biomaterials, and The Australian Society for Biomaterials and the Korean Society for Biomaterials, 2003. 66(2): p. 224-232.
61. Ueno, H., T. Mori, and T. Fujinaga, *Topical formulations and wound healing applications of chitosan.* Advanced drug delivery reviews, 2001. 52(2): p. 105-115.
62. Kim, I.-Y., et al., *Chitosan and its derivatives for tissue engineering applications.* Biotechnology advances, 2008. 26(1): p. 1-21.
63. Muzzarelli, R.A., *Chitins and chitosans for the repair of wounded skin, nerve, cartilage and bone.* Carbohydrate polymers, 2009. 76(2): p. 167-182.
64. Kumar, M.N.R., *A review of chitin and chitosan applications.* Reactive and functional polymers, 2000. 46(1): p. 1-27.
65. Hermans, M.H., *Silver-containing dressings and the need for evidence.* Advances in skin & wound care, 2007. 20(3): p. 166-173.
66. Lansdown, A.B., *Silver I: its antibacterial properties and mechanism of action.* Journal of wound care, 2002. 11(4): p. 125-130.
67. Percival, S.L., P. Bowler, and D. Russell, *Bacterial resistance to silver in wound care.* Journal of hospital infection, 2005. 60(1): p. 1-7.
68. Woodward, M., *Silver dressings in wound healing: what is the evidence?* Primary Intention: The Australian Journal of Wound Management, 2005. 13(4): p. 153.
69. Nadworny, P. and R. Burrell, *A Review of Assessment Techniques for Silver Technology in Wound Care Part 1: In VitroMethods for Assessing Antimicrobial Activity.* Journal of Wound Technology, 2008. 2(I): p. 6-13.
70. Nadworny, P. and R. Burrell, *A Review of Assessment Techniques for Silver Technology in Wound Care Part II.* Journal of Wound Technology, 2008. 2(I): p. 14-22.
71. Ip, M., et al., *Antimicrobial activities of silver dressings: an in vitro comparison.* Journal of medical microbiology, 2006. 55(1): p. 59-63.

72. Bowler, P., et al., *Microbicidal properties of a silver-containing Hydrofiber® dressing against a variety of burn wound pathogens.* Journal of Burn Care & Rehabilitation, 2004. 25(2): p. 192-196.
73. Parsons, D., et al., *Silver antimicrobial dressings in wound management: a comparison of antibacterial, physical, and chemical characteristics.* Wounds-A Compendium of Clinical Research and Practice, 2005. 17(8): p. 222-232.
74. Chaw, K., M. Manimaran, and F.E. Tay, *Role of silver ions in destabilization of intermolecular adhesion forces measured by atomic force microscopy in Staphylococcus epidermidis biofilms.* Antimicrobial agents and chemotherapy, 2005. 49(12): p. 4853-4859.
75. Percival, S.L., P. Bowler, and E.J. Woods, *Assessing the effect of an antimicrobial wound dressing on biofilms.* Wound repair and regeneration, 2008. 16(1): p. 52-57.
76. Thorn, R., et al., *In vitro comparison of antimicrobial activity of iodine and silver dressings against biofilms.* Journal of wound care, 2009. 18(8): p. 343-346.
77. Kostenko, V., et al., *Impact of silver-containing wound dressings on bacterial biofilm viability and susceptibility to antibiotics during prolonged treatment.* Antimicrobial agents and chemotherapy, 2010. 54(12): p. 5120-5131.
78. Lansdown, A., et al., *Silver aids healing in the sterile skin wound: experimental studies in the laboratory rat.* British Journal of Dermatology, 1997. 137(5): p. 728-735.
79. Lansdown, A.B., *A pharmacological and toxicological profile of silver as an antimicrobial agent in medical devices.* Advances in pharmacological sciences, 2010. 2010.
80. Wilkinson, L., R. White, and J. Chipman, *Silver and nanoparticles of silver in wound dressings: a review of efficacy and safety.* Journal of wound care, 2011. 20(11): p. 543-549.
81. Lansdown, A. and A. Williams, *How safe is silver in wound care?* Journal of wound care, 2004. 13(4): p. 131-136.
82. Walker, M., P.G. Bowler, and C.A. Cochrane, *In vitro studies to show sequestration of matrix metalloproteinases by silver-containing wound care products.* Ostomy Wound Management, 2007. 53(9): p. 18.
83. Jebahi, S., et al., *Chitosan-based bioglass composite for bone tissue healing: oxidative stress status and antiosteoporotic performance in a ovariectomized rat model.* Korean Journal of Chemical Engineering, 2014. 31(9): p. 1616-1623.
84. Peter, M., et al., *Novel biodegradable chitosan–gelatin/nano-bioactive glass ceramic composite scaffolds for alveolar bone tissue engineering.* Chemical Engineering Journal, 2010. 158(2): p. 353-361.

85. Peter, M., et al., *Nanocomposite scaffolds of bioactive glass ceramic nanoparticles disseminated chitosan matrix for tissue engineering applications.* Carbohydrate Polymers, 2010. 79(2): p. 284-289.
86. Oudadesse, H., et al., *Chitosan effects on glass matrices evaluated by biomaterial. MAS-NMR and biological investigations.* Korean Journal of Chemical Engineering, 2013. 30(9): p. 1775-1783.
87. Yang, J., et al., *Fabrication of a chitosan/bioglass three-dimensional porous scaffold for bone tissue engineering applications.* Journal of Materials Chemistry B, 2014. 2(38): p. 6611-6618.
88. Kaur, G., et al., *Review and the state of the art: sol–gel and melt quenched bioactive glasses for tissue engineering.* Journal of Biomedical Materials Research Part B: Applied Biomaterials, 2016. 104(6): p. 1248-1275.
89. Shih, S.-J., et al., *The correlation of surfactant concentrations on the properties of mesoporous bioactive glass.* Materials, 2016. 9(1): p. 58.
90. Chen, C.-Y., et al., *High supercapacitive performance of sol–gel ZnO-doped manganese oxide coatings.* Thin Solid Films, 2013. 528: p. 61-66.
91. PromoCell. *DetachKit-Manual*. 01/2017 15 April, 2019]; Available from: https://www.promocell.com/f/product-information/manual/C-41200.pdf.
92. Doyle, K., J. Miles, and P. Corporation, *Protocols and applications guide*. 1996: Promega Corporation.
93. Testing, E.C.o.A.S., *Antimicrobial susceptibility testing EUCAST disk diffusion method.* Available: Accessed, 2012. 27.
94. Cockerill, F.R., *Performance standards for antimicrobial susceptibility testing: twenty-first informational supplement*. 2011: Clinical and Laboratory Standards Institute (CLSI).
95. Jorgensen, J.H., *Methods for dilution antimicrobial susceptibility tests for bacteria that grow aerobically: approved standard: NCCLS document M7-A3*. 1993: Nccls.
96. Sayah, E., et al., *A TEM and UV–visible study of silver reduction by ethanol in Ag–alumina catalysts.* Applied Catalysis A: General, 2011. 406(1-2): p. 94-101.
97. Chen, S., G. Wu, and H. Zeng, *Preparation of high antimicrobial activity thiourea chitosan–Ag+ complex.* Carbohydrate Polymers, 2005. 60(1): p. 33-38.
98. Kong, M., et al., *Antimicrobial properties of chitosan and mode of action: a state of the art review.* International journal of food microbiology, 2010. 144(1): p. 51-63.
99[A]. Younes, I., et al., *Influence of acetylation degree and molecular weight of homogeneous chitosans on antibacterial and antifungal activities.* International journal of food microbiology, 2014. 185: p. 57-63.
99[B]. esting, E.C.o.A.S., Setting breakpoints for new antimicrobial agents, EUCAST SOP 1.1, 2013. Växjö: EUCAST. 1 Jun 2013.

100. Kokubo, T. and H. Takadama, *How useful is SBF in predicting in vivo bone bioactivity?* Biomaterials, 2006. 27(15): p. 2907-2915.

7.4 Appendix C

MBGs synthesis (in detail)

7.4.1 Non-surfactant sol-gel method – Non-ordered MBGs

Non-ordered und. MBG

The sol-gel precursors included: tetraethyl orthosilicate (TEOS, 98%, Sigma-Aldrich), triethylphosphate (TEP, 99.8%, Sigma-Aldrich) and calcium nitrate tetrahydrate (Ca $(NO_3)_2 \cdot 4H_2O$, 99%, Sigma-Aldrich). TEOS and TEP were hydrolysed, while other precursors were solubilized in the presence of 0.5M aq. hydrochloric acid (HCl, 37%, Sigma-Aldrich). First, 50mL of TEOS was mixed with 33.12mL of distilled water and 6.80mL of 0.5M HCl as a catalyst for 30 min. Once TEOS completely dissolved, 4.76mL of TEP was added and mixed for 30 min. Finally, 9.87g of Ca $(NO3)_2 \cdot 4H_2O$ was added to this solution and stirred for 1 h. After the subsequent aging at room temperature for 3 days, the gels were dried at 70°C for 24 h, leading to heat-treatment at 700°C (heating rate: 233.3°C/h) for 3 h.

Non-ordered Ag- MBG

The respective wt.% composition was: $71SiO_2$-13CaO-$11P_2O_5$-$5Ag_2O$. The sol-gel precursors included: TEOS, TEP, (Ca $(NO_3)_2 \cdot 4H_2O$, and silver nitrate ($AgNO_3$, 99.5%, Sigma-Aldrich). TEOS and TEP were hydrolyzed, while other precursors were solubilized in the presence of 0.5M aqueous nitric acid (HNO_3, 69%, Sigma-Aldrich) solution. First, 46.80mL of TEOS was mixed with 32.12 mL of distilled water and with 24.04mL of 0.5M HNO_3 as a catalyst for 30 min. Once TEOS completely dissolved, 4.76mL of TEP was added and mixed for 30 min. Then, 9.87g of Ca $(NO_3)_2 \cdot 4H_2O$ was added to the solution and stirred for 1h. Lastly, 1.30g of $AgNO_3$ was added and mixed for 1 h. After the subsequent aging for 3 days, the gels were dried at 70°C for 24 h, leading to heat-treatment at 500°C (heating rate: 166.6°C/h) for 5 h.

7.4.2 Surfactant-assisted sol-gel method – Ordered MBGs

Ord. und. MBG

The respective wt.% composition was: $76SiO_2$-13CaO-$11P_2O_5$. The sol-gel precursors included: TEOS, TEP, (Ca $(NO_3)_2 \cdot 4H_2O$, Pluronic P123 (M_n 5800, Sigma-Aldrich used as a surfactant to introduce mesoporosity). 4.00g of P123 was dissolved in 76mL of 96 vol% ethanol (C_2H_5OH, 96%, Sigma-Aldrich) and 1 mL 0.5M of aq. HCl solution for 1 day. 7.13mL of TEOS was added to the solution and dissolved for 30min. Then, 0.67mL of TEP was added and stirred for 30min. 1.40g of Ca $(NO_3)_2 \cdot 4H_2O$ was added and stirred for 1 day. The prepared solution (sol) was left for evaporation-induced self-assembly

process (EISA) for 5 days in petri dishes under a fume hood. The obtained gels were calcined at 700°C (heating rate: 233.3 °C/h) for 3 h.

Ord. Ag- MBG

The respective wt.% composition was: $71SiO_2$-$13CaO$-$11P_2O_5$-$5Ag_2O$. The sol-gel precursors included: TEOS, TEP, (Ca $(NO_3)_2 \cdot 4H_2O$, and $AgNO_3$. 4.00g P123 was dissolved in 76mL of 96 vol% ethanol and 1mL of 0.5M aq. HNO_3 solution for 1 day. 6.65mL of TEOS was added and dissolved for 30 min. 0.67mL of TEP was added and stirred for 30min. 1.40 g of Ca $(NO_3)_2 \cdot 4H_2O$ was added and stirred for 1 h. Finally, 0.19g $AgNO_3$ was dissolved in the solution and the mixture was stirred for 1 day. The prepared sol was left for EISA for 5 days in petri dishes under a fume hood. The obtained gels were calcined at 500°C (heating rate:166.6°C/h) for 5 h.

Chapter 08: Cytotoxicity and Antibacterial Activity of Hydrogen Peroxide (H_2O_2)

Table of contents

List of figures

List of tables

Abbreviations

A. baumannii: Acinetobacter baumannii
AMPBs: Antimicrobial polymeric biomaterials
ATCC: American type culture collection
BF: Bright field microscopy
CLSI: Clinical & laboratory standards institute guidelines
COPD: Chronic obstructive lung disease
CTB: CellTiter-Blue® assay
CTO: CytoTox-ONE™ assay
$C_{31}H_{28}N_2Na_4O_{13}S$: Xylenol orange
$C_6H_{14}O_6$: Sorbitol
DSMZ: German collection of microorganisms and cell cultures
E. coli: Escherichia coli
E. faecalis: Enterococcus faecalis
Em: Emission
EU: European Union
EUCAST: European committee on antimicrobial susceptibility testing
ESR01: Early stage researcher, Jeddah Marie Vasquez
Ex: Excitation
FAK: Focal adhesion kinase
FBS: Foetal bovine serum
FOX: Ferrous oxidation-xylenol orange assay
GA: Grant agreement
Gram +ve: Gram positive bacteria
Gram -ve: Gram negative bacteria
GO: Glucose oxidase
G: Glucose
GC: Growth control
H_2O_2: Hydrogen peroxide
H_2SO_4: Sulfuric acid
K. pneumoniae: Klebsiella pneumoniae
L929: Murine fibroblast cell line
LDH: Lactate dehydrogenase
MIC: Minimum inhibitory concentration
MBC: Minimum bactericidal concentration
MHB: Mueller-Hinton broth
$NaHCO_3$: Sodium bicarbonate
$(NH_4)_2$ Fe $(SO_4)_2$: Ammonium ferrous sulphate
P. aeruginosa: Pseudomonas aeruginosa

RPMI1640: Roswell Park memorial institute cell culture medium
S. aureus: Staphylococcus aureus
S. epidermidis: Staphylococcus epidermidis
S. lugdunensis: Staphylococcus lugdunensis
StDev: Standard deviation
SUMO: Small ubiquitin-related modifier
SC: Sterility control
TCPS: Tissue culture polystyrene
T_{4h}, T_{8h}, T_{24h}: Time points at 4, 8 and 24 hours
VEGF: Vascular endothelial growth factor

Chapter 08: Cytotoxicity and Antibacterial Activity of Hydrogen Peroxide (H_2O_2)

Abstract

With an increasing need to develop novel antimicrobial polymeric biomaterials (AMPBs) for treating infected wounds, hydrogen peroxide (H_2O_2) was selected as an antibacterial agent (to be released from a hydrogel developed by the PhD student and Early Stage Researcher (ESR01) of the EU-funded project HyMedPoly (GA ID: 643050) Jeddah Marie Vasquez. Hence the agent was here investigated for its cytotoxic and antibacterial activity.

H_2O_2 at different concentrations was tested with L929 cell monolayer culture. The cytotoxicity and cell viability of the cells were assessed by CytoTox-ONE™ and CellTiter-Blue® assays (Promega). Evaluations for changes in cell morphology were made at different time points of H_2O_2 exposure. The antibacterial activity of H_2O_2 in aqueous solutions was evaluated by MIC and MBC determination through microdilution method against *Staphylococcus aureus*, *Staphylococcus epidermidis*, *Staphylococcus lugdunensis, Enterococcus faecalis, Escherichia coli*, *Pseudomonas aeruginosa*, *Klebsiella pneumoniae,* and *A. baumanii*.

Our data suggested that the exposure of cultured L929 cells to H_2O_2 can induce cell damage within 1 hour, as assessed by cytotoxicity, and morphological measures. The time required to reach the maximal cytotoxicity was used as a mode to assess the sensitivity of L929 cells towards H_2O_2 concentrations and was demonstrated as an altered morphological appearance. Concentrations of H_2O_2 of 20mM and 10mM induced rapid cell killing detectable within 60 min. In contrast, exposure to 1mM H_2O_2 resulted in a slightly slower kinetics of L929 cytotoxicity that was detectable within 4-8 hours. When the H_2O_2 concentration was further decreased to 100µM, the detection of a significant cytotoxicity was delayed and hardly detectable even after 24 hours of exposure.

H_2O_2, in general, performed better against Gram +ve (MIC of 0.5mM) than against Gram -ve bacteria (MIC in a range of 0.5-2.5mM) demonstrating MIC values comparatively higher in later.

The cell viability results showed an IC50 of 75.6µM with L929 cells in our experimental set-up, while the MIC and MBC (99.9% bacterial reduction) against *S. aureus* was measured as 500µM.

The redox environment at wound site might induce wound healing by promoting cells. However, H_2O_2 should be used carefully for wound cleaning to kill pathogens, as at higher concentrations it might harm newly proliferating cells surrounding the wound

area. This should be taken under consideration while choosing H_2O_2 based antibacterial wound dressings.

Further *in vitro* tests with a range of FBS supplementation in cell culture media would provide additional insights about H_2O_2 induced cytotoxicity and its consumption at wound site.

Keywords: Hydrogen peroxide (H_2O_2), cytotoxicity, antibacterial activity, H_2O_2 consumption-

Introduction

Inside body, hydrogen peroxide (H_2O_2) is produced as an intermediate molecule during cell's antioxidant defense mechanism against superoxide anions by an action of superoxide dismutase. It is then converted to water and oxygen by catalases/glutathione peroxidases. H_2O_2 is freely miscible in water and can diffuse across biological membranes quickly [1].

H_2O_2 has been implicated to have a role in degenerative diseases by catalyzing oxidative reactions e.g. Alzheimer's disease [2, 3], amyotrophic lateral sclerosis [4], and pulmonary diseases like asthma, and chronic obstructive lung disease (COPD) [5]. etc. On the other hand, H_2O_2 plays a role in regulating renal function and act as an antibacterial agent in urine [6]. The anticipated mechanism of H_2O_2 for its potential antibacterial activity was nicely described in Figure 8.1.

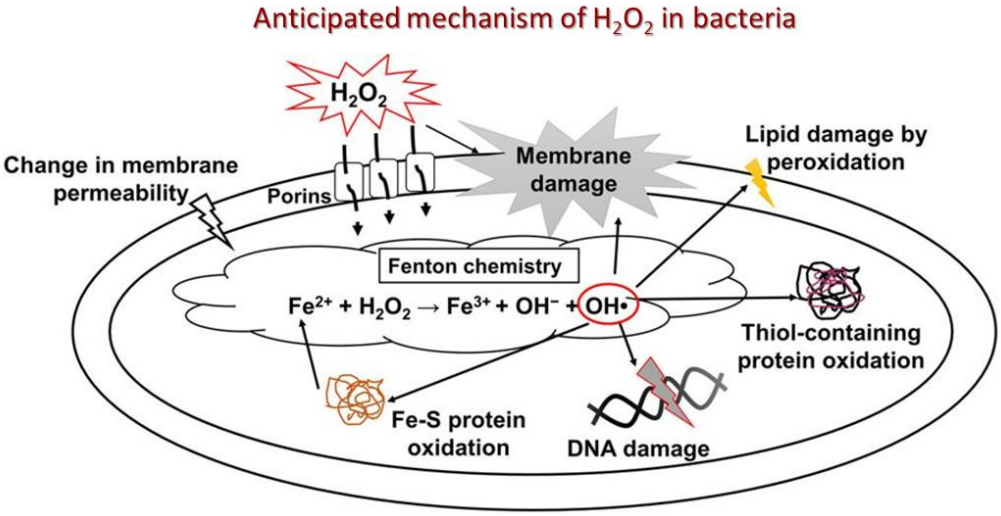

Figure 8.1 Schematic representation of the antimicrobial mechanism of an electrochemical scaffold generating H_2O_2 and enhancing the antibiotic susceptibility in bacteria. The extracellularly generated H_2O_2 diffuses through the bacterial envelope, forms radicals upon reacting with intracellular Fe^{2+}, and oxidizes cellular lipids, proteins, and DNA, inducing cell death. Since the membrane is damaged or now has a changed permeability, antibiotics can penetrate through cells, enhancing their antibiotic susceptibility. This image is licensed under © Creative Commons Attribution 4.0 International License (CC BY 4.0) [7].

Additionally, H_2O_2, has been proposed to have an important role as a secondary messenger in signal transduction molecular pathways [8-10]. Figure 8.2 was shown to demonstrate the concentration dependent effects of H_2O_2 inside body.

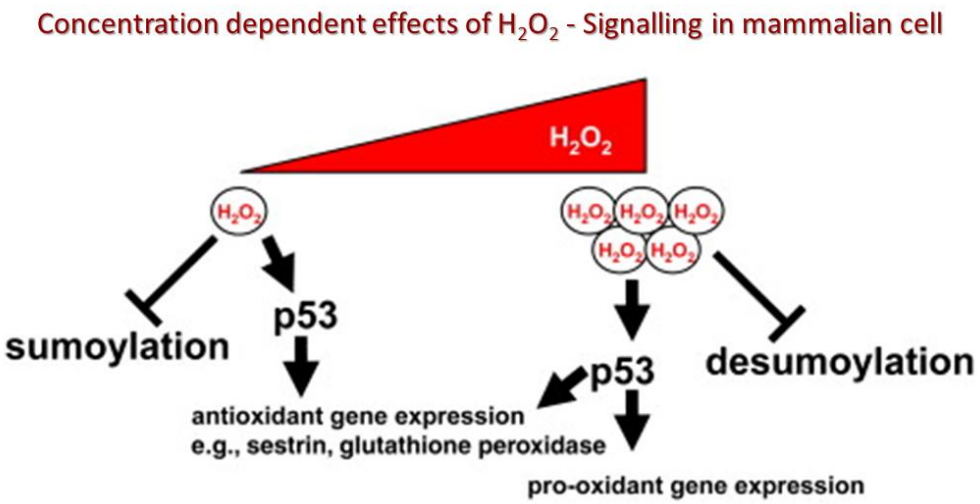

Figure 8.2 Concentration dependent effects of H_2O_2 - Signaling in mammalian cell. As the concentration of H_2O_2 increases, the cell signaling pathways are differentially affected. E.g. level of H_2O_2 determines the level of sumoylation (small ubiquitin-related modifier - SUMO) of proteins [11]. Moreover, p53, a transcription factor would activate the antioxidant genes at sublethal H_2O_2 concentration, but further pro-oxidant genes would get activated as H_2O_2 continues to increase to lethal level [12]. The image [13] has been used with copyright permission.

A two-component based hydrogel has been recently used to encapsulate glucose oxidase (GO) and glucose (G) as a drug-free antibacterial system by J.M. Vasquez (ESR01, HyMedPoly project, https://hymedpoly.eu/). The released H_2O_2 (with an aimed concentration of 10-20mM by ESR01 according to previous literature [14]) was intended for decolonizing bacteria-infected wounds without harming eukaryotic cells at wound site. For this purpose, the current study focused to investigate the cytotoxic and antibacterial activity of H_2O_2, as an active antimicrobial agent.

Depending on its concentration specific to each cell type, H_2O_2 might broadly be known as cell apoptosis-inducer [15]. However, H_2O_2 can induce necrotic and apoptotic forms of cell death [16, 17], or it can lead to the features of cell senescence (G0 phase of cell cycle) [18]. Usually, ≥50µM levels of H_2O_2 are considered cytotoxic. However, the mode of cell death induced by H_2O_2 depends on its concentration and exposure time to the agent [1, 19-23].

A study reported that when the cells (Jurkat cells) were exposed to continuously generating H_2O_2 at low rates such as the one produced by GO, H_2O_2 attained a steady state condition, and inhibited the occurrence of any apoptotic event [24]. On the other hand, providing H_2O_2 directly to cells (bolus addition), H_2O_2 was eliminated by the cellular defense mechanism following first order kinetic reaction [24], and induced apoptosis. These results suggested that besides genotoxic and proapoptotic effects, H_2O_2 may also exert antiapoptotic effect depending on release kinetics [24].

In this study, H_2O_2 induced cytotoxicity and antibacterial activity would provide the initial insights for the optimization of subsequent GO/G based H_2O_2 releasing hydrogel systems.

Materials and Methods

8.1.1 *Cytotoxicity evaluation*

Cells and cell culture maintenance

L929 cells (mouse fibroblast cell line) were obtained from DSMZ (German Collection of Microorganisms and Cell Cultures) and maintained in cell culture media RPMI 1640 with stable glutamine (P04-16530, PAN Biotech), without glucose, without phenol red supplemented with 5% foetal bovine serum (FBS; PAN Biotech) under physiological culture conditions (37°C, 5% CO_2), and sub-cultured using 0.25% trypsin (Gibco).

Cytotoxicity and cell viability evaluation

Defined aliquots of cell suspension (3 x 10^5 cells per well) at early passage numbers (P6 to P12) were pipetted in TC 6 well plate (growth surface area of 9.5cm^2). The plates were incubated at 37°C and 5% CO_2 for 24 hours. The cell sub-confluency and morphology were verified before exposing the cells to test samples. Culture medium was removed and replaced with fresh medium (5mL per well) before starting the test.

H_2O_2 solutions were prepared as ten-folds dilutions in cell culture media at concentrations of 20mM, 10 mM, 1mM, 100µM, 10µM, 1µM, 0.1µM and were tested with above prepared cell monolayer culture. The wells without any sample exposure served as TCPS control (Tissue Culture Treated Polystyrene), while the wells treated with lysis solution (9% Triton® X-100; Promega) served as Lysis control.

The well plate was then incubated at 37°C, 5% CO_2 for 24 hours. The next day, CytoTox-ONE™ assay (CTO, Promega) and CellTiter-Blue® assay (CTB, Promega) were performed for measuring the cytotoxicity and cell viability, respectively according to Promega standard protocols [25] in a multiplex manner. To this aim, first the CTO assay was performed by transferring 100µL of cell supernatant into black microtiter 96-well plate and allowed to reach ambient temperature (~20 min). The 100µL of CTO reagent was added to each well, mixed, and incubated for 15 min at room temperature. Finally, 50µl of stop solution was added to each well, mixed, and protected from light until measurement at excitation (Ex) of 560nm and emission (Em) of 590nm. The CTO assay was performed at 4, 8, and 24 hours (T_{4h}, T_{8h}, T_{24h}) after H_2O_2 exposure to cells.

For CTB assay, the supernatant culture medium was removed, and 2mL CTB reagent (this vol. is enough to cover the surface of TC 6 well) was pipetted per well for 2h at 37°C and 5% CO_2. The cell supernatant was transferred to black microtiter 96-well plates. Fluorescence intensity was measured at Ex of 560nm and Em of 590nm.

Cell morphological analysis

Changes in morphological appearance of L929 cells were evaluated using bright field (BF) microscopy at 0, 1, 4, 8, and 24 hours after H_2O_2 exposure. Such results were used in combination with CTO assay data to evaluate early cytotoxic effects upon exposure of different H_2O_2 concentrations to L929 cells.

8.1.2 *H_2O_2 elimination by L929 over time – FOX (ferrous oxidation-xylenol orange) assay*

The H_2O_2 levels in cell culture system were measured using FOX assay according to previously described protocols [23, 26, 27]. The reagent was incubated with the peroxide containing cell supernatant. Fe^{2+} ions upon oxidation by peroxides resulted into Fe^{3+} ions formation that were able to bind xylenol orange dye. The formation of this Fe^{3+}/xylenol orange complex (colour change) was detected by measuring absorbance intensity at 570nm.

H_2O_2 containing L929 cell cultures at various incubation times (0, 2, 4, 8, 24 hours) were tested to measure the amount of peroxides present at that time point. To this purpose, 10µl samples of cell supernatant were collected and added to 140µl of 25mM H_2SO_4 (sulfuric acid) in a 96 plate well. The prepared reaction solution contained 0.5mM $(NH_4)_2$ Fe $(SO_4)_2$ (ammonium ferrous sulphate), 200µM xylenol orange, and 200mM sorbitol in 25mM H_2SO_4 (Table 8.1). 150µl of this reaction solution was added to each well and the plates were shaken gently for 45 min. The absorption intensity at 570nm was read using a microtiter plate reader. Stock solutions and reagent mixture should be prepared immediately before performing the FOX assay.

Standard peroxide solutions (2-fold dilutions) were freshly prepared (20mM - 0.00015mM) in the same cell culture media in which cells were incubated. A volume of 10µl samples in culture medium (but without cells) was collected and processed for the measurement of the peroxide concentration as mentioned above.

Table 8.1 Reagents with required concentration – FOX assay.

Chemicals	Required concentration	Volume of diluent	Calculations
Hydrogen peroxide-H_2O_2-(30% w/w)-ROTH	20mM and 10mM [10-fold dilutions of 10 mM: 1 mM, 0.1 mM, 0.01 mM, 0.001 mM]	10mL incubation media	$\therefore Density=1.11g/mL,\ Molarity = 9.79M$ $C1V1 = C2V2$ For 20mM in 10mL: Add 20.42µL from H_2O_2 stock into 9.9795mL media.
Sulfuric acid-H_2SO_4-(95-98%)-ROTH	25mM	500mL H_2O	$\therefore Density=1.84g/mL,\ Molarity = 18.12M$ $C1V1 = C2V2$ For 1M stock in 50mL: Add 2.7mL from original H_2SO_4 into 47.24mL H_2O.

			For 25mM in 500mL: Add 12.5mL from stock to 487.5mL media.
Ammonium ferrous sulfate-$(NH_4)_2$ Fe $(SO_4)_2 \cdot 6H_2O$- (≥99%)-ROTH Solubility: 270g/L (H_2O, 20°C)	0.5mM	30mL of 25mM H_2SO_4	*∴Molar mass=392.14g/mol* For 1M stock solution in 1mL: Dissolve 0.39g in 1mL H_2O. $C1V1 = C2V2$ For 0.5mM in 30 mL H_2SO_4: Add 15µL from stock to 30mL of 25mM H_2SO_4.
Xylenol orange tetrasodium salt-$C_{31}H_{28}N_2Na_4O_{13}S$- ROTH Solubility: 510g/L (H_2O, 20°C)	200µM	30mL of 25mM H_2SO_4	*∴Molar mass=760.59g/mol* For 1M stock solution: 0.76g in 1mL H_2O. $C1V1 = C2V2$ For 200µM in 30mL H_2SO_4: Add 6µL from stock to 30mL of 25mM H_2SO_4.
D-sorbitol-$C_6H_{14}O_6$- (≥98 %)-ROTH Solubility: 2350g/L (H_2O, 20°C)	200mM	30mL of 25mM H_2SO_4	*∴Molar mass=182.18g/mol* For 1M stock solution in 1mL: Dissolve 1.821g in 10mL H_2O. $C1V1 = C2V2$ 200mM in 30mL: Add 6mL from stock into 30mL of 25mM H_2SO_4.

8.1.3 *Antibacterial activity of H_2O_2 - MIC and MBC determination*

Staphylococcus aureus (ATCC 29213 of wound source), *Staphylococcus epidermidis* (ATCC 12228), *Staphylococcus lugdunensis* (ATCC 43809), *Enterococcus faecalis* (ATCC 29212), *Escherichia coli* (ATCC 25922), *Pseudomonas aeruginosa* (ATCC 27853), *Klebsiella pneumoniae* (ATCC 10031), and *A. baumanii* were used to evaluate antibacterial activity of H_2O_2.

The MIC (minimum inhibitory concentration) and MBC (minimum bactericidal concentration) determination was performed by microdilution method according to CLSI (Clinical & Laboratory Standards Institute) guidelines [28]. The detailed protocol was described as following:

1. Bacterial strains were revived by culturing on fresh blood agar one day before testing.

2. The tested antibacterial agent's stock solution of H_2O_2 was prepared at a double concentration respect to the target final concentration, using 30% (w/w) H_2O_2 solution (Carl Roth) in MHB (Mueller-Hinton broth from Becton Dickinson, BD 212322) aseptically. To this purpose, the amount of the volume to be taken from the 30% w/w H_2O_2 solution (i.e. 9.79 M) was calculated (C1V1=C2V2) as 20.42µL and was mixed with 9.9795mL MHB to obtain 20mM stock solution.

3. 50µL MHB was pipetted in all wells.

Note: 50µL MHB was pipetted in the growth control (GC) well and 100µL in the sterility control (SC) well.

4. 50µL of tested compound was pipetted into the first well and two-fold dilutions were prepared by pipetting 50µL of each dilution into the next respective wells, and 50µL was discarded from the last dilution.

5. The well-isolated colonies were suspended in 0.9% normal saline by direct colony suspension method and adjusted to McFarland 0.5 [29, 30].

6. Each well containing 50µL of tested compound's dilutions as well as the GC were inoculated with 50µL of the bacterial suspension (using automatic dispensing pipette for accuracy). This resulted in the final desired inoculum of 3.75 X 10^5 CFU ml^{-1} (Table 8.2).

Table 8.2 Calculation for bacterial seeding density according to CLSI standards.

Turbidity		**Calculation (according to CLSI standards final bacterial concentration in each well should be between 2 - 8 x 10^5 CFU/mL)**	
0.5McFarland in 0.9% saline 1 - 2 x 10^8 CFU/mL	1 x 10^8 CFU/mL	1:100 → 1 x 10^6 CFU/mL	1:200 → 0.5 x 10^6 CFU/mL
		(50uL inoculum + 50µL compound) 5 x 10^5 CFU/mL or 5 x 10^4 CFU/well	(50uL inoculum + 50µL compound) 2.5 x 10^5 CFU/mL or 2.5 x 10^4 CFU/well
	1.5 x 10^8 CFU/mL	1:100 → 1.5 x 10^6 CFU/mL	1:200 → 0.75 x 10^6 CFU/mL
		(50uL inoculum + 50µL compound) 7.5 x 10^5 CFU/mL or 7.5 x 10^4 CFU/well	(50uL inoculum + 50µL compound) **3.75 x 10^5 CFU/mL or 3.75 x 10^4 CFU/well**
	2 x 10^8 CFU/mL	1:100 → 2 x 10^6 CFU/mL	1:200 → 1 x 10^6 CFU/mL
		(50uL inoculum + 50µL compound) 1 x 10^5 CFU/mL or 1 x 10^4 CFU/well	(50uL inoculum + 50µL compound) 5 x 10^5 CFU/mL or 5 x 10^4 CFU/well

The most likely value for CFU/mL at 0.5 McFarland was bolded.

7. Colony counts of inoculum suspensions: aliquot from the GC immediately after inoculation was diluted as 1:100 and 1:1000 by transferring 10µL aliquot in 990µL saline and 10µL aliquot in 1990µL of saline. These dilutions were plated by pipetting 100µL aliquots on blood agar plates in duplicates. After incubation, the presence of approximately 50 colonies indicated an inoculum density of 5 × 10^5 CFU ml^{-1}.

8. The inoculated microdilution trays were placed at 35±2°C for 16-20 hours in an ambient air incubator. If necessary, each tray can be sealed with plastic tape and placed in a plastic bag to prevent drying.

9. The results can be read next day after wiping off the bottom of the microtiter plate. SC should be clear. The MIC was defined as the lowest concentration of the antimicrobial agent that inhibited the visible growth of the tested isolate. To determine

the MBC, the dilution representing the MIC and at least two of the more concentrated dilutions were plated and enumerated next day to determine viable CFU/ml.

Results & Discussion

The redox environment at wound site might have an important role on wound healing outcomes. For example, H_2O_2 demonstrated to promote wound healing by inducing VEGF (vascular endothelial growth factor) expression in human keratinocytes *in vitro* [31]. It was also reported that H_2O_2 can stimulate wound healing by inducing keratinocytes proliferation to promote re-epithelization *in vitro* [32]. Moreover, it was demonstrated *in vivo* (mice) that wound site contained micromolar concentrations of H_2O_2. At higher doses, H_2O_2 adversely affected the healing process. While at lower concentrations, H_2O_2 supported the wound healing process by facilitating angiogenesis. H_2O_2 promoted wound healing by inducing site-specific (Tyr-925 and Tyr-861) FAK (focal adhesion kinase) phosphorylation in endothelial cells at wound edge [33].

Cell viability

CTB assay measured cell viability and was based on the ability of living cells to convert a redox dye (resazurin) into a fluorescent end-product (resorufin). On the other hand, CTO assay evaluated the cytotoxicity by measuring the release of lactate dehydrogenase (LDH) from cells with a damaged membrane. Both assays were performed in multiplexed format to get more information from the same sample. L929 viability data showed that H_2O_2 did not favour the cell viability at 20mM, 10mM, and 1mM concentrations (Figure 8.3). Cytotoxic effects were less pronounced at 100µM H_2O_2 concentration and were no more relevant at further lower concentrations (i.e. 10µM, 1µM, 0.1µM) (Figure 8.3). H_2O_2 concentration of 10µM did not alter cell viability respect to TCPS control and indeed it has been reported to stimulate cell growth [34, 35]. However, sensitivity of cells to H_2O_2 depends on the cell type [36], their physiological state, and adaptation to oxidative stress [34, 37-39].

H_2O_2-induced cytotoxicity depending on its concentration might be involved in distinct pathways of cell damage. For example, a study reported that H_2O_2 at higher concentration than 10mM caused necrotic cell death, suggested by smeared patterns of digested DNA and morphological evidences of damaged cell membrane. At 10-5mM concentrations, H_2O_2 was found to induce apoptotic cell death, as shown by ladder formation of endonucleosomally digested DNA, accompanied by morphological evidence of apoptosis. At lower concentrations of 0.5-0.1mM, H_2O_2 induced delayed cytotoxicity after 24 and 4 hours of exposure without any evidence of apoptosis [40].

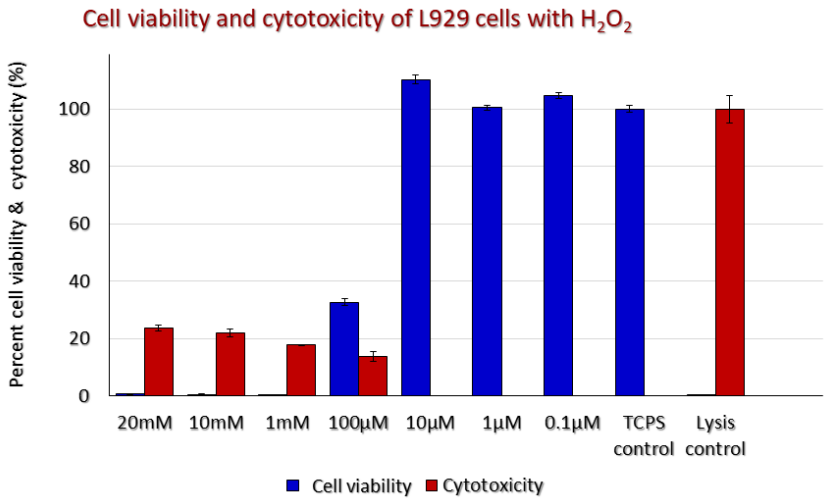

Figure 8.3 Cell viability and cytotoxicity of L929 cells incubated with H_2O_2.

Cytotoxicity and morphological analysis

Cytotoxic effects of H_2O_2 with L929 cells over time, were measured by recording morphological changes (BF images) and cell membrane integrity (CTO assay) in parallel (Figure 8.4 A & B). H_2O_2 at concentrations of 20mM and 10mM, affected the cell morphology (shrunken, rounded, and detaching cells) as early as within 1 h (Figure 8.4 A-ii & -iii). Morphological changes could be attributed to alterations in intermediate filaments of cell cytoskeleton as a result of H_2O_2-induced oxidative damage and cell stress [41, 42]. Morphological results correlated with cytotoxicity data (CTO values): after 4 h exposure time, 20mM and 10mM H_2O_2 concentrations caused 84% and 69% cytotoxicity (at T_{4h}) respectively, which explained the observed damages to cell membrane integrity (Figure 8.4 B).

At H_2O_2 concentration of 100µM, L929 cells did not show immediate alteration in cell morphology, while the cytotoxic effect increased with time (Figure 8.4 A-iv) suggesting delayed cytotoxic effect (Figure 8.4 A-v). H_2O_2 concentration of 10µM did not cause cytotoxicity up to 24h exposure time.

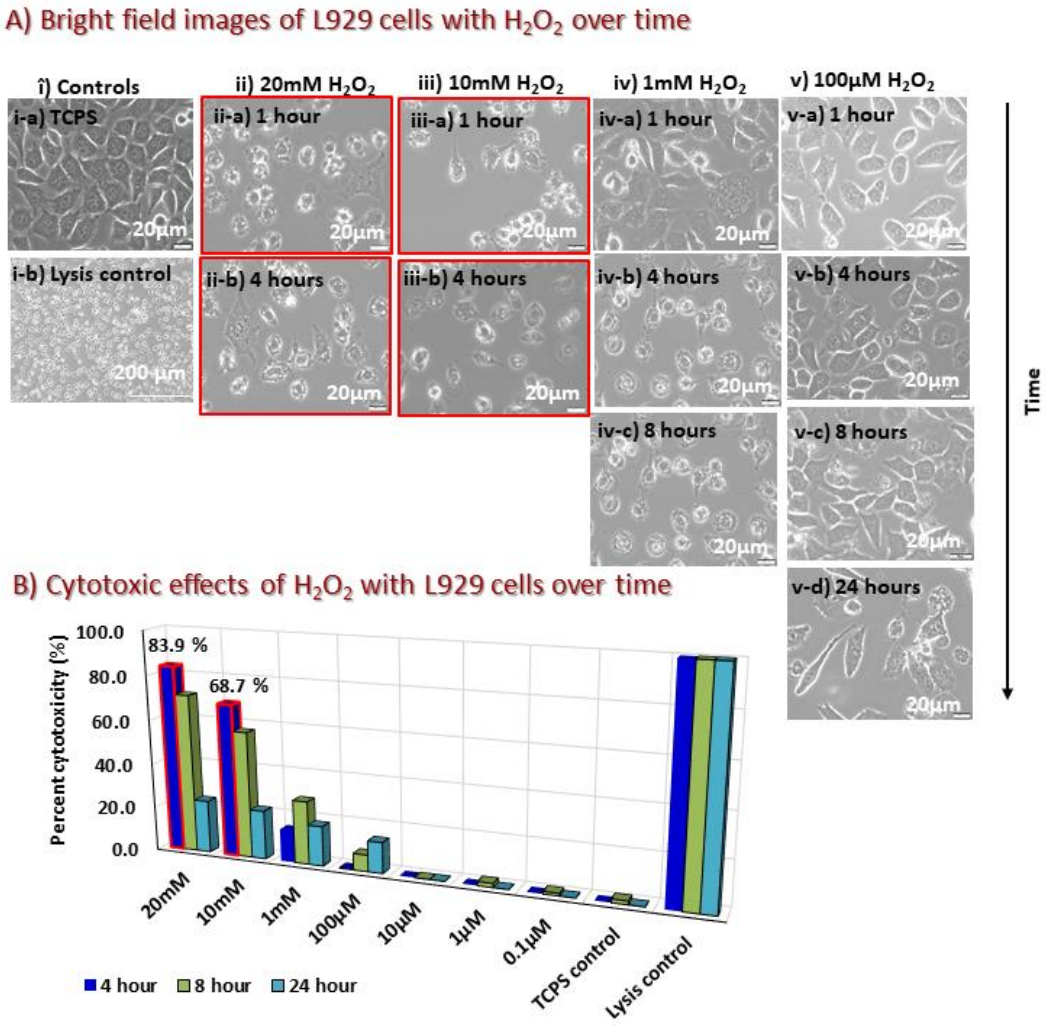

Figure 8.4 A) Bright field images of L929 cells incubated with H_2O_2 over time. B) Cytotoxic effects (CTO assay) of H_2O_2 incubated with L929 cells over time.

Moreover, 1mM H_2O_2 concentration caused changes in morphology during 4-8h exposure (Figure 8.4 A-iv), while the CTO values were not apparently high (Figure 8.4 B). The effect might be related with other forms of cell death than the one involving LDH release from compromised cell membrane into the surrounding medium. Besides, it would be worth considering that the half-life of LDH released from cells was approx. 9 hours. Consequently, despite the evidence of affected morphology, if the maximal membrane damage (thus, LDH release) began only after initial 8 hours, the quantity of active LDH remaining in the cell culture medium at 24 h, might be an underestimation of the actual LDH quantity released. The average and StDev values of cytotoxicity data (Figure 8.4 B) are shown in Table 8.3.

Table 8.3 Average ± StDev of cytotoxicity of L929 by H_2O_2 (the data plotted in Figure 8.4B)

H_2O_2 concentration	Percent cytotoxicity (%) (04 hour)	Percent cytotoxicity (%) (08 hour)	Percent cytotoxicity (%) (24 hour)
	Average ± StDev		
20mM	83.85±13.85	71.36±6.52	23.63±0.99
10mM	68.71±14.55	56.87±2.78	21.93±1.33
1mM	14.57±4.41	28.41±1.38	17.92±0.13
100µM	00.00±4.48	7.47±0.15	13.89±1.76
10µM	00.00±2.25	00.00±4.29	00.00±0.17
1µM	00.00±1.74	1.82±1.33	00.00±0.29
0.1µM	00.00±3.55	1.14±0.31	00.00±0.56
TCPS control	00.00±4.62	1.60±1.46	00.00±1.17
Lysis control	99.69±0.44	100.00±12.71	99.99±4.85

Elimination of H_2O_2 by L929 cells

The FOX assay was used to analyse the elimination of H_2O_2 by cultured L929 cells as a function of time (Figure 8.5). At H_2O_2 concentrations lower than 1mM, cells were able to detoxify H_2O_2 by ~87% during a period of 24h (as indicated by black arrow in Figure 8.5 B). As the H_2O_2 elimination proceeded, H_2O_2 could approach a steady concentration, lower than that initially applied [23]. However, at higher H_2O_2 concentration (i.e. 20mM and 10mM), no apparent H_2O_2 elimination was observed, demonstrating that the cells were not able to clear H_2O_2 effects. Such data can also be correlated with the serious cell damages observed at these concentrations, during the first hour (1 h) of exposure (Figure 8.4 A-ii & -iii).

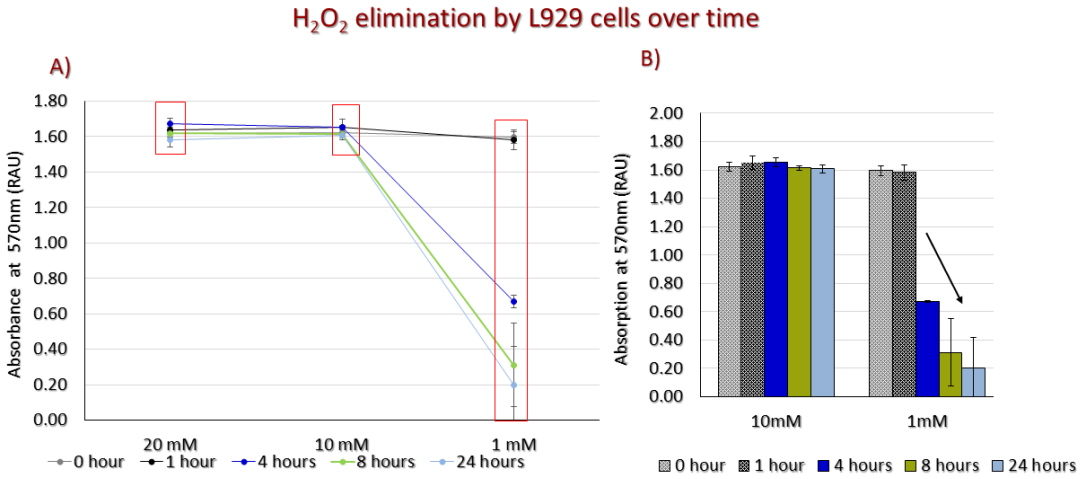

Figure 8.5 H_2O_2 elimination by L929 cells over time (A, B).

These results were preliminary and assay tuning would be necessary to standardize the method for H_2O_2 detoxification measurements by circumventing the problems related to assay linearity (data not shown). Similar effect was described previously for detection

of lipid hydroperoxides in plant tissues [43]. The time required for max. colour development was inconsistent and the set 10-min period incubation developed the linearity [43].

The ability of cells to withstand H_2O_2 induced toxicity and perform its clearance from cell culture system depends on cell concentration [23], cell metabolism [23], adaptation to oxidative stress [34, 37-39], H_2O_2 concentration and exposure time [1, 19-23], supplementation of cell culture media with antioxidants (e.g. glutathione or precursors) [44, 45], contents of peroxide consuming additives (e.g. pyruvate) [46, 47] and serum albumin [8]. The differences in any of these factors would add the noticeable variability in peroxides-induced cytotoxicity outcomes.

Among the factors affecting the ascorbate- & phenolic-mediated H_2O_2 generation, sodium bicarbonate as a constituent of cell culture medium was found to evidently accelerate H_2O_2 production by polyphenols. However, H_2O_2 formation was dependent on pH, and its decomposition might result from the metabolic acidification of cell culture medium [48, 49].

In this experiment, the L929 cells were maintained in RPMI 1640 w/o phenol red and pyruvate. It contained glutathione (1mg/L) & $NaHCO_3$ (2.0g/L) as medium constituents and was supplemented with 5% FBS. The detailed composition of the media (P04-16530, PAN Biotech) has been described [50].

Antibacterial activity

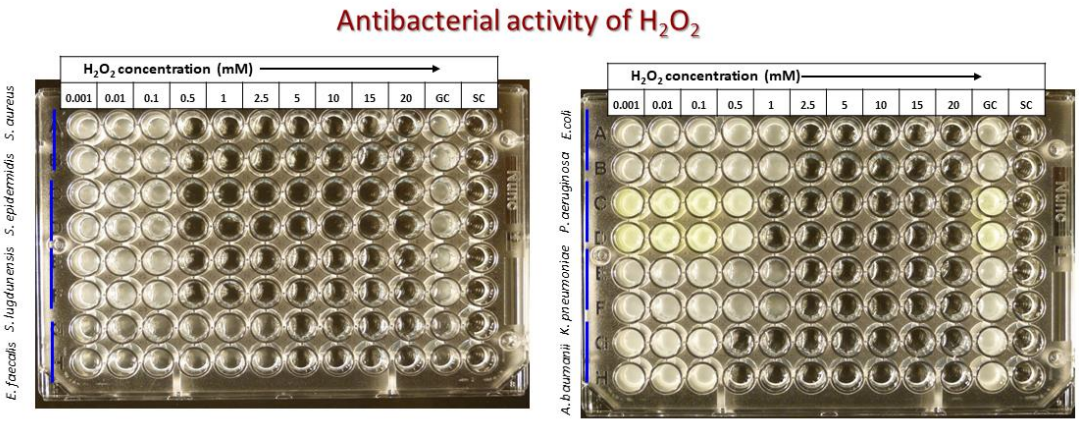

Figure 8.6 Antibacterial activity of H_2O_2.

In this study, H_2O_2 was examined for both its MIC and MBC against selected Gram +ve and Gram -ve bacteria through a microtiter dilution assay (Figure 8.6). The tested *staphylococcal* bacteria exhibited MIC value of 0.5mM. Among Gram +ve bacteria, *E. faecalis* demonstrated highest MIC of 5mM. *Enterococci* are naturally tolerant to antibiotics as demonstrated by their high MIC and MBC values. This is due to their

resistance against bactericidal activity of cell-wall active antimicrobial agents, e.g. β–lactam antibiotics and vancomycin [51].

On the other hand, against Gram-ve bacteria, H_2O_2 demonstrated MIC within 0.5-2.5mM range. *S. aureus*, *P. aeruginosa* and *E. coli* are among the most commonly found pathogens in infected wounds and each of them showed equal values for MIC and MBC of 0.5, 1.0, and 2.5mM, respectively. The MIC and MBC values against the tested bacteria were summarized in Table 8.4.

Table 8.4 The MIC and MBC values of H_2O_2 against the tested bacteria.

	Bacterial species	MIC (mM)	MBC (mM)
Gram +ve	***S. aureus***	0.5	0.5
	S. epidermidis	0.5	5.0
	S. lugdunensis	0.5	2.5
	E. faecalis	5.0	5.0
Gram -ve	***E. coli***	2.5	2.5
	P. aeruginosa	1.0	1.0
	K. pneumoniae	2.5	2.5
	A. baumanii	0.5	1.0

The intrinsic resistance of Gram -ve bacteria attributed to their outer membrane and the presence of very narrow porins to prevent penetration of even very small molecules.

There might be several different pathways of H_2O_2 induced cytotoxicity, though the degree of oxidative damage determines the triggered pathway. For example, low H_2O_2 concentration-induced toxicity reported in *E. coli* [19] depended on bacterial ability to metabolise and generate the reducing equivalents. The H_2O_2 derived oxidative species generated the "DNA oxidants" that in turn depend upon the availability of both reducing equivalents and iron species in cell (Fenton reaction) [52]. On the other hand, higher H_2O_2 concentration suppressed the DNA damage in *E. coli* due to the metabolic starvation to mediate the above mentioned Fenton reaction [52]. A similar effect has been recently observed for mammalian cells as well [53, 54].

H_2O_2 is naturally produced within bacteria due to an autoxidation of redox enzymes, especially in aerobic bacteria or by a deliberate production to compete with other microbial organisms. Because H_2O_2 is acutely toxic, bacteria tend to scavenge H_2O_2 keeping it at nanomolar intracellular levels. Catalases and NADH peroxidases are the

two primary scavengers present in many bacteria. These enzymes are capable of degrading H_2O_2 *in vitro*, although their *in vivo* mechanism is not known up to now [55].

Moreover, as a topical antiseptic since 1920s, H_2O_2 has been extensively used in wound cleaning by killing pathogens through an oxidation burst [56]. However, many clinicians advise exactly against the use of H_2O_2, as it has been observed to slow down the tissue healing process that might be due to oxidative damage to newly proliferating cells surrounding the wound area [57]. Therefore, its rational potential use has been an area of debate.

Conclusion

H_2O_2 showed IC50 of 75.6µM against L929 cells in our experimental set-up, while MIC and MBC (99.9% bacterial reduction) against *S. aureus* was measured to be 500µM. Based on that, the target H_2O_2 concentration of 10-20mM for H_2O_2 releasing hydrogels, adopted by ESR01 from literature [14], appears excessively. However, it has to be considered that *in vitro* and *in vivo* wound environments are completely different. Thus, it might be assumed that H_2O_2 initially at higher concentrations might be consumed by bacterial burden and wound exudate before its possible direct cytotoxic effects towards cells. On the contrary, H_2O_2 at lower concentration might help wound healing [33], preserving the wound from bacterial colonization.

Moreover, further *in vitro* tests with differential supplementation with FBS in cell culture media would provide additional insights on H_2O_2 induced cytotoxicity. L929 cells used in this study was an ISO standardized cell line according to ISO 10993-5 [58]. Further tests with keratinocytes and endothelial cells would help to understand the role of H_2O_2 in wound healing. In Chapter 09, H_2O_2 releasing hydrogels (developed by ESR01) were tested with multiple cell types including human fibroblasts & keratinocytes under different experimental designs as well as with 3D skin model (HSE) to better understand the materials effect.

Collaboration work

The present study was performed as supportive information for collaboration between Ayesha Idrees (ESR14) and Jeddah Marie Vasquez (ESR01) under HyMedPoly project (Grant agreement No. 643050). ESR01 worked with GO/G encapsulated H_2O_2 releasing hydrogels whose bio-evaluations were performed by Ayesha Idrees, as discussed in Chapter 09.

Here are the descriptions of ESR01, Jeddah Marie Vasquez PhD thesis: "Design of a Multilayer Honey-Mimetic Antibacterial Wound Healing Device" PhD Program in Bioengineering and Medical-Surgical Sciences - 31st cycle (2019) - Department of Mechanical and Aerospace Engineering (DIMEAS), Politecnico di Torino, Turin, Italy - Tutor: Valeria Chiono. Co-tutor(s): Prof. Gianluca Ciardelli, Dr. Udo Greiser (external advisor), Prof. Wenxin Wang (external advisor

References

1. Halliwell, B. and J. Gutteridge, *Free radicals in biology and medicine, 3rd edn Oxford University Press.* New York, 1999.
2. Behl, C., et al., *Hydrogen peroxide mediates amyloid β protein toxicity.* Cell, 1994. 77(6): p. 817-827.
3. Busciglio, J. and B.A. Yankner, *Apoptosis and increased generation of reactive oxygen species in Down's syndrome neurons in vitro.* Nature, 1995. 378(6559): p. 776.
4. Wiedau-Pazos, M., et al., *Altered reactivity of superoxide dismutase in familial amyotrophic lateral sclerosis.* Science, 1996. 271(5248): p. 515-518.
5. Van Eeden, S.F. and D.D. Sin, *Oxidative stress in chronic obstructive pulmonary disease: a lung and systemic process.* Canadian respiratory journal, 2013. 20(1): p. 27-29.
6. Halliwell, B., M.V. Clement, and L.H. Long, *Hydrogen peroxide in the human body.* FEBS letters, 2000. 486(1): p. 10-13.
7. Sultana, S.T., D.R. Call, and H. Beyenal, *Eradication of Pseudomonas aeruginosa biofilms and persister cells using an electrochemical scaffold and enhanced antibiotic susceptibility.* NPJ biofilms and microbiomes, 2016. 2(1): p. 2.
8. Carballal, S., et al., *Sulfenic acid formation in human serum albumin by hydrogen peroxide and peroxynitrite.* Biochemistry, 2003. 42(33): p. 9906-9914.
9. Schmidt, K.N., et al., *The roles of hydrogen peroxide and superoxide as messengers in the activation of transcription factor NF-κB.* Chemistry & biology, 1995. 2(1): p. 13-22.
10. Sundaresan, M., et al., *Requirement for generation of H2O2 for platelet-derived growth factor signal transduction.* Science, 1995. 270(5234): p. 296-299.
11. Bossis, G. and F. Melchior, *Regulation of SUMOylation by reversible oxidation of SUMO conjugating enzymes.* Molecular cell, 2006. 21(3): p. 349-357.
12. Sablina, A.A., et al., *The antioxidant function of the p53 tumor suppressor.* Nature medicine, 2005. 11(12): p. 1306.
13. Veal, E.A., A.M. Day, and B.A. Morgan, *Hydrogen peroxide sensing and signaling.* Molecular cell, 2007. 26(1): p. 1-14.
14. Loo, A.E.K., et al., *Effects of hydrogen peroxide on wound healing in mice in relation to oxidative damage.* PloS one, 2012. 7(11): p. e49215.
15. Xiang, J., et al., *Is hydrogen peroxide a suitable apoptosis inducer for all cell types?* BioMed research international, 2016. 2016.
16. Escargueil-Blanc, I., R. Salvayre, and A. Negre-Salvayre, *Necrosis and apoptosis induced by oxidized low density lipoproteins occur through two*

calcium-dependent pathways in lymphoblastoid cells. The FASEB journal, 1994. 8(13): p. 1075-1080.
17. Lennon, S., S. Martin, and T. Cotter, *Dose-dependent induction of apoptosis in human tumour cell lines by widely diverging stimuli.* Cell proliferation, 1991. 24(2): p. 203-214.
18. Bladier, C., et al., *Response of a primary human fibroblast cell line to H2O2: senescence-like growth arrest or apoptosis?* Cell growth & differentiation: the molecular biology journal of the American Association for Cancer Research, 1997. 8(5): p. 589-598.
19. Imlay, J.A. and S. Linn, *Mutagenesis and stress responses induced in Escherichia coli by hydrogen peroxide.* Journal of Bacteriology, 1987. 169(7): p. 2967-2976.
20. Hampton, M.B. and S. Orrenius, *Dual regulation of caspase activity by hydrogen peroxide: implications for apoptosis.* FEBS letters, 1997. 414(3): p. 552-556.
21. Clément, M.-V., A. Ponton, and S. Pervaiz, *Apoptosis induced by hydrogen peroxide is mediated by decreased superoxide anion concentration and reduction of intracellular milieu.* FEBS letters, 1998. 440(1-2): p. 13-18.
22. Gonzalez-Flecha, B. and B. Demple, *Homeostatic regulation of intracellular hydrogen peroxide concentration in aerobically growing Escherichia coli.* Journal of Bacteriology, 1997. 179(2): p. 382-388.
23. Gülden, M., et al., *Cytotoxic potency of H2O2 in cell cultures: impact of cell concentration and exposure time.* Free Radical Biology and Medicine, 2010. 49(8): p. 1298-1305.
24. Barbouti, A., et al., *DNA damage and apoptosis in hydrogen peroxide-exposed Jurkat cells: bolus addition versus continuous generation of H2O2.* Free Radical Biology and Medicine, 2002. 33(5): p. 691-702.
25. Doyle, K., J. Miles, and P. Corporation, *Protocols and applications guide*. 1996: Promega Corporation.
26. Jiang, Z.-Y., A.C. Woollard, and S.P. Wolff, *Hydrogen peroxide production during experimental protein glycation.* Febs Letters, 1990. 268(1): p. 69-71.
27. Dringen, R., L. Kussmaul, and B. Hamprecht, *Detoxification of exogenous hydrogen peroxide and organic hydroperoxides by cultured astroglial cells assessed by microtiter plate assay.* Brain Research Protocols, 1998. 2(3): p. 223-228.
28. CLSI, *M26-A: Methods for Determining Bactericidal Activity of Antimicrobial Agnets;Approved Guidline.* (Clinical & Laboratory Standards Institute: CLSI Guidelines), September 1999.
29. Cockerill, F.R., *Performance standards for antimicrobial susceptibility testing: twenty-first informational supplement*. 2011: Clinical and Laboratory Standards Institute (CLSI).

30. Jorgensen, J.H., *Methods for dilution antimicrobial susceptibility tests for bacteria that grow aerobically: approved standard: NCCLS document M7-A3*. 1993: Nccls.
31. Sen, C.K., et al., *Oxidant-induced vascular endothelial growth factor expression in human keratinocytes and cutaneous wound healing.* Journal of Biological Chemistry, 2002. 277(36): p. 33284-33290.
32. Loo, A.E.K. and B. Halliwell, *Effects of hydrogen peroxide in a keratinocyte-fibroblast co-culture model of wound healing.* Biochemical and biophysical research communications, 2012. 423(2): p. 253-258.
33. Roy, S., et al., *Dermal wound healing is subject to redox control.* Molecular Therapy, 2006. 13(1): p. 211-220.
34. Wiese, A.G., R.E. Pacifici, and K.J. Davies, *Transient adaptation to oxidative stress in mammalian cells.* Archives of biochemistry and biophysics, 1995. 318(1): p. 231-240.
35. Burdon, R.H., *Superoxide and hydrogen peroxide in relation to mammalian cell proliferation.* Free Radical Biology and Medicine, 1995. 18(4): p. 775-794.
36. Dringen, R., P.G. Pawlowski, and J. Hirrlinger, *Peroxide detoxification by brain cells.* Journal of neuroscience research, 2005. 79(1-2): p. 157-165.
37. Cao, C., Y. Leng, and D. Kufe, *Catalase activity is regulated by c-Abl and Arg in the oxidative stress response.* Journal of Biological Chemistry, 2003. 278(32): p. 29667-29675.
38. Spitz, D.R., W. Dewey, and G.C. Li, *Hydrogen peroxide or heat shock induces resistance to hydrogen peroxide in Chinese hamster fibroblasts.* Journal of cellular physiology, 1987. 131(3): p. 364-373.
39. Davies, K.J., *The broad spectrum of responses to oxidants in proliferating cells: a new paradigm for oxidative stress.* IUBMB life, 1999. 48(1): p. 41-47.
40. Gardner, A.M., et al., *Apoptotic vs. nonapoptotic cytotoxicity induced by hydrogen peroxide.* Free radical biology and medicine, 1997. 22(1-2): p. 73-83.
41. Lin, J.J.-C. and J.R. Feramisco, *Disruption of the in vivo distribution of the intermediate filaments in fibroblasts through the microinjection of a specific monoclonal antibody.* Cell, 1981. 24(1): p. 185-193.
42. Welch, W.J. and J.P. Suhan, *Morphological study of the mammalian stress response: characterization of changes in cytoplasmic organelles, cytoskeleton, and nucleoli, and appearance of intranuclear actin filaments in rat fibroblasts after heat-shock treatment.* The Journal of cell biology, 1985. 101(4): p. 1198-1211.
43. DeLong, J.M., et al., *Using a modified ferrous oxidation− xylenol orange (FOX) assay for detection of lipid hydroperoxides in plant tissue.* Journal of Agricultural and Food Chemistry, 2002. 50(2): p. 248-254.

44. Leist, M., et al., *Conventional cell culture media do not adequately supply cells with antioxidants and thus facilitate peroxide-induced genotoxicity.* Free Radical Biology and Medicine, 1996. 21(3): p. 297-306.
45. Brenner, S., et al., *Lasting effect of preceding culture conditions on the susceptibility of C6 cells to peroxide-induced oxidative stress.* Toxicology in Vitro, 2010. 24(8): p. 2090-2096.
46. Andrae, U., J. Singh, and K. Ziegler-Skylakakis, *Pyruvate and related α-ketoacids protect mammalian cells in culture against hydrogen peroxide-induced cytotoxicity.* Toxicology letters, 1985. 28(2-3): p. 93-98.
47. Sasaki, K., S. Bannai, and N. Makino, *Kinetics of hydrogen peroxide elimination by human umbilical vein endothelial cells in culture.* Biochimica et Biophysica Acta (BBA)-General Subjects, 1998. 1380(2): p. 275-288.
48. Bellion, P., et al., *Formation of hydrogen peroxide in cell culture media by apple polyphenols and its effect on antioxidant biomarkers in the colon cell line HT-29.* Molecular nutrition & food research, 2009. 53(10): p. 1226-1236.
49. Wee, L.M., et al., *Factors affecting the ascorbate-and phenolic-dependent generation of hydrogen peroxide in Dulbecco's Modified Eagles Medium.* Free radical research, 2003. 37(10): p. 1123-1130.
50. BIOTECH, P. *RPMI 1640 Composition*. [cited 13 April, 2019; Available from: https://www.pan-biotech.de/media-catalog/cell-culture-media/rpmi-1640.html.
51. Kristich, C.J., L.B. Rice, and C.A. Arias, *Enterococcal infection—treatment and antibiotic resistance*, in *Enterococci: From commensals to leading causes of drug resistant infection [Internet]*. 2014, Massachusetts Eye and Ear Infirmary.
52. Imlay, J.A., S.M. Chin, and S. Linn, *Toxic DNA damage by hydrogen peroxide through the Fenton reaction in vivo and in vitro.* Science, 1988. 240(4852): p. 640-642.
53. Kaneko, M., M. Kodama, and F. Inoue, *Bimodal pattern of killing of Chinese hamster V79 variant cells by hydrogen peroxide.* Free radical research, 1994. 20(4): p. 229-239.
54. Enright, H.U., W.J. Miller, and R.P. Hebbel, *Nucleosomal histone protein protects DNA from iron-mediated damage.* Nucleic acids research, 1992. 20(13): p. 3341-3346.
55. Mishra, S. and J. Imlay, *Why do bacteria use so many enzymes to scavenge hydrogen peroxide?* Archives of biochemistry and biophysics, 2012. 525(2): p. 145-160.
56. Zhu, G., et al., *Hydrogen peroxide: A potential wound therapeutic target.* Medical Principles and Practice, 2017. 26(4): p. 301-308.
57. Oberg, M.S. and D. Lindsey, *Do not put hydrogen peroxide or povidone iodine into wounds!* American Journal of Diseases of Children, 1987. 141(1): p. 27-28.

58. ISO, P., *10993–5: 2009 Biological Evaluation of Medical Devices—Part 5: Tests for In Vitro Cytotoxicity.* ISO: Geneva, Switzerland, 2009.

Chapter 09: Bio-evaluation of H_2O_2 Releasing HB-PEGDA/HA-SH (Hyperbranched Polyethylene Glycol Diacrylate/ Thiolated Hyaluronic Acid) Hydrogels as Antibacterial *In situ* Forming Hydrogel Wound Dressing

Table of contents

List of figures

List of tables

Abbreviations

10% HB-PEGDA/1% HA-SH:10% (w/w) hyperbranched polyethylene glycol diacrylate /1% (w/w) thiolated hyaluronic acid
125U/L hydrogel: 10% HB-PEGDA/1% HA-SH with 125U/L of encapsulated GO and 2.5% glucose
2.5% glucose: 2.5% (w/w) glucose
250U/L hydrogel: 10% HB-PEGDA/1% HA-SH with 250U/L of encapsulated GO and 2.5% glucose
25U/L hydrogel: 10% HB-PEGDA/1% HA-SH with 25U/L of encapsulated GO and 2.5% glucose
3D: Three-dimensional
500U/L hydrogel: 10% HB-PEGDA/1% HA-SH with 500U/L of encapsulated GO and 2.5% glucose
50U/L hydrogel: 10% HB-PEGDA/1% HA-SH with 50U/L of encapsulated GO and 2.5% glucose
A. baumannii: Acinetobacter baumannii
A-area: Area around the specimen (incl. N- & F-areas)
AIBN: Azobisisobutyronitrile, 2,2'-Azobis(2-methylpropionitrile)
ATCC: American type culture collection
BF: Bright field microscopy
Carbapenemases: A diverse group of β-lactamases
CLS: Cell line services, Germany
CnT: CELLnTECH
CnT-PR: CnT-Prime epithelial cell culture medium
CnT-PR-3D: CnT-Prime 3D barrier cell culture medium
CnT-PR-F: CnT-Prime fibroblast cell culture medium
COCA: Murine epidermal cell line
Col. I: Collagen type I
CTB: CellTiter-Blue® assay
DB: Degree of branching
Disulfiram: 1-(diethylthiocarbamoyldisulfanyl)-N, N-diethyl-methanethioamid
DMEM: Dulbecco's modified Eagle's cell culture medium
DS: Disulfiram
DSMZ: German collection of microorganisms and cell cultures
E. coli: Escherichia coli
E. faecalis: Enterococcus faecalis
ECACC: European collection of authenticated cell cultures
ECM: Extracellular matrix
ESR01: Early stage researcher (Jeddah Marie Vasquez)
EthD-III: Ethidium homodimer III

EUCAST: European committee on antimicrobial susceptibility testing
FAD: Flavin adenine dinucleotide
FADH2: Hydroquinone form (an oxidized form) of FAD
F-area: Area far from the specimen
FBS: Foetal bovine serum
GO/G: Encapsulated glucose oxidase and glucose
GO: Glucose oxidase
GPC: Gel permeation chromatography, a type of size exclusion chromatography
Gram +ve: Gram positive bacteria
Gram -ve: Gram negative bacteria
H_2O_2: Hydrogen peroxide
H_2TiO_4: Pertitanic acid
HaCaT: Human keratinocyte cell line
HEPES BSS: (4-(2-hydroxyethyl)-1-piperazineethanesulfonic acid buffered saline solution
HSE: Human skin equivalent
KPC-2: Klebsiella pneumoniae carbapenemase-2 (Class A carbapenemases)
L929: Murine fibroblast cell line
MDR: Multi drug resistance
mecA: Gene for methicillin resistance
MH agar: Mueller-Hinton agar
MRSA: Methicillin resistant Staphylococcus aureus
MRSE: Methicillin-resistant Staphylococcus epidermidis
Mw: Molecular weight
NAD: Nicotinamide adenine dinucleotide
NADH: A reduced form of nicotinamide adenine dinucleotide
N-area: Area near the specimen
NHDF: Normal human dermal fibroblasts
NHEK: Normal human epidermal keratinocytes
NMR: Nuclear magnetic resonance spectroscopy
P. aeruginosa: Pseudomonas aeruginosa
Pbp2a: Gene for penicillin binding protein 2A
PEGMEMA: Poly (ethylene glycol) methyl methacrylate
PET membrane: Polyethylene terephthalate membrane
RAFT: Reversible-addition-fragmentation chain-transfer polymerization
ROS: Reactive oxygen species
RPMI1640: Roswell Park memorial institute cell culture medium
S. aureus: Staphylococcus aureus
S. epidermidis: Staphylococcus epidermidis
TCPS: Tissue culture polystyrene surface

TNS: Trypsin Neutralizing Solution
U-area: Area right under the specimen
UV/VIS: Ultraviolet–visible spectroscopy
VIM-2: Verona integron-encoded metallo-β-lactamase (class B carbapenemases)
ZOI: Zone of inhibition

Chapter 09: Bio-evaluation of H_2O_2 Releasing HB-PEGDA/HA-SH (Hyperbranched Polyethylene Glycol Diacrylate/ Thiolated Hyaluronic Acid) Hydrogels as Antibacterial *In situ* Forming Hydrogel Wound Dressing

Abstract

With the emergence of antibiotic resistance, drug-free antibacterial strategies are becoming highly popular. For this purpose, a honey-inspired H_2O_2 releasing system was fabricated by encapsulating glucose oxidase (GO) and glucose (G) in a two component-based hydrogel based on hyperbranched polyethylene glycol (HB-PEGDA) and thiolated hyaluronic acid (HA-SH). The HB-PEGDA was synthesized by an *in situ* RAFT polymerization and crosslinked with HA-SH to generate HB-PEGDA/HA-SH hydrogels *via* thiol-ene click reaction, as described in [1-3], making these polymers promising materials for biological applications. In this study, HB-PEGDA/HA-SH based hydrogels containing different ratios of GO/G were bio-evaluated as drug-free antibacterial systems for healing infected wounds. 10% (w/w) HB-PEGDA/1% (w/w) HA-SH hydrogel samples were encapsulated with glucose (2.5%, w/w) and GO at various concentrations (25U/L, 50U/L, 125U/L, 250U/L, 500U/L).

H_2O_2 releasing hydrogels were evaluated for cytotoxicity with fibroblast and keratinocyte cell line such as L929, HaCaT, and COCA cells. On the other hand, primary cells being clinically more relevant, such as normal human dermal fibroblasts (NHDF) and normal human epidermal keratinocytes (NHEK) were used to evaluate the specific cytotoxicity. Additionally, as *in vitro* bio-evaluation is more accurate in 3D systems, the H_2O_2 releasing hydrogels were also evaluated using an in-house 3D *in vitro* skin model. The cell culture medium is designed for optimal growth of a specific cell type. Therefore, the total glucose content of each cell culture media was different from one another. Being complicated systems for *in vitro* cytotoxicity analysis, GO/G encapsulated hydrogel systems were investigated under three different test designs by direct contact, indirect contact, and adapted direct contact methods. The cell viability was evaluated by CellTiter-Blue® assay (CTB assay, Promega). The changes in cell morphology and cytotoxicity visualization (Live/Dead staining, Promokine) were performed by bright field (BF) and fluorescent microscopy, respectively.

The antibacterial activity was determined by disc-diffusion test against *Staphylococcus aureus, Staphylococcus epidermidis, Escherichia coli, Pseudomonas aeruginosa, Enterococcus faecalis,* and *Acinetobacter baumannii* being the most relevant bacteria in infected wounds. Additionally, resistant strains with most commonly found resistance-phenotypes were also tested including *Methicillin-resistant Staphylococcus aureus*

(MRSA), *Methicillin-resistant Staphylococcus epidermidis (MRSE), VIM-2 producing drug resistant Pseudomonas aeruginosa, KPC-2 producing drug resistant Escherichia coli.*

The optimal hydrogel composition was 10% HB-PEGDA/1% HA-SH due to its closeness to the desired properties of hydrogel gelation time, structure stability, and H_2O_2 release. 10% HB-PEGDA/1% HA-SH was able to form a gel within 63 seconds making it suitable for *in situ* forming hydrogel wound dressings. 10% HB-PEGDA/1% HA-SH hydrogel with 250U/L GO produced 9.11±0.92mM H_2O_2 for 24 hours, which was within the aimed concentration of 10-20mM H_2O_2. However, approx. 50% of the H_2O_2 concentration was produced during the first two hours with a decrease in later hours.

The cytotoxic effects demonstrated by hydrogels were highly dependent on the type of the test procedure as well as concentration of encapsulated GO. For example, under direct contact test, ≤50U/L hydrogels demonstrated the minimum cytotoxic effect of ~25% with NHDF. While under indirect contact test, even 250U/L hydrogels demonstrated approx. ~≤32% cytotoxicity with both NHDF and NHEK. However, under adapted direct contact test, 250U/L hydrogels demonstrated approx. ≤13% cytotoxicity with both NHDF and NHEK. These results also suggested the importance of microscopic analysis and Live/Dead staining for the visualization of the cytotoxic effects, in complementarity to CTB assay i.e. a quantitative analysis of cell viability. The cytotoxic effects were more apparent in Live/Dead imaging than were in CTB assay, demonstrating that the cytotoxic effects of materials can be better understood this way.

H_2O_2 releasing hydrogels, in general, performed better against Gram +ve than against Gram -ve bacteria, demonstrating antibacterial activity at comparatively higher GO concentrations for Gram -ve bacteria. This might be due to the intrinsic resistance attributed by the presence of the outer membrane and narrow porins in Gram -ve bacteria to prevent penetration of even small molecules. Among the tested compositions, 250U/L H_2O_2 releasing hydrogels demonstrated a strong antibacterial effect against a wide range of wound associated pathogens.

The H_2O_2 releasing hydrogels at higher GO (e.g. 125-250U/L) concentrations with respect to lower GO concentrations (e.g. 25U/L and 50U/L) can be eliminated by bacteria and wound exudate in infected wounds, thus, avoiding the possible direct cytotoxic effect towards eukaryotic cells to help wound in healing. An initial robust H_2O_2 release might help to reduce bacterial burden at initial stages, while a further constant H_2O_2 release might help preventing recurring bacterial colonization of wounds.

Different types of procedures were executed to investigate cytotoxic effects possibly provoked by the polymer, though, the H_2O_2 releasing system has to be better characterized for optimal immobilization of GO within cross-linked hydrogels and the

presence/release of unpolymerized PEGDA. Additionally, knowledge of H_2O_2 consumption by different types of cell culture media and cell types would be highly relevant to understand the cytotoxicity of H_2O_2 releasing hydrogels. Moreover, immunohistological and gene expression analysis would help to understand the underlying cellular and molecular mechanism. Moreover, peroxidase scavengers present in many bacteria have to be considered during *in vitro* bio-evaluation of H_2O_2 as an antibacterial agent.

Keywords: Bio-evaluation, cytotoxicity, antibacterial activity, infected wounds, H_2O_2, glucose oxidase, HB-PEGDA/HA-SH hydrogel.

9.1 Introduction

9.1.1 H_2O_2 as antibacterial agent

With the emergence of antibiotic resistance, drug-free antibacterial strategies are becoming highly popular. In this context, honey as a natural product, has been used since ancient times and traditionally demonstrated to be effective in wound healing due to its anti-inflammatory properties [4]. Honey has also been shown to possess antibacterial properties for treating infected wounds [5-7]. Depending on the type of honey, its antibacterial properties might be attributed by various factors such as, its acidity, osmotic effect, antioxidant and hydrogen peroxide (H_2O_2) content [8, 9]. In this study, H_2O_2 as a Reactive oxygen species (ROS) was investigated as a wound healing and antibacterial agent. For this purpose, a H_2O_2 releasing system was focused on exploiting intracellular production process of H_2O_2 by glucose oxidase (GO) and glucose (as shown in Figure 9.1).

Topically applied GO at wound site, might result in burst release of ROS or inactivation of the enzyme caused by the complexity of wound fluids, thus a controlled release of H_2O_2 was ensured by encapsulating GO and glucose in the two component-based crosslinked hydrogels. *V. Arul et al.* and others have observed beneficial role of sustained release of ROS for treating diabetic wounds by using a GO incorporated collagen matrix to directly apply on diabetic wounds [10]. Among other examples, Oxyzyme™ (trademark) and Surgihoney (SH, a general term used by [11]) both are ROS-based hydrogel technologies for wound healing applications [11-13]. They consist of two individual hydrogel patches i.e. embedded with glucose (G) and GO. Oxyzyme™ was developed to shorten the wound healing period by *in situ* production of active oxygen inducing angiogenesis. Though, Oxyzyme™ contains iodine as an antimicrobial agent and the dressing is still not indicated to treat infected wounds [12]. On the other hand, SH was reported to demonstrate antibacterial effects by reactive oxygen (RO) production from the breakdown of H_2O_2 (a release of 1.5-2.5mM was measured for 24 hours) [11].

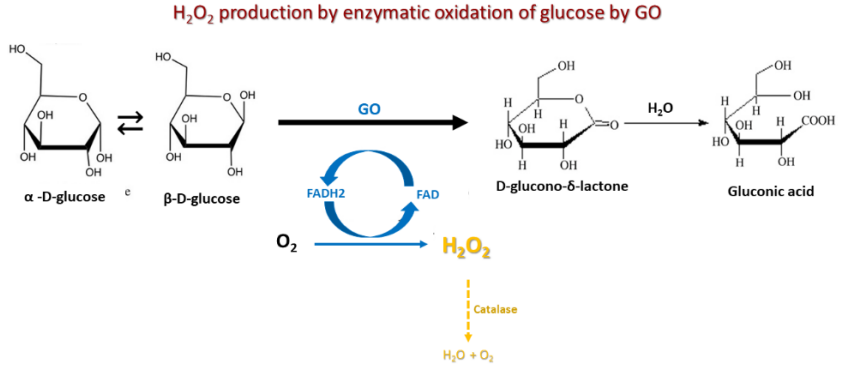

Figure 9.1 H_2O_2 production by enzymatic oxidation of glucose by GO. GO catalyzes the oxidation of β-D-glucose into gluconic acid, by using molecular oxygen (O_2) as an e^- acceptor producing H_2O_2 [14].

Intracellular FAD (flavin adenine dinucleotide) is oxidised to FADH2 (hydroquinone form) i.e. its fully oxidized form. H_2O_2 might be decomposed by catalase to water and oxygen. This is a second enzyme that protects cells from oxidative damage of ROS. The image was modified and used with copyright permission [14].

9.1.2 Hydrogel matrix for GO/glucose encapsulation

Hyperbranched (HB) polymers are rich in functional groups, have a 3D structure, high solubility, and low viscosity [15]. This makes them ideal as pre-hydrogel solution that can be easily cross-linked using thiolated nature polymer e.g. thiolated hyaluronic acid (HA-SH) to make a stable hydrogel [15].

Hyaluronic acid (HA) being an important component of extracellular matrix (ECM) especially in soft connective tissues, serves an attractive biomaterial for biomedical applications [16].

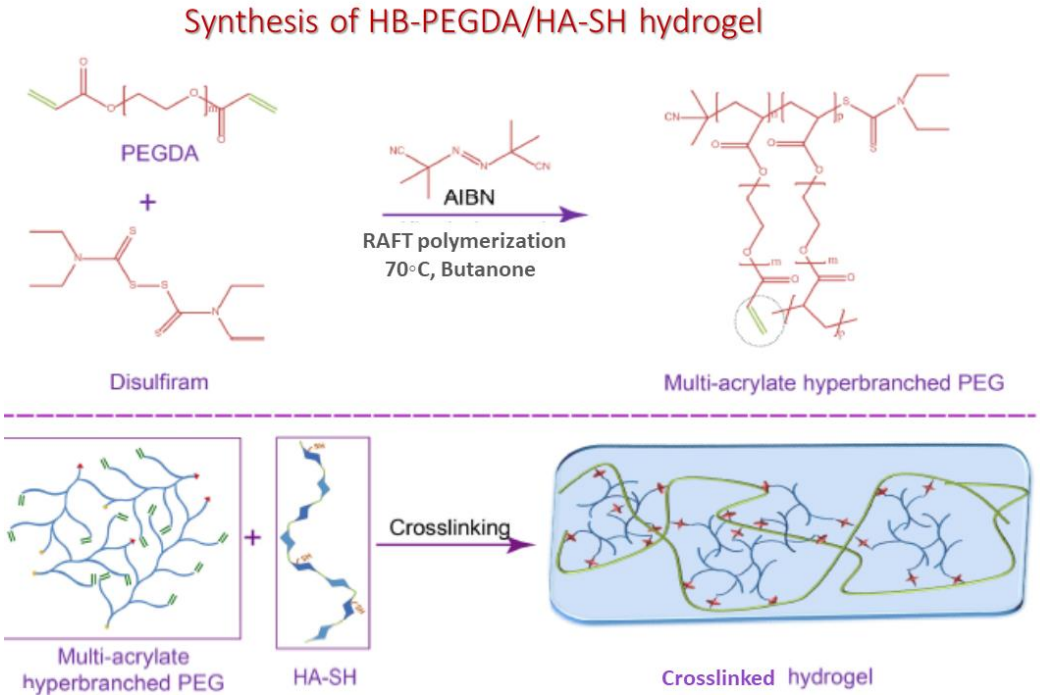

Figure 9.2 Synthesis of HB-PEGDA/HA-SH hydrogel. The image was used with copyright permission [3].

In literature as shown in Figure 9.2, the hyperbranched polyethylene glycol with numerous acrylate groups (HB-PEGDA) were synthesized by an *in situ* RAFT polymerization (reversible-addition-fragmentation chain-transfer polymerization) of PEGDA (polyethylene glycol diacrylate monomers) using AIBN (2,2'-Azobis(2-methylpropionitrile)) as initiator and disulfiram (DS) as a precursor agent [2, 3]. The HA-SH was then used to crosslink HB-PEGDA to generate hydrogels *via* thiol-ene click reaction [2, 3], making these polymers very promising materials for biological applications. The electron deficient acrylate groups react with thiol groups via Michael addition without side product formation [17]. The R–CH_2–CH_2–S–R' crosslink binds the

two components together making a complex hydrogel network (Figure 9.3) which can expand or shrink in the presence or absence of water [3].

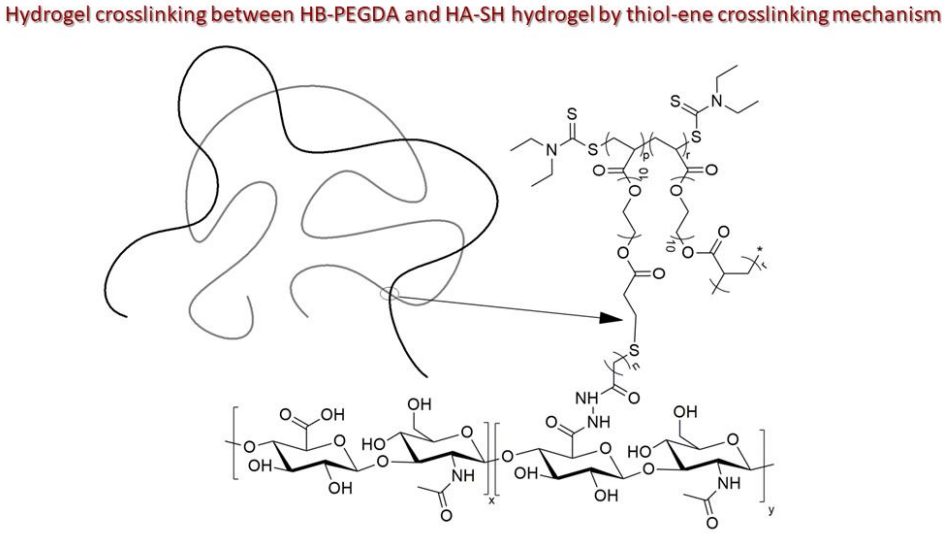

Figure 9.3 Hydrogel crosslinking between HB-PEGDA and HA-SH hydrogel by thiol-ene crosslinking mechanism. The image has been drawn by ESR01.

These HB-PEGDA/HA-SH based hydrogel systems have been reported for wound healing, cartilage regeneration, and stem cell delivery applications [1-3]. Another study used HB-PEGDA/PEGMEMA/HA-SH copolymer hydrogel to encapsulate silver sulfadiazine (SSD) as an antimicrobial agent for antimicrobial wound care application [18]. In this study, HB-PEGDA/HA-SH based hydrogel was used to encapsulate GO and glucose as a drug-free antibacterial system for healing infected wounds. For this purpose, hydrogel system was optimized for an optimum and controlled H_2O_2 release.

9.2 Materials and methods

9.2.1 HB-PEGDA/HA-SH hydrogel preparation

Briefly, HB-PEGDA polymer (Blafar Ltd., Ireland [19]) was polymerized as described above using PEGDA monomers (M_W=575Da monomers), AIBN (reaction initiator), and DS (chain transfer agent) in butanone as solvent and purged under Argon atmosphere at 70°C through RAFT polymerization reaction [3, 18, 19] where molecular weight, branching degree, as well as vinyl group content of the polymers can be easily tuned. The increase in Mw and the molar conversion of polymer was monitored through GPC (gel permeation chromatography), and the reaction was stopped when Mw of polymer reached 10-20kDa. After the polymer was purified, it was dialysed at molecular weight cut-off (MWCO) of 3500Da and stored at -20°C until next use. HB-PEGDA was crosslinked as described above using HA-SH (Blafar Ltd., Ireland [20], with 80% degree of thiolation, Mw=400kDa) through thiol-ene click chemistry [3, 18, 20].

9.2.2 GO and glucose encapsulation in HB-PEGDA/HA-SH hydrogel

The H_2O_2 releasing hydrogel samples were prepared by mixing of HB-PEGDA polymer, containing different concentrations of GO (E.C. 1.1.3.4 from Sigma) with HA-SH solution, containing a constant glucose concentration (Figure 9.4).

In detail, first HB-PEGDA polymer was dissolved in 1X PBS to prepare a 40% (w/w) stock solution. 1U is the amount of GO that catalyzes the 1µM glucose substrate into 1µM H_2O_2 within one minute [21]. The purchased GO was a lyophilized product that had an activity of 19.290 U/mg. Enzyme stock solution was prepared as 10,000U/L in 1X PBS. Enzyme solutions (named as *Solution A*, as shown in Table 9.1 and Figure 9.4) were prepared from enzyme stock solution by diluting in PBS. An equal volume of *Solution A* was mixed with 40% (w/w) HB-PEGDA solution to obtain *Solution B* (Table 9.1 and Figure 9.4).

2% (w/w) HA-SH stock solution was prepared directly in 5% (w/w) glucose stock solution (*Solution C*, as shown in Table 9.2 and Figure 9.4).

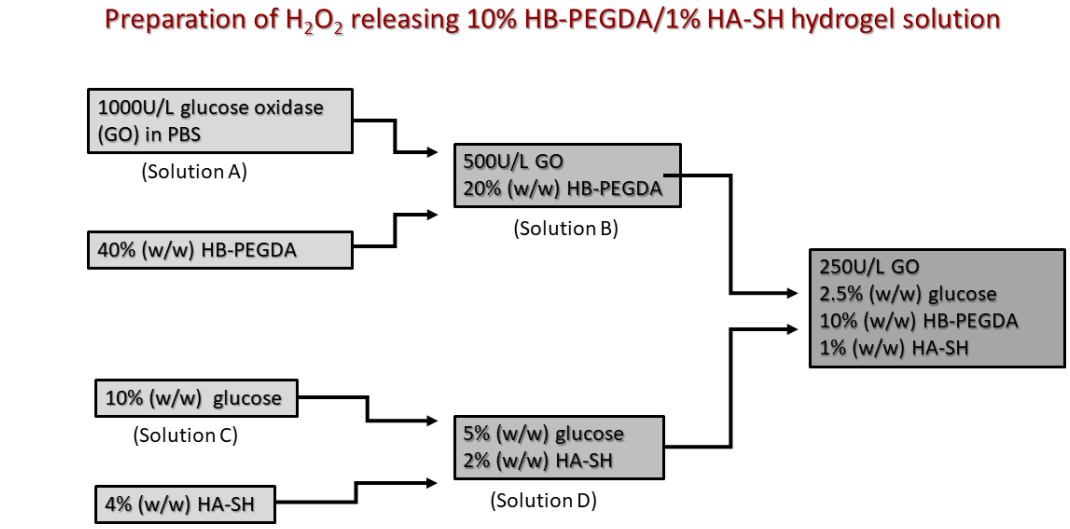

Figure 9.4 Preparation of H_2O_2 releasing 10% HB-PEGDA/1% HA-SH hydrogel solution.

Table 9.1 Enzyme concentrations prepared to form hydrogel samples.

GO solution in PBS (U/L) *(Solution A)*	GO concentration in HB-PEGDA (U/L) *(Solution B)*	GO concentration in HB-PEGDA/HA-SH crosslinked hydrogel (U/L)
0	0	0
100	50	25
200	100	50
500	250	125
1000	500	250
2000	1000	500

Table 9.2 Glucose concentration prepared to form hydrogel samples.

Glucose solution (%, w/w) prepared *(Solution C)*	Glucose concentration (%, w/w) in HA-SH *(Solution D)*	Glucose concentration (%, w/w) in hydrogel
5	5	2.5

Then *Solution B* (e.g. 15µL) was mixed with an equal volume of *Solution D* (e.g. 15µL) and waiting a few seconds until properly dispersed before pipetting (a total volume of 30µL) onto a Teflon™ surface. Following this protocol semi-spherical hydrogel beads with 5mm in diameter at the bottom side could be achieved (Figure 9.5). The 10% HB-PEGDA/1% HA-SH hydrogel samples were named according to the concentration of encapsulated GO such as 500U/L, 250U/L, 125U/L, 50U/L, 25U/L.

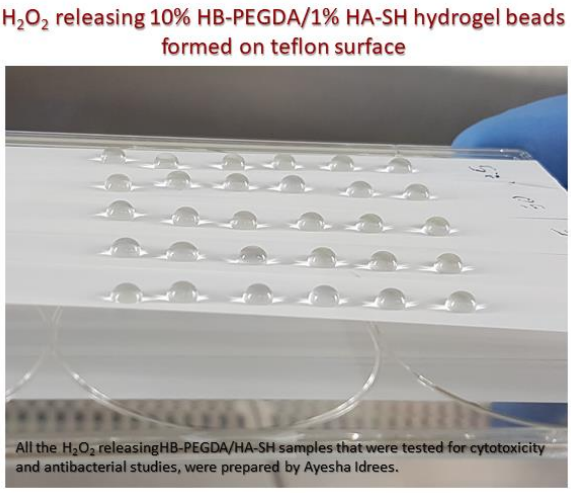

Figure 9.5 H_2O_2 releasing 10% HB-PEGDA/1% HA-SH hydrogel beads formed on a teflon surface.

9.2.3 Measurement of H_2O_2 release from 10% HBPEGDA/1% HA-SH hydrogel

H_2O_2 release from hydrogel was measured by a colorimetric pertitanic acid (H_2TiO_4) method as described in [22] for 2-48 hours. For this purpose, 100µL of HB-PEGDA/GO and 100µL of HA-SH/glucose solutions were pipetted in an Eppendorf tube, mixed well and allowed to gelatinize. Then, 9800µL of deionized water was added to this 200µL of hydrogel sample and placed at 37°C. The H_2O_2 release at a given time point was quantified by pipetting 100µL of this solution and mixing it with 50µL of titanium sulphate solution. *In situ* generated H_2O_2 reacting with Ti^{4+} changed the color of the solution to yellow. This color change was analyzed by UV/VIS spectrophotometry and absorbance was measured at 407nm. Measured concentrations of diluted H_2O_2 were calculated based on a standard calibration curve that was obtained by pipetting 100µL of each of the known concentration of H_2O_2 (conc. range of 0-20mM) in a 96-well plate format (Figure 9.6). 50µL of assay solution was added into each well and the plate was shaken for 15sec. The absorbance was measured using SpectraMax (M3) multi-mode microplate reader from Molecular Devices.

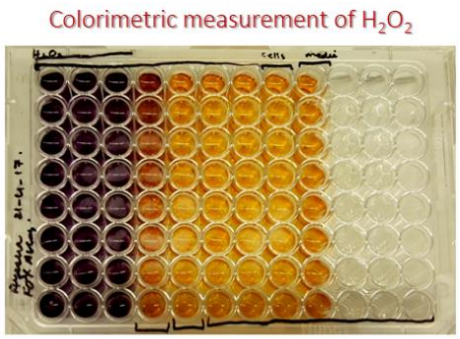

Figure 9.6 Colorimetric measurement of H_2O_2.

9.2.4 Cytotoxicity evaluation

Cells and cell culture maintenance

Primary cells including normal human dermal fibroblasts (NHDF) and normal human epidermal keratinocytes (NHEK) were obtained from PromoCell. Cell lines including L929 (murine fibroblast cell line), HaCaT (a transformed human keratinocyte cell line), and COCA (a non-transformed murine epidermal cell line), were obtained from DSMZ (German collection of microorganisms and cell cultures), CLS (cell line services Germany), and ECACC (European collection of authenticated cell cultures), respectively.

NHDF were maintained in CnT-Prime fibroblast medium (CnT-PR-F, CELLnTECH) while NHEK and COCA were maintained in CnT-Prime epithelial culture medium (CnT-PR, CELLnTECH) under the physiological culture conditions (37°C, 5% CO_2), and sub-cultured using DetachKit-Promocell HEPES BSS (2-[4-(2-hydroxyethyl)piperazine-1-yl] ethanesulfonic acid buffered saline solution); 0.04% Trypsin/0.03% EDTA (ethylenediaminetetraacetic acid); and TNS (trypsin neutralizing solution) containing 0.05% trypsin inhibitor from soybean/0.1% bovine serum albumin). L929 cells were maintained in RPMI 1640 cell culture medium with stable glutamine without glucose (PAN Biotech, P04-18500), containing 10% foetal bovine serum (FBS; PAN Biotech) under physiological culture conditions (37°C, 5% CO_2), and sub-cultured using 0.25% trypsin (Gibco). HaCaT cells were maintained in DMEM cell culture medium (PAN Biotech) containing 10% FBS under physiological culture conditions (37°C, 5% CO_2), and sub-cultured using TrypLE^{TM} Express (Thermo Fisher).

Fabrication of in vitro 3D skin model

The *in vitro* 3D skin model (named as human skin equivalent or HSE) was obtained having both a dermal and an epidermal compartment, by first embedding NHDF in rat tail tendon collagen type I (Col. I) hydrogel from Ibidi (mimicking dermal extracellular matrix or ECM) to fabricate the dermal construct and then later seeding NHEK on it to generate the epidermis. The 3D cell culture conditions were optimized to obtain a closely

in vivo tissue mimicking HSE. The HSE development and full characterization were described in detail in Chapter 04.

Cytotoxicity evaluation of hydrogels with cells – Direct contact, indirect contact, adapted direct contact tests

Defined aliquots of cell suspensions for each cell type were used as: NHDF (P4 to P6) 0.6 X 10^5 cells/well, NHEK (P4 to P6) 1.3 X 10^5 cells/well, L929 (P7 to P10) 0.7 X 10^5 cells/well, COCA (P7 to P10) 0.7 X 10^5 cells/well, and HaCaT (P35 to P37) 2.5 X 10^5 cells/well were pipetted in 24 well plates. The culture was incubated at 37°C, 5% CO_2 for 24 hours. The cell's sub-confluency and morphology were verified before exposing the cells with hydrogel samples. Culture medium was removed and replaced with fresh medium (1mL) before starting the test.

The GO encapsulated hydrogel samples were freshly prepared right before exposing them with cell monolayer culture either through direct, indirect, or adapted direct contact method (Figure 9.7). For direct contact test, freshly prepared hydrogel samples were placed directly on the cell monolayer in the centre of wells without making unnecessary movements of the specimens. Thus, each sample of 5mm in diameter covered approx. 1/3rd growth area of the well surface of 24-well cell culture plate.

For indirect contact test, the hydrogel samples were exposed to L929 cells through 24 well Transwell inserts (PET membrane, 1µm pore size, 6.5mm in diameter, Sarstedt.), in 24 well cell culture plate. The cell culture media volume at apical (250µL) and basal sides (800µL) of inserts was maintained at the same level outside and inside the Transwell inserts.

For adapted direct contact test, freshly prepared hydrogel samples were pretreated (or equilibrated) in respective cell culture media for 5+5 min and placed in the centre of cell monolayer culture without making unnecessary movements of the specimens.

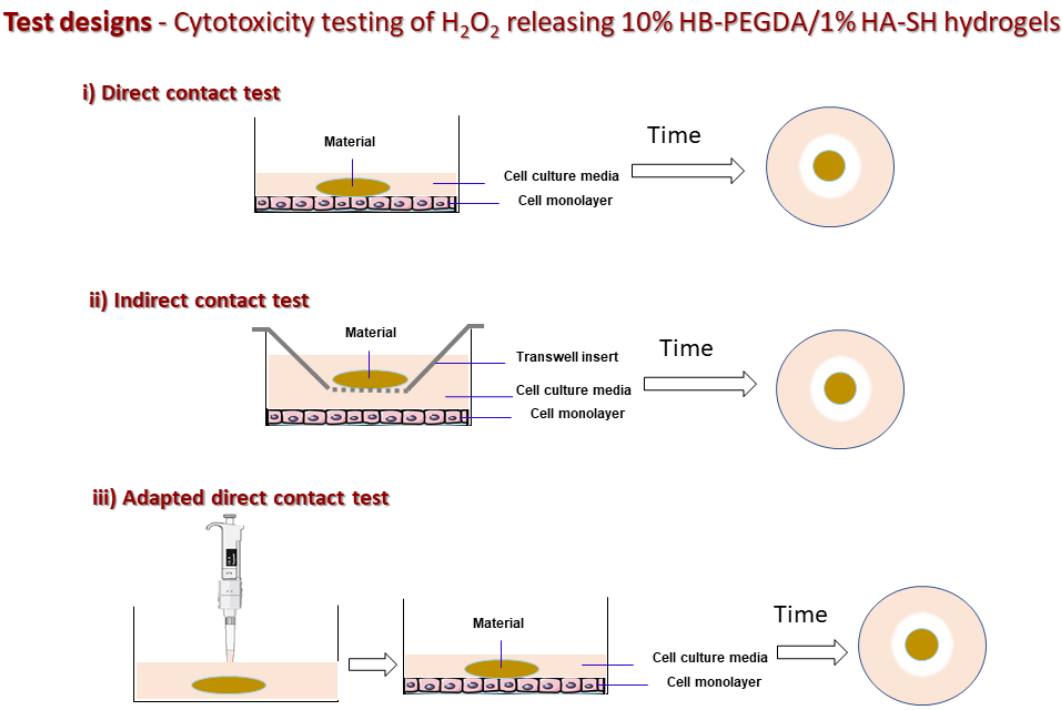

Figure 9.7 Test designs - Cytotoxicity testing of H_2O_2 releasing 10% HB-PEGDA/1% HA-SH hydrogels. i) Direct contact, ii) indirect contact, iii) adapted direct contact tests

The wells without any sample exposure served as "TCPS (tissue culture treated polystyrene) control", while the sample treated with lysis solution (9% Triton® X-100 in water from Promega) served as "lysis control". 10% HB PEGDA/1% HA-SH hydrogels without any loaded or encapsulated GO were named as 0U/L (or so-called polymer control). The well plate was then incubated at 37°C, 5% CO_2 for 24 hours. The next day, supernatant culture medium and specimens were carefully removed, and CellTiter-Blue® assay (CTB, Promega) was performed for measuring the cell viability according to standard protocols [19]. To this aim, 400µL CTB reagent (this vol. was enough to cover the surface of TC 24 well) was pipetted per well for 2 h at 37°C and 5% CO_2. The cell supernatant was transferred to black microtiter 96-well plates. The fluorescence was measured at excitation (Ex) of 560nm and emission (Em) of 590nm.

Cytotoxicity evaluation of hydrogels with in vitro 3D skin model

The cytotoxicity evaluation of hydrogels onto HSE was measured by direct contact test (Figure 9.8), and the detailed protocol is as followed. Hydrogel samples were placed on the top of HSE carefully using the sterile forceps and 500µL CnT-PR-3D medium was pipetted to wet the material. The level of the medium was kept similar outside and inside the HSE containing Transwell inserts.

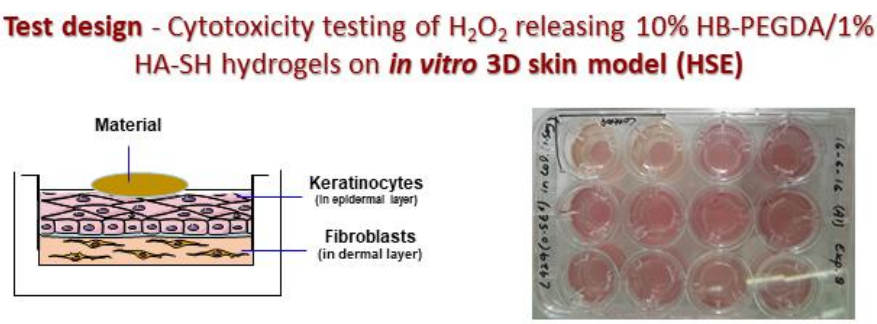

Figure 9.8 Test design - Cytotoxicity testing of H_2O_2 releasing 10% HB-PEGDA/1% HA-SH hydrogels on in vitro 3D skin model (HSE).

The hydrogel treated HSEs were placed at 37° C and 5% CO_2 for 24 hours. After the incubation, the tested samples were removed using forceps and HSEs were rinsed thoroughly with sterile PBS 3 times to remove all the residual material. The remaining PBS was gently removed and HSE were transferred to 24 well plate by cutting the Transwell membrane. The cell viability was measured by CTB assay. For this 400µL CTB reagent per well (this vol. is enough to completely dip the HSEs) was pipetted and incubated for 3h at 37°C and 5% CO_2. The cell supernatant was transferred to black microtiter 96-well plates. The fluorescence was measured at Ex/Em 560/590 nm. PBS treated HSE served as negative control and 5%SDS treated HSE served as positive controls for cytotoxicity evaluation of samples. The relative tissue viability of each tissue was calculated as a percentage of the viability of the mean of the negative controls

Microscopic analysis

Changes in morphological appearance and visualization of live and dead cells, were evaluated using bright field and fluorescent microscopy (Olympus IX51). Fluorescent staining was performed using Live/Dead imaging (Promokine) using calcein-AM and ethidium homodimer III (EthD-III) to see live (green-fluorescence for live cells by enzymatic conversion of non-fluorescent substrate, Ex/Em ~495nm/~515nm) and dead (red-fluorescence for dead cells upon binding to nucleic acid, Ex/Em ~530nm/~635nm) cells.

9.2.5 Antibacterial activity

Staphylococcus aureus (ATCC 29213), *Staphylococcus epidermidis* (ATCC 12228), *Escherichia coli* (ATCC 25922), *Pseudomonas aeruginosa* (ATCC 27853), *Enterococcus faecalis* (ATCC 29212), and *Acinetobacter baumannii* being the most relevant bacteria in infected wounds, were used to evaluate antibacterial activity of H_2O_2 releasing hydrogels. Additionally, resistant strains with most commonly found resistance-phenotypes were also tested including *Methicillin-resistant Staphylococcus aureus (MRSA)*, *Methicillin-resistant Staphylococcus epidermidis (MRSE), VIM-2*

producing drug resistant Pseudomonas aeruginosa [20] (VIM-2 β-lactamases producing multidrug-resistant *P. aeruginosa*)*, KPC-2 producing drug resistant Escherichia coli [21]* (*Klebsiella pneumoniae* carbapenemase-producing *E. coli*) (national reference center for gram negatives). The disc-diffusion test was performed for antimicrobial susceptibility testing according to EUCAST (European Committee on Antimicrobial Susceptibility Testing) guidelines [22]. Bacterial strains were revived and cultured on fresh Mueller-Hinton (MH) agar one day before testing. The well-isolated colonies were suspended in 0.9% normal saline and adjusted to McFarland 0.5 [23]. The inoculum was spread evenly over the entire surface of MH agar using a sterile cotton swab. The freshly prepared hydrogel samples (30µL) constituted ~5mm in diameter bead-shaped discs, that were applied on agar plate within 15 min of bacterial inoculation. The plates were then incubated at 37°C for 16-20 hours (within 15 min of disc application). The zone of inhibition (ZOI, in mm) was measured using a scale bar by reading the MH plates from the back against a dark background and zone edges were read at the point of complete inhibition.

9.3 Results & Discussion

This section initially discusses the main physicochemical properties of HB-PEGDA/HA-SH hydrogels, including their ability to release H_2O_2 when loaded with glucose (G) and GO enzyme. This data was provided by the Ph.D. student Jeddah Marie Vasquez (ESR01) (Politecnico di Torino, Italy) who carried out this activity.

Based on the underlined physicochemical properties, the second part of the section discusses the biological properties of HB-PEGDA/HA-SH hydrogels, including cell viability by direct contact, indirect contact and "modified (or adapted)" direct-contact tests, using both primary cells and cell lines, as well as hydrogel antibacterial properties. This part of the activity, including G/GO encapsulation in HB-PEGDA/HA-SH hydrogels was carried out by the Ph.D. candidate Ayesha Idrees.

9.3.1 HB-PEGDA polymer and HB-PEGDA/HA-SH hydrogel

The HB-PEGDA had a vinyl content of 0.99mmol/g (vinyl ratio of 57mol%), Mw of 16.656kDa, and a polydispersity (PD) of 1.5. The higher vinyl content (as analyzed by NMR spectra) was associated with greater chances of polymer crosslinking. Thus, the degree of branching (DB) for the HB-PEGDA was 40-60%, indicating a highly branched polymer structure due to the availability of numerous vinyl functional groups [23].

Moreover, the HB-PEGDA/HA-SH hydrogel had a quick forming property. The gelation speed and the mechanical properties of HB-PEGDA/HA-SH hydrogels could be adjusted by varying the crosslinking conditions [1]. 10% HB-PEGDA/1% HA-SH was the selected composition of polymer/crosslinker-based hydrogel due to its rapid gelation time (63 sec) as compared to 5% HB-PEGDA/1% HA-SH with 532 sec (approx. 9 min), making 10% HB-PEGDA/1% HA-SH suitable for an *in situ* forming hydrogel wound dressing. A higher amount of HB-PEGDA reduced the gelation time due to the higher number of acrylate groups available for crosslinking, demonstrating more concentrated hydrogel accelerated the gelation.

The water absorbed by hydrogel was <10% of its mass during the first two weeks. Though, 10% HB-PEGDA/1% HA-SH was able to keep its semi-rigid structure even by 64 days and maximum water uptake (131%), demonstrating the stability of hydrogel matrix.

9.3.2 H_2O_2 release from HB-PEGDA/HA-SH hydrogel

Glucose being very low in molecular weight (180g/mol) would freely diffuse through the liquid phase within the 3D hydrogel matrix to interact with the physically encapsulated GO (molecular weight 160kDa [24]). Results showed that H_2O_2 release increased with time, however, approx. 50% of the H_2O_2 concentration was produced during the first two hours, with a decreasing rate in later hours (Figure 9.9). This might

be due to the higher possibility of contact between GO and mobile glucose molecules in the initial stages through the liquid phase of hydrogel. 5% HB-PEGDA/1% HA-SH produced more H_2O_2 than 10% HB-PEGDA/1% HA-SH. This might be a result of higher porosity due to lower polymer concentration thus, favoring more free interaction between encapsulated GO and glucose (Figure 9.9). Based on the literature study, where 10mM H_2O_2 stimulated the wound healing in mice [25], 10-20mM H_2O_2 release by hydrogels was the aimed concentration by ESR01. 10% HB-PEGDA/1% HA-SH Hydrogel with 250U/L GO produced 16.02±4.16mM H_2O_2 for 24 hours that slightly increased for 48 hours. Thus, 10% HB-PEGDA/1% HA-SH Hydrogel with 250U/L encapsulated GO produced an H_2O_2 concentration in 24 hours more close to the target H_2O_2 concentration than 5% HB-PEGDA/1% HA-SH Hydrogel with 250U/L encapsulated GO (Figure 9.9).

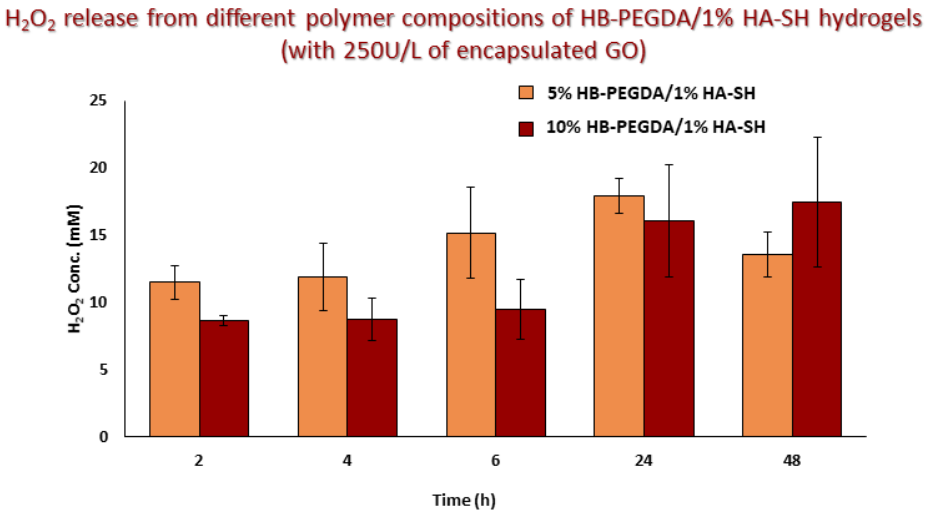

Figure 9.9 H_2O_2 release from different polymer compositions of HB-PEGDA/1% HA-SH hydrogels (with 250U/L of encapsulated GO). This release data was obtained under stirring (dynamic) conditions.

The GO is the limiting agent that can produce H_2O_2 at a specific rate with respect to its activity until the saturation curve is reached depending on the substrate concentration (i.e. glucose). The effect of encapsulated glucose concentration was evaluated as shown in Figure 9.10. H_2O_2 release data comparing 2.5% (w/w) and 5.0% (w/w) glucose concentrations at each time (24 h or 48 h) showed that the hydrogels with 2.5% glucose were able to show an increase in H_2O_2 production when the GO conc. was increased from 250U/L to 500U/L (as indicated by black solid arrow), as compared to the effect observed with 5% glucose. Thus, 2.5% was chosen as encapsulated glucose concentration.

The graph also showed that 250U/L hydrogel [with 2.5% (w/w) glucose] was able to produce H_2O_2 until 48 hours (as indicated by dotted arrow), though the release was only slightly higher at T_{48h} with respect to T_{24h} (but differences were not statistically

significant). As 500U/L GO did not increase significantly H_2O_2 production with time, 250U/L was selected.

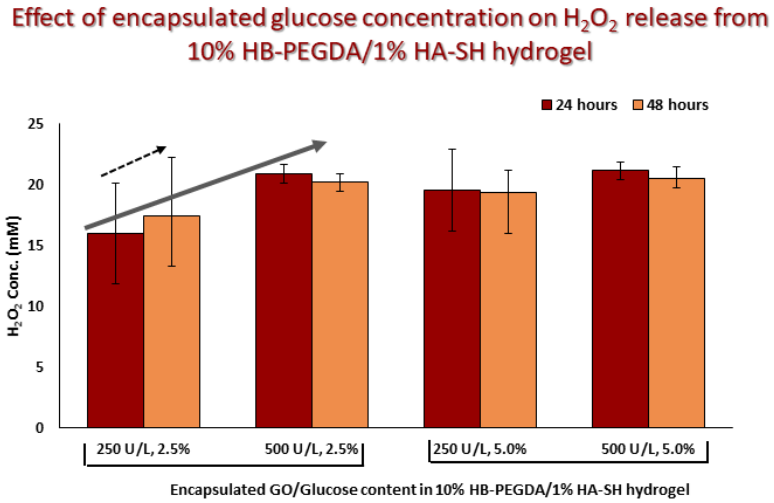

Figure 9.10 Effect of encapsulated glucose concentration on H_2O_2 release from 10% HB-PEGDA/1% HA-SH hydrogel. This release data was obtained under stirring conditions. The mean values of 250U/L hydrogels between 2.5% and 5% glucose content demonstrated higher glucose concentration had an effect on H_2O_2 production, though the effect was not statistically significant.

H_2O_2 release from 10% HB-PEGDA/1% HA-SH Hydrogel with 250U/L GO and 2.5% glucose was 9.11±0.92mM after 24 h while it was 8.21±0.47mM for the same hydrogel with 500U/L GO (Figure 9.11).

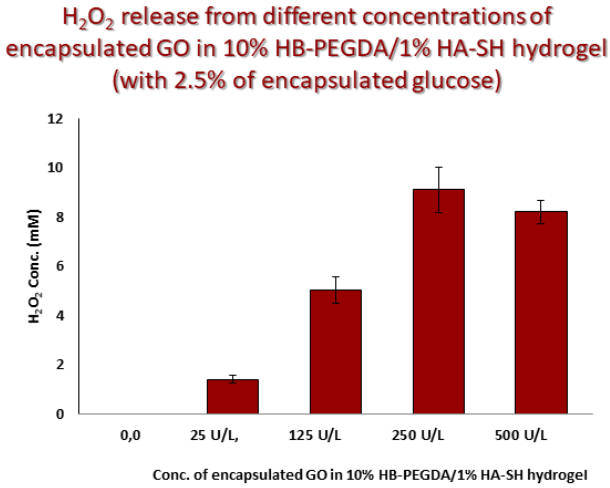

Figure 9.11 H_2O_2 release from different concentrations of encapsulated GO in 10% HB-PEGDA/1% HA-SH hydrogel (with 2.5% of encapsulated glucose). This release data was obtained under non-stirring conditions and considered to correlate with bio-evaluation data that were also performed under non-stirring conditions (static conditions).

An increasing release of H_2O_2 was observed with an increasing amount of encapsulated GO (Figure 9.11). However, the release test results in static and dynamic conditions

demonstrated significant differences. For example, the release measured was 16.02±4.16mM and 20.93±00.78mM by 250U/L and 500U/L GO hydrogel, respectively under stirring conditions (Figure 9.10). While under non-stirring conditions, the release values were 9.11±0.92mM and 8.21±0.47mM by 250U/L and 500U/L GO hydrogels, respectively (Figure 9.11). The release data obtained under non-stirring conditions were considered to correlate with bio-evaluation data (e.g. cytotoxicity) that were also performed under static conditions.

9.3.3 Cytotoxicity analysis

The optimal polymer/crosslinker-based hydrogel composition was 10% HB-PEGDA/1% HA-SH due to its closeness to the desired properties of hydrogel gelation time, structure stability, and H_2O_2 release as selected by ESR01. Particularly, the ROS release analysis showed that 10% HB-PEGDA/1% HA-SH hydrogel samples with encapsulated glucose (2.5%) and GO at various concentrations (25U/L, 50U/L, 125U/L, 250U/L, 500U/L) resulted in varying amount of H_2O_2 release, demonstrating 10%HB-PEGDA/1%HA-SH hydrogel with 250U/L and 2.5% glucose as optimal for targeted concentration of H_2O_2 release. Therefore, this composition was proceeded for subsequent cytotoxicity and antibacterial evaluation.

Though, the released H_2O_2 interaction with cells would determine the optimal GO concentration to be encapsulated in these hydrogels. That would be able to induce the cells for wound healing as well as still retaining antibacterial activity against colonized bacteria (which is a very ideal condition).

is important for these hydrogels to be antibacterial and still cytocompatibility on wounds.

on wounds that are yet able to show ROS-induced antibacterial activity.

Cell lines were used to assess general *in vitro* cytotoxicity based on DIN EN ISO 10993-5 e.g. L929, HaCaT, and COCA. While primary cells being clinically more relevant [26] were used to evaluate the specific cytotoxicity e.g. using specific primary cells such as NHDF and NHEK. Additionally, *in vitro* bio-evaluation being more accurate in 3D systems [25-27], the *in vitro* skin model was also used to evaluate the cytotoxicity of hydrogel samples.

Cell-based assays being routinely used are based on a specific biomarker for detecting cytotoxicity. In this study, the cell viability was evaluated by CTB assay that measures the resazurin reduction into a highly fluorescent product resorufin by mitochondrial, cytosolic, and microsomal enzymes [27] of living cells. Non-viable cells being metabolically affected were no longer able to reduce the indicator dye.

Moreover, the type of test procedure depends on the type of assessment in question e.g. the effect of extract, diffusible leachable, or the test sample itself. The cytotoxicity results highly depend on the test design used to evaluate the respective materials. For

this reason, in this study, H_2O_2 releasing hydrogels were evaluated by direct contact, indirect contact, and adapted direct contact methods.

Direct contact test

Direct contact test with L929

In the direct contact method, H_2O_2 releasing hydrogel samples (5mm in diameter) were placed in direct contact with cell monolayer on 24 well plate (15mm in diameter). The graph demonstrated a decrease in cell viability with an increase in GO and thus H_2O_2 production (Figure 9.12-A).

The effect of polymer concentration on cell viability was tested by encapsulating a constant GO (i.e 250U/L) in 5% and 10% HB-PEGDA hydrogels. The results demonstrated an increase in cell viability by 28% with the decrease in polymer concentration (Figure 9.12-B). It can be speculated that some residue was leached out from the polymer (e.g. unpolymerized polymer chains), and such leachable amount increased with increasing the polymer concentration, leading to higher cytotoxicity. The cytotoxicity of the cytotoxic agent (mechanism) might be due to its adsorbance to the TCPS surface subsequently preventing the attachment of cells, or causing the already attached cells to detach, or the agent was surface active thus disturbing the cell membrane integrity. To understand the mechanism of action, further experiments should be carried out. However it is interesting to note that hydrogels with lower polymer conc. (5% HB-PEGDA) demonstrated comparatively higher H_2O_2 release than 10%HB-PEGDA hydrogels (Figure 9.9), due to their higher porosity.

A cell culture media with glucose showed comparatively increased cytotoxicity as tested at constant GO i.e. 250U/L (Figure 9.12-C), demonstrating that glucose presence in cell culture media had an impact on H_2O_2 production. For example, 250U/L GO hydrogels demonstrated ~35% cytotoxicity in glucose-free media as compared to ~92% cytotoxicity in glucose-containing media, with a total difference by 57% (Figure 9.12-B and -C). This data can also be correlated with H_2O_2 release data (Figure 9.10) where increasing the encapsulated glucose conc. from 2.5 to 5% at constant GO conc. (i.e. 250U/L) resulted in higher H_2O_2 release from 16mM to 19.5mM, respectively. This demonstrated a proportional effect of glucose conc. on enzymatic activity and the amount of H_2O_2 production. Since L929 cells are most easy and rapidly growing cell line, GO/G encapsulated hydrogels were also tested in glucose-free media. Related to this, it would be worth mentioning that the nutritional value (including glucose content) of each cell culture media is highly specific to the growth requirements of different cell types. For example, the glucose content of cell culture media used in this study was as following: 2mg/mL of RPMI 1640, 4mg/mL of DMEM, 0.9mg/mL of CnT-F, CnT-P, and CnT-PR-3D each. While a 5mm hydrogel bead, that was constituted by 30µL of hydrogel contained a total of 0.75mg glucose per hydrogel bead sample. This

demonstrated the inter-variation in total glucose content per system. It is scientifically neither achievable nor suitable to exclude glucose from the various cell culture media to study the sole impact of GO/G encapsulated hydrogel system, as it would add the variables related to abnormal cell growth and/or associated unseen molecular mechanisms in cells, resulting in false and invalid outcomes. Moreover, "peroxide consumption" by serum proteins had a great impact on cytotoxicity, resulting in different levels of available H_2O_2 for different cell types. For examples, L929 and HaCaT were grown in 10%FBS containing cell culture media. While COCA and human primary cells were grown in fully-defined and animal component-free cell culture media. Being a complicated system for *in vitro* cytotoxicity analysis, GO/G encapsulated hydrogel system was investigated under normal (most optimal per cell type) cell culture conditions, however, evaluated under three different test designs and with five different cell types.

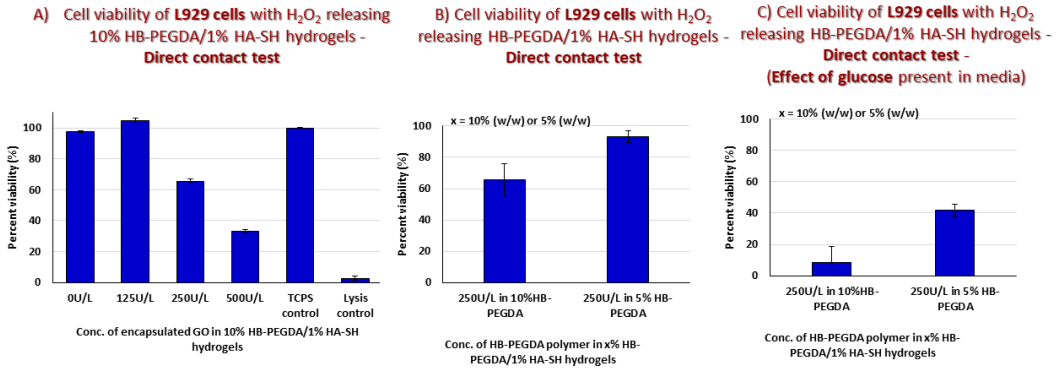

Figure 9.12 A) Cell viability of L929 cells with H_2O_2 releasing 10% HB-PEGDA/1% HA-SH hydrogels - Direct contact test. B) Cell viability of L929 cells with H_2O_2 releasing x% HB-PEGDA/1% HA-SH hydrogels - Direct contact test. C) Cell viability of L929 cells with H_2O_2 releasing HB-PEGDA/1% HA-SH hydrogels - Direct contact test - (Effect of glucose present in media).

Direct contact test with HaCaT

An increased HaCaT cells cell viability was found for hydrogel exposed wells as compared to TCPS control, indicating that the material might have stimulated the HaCaT cells (Figure 9.13). The observed effect might be either due to higher proliferation or increased metabolism. Expression profile for cell division and energy metabolism genes would provide the next hint.

The graph demonstrated a decrease in cell viability with an increase in H_2O_2 production. Though, as compared to L929 (a fibroblast cell line), HaCaT (a keratinocyte cell line) appeared to be more resistant to H_2O_2 induced cytotoxicity.

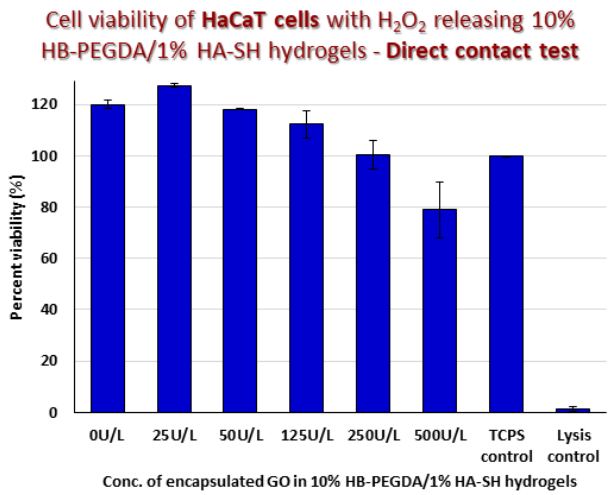

Figure 9.13 Cell viability of HaCaT cells with H_2O_2 releasing 10% HB-PEGDA/1% HA-SH hydrogels - Direct contact test.

Direct contact test with NHDF and NHEK

Due to the observed cytotoxicity of higher GO concentrations with L929 fibroblasts, hydrogels with lower GO concentrations (<125U/L) were also prepared and evaluated with human primary cells. The next graphs demonstrated a decrease in cell viability with an increase in H_2O_2 production (Figure 9.14 & Figure 9.15). Though, as compared to L929, primary cells i.e. NHDF and NHEK demonstrated higher sensitivity towards H_2O_2 induced cytotoxicity. Moreover, between these two primary cell types, NHEK appeared more vulnerable to cytotoxic damage than NHDF. For example, 25U/L caused ~50% cytotoxicity with NHEK, while in case of NHDF, a same amount of cytotoxicity (~50%) was caused by a higher GO conc. of 125U/L.

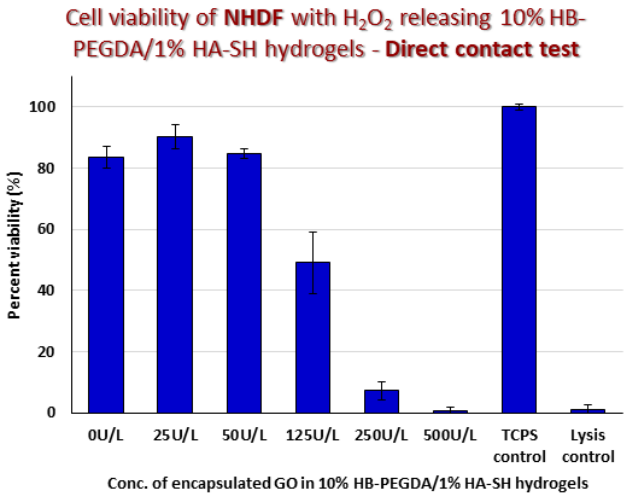

Figure 9.14 Cell viability of NHDF with H_2O_2 releasing 10% HB-PEGDA/1% HA-SH hydrogels - Direct contact test.

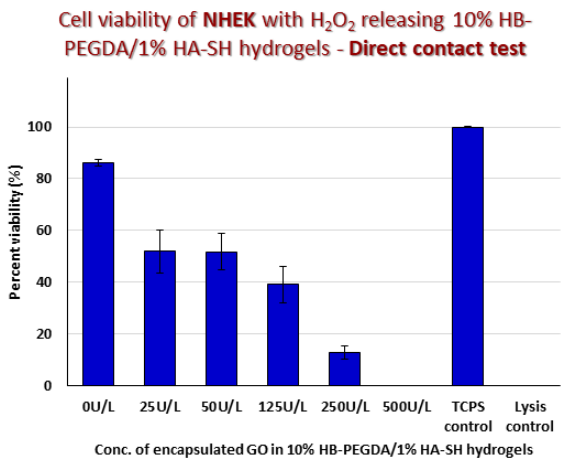

Figure 9.15 Cell viability of NHEK with H_2O_2 releasing 10% HB-PEGDA/1% HA-SH hydrogels - Direct contact test.

Direct contact with COCA cells

HaCaT is an immortalized human keratinocyte cell line and is widely used as an alternative of primary keratinocytes for cytotoxicity evaluation of materials. But HaCaT cells are deficient in the intrinsic genetic variability of primary cells, hardly capable of differentiation, and have very high tendency to proliferate [28-30]. On the other hand, COCA is a non-transformed murine epidermal cell line with non-tumorigenic behavior. Like human keratinocytes it has the capacity to normally grow and differentiate into 3D tissue under optimal 3D cell culture conditions. Therefore, besides using HaCaT cell line, we also used a more closely simulating keratinocyte cell line i.e. COCA cells. The results demonstrated that the cytotoxic effect was similar to the one demonstrated by NHEK (Figure 9.16 & Figure 9.15). The graph demonstrated a steep decrease in cell viability with an increase in H_2O_2 production (Figure 9.16).

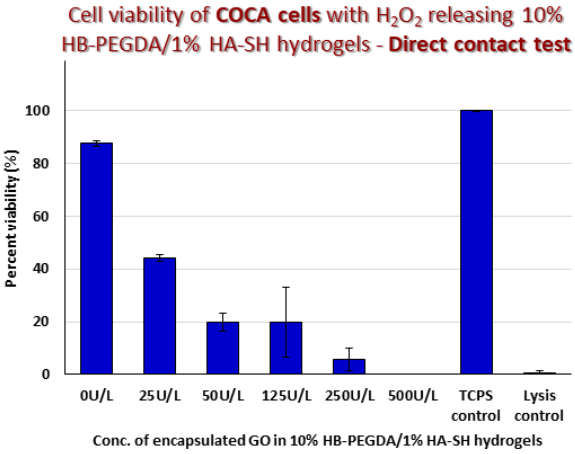

Figure 9.16 Cell viability of COCA cells with H_2O_2 releasing 10% HB-PEGDA/1% HA-SH hydrogels - Direct contact test.

Direct contact test with *in vitro* 3D skin model

H_2O_2 releasing hydrogel samples were also tested in an *in vitro* 3D skin model as an in-house advanced and complex cell culture system. The graph demonstrated an increased cell viability of hydrogel exposed-3D skin constructs as compared to untreated 3D skin constructs (Figure 9.17). The observed effect might be a result of an activated state of skin due to a combined effect from the polymer and released H_2O_2. ROS at sub-micromolar levels might act as intra- and intercellular "messengers" promoting growth responses in cell culture either by interacting with certain receptors or by oxidizing signal transduction molecules [31, 32].

Human keratinocytes are usually very responsive to external stimuli, when cultured *in vitro*. A damage can cause the cells to undergo a re-epithelialization process (a process happens upon wounding *in vivo*) [63, 103], causing them to stay in an activated phase. The effect is a hyperproliferative stimuli [104, 105]: K6/K16 expression in the basal layer that is normally absent in interfollicular epidermis is induced. The occurrence of this phenomenon can be evaluated by examining the phenotypic differences in keratins expression.

Moreover, NHDF and NHEK-based 3D skin construct (acting like a tissue) demonstrated more resistant behaviour towards H_2O_2 induced cytotoxicity than NHDF- and NHEK-based 2D monolayer culture systems alone (Figure 9.14 & Figure 9.15). For example, there was no damage observed in 250U/L-exposed 3D skin construct as compared to the ~90% damage observed in 250U/L-exposed NHDF and NHEK monolayer cell cultures.

Moreover, the graph demonstrated a very gradual decrease in cell viability with an increase in H_2O_2 production though this effect was not significant.

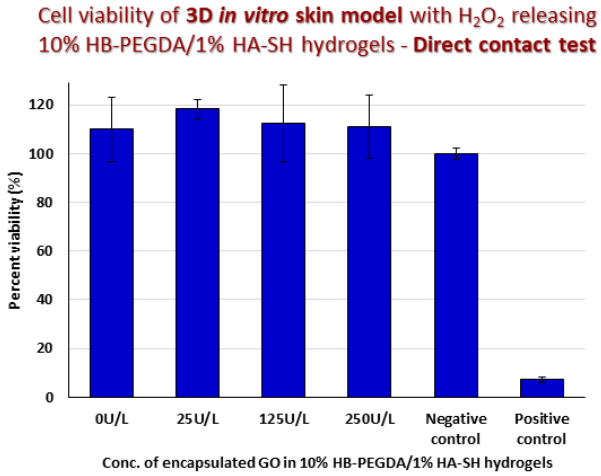

Figure 9.17 Cell viability of 3D in vitro skin model with H_2O_2 releasing 10% HB-PEGDA/1% HA-SH hydrogels - Direct contact test.

Indirect contact test

Indirect contact test with L929

Additional experiments were carried out to exclude certain factors observed in direct contact test. For example, a direct contact of a biomaterial on top of a 2D cell monolayer reduces the interface space of medium on top of the cells, that could lead to a local hypoxia (hypoxia induced cell stress). For this, the hydrogel samples were exposed to cells via an indirect contact test (through Transwell insert membrane). This time, all H_2O_2 releasing samples demonstrated comparatively higher cell viability (~75-83%) (Figure 9.18-A) than they demonstrated upon direct contact with L929 cells (Figure 9.12). Additionally, the effect of polymer concentration on cytotoxicity was also evaluated by encapsulating an equal GO (i.e. 250U/L) in 5% and 10% HB-PEGDA hydrogels. However, this time the results demonstrated no difference in cell viability between two different polymer concentrations (Figure 9.18-B). These results indicated the importance of the test design being applied for cytotoxicity evaluation. It might be that some of the released polymer chains of unpolymerized PEGDA were too high in molecular weight to cross the Transwell membrane, and thus a reduced cytotoxicity was detected upon indirect contact with cells. The indirect contact test would also serve as a supporting information for the results obtained by direct contact test (Figure 9.12 & Figure 9.18).

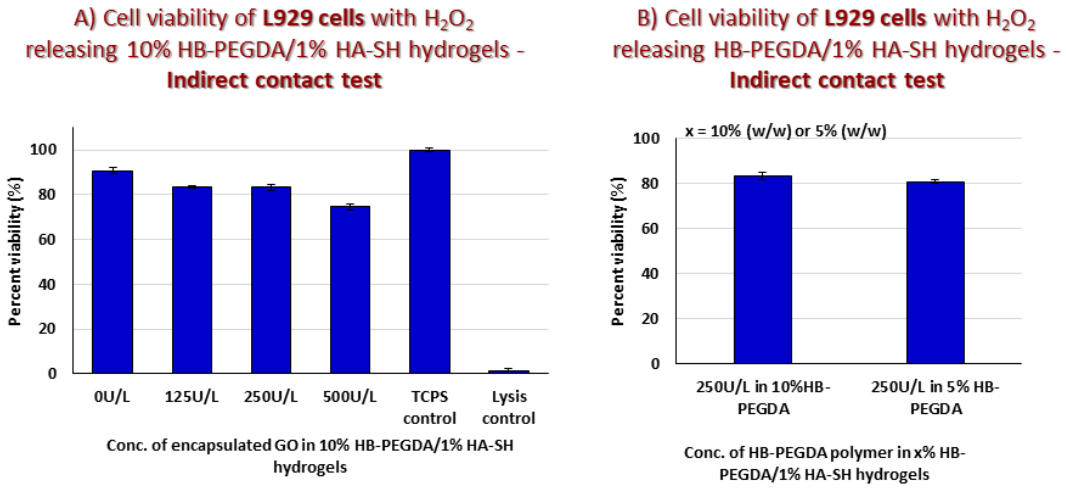

Figure 9.18 A) Cell viability of L929 cells with H_2O_2 releasing 10% HB-PEGDA/1% HA-SH hydrogels - Indirect contact test. B) Cell viability of L929 cells with H_2O_2 releasing x% HB-PEGDA/1% HA-SH hydrogels - Indirect contact test.

Indirect contact test with HaCaT and COCA cells

HaCaT cells demonstrated a good cell viability in direct contact with samples (as shown before in Figure 9.13) and similarly they behaved upon indirect contact test as well (Figure 9.19). Like direct contact test, hydrogel exposed wells demonstrated an increased

cell viability as compared to TCPS control, indicating that in case of HaCaT cells, the stimulatory effect of materials stayed as it was irrespective of used test design (Figure 9.13 & Figure 9.19). Likewise, the graph demonstrated a slight decreasing pattern in cell viability with an increase in H_2O_2 production, though this effect was not very sharp.

Similarly, to L929 cells, COCA cells also demonstrated higher viability values at all GO concentrations upon indirect contact as compared to direct contact (Figure 9.20).

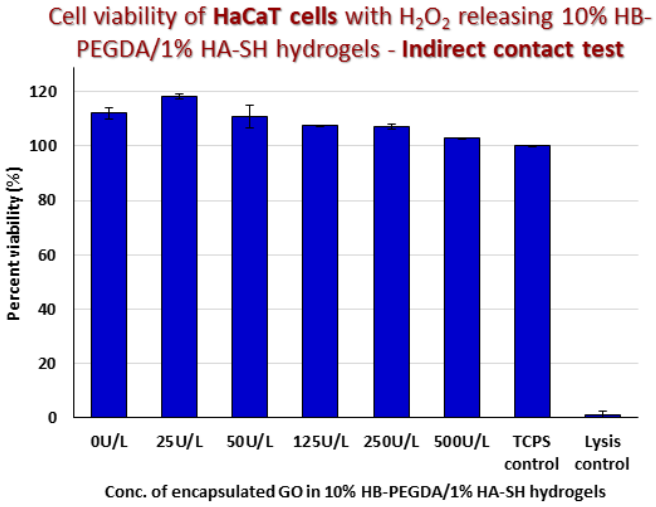

Figure 9.19 Cell viability of HaCaT cells with H_2O_2 releasing 10% HB-PEGDA/1% HA-SH hydrogels - Indirect contact test.

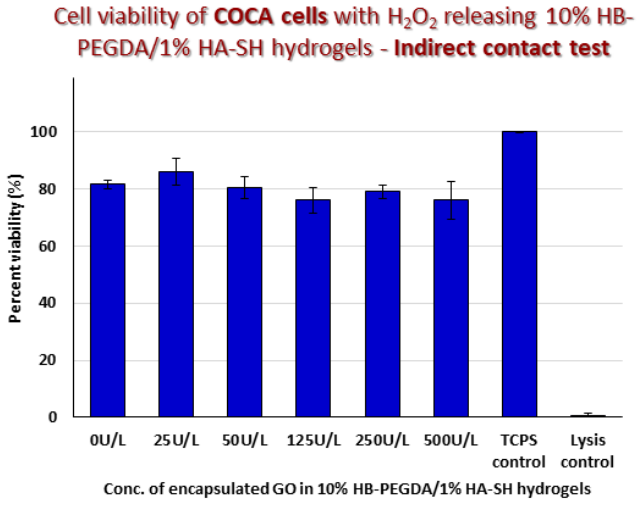

Figure 9.20 Cell viability of COCA cells with H_2O_2 releasing 10% HB-PEGDA/1% HA-SH hydrogels - Indirect contact test.

Indirect contact test with NHDF and NHEK

All H_2O_2 releasing samples (25U/L, 50U/L, 125U/L, 250U/L, 500U/L) demonstrated comparatively higher cell viability upon an indirect contact with cells (Figure 9.21 & Figure 9.22) in a range of ~68-93% with NHDF and ~83-97% with NHEK) than they demonstrated upon direct contact with cells (Figure 9.14 & Figure 9.15 in a range of ~0-90% with NHDF and ~0-52% with NHEK). Additionally, the graph demonstrated a slight decreasing pattern in cell viability with an increase in H_2O_2 production (25U/L to 250U7L), though this effect was not as sharp as it was detected under direct contact test. Interestingly this inversely proportional relationship between cell viability and GO concentrations did not stay true for 500U/L GO concentration. Enzymes have an optimal window of activation while consuming the substrate. Probably this was not an ideal GO concentration for maximal enzyme activity, and something might be competing at this concentration. Upon exceeding the encapsulated GO concentration above a certain amount (e.g. in this case >250U/L) might result in a non-uniform enzyme distribution where immobilized enzyme molecules might be located very close to each other, blocking the substrate pockets, and thus decreasing the enzyme optimal activity at this concentration, disturbing the proportional relationship between GO concentration and subsequent H_2O_2 production. These results can be correlated with H_2O_2 release (Figure 9.11) that showed that maximum H_2O_2 release was obtained at 250U/L of encapsulated GO as compared to lower and higher encapsulated GO concentrations. For example, 9.11±0.92mM H_2O_2 was released by 250U/L GO hydrogels and 8.21±0.47mM H_2O_2 was released by 500U/L GO hydrogels, though the difference was not significant (Figure 9.11).

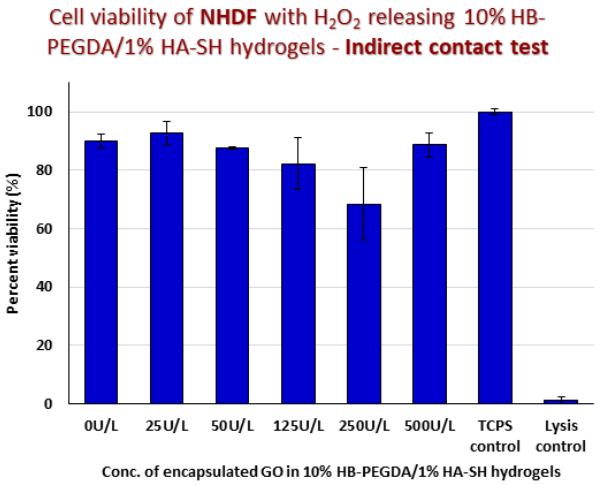

Figure 9.21 Cell viability of NHDF with H_2O_2 releasing 10% HB-PEGDA/1% HA-SH hydrogels - Indirect contact test.

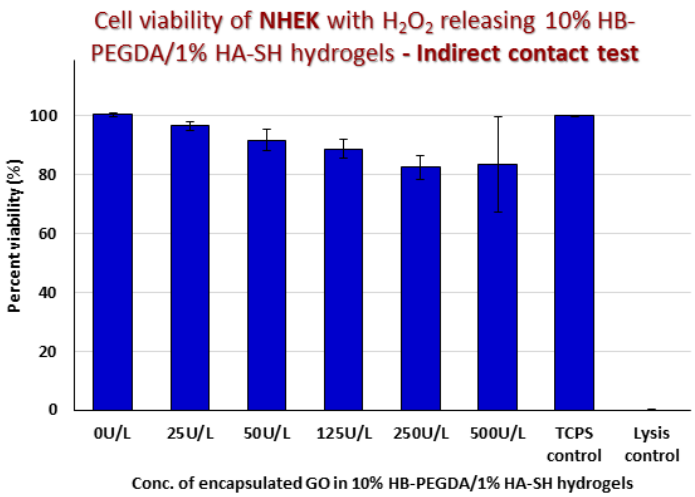

Figure 9.22 Cell viability of NHEK with H_2O_2 releasing 10% HB-PEGDA/1% HA-SH hydrogels - Indirect contact test.

If the enzyme is not homogenously distributed, it cannot be freely and appropriately reachable by substrate (i.e. glucose). Assuming two-components-based cross-linked 3D hydrogel system with multiple anchor points to immobilize GO, the GO encapsulation at high conc. (e.g. 500U/L) might change the hydrogel preparation, resulting in a higher StDev (Figure 9.22).

Adapted direct contact test

Considering the presence of wound fluid (WF) at wound site and the subsequent consumption of ROS by WF proteins [33-36], the H_2O_2 releasing hydrogels were tested in another experimental set-up named as adapted direct contact test. For this purpose, hydrogel samples were pre-exposed or pre-treated with cell culture media as a strategical approach to ensure peroxide consumption to some extent. The differences in H_2O_2 induced cytotoxicity were now evaluated by direct contact between hydrogels and cell monolayer culture.

Moreover, this experimental set-up would exclude certain factors observed in direct contact test. For example, the hydrogel samples placed directly on top of cell monolayer culture would swell over time (until swelling equilibrium is reached), squeezing the cells underneath them, causing a mechanical force-induced stress on cells. This is not the case when hydrogels samples are pre-treated, as it gives the material enough time or more time to swell and equilibrate before

As expected, the cell viability in contact with hydrogels treated according to this procedure had increased (Figure 9.23 & Figure 9.24) as compared to cell viability observed previously (Figure 9.14 & Figure 9.15), due to the peroxide consumption by proteins during pre-treatment step. Additionally, in this set-up, the polymer control (0U/L) was able to show ~100% cell viability with NHDF and NHEK as compared to

TCPS control suggesting that an assumed non-polymerized HB-PEGDA might have washed out during pre-treatment step. In previous direct contact test, NHEK demonstrated more damage than did the NHDF (Figure 9.14 & Figure 9.15). However, in this set-up the cell type-associated cytotoxic difference was no more obvious at GO conc. of ≤250U/L, demonstrating the similar extent of cell-damage towards both cell types i.e. NHDF and NHEK (Figure 9.23 & Figure 9.24). However, at 500U/L, NHDF appeared to be more damaged (54% cytotoxicity) than NHEK (26% cytotoxicity). It was speculated before that sub-optimal enzyme activity of encapsulated GO at 500U/L might be due to overloaded enzyme molecules in a cross-linked hydrogel. The pre-treatment step might compensate to recover enzyme optimal activity by removing the loosely attached molecules of GO. These findings suggest different susceptibilities of human fibroblasts and keratinocytes towards H_2O_2 induced cytotoxicity that might be linked to the differences in their antioxidant capacities and thus cell response. A study on cell defense against UV damage in cutaneous fibroblasts and keratinocytes demonstrated the presence of different levels of glutathione peroxidase, superoxide dismutase, and lipid peroxidation in these two cell types. The levels of antioxidants were found higher and lipid peroxidation lower in keratinocytes than in fibroblasts [37].

However, previous results showed cytotoxic effect of H_2O_2 hydrogels towards NHDF and NHEK upon direct contact (Figure 9.14 and Figure 9.15), where NHEK appeared more sensitive to peroxide damage than NHDF. It might be that without pre-treatment, NHEK were more susceptible towards mechanical force-induced cell stress at material-cell interface, exerted by hydrogels that started to swell in cell culture media.

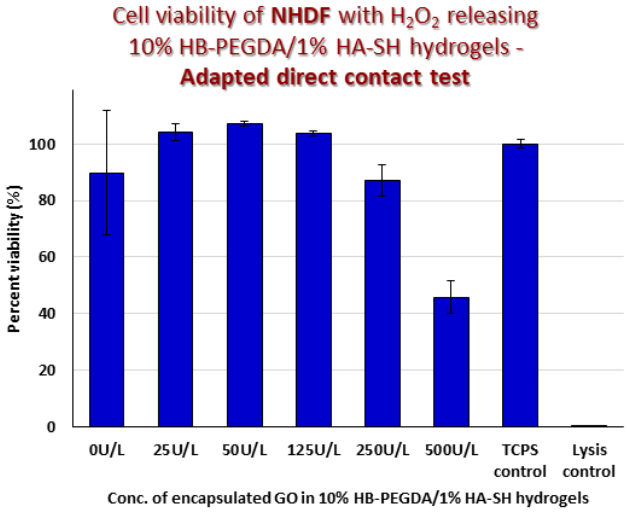

Figure 9.23 Cell viability of NHDF with H_2O_2 releasing 10% HB-PEGDA/1% HA-SH hydrogels - Adapted direct contact test.

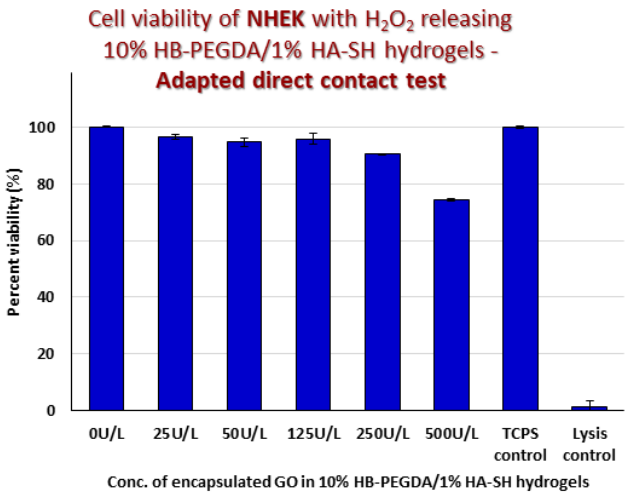

Figure 9.24 Cell viability of NHEK with H_2O_2 releasing 10% HB-PEGDA/1% HA-SH hydrogels - Adapted direct contact test.

The effects of H_2O_2 releasing hydrogels on cells were visualized by bright field (BF) microscopy and Live/Dead stained fluorescent microscopy for morphological changes and cytotoxicity visualization, respectively. For Live/Dead staining, a simultaneous staining with calcein-AM (green-fluorescence by live cells) indicated the presence of intracellular esterase activity, while EthD-III (red-fluorescent by dead cells) indicated the loss of plasma membrane integrity. TCPS (served as a negative control for cytotoxicity evaluation) was an ideal cell culture surface for adhering cells and thus demonstrated well-spread cells with normal morphology (BF micrographs) and a uniform green signal (fluorescent micrographs). While lysis control (served as a positive control for cytotoxicity evaluation) showed lysed cells and red signal as an indication of dead cells. Figure 9.25 showed BF micrographs of NHDF around the hydrogels after 24 hours exposure with hydrogen peroxide releasing hydrogel samples. The 250U/L and 500U/L hydrogels demonstrated a shrunken appearance of NHDF as compared to untreated TCPS control (Figure 9.25-i vs. -vi, -vii). Changes in morphology is a cell stress response that can be a result of fragmentation of Golgi complex, swelling of mitochondria, or alterations in cytoskeleton especially in intermediate filaments [38, 39]. On the other hand, the fluorescent images were recorded in the areas that were right under (U) and around (A) the hydrogel samples. Moreover, green and red fluorescence channels were shown separately as two individual micrographs from the same microscopic field to better visualized the live and dead cells in these areas. The fluorescent micrographs showed red signal by NHDF in U-areas and the green fluorescent signal around the hydrogels in A-areas. However, in case of 500U/L, the green fluorescent signal even in A-areas appeared to be evidently reduced, demonstrating an abundant of red signal due to induced cytotoxicity (Figure 9.26-iv). However, the simultaneous presence of green signal along with red signal demonstrated that cells cannot be considered completely dead (Figure 9.26-iv) and they still retained

some metabolic activity even at 500U/L. This result also correlated with the viability data of NHDF where cells demonstrated minimum cell viability of 46% at highest GO conc. of 500U/L (Figure 9.23). These results suggested the importance of Live/Dead staining for the visualization of the cytotoxic effects, in complementary to CTB assay i.e. a quantitative analysis of cell viability. The cytotoxic effects were more apparent in Live/Dead imaging than were in CTB assay, demonstrating that the cytotoxic effects of materials can be better understood this way. But even better by applying apoptosis analysis, transcriptomics, and proteomics in future. H_2O_2 induced cytotoxicity mechanism (either necrosis or apoptosis induced cell death) is highly dependent on the H_2O_2 concentration cells are exposed to [40]. It was reported that H_2O_2 induced cytotoxicity in human fibroblasts mainly involved a direct damage to DNA strands by generation of hydroxyl free radicals in close proximity to DNA [41, 42]. However, cells have a defensive system against oxidants including scavengers (ascorbic acid, thiols, quinols, carotenoids etc.), enzymes (superoxide dismutases, glutathione peroxidases and catalases etc), and damage repairing enzymes (methionine sulfoxide reductases, disulfide reductases or isomerases, DNA repair enzymes etc) to limit the damage [43]

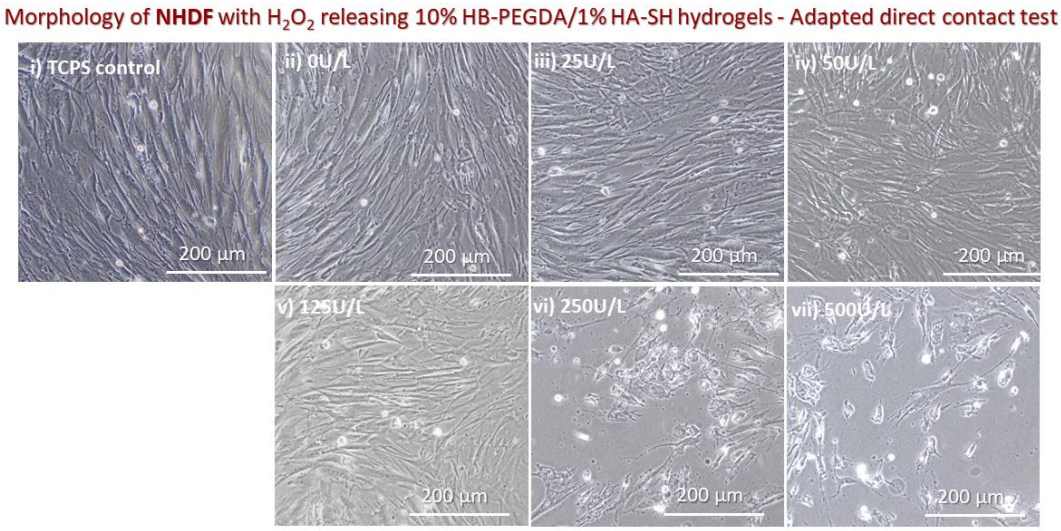

Figure 9.25 Morphology of NHDF with H_2O_2 releasing 10% HB-PEGDA/1% HA-SH hydrogels - Adapted direct contact test. The sub-images showed the cell monolayer exposed with i) TCPS, ii) 0U/L hydrogel, iii) 25U/L hydrogel, iv) 50U/L hydrogel, v) 125U/L hydrogel, vi) 250U/L hydrogel, and vii) 500U/L hydrogel.

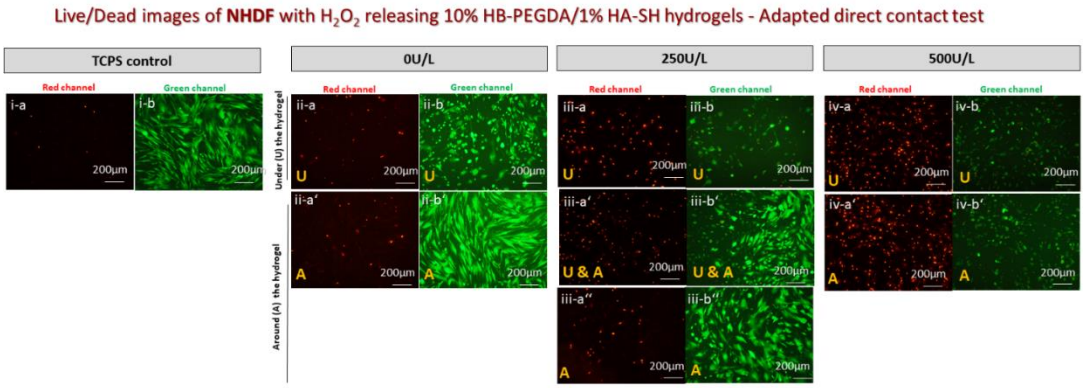

Figure 9.26 Live/Dead images of NHDF with H_2O_2 releasing 10% HB-PEGDA/1% HA-SH hydrogels - Adapted direct contact test. The sub-images showed the cell monolayer exposed with i) TCPS controls, ii) 0U/L hydrogel, iii) 250U/L hydrogel, and iv) 500U/L hydrogel. The microscopic fields showed the area under (U) and around (A) the hydrogel samples, labelled as -a & -a' for red channel in U-area and A-area, respectively. While -b & -b' for green channel in U-area and A-area, respectively.

NHEK did not show evident differences in their morphology at any concentration of encapsulated GO (Figure 9.27). Keratinocytes monolayer cultures, in general, are difficult to dissociate, as has been observed in their difficulty to detach during trypsinization *in vitro*. While COCA cells, that have a cell morphology closer to NHEK than HaCaT cells, showed an affected cell morphology at 250U/L to 500U/L based on BF micrographs (Figure 9.28-vi & - vii). Additionally, 0U/L hydrogel control also affected the cell morphology of COCA cells to some extent. This data also correlated with the CTB data, that demonstrated 77% and 25% cell viability for 250U/L and 500U/L, respectively. While 0U/L demonstrated 85% of cell viability as compared to the viability values of 94%-98% for lower concentrations of encapsulated GO (<250U/L) (Figure 9.29).

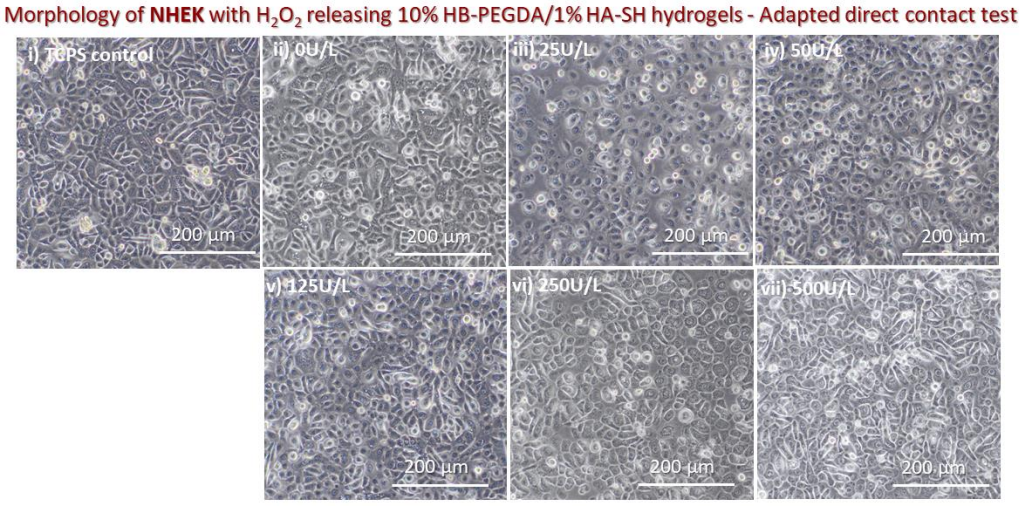

Figure 9.27 Morphology of NHEK with H_2O_2 releasing 10% HB-PEGDA/1% HA-SH hydrogels - Adapted direct contact test. The sub-images showed the cell monolayer exposed with i) TCPS, ii) 0U/L hydrogel, iii) 25U/L hydrogel, iv) 50U/L hydrogel, v) 125U/L hydrogel, vi) 250U/L hydrogel, and vii) 500U/L hydrogel.

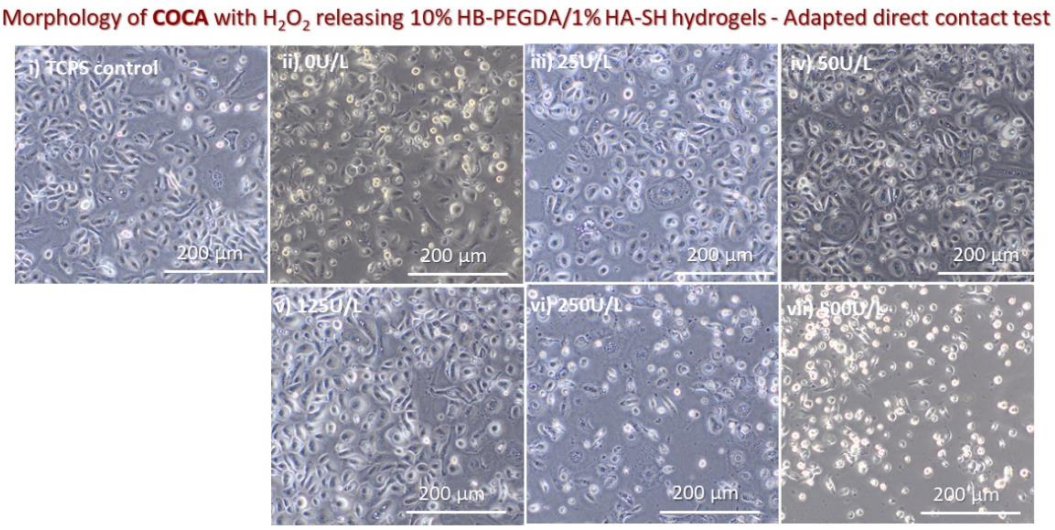

Figure 9.28 Morphology of COCA with H_2O_2 releasing 10% HB-PEGDA/1% HA-SH hydrogels - Adapted direct contact test. The sub-images showed the cell monolayer exposed with i) TCPS, ii) 0U/L hydrogel, iii) 25U/L hydrogel, iv) 50U/L hydrogel, v) 125U/L hydrogel, vi) 250U/L hydrogel, and vii) 500U/L hydrogel.

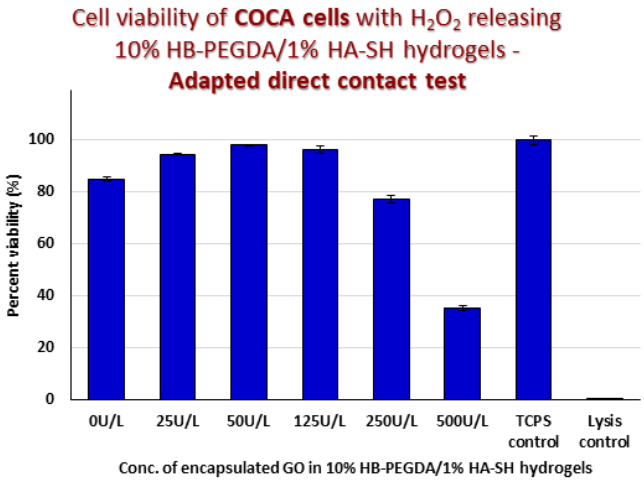

Figure 9.29 Cell viability of COCA cells with H_2O_2 releasing 10% HB-PEGDA/1% HA-SH hydrogels - Adapted direct contact test.

The fluorescent micrographs of NHEK demonstrated that the green signal evidently decreased (and thus, red signal increased) from 125U/L to 500U/L GO hydrogel wells in U- areas only, as compared to A-areas that still showed abundant of green signal (Figure 9.30-v, -vi, -vii). This might be related with hypoxic effects directly under the sample, as described above. However, when correlated with the CTB data, NHEK still demonstrated the cell viability of ~96% to 74% for the encapsulated GO concentrations of 125U/L to 500U/L (Figure 9.24).

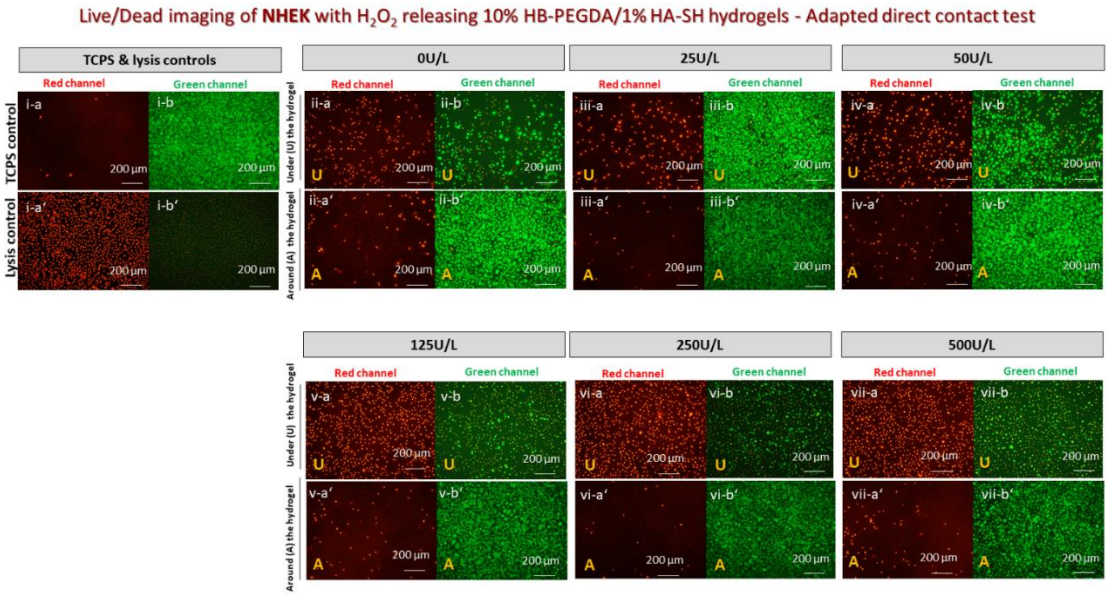

Figure 9.30 Live/Dead imaging of NHEK with H_2O_2 releasing 10% HB-PEGDA/1% HA-SH hydrogels - Adapted direct contact test. The sub-images showed the cell monolayer exposed with i) Lysis & TCPS controls, ii) 0U/L hydrogel, iii) 25U/L hydrogel, iv) 50U/L hydrogel, v) 125U/L hydrogel, vi) 250U/L hydrogel, and iii) 500U/L hydrogel. The microscopic fields showed the area under (U) and around (A) the hydrogel samples, labelled as -a & -a' for red channel in U-area and A-area, respectively. While -b & -b' for green channel in U-area and A-area, respectively.

On the other hand, the fluorescent micrographs of L929 and HaCaT cell lines demonstrated that the green signal evidently started to decrease even at lower GO concentration of 50U/L and progressively decreased until 500U/L in U-areas only, while A-areas still demonstrated abundant of green signal (Figure 9.31-iv to -vii & Figure 9.32-iv to -vii). Moreover, the CTB assay with L929 demonstrated cell viability in a range of 85% to 60% at the respective GO concentrations (Figure 9.33). Furthermore, BF micrographs of L929 cells demonstrated morphological differences in the microscopic fields that were right under (U), near (N), and far (F) from the hydrogel specimen and thus, images were recorded in these microscopic fields for better examining the precise differences in H_2O_2 induced cytotoxicity by different GO concentrations (Figure 9.34).

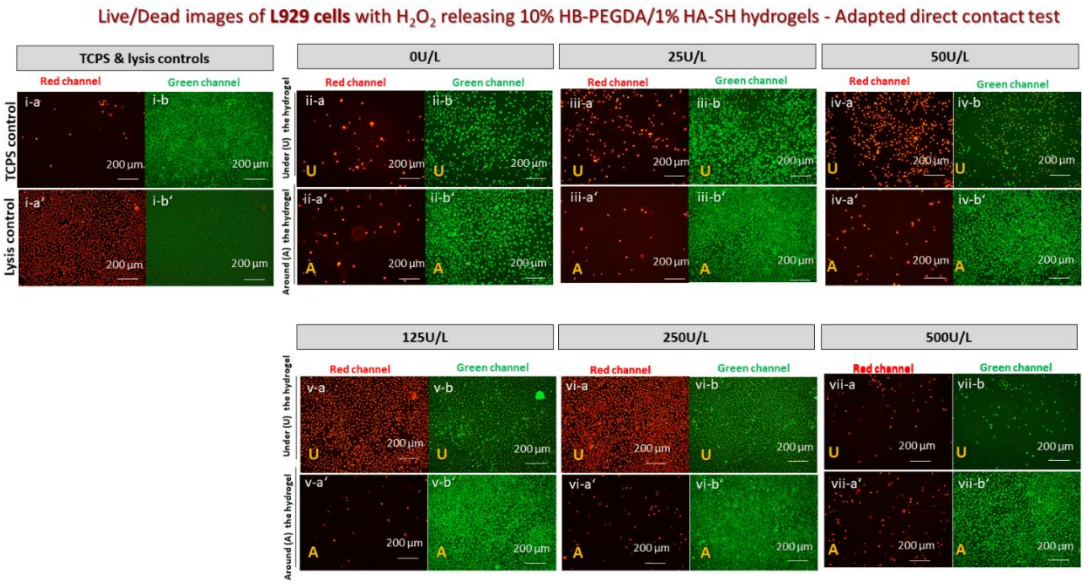

Figure 9.31 Live/Dead images of L929 cells with H_2O_2 releasing 10% HB-PEGDA/1% HA-SH hydrogels - Adapted direct contact test. The sub-images showed the cell monolayer exposed with i) Lysis & TCPS controls, ii) 0U/L hydrogel, iii) 25U/L hydrogel, iv) 50U/L hydrogel, v) 125U/L hydrogel, vi) 250U/L hydrogel, and iii) 500U/L hydrogel. The microscopic fields showed the area under (U) and around (A) the hydrogel samples, labelled as -a & -a' for red channel in U-area and A-area, respectively. While -b & -b' for green channel in U-area and A-area, respectively.

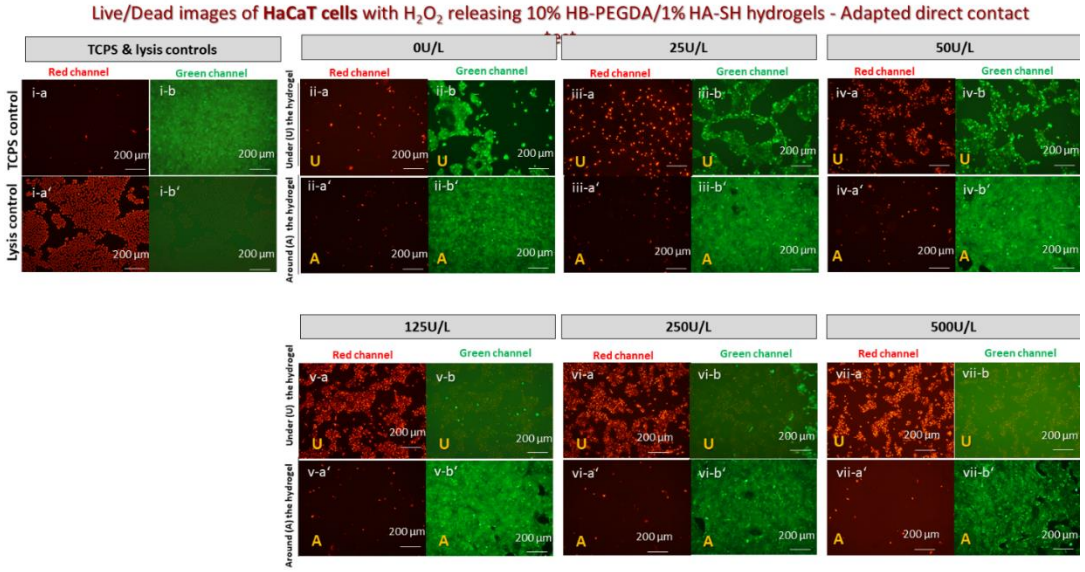

Figure 9.32 Live/Dead images of HaCat cells with H_2O_2 releasing 10% HB-PEGDA/1% HA-SH hydrogels - Adapted direct contact test. The sub-images showed the cell monolayer exposed with i) Lysis & TCPS controls, ii) 0U/L hydrogel, iii) 25U/L hydrogel, iv) 50U/L hydrogel, v) 125U/L hydrogel, vi) 250U/L hydrogel, and iii) 500U/L hydrogel. The microscopic fields showed the area under (U) and around (A) the hydrogel samples, labelled as -a & -a' for red channel in U-area and A-area, respectively. While -b & -b' for green channel in U-area and A-area, respectively.

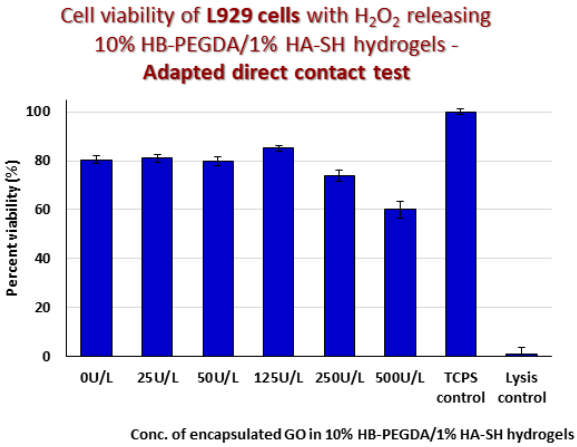

Figure 9.33 Cell viability of L929 cells with H_2O_2 releasing 10% HB-PEGDA/1% HA-SH hydrogels - Adapted direct contact test.

When the before mentioned results (fluorescent micrographs and CTB) of L929 cells were correlated with their BF micrographs, the images showed that 125U/L to 500U/L hydrogels affected the cells morphology in U-, and N- areas (Figure 9.34-v to -vii), as compared to 25U/L to 50U/L which showed that this effect was restricted to U-areas only (Figure 9.34-iii & -iv). The affected cells had either rounded or shrunken cell morphology than the well-spread healthy cell morphology in case of TCPS control. The lower cell density in the affected areas was due to the detachment of damaged cells from the surface that then appeared floating in cell culture media. Additionally, it was worth noticing that the 0U/L hydrogel sample demonstrated the cell damage in U- as well as N- areas, demonstrating that the polymer itself had some cytotoxic effects on cells, as has been observed so far with other cell types as well, that might also be related with hypoxic effect at material-cell interface.

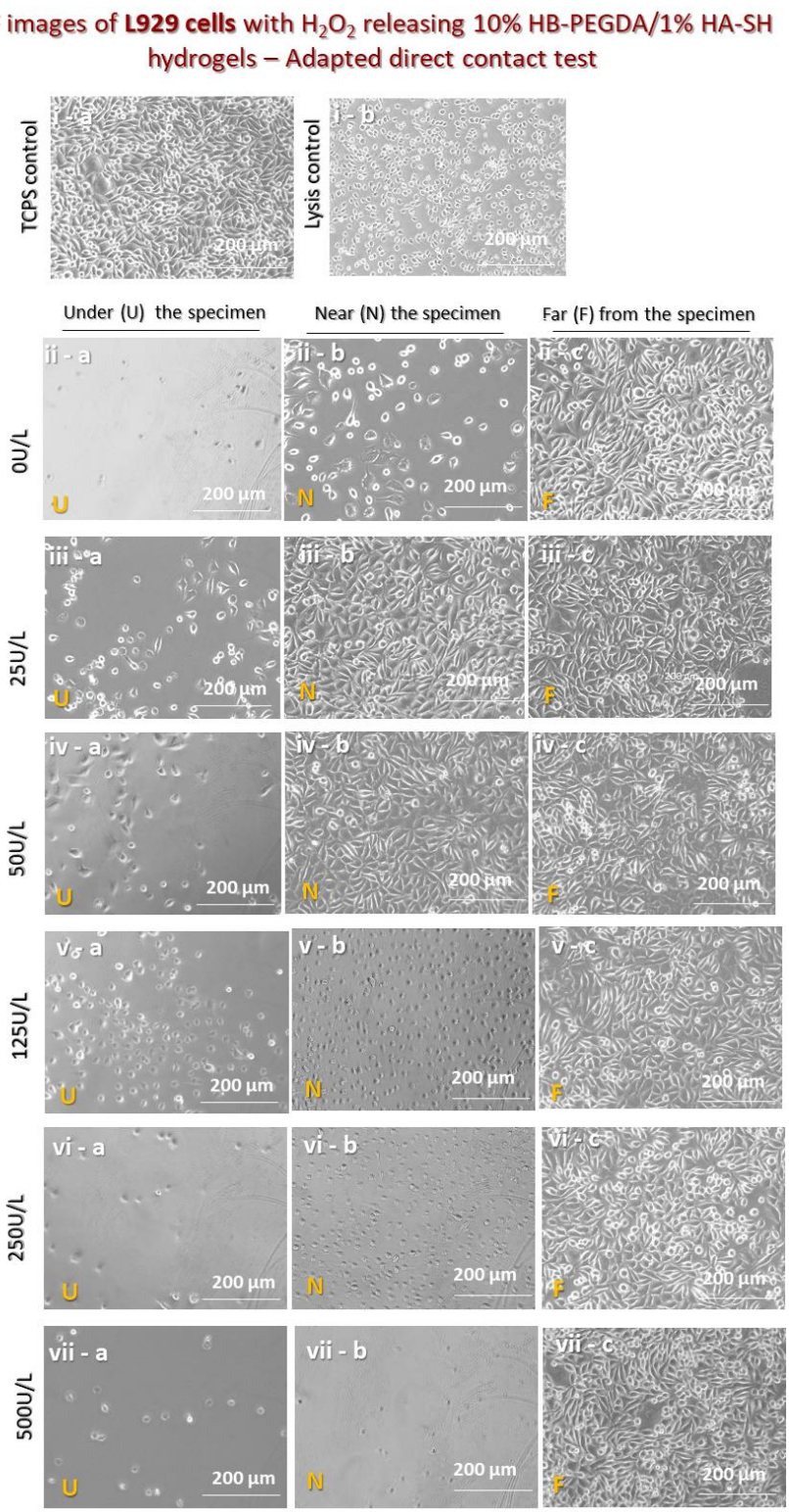

Figure 9.34 BF images of L929 cells with H_2O_2 releasing 10% HB-PEGDA/1% HA-SH hydrogels – Adapted direct contact test. The sub-images showed the cell monolayer exposed with i-a & i-b) TCPS & Lysis controls, ii) 0U/L hydrogel, iii) 25U/L hydrogel, iv) 50U/L hydrogel, v) 125U/L hydrogel, vi) 250U/L hydrogel, and vii) 500U/L hydrogel. The microscopic fields showed the area under (U) and near (N), and far (F) from the hydrogel samples, labelled as -a, - b, and -c respectively.

On the other hand, the BF micrographs of HaCaT cells were recorded in the areas that were under (U), and around (A) the hydrogel exposure. The BF micrographs, due to an inherent ability of HaCaT cells to grow in dense groups (cells islets) did not provide a clear outcome of an affected cells morphology or damaged cell growth (as can be seen in Figure 9.35). Though, the results were somehow understandable in fluorescent micrographs as described before (Figure 9.32).

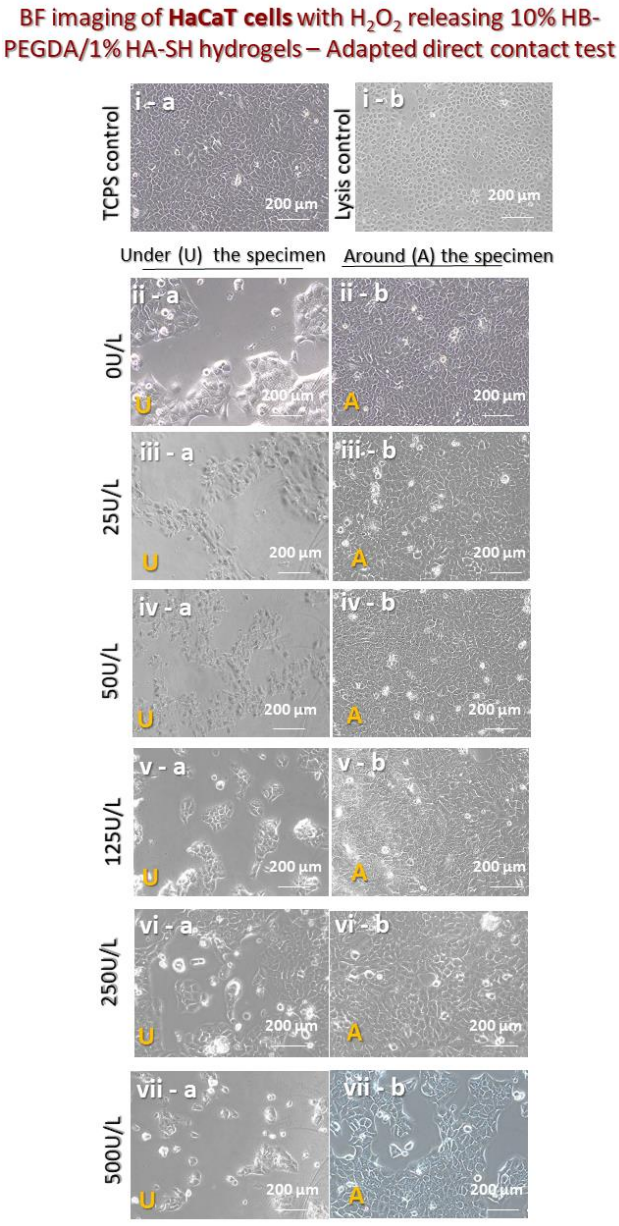

Figure 9.35 BF imaging of HaCaT cells with H_2O_2 releasing 10% HB-PEGDA/1% HA-SH hydrogels – Adapted direct contact test. The sub-images showed the cell monolayer exposed with i-a & i-b) TCPS & Lysis controls, ii) 0U/L hydrogel, iii) 25U/L hydrogel, iv) 50U/L hydrogel, v) 125U/L hydrogel, vi) 250U/L hydrogel, and vii) 500U/L hydrogel. The microscopic fields showed the area under (U) and around (A) the hydrogel samples, labelled as -a and -b respectively.

9.3.4 *Antibacterial Activity*

The antibacterial activity was evaluated by disc-diffusion assay and was demonstrated as zone of inhibition (ZOI) (Figure 9.36). The ZOI increased with an increase in GO concentration, demonstrating the biggest zones were obtained at 250U/L and 500U/L GO concentrations (Figure 9.36 & Figure 9.37).

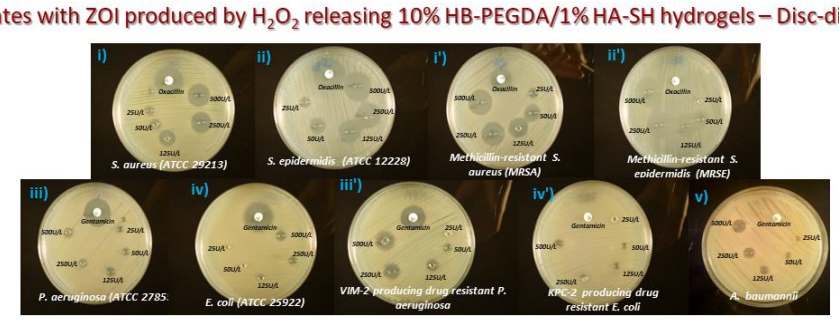

Figure 9.36 Agar plates with ZOI produced by H_2O_2 releasing 10% HB-PEGDA/1% HA-SH hydrogels – Disc-diffusion assay. against i) S. aureus, ii) S. epidermidis, iii) P. aeruginosa, iv) E. coli, v) A. baumannii, i') Methicillin-resistant S. aureus (MRSA), ii') Methicillin-resistant S. epidermidis (MRSE), iii') VIM-2 producing drug resistant P. aeruginosa, and iv') KPC-2 producing drug resistant E. coli.

The H_2O_2 releasing hydrogels were equally effective in inhibiting bacterial growth of both "methicillin sensitive" (*S. aureus* and *S. epidermidis)* as well as "methicillin resistant" bacterial strains (MRSA and MRSE) (Figure 9.36-i, -ii -i', -ii' & Figure 9.37). The resistance-phenotype against methicillin is due to an alternative transpeptidase Pbp2a encoded by *mec*A which is not affected by beta-lactams [44]. H_2O_2 releasing hydrogels might have shown antibacterial activity against them by hydroxyl free radicals that can directly impair the biomolecules most significantly causing DNA lesions at multiple sites [45].

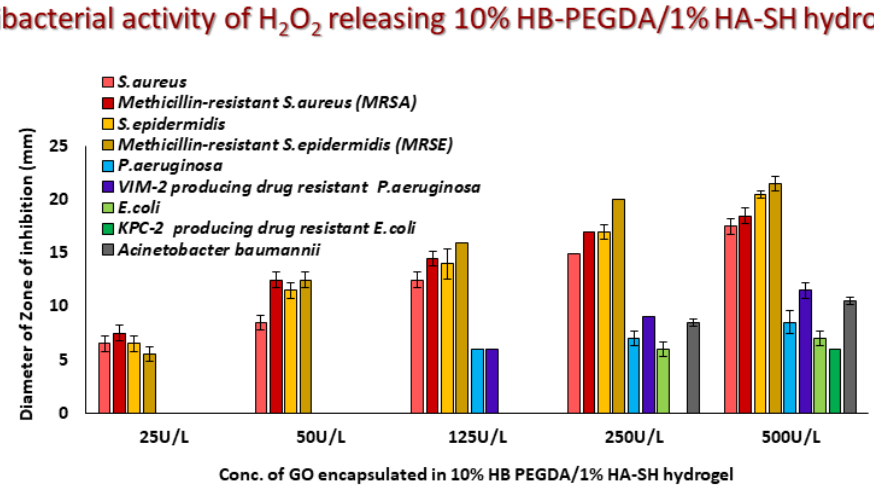

Figure 9.37 Antibacterial activity of H_2O_2 releasing 10% HB-PEGDA/1% HA-SH hydrogels.

Unlike Gram-positive bacteria, Gram-negative bacteria were inhibited at higher GO concentrations i.e. ≥125U/L, for example *P. aeruginosa* as well as its resistant strain (Figure 9.36-iii & -iii' & Figure 9.37). However, in case of *E. coli,* the minimum GO concentration that showed inhibition was 250U/L, its resistant strain was inhibited only at 500U/L (Figure 9.36-iv &-iv' & Figure 9.37).

A. baumannii being a multidrug-resistant (MDR) bacteria and as an emerging serious threat for injuries associated infections [46] demonstrated an inhibition at higher GO concentrations of 250U/L and 500U/L (Figure 9.36-v & Figure 9.37). The ZOI measured were summarized in Table 9.3.

Table 9.3 ZOI (mm) demonstrated by H_2O_2 releasing 10% HB-PEGDA/1% HA-SH hydrogels.

Conc. of GO in 10% HB-PEGDA/1% HA-SH hydrogel	*S. aureus* (ATCC 29213)	*S. epidermidis* (ATCC 12228)	*E. coli* (ATCC 25922)	*P. aeruginosa* (ATCC 27853)	*E. faecalis* (ATCC 29212)	*Methicillin-resistant S. aureus (MRSA)*	*Methicillin-resistant S. epidermidis (MRSE)*	*VIM-2 producing drug resistant P. aeruginosa*	*KPC-2 producing drug resistant E. coli*	*A. baumannii*
	ZOI (mm)									
25U/L	6.5±0.70	6.5±0.70	0.0±0.0	0.0±0.0	0.0±0.0	7.5± 0.70	5.5±0.70	0.0±0.0	0.0±0.0	0.0±0.0
50U/L	8.5±0.70	11.5±0.70	0.0±0.0	0.0±0.0	0.0±0.0	12.5± 0.70	12.5±0.70	0.0±0.0	0.0±0.0	0.0±0.0
125U/L	12.5±0.70	14.0±1.4	0.0±0.0	6.0±0.0	0.0±0.0	14.5± 0.70	16.0±0.0	6.0±0.0	0.0±0.0	0.0±0.0
250U/L	15.0±0.0	17.0±0.70	6.0±0.70	7.0±0.70	0.0±0.0	17.0±0.0	20.0±0.0	9.0±0.0	0.0±0.0	8.5±0.35
500U/L	17.5±0.70	20.5±0.35	7.0±0.70	8.5±1.06	0.0±0.0	18.5±0.70	21.5±0.70	11.5± 0.70	6.0±0.0	10.5±0.35

H_2O_2 releasing hydrogels, in general, performed better against Gram +ve bacteria demonstrating ZOI at all GO concentrations than against Gram-ve bacteria where hydrogels worked at comparatively higher GO concentrations. Among other differences, the main difference between Gram +ve and Gram -ve bacteria exists in the intrinsic

resistance attributed by the presence of the outer membrane in Gram -ve bacteria as well as the presence of very narrow porins to prevent penetration of even small molecules [47].

Additionally, H_2O_2 is naturally produced within cell due to an autoxidation of redox enzymes especially in aerobic bacteria or by a deliberate production to compete with other microbial organisms. Because H_2O_2 is acutely toxic to cells, bacteria tend to scavenge it to keep it at nanomolar intracellular levels. Catalases and NADH peroxidases are two primary scavengers present in many bacteria, therefore, it must be considered while using H_2O_2 as an antibacterial agent. These enzymes are entirely capable of degrading H_2O_2 *in vitro*, though what is their contributions *in vivo* is still not clear [48].

These finding were based on preliminary experiments. The bio-evaluations were repeated (number of experiments i.e. n=2) with biological replicates in duplicates per experiment. This was due to limited amount of hydrogel components (in this case HA-SH) accessible. It would be better to repeat the experiments with higher number of replicates per experiment to validate the results observed. Based on the complexity of the present H_2O_2 releasing hydrogel system and the statistical reasons, we must be careful with the interpretation of the current data.

Conclusion

250U/L H_2O_2 releasing hydrogels demonstrated a strong antibacterial effect against a wide range of wound associated pathogens. However, the cytotoxic effects demonstrated by 10% HB-PEGDA/1% HA-SH hydrogels were highly dependent on the type of the test procedure as well as concentration of encapsulated GO. For example, under direct contact test, ≤50U/L hydrogels demonstrated the minimum cytotoxic effect of ~25% with NHDF. While under indirect contact test, even 250U/L hydrogels demonstrated approx. ≤32% cytotoxicity with both NHDF and NHEK. However, under adapted direct contact test, 250U/L hydrogels demonstrated approx. ≤13% cytotoxicity with both NHDF and NHEK. Moreover, 3D skin model demonstrated a slightly activated state at all GO concentrations with no apparent cytotoxic effects, however, this data must be complemented with histological findings. The involvement of cross-talk between cell types contributes towards an advanced and combined response towards a stimulus, and thus served as a more reliable test system [49].

The H_2O_2 releasing hydrogels at higher GO concentrations can be consumed by bacterial burden and wound exudate to kill the bacteria in infected wounds, thus avoiding the possible direct cytotoxic effect towards cells to help wound in healing. An initial robust H_2O_2 release might help to reduce bacterial burden at initial stages, while a constant H_2O_2 release, later on might help keeping the wound away from bacterial re-colonization.

Different types of procedures were employed to understand the cytotoxic effect by polymer, released H_2O_2, or their combined effect. However, the H_2O_2 releasing system has to be better characterized as well, such as optimal immobilization of GO within cross-linked hydrogels, optimal concentration of encapsulated glucose, presence/ release of unpolymerized PEGDA , the amount of immediate (robust) production of H_2O_2 during the hydrogel cross-linking and after its complete gel formation, H_2O_2 release in different types of cell culture media, H_2O_2 consumption in different types cell culture media and by different cell types, consumed amount of H_2O_2 by proteins during pre-treatment step, etc. In biological side, the expression profile of different cell types with respect to different exposed GO concentrations, histological, and immunohistological analysis would be very helpful to address many unanswered questions.

Initially, another hydrogel system based on PLGA (poly L-lactide-co-glycolide) - PEG (poly ethylene glycol) – PLGA copolymer was also used for G/GO encapsulation by ESR01 as a preliminary H_2O_2 releasing hydrogel system. Main findings about the bio-evaluation of this system were described in Appendix D.

Collaboration work

This chapter describes the collaboration work between Ayesha Idrees (as ESR14) and Jeddah Marie Vasquez (as ESR01) under HyMedPoly project (Grant agreement No. 643050). The HB-PEGDA polymer synthesis, GO/G encapsulated HB-PEGDA/HA-SH hydrogel, and its characterization were performed by Jeddah Marie Vasquez. While GO/G encapsulated HB-PEGDA/HA-SH hydrogel samples preparation, their cytotoxicity, and antibacterial evaluations were performed by Ayesha Idrees.

Here are the descriptions of ESR01, Jeddah Marie Vasquez Ph.D. thesis: "Design of a Multilayer Honey-Mimetic Antibacterial Wound Healing Device" Ph.D. Program in Bioengineering and Medical-Surgical Sciences - 31st cycle (2019) - Department of Mechanical and Aerospace Engineering (DIMEAS), Politecnico di Torino, Turin, Italy - Tutor: Valeria Chiono. Co-tutor(s): Prof. Gianluca Ciardelli, Dr. Udo Greiser (external advisor), Prof. Wenxin Wang (external advisor).

References

1. Dong, Y., et al., *A rapid crosslinking injectable hydrogel for stem cell delivery, from multifunctional hyperbranched polymers via RAFT homopolymerization of PEGDA.* Polymer chemistry, 2015. 6(34): p. 6182-6192.
2. Li, J., et al., *Cartilage regeneration using arthroscopic flushing fluid-derived mesenchymal stem cells encapsulated in a one-step rapid cross-linked hydrogel.* Acta biomaterialia, 2018. 79: p. 202-215.
3. Xu, Q., et al., *A hybrid injectable hydrogel from hyperbranched PEG macromer as a stem cell delivery and retention platform for diabetic wound healing.* Acta biomaterialia, 2018. 75: p. 63-74.
4. Efem, S., *Clinical observations on the wound healing properties of honey.* British journal of Surgery, 1988. 75(7): p. 679-681.
5. Molan, P.C., *Honey as a topical antibacterial agent for treatment of infected wounds.* World Wide Wounds, 2001. 1: p. 1-13.
6. Cooper, R., P. Molan, and K. Harding, *Antibacterial activity of honey against strains of Staphylococcus aureus from infected wounds.* Journal of the royal society of medicine, 1999. 92(6): p. 283-285.
7. Cooke, J., et al., *The antimicrobial activity of prototype modified honeys that generate reactive oxygen species (ROS) hydrogen peroxide.* BMC research notes, 2015. 8(1): p. 20.
8. Bogdanov, S., *Nature and origin of the antibacterial substances in honey.* LWT-Food Science and Technology, 1997. 30(7): p. 748-753.
9. Yaghoobi, R. and A. Kazerouni, *Evidence for clinical use of honey in wound healing as an anti-bacterial, anti-inflammatory anti-oxidant and anti-viral agent: A review.* Jundishapur journal of natural pharmaceutical products, 2013. 8(3): p. 100.
10. Arul, V., et al., *Glucose oxidase incorporated collagen matrices for dermal wound repair in diabetic rat models: a biochemical study.* Journal of biomaterials applications, 2012. 26(8): p. 917-938.
11. hrhealthcare.co.uk. *SurgihoneyRO™*. 2019 06 April, 2019]; Available from: http://hrhealthcare.co.uk/product/surgihoneyro/.
12. Dressings.org. *SMTL Dressings Datacard* 07 Jan, 2014 06 April, 2018]; Available from: http://www.dressings.org/Dressings/oxyzyme.html.
13. Moffatt, C.J., et al., *A randomised trial to compare the performance of Oxyzyme® and Iodozyme® with standard care in the treatment of patients with venous and mixed venous/arterial ulceration.* Wound Medicine, 2014. 6: p. 1-10.
14. Bankar, S.B., et al., *Glucose oxidase—an overview.* Biotechnology advances, 2009. 27(4): p. 489-501.

15. Zheng, Y., et al., *Hyperbranched polymers: advances from synthesis to applications.* Chemical Society Reviews, 2015. 44(12): p. 4091-4130.
16. Juhlin, L., *Hyaluronan in skin.* Journal of internal medicine, 1997. 242(1): p. 61-66.
17. Nair, D.P., et al., *The thiol-Michael addition click reaction: a powerful and widely used tool in materials chemistry.* Chemistry of Materials, 2013. 26(1): p. 724-744.
18. McMahon, S., et al., *Poly (ethylene glycol)-based hyperbranched polymer from RAFT and its application as a silver-sulfadiazine-loaded antibacterial hydrogel in wound care.* ACS applied materials & interfaces, 2016. 8(40): p. 26648-26656.
19. Blafar. *Hyperbranched PEG-Based Multi-Acrylate Polymer (HB-PEG)*. 06 April, 2019]; Available from: http://blafar.com/product/hb-peg/.
20. Blafar. *Thiolated Hyaluronic Acid (HA-SH)*. 06 April, 2019]; Available from: http://blafar.com/product/ha-sh/.
21. Biochemistry), N.-I.N.C.o.t.I.U.o., *Units of Enzyme Activity - 1979.* Eur. J. Biochem. Y7, 319-320 (197Y)
22. Eisenberg, G., *Colorimetric determination of hydrogen peroxide.* Industrial & Engineering Chemistry Analytical Edition, 1943. 15(5): p. 327-328.
23. Wang, D., et al., *Bioapplications of hyperbranched polymers.* Chemical Society Reviews, 2015. 44(12): p. 4023-4071.
24. Sigma-Aldrich. *Glucose Oxidase (G2133) - Product Information Sheet - Sigma-Aldrich*. 09 April, 2019]; Available from: https://www.sigmaaldrich.com/content/dam/sigma-aldrich/docs/Sigma/Datasheet/7/g2133dat.pdf.
25. Loo, A.E.K., et al., *Effects of hydrogen peroxide on wound healing in mice in relation to oxidative damage.* PloS one, 2012. 7(11): p. e49215.
26. Idrees, A., et al., *Validation of in vitro assays in three-dimensional human dermal constructs.* The International journal of artificial organs, 2018: p. 0391398818775519.
27. Gonzalez, R. and J. Tarloff, *Evaluation of hepatic subcellular fractions for Alamar blue and MTT reductase activity.* Toxicology in vitro, 2001. 15(3): p. 257-259.
28. Lebonvallet, N., et al., *The evolution and use of skin explants: potential and limitations for dermatological research.* European Journal of Dermatology, 2010. 20(6): p. 671-684.
29. Boelsma, E., M.C. Verhoeven, and M. Ponec, *Reconstruction of a human skin equivalent using a spontaneously transformed keratinocyte cell line (HaCaT).* Journal of investigative dermatology, 1999. 112(4): p. 489-498.

30. Maas-Szabowski, N., A. Stärker, and N.E. Fusenig, *Epidermal tissue regeneration and stromal interaction in HaCaT cells is initiated by TGF-α.* Journal of cell science, 2003. 116(14): p. 2937-2948.
31. Burdon, R.H., *Superoxide and hydrogen peroxide in relation to mammalian cell proliferation.* Free Radical Biology and Medicine, 1995. 18(4): p. 775-794.
32. Wiese, A.G., R.E. Pacifici, and K.J. Davies, *Transient adaptation to oxidative stress in mammalian cells.* Archives of biochemistry and biophysics, 1995. 318(1): p. 231-240.
33. Brenner, S., et al., *Lasting effect of preceding culture conditions on the susceptibility of C6 cells to peroxide-induced oxidative stress.* Toxicology in Vitro, 2010. 24(8): p. 2090-2096.
34. Leist, M., et al., *Conventional cell culture media do not adequately supply cells with antioxidants and thus facilitate peroxide-induced genotoxicity.* Free Radical Biology and Medicine, 1996. 21(3): p. 297-306.
35. Andrae, U., J. Singh, and K. Ziegler-Skylakakis, *Pyruvate and related α-ketoacids protect mammalian cells in culture against hydrogen peroxide-induced cytotoxicity.* Toxicology letters, 1985. 28(2-3): p. 93-98.
36. Cao, C., Y. Leng, and D. Kufe, *Catalase activity is regulated by c-Abl and Arg in the oxidative stress response.* Journal of Biological Chemistry, 2003. 278(32): p. 29667-29675.
37. Leccia, M.-T., et al., *UV-A1 cytotoxicity and antioxidant defence in keratinocytes and fibroblasts.* European journal of dermatology: EJD, 1998. 8(7): p. 478-482.
38. Lin, J.J.-C. and J.R. Feramisco, *Disruption of the in vivo distribution of the intermediate filaments in fibroblasts through the microinjection of a specific monoclonal antibody.* Cell, 1981. 24(1): p. 185-193.
39. Welch, W.J. and J.P. Suhan, *Morphological study of the mammalian stress response: characterization of changes in cytoplasmic organelles, cytoskeleton, and nucleoli, and appearance of intranuclear actin filaments in rat fibroblasts after heat-shock treatment.* The Journal of cell biology, 1985. 101(4): p. 1198-1211.
40. Gardner, A.M., et al., *Apoptotic vs. nonapoptotic cytotoxicity induced by hydrogen peroxide.* Free radical biology and medicine, 1997. 22(1-2): p. 73-83.
41. Jonas, S.K., P.A. Riley, and R.L. Willson, *Hydrogen peroxide cytotoxicity. Low-temperature enhancement by ascorbate or reduced lipoate.* Biochemical Journal, 1989. 264(3): p. 651-655.
42. Mello Filho, A.C. and R. Meneghini, *In vivo formation of single-strand breaks in DNA by hydrogen peroxide is mediated by the Haber-Weiss reaction.* Biochimica et Biophysica Acta (BBA)-Gene Structure and Expression, 1984. 781(1-2): p. 56-63.

43. Davies, M.J., *Protein oxidation and peroxidation.* Biochemical Journal, 2016. 473(7): p. 805-825.
44. Chambers, H.F., *Methicillin resistance in staphylococci: molecular and biochemical basis and clinical implications.* Clinical microbiology reviews, 1997. 10(4): p. 781-791.
45. Imlay, J.A., *Pathways of oxidative damage.* Annual Reviews in Microbiology, 2003. 57(1): p. 395-418.
46. Dijkshoorn, L., A. Nemec, and H. Seifert, *An increasing threat in hospitals: multidrug-resistant Acinetobacter baumannii.* Nature reviews microbiology, 2007. 5(12): p. 939.
47. Nikaido, H. and M. Vaara, *Molecular basis of bacterial outer membrane permeability.* Microbiological reviews, 1985. 49(1): p. 1.
48. Mishra, S. and J. Imlay, *Why do bacteria use so many enzymes to scavenge hydrogen peroxide?* Archives of biochemistry and biophysics, 2012. 525(2): p. 145-160.
49. Wojtowicz, A.M., et al., *The importance of both fibroblasts and keratinocytes in a bilayered living cellular construct used in wound healing.* Wound Repair and Regeneration, 2014. 22(2): p. 246-255.
50. Biomaterials, V. *Vornia Bioresorbable Thermoresponsive Hydrogel Technology - PLGA-PEG-PLGA*. 24 April, 2019]; Available from: http://www.vornia.com/wp-content/uploads/2017/02/Vornia-PLGA-PEG-PLGA.pdf.
51. Biomaterials, V. *PLGA-PEG-PLGA*. June 2017 24 April, 2019]; Rev. No.1:[Available from: http://www.vornia.com/wp-content/uploads/2017/10/PLGA-PEG-PLGA-Product-Brochure.pdf.
52. Nandi, N., et al., *Hydrogen peroxide induces apoptosis-like death in Entamoeba histolytica trophozoites.* Microbiology, 2010. 156(7): p. 1926-1941.
53. Oney, I., I.A. Kurnaz, and M.L. Kurnaz, *Cytoplasmic-to-nuclear volume ratio affects AP-1 complex formation as an indicator of cell cycle responsiveness.* FEBS letters, 2005. 579(2): p. 433-440.
54. Liang, X., et al., *Nanoparticles with CD44 Targeting and ROS Triggering Properties as Effective in Vivo Antigen Delivery System.* Molecular pharmaceutics, 2018. 15(2): p. 508-518.
55. Liang, X., et al., *Improved vaccine-induced immune responses via a ROS-triggered nanoparticle-based antigen delivery system.* Nanoscale, 2018. 10(20): p. 9489-9503.

9.4 Appendix D

9.4.1 PLGA (poly L-lactide-co-glycolide) - PEG (poly ethylene glycol) – PLGA copolymer (As a preliminary H_2O_2 releasing hydrogel system)

PLGA-PEG-PLGA (Vornia Ltd. Ireland [50, 51]) a triblock copolymer was synthesized via a "green" manufacturing procedure. The procedure referred to as an innovative production technology which cannot be disclosed due to the sensitive nature of the intellectual property associated. As a drug-free antibacterial strategy, this copolymer was used to encapsulate G/GO (a preliminary H_2O_2 releasing hydrogel system) by ESR01 for infected wound healing applications.

Due to its gel forming ability, biodegradability (of PLGA), bioresorbablity (of PEG i.e. releasable by kidney), and biocompatibility (due to PEG segment) [50, 51], PLGA-PEG-PLGA selected as a suitable matrix for G/GO to encapsulation. PLGA-PEG-PLGA is an amphiphilic copolymer that can self-assemble to form micelles in aq. medium. This is due to the PLGA segment that forms hydrophobic core and PEG section imparts hydrophilicity. This makes these copolymers ideal for sustained release of drugs [50, 51].

20wt% PLGA-PEG-PLGA hydrogel was used to encapsulate different G/GO concentrations (Table 9.4) and tested for its antimicrobial and cytotoxicity evaluation (briefly described here).

Table 9.4 20wt% PLGA-PEG-PLGA hydrogel samples with different G/GO concentrations.

G10/E1000 hydrogel [10wt% glucose containing polymer solution (G10) + 1000U/L enzyme containing polymer solution (E1000)]	**G10/E2000 hydrogel** [10wt% glucose containing polymer solution (G10) + 2000U/L enzyme containing polymer solution (E2000)]
G20/E1000 hydrogel [20wt% glucose containing polymer solution (G20) + 1000U/L enzyme containing polymer solution (E1000)]	**G20/E2000 hydrogel** [20wt% glucose containing polymer solution (G20) + 2000U/L enzyme containing polymer solution (E2000)]
Polymer control: Polymer without G/GO	**GO control: Polymer with GO (E2000)**

Here, E (enzyme) presented GO (glucose oxidase).

G/GO encapsulated 20wt% PLGA-PEG-PLGA polymer solution preparation at Universitätsklinikum Knappschaftskrankenhaus Bochum, Germany offered serious practical challenges. 20wt% PLGA-PEG-PLGA polymer solution were prepared in water at 60-70°C with 4h shaking. The polymer solution was allowed to stand at room

temperature (48 h) to take up the water and attain hydrogel-like consistency. Addition of glucose solution to polymer solution caused polymer to clump together. This was brought to uniformly-viscous consistency by sonication & vortexing (24h) and letting the solution to stand at room temperature (48 h). In the end, G20 solution appeared as whitish thick gel as compared to G10 solution that was comparatively clear. Though, if hydrogels didn't test immediately upon preparation, clumping re-appeared during polymer solutions storage at 4°C. Therefore, G10 hydrogels i.e. G10/E1000 and G10/E2000 hydrogels were mostly proceeded for antibacterial and cytotoxicity evaluations.

9.4.2 Antibacterial activity

Antibacterial activity of H_2O_2 releasing hydrogels (80µL per well) were evaluated against *S. aureus* (ATCC 25923) and *E. coli* (ATCC 25922) through well-diffusion assay (well diameter of 5mm). G10/E2000 hydrogels demonstrated larger ZOI than G10/E1000 indicating higher the encapsulated GO concentration (Table 9.5), more would be the H_2O_2 release, and so would be the antibacterial effect. Prominent antibacterial activity of H_2O_2 releasing hydrogel was observed against *S. aureus* MHA after 24h incubation. The size of ZOI was similar after 48 h incubation, however, single bacterial colonies were detected inside the inhibition zone (Figure 9.38).

The reappearance of colonies inside ZOI after 24 hours indicated that bacteria weren't killed 100% or H_2O_2 was no more effective or available to stop bacterial growth. Thus, the bacteria were able to grow (or recover) as the released H_2O_2 decreased over time. The hydrogen peroxide might have a burst release and up from a certain point H_2O_2 generation and thus, release from 20wt% PLGA-PEG-PLGA hydrogels dropped down. How uniform was the distribution of GO inside 20wt% PLGA-PEG-PLGA matrix, what is the activity of enzyme in this polymer matrix, and H_2O_2 generation/release profile over time are missing from materials' side and still has to be carried out by ESR01.

Blood agar (BA) being complex medium contains numerous unspecified nutrients and demonstrated comparatively smaller ZOI than MHA, indicating that peroxide consumption of diffusible H_2O_2 by medium constituents (proteins) decreased its antibacterial effect.

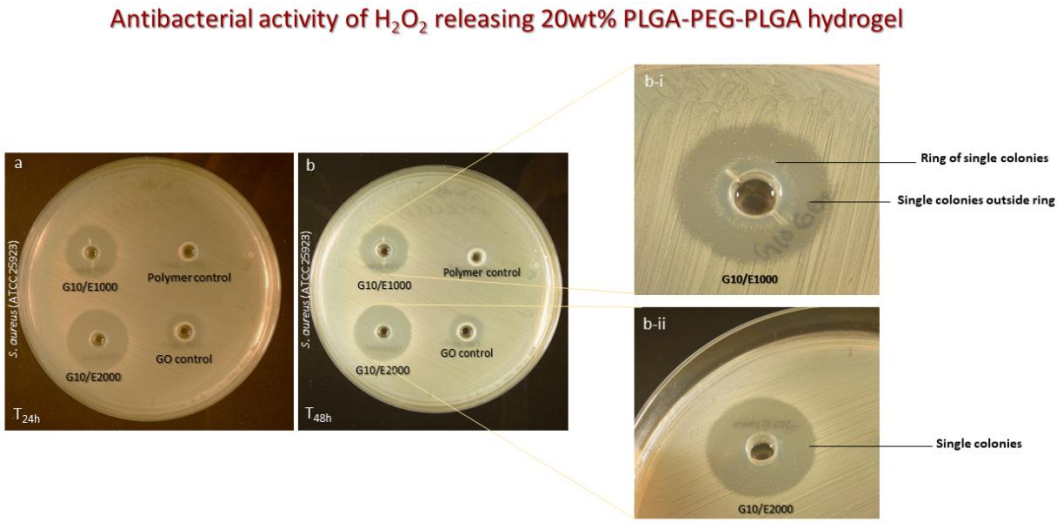

Figure 9.38 Antibacterial activity of H_2O_2 releasing 20wt% PLGA-PEG-PLGA hydrogel. The sub-images showed ZOI by H_2O_2 releasing 20wt% PLGA-PEG-PLGA against S. aureus on MHA after (a) 24 hours and (b) 48 hours exposure times. The sub-images b-i) and b-ii) were at higher magnification that showed the re-appearance of single colonies inside ZOI after 48 hours exposure with G10/E1000 and G10/E2000 hydrogel compositions, respectively.

Table 9.5 ZOI of different hydrogel samples at T_{24h}.

Hydrogel samples	***S. aureus* (ATCC 25923)**		***E. coli* (ATCC 25922)**	
	ZOI (mm)			
	MHA	**BA**	**MHA**	**BA**
G10/E1000	16	09	06	<06
G10/E2000	20	09	08	<06
GO control	11	08	00	<06
Polymer control	<06	06	<06	00

Mueller-Hinton agar (MHA) and Blood agar (BA)

9.4.3 Cytotoxicity analysis

L929 cells (1 x 10^5 cells per well) were cultured on 6-well TC plate in RPMI1640 (without FBS supplementation). The hydrogel samples (100µL per well) were indirectly exposed to cells using 12 well plate Transwell inserts (via spacers) for 24 h.

H_2O_2 releasing hydrogels demonstrated a severely affected cell metabolic activity (0% cell viability by CTB assay) and cell membrane integrity (CTO assay) at all G/GO

compositions (Figure 9.39 Cell viability and cytotoxicity of L929 cells with H2O2 releasing 20wt% PLGA-PEG-PLGA hydrogel - Indirect contact test.

), possibly due to an induced oxidative stress caused by H_2O_2 release from hydrogels. GO control demonstrated the similar cytotoxic results. This demonstrated that GO was able to interact with glucose in cell culture media producing H_2O_2 the same way as H_2O_2 releasing hydrogels of different G/GO compositions. Thus, the constituents of cell culture media would have an important role on the cytotoxicity outcomes of G/GO encapsulated hydrogel systems.

Polymer control showed the similar cell viability as TCPS control, demonstrating that polymer itself was not the contributing factor for the observed cytotoxic effect.

Live/Dead images confirmed the cytotoxic effect of H_2O_2 releasing hydrogels (Figure 9.40). Additionally, BF images indicated the affected morphological changes demonstrating increased vacuolization (presence of clear vacuoles inside cytoplasm) [52], cytoplasmic-to-nuclear ratio [53], and shrunken cells after exposure of H_2O_2 releasing hydrogels of different G/GO compositions with L929 cells (Figure 9.41). Cell morphological changes were measured at 1 h, 2 h, 3 h, 4 h, 8 h, 24 h, and 48 h. The results showed that the changes started at very early stage (4-8 h) (Figure 9.42).

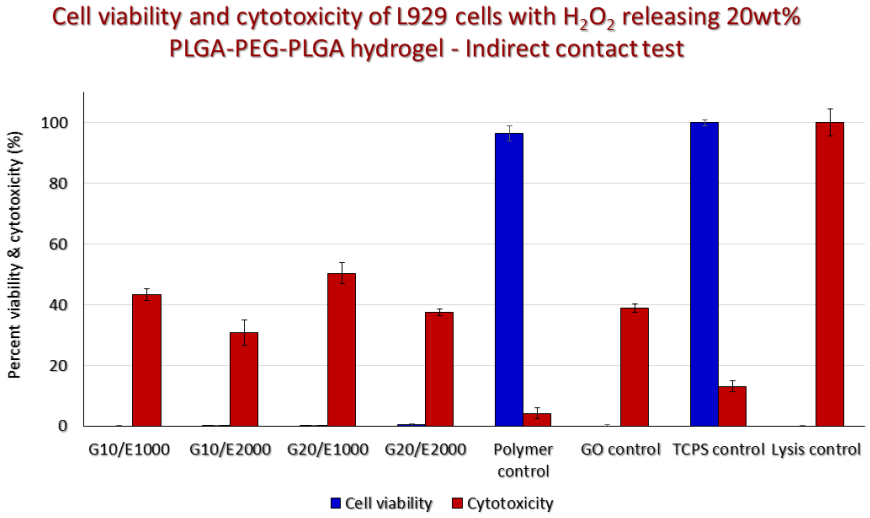

Figure 9.39 Cell viability and cytotoxicity of L929 cells with H_2O_2 releasing 20wt% PLGA-PEG-PLGA hydrogel - Indirect contact test.

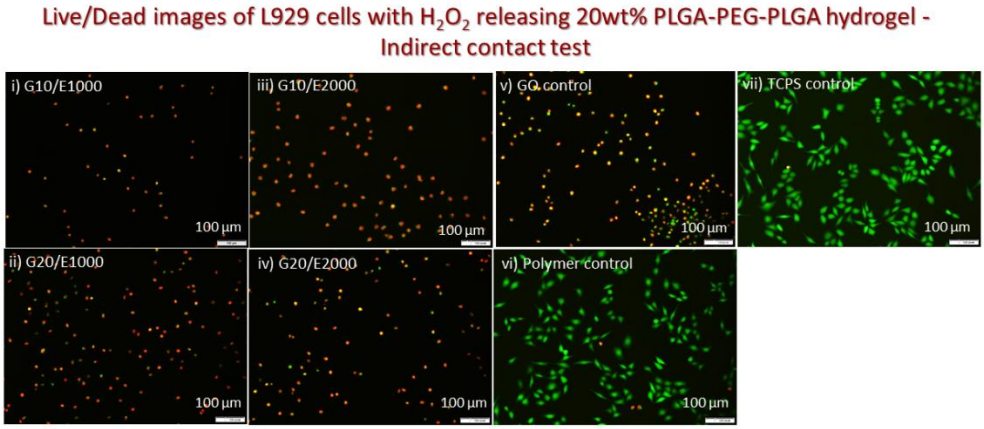

Figure 9.40 Live/Dead images of L929 cells with H_2O_2 releasing 20wt% PLGA-PEG-PLGA hydrogel - Indirect contact test. The sub-images i, ii, iii, and iv showed L929 cells after 24 hours of exposure with G10/E1000, G10/E2000, G20/E1000, G20/E2000 hydrogel samples, respectively. The sub-images v, vi, and vii showed L929 cells with GO, Polymer, and TCPS controls, respectively.

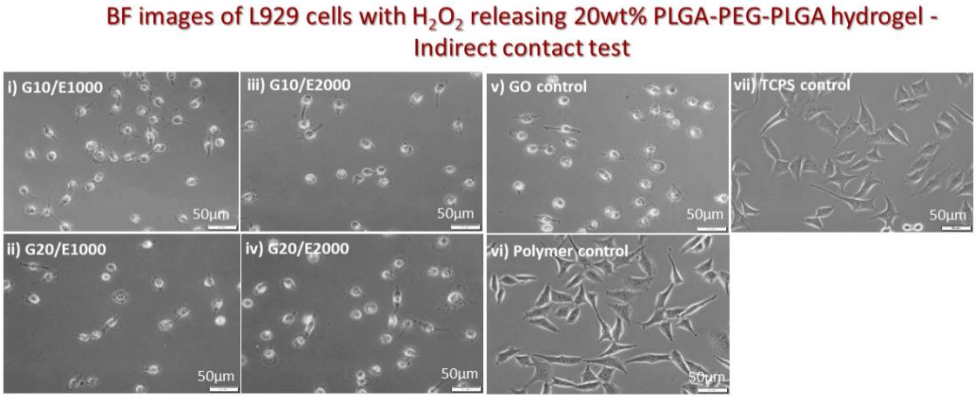

Figure 9.41 BF images of L929 cells with H_2O_2 releasing 20wt% PLGA-PEG-PLGA hydrogel - Indirect contact test. The sub-images i, ii, iii, and iv showed L929 cells after 24 hours of exposure with G10/E1000, G10/E2000, G20/E1000, G20/E2000 hydrogel samples, respectively. The sub-images v, vi, and vii showed L929 cells with GO, Polymer, and TCPS controls, respectively.

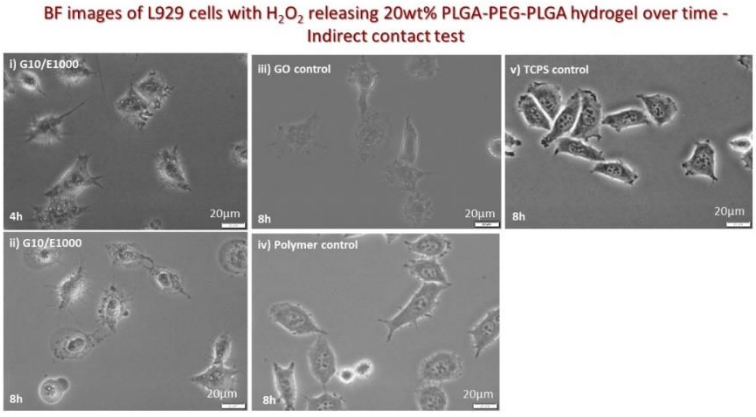

Figure 9.42 BF images of L929 cells with H_2O_2 releasing 20wt% PLGA-PEG-PLGA hydrogel over time - Indirect contact test. The sub-images i, and ii, showed L929 cells after 4 and 8 hours of exposure with G10/E1000 hydrogel. respectively. The sub-images iii, iv, and v showed L929 cells with GO, Polymer, and TCPS controls, respectively.

9.4.4 Cytotoxicity analysis – Experimental set-up II

L929 cells (1 x 10^5 cells per well) were cultured on 6-well TC plate in RPMI1640 (supplemented with 10% FBS). The G10/E1000 hydrogel sample (supposedly being able to release minimum H_2O_2 as compared to other G/GO compositions) (100µL per well) were indirectly exposed to cells using 12 well plate Transwell inserts. The hydrogel with lowest G/GO i.e. G10/E1000 was tested in this experimental set-up assuming that "peroxide consumption" by serum proteins might have an impact on the extent of H_2O_2-induced cytotoxicity. Results demonstrated that morphological changes started as early as 2-3 hours (Figure 9.43). Though, in this case, cells demonstrated an affected cell morphology in the microscopic area directly under (U) the sample-carrying-insert, while cell areas around (A) the sample exposure demonstrated a normal morphology at this time point (Figure 9.44).

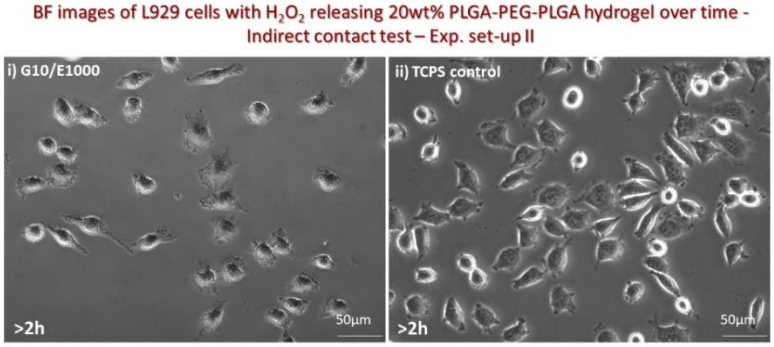

Figure 9.43 BF images of L929 cells with H_2O_2 releasing 20wt% PLGA-PEG-PLGA hydrogel over time - Indirect contact test – Exp. set-up II. The sub-image i) showed L929 cells after >2 hours of exposure with G10/E1000 hydrogel. The sub-image ii) showed L929 cells with TCPS control.

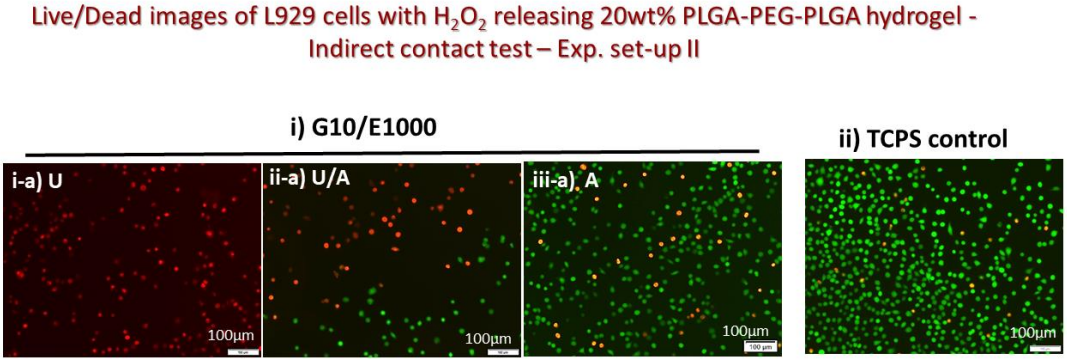

Figure 9.44 Live/Dead images of L929 cells with H_2O_2 releasing 20wt% PLGA-PEG-PLGA hydrogel - Indirect contact test – Exp. set-up II. The sub-image i-a, i-b, i-c showed L929 cells after >2 hours of exposure with G10/E1000 hydrogel in U-area, U/A-area, and A-area, respectively. The sub-image ii) showed L929 cells with TCPS control.

Antibacterial tests and cytocompatibility analysis are clearly showing that neither the G/GO loading of PLGA-PEG-PLGA hydrogels nor their H_2O_2 generation and release were working properly. Based on the results, this hydrogel matrix system was not

suitable as H_2O_2 releasing wound covering. This is because H_2O_2 encapsulation, generation, and release was not regulated. Moreover, water uptake (swelling properties), and how fast H_2O_2 was being released (or diffusing) from the polymeric matrix into the surrounding medium, were missing information from materials' side. Thus, the explanation of bio-evaluation data would currently be too speculative to interpret. Further investigations on the materials design and processing (for G/GO encapsulation as well as preservation of GO's activity over time) would be necessary to be carried out. Moreover, the study about stability of ester bond between PLGA and PEG towards peroxidation would be important to investigate [54, 55].

General discussion

Healing of infected wounds represents a great challenge in public health. With an increasing need for novel strategies to treat wounds colonized with resistant microbes, more reliable preclinical trials are needed to analyze antimicrobial polymeric biomaterials (AMPBs). The here developed 3D human skin equivalent (HSE) and infected 3D human skin equivalent (c-HSE) as wound infection model represent biomimetic systems for the testing of AMPBs.

Relevance of in vitro models as biomimetic replica of healthy and infected skin

Single-cell assays under submerged 2D culture conditions (cell lines and/or human primary cells), or 3D systems, like dermal equivalents, epidermal equivalents, and full-thickness skin equivalents under air-liquid interface (ALI) culture conditions, are different types of model systems with different advantages and disadvantages [1]. The degree of complexity of a selected test system depends on the final aim (e.g. *in vitro* toxicity measurement, wound healing, penetration studies etc.) and application (e.g. regulatory, industrial screening, or research purposes).

An *in vitro* model able to assess toxicity as an alternative to animal model should be able to distinguish should be able to distinguish a toxic from a non-toxic substance. For regulatory purposes, a skin model has to be validated for its relevance and reliability as per international standard procedures [2]. On the other hand, for industrial screening purposes, the model preparation and the assay design should allow medium to high throughput testing of compounds/products in a dose-response manner. For research purposes, the model should be physiologically relevant.

Single cell assays are simple providing high-throughput screening in a 96-well plate format and allowing to investigate the events happening within one cell. However, 2D cell cultures do not reproduce the natural tissue microenvironment and complexity of a 3D system. Current well-differentiated 3D epidermal equivalents are going to be used as stand-alone irritancy test replacements of rabbit Draize test [3]. However, they exhibit only a partial barrier to the topically applied substances, as compared to *in vivo* human skin [4]. A wide variety of skin equivalents (as described in Chapter 01) exists but are not as much studied as epidermal models. Being more complex, the full-thickness skin models based on dermal and epidermal compartments exhibit a crosstalk between fibroblasts and keratinocytes and are physiologically more relevant skin models.

Freshly excised skin are also advanced models, containing multiple cell types. The major drawback is the availability and transport of a large amount of freshly excised skin directly to the research lab for performing industrial- or research-based screening. This model also has ethical constrains. Such drawbacks could be overcome by using the cells and constructing the model *in vitro*.

Need of an alternative of animal testing

Animal models have been used to perform *in vivo* studies for testing new therapeutics and chronic wound healing. Related to the irritancy evaluation, Draize assay is performed on albino rabbit skin by applying the test substance to investigate the tissue harm [5]. Despite being ethically questionable (animals suffering pain), the test has provided incorrect information in the past [6, 7]. On the other hand, murine models have also been extensively used for skin biology experiments, wound healing and skin cancer studies [8-10]. However, there are some basic dissimilarities between mouse and human skin architecture [11]. Mouse skin being furry is densely packed with hair follicles, epidermis is quite thin (thus has less water barrier properties [12]), and cutaneous muscle layer i.e. panniculous carnosus is present (that promotes rapid wound contraction than hypertrophic scar (keloids) formation as happens in human [13]). On the other hand, porcine skin has physiologically and anatomically similarity to human skin e.g. thick dermal /epidermal layers, presence of sparse hair, presence of apocrine glands, wound healing through re-epithelization, and wound healing dependency on exogenous vitamin C source [14]. However, porcine dermis is less vascularized compared to human dermis [15]. Regardless of these similarities, pig is still not considered a suitable animal model because of its high cost and unfeasibility for large experimental set-ups.

Amendments in EU regulations and current policies have further pushed the development of *in vitro* testing systems as alternatives to animal testing. The European Union (EU) 7th amendment (Dir. 2003/15/EC) of the "Cosmetics Directive" (76/768/EEC) made it obligatory to replace animal trials for cutaneous resorption with reliable *in vitro* tests by the year 2009 [16]. This gave rise to the development of the 3Rs principle "replacement, reduction and refinement" [17]. Moreover, REACH, a European regulatory program for "registration, evaluation, authorization and restriction of chemicals" highlights human health and environment by emphasizing early characterization of chemicals' properties for risk assessment [18, 19].

Development and Characterisation of HSE and c-HSE

In this regard, the here developed in-house built HSE has a great potential for the safety assessment of antibacterial biomaterials. The HSE was obtained having both a dermal and an epidermal compartment, by embedding NHDF (normal human dermal fibroblasts) in rat tail tendon collagen type I hydrogel (mimicking dermal extracellular matrix) and then seeding NHEK (normal human epidermal keratinocytes) on it to generate the epidermis. Three-dimensional cell culture conditions (3D-CCs) based on commercially available serum/animal component-free and/or fully-defined media were applied to optimize the epidermal differentiation mimicking as closely as possible native human skin (NHS). (Chapter 04)

Histological results of HSE showed the formation of a dermal layer demonstrating NHDF with typical elongated filopodia-like morphology, that were uniformly

distributed all along the dermal length. Histological results for epidermis showed characteristic multi-layered epidermis with well-differentiated layers of stratum basale, spinosum, granulosum, and corneum (Figure 4.10). IHC results showed that keratinocytes in basal layer were positive for Ki-67, demonstrating their active state of proliferation. Immunoreactivity for Keratins (K) indicated that K14 expression was displayed by keratinocytes in the basal layer while K10 (marker of early differentiation) was restricted to the supra-basal layers. Terminal differentiation was demonstrated as spotted expression of Filaggrin (Flg) and Loricin (Lor) in the sub-corneal and corneal layers of the epidermis. The basement membrane protein Laminin 5 (Lam 5) was displayed as a continuous line at Dermal-Epidermal Junction (DEJ) (Figure 4.15). TEM revealed basement membrane with lamina lucida (LL), lamina densa (LD), regular hemidesmosomes and anchoring fibres. The epidermal layers showed abundant intracellular keratin filaments, desmosomes, and tight junction (TJ) between keratinocytes (Figure 4.21). SEM revealed the interwoven network and architecture of ECM with embedded dermal fibroblasts lying along collagen fibres; on the other hand, epidermal layers closer to the surface were increasingly flattened (Figure 4.22). The static contact angle of HSE was 82.5°±8.9° demonstrating the barrier function of HSE, which was highly comparable to the reported measurement of 90.0°±5.1° for NHS [20] (Figure 4.26). In this study, we successfully created an *in vitro* three-dimensional dermal-epidermal based interfollicular full-thickness human skin construct recapitulating the skin morphogenesis, epidermal differentiation, ultra-structure features, tissue architecture, and barrier function properties, closely imitating the properties of NHS and thus named as HSE. (Chapter 04)

Skin infection model was created by full-thickness incision and colonization with *S. aureus* to construct *S aureus* colonized HSE (c-HSE) (Chapter 05). Bacterial aggregations and early biofilm formation were observed at wound site on c-HSE (Figures 5.9, 5.12, & 5.13). In the present study, c-HSE was used as an advanced model to investigate antibacterial effects of silver and Ag-dressing on HSE adhered and colonized bacteria (Chapter 06).

Relevance of in vitro models as testing systems

The cytotoxicity and antibacterial outcomes of antibacterial wound products vary significantly under different laboratories as well as in clinical situations [21]. The sensitivity of the cells and the lethal effects of tested compound towards bacteria are decreased when the cells and/or bacteria are grown in complex arrangements to simulate the clinical environment.

The promotion of the antibacterial feature of a silver dressing is more of a marketing tact [22]. The clinical evidence of antibacterial activity is speculative to some extent [23], as the quantitative microbial count is necessary to prove its antibacterial activity in clinical practice. Therefore, doubts exist on the efficient antibacterial properties of silver

dressings in the clinics. Industrial trials make use of different microbes and microbial methodologies. This cause difficulty in data interpretation, correlation, and extrapolation of these *in vitro* findings with clinical outcomes. The antibacterial products may result effective in controlled laboratory set-up, while their functionality on patients may decrease. Traditional microbiological research has approached bacterial susceptibility, considering that bacterial cells live in a liquid free-floating medium, containing a low number of organisms and without sufficient organic matter in the medium.

Bacterial adherence and biofilm formation on plastic and human cells are two distinct events, presenting bacterial interactions with abiotic and biotic surfaces. However, these systems do not adequately imitate bacterial interaction with the human skin: the process occurs under relatively dry conditions [24], depends on physicochemical barrier properties of the skin and is strongly influenced by environmental conditions [25].

Clinical evidence of antibacterial activity of Ag-dressings

Considering the clinical evidence, silver wound dressings have been evaluated in several different types of studies. These studies involved partial thickness burns, donor site wounds, as well chronic wounds from: pressure ulcers (grades III & IV), venous leg ulcers (at risk of infection, colonised, critically colonised, critically colonised with delayed healing, infected, or infected with critical inflammation), and diabetic foot ulcer. A meta-analysis study combines the results from multiple studies in order to understand the efficacy of silver wound dressings [26]. Some studies have found Ag-dressings to exert a positive impact on overall wound healing [27-38], while others have found no significant differences respect to controls [39, 40]. The difficulties in interpretation and comparisons mainly arise from the small number of patients (problems with randomization), a wide range of different criteria, study protocols and study endpoints used. Many of the studies have used an endpoint associated with healing. However, more appropriate endpoint should relate to measurement of microbial burden and assessment of clinical indicators of infection [41]. A study that examined pre-specified indicators of infection, observed significant differences in Ag-dressings treated group showing no signs of heavy bacterial colonisation after 4-8 weeks of treatment [30]. However, another smaller study that used clinical infection scores, observed no significant difference between silver dressing treated and control groups after 2 weeks of treatment [42].

A particularly controversial study called VULCAN study [40, 43] used randomised patients (n=213) with venous leg ulcers receiving Ag- dressings. The main outcome considered was rate of complete wound healing after 12 weeks. The study concluded no significant difference between Ag-dressings treated and the control group, although cost analysis showed a higher cost associated with Ag-dressings. Despite the care involved in the study design, many researchers expressed their concerns on the potentially misleading outcomes [44-46]. The major concern was that the study did not use Ag-dressings in line with existing recommendations, for example, the study did not report

the risk of infection, and did not evaluate the wounds for presence of infection. Furthermore, silver dressings are not intended to be used for extended periods, whereas in the study the dressings were applied for 12 weeks. More importantly, the endpoint or the goal of the care using Ag-dressings should not be wound healing, rather it should be the reduction in wound bioburden. Some studies generalized the findings suggesting the invalid use of Ag-dressings in clinics. However, the study designs and clinical outcomes must be carefully concluded.

Clinical evidence of toxicity of silver and Ag-dressings

Some cases of dermatitis and eye irritation have been reported in humans, but in general silver was observed to have low chances of skin irritation if exposed through intact skin [21]. Exposure of dermal, mucosal and compromised skin to silver resulted in the deposition of particles causing discoloration (argyria). After exposure to dermal and mucosal surface, silver is excreted in urine and faeces, though the elimination from plasma takes hundreds of days [21]. Regarding the silver toxicities, hepatic, renal, neurological, hematological, and carcinogenic/genotoxic (where additional data is needed) effects have been observed in human body [21]. A mortality case was shown at an intrauterine exposure of ionic silver of 64mg/Kg body weight [21]. Argyria with ionic and nanocrystalline silver was reported at cumulative range of 70-1500mg/Kg body weight in humans [21]. Silver-containing formulations studied for their toxicity in various animal models were described in a recent review article [21] that clearly showed the existing discrepancies between human and animal data. There are valuable, suitable, and independent studies available on Ag-based dressings investigated in this thesis, except the ones carried out by industry.

Concerning the toxicity of silver dressings in general, an increasing amount of silver available for antimicrobial purposes caused increased toxicity to host cells, but in most *in vitro* studies, the microenvironment of wound tissue has not been reproduced as it is present *in vivo*. Moreover, the frequency of dressing change and thus the ability of the antimicrobial wound dressing to handle wound exudate (and bioburden) is hard to be precisely taken into account. Nanocrystalline silver based antimicrobial dressings tested using contaminated cultured skin substitutes that were grafted to athymic mice, were found non-toxic. Whereas these dressings resulted toxicity using fibroblasts and keratinocytes cells based *in vitro* tests [47-51]. The same dressings in a study of 17 clinical donor sites were found to be toxic. It is important to note that these donor sites were free from bioburden and dressings were soaked prior to exposure to wounds. Overhydration of the wound and surrounding healthy skin caused the maceration problems and might have an impact on the observed outcome about silver dressing toxicity [52].

On the other hand, nanocrystalline silver dressings through their direct antibacterial activity have been clinically shown to reduce metalloproteinases (MMPs) reducing

inflammation and thus promoting healing [53]. Similar results were shown in an *in vivo* study (microbial contaminated porcine model) that showed reduced *Pseudomonas* and *Staphylococci* number, reducing MMPs and enhancing granulation tissue formation [54].

HSE and c-HSE models as advanced in vitro testing systems

Comparative 2D vs. 3D bio-evaluation tools

To validate our 3D systems, Ag^+ as an antibacterial agent and most commonly clinically applied Ag containing antimicrobial wound dressings (Ag-dressings) [namely PolyMem Ag (Ferris), Biatain® Alginate Ag (Coloplast), Biatain® Ag (Coloplast), Atrauman® Ag (Hartmann)] along with their controls without silver, were tested for cytocompatibility and antimicrobial properties using HSE and c-HSE imitating an *in vivo* like setting. (Chapter 06)

On the other hand, L929 cells, COCA cells, NHDF, and NHEK monolayer cell cultures were used as 2D cytocompatibility evaluation systems. Ag^+ and Ag-dressings were evaluated for their antibacterial activities (e.g. MIC, MBC, CFU percentage reduction) against clinically relevant pathogens (*Staphylococcus aureus, Pseudomonas aeruginosa* etc.) under different growth media [tryptic soy broth (TSB) and simulated wound fluid (SWF)] over time to assess the effects of culture 'environment' on bacterial susceptibility to the toxic action of silver. (Chapter 06)

1. In vitro cytotoxicity testing

The cytotoxicity was represented as IC50 (half maximal inhibitory concentration), while assaying cytotoxicity, IC50 is the concentration of cytotoxic compound that gives 50% viability.

Ag^+ showed IC50 of 2.3µg/mL, 10.8µg/mL, 10.3µg/mL and 11.8µg/mL in 2D monolayer cultures of L929, COCA, NHDF and NHEK, respectively, while IC50 was three times higher (34.2µg/mL) when using HSE (Figures 6.12, 6.13, & 6.14). Tissue culture models indicated an 'environmental effect' on cytotoxicity, with decreased sensitivity to Ag^+ cytotoxicity for cells in 3D with respect to cells in 2D cultures.

Among tested Ag-dressings, the cytotoxicity tests using NHDF and NHEK indicated that silver released from Biatain® Ag (1% cell viability) and Biatain® Alginate Ag (53% cell viability) was lethal for both fibroblasts and keratinocytes (Figure 6.21). On the other hand, Biatain® Ag and Biatain® Alginate Ag demonstrated 77±21.8% and 92.5±10.6% cell viability with HSE, that was not significantly different than negative control (Figure 6.23). Biatain® Ag caused 77 ± 21.8% cell viability in HSE as compared to 1% cell viability in 2D monolayer cultures (Figures 6.21 & 6.23).

2. In vitro antibacterial testing

Ag^+ showed MIC (minimum inhibitory concentration) in a range of 4.2-8.4µg/mL and MBC (minimum bactericidal concentration) in a range of 4.2-33µg/mL against the tested Gram+ve and Gram-ve bacteria.

The antibacterial activity of Ag^+ showed 99.99% *S. aureus* reduction in TSB (tryptic soy broth), while 0% reduction in SWF (simulated wound fluid) indicating the significance of wound extracellular micro-environment (e.g. wound fluid, interstitial fluid).

Biatain® Ag demonstrated 99.99% bacterial reduction against *S. aureus*, and Gram-ve (e.g. *P. aeruginosa*, and/or *E. coli*) in both TSB and SWF testing environments at all time points (Figures 6.24, 6.25, 6.26, & 6.27). On the contrary, Biatain® Alginate Ag showed 99% bacterial reduction against *S. aureus* and Gram-ve (e.g. *P. aeruginosa*) only in TSB but not in SWF environment (Figures 6.24, 6.25, 6.26, & 6.27). When tested in a more complex *S. aureus* colonized HSE model (c-HSE), Biatain® Ag was still able to reduce bacterial burden and demonstrated significantly less (P=0.0085, **) Log CFU in Biatain® Ag treated c-HSE, while Biatain® Alginate Ag showed no significant reduction (Figure 6.28). These results demonstrated that as the cell viability decreased, the antibacterial effect increased. Among the tested Ag-dressings, Biatain® Ag was able to significantly reduce bacteria in c-HSE without significantly compromising cell viability of HSE in our advanced experimental set-ups. Other Ag-products were highly compatible with cells but were not significantly lethal to bacteria.

This study analysed antibacterial activity and cytocompatibility of Ag^+ and Ag-products under commonly used antibacterial evaluation methods (broth inoculation method) and 2D cell culture system respectively. The outcomes were compared to the results obtained from advanced HSE & c-HSE based 3D testing systems, demonstrating considerable variations among the two set-ups. In this context, a quick extrapolation of results from laboratory experiments to clinical outcomes must be taken with extreme care. Moreover, results evidenced that a critical approach is required when using specific Ag-containing compounds/materials for wound care needs depending on the patient and the wound situation.

With an increasing need for reliable *in vitro* testing systems, we were successfully able to verify our advanced 3D models, to serve as a risk assessment platform for cytocompatibility and antibacterial properties. HSE and c-HSE have great potential to develop even more complex skin models including micro-vasculature (in dynamic flow) and immunocompetent cells, e.g. monocytes and dendritic cells (mimicking partially the human immune system) for testing skin treatment strategies and designing new antibacterial agents.

For the treatment of chronic wounds, the antibacterial products should also be evaluated for anti-inflammatory properties. In this context, Ag^+ and Ag-products have been shown to have anti-inflammatory and neovascularization effects *in vitro* [55-58], though this needs further experimentation to prove clinical relevance. For this purpose, our 3D system can be used as a base to build more complex immunocompetent models. Despite a few ongoing efforts, there is no immunocompetent model existing at the moment. However, for safety assessment and robust toxicity screening, an immunocompetent model is not necessarily required. The major requirement of HSE model is to predict the cytotoxicity effect of tested compounds, and thus can be used as an alternative to animal testing.

Costs consideration

Our one 12mm diameter HSE tissue preparation (including costs for cells, collagen, inserts, cell culture media, all other ingredients & growth factors, cytotoxicity analysis, and laboratory and personnel costs - as calculated by the researcher herself) together with cytotoxicity analysis costs 120€. Small animal trials [including costs for animal itself, animal maintenance, i.e. for a 6 weeks-study, stock breeding included and included laboratory cost, and personnel costs, as calculated on the basis of data from Charles River Laboratories Ltd., US; Charles River Laboratories GmbH, Germany; Small Animal Facility (SAF) of the Centre for Clinical Research/Medical Faculty, RUB, Bochum, Germany; Large Animal Facility (LAF) of the University Hospital Essen, University Essen-Duisburg, Germany; and the company Life & Device S.r.l., Italy] together with blood tests cost 150€/mice, 250€/immunodeficient mice, 150 €/rat, 300 €/ immunodeficient rat, 300€/ guinea pig, 2,100€/pig. These data are exclusive of the costs for operation, special post-op care, special diagnostics (X-ray, CT, MRI, ultrasonography etc.), all post-mortem analytics, and treatments if necessary, for animals in case of acquired infection etc.

For specific sero-immunological and IHC diagnostics, specific antibodies are routinely and available at affordable costs for mice and rats. For all other species, they are very expensive.

Evaluation of novel biomaterials products for wound treatment

Additional efforts were addressed to the evaluation of the antibacterial properties and cytotoxicity of novel biomaterials: (1) Chitosan/Ag-doped mesoporous bioactive glass composite films (CS/ Ag-MBG) (either using ordered or non-ordered MBGs) (Chapter 07) and (2) Glucose and glucose oxidase (G/GO) encapsulated H_2O_2 releasing HB-PEGDA (hyperbranched polyethylene glycol with numerous acrylate groups)/HA-SH (thiolated hyaluronic acid) based hydrogels (Chapter 08 & 09) developed under HyMedPoly project (https://hymedpoly.eu/).

1. CS/ Ag-MBG composite films

Ag-doped composites (CS/ Ag-MBG) showed a decrease in CTB-derived L929 viability with respect to untreated control (as indicated by direct contact test) of approx. 60% for the CS/ non-ord. Ag-MBG and approx. 23% for the CS/ ord. Ag-MBG composites (Figures 7.5 & 7.6). However, in case of NHEK, the cytotoxic effects were reduced to approx. <20% for both Ag-doped composites as compared to their undoped composite counterparts (Figures 7.11 & 7.12). In the case of CS/ ord. Ag-.MBG composite, Ag release (0.9ppm after 3 days – Table 7.2) could explain the cytotoxicity towards L929 cells, which were indeed more sensitive to silver than were NHEK. However, the low L929 cell viability in contact with CS/ non-ord. Ag-MBG composite could not be correlated to Ag release (0.0ppm for 3 days – Table 7.2), but rather to other factors, such as surface topography, porosity, particle size distribution, wettability, chemical, and mechanical properties (Figures 7.7, 7.8, 7.9, 7.10, & 7.15; and Tables 7.3 & 7.4). Additionally, Ag release was evaluated in SBF, while cell tests were performed in culture medium: probably the interaction of the substrate with SBF during Ag release tests affected the kinetics of Ag release. This means that the measured release data did not reproduce Ag release in culture medium during cell tests. In support to this hypothesis, both Ag-doped composites demonstrated antibacterial activity against tested bacteria, and zone of inhibition (ZOI) values were found similar between CS/ non-ord. Ag-MBG and CS/ ord. Ag-MBG composites (Figures 13 &14; and Table 7.5). Thus, due to antibacterial, cytocompatibility, and water retaining properties, in general, Ag-doped composites especially CS/ ord. Ag-MBG composite might have a potential for wound application. (Chapter 07)

2. H_2O_2 releasing HB-PEGDA/HA-SH based hydrogels

The cytotoxic effects of 10% (w/w) HB-PEGDA/1% (w/w) HA-SH hydrogel samples encapsulated with glucose (2.5%, w/w) and GO at various concentrations (25U/L, 50U/L, 125U/L, 250U/L, 500U/L – Table 9.1) was highly dependent on the type of test procedure -direct contact, indirect contact, and adapted direct contact methods (where samples were pre-treated in cell culture medium)-, and concentration of encapsulated GO. For example, under direct contact test, hydrogels with GO ≤50U/L demonstrated the minimum cytotoxic effect of ~25% with NHDF (Figure 9.14). On the other hand, under indirect contact test, 250U/L GO hydrogels demonstrated approx.~≤32% cytotoxicity with both NHDF and NHEK (Figures 9.21 & 9.22). However, under adapted direct contact test, 250U/L GO hydrogels demonstrated approx. ≤13% cytotoxicity with both NHDF and NHEK (Figures 9.23 & 9.24). (Chapter 09)

H_2O_2 releasing hydrogels, in general, performed better against Gram+ve than against Gram-ve bacteria where hydrogels demonstrated antibacterial activity at comparatively higher GO concentrations (Figure 9.37). Among other differences, the main difference

between Gram+ve and Gram-ve bacteria exists in the intrinsic resistance attributed by the presence of the outer membrane in Gram-ve bacteria as well as the presence of very narrow porins to prevent penetration of even small molecules [59]. H_2O_2 releasing hydrogels prepared using 250U/L GO demonstrated a strong antibacterial effect against a wide range of wound associated pathogens (Figure 9.37). H_2O_2 released from hydrogels at high GO concentrations could be reduced by bacterial burden and wound exudate, decreasing the possible direct cytotoxic effects towards cells. Ideally, burst H_2O_2 release could reduce bacterial burden at initial stages, followed by a sustained lower H_2O_2 release to prevent bacterial re-colonization. (Chapter 09)

As a preliminary H_2O_2 releasing hydrogel system, PLGA (poly L-lactide-co-glycolide)-PEG (polyethylene glycol)-PLGA copolymer was encapsulated with G/GO [G10(w/w) / E1000(U/L), G10/E2000, G20/E1000, and G20/E2000] (Table 9.4). H_2O_2 releasing hydrogels severely affected cell metabolic activity, cell membrane integrity, and cell morphology at all tested G/GO concentrations (Figures 9.39-9.42). Based on that, an optimization of the G/GO relative amount would be needed as to optimize H_2O_2 release. (Appendix-D)

H_2O_2 alone as an active agent was also investigated at a concentration range of 20mM-0.1µM and the cell viability results showed an IC50 of 75.6µM with L929 cells in our experimental set-up (Figure 8.3), while the MIC and MBC (99.9% bacterial reduction) against *S. aureus* was measured to be 500µM (Table 8.4). (Chapter 08)

As a conclusion, H_2O_2 as an antibacterial agent should be used carefully for wound cleaning to kill pathogens, as at high concentrations it might damage newly proliferating cells surrounding the wound area. This should be taken into consideration while choosing H_2O_2 based antibacterial wound dressings.

Moreover, it must be considered that H_2O_2 is naturally produced within cell due to an autoxidation of redox enzymes especially in aerobic bacteria or by a deliberate production to compete with other microbial organisms. Because H_2O_2 is acutely toxic to cells, bacteria tend to scavenge it to keep it at nanomolar intracellular levels. Catalases and NADH peroxidases are two primary scavengers present in many bacteria, therefore, it must be considered while using H_2O_2 as an antibacterial agent. These enzymes are entirely capable of degrading H_2O_2 *in vitro*, though what is their contributions *in vivo* is still not clear [60].

Moreover, the suitability of a certain hydrogel matrix system for G/GO encapsulation, the uniform distribution of GO & its activity inside this polymer matrix, and the susceptibility of covalent linkages of polymers towards peroxidation damage are important to be considered and investigated rationally.

Future developments – Perspective & outlook

Future plans will involve *in vivo* studies on animals to compare results with data obtained using the here developed advanced *in vitro* skin models. Additionally, it will be possible to compare clinical outcomes of the commercially available dressings tested in this study with the results obtained from *in vitro* models.

Meanwhile, we intend to replace the rat tail collagen I used to construct dermal layer of HSE with human-based collagen matrix. For this purpose, we have initiated the experiments using transgenic plants-derived human collagen from an Israeli company CollPlant Ltd.

The toxicity and antibacterial evaluations of novel antimicrobial polymeric materials produced in HyMedPoly was a piece of collaborative work. We intend to continue these collaborations to bio-evaluate the successfully produced antimicrobial materials using our advanced HSE and c-HSE based 3D systems.

Regarding the evaluation of CS/ Ag-MBG composite films, the measured release data (in SBF) did not reproduce Ag release in culture medium used during cell tests. To reproduce the kinetics of Ag release, future release tests should be redone in culture medium or simply in PBS.

Regarding the evaluation of H_2O_2 releasing system, different types of procedures were employed to understand the cytotoxic effect by polymer, released H_2O_2, or their combined effect. However, the H_2O_2 releasing system has to be better characterized as well (as mentioned above), such as optimal immobilization of GO within cross-linked hydrogels, optimal concentration of encapsulated glucose, presence/ release of unpolymerized PEGDA , the amount of immediate (robust) production of H_2O_2 during the hydrogel cross-linking and after its complete gel formation, H_2O_2 release in different types of cell culture media, H_2O_2 consumption in different types cell culture media and by different cell types, consumed amount of H_2O_2 by proteins during pre-treatment step, etc. In biological side, the expression profile of different cell types with respect to different exposed GO concentrations, histological, and immunohistological analysis would be very helpful to address many unanswered questions.

References

1. Gibbs, S., *In vitro irritation models and immune reactions.* Skin pharmacology and physiology, 2009. 22(2): p. 103-113.
2. 2005, *OECD SERIES ON TESTING AND ASSESSMENT Number 34 GUIDANCE DOCUMENT ON THE VALIDATION AND INTERNATIONAL ACCEPTANCE OF NEW OR UPDATED TEST METHODS FOR HAZARD ASSESSMENT.*
3. McNamee, P., et al., *A tiered approach to the use of alternatives to animal testing for the safety assessment of cosmetics: eye irritation.* Regulatory toxicology and pharmacology, 2009. 54(2): p. 197-209.
4. Gibbs, S., et al., *Effect of skin barrier competence on SLS and water-induced IL-1α expression.* Experimental dermatology, 2002. 11(3): p. 217-223.
5. Draize, J.H., G. Woodard, and H.O. Calvery, *Methods for the study of irritation and toxicity of substances applied topically to the skin and mucous membranes.* Journal of pharmacology and Experimental Therapeutics, 1944. 82(3): p. 377-390.
6. Campbell, R.L. and R.D. Bruce, *Comparative dermatotoxicology: I. Direct comparison of rabbit and human primary skin irritation responses to isopropylmyristate.* Toxicology and applied pharmacology, 1981. 59(3): p. 555-563.
7. Phillips II, L., et al., *A comparison of rabbit and human skin response to certain irritants.* Toxicology and Applied Pharmacology, 1972. 21(3): p. 369-382.
8. Youssef, K.K., et al., *Identification of the cell lineage at the origin of basal cell carcinoma.* Nature cell biology, 2010. 12(3): p. 299.
9. Paulitschke, V., et al., *3, 3', 4, 4', 5, 5'-hexahydroxystilbene impairs melanoma progression in a metastatic mouse model.* Journal of Investigative Dermatology, 2010. 130(6): p. 1668-1679.
10. Mancuso, M., et al., *Modulation of basal and squamous cell carcinoma by endogenous estrogen in mouse models of skin cancer.* Carcinogenesis, 2008. 30(2): p. 340-347.
11. Groeber, F., et al., *Skin tissue engineering—in vivo and in vitro applications.* Advanced drug delivery reviews, 2011. 63(4-5): p. 352-366.
12. Menon, G.K., *New insights into skin structure: scratching the surface.* Advanced drug delivery reviews, 2002. 54: p. S3-S17.
13. Khorshid, F.A., *Comparative study of keloid formation in humans and laboratory animals.* Medical science monitor, 2005. 11(7): p. BR212-BR219.
14. Seaton, M., A. Hocking, and N.S. Gibran, *Porcine models of cutaneous wound healing.* ILAR journal, 2015. 56(1): p. 127-138.

15. Summerfield, A., F. Meurens, and M.E. Ricklin, *The immunology of the porcine skin and its value as a model for human skin.* Molecular immunology, 2015. 66(1): p. 14-21.
16. *Council of the European Union. Seventh Amendment to the EU and Cosmetics Directive 76/768/EEC. Brussels: The European Parliament and the Council of the European Union.* 2003.
17. Becker, R.A., et al., *Report of an ISRTP Workshop: Progress and barriers to incorporating alternative toxicological methods in the US.* Regulatory Toxicology and Pharmacology, 2006. 46(1): p. 18-22.
18. Kuroyanagi, Y., et al., *Establishment of banking system for allogeneic cultured dermal substitute.* Artificial organs, 2004. 28(1): p. 13-21.
19. UNION, P., *Regulation (EC) No 1907/2006 of the european parliament and of the council*. 2006.
20. Casale, C., et al., *Endogenous human skin equivalent promotes in vitro morphogenesis of follicle-like structures.* Biomaterials, 2016. 101: p. 86-95.
21. Hadrup, N., A.K. Sharma, and K. Loeschner, *Toxicity of silver ions, metallic silver, and silver nanoparticle materials after in vivo dermal and mucosal surface exposure: A review.* Regulatory Toxicology and Pharmacology, 2018.
22. Mooney, E., C. Lippitt, and J. Friedman, *Plastic surgery educational foundation DC. Silver dressings.* Plast Reconstr Surg, 2006. 117: p. 666-9.
23. Parsons, D., P. Bowler, and M. Walker, *Polishing the information on silver.* Ostomy/wound management, 2003. 49(8): p. 10.
24. Shepherd, J., et al., *Development of three-dimensional tissue-engineered models of bacterial infected human skin wounds.* Tissue Engineering Part C: Methods, 2009. 15(3): p. 475-484.
25. O'Toole, G., H.B. Kaplan, and R. Kolter, *Biofilm formation as microbial development.* Annual Reviews in Microbiology, 2000. 54(1): p. 49-79.
26. Leaper, D., *Appropriate use of silver dressings in wounds: international consensus document.* International wound journal, 2012. 9(5): p. 461-464.
27. Opasanon, S., P. Muangman, and N. Namviriyachote, *Clinical effectiveness of alginate silver dressing in outpatient management of partial-thickness burns.* International wound journal, 2010. 7(6): p. 467-471.
28. Muangman, P., et al., *A prospective, randomized trial of silver containing hydrofiber dressing versus 1% silver sulfadiazine for the treatment of partial thickness burns.* International wound journal, 2010. 7(4): p. 271-276.
29. Dimakakos, E., et al., *Infected Venous Leg Ulcers: Management With Silver-releasing Foam Dressing.* Wounds: a compendium of clinical research and practice, 2009. 21(1): p. 4-8.
30. Lazareth, I., et al., *The Role of a Silver Releasing Lipido-colloid Contact Layer in Venous Leg Ulcers Presenting Inflammatory Signs Suggesting Heavy*

Bacterial Colonization: Results of a Randomized Controlled Study. Wounds: a compendium of clinical research and practice, 2008. 20(6): p. 158-166.

31. Munter, K.-C., et al., *Effect of a sustained silver-releasing dressing on ulcers with delayed healing: the CONTOP study.* Journal of wound care, 2006. 15(5): p. 199-206.
32. Jude, E., et al., *Prospective randomized controlled study of Hydrofiber® dressing containing ionic silver or calcium alginate dressings in non-ischaemic diabetic foot ulcers.* Diabetic Medicine, 2007. 24(3): p. 280-288.
33. Jørgensen, B., et al., *The silver-releasing foam dressing, Contreet Foam, promotes faster healing of critically colonised venous leg ulcers: a randomised, controlled trial.* International Wound Journal, 2005. 2(1): p. 64-73.
34. Meaume, S., et al., *Evaluation of a silver-releasing hydroalginate dressing in chronic wounds with signs of local infection.* Journal of wound care, 2005. 14(9): p. 411-419.
35. Romanelli, M. and P. Price, *Health-related quality of life aspects after treatment with a foam dressing and a silver-containing foam dressing in chronic leg ulcers.* Journal of the American Academy of Dermatology, 2005. 52(3): p. P211.
36. Russell, L., *The CONTOP multinational study: preliminary data from the UK arm.* WOUNDS UK, 2005. 1(1): p. 44.
37. Verd Soriano, J., et al., *Effects of an activated charcoal silver dressing on chronic wounds with no clinical signs of infection.* Journal of wound care, 2004. 13(10): p. 419-423.
38. Wunderlich, U. and C. Orfanos, *Treatment of venous ulcera cruris with dry wound dressings. Phase overlapping use of silver impregnated activated charcoal xerodressing.* Der Hautarzt; Zeitschrift fur Dermatologie, Venerologie, und verwandte Gebiete, 1991. 42(7): p. 446-450.
39. Jurczak, F., et al., *Randomised clinical trial of Hydrofiber dressing with silver versus povidone–iodine gauze in the management of open surgical and traumatic wounds.* International wound journal, 2007. 4(1): p. 66-76.
40. Michaels, J., et al., *Randomized controlled trial and cost-effectiveness analysis of silver-donating antimicrobial dressings for venous leg ulcers (VULCAN trial).* British Journal of Surgery: Incorporating European Journal of Surgery and Swiss Surgery, 2009. 96(10): p. 1147-1156.
41. *Best Practice Statement: The use of topical antiseptic/antimicrobial agents in wound management, 2nd edition.* Wounds UK, 2011.
42. Trial, C., et al., *Assessment of the antimicrobial effectiveness of a new silver alginate wound dressing: a RCT.* Journal of Wound Care, 2010. 19(1): p. 20-26.
43. Michaels, J., et al., *A prospective randomised controlled trial and economic modelling of antimicrobial silver dressings versus non-adherent control dressings for venous leg ulcers: the VULCAN trial.* Health Technol Assess, 2009. 13(56): p. 1-114.

44. Leaper, D. and R. Drake, *Should one size fit all? An overview and critique of the VULCAN study on silver dressings.* International wound journal, 2011. 8(1): p. 1-4.
45. Gottrup, F. and J. Apelqvist, *The challenge of using randomized trials in wound healing.* British Journal of Surgery: Incorporating European Journal of Surgery and Swiss Surgery, 2010. 97(3): p. 303-304.
46. White, R., et al., *Randomized controlled trial and cost-effectiveness analysis of silver-donating antimicrobial dressings for venous leg ulcers (VULCAN trial)(Br J Surg 2009; 96: 1147–1156).* British Journal of Surgery: Incorporating European Journal of Surgery and Swiss Surgery, 2010. 97(3): p. 459-460.
47. Poon, V.K. and A. Burd, *In vitro cytotoxity of silver: implication for clinical wound care.* Burns, 2004. 30(2): p. 140-147.
48. Supp, A.P., et al., *Evaluation of cytotoxicity and antimicrobial activity of Acticoat® burn dressing for management of microbial contamination in cultured skin substitutes grafted to athymic mice.* Journal of Burn Care & Rehabilitation, 2005. 26(3): p. 238-246.
49. Cochrane, C., et al., *The effect of several silver-containing wound dressings on fibroblast function in vitro using the collagen lattice contraction model.* WOUNDS-A COMPENDIUM OF CLINICAL RESEARCH AND PRACTICE, 2006. 18(2): p. 29-34.
50. Lam, P., et al., *In vitro cytotoxicity testing of a nanocrystalline silver dressing (Acticoat) on cultured keratinocytes.* British journal of biomedical science, 2004. 61(3): p. 125-127.
51. Leaper, D.J., *Silver dressings: their role in wound management.* International wound journal, 2006. 3(4): p. 282-294.
52. Innes, M.E., et al., *The use of silver coated dressings on donor site wounds: a prospective, controlled matched pair study.* Burns, 2001. 27(6): p. 621-627.
53. Dunn, K. and V. Edwards-Jones, *The role of Acticoat™ with nanocrystalline silver in the management of burns.* Burns, 2004. 30: p. S1-S9.
54. Wright, J.B., et al., *Early healing events in a porcine model of contaminated wounds: effects of nanocrystalline silver on matrix metalloproteinases, cell apoptosis, and healing.* Wound Repair and Regeneration, 2002. 10(3): p. 141-151.
55. Lansdown, A. and A. Williams, *How safe is silver in wound care?* Journal of wound care, 2004. 13(4): p. 131-136.
56. Lansdown, A.B., *A pharmacological and toxicological profile of silver as an antimicrobial agent in medical devices.* Advances in pharmacological sciences, 2010. 2010.
57. Walker, M., P.G. Bowler, and C.A. Cochrane, *In vitro studies to show sequestration of matrix metalloproteinases by silver-containing wound care products.* Ostomy Wound Management, 2007. 53(9): p. 18.

58. Wilkinson, L., R. White, and J. Chipman, *Silver and nanoparticles of silver in wound dressings: a review of efficacy and safety.* Journal of wound care, 2011. 20(11): p. 543-549.
59. Nikaido, H. and M. Vaara, Molecular basis of bacterial outer membrane permeability. Microbiological reviews, 1985. 49(1): p. 1.
60. Mishra, S. and J. Imlay, Why do bacteria use so many enzymes to scavenge hydrogen peroxide? Archives of biochemistry and biophysics, 2012. 525(2): p. 145-160.